

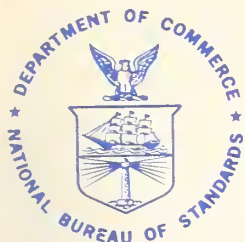
A11100 985894

NATL INST OF STANDARDS & TECH R.I.C.



A1100985894

/Applications of phase diagrams in metal
QC100 .U57 V496,2:1978 C.2 NBS-PUB-C 197



NBS SPECIAL PUBLICATION 496

U.S. DEPARTMENT OF COMMERCE / National Bureau of Standards



National Bureau of Standards
Library, E-01 Admin. Bldg.

OCT 1 1981

191051

QC

100

.U57

Applications of Phase Diagrams in Metallurgy and Ceramics

Volume 2

NATIONAL BUREAU OF STANDARDS

The National Bureau of Standards¹ was established by an act of Congress March 3, 1901. The Bureau's overall goal is to strengthen and advance the Nation's science and technology and facilitate their effective application for public benefit. To this end, the Bureau conducts research and provides: (1) a basis for the Nation's physical measurement system, (2) scientific and technological services for industry and government, (3) a technical basis for equity in trade, and (4) technical services to promote public safety. The Bureau consists of the Institute for Basic Standards, the Institute for Materials Research, the Institute for Applied Technology, the Institute for Computer Sciences and Technology, the Office for Information Programs, and the Office of Experimental Technology Incentives Program.

THE INSTITUTE FOR BASIC STANDARDS provides the central basis within the United States of a complete and consistent system of physical measurement; coordinates that system with measurement systems of other nations; and furnishes essential services leading to accurate and uniform physical measurements throughout the Nation's scientific community, industry, and commerce. The Institute consists of the Office of Measurement Services, and the following center and divisions:

Applied Mathematics — Electricity — Mechanics — Heat — Optical Physics — Center for Radiation Research — Laboratory Astrophysics² — Cryogenics² — Electromagnetics² — Time and Frequency².

THE INSTITUTE FOR MATERIALS RESEARCH conducts materials research leading to improved methods of measurement, standards, and data on the properties of well-characterized materials needed by industry, commerce, educational institutions, and Government; provides advisory and research services to other Government agencies; and develops, produces, and distributes standard reference materials. The Institute consists of the Office of Standard Reference Materials, the Office of Air and Water Measurement, and the following divisions:

Analytical Chemistry — Polymers — Metallurgy — Inorganic Materials — Reactor Radiation — Physical Chemistry.

THE INSTITUTE FOR APPLIED TECHNOLOGY provides technical services developing and promoting the use of available technology; cooperates with public and private organizations in developing technological standards, codes, and test methods; and provides technical advice services, and information to Government agencies and the public. The Institute consists of the following divisions and centers:

Standards Application and Analysis — Electronic Technology — Center for Consumer Product Technology: Product Systems Analysis; Product Engineering — Center for Building Technology: Structures, Materials, and Safety; Building Environment; Technical Evaluation and Application — Center for Fire Research: Fire Science; Fire Safety Engineering.

THE INSTITUTE FOR COMPUTER SCIENCES AND TECHNOLOGY conducts research and provides technical services designed to aid Government agencies in improving cost effectiveness in the conduct of their programs through the selection, acquisition, and effective utilization of automatic data processing equipment; and serves as the principal focus within the executive branch for the development of Federal standards for automatic data processing equipment, techniques, and computer languages. The Institute consist of the following divisions:

Computer Services — Systems and Software — Computer Systems Engineering — Information Technology.

THE OFFICE OF EXPERIMENTAL TECHNOLOGY INCENTIVES PROGRAM seeks to affect public policy and process to facilitate technological change in the private sector by examining and experimenting with Government policies and practices in order to identify and remove Government-related barriers and to correct inherent market imperfections that impede the innovation process.

THE OFFICE FOR INFORMATION PROGRAMS promotes optimum dissemination and accessibility of scientific information generated within NBS; promotes the development of the National Standard Reference Data System and a system of information analysis centers dealing with the broader aspects of the National Measurement System; provides appropriate services to ensure that the NBS staff has optimum accessibility to the scientific information of the world. The Office consists of the following organizational units:

Office of Standard Reference Data — Office of Information Activities — Office of Technical Publications — Library — Office of International Standards — Office of International Relations.

¹ Headquarters and Laboratories at Gaithersburg, Maryland, unless otherwise noted; mailing address Washington, D.C. 20234.

² Located at Boulder, Colorado 80302.

APR 26 1978

Applications of Phase Diagrams in Metallurgy and Ceramics

Volume 2

Proceedings of a Workshop Held at the
National Bureau of Standards
Gaithersburg, Maryland, January 10-12, 1977

Edited by

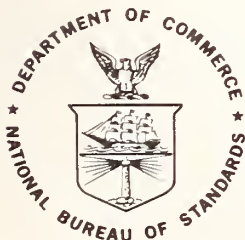
G.C. Carter

Institute for Materials Research
National Bureau of Standards
Washington, D.C. 20234

Sponsored by:

Institute for Materials Research and
Office of Standard Reference Data, NBS
and by

National Science Foundation
Defense Advanced Research Projects Agency
Office of Naval Research
National Aeronautics and Space Administration
Energy Research and Development Administration
U.S. Army Research Office



U.S. DEPARTMENT OF COMMERCE, Juanita M. Kreps, Secretary

Dr. Sidney Harman, Under Secretary

Jordan J. Baruch, Assistant Secretary for Science and Technology

NATIONAL BUREAU OF STANDARDS, Ernest Ambler, Director

Issued March 1978

Library of Congress Catalog Card Number: 78-2201

National Bureau of Standards Special Publication 496/2

Nat. Bur. Stand. (U.S.) Spec. Publ. 496/2, 847 pages (March 1978)

CODEN: XNBSAV

U.S. GOVERNMENT PRINTING OFFICE
WASHINGTON: 1978

For sale by the Superintendent of Documents, U.S. Government Printing Office, Washington, D.C. 20402

Stock No. 003-003-01895-3

2-volume set; sold in sets only.

(Add 25 percent additional for other than U.S. mailing).

General Abstract

The proceedings of a Workshop on Applications of Phase Diagrams in Metallurgy and Ceramics, held at the National Bureau of Standards, Gaithersburg, Maryland, on January 10-12, 1977, is presented in this NBS Special Publication. The Workshop was co-sponsored by the Institute for Materials Research and the Office of Standard Reference Data, NBS, and the National Science Foundation, the Defense Advanced Research Projects Agency, the Office of Naval Research, the National Aeronautics and Space Administration, the Energy Research and Development Administration, and the U. S. Army Research Office.

The purpose of the Workshop was to assess the current national and international status of phase diagram determinations and evaluations for alloys, ceramics and semiconductors; to determine the needs and priorities, especially technological, for phase diagram determinations and evaluations; and to estimate the resources being used and potentially available for phase diagram evaluation. These proceedings reflect the detailed contents of the Workshop for both the tutorial and review sessions as well as four poster sessions and four panel sessions covering the subjects; critical phase diagram availability, user needs of phase diagrams, experimental methods of determination, theoretical methods of calculation and prediction, methods of phase diagram representations of calculation and prediction, methods of phase diagram representations (especially multicomponent) and distribution to the user. Three of the panels addressed the subject of phase diagram needs in industrial applications.

These proceedings represent documentation of this assessment, and constitute a valuable resource to workers in these areas, especially those planning to initiate phase diagram programs. Most subjects within the overall scope have been dealt with substantially in these proceedings; a few specialized topics such as surface and small particle phases, needed for the study of catalysis, have not been treated in detail. As the Alloy Data Center maintains a continuing phase diagram program, we would like to receive suggestions for similar topics of current and future interest, descriptions of new needs, or addenda and corrigenda to these proceedings. A tear-off sheet has been provided at the end of these proceedings for this purpose to be sent to the NBS Alloy Data Center.

KEY WORDS: Ceramics; computer predictions; critical evaluations; data compilations; electronic materials; industrial needs; metallurgy; phase diagrams; theory of phase diagrams; thermodynamics.

Foreword

Quantitative data on physical and chemical properties of materials form a key resource of modern technology. In the past a few dedicated scientists and engineers have performed an important service by compiling and evaluating such data for use by the technical community; an outstanding example is the work of Hansen on alloy phase diagrams. With the rapid growth of science and technology, this task has become too large and complex for a single individual. Organized programs with proper funding and continuity are essential if the technical community is to have the reliable data needed to solve the problems of modern society.

This Workshop represents an effort to coordinate and reinforce the current efforts on compilation of phase diagrams of alloys and ceramics. Many research groups and individual scientists throughout the world are concerned with phase equilibrium data.

Specialized expertise exists in small institutions as well as large laboratories. If this talent can be effectively utilized through a cooperative effort, the needs for such data can be met. The Office of Standard Reference Data, which serves as the program management office for the National Standard Reference Data System, is eager to work with all groups concerned with this problem. Through a cooperative international effort we can carry out a task which has become too large for an individual.

David R. Lide, Jr.
Chief
Office of Standard Reference Data
National Bureau of Standards

CONTENTS

	Page
General Abstract.....	iii
Foreword.....	v
Welcome - E. Ambler.....	xv
Overview of the Workshop - G.C. Carter.....	xvii
Workshop Organizing Committee	xviii

VOLUME 1

Present Status of Phase Diagram Compilation Activities

Phase Diagram Compilation Activities in Ceramics	
R.S. Roth, L.P. Cook, T. Negas, G.W. Cleek, and J.B. Wachtman, Jr.	1
Discussion	22
Present Status of Phase Diagram Compilation Activity for Semiconductors	
C.D. Thurmond.....	23
Phase Diagram Compilations for Metallic Systems - An Assessment of Ongoing Activities	
G.C. Carter.....	36
Organization of Phase Diagram Information in the Soviet Union	
N.V. Ageev, D.L. Ageeva, T.P. Kolesnikova, and L.A. Petrova.....	90
Discussion.....	95
A Survey of High Pressure Phases of Materials	
L. Merrill.....	100
Discussion (Jan. 10 - AM Session)	121
Phase Diagram Information from Computer Banks	
I. Ansara.....	123
An Overview of the Determination of Phase Diagrams	
F.N. Rhines.....	142
Discussion.....	163

Phase Diagram Compilation and Data Evaluation Activities

Proposal for a Comprehensive Handbook on "Ternary Phase Diagrams of Metals"	
F. Aldinger, E.-Th. Henig, H.L. Lukas, and G. Petzow	164
Phases and Phase Relations in the Binary Oxide Systems Containing WO ₃	
Luke L.Y. Chang.....	165

RIC in Phase with Rare-Earth Constitutional Diagrams K.A. Gschneidner, Jr., M.E. Verkade and B.L. Evans.....	226
Evaluations of Phase Diagrams and Thermodynamic Properties of Ternary Copper Alloy Systems Y.A. Chang, J.P. Neumann, U.V. Choudary.....	229
Phase Equilibria in Variable Valence Oxide Systems W.B. White.....	251
Phase Diagrams for Ceramists L.P. Cook, R.S. Roth, T. Negas and G.W. Cleek.....	257
NBS Crystal-Data Center A. Mighell, H. Ondik, J. Stalick, R. Boreni.....	259
The NBS Alloy Data Center G.C. Carter, D.J. Kahan, and L.H. Bennett.....	261
A Review of Phase Equilibria in the $\text{Na}_3\text{AlF}_6\text{-LiF-CaF}_2\text{-AlF}_3\text{-Al}_2\text{O}_3$ System D.F. Craig, R.T. Cassidy, and J.J. Brown, Jr.	272
Methods of Compiling and Editing "Structure and Properties of Binary Metallic Systems" A.E. Vol and I.K. Kagan.....	346
English Translation	351
Experimental Techniques in Phase Diagram Determinations	
The Determination of Phase Diagrams for Liquid Oxides and Metallurgical Slags by Hot-Wire Microscopy H.A. Fine.....	355
Experimental Techniques in Phase Diagram Determination of Superconducting Compounds Containing Volatile Components at Temperatures up to 2200°C R. Flukiger and J.-L. Jorda	375
Application of Experimental Techniques and the Critical Determination of Phase Equilibria in Oxide Systems F.P. Glasser.....	407
Protective Coatings for Superalloys and the Use of Phase Diagrams M.R. Jackson and J.R. Rairden	423
Application of the Scanning Electron Microscope to the Study of High Temperature Oxide Phase Equilibria L.P. Cook and D.B. Minor.....	440

Hyperfine Techniques and the Determination of Phase Diagrams	
R.C. Reno, L.J. Swartzendruber, G.C. Carter , and L.H. Bennett.....	450
Experimental Determination of Phase Diagrams with the Electron Microprobe and Scanning Transmission Electron Microscope	
A.D. Romig, Jr. and J.I. Goldstein.....	462
Interrelations Between Phase Diagrams and Hydriding Properties for Alloys Based on the Intermetallic Compound FeTi	
G.D. Sandrock, J.J. Reilly, and J.R. Johnson.....	483
Phase Equilibria in the System MgO-RCl (R=Li, Na and K) Solution Under Hydrothermal Conditions by Means of a Capsule Bursting Method	
Shigeyuki Sōmiya, Kazuo Nakamura, Shin-ichi Hirano and Shinroku Saito	508
High-Energy Ion Beams in Phase Diagram Determination	
J.E. Smugeresky, and S.M. Myers.....	516
Phase Equilibrium Diagrams in Terms of Electronic Structure	
F. E. Wang.....	545
Use of Segregation Phenomena in Solid Solutions as a Method for Determining Solidification Diagrams. Application to some Sc_2O_3 - Ho_2O_3 and Sc_2O_3 - Dy_2O_3 Systems	
J.M. Badie.....	550
Studies of the Fe-C-B Phase Diagram by Autoradiography	
T.B. Cameron and J.E. Morral.....	566
User Needs for Phase Diagrams	
P. J. Fopiano.....	567
Phase Diagram of a Specimen at High Temperatures Under External Tensile or Shear Stress or Both	
K.M. Khanna.....	575
Phase Diagram of a Metal-Gas System	
V.K. Sinha.....	578
Methods of Phase Diagram Calculations	
Theory of Alloy Phases	
R.E. Watson, H.Ehrenreich and L.H.Bennett.....	592
Discussion.....	620

Computation and Prediction of Phase Diagrams (Panel I)

Estimation of Conjugate γ and γ' Compositions in Ni-Base Superalloys R.L. Dreshfield.....	624
Discussion (Panel I - Jan. 11).....	658

Review of Phase Diagram Representations, Format, and Distribution

The Representation of Phase Equilibria A. Prince.....	660
Phase-Diagram Compilations - A User's View J.D. Livingston.....	703
Some Thoughts on the Distribution of Reference Data H. J. White, Jr.....	709
Remarks on Producing and Publishing Critically Evaluated Data W.B. Pearson.....	720
Discussion (Jan. 11 - PM Session).....	725
AUTHOR INDEX	725-A
SUBJECT INDEX	725-C
MATERIALS INDEX	725-J

VOLUME 2

Computational Techniques for Phase Diagram Construction

Computerized Characterization of the Au-Cu-Ni Ternary System S.K. Tarby, C.J. Van Tyne, and M.L. Boyle.....	726
Correlations and Predictions of Metal-Boron Phase Equilibria K.E. Spear.....	744
A Valence Bond Test for the Validity of Intermetallic and Semiconducting Structures F.L. Carter.....	763
Computation of the Component Activities from Ternary Miscibility Gap Data: The Cu-Ag-S and Cu-Ag-Se Systems U.V. Choudary and Y.A. Chang.....	774
The Mathematical Representation of Activity Data in Three Component Systems I. Eliezer and R.A. Howald.....	803
A Program for Binary Phase Equilibria Using the Redlich- Kister Equations I. Eliezer and R. A. Howald.....	846
Polynomial Representation of the Excess Free Energy of Multicomponent Systems and Their Use in Phase Diagram Calculations H. Gaye and C.H. P. Lupis	907

Thermodynamic Data for the Fe-O System Evaluated Using a New Computer-Aided Strategy J.L. Haas, Jr. and J.R. Fisher.....	909
Analysis and Synthesis of Phase Diagrams of the Fe-Cr-Ni, Fe-Cu-Mn and Fe-Cu-Ni Systems M. Hasebe and T. Nishizawa.....	911
Optimization of Phase Diagrams by a Least Squares Method Using Simultaneously Different Types of Data E.-Th. Henig, H.L. Lukas, B. Zimmermann and G. Petzow ..	955
Theoretical Calculation of Phase Diagrams Using the Cluster Variation Method R. Kikuchi and D. de Fontaine	967
Fundamental Calculations of Coherent Phase Diagrams D. de Fontaine and R. Kikuchi.....	999
Discussion.....	1017
Generation of Self-Consistent Gibbs Energy Functions for Binary Systems: The Fe-Cu System as an Example J.F. Smith, D.M. Bailey and O. Kubaschewski.....	1027
Characteristics and Calculation of Stability Diagrams S. McCormick and Y. Bilimoria.....	1047
The Effect of Irradiation on Phase Stability L. Kaufman, J.S. Watkin, J.H. Gittus. and A.P. Miodownik	1065
Facility for the Analysis of Chemical Thermodynamics (F*A*C*T) - A Computerized Canadian Thermodynamic Data Treatment Centre A.D. Pelton, C.W. Bale, and W.T. Thompson.....	1077
The Calculation of Pourbaix Diagrams Using a Modified Linear Programming Technique B.H. Rosof.....	1090
Theoretical Concepts Useful in the Calculation or Storage of Phase Diagrams of Ionic Systems M.-L. Saboungi and M. Blander.....	1093
Estimation of Isothermal Sections of Ternary Phase Diagrams of Lithium Containing Systems: The Al-Li-Mg System M.-L. Saboungi and C.C. Hsu.....	1109
Cybernetic Prediction of the Formation of Chemical Compounds in Uninvestigated Systems E.M. Savitskii, V.P. Gribulya, and N.N. Kiselyeva	1139
English Translation.....	1151

The Determination and Representation of Metastable Phase Diagram Features and Other Thermal Characteristics of Metastable Alloys, Especially Amorphous Metals	
B.C. Giessen.....	1161
Discussion.....	1183
 The Calculation of Multicomponent Alloy Phase Diagrams at the National Physical Laboratory	
T.G. Chart.....	1186
 Synthesis of Binary Metallic Systems I. Isomorphous Systems II. Simple Eutectic Systems	
S.S. Balakrishna, and A. K. Mallik.....	1200
 Quantitative Fits to Phase Lines and High Temperature Thermodynamic Data for Systems Forming Semiconductor Compounds	
R.F. Brebrick.....	1220
 Format and Distribution of Phase Diagram Data	
Table of Contents and Cumulative Subject Index for "Phase Diagrams of Metallic Systems," N.V. Ageev, editor, Volumes 1-19	
C.M. Scheuermann	1237
 Standards for Publication of Phase Equilibrium Studies	
E.R. Kreidler.....	1307
 Formatting and Distributing Evaluated Reference Data: The Office of Standard Reference Data at the National Bureau of Standards	
S.P. Fivozinsky and G.B. Sherwood.....	1325
 User Needs for Phase Diagram Information (Panel II)	
Panel Discussion: Primary Metal Production	
J.F. Elliott.....	1332
 Needs for Phase Diagram Information in Non-Ferrous Industry	
P.R. Ammann.....	1334
Discussion.....	1353
 Primary Metals Production	
H.R. Larson.....	1354
Discussion.....	1357
 Use of Phase Diagrams in Iron and Steelmaking	
R.D. Pehlke.....	1360
Discussion.....	1371

Materials Processing (Fabricating, Machining, Heat Treating, etc.)
(Panel III)

User Needs for Phase Diagrams for Materials Processing:

Glasses

R.C. Doman, and R.N. McNally 1378

Equilibrium Diagrams in Non-Ferrous Alloys

L.F. Mondolfo..... 1382

Phase Equilibria in the Development of High Temperature
Structural Ceramics

S. Prochazka..... 1409

Phase Diagram Information for Processing of Superconductors

D. Dew-Hughes..... 1411

Product Applications (User Needs for Phase Diagram Information)
(Panel IV)

Panel Discussion: Product Applications

F.L. VerSnyder..... 1418

Importance of Phase Diagrams in the Electric Power Industry

R.I. Jaffee..... 1420

Summary of Presentation on User Needs of Phase Diagrams:
The Solar Energy Field

A.I. Mlavsky..... 1426

The Use of Phase Equilibria in the Manufacture of Spinel
Ferrites

P. Slick..... 1427

The Application of the Phase Diagram to Thermal Energy
Storage Technology

J.E. Beam and J.E. Davison..... 1428

The Needs for Phase Equilibria Data in the Development
of Magnetohydrodynamics

R.A. Howald and I. Eliezer..... 1440

Discussion..... 1451

Summary Remarks

J. F. Elliott..... 1453

Evaluation of Conference

R.A. Howald..... 1470

Evaluation of Conference

J.E. Selle..... 1471

Comments on the Phase Diagram Workshop	
D. de Fontaine.....	1472
Additional Contributed Papers to the Workshop	
The Relation Between Bond Length and Crystal Structures in Metals	
A.P. Miodownik.....	1479
On Computerized Construction of Multidimensional Phase Diagrams in a Factographic IRS	
I.V. Tulupova and V.S. Stein.....	1506
REGISTRATION LIST.....	1520
AUTHOR INDEX.....	1529
SUBJECT INDEX.....	1531
MATERIALS INDEX.....	1538

Disclaimer

Certain commercial products and instruments are identified in this publication in order to specify adequately the experimental procedure. In no case does such identification imply recommendation or endorsement by the National Bureau of Standards, nor does it imply that the products or equipment identified are necessarily the best available for the purpose.

Welcome to the Workshop on Applications of
Phase Diagrams in Metallurgy and Ceramics

E. Ambler

Good morning. It is my pleasure to welcome you this morning to the National Bureau of Standards and this Workshop on Applications of Phase Diagrams in Metallurgy and Ceramics. Evidence of the broad interest in and importance of this subject matter is seen when one notes that the National Science Foundation, Defense Advance Research Project Agency, Office of Naval Research, National Aeronautics and Space Administration, and U. S. Army Research Office have joined with the NBS Institute for Materials Research and NBS Office of Standard Reference Data in the sponsorship of this workshop.

As I looked over the material for this workshop, I found this group to be truly international and interdisciplinary in scope. There are participants here from Canada, France, Germany, India, Japan, the United Kingdom, Switzerland, the Union of Soviet Socialist Republics, and our own United States. You include representatives from data compilation groups, major industries and trade associations, and scientists from industry, government and university laboratories.

Of special interest to me is your banquet speaker, W. Dale Compton, who is the Vice President for Scientific Research at the Ford Motor Company. In addition, Dale is also a member of the NBS Visiting Committee - our Board of Directors so to speak - and the former chairman of the National Science Foundation Numerical Advisory Board. I look forward to joining you for the banquet and Dale's presentation.

For more than 100 years, phase diagrams have been a recognized and important tool in the development of science and technology. As one example, phase diagrams formed the basis for the development of new alloys and the respective heat treatments for these alloys. This resulted in new materials highly characterized and tailored to a host of specific uses. Today, phase diagrams are increasingly relevant to the development of new and substitute materials.

Now, as we stand at the threshold of this Workshop, it seems an appropriate time to spend a brief moment clarifying our perspective concerning the development of phase diagrams. Where do we stand in the study of phase diagrams and the compilation of phase diagram data? Clearly, the studies of and the techniques used today are vastly different than those of yesterday.

The optical microscope was used 100 years ago to study the character of alloys and minerals. By 1914, x-rays were used to confirm the crystalline structure of materials. The 1930's brought the advent of the electron microscope and a higher resolution of the materials being studied. From that evolved the electron microprobe which allowed us to determine the chemical composition of an individual phase on a spatial resolution of two to three μm in diameter. More recently, we have seen the development of the scanning electron microscope, the field ion microscope, and the Auger electron spectrometer.

Over the past 30 - 35 years, we have witnessed and participated in an evolution in experimental techniques. Today, we are able to determine phase diagrams to a high level and detail of accuracy. Certainly, our techniques are vastly improved. But the task we face is still enormous. Just consider the study of alloys. In the study of binarys, there are 1770 possible diagrams; with ternaries, there are 34,200 possible phase diagrams; and with quaternaries, there are many, many possible diagrams. To compound this task is the fact that it is the multicomponent materials which are of the greatest interest today.

To meet this problem, new techniques are now being developed which are based on a theoretical understanding of materials. We find that we can achieve "paper calculations" through theoretical prediction of phase diagrams. In addition, we can develop mathematical models that are predictive. However, the validity of these models is dependent on the availability of accurate data. Thus, while we strive to predict complicated phenomena, we do so with the clear understanding that we must first develop a simple, accurate data base.

An assessment of today's environment then shows that although we possess many new and improved tools, they are still not sufficient to perform the task that faces us. Therefore, we stand in a position where our first order of business should be an assessment of priorities. The goals of this workshop:

- ° To assess the current national and international status of phase diagram determination and evaluation for alloys, ceramics and semi-conductors;
- ° To determine the needs and priorities, especially technological, for phase diagram determinations and evaluations; and
- ° To estimate the resources being used and potentially available for phase diagram evaluation;

are quite timely. In fact, I think that the key statement for this workshop is found on page 1 of your program: "It is hoped that the workshop will provide the stimulus for the production of more relevant more useful, and more useable phase diagram data."

I concur with that statement and heartily endorse the goals of this workshop. Moreover, it is my personal belief that communication, such as this workshop is intended to foster, is a critical component to all scientific and technological ventures.

In closing, again let me welcome you to NBS. Our facilities are at your disposal and we would invite any inquiries about our specific programs that are of interest to you. I look forward to joining you Tuesday evening and I hope that your workshop is both stimulating and productive.

Overview of the Workshop

G. C. Carter

Knowledge of the structure of materials is important in understanding several industrially significant phenomena and applications such as aging, hardness, occurrence of brittle intermetallic compounds, magnetic transition temperatures, high-temperature solubility of impurities, corrosion resistance, solid electrolytes and non-crystalline solids. The study of a phase diagram appropriate to a particular material can often provide information important to its scientific and technical application.

Wide participation by industry, government, and university representatives was achieved at the Workshop. International participation was particularly successful among the data evaluation groups including important representations from the Soviet Union, Germany, France, the UK, Japan, and Canada. Other countries were represented; experimentalists and theorists determining phase diagrams were among the participants, as were a substantial fraction of phase diagram users from industry.

Specific subjects of investigation were:

- ... to assess the current national and international status of phase diagram determinations and evaluations for alloys, ceramics and semiconductors; to identify resources being expended that could be made more useful by appropriate coordination; to recognize unnecessarily overlapping efforts in determining phase diagrams; to suggest areas of international cooperation.
- ... to determine the needs and priorities, especially technological, for phase diagram determinations and evaluations; to gauge the relative importance of depth of coverage and range of materials including factors such as a) high precision, b) metastable phases, c) binary and higher order systems, d) magnetic, metal nonmetal and other phase transitions, e) high pressure data, f) integration of collateral information, and g) the role of impurities or trace additions.
- ... to review the strengths and limitations of various experimental techniques for determining phase diagrams,
- ... to briefly survey the status and merits of various predictive methods (CALPHAD, PHACOMP, pseudopotential, etc.),
- ... to discuss diverse presentation methods, and
- ... to discuss effective and alternative means for dissemination of phase diagram data.

The workshop program was designed to stimulate interactions between (i) phase diagram data providers and users, (ii) metallurgists, geochemists, thermochemists, ceramics, solid state chemists, physicists, and scientists in other disciplines, (iii) representatives from industry, government, and the academia, (iv) phase diagram data centers throughout the world.

Plenary lectures introduced the subjects of present status of data availability from reference books, data centers and computerized files, the status of experimental data and theory of alloy phases. A panel on computation and prediction gave a more thorough introduction to that subject, and short reviews introduced the subjects of phase diagram representations and methods of distribution. Lively poster sessions followed these introductions. Three panel sessions were devoted to industrial needs in (i) Primary Metals Production, (ii) Materials Processing, and (iii) Product Applications. Discussion covered needs for multicomponent diagrams (up to 9 or 10 components) for industrial applications down to binary equilibrium diagrams, for various R & D programs, theoretical and prediction models, and other applications.

Four on-line demonstrations of computer-data handling systems related to phase diagrams were held and short instructional movies were shown during the poster session.

The workshop was organized by the Alloy Data Center and the group compiling "Phase Diagrams for Ceramists". The success of the Workshop program could not have been realized without invaluable assistance received from our very able organizing committee.

WORKSHOP ORGANIZING COMMITTEE

Members from NBS

L. H. Bennett, chairman
G. T. Armstrong, C. J. Bechtoldt, D. B. Butrymowicz, G. C. Carter, L. P. Cook, J. R. Cuthill, P. R. deBruyn, D. J. Kahan, M. B. McNeil, R. L. Parker, R. M. Waterstrat, H. J. White

Members from other Organizations

N. Ault, Norton Co., Worcester, MA
J. Elliott, M.I.T., Cambridge, MA
S. G. Epstein, Aluminum Association, New York, NY
L. Kaufman, ManLabs, Cambridge, MA
R. Laudise, Bell Telephone Laboratories, Murray Hill, NJ
J. D. Livingston, General Electric, Schenectady, NY
E. S. Osborne, Carnegie Geophysical Lab., Washington, DC
E. C. Van Reuth, Defense Advanced Res. Projects Agency, Arlington, VA
Schrade F. Radtke, Intl. Lead-Zinc Research Organization, New York, NY
R. Reynik, National Science Foundation, Washington, DC
E. Salkovitz, Office of Naval Research, Arlington, VA
L. M. Schetky, International Copper Research Assoc., New York, NY
C. Scheuermann, NASA Lewis Research Center, Cleveland, OH
M. Semchyschen, Climax Molybdenum Corp., Ann Arbor, MI
J. Swisher, Energy Research & Development Admin., Washington, DC

ARRANGEMENTS COMMITTEE

Ronald B. Johnson, Chairman
Sara R. Torrence



COMPUTERIZED CHARACTERIZATION OF THE Au-Cu-Ni TERNARY SYSTEM

by

S. K. Tarby, C. J. Van Tyne, and M. L. Boyle
Department of Metallurgy and Materials Science
Lehigh University, Bethlehem, Pa. 18015

Abstract

Information synthesized from binary systems by a computer method was used to characterize the Au-Cu, Au-Ni, and Cu-Ni binary systems. This characterization allows for the calculation of binary thermodynamic properties and binary phase equilibria. An extension of this characterization to the ternary Au-Cu-Ni system was made through the use of Kohler's equation of mixing. Not only did this yield thermodynamic information about the ternary, but it also permitted the calculation of a miscibility gap in the system. The predicted miscibility gap agrees extremely well with one determined experimentally. Currently, work with a computer optimization technique is being performed for the prediction of solid-liquid, two-phase equilibria in a ternary system.

Introduction

A computer program¹ employing a least squares technique has been developed to analyze concurrently activity data, integral heat of mixing data, and phase diagram data in order to generate a set of α -parameters for binary systems. The α -parameter is defined as

$$\alpha_{12} = \ln \gamma_1 / (1-X_1)^2 \quad (1)$$

where γ_1 is the Raoultian activity coefficient and X_1 is the atom fraction of component 1. These α -parameters were given a composition and inverse temperature dependence of the form

$$\alpha_{12} = \sum_{i=0}^n (A_{2i} + A_{2i+1}/T) \cdot X_2^i \quad (2)$$

where n is the order of the α -parameter representation, the A_j 's are constants determined by the least squares analysis, and T is absolute temperature. Each α -parameter characterizes a single phase region in a binary system. The integral and partial molar solution thermodynamic quantities as well as the activities of each component can be calculated from the α -parameter for any given temperature and composition in a one phase region. A pair of α -parameters for two different phases can be used to predict two phase equilibria in a binary system.

The Cu-Ni, Au-Ni, and Au-Cu binary systems have been analyzed by such a technique¹ and the constants for the α -parameter representation are given in Table I.

TABLE I - Calculated Liquid and Solid α -Parameter Constants for the Cu-Ni, Au-Ni, and Au-Cu Binary Systems

	$\alpha_{\text{Cu-Ni}}^{\text{L}}$	$\alpha_{\text{Cu-Ni}}^{\text{S}}$	$\alpha_{\text{Au-Ni}}^{\text{L}}$	$\alpha_{\text{Au-Ni}}^{\text{S}}$	$\alpha_{\text{Au-Cu}}^{\text{L}}$	$\alpha_{\text{Au-Cu}}^{\text{S}}$
A_1	1.590	.8909	-18.34	-1.994	5.483	-3.654
A_2	-1538.	-816.4	27000.	2757.	-10750.	1252.
A_3	-3.076	-.6033	46.22	10.31	-7.777	5.391
A_4	5702.	2229.	-80160.	-4737.	11260.	-4859.
A_5	-	-	-55.90	-18.73	-	-
A_6	-	-	116500.	7813.	-	-
A_7	-	-	32.33	9.100	-	-
A_8	-	-	-69830.	-1267.	-	-

This study shows how the α -parameter representation can be utilized in the prediction of solution thermodynamic and phase equilibria properties of ternary systems.

α -Parameter Representation of Ternary Systems

A simple approach to the prediction of thermodynamic properties and phase diagrams in multicomponent systems is to employ a formalism based entirely on binary and pure component data. Ansara² has presented the highlights of several models that have been proposed for an approach of this sort. The equations developed by Kohler³ have been selected from this group. According to Kohler, the excess molar free energy of a ternary solution can be given as

$$\frac{G_{123}^{XS}}{RT} = (1 - X_3)^2 \left. \frac{G_{12}^{XS}}{RT} \right|_{X_1/X_2} + (1 - X_2)^2 \left. \frac{G_{13}^{XS}}{RT} \right|_{X_1/X_3} + (1 - X_1)^2 \left. \frac{G_{23}^{XS}}{RT} \right|_{X_2/X_3} \quad (3)$$

where along the constant composition path X_1/X_2

$$\left. \frac{G_{12}^{XS}}{RT} \right|_{X_1/X_2} = \frac{X_1}{1 - X_3} \frac{X_2}{1 - X_3} \alpha_{12} \quad (4)$$

Similar relations hold for $\left. \frac{G_{13}^{XS}}{RT} \right|_{X_1/X_3}$ and $\left. \frac{G_{23}^{XS}}{RT} \right|_{X_2/X_3}$.

If the α functions are constant, then Eq. (3) reduces to the so-called regular solution form, i.e.,

$$\frac{G_{123}^{XS}}{RT} = \alpha_{12} X_1 X_2 + \alpha_{13} X_1 X_3 + \alpha_{23} X_2 X_3 \quad (5)$$

This symmetrical form has been used by many investigators including Meijering,^{4,5} Benedict et al.,⁶ Oriani and Alcock,⁷ Toop,⁸ Olson and Toop,^{9,10} and Wohl.¹¹

In this study the α -parameters were not constant but were given the variability described by Eq. (2).

The activity coefficient of component 1 in a ternary solution may be expressed in terms of the binary data by differentiating Eq. (3) with

respect to X_1 at constant X_2/X_3 . The result⁽¹⁰⁾ is

$$\begin{aligned} \ln \gamma_1^{123} = & ((1-X_3) \ln \gamma_1^{12} + X_3(1-X_3) [\ln \gamma_1^{12} + \ln \gamma_2^{12}]) \Big|_{X_1/X_2} \\ & + ((1-X_2) \ln \gamma_1^{13} + X_2(1-X_2) [\ln \gamma_1^{13} + \ln \gamma_3^{13}]) \Big|_{X_1/X_3} \\ & - (1-X_1)^2 [\ln \gamma_2^{23} + \ln \gamma_3^{23}] \Big|_{X_2/X_3} \end{aligned} \quad (6)$$

Similar relations for $\ln \gamma_2^{123}$ and $\ln \gamma_3^{123}$ can also be formulated. Olson and Toop⁹ have shown that both Eqs. (3) and (6) can be applied to systems that are non-regular. Thus, these equations can be quite useful for making predictions of ternary thermodynamic properties of non-regular systems where measured data are often lacking.

The addition of the ideal terms to Eq. (3) gives the molar free energy of mixing, i.e.,

$$\begin{aligned} \frac{\Delta G_{123}^M}{RT} = & (1-X_3)^2 \frac{G_{12}^{XS}}{RT} \Big|_{X_1/X_2} + (1-X_2)^2 \frac{G_{13}^{XS}}{RT} \Big|_{X_1/X_3} \\ & + (1-X_1)^2 \frac{G_{23}^{XS}}{RT} \Big|_{X_2/X_3} + X_1 \ln X_1 + X_2 \ln X_2 + X_3 \ln X_3 \end{aligned} \quad (7)$$

Results of Calculation

Figures 1, 2, and 3 show the iso-free energy of mixing curves, determined from Eq. (7), for solid Au-Cu-Ni alloys at 500°, 800°, and 1100°K, respectively. Figure 4 is a three dimensional representation of the free energy of mixing values at 800°K. Table II lists the 1100°K values of the free energy of mixing across the ternary system. Because of the temperature dependency assigned to the α -parameters, enthalpy of mixing and entropy of mixing values can also be determined for the ternary.

TABLE II - Free Energy of Mixing for the Au-Cu-Ni Ternary
at 1100°K (J/mole).

x_{Au}	$x_{\text{Cu}}/x_{\text{Ni}}$										
	10/0	9/1	8/2	7/3	6/4	5/5	4/6	3/7	2/8	1/9	0/10
0.0	0	-2206	-3109	-3525	-3642	-3559	-3330	-2978	-2485	-1738	0
0.1	-4282	-6050	-6614	-6714	-6522	-6126	-5575	-4886	-4040	-2929	-878
0.2	-6975	-8366	-8678	-8562	-8168	-7567	-6801	-5882	-4789	-3423	-1176
0.3	-8829	-9887	-9990	-9713	-9180	-8451	-7555	-6500	-5263	-3753	-1438
0.4	-9967	-10736	-10677	-10282	-9660	-8858	-7898	-6783	-5491	-3940	-1673
0.5	-10422	-10943	-10768	-10305	-9643	-8822	-7858	-6752	-5482	-3980	-1864
0.6	-10181	-10499	-10256	-9776	-9129	-8346	-7440	-6410	-5238	-3869	-1996
0.7	-9203	-9362	-9100	-8657	-8083	-7401	-6620	-5738	-4741	-3588	-2048
0.8	-7403	-7453	-7223	-6872	-6431	-5914	-5326	-4667	-3927	-3076	-1961
0.9	-4603	-4598	-4455	-4250	-4001	-3713	-3388	-3026	-2620	-2156	-1558

Olson and Toop⁹ have proposed a method for determining ternary phase boundaries. The technique gives a fair approximation of ternary phase diagrams exhibiting miscibility gaps and was used to investigate the miscibility gap in the Au-Cu-Ni system. The underlying principle of this method is that the ends of the tie lines connecting two phases are located where each of the three components has the same activity in both phases. These tie lines may be determined by plotting the ternary activities of two components along an isoactivity line for the third component and then graphically locating the unique points where the activities of these two components are the same in both phases.

With the use of Eq. (6) in a computer program, the ternary compositional grid of the Au-Cu-Ni system was scanned to find points of equal activity for any component in this ternary system. Figure 5 shows the results of one of these scans. For this figure and in the activity search, nickel was chosen as component 1 and points of nickel activity equal to 0.92 in solid Au-Cu-Ni

alloys at 1100°K were determined by the grid search program. With the grid points of the isoactivity of nickel known, the activities of gold and copper were calculated directly from Eq. (6). The activities of gold and copper were plotted versus a composition ratio to find the unique set of points $a_{\text{Au}}(\text{PHASE 1}) = a_{\text{Au}}(\text{PHASE 2})$ and $a_{\text{Cu}}(\text{PHASE 1}) = a_{\text{Cu}}(\text{PHASE 2})$. An example of this determination may be seen in Figure 6. Here, the unique pair of points were found to be

$$\frac{X_{\text{Ni}}}{1-X_{\text{Cu}}} = 0.4575 \text{ and } \frac{X_{\text{Ni}}}{1-X_{\text{Cu}}} = 0.9517$$

Figure 7 shows the two points where the above composition ratios occur along the nickel isoactivity curve; hence, the ends of the tie line are now defined. A range of nickel isoactivity curves and associated tie lines are presented in Fig. 8. This technique was applied at several temperatures and the resulting calculated miscibility gap is shown in Fig. 9. It was estimated by this graphical method that the ternary critical point is between 1225° and 1250°K.

Discussion

Raub and Engel^{12,13} have conducted the only extensive phase boundary determinations of the Au-Cu-Ni miscibility gap. The results of their experiments are found in Figs. 10a and 10b. The difference between the calculated and experimentally determined phase boundaries for this system is extraordinarily small. The only major difference is the predicted intersection of the miscibility gap with the Cu-Ni binary.

Although the approach of Olson and Toop is suitable for predicting the phase equilibria of a miscibility gap, a different approach is required for the more general case of two phase equilibria in a ternary system. A method currently under investigation is described below.

The ends of a two phase tie line are determined by the compositions which cause the partial molar Gibbs free energy of a component to be equal in the two phases. In essence, the problem becomes one of determining four unknowns--the atom fractions of two components in each of two phases. To obtain a unique solution for the location of the phase boundaries, it is necessary to have four equations for these unknown compositions. Three equations can be generated by equating the partial molar Gibbs free energy for each component in the two phases

$$\bar{G}_1 \text{ (PHASE 1)} = \bar{G}_1 \text{ (PHASE 2)} \quad (8a)$$

$$\bar{G}_2 \text{ (PHASE 1)} = \bar{G}_2 \text{ (PHASE 2)} \quad (8b)$$

$$\bar{G}_3 \text{ (PHASE 1)} = \bar{G}_3 \text{ (PHASE 2)} \quad (8c)$$

The fact that tie lines are straight lines allows for the development of a fourth equation from geometrical considerations.

With the use of α -parameters synthesized from the three binaries, the problem of phase boundary determination in the ternary system ultimately reduces to one of solving four non-linear equations for four unknowns. In our present study of this problem, the approach being used sets all the equations equal to zero, e.g.,

$$\bar{G}_1 \text{ (PHASE 1)} - \bar{G}_1 \text{ (PHASE 2)} = 0 \quad (9)$$

and then an optimization procedure is used to determine the four composition values which minimize on the error between the actual value of these equations and zero. Preliminary results from the determination of liquidus and solidus lines on isotherms of the Ag-Au-Cu system are very encouraging.

Conclusion

It appears that α -parameters which have been synthesized from data on binary systems can be used to predict solution thermodynamic and phase equilibria properties in ternary systems. Indeed, calculations made in this study gave a predicted miscibility gap in solid Au-Cu-Ni alloys that

was in excellent agreement with an experimentally determined one. Although the method described here is purely predictive since it relies only on binary and pure component data, it could prove useful in estimating properties of ternary systems for which experimental data are lacking.

References

1. M. L. Boyle: M.S. Thesis, Lehigh University, Bethlehem, Pa., 1976.
2. I. Ansara: Metallurgical Chemistry Symposium 1971, O. Kubaschewski, Ed., pp. 403-430, Her Majesty's Stationary Office, London, 1972.
3. F. Kohler: Monatshefte für Chemie, 1960, vol. 91, pp. 738-740.
4. J. L. Meijering: Philips Research Reports, 1950, vol. 5, pp. 333-356.
5. J. L. Meijering: Philips Research Reports, 1951, vol. 6, pp. 183-210.
6. M. Benedict, C. A. Johnson, E. Solomon and L. C. Rubin: Transactions A.I.Ch.E., 1945, vol. 41, pp. 371-392.
7. R. A. Oriani and C. B. Alcock: Transactions TMS-AIME, 1962, vol. 224, pp. 1104-1115.
8. G. W. Toop: Transactions TMS-AIME, 1965, vol. 233, pp. 850-855.
9. N. J. Olson and G. W. Toop: Transactions TMS-AIME, 1969, vol. 245, pp. 905-910.
10. N. J. Olson and G. W. Toop: Transactions TMS-AIME, 1966, vol. 236, pp. 590-592.
11. K. Wohl: Transactions A.I.Ch.E., 1946, vol. 42, pp. 215-249.
12. E. Raub and A. Engel: Zeitschrift für Metalkunde, 1947, vol. 2, pp. 11-16.
13. E. Raub and A. Engel: Zeitschrift für Metalkunde, 1947, vol. 2, pp. 147-158.

Acknowledgement

We wish to thank the United States Steel Foundation for their support of the Chemical Metallurgy Program at Lehigh University.

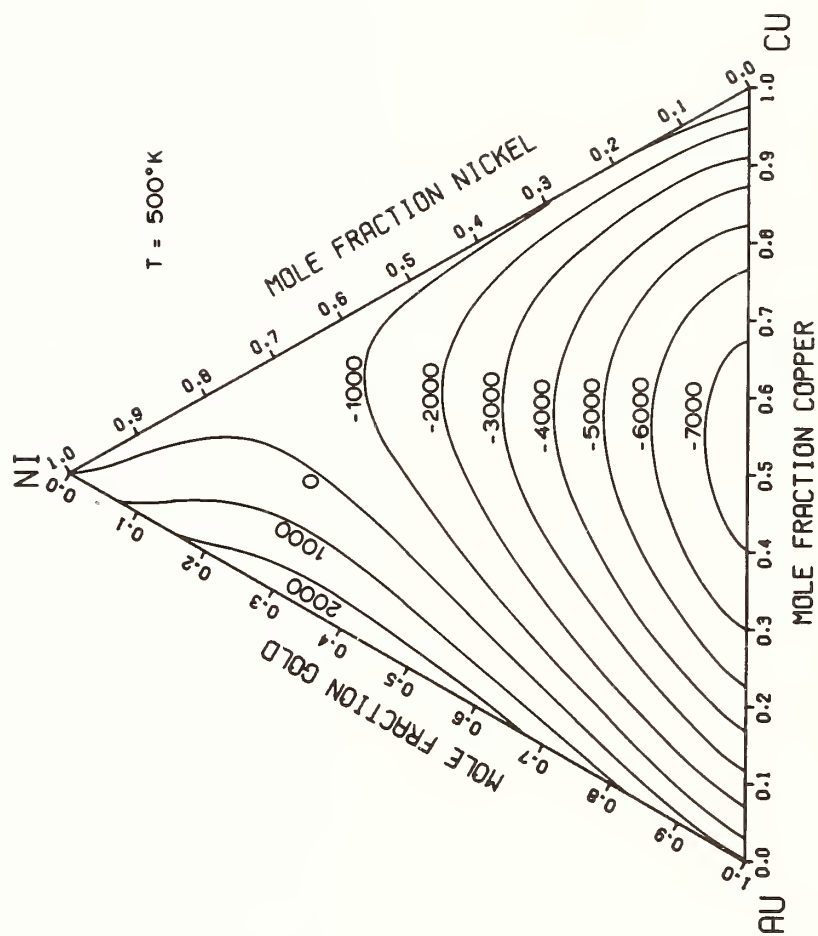


Figure 1. Iso-Free Energy of Mixing Curves for Solid Au-Cu-Ni Alloys at 500°K. Energy in units of J mol^{-1} .

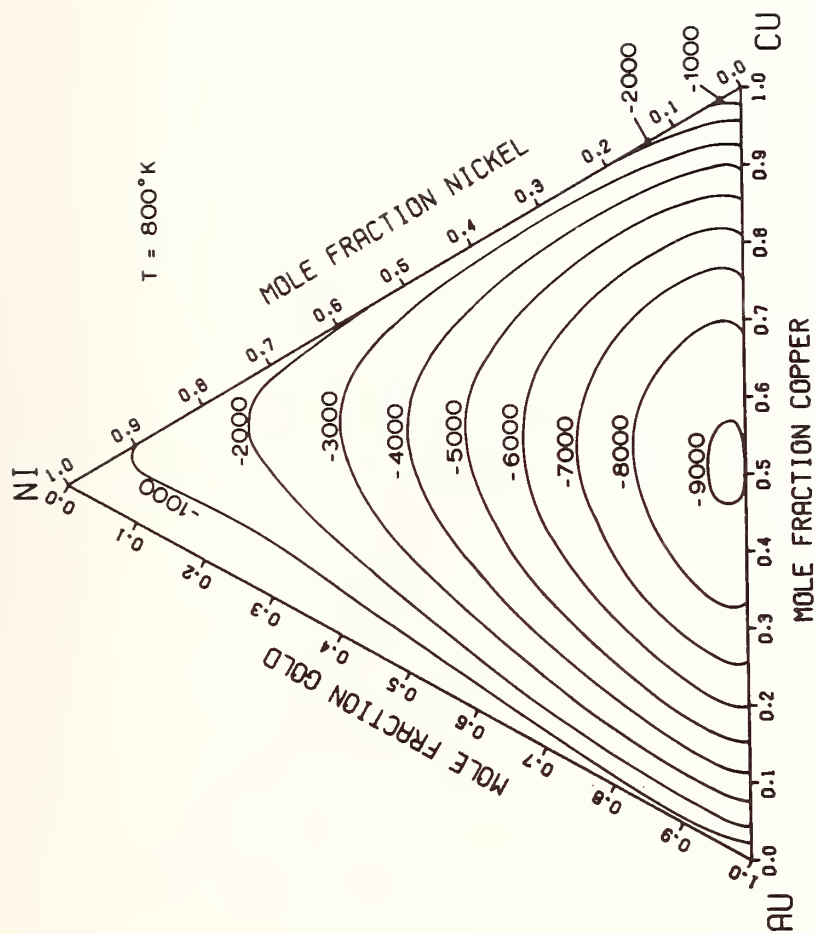


Figure 2. Iso-Free Energy of Mixing Curves for Solid Au-Cu-Ni Alloys at 800°K.
Energy in units of J mol^{-1} .

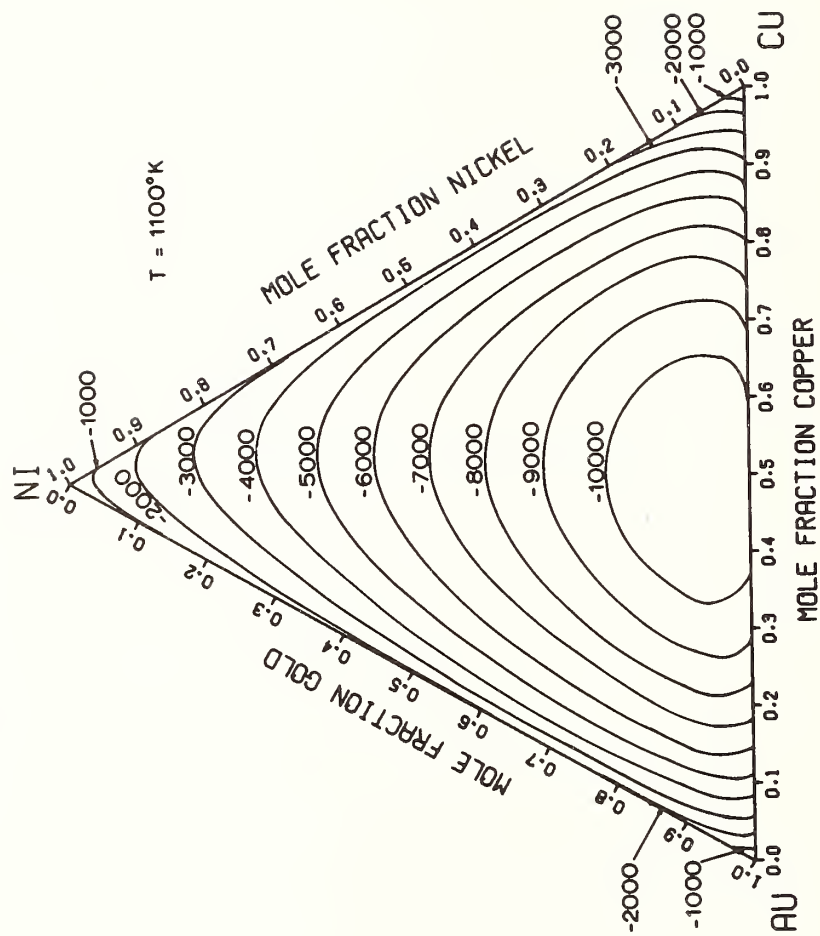


Figure 3. Iso-Free Energy of Mixing Curves for Solid Au-Cu-Ni Alloys at 1100°K.
Energy in units of J mol⁻¹.

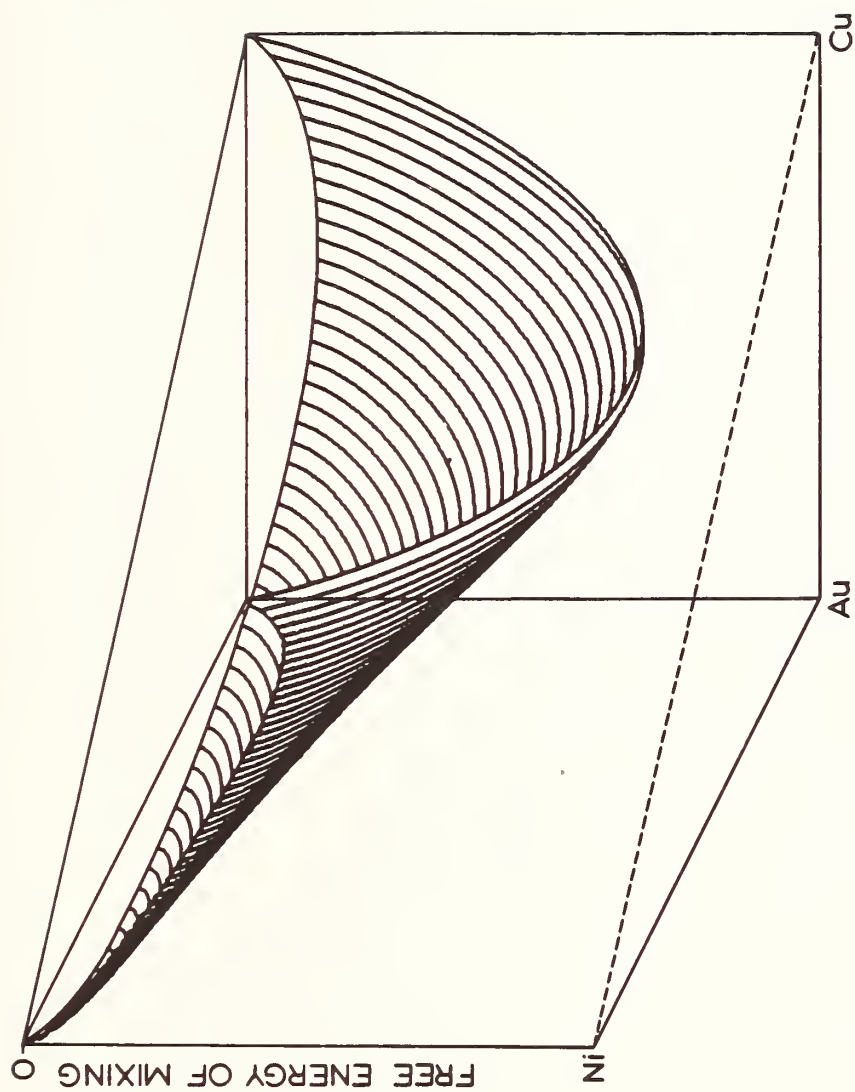


Figure 4. Three Dimensional Representation of the Free Energy of Mixing for Solid Au-Cu-Ni Alloys at 800°K.

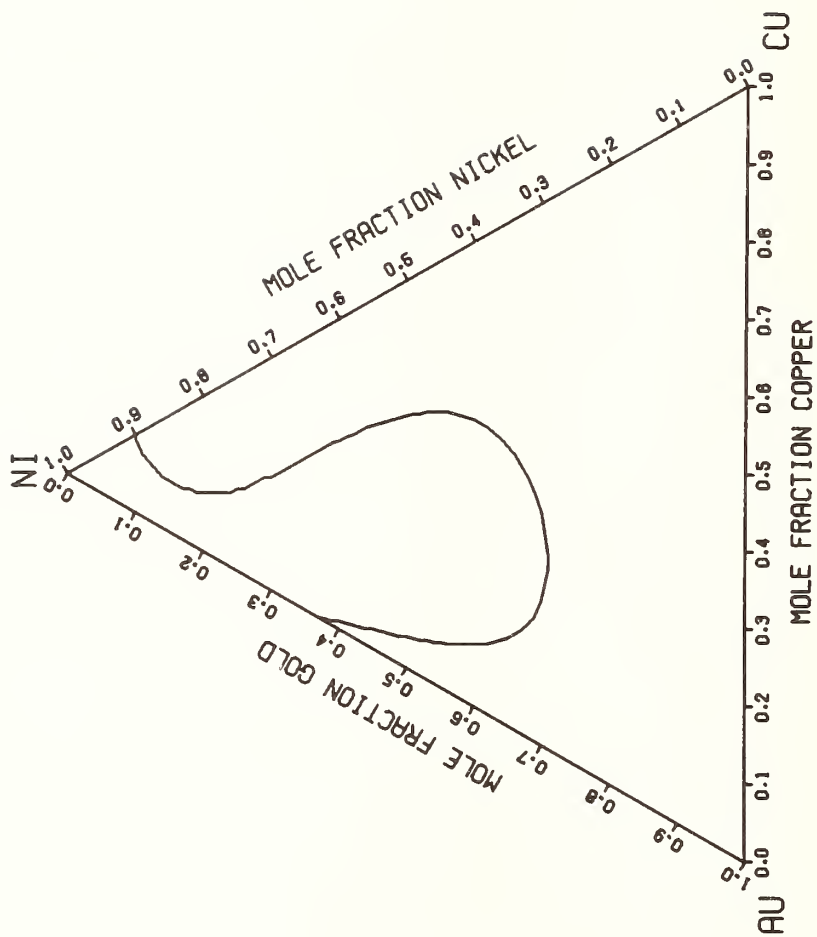


Figure 5. Iso-Activity of Nickel Curve Equal to 0.92 in Solid Au-Cu-Ni Alloys at 1100°K.

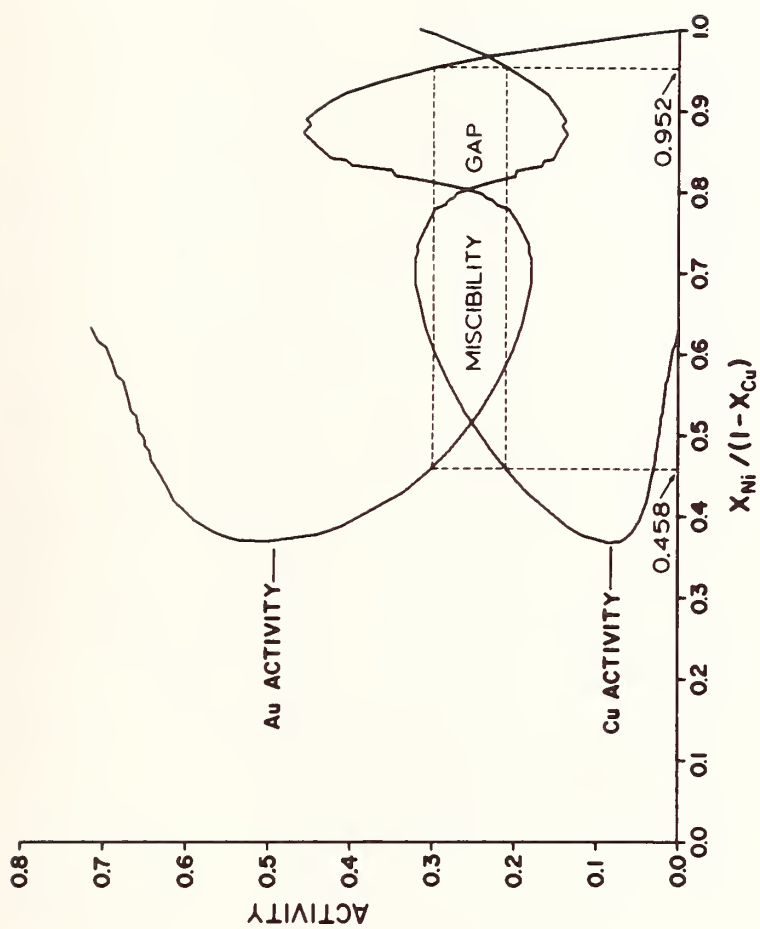


Figure 6. Graphical Determination of Miscibility Gap Boundaries as Proposed by Olson and Toop⁹ in Solid Au-Cu-Ni Alloys at 1100°K.

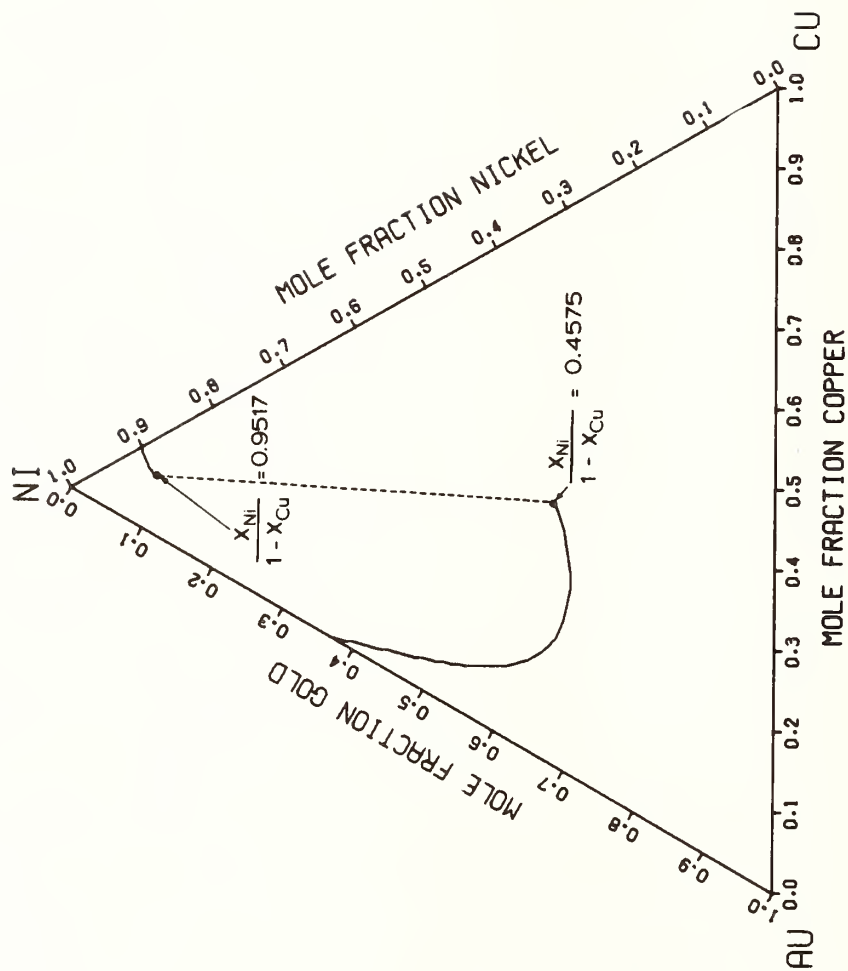


Figure 7. Placement of the Ends of the Graphically Determined Miscibility Gap Boundary in Solid Au-Cu-Ni Alloys at 1100°K.

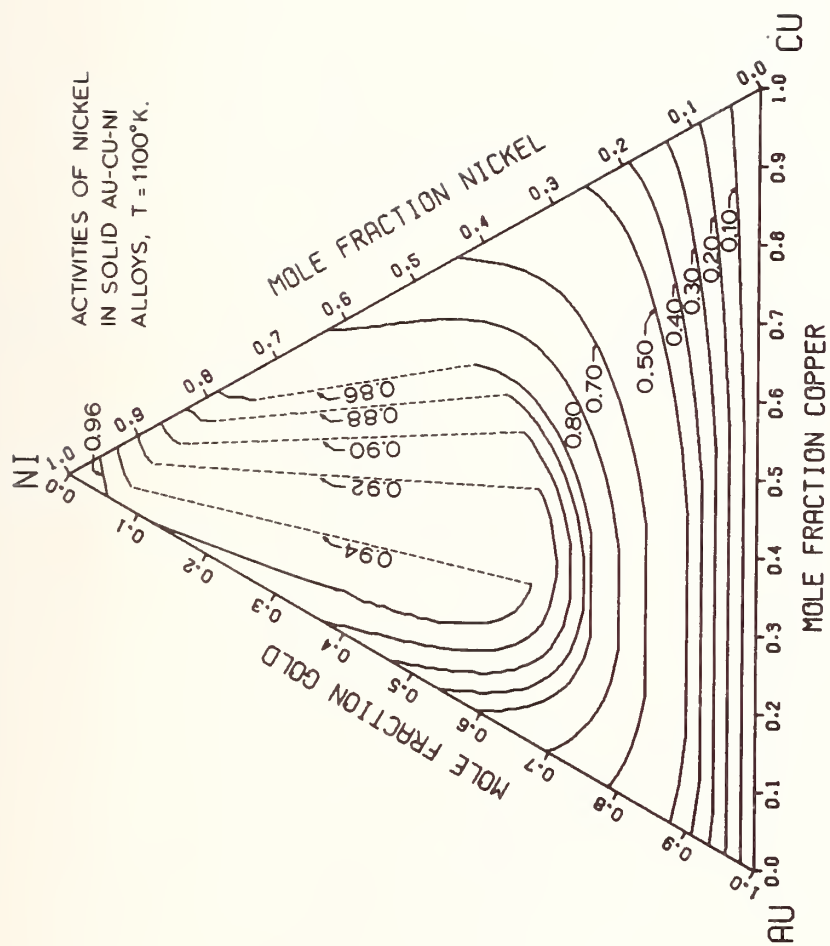


Figure 8. Miscibility Gap Tie Lines and Associated Nickel Iso-Activity Curves in Solid Au-Cu-Ni Alloys at 1100°K .

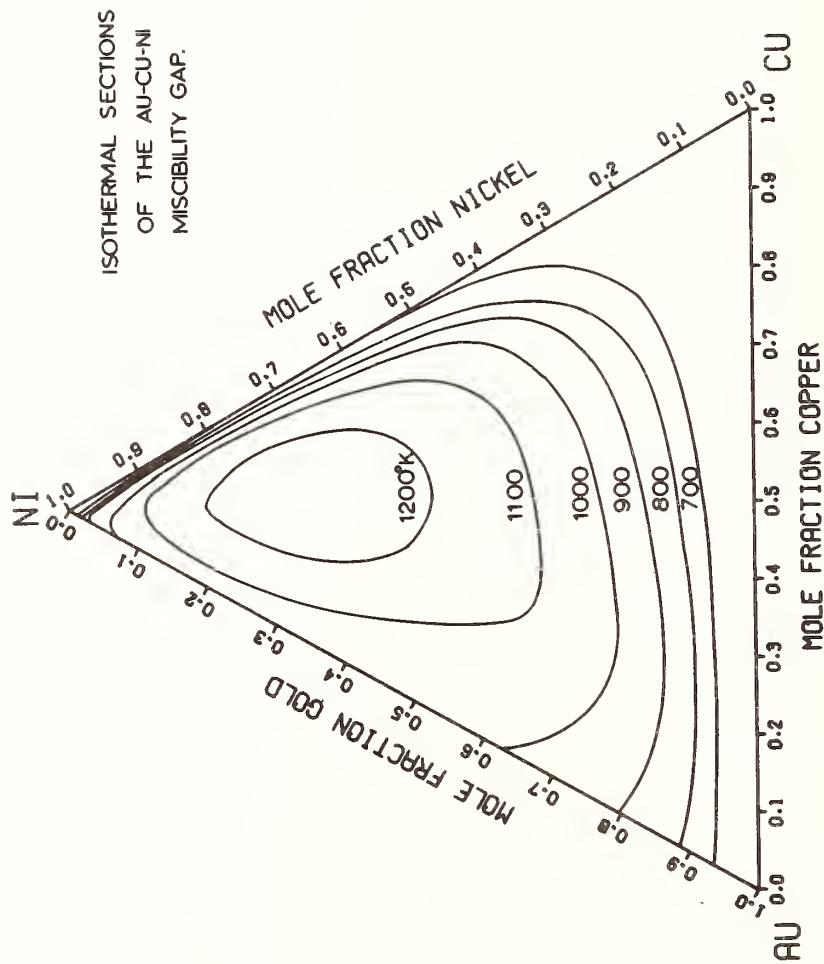


Figure 9. Graphically Determined Isothermal Sections of the Au-Cu-Ni Miscibility Gap.

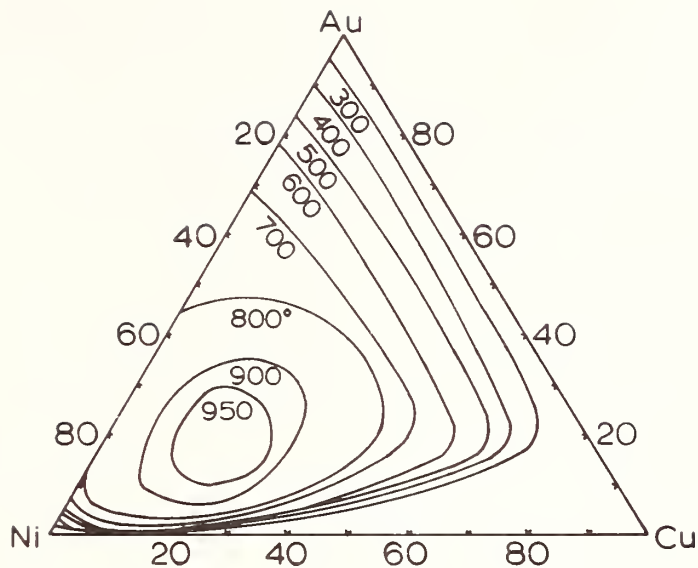


Figure 10a. Experimentally Determined Isothermal Sections of the Au-Cu-Ni Miscibility Gap from Raub and Engel.^{12,13} (Temperature in °C, Composition in Atomic Percent.)

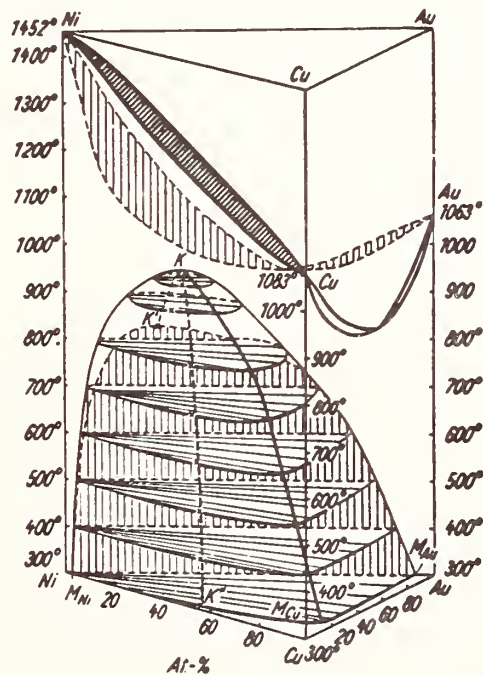


Figure 10b. Three Dimensional View of the Au-Cu-Ni Miscibility Gap from Raub and Engel.^{12,13} (Temperature in °C.)



CORRELATIONS AND PREDICTIONS OF METAL-BORON PHASE EQUILIBRIA*

Karl E. Spear
Materials Research Laboratory
Materials Science Department
The Pennsylvania State University
University Park, Pennsylvania 16802

ABSTRACT

Attempts have been made to find correlations relating the binary metal boride phase equilibria, the boride crystal chemistry, and the positions of the metals in the periodic chart. These correlations are used along with available experimental data and phase equilibria logic to predict unmeasured properties and to construct phase diagrams for binary metal-boron systems. Earlier research of this type on rare-earth boride systems was recently completed in the form of a critical analysis and compilation; the research published here is not yet that complete and should be considered as an interim report for the Workshop.

I. INTRODUCTION

This paper briefly summarizes our attempts to correlate and predict phase equilibria information for binary metal-boron systems. Our early research in this area (see Spear, 1976) emphasized RE-B systems, where RE is one of the metals Sc, Y, La, or a rare-earth Ce through Lu. We compiled and critically analyzed reported data for these systems and predicted unmeasured properties with the help of correlations, published limits, and phase equilibria logic so that we could construct phase diagrams for all 17 RE-B systems. These diagrams serve as graphical summaries of reported information, indicate reasonable estimates of unmeasured properties, and point out needed experimental research.

Our current efforts are aimed at extending the RE-B research to include transition metal and actinide metal boride systems as well as what little information has been published about the borides of metals from groups IA, IIA, and IIIA. This extended research is not yet a "critical analysis and compilation" as is the rare-earth boride publication, but is a current study being documented in the spirit of the Workshop at which this research was first presented.

* Research supported by the National Science Foundation, grant No. DMR76-14448.

The heart of this paper is presented in four sections. Section II outlines crystal chemical correlations for metal-boron phases and systems. An understanding of these correlations is particularly helpful in understanding and predicting the relationships among the boride phase equilibria properties since boron-boron bonding is so prominent in the majority of borides. Correlations and predictions of phase behavior are given in Section III, and are based on methods similar to those used in the RE-B studies.

Phase diagrams are given in Section IV for 37 metal-boron systems which form intermediate binary compounds. Not given are the RE-B diagrams for Ce through Lu since they have been published elsewhere (Spear, 1976), nor are the alkali metal-boron diagrams which have not yet been reviewed in enough detail to make predications.

We have not given specific references for information tabulated in the subsequent tables and figures, but instead have listed our main sources of information in Section V, the reference section at the end of the text. The references are listed under five topical headings to aid in finding information. A critical assessment and compilation which includes more specific references will be published later.

II. BORIDE CRYSTAL CHEMISTRY

The crystal chemistry of metal boride phases is dominated by the boron configurations in the structures. Boron-boron bonding occurs in most borides containing greater than 35 at.% boron. The B-B bond distances are practically identical in these boride structures and in pure boron.

The common types of boron configurations found in metal boride structures are shown in Figure 1. These configurations include (i) the "no connections" exhibited by metal-rich structures which exhibit no boron-boron bonding, (ii) the various types of boron chains, (iii) two-dimensional graphite-like nets, and (iv) a number of three-dimensional frameworks which are found in the boron-rich phases. The structure types which exhibit these configurations are listed in Table 1.

Figure 2 shows that the larger metals and those with unfilled d-shells favor the formation of the boron-rich phases, the phases which exhibit 2- and 3-dimensional boron frameworks. The smaller metals, and particularly those with a significant number of d-electrons, tend to form metal-rich phases which have few boron-boron bonds. The more noble metals such as Ru, Rh, and Pd have a greater tendency than the other metals to form defect structures. For the re

crystal chemical details, one should refer to Aronsson et al. (1965), Lundstrom (1969, 1977), and Spear (1976).

III. PHASE EQUILIBRIA CORRELATIONS AND PREDICTIONS

A few specific correlations used to help in predicting phase equilibria properties are discussed in this section. Other estimates based on drawing "reasonable" phase diagrams which do not violate the phase rule are not discussed, but are evident from the constructed diagrams shown in Section IV.

In the previous section, the crystal chemical compositional trends with the position of the metal in the periodic chart were mentioned. The highest melting metal boride in a given M-B system tends to follow similar compositional trends with the size and number of metal d-electrons. The MB_6 phase is the highest melting in systems containing the larger rare-earth metals. This shifts to the MB_4 phases for the smaller rare-earths, then to the MB_2 phases for Sc, the Ti group metals, V and Nb, and Cr. The more metal-rich borides or defect diborides are the highest melting intermediate phases in systems with metals further to the right in the periodic chart.

The diboride with the AlB_2 -type structure is the most common metal boride phase found. This group includes the most stable and the highest melting metal borides known. The metals forming this phase possess a wide range of sizes and electronic configurations. The reason for the common occurrence of this phase appears to be related to the ability of the metals in this structure to deform their electron cloud from an approximately spherical shape. The bond strengths between the metals are enhanced without drastically reducing the boron-boron bond strengths (Spear, 1976).

Correlations of the diboride melting temperatures along with those for other boron-rich phases are shown in Table 2. The fact that 2- and 3-dimensional boron frameworks dominate the structures of boron-rich compounds causes one to expect similar melting temperatures for these phases, particularly for those within a group exhibiting the same structure. The general correlations shown in Table 2 confirm these expectations. Unmeasured melting temperatures for similar phases are expected to lie approximately within the given range for the particular structure type and subgroup listed in the table.

The metals forming only intermediate boride phases with B/M atomic ratios of two and greater can be grouped into families, as is shown in Table 3. The

metals involved include the alkaline-earths, all the group III metals, the rare-earths, and the actinides. Zirconium also fits into this scheme. These metals are all fairly large and do not possess a large number of d-electrons. The RE-B systems have already been thoroughly analyzed and correlated (Spear, 1976), so only the other metal-boron systems will be discussed to a significant extent. This correlation does not include the new Sm_2B_5 -type phase formed by Sm and Gd, nor the recently discovered REB_x ($x < 4$) phases in the Nd and Pr system.

The metals within a given family are expected to show similarities in their binary phase diagrams, as well as in their other properties. The alkaline earths Ca, Sr, and Ba have only one confirmed intermediate boride phase, the hexaboride. They are similar to Eu in this respect, and in the fact that Eu is divalent in its hexaboride phase (Spear, 1976). (The YbB_6 phase is similar to EuB_6 , but Yb forms other borides and converts to a trivalent state like most of the other rare earths. These phenomena will not be discussed further here.) The respective melting and boiling temperatures for Eu and the alkaline earth metals are also very similar, as is shown below, so it would be very surprising if their respective binary M-B phase diagrams were not also similar.

<u>Metal</u>	<u>T°C(fusion)</u>	<u>T°C(boiling)</u>
Eu	826	1491
Ca	850	1483
Sr	770	1367
Ba	710	1622
Ra	700	1527

Data are from Hultgren et al. (1973)

If Ra is not too large to form a hexaboride, its phase diagram would also be expected to be similar.

The Ac-B system has not been studied because of the extreme radioactivity of Ac, but its diagram is expected to be similar to La-B; both metals belong to group III. The Am-B system is expected to be similar to the next family forming three phases. The AmB_6 phase is congruently vaporizing, just like the hexaborides in the RE-B systems of the same family. The next smaller rare-earth, Gd, has a congruently vaporizing tetraboride. The lattice constants for AmB_4 are slightly smaller than those for ThB_4 , indicating that Am is not too large to form the AmB_{66} phase, even though only AmB_4 and AmB_6 have been reported.

The unstudied Pa-B system should be intermediate between Th-B and U-B in behavior. It is assumed that it is similar to the Gd-B system. The Pu-B and Np-B systems clearly fall in the next family containing Tb-B, Y-B, Dy-B, and Ho-B systems. The phase behavior of these four RE-B systems is very similar, and the diagrams of Pu-B and Np-B are expected to be similar as well. All six systems have a congruently vaporizing tetraboride phase. The NpB_{66} phase has not been reported, but no other metal is known to exhibit the UB_{12} , AlB_2 , ThB_4 , and CaB_6 type phases without also forming a stable YB_{66} type phase.

The next actinide metal boride system is U-B, and it appears to fall in an intermediate stage between the Lu-B and the Sc-B systems. The UB_{66} phase has been searched for, but not found. The last family represents the smallest metals to form the dodecaboride phase.

IV. BINARY METAL-BORON PHASE DIAGRAMS

Binary temperature-composition phase diagrams for 37 metal-boron systems have been constructed and are shown in Figures 3-8. The metals include the alkaline earths, aluminum, the transition metals in groups III through VIII, and the actinide metals Ac through Am. These diagrams do not yet represent a thorough critical assessment in many cases, and much of the information has been estimated. The estimates of the alkaline earth and actinide boride diagrams are probably more reliable than those of the later transition metals. In order that the reader may better judge the reliability of the diagrams, some specific comments and references are given below for each system. The comments for diagrams given in the same figure are grouped together. The figures contain groups of systems organized according to the positions of the metals in the periodic chart. The actinide boride systems are given last.

Figure 3:

- Be-B : Based on information from Stecher and Aldinger (1973). The composition of the dashed boron-rich phase lies somewhere between BeB_6 and BeB_{12} .
- Mg-B : The decomposition temperatures for 1 atm vapor are strictly guesses. The general type of diagram shown is the type that the Mg-B system will exhibit, but the given critical temperatures may be grossly in error.
- Ca-B, Sr-B, Ba-B: A discussion of the similarities of these estimated diagrams and the Eu-B diagram is given in Section III of the text..

Al-B : Many of the boron-rich phases reported have been shown to be impurity stabilized phases (Shunk, 1968). Otherwise, the diagram is generally the same as is given by Elliott (1965).

Figure 4:

Sc-B, Y-B, La-B: Based on diagrams from Spear (1976).

Ti-B, Zr-B, Hf-B: Based on diagrams from Rudy (1969).

Figure 5:

V-B, Nb-B, Ta-B: Based on diagrams from Rudy (1969), except for the addition of the V_5B_6 and V_2B_3 phases to the V-B system based on data by Spear and Gilles (1969).

Cr-B : Based on diagram by Portnoi and Romashov (1972), plus possible formation of Cr_4B phase, and the CrB_4 phase discussed by Lundstrom (1977).

Mo-B, W-B: Based on diagrams by Rudy (1969).

Figure 6:

Mn-B : Diagram estimated to be similar to Cr-B system; both systems form similar intermediate phases.

Tc-B : Diagram estimated to be similar to Re-B system. Both systems form similar intermediate phases.

Re-B : Based on diagram by Portnoi and Romashov (1972).

Fe-B : Based on diagram by Portnoi and Romashov (1972), but leaving out B-rich FeB_n phase shown by Carlsson and Lundstrom (1970) to be a solution of Fe in B.

Ru-B, Os-B: Estimated to be similar to neighboring diagrams, with the trend toward lower boride melting temperatures with an increase in metal d-electrons being observed. The defect diborides are estimated to have relatively high melting temperatures since all diborides appear to be relatively stable.

Figure 7:

Co-B : Based on diagram by Schobel and Stadelmaier (1966).

Rh-B, Ir-B: Estimated to have lower melting temperatures for their intermediate boride phases, as appears to be the trend with increasing number of metal d-electrons.

- Ni-B : Based on diagram by Portnoi and Romashov (1972), but with slight modifications in Ni_4B_3 and NiB region to show similarities with Fe-B and Co-B diagrams. The B-rich NiB_n phase was left out since Carlsson and Lundstrom (1970) have shown this to be a solution of Ni in boron.
- Pd-B : Estimated to be similar to its neighboring M-B systems.
- Pt-B : Based primarily on diagram by Wald and Rosenberg (1965).

Figure 8:

A more detailed discussion of these seven actinide-boron systems and the correlations involved in the predictions of their properties is given in Section III. The papers published on the actinide borides are listed in the reference section.

Each phase diagram in Figures 3-8 is for a constant total pressure of 1 atm. A vapor phase is shown only when the total metal plus boron vapor pressure reaches 1 atm., which for these systems occurs first at the boiling (or 1 atm. sublimation) temperature for the metal. Data for the elements, including boron, were taken from Hultgren et al. (1973).

On the constructed diagrams shown in the figures, a fine line was used to represent estimated parts of the diagrams and a heavier line was used when at least some experimental evidence was available.

The (B/M) atomic ratios for common metal boride phases are shown on each diagram, with the tic-marks representing these ratios being drawn outside the diagram. The ratios of phases existing in a particular binary system are indicated by extending the specific tic-marks downwards into the graphed region of the diagram. No attempt has been made to indicate specific compositions of defect structures, or the homogeneity ranges of phases (although most boride homogeneity ranges are relatively small).

Again, the reader is reminded that the given diagrams are intended to serve as graphical summaries of reported information and reasonable estimates of unmeasured properties. Researchers are encouraged to send new information to the author of this paper so that a continual updating of these diagrams can be accomplished.

V. REFERENCES

General For Elements and For Borides

- R. Hultgren, P. D. Desai, D. T. Hawkins, M. Gleiser, K. K. Kelley, and D. D. Wagman (1973). Selected Values of The Thermodynamic Properties of the Elements, Am. Soc. Metals, Metals Park, Ohio.
- M. Hansen and K. Anderko (1958). Constitution of Binary Alloys, McGraw-Hill, New York.
- R. P. Elliott (1965). *ibid.*, First Supplement.
- F. A. Shunk (1968). *ibid.*, Second Supplement.
- B. Aronsson, T. Lundstrom, and S. Rundqvist (1965). Borides, Silicides, and Phosphides, Wiley (Methuen), New York.

Reviews of Transition Metal-Boron Systems

- E. Rudy (1969). "Compendium of Phase Diagram Data," AFML-TR-65-2, Part V, Air Force Materials Laboratory, Wright-Patterson Air Force Base, Ohio.
- K. I. Portnoi and V. M. Romashov (1972). "Binary Constitution Diagrams of Systems Composed of Various Elements and Boron - A Review," Russ. Powder Met. 5 (113), 378-384.
- T. Lundstrom (1969). "Preparation and Crystal Chemistry of Some Refractory Borides and Phosphides," Arkiv fur Kemi 31 (19), 227-266.
- T. Lundstrom (1977). "Transition Metal Borides," Chapter in Boron and Refractory Borides (V.I. Matkovich, ed.) Springer-Verlag, Berlin (in press).

Review of Rare-Earth Metal-Boron Systems

- K. E. Spear (1976), "Phase Behavior and Related Properties of Rare-Earth Borides," Chapter II in Phase Diagrams: Materials Science and Technology, Vol. IV (A. M. Alper, ed.) Academic Press, New York, pp. 91-159.

Actinide Metal-Boron Systems

- Th-B P. Stecher, F. Benesovsky and H. Nowotny (1965), "Study of the Alloy Behavior of Borides in the Ternary Systems Cerium-Thorium (Uranium)-Boron," Planseeber. Pulvermet. 13, 37-46.
- U-B B. W. Howlett (1959), "A Note on the Uranium-Boron Alloy System," J. Inst. Metals 88, 91-92.
- R. W. Mar (1975). "The U-B System," J. Am. Ceram. Soc. 58 (2), 145-146.
- Pu-B H. A. Eick (1965), "Plutonium Borides," Inorg. Chem. 4 (8), 1237-1239.
- Am-B, Np-B H. A. Eick and R. N. R. Mulford (1969), "Americium and Neptunium Borides," J. Inorg. Nucl. Chem. 31, 371-375.

Other Specific Systems and Phases Types

- AlB₂-Type K. E. Spear (1976), "Chemical Bonding in AlB₂-Type Borides," J. Less-Common Metals 47, 195-201
- Be-B J. Stecher and F. Aldinger (1973), "Über den Aufbau des Systems Beryllium-Bor," Z. Metallkde. 64 (10), 684-689.
- Co-B J. D. Schobel and H. H. Stadelmaier (1966). "Das Zweistoffsystem Kobalt-Bor," Z. Metallkde. 57 (4), 323-325.
- Pt-B F. Wald and A. J. Rosenberg (1965), "Constitutional Investigations in the Boron-Platinum System," Trans. AIME 233, 796-799.
- V-B K. E. Spear and P. W. Gilles (1969), "Phase and Structure Relationships in the Vanadium-Boron System", High Temp. Sci. 1 (1), 86-97.
- B-Rich J. O. Carlsson and T. Lundstrom (1970). "The Solution Hardening of β -Rhombohedral Boron," J. Less-Common Metals 22, 317-320.

Table 1: Metal Boride Structures Which Exhibit Specific Types of Boron Configurations.

BORON CONFIGURATION*	STRUCTURE TYPES EXHIBITING THESE CONFIGURATIONS
No Connections	Mn ₄ B, Re ₃ B, Ni ₃ B, Pd ₅ B ₂ , Ru ₇ B ₃ , Fe ₂ B, PtB, RuB, IrB _{1.1}
Partial Chains	Cr ₅ B ₃ , V ₃ B ₂ , Ru ₁₁ B ₈ , Ni ₄ B ₃
Single Chains	FeB, CrB, MoB
Multiple Chains	V ₅ B ₆ , Ta ₃ B ₄ , V ₂ B ₃
2-D Nets (Perfect)	AlB ₂
2-D Nets (Defect AlB ₂)	Ir ₂ B _{3-x} (IrB _{1.35}), Ru ₂ B _{3-x} (Ru ₂ B ₃), RuB ₂ , ReB ₂ , Mo ₂ B _{5-x} (Mo ₂ B ₅), W ₂ B _{5-x} (W ₂ B ₅), Mo _{1-x} B ₃ (MoB ₄₋₆)
3-D Frameworks	Sm ₂ B ₅ , CrB ₄ , ThB ₄ , NaB ₆ , CaB ₆ , AlB ₁₂ , UB ₁₂ , YB ₆₆

* See Fig. 1 for illustrations of the Boron Configurations.

Table 2: Correlations of Melting Temperatures of Boron-Rich Metal Boride Phase Types.

Structure Type	Subgroups	Limiting Melting Temperatures Observed	
		Lowest T_{fus} °C	Highest T_{fus} °C
AlB_2	Groups IVA, VA	>2500	3400
	Other Metals	2000	< 2500
ThB_4	Congruent Melting	2500	2800
	Peritectic Melting*	2350	2400
CaB_6	Congruent Melting	2550	2715
	Peritectic Melting	2200	2600
UB_{12}	All Phases	2000	2250
YB_{66}	All Phases	2050	2150

* LaB_4 melts at 1800°C. The limited stability of LaB_4 with respect to decomposition to LaB_6 and a metal-rich melt is explained by the fact that La is the largest metal to form this phase.

Table 3: Families of Metals Forming Higher Borides.

Metal in M-B System	Phase Types				
	UB_{12}	AlB_2	YB_{66}	ThB_4	CaB_6
Ba, Sr, Eu, Ca, Yb ^a					X
La, Ce, Pr, (Ac) ^b				X	X
Th, Nd, Sm, (Pm) ^b , Am			X	X	X
Gd, (Pa) ^b		X	X	X	X
Tb, Y, Dy, Ho, Pu, Np	X	X	X	X	X
Er, Tm, Yb ^a , Lu	X	X	X	X	
U	X	X		X	
Sc, Zr, Al	X	X			

(a) Yb is listed in both the first and sixth groups because it is divalent in YbB_6 while it is trivalent in its other borides.

(b) These M-B systems have not been studied, but are predicted to form the indicated compounds.

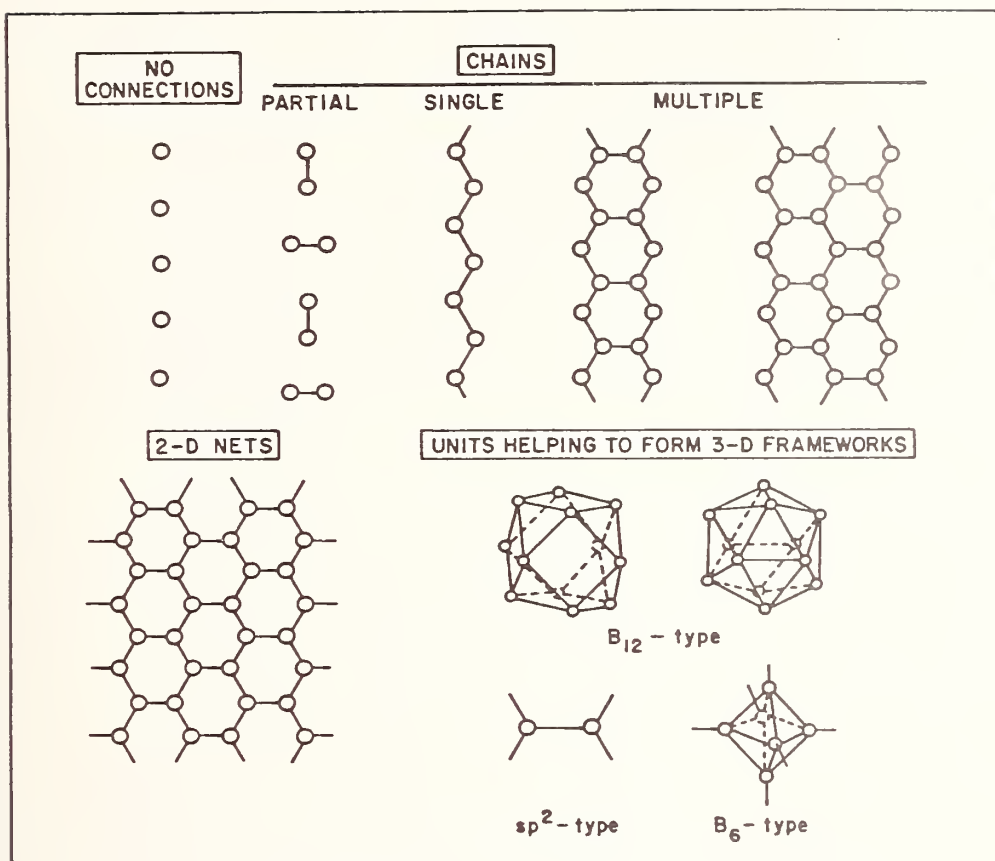


Figure 1: Common Types of Boron Configurations Found in Metal Boride Structures.

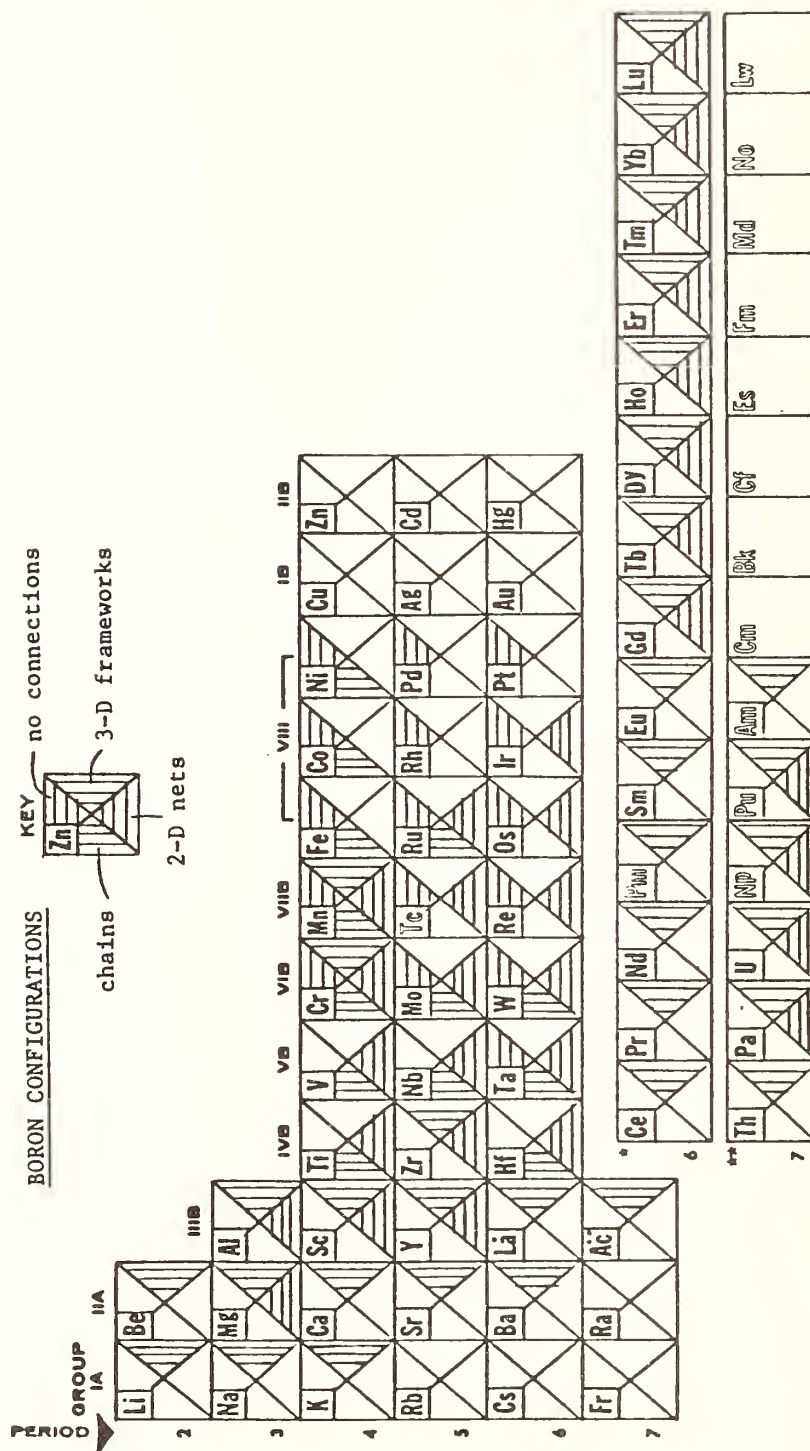


Figure 2: Partial Periodic Chart Showing the Types of Boron Configurations Exhibited by the Borides of the Various Metals.

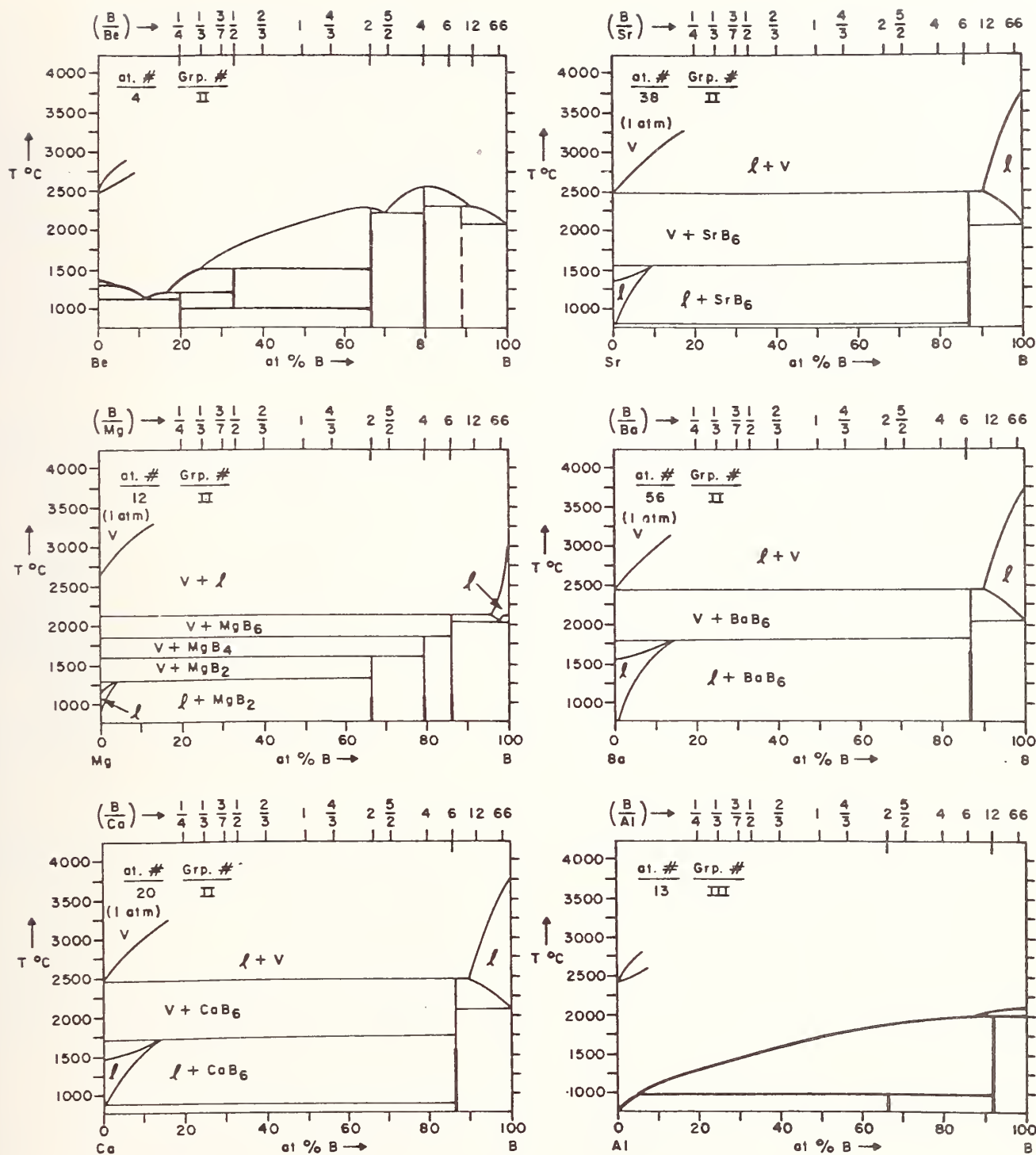


Figure 3: Phase Diagrams for the Metal-Boron Systems of the Alkaline-Earth Metals and Aluminum.

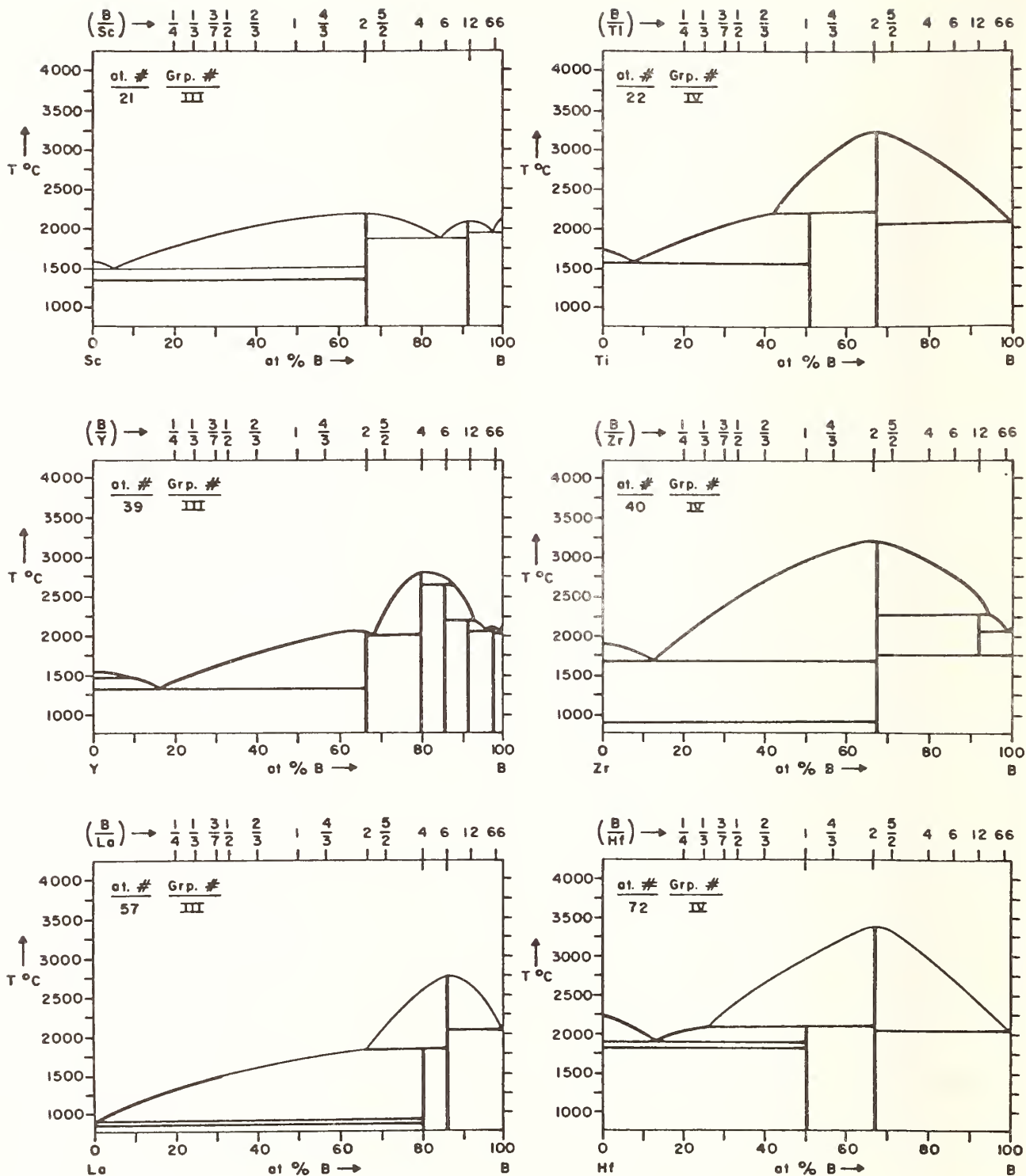


Figure 4: Phase Diagrams for the Metal-Boron Systems of the Transition Metals from Groups II and IV.

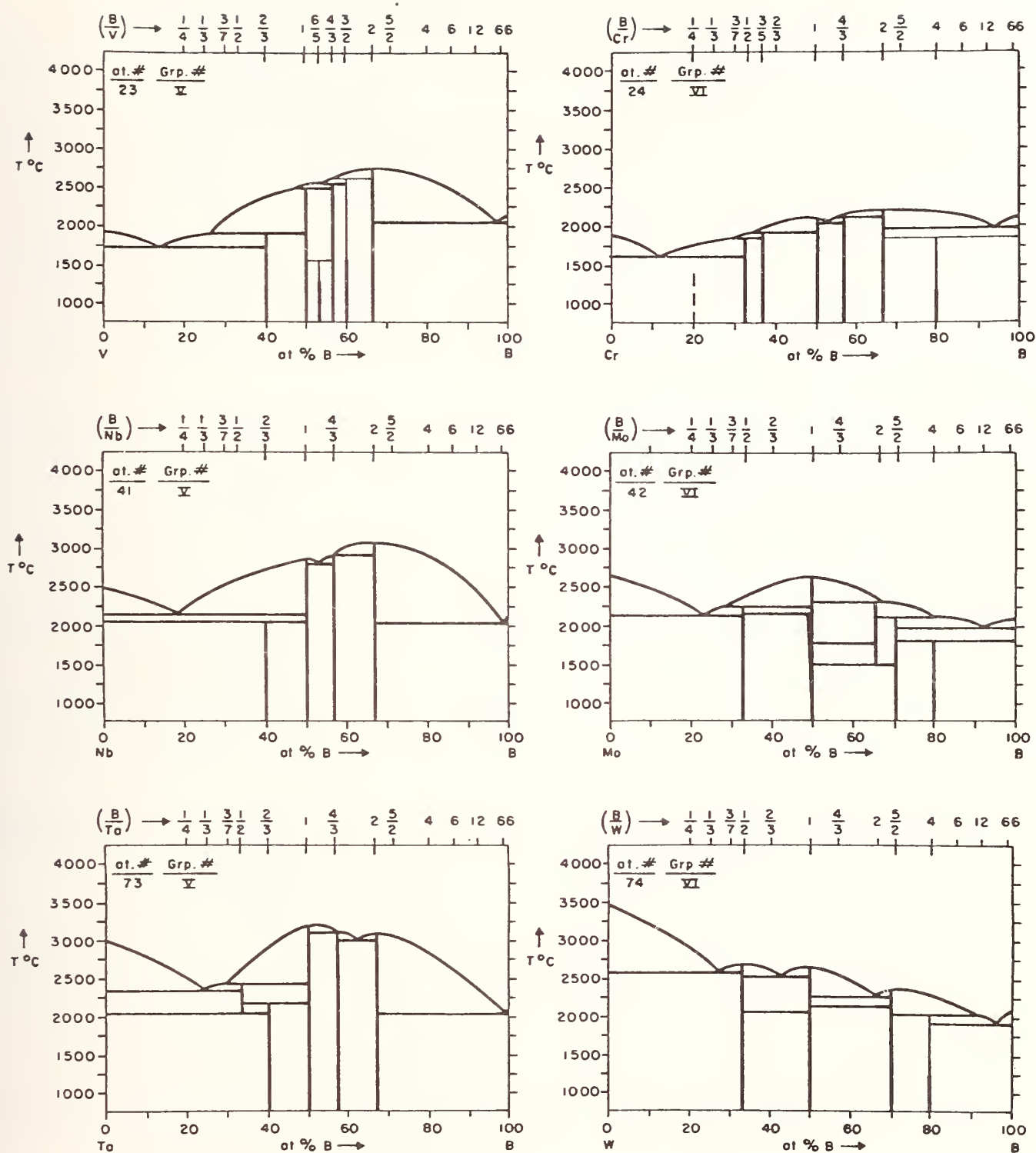


Figure 5: Phase Diagrams for the Metal-Boron Systems of the Transition Metals from Groups V and VI.

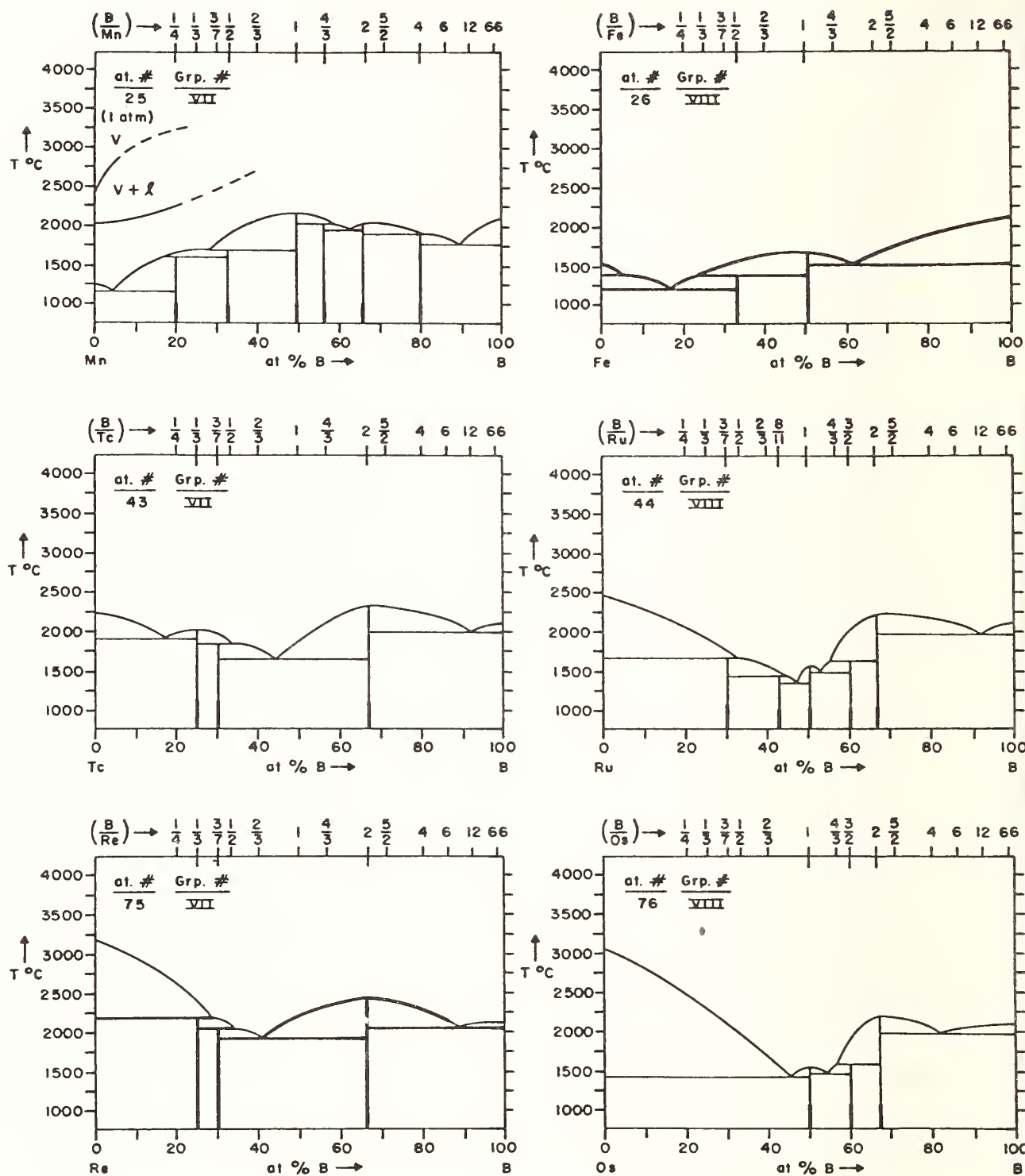


Figure 6: Phase Diagrams for the Metal-Boron Systems of the Transition Metals from Groups VII and VIII.

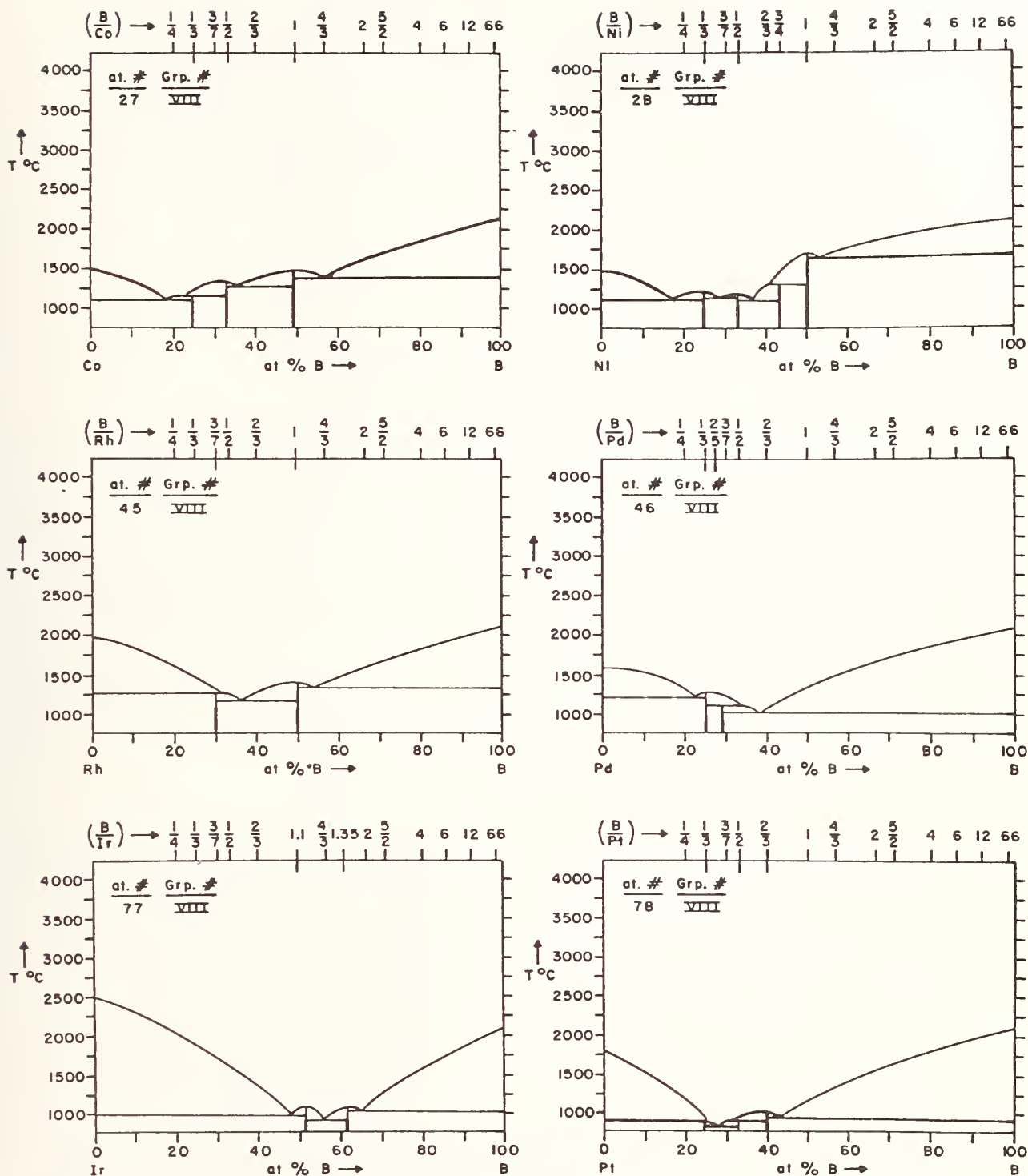


Figure 7: Phase Diagrams for the Metal-Boron Systems of the Transition Metals from Group VIII.

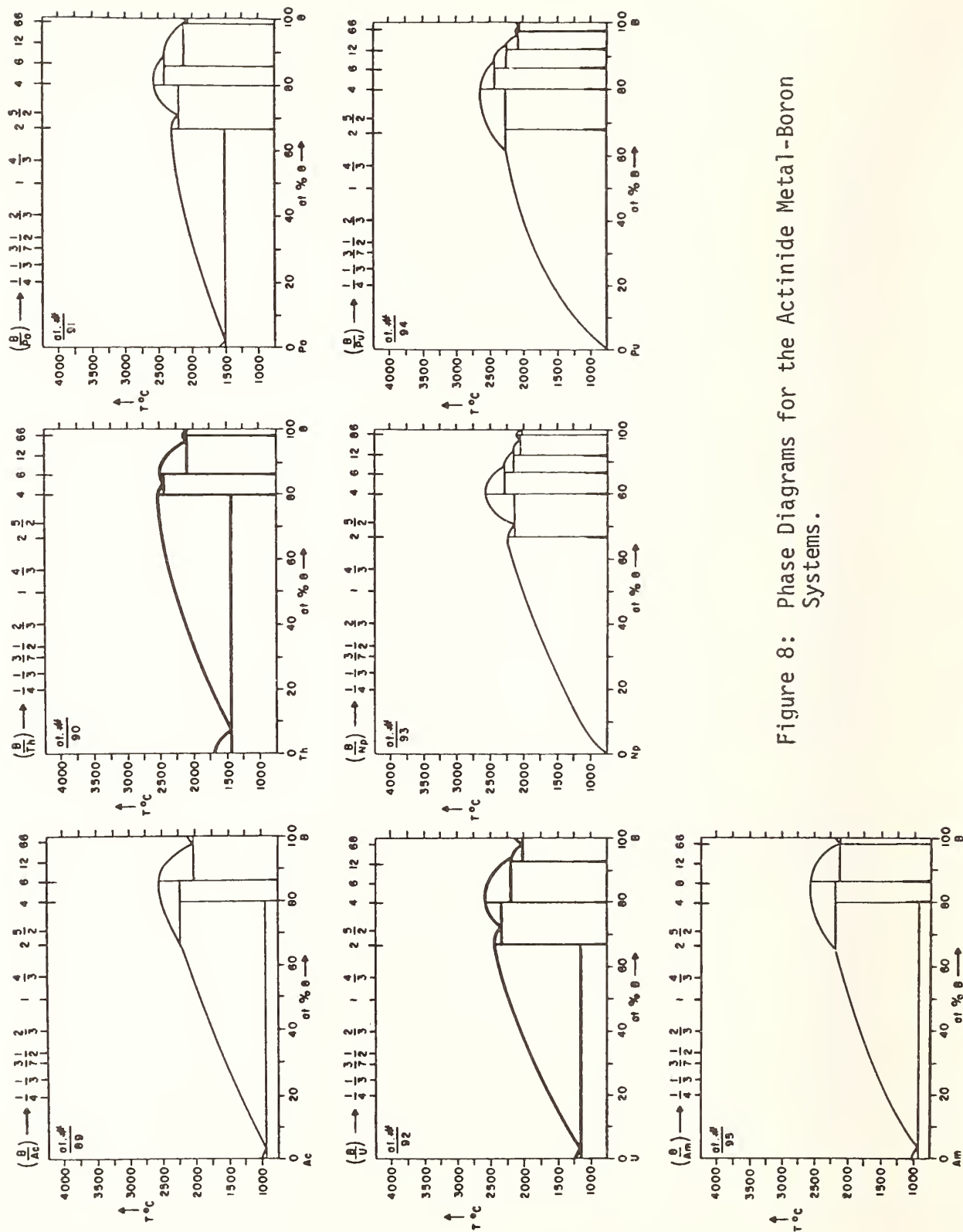


Figure 8: Phase Diagrams for the Actinide Metal-Boron Systems.



A VALENCE BOND TEST FOR THE VALIDITY OF INTERMETALLIC AND SEMICONDUCTING STRUCTURES

Forrest L. Carter
Naval Research Laboratory
Washington, D.C. 20375

Abstract

The existence and stability of compounds is reflected primarily by the local coordination of and atomic distances between the constitute atoms. The most universally valid method to make use of this important primary information is the system of metallic radii developed by Pauling. We have found that if these metallic radii cannot be applied in a self-consistent manner to reputedly "known" compounds, then the crystal structure and/or composition of the "known" compound should be questioned. Examples are primarily drawn from the transition metal borides, pnictides, and intermetallic compounds, including those of the rare earths. The advantages and limitations of this approach are discussed, and the plan for its future development as a sharper diagnostic, as well as predictive, tool is indicated.

Introduction

The validity of intermetallic and semiconducting structures can be tested via the use of Pauling's single bond metallic radii [1]. The general correctness of this assertion has become increasingly clear during the course of our several studies of chemical bond formation in transition metal and rare earth compounds. With experience, we have learned that if the semiempirical approach of Pauling cannot be self-consistently applied within certain limits (to be discussed), then either the structure or composition is seriously in error. In short, for a very wide selection of compounds, one has a test for the correctness of a phase description, provided x-ray data are available.

After discussing the basis of Pauling's metallic radii in the next section, we will then describe its advantages as well as its limitations. The succeeding sections will then provide examples where this approach suggests (a) crystallographic refinement is desirable, (b) structural instability exists, (c) compositional data are incorrect, and (d) failure of the material to exist as reported. The final section will indicate our plans to strengthen the powers of this approach to include a predictive capability.

Pauling's Metallic Radii:

The semiempirical single bond metallic radii, $R(1)$, of Pauling are much more than a set of hard sphere radii of a few elements useful only for a particular class of compounds. Rather, they are a set of radii for most of the periodic table, calculable from a few simple equations firmly based on the chemical concepts of covalency and hybridization.

From the observed crystallographic interatomic distances d_{ij} , the corresponding bond order n_{ij} between atoms i and j may be readily calculated from Eq. (1):

$$d_{ij} = R_i(1) + R_j(1) - 0.600 \log n_{ij} \quad (1)$$

If atoms i and j form a single bond between them, then $n_{ij} = 1$, since each atom contributes one electron to the formation of that bond. From Eq. (1) we see that d_{ij} is then the sum of the single bond radii, $R_i(1) + R_j(1)$. Usually, however, d_{ij} is larger than the sum of the $R(1)$, corresponding to a bond order less than 1.0; double bonds ($n_{ij} = 2$) are very rare in transition metal semiconductors and intermetallics. From the observed bond distances, one may calculate the valence of atom i by summing up the corresponding n_{ij} , Eq. 2:

$$V_i = \sum_j n_{ij} \quad (2)$$

The single bond radii $R_i(1)$ are readily calculated for the Fe-transition elements as:

$$R_i(1) = 1.825 - 0.043z_i - (1.600 - 0.100z_i) \delta_i, \quad (3)$$

where z_i is the number of electrons outside the rare gas core minus Q_i , the number of electrons transferred from atom i to its neighbors j . The d -character, δ_i , associated with the bond of atom i has a strong influence on the $R_i(1)$ of the transition elements, as we shall see shortly. As seen from Fig. 1, the equation for $R_i(1)$ of the Pd-transition elements is very similar to that of Eq. (3) and, excepting the interruption caused by the lanthanides, the equation for $R(1)$ of the long row of Pt-transition elements is also closely related.

In Fig. 1 we note that the single bond radii $R_i(1)$ are marked by circles and linked by solid lines. The dotted lines correspond to tetrahedral radii of sp^3 type hybridization with the radii $R(\text{tet})$ having the form of Eq. (3) with zero d character, $\delta_i = 0$, thusly:

$$R_i(\text{tet}) = 1.825 - 0.043z_i \quad (4)$$

METALLIC RADII

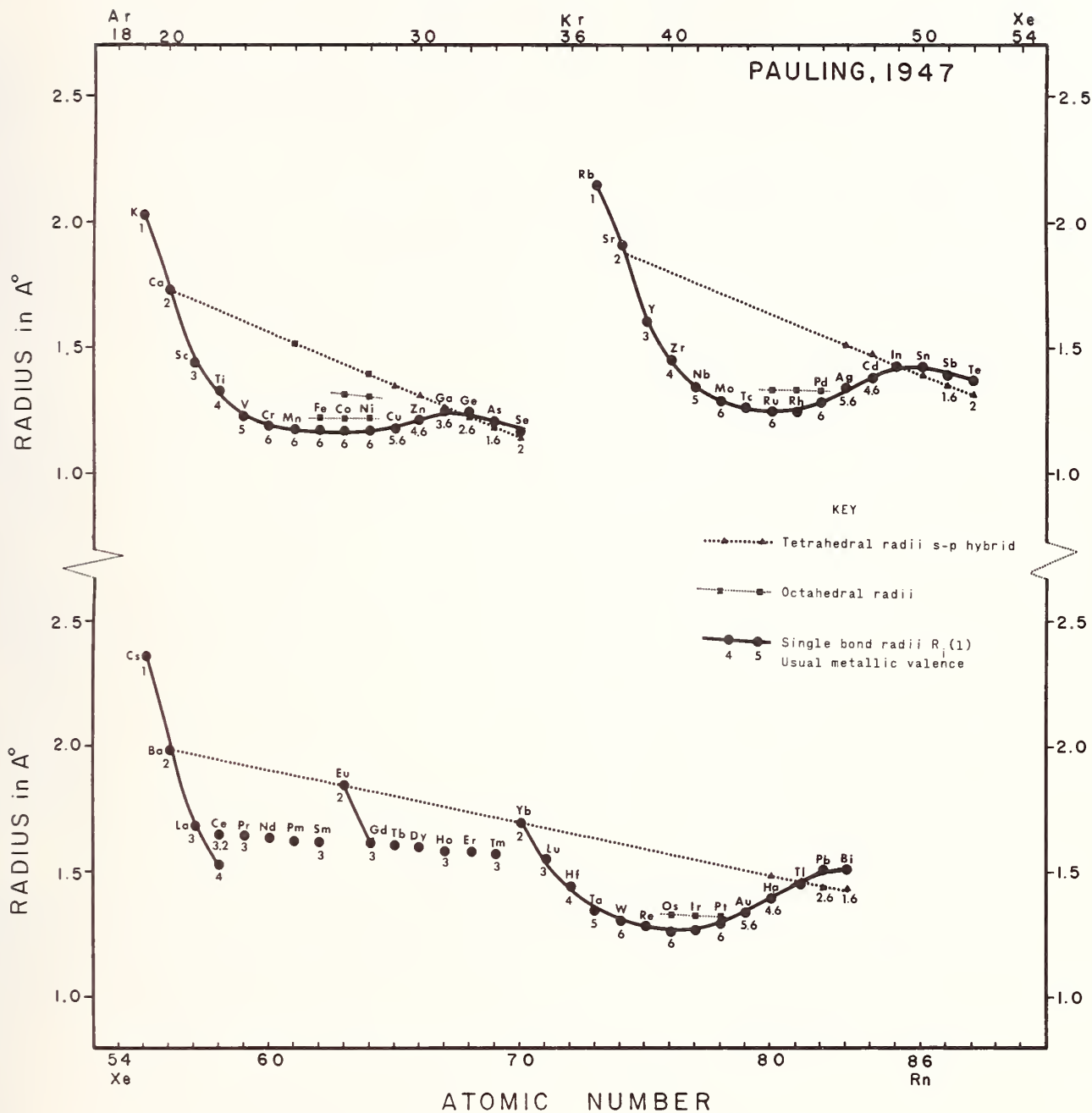


Fig. 1. The single bond radii of Pauling depend on valence and hybridization in a readily understandable fashion (see text).

We further note that the slope for the tetrahedral radii (-0.043) is the same for both the Fe- and the Pd-transition series elements and similar to that of the Pt-transition elements (-0.030). Further, Pauling provided for pure p-hybridization bonding by changing the constant of Eqs. 3 and 4, $1.825(sp^3)$ to $1.855(p)$. Accordingly, we can see (as a chemist would expect) a systematic dependence of $R_i(1)$ on the atomic number and hence on the hybridization.

The valence of the element also plays an important role in the single bond radius. This is suggested in several ways. For example: (1) in the beginning of each series, the sharp decline in $R_i(1)$ is due both to valence increases, as in the sequence $K(1) \rightarrow Ca(2) \rightarrow Sc(3) \rightarrow Ti(4)$, and to hybridization changes $s \rightarrow sp \rightarrow spd$. (2) For Fe, Co, and Ni, we find octahedral radii for different valent states midway between the solid $R(1)$ curve and the dotted $R(tet)$ line. For the rare earths, the divalent states of Eu and Yb are on the tetrahedral dotted line while the trivalent rare earths are significantly smaller. Thus it is quite clear from Fig. 1 that the atomic size is a significant function of both bond hybridization and valence. In contrast to the ionic picture, the single bond radii are only a weak function of formal charge Q_i (via the z_i parameter), usually with $|Q_i| < 1.5$.

In the application of Pauling's metallic radii to a given structure, it is usually desirable and often necessary to perform the calculation in an iterative manner to obtain self-consistent results. Starting with an atom's normal valence as an estimated valence, $V(est)$, one calculates from the known interatomic distances d_{ij} , the associated bond orders n_{ij} (Eq. 1) and then a calculated valence $V(calc)$ via Eq. 2. A new $V(est)$ may be taken as an average of $V(calc)$ and the prior $V(est)$. During the iterative process, charge transfer and/or some hybridization change in δ_i may be necessary to achieve the self-consistency in which for each atom $V_i(est) = V_i(calc)$. Generally, charge transfer is allowed to take place only to maintain a filled octet (as for sulfur) or to increase the bonding power of one atom without impairing that of a neighbor. From the formal charges and adjusted electronegativity differences, one may estimate ionic bond character and hence the bond polarization. The resultant effective charge for an atom is then

$$Q_i(eff) = Q_i(formal) - \sum_j n_{ij} (1 - \exp(-(x_i - x_j)^2/4)) * \text{sign}(x_i - x_j) \quad (5)$$

where x_i is the electronegativity of the i th atom. Usually the bond polarization occurs in such a way as to reduce the formal charge.

Advantages and Limitations:

Compared to any hard sphere model, the use of Pauling's metallic radii has several advantages. First of all, it can handle compounds involving combinations of any of more than 75 elements. It also provides approximate atomic valences and, through bond order calculations, an estimate of the relative strength and importance of various bonds. In addition, the method permits an estimate of effective charges which are generally in reasonable agreement with ESCA results (but not with the naive ionic models). Further, the method calls attention to any unusual hybridization conditions. From the simple bookkeeping of electrons and their relative s-, p-, and d-character, one may estimate the maximum number of unpaired d-electrons for comparison with magnetic and neutron diffraction data.

Two additional advantages are associated with the use of a self-consistent set of single bond radii for a compound: (1) the metallic radii can serve as atom sizes for a computer program [2,3] that calculates polyhedral atomic volumes (PAV) using a Voronoi-like cell construction. This result is useful for unequivocally establishing which atom undergoes a volume change upon compound formation and how much change there is. (2) The second use permits one to calculate generalized coordination numbers, CN_i , for non-symmetric as well as symmetric coordinations via the formula of Eq. 6 [2.4].

$$\frac{1}{CN_i} = \sum \left(\frac{n_{ij}}{V_i} \right)^2 \quad (6)$$

Hard sphere models offer none of these special chemical advantages.

The limitations of Pauling's metallic radii are of various sorts. First of all, the approach is not generally applicable to extremely ionic materials like halides or oxides, although the application to conducting halides and oxides might be both interesting and useful. Secondly, values of $R_i(1)$ and the variation of $R_i(1)$ with valence and d- or f-hybridization have not been developed for the actinide elements. Further, we note two kinds of difficulties with the rare earths: (1) the polyhedral atomic volumes of rare earths in most of their compounds are 10 to 15% smaller than calculated from the elements (see refs. 3 and 5), which indicates that the elemental $R_i(1)$ are generally too large (or the δ value is too small). The second problem is that in the rare earths, there is some evidence that bond hybridization is not isotropic, namely that f orbital participation may be strong for some bonds but not for others.

Finally, we note that the successful application of Pauling's metallic radii often requires some experience with the method. For example, for a particular compound it may be possible to achieve self-consistency via either a large charge transfer or through a vastly increased d-character. In such a case, it is difficult to know a priori which is more reasonable or what combination of these two approaches to use. In the future we hope to avoid this problem via the minimization of energy terms while iterating for self-consistency (details to be discussed later).

In summary of this section, we have found as a user (and not the originator) that the advantages of Pauling's metallic radii scheme render it far superior to any other proposed approach and that the method provides much useful information on innumerable phases, notwithstanding the limitations.

Applications:

Examples of the application of Pauling's metallic radii will be wholly drawn from our own experience, although the literature bulges with Pauling's contributions to elemental, compound, and alloy phases (for Si, see [6]). It is conceivable that the reader will be more convinced of the correctness of this method if it is argued by someone without Pauling's easy facility. In the examples we have chosen, we hope to demonstrate both the variation in criticality and the usefulness of this test for the validation of phases.

Refinement of Structure: Pauling's metallic radii can be used to indicate that a structure is probably correct but that refinement is necessary. In the case of ZnSb, the structure was solved in essence by Almin [7] using powder data. However, when it appeared that a Zn-Zn single bond was present as well as an Sb-Sb single bond, and that the metallic valence of Zn approached 4, it was decided that a structural redetermination was in order using a single crystal. In the results of Carter and Mazelsky [8], the Sb-Sb single bond was found correct, but the Zn-Zn bond order decreased to a more normal 0.31. The coordination of Sb is tetrahedral, while that of Zn is nearly trigonal planar. The use of Pauling's metallic radii suggests that antimony transfers approximately one electron to Zn, thereby permitting each to increase its valence by one (to 4 and 3, respectively, in agreement with their coordination). This increased bonding power presumably more than compensates for the energy cost of the electron transfer.

In the second example, we consider the isomorphous series Cr_3B_4 , Mn_3B_4 , Nb_3B_4 , and Ta_3B_4 , where accurate position parameters are available only for Cr_3B_4 (see Pearson [9]), and where the latter compounds probably were deemed too simple to be worthy of a full structure analysis. In using the metallic radii approach, the primary problem appears in terms of the valence of B2 (boron

No. 2, as catalogued by Pearson [9]), which increases from a reasonable value of 3.31 for Cr_3B_4 to 4.0 for Mn_3B_4 , and in excess of 4.0 for the Nb and Ta analogues. A boron valence greater than 4 is not chemically reasonable, since there are only four atomic orbitals available ($2s2p^3$). An analysis of the bond orders for B2 shows that there is an unusually strong B2-B2 bond ($n \approx 0.95$), which is much too strong for this composition. The metallic radii approach, then, suggests that structural refinement is in order and the parameters of B2 should change in such a way that the B2-B2 bond should lengthen. As a third example, in [2], we consider the single crystal structure determination of Ru_{11}B_8 in which light atoms are sought in the presence of heavy ones. Again, the valences of boron are too high (B2, $V = 4.04$; B4, $V = 4.61$), indicating too many short contacts. Here it is unfortunate that neutron diffraction techniques cannot be of ready assistance.

Structural Instability: In our next two examples, we indicate how the application of Pauling's metallic radii suggests structural instability for two unusual materials which are important for special purposes in DoD devices. As our first example, we will discuss TiNi, a material known both for its "memory" and its sound attenuation properties. Its high temperature structure is CsCl-type, but upon cooling below 700°C , it undergoes a diffusion-controlled transition to a trigonal unit cell. Cooling further below 160°C , TiNi begins a long series of poorly understood, martensitic transitions that are involved in both its memory and its sound attenuation properties [10]. The room temperature powder pattern, however, still appears to be closely related to the CsCl structure. In an attempt to understand this material and how it might transform, we applied the metallic radii approach to TiNi as if it were CsCl type (since the real structure was unknown). The large size of elemental Ti prevented the attainment of self-consistency and suggested an excessive Ti valence of $V(\text{calc}) = 5.6$, and a corresponding excessive Ti charge of -1.6 . However, Ni in the structure seemed to possess a near-normal valence of 5.40. In order to obtain self-consistency without charge transfer, it was necessary to increase the d-character of Ti from $\delta = 0.27$ to 0.37. Not only was such a d-character objectionably high for Ti, but it also resulted in abnormally low valences for both Ti and Ni. In short, no reasonable adjustment of the parameters available in the metallic radii method resulted in a useful discussion of the bonding in TiNi as an ambient CsCl structure. This result was in agreement with the experimental facts; namely, TiNi was CsCl only above 700°C .

In a similar treatment of the super-permanent magnet material, SmCo_5 , the two different kinds of cobalt (trigonal and icosahedral coordination) appeared as normal cobalts, but the Sm radius was obviously too large. In order to achieve a self-consistent treatment, Sm required not only an increased d-character and some charge transfer, but an anisotropic hybridization as well. Thus the final

model suggested f-orbital hybridization in the basal plane where Sm is encircled by a small ring of six cobalts. This structure prompted us to predict [3] that the structure was unstable at ambient conditions, which was found later to be the case experimentally by the co-workers of Buschow[11]. In short, if Pauling's metallic radii cannot be readily applied, then the stability and/or existence of the phase should be questioned.

Predicted Non-stoichiometry: In a consideration of the reported transition metal diborides of the AlB_2 structure, several reported diborides failed to iterate to self-consistent results at the ideal stoichiometry. Compounds for which this was the case and which might be non-stoichiometric members of the AlB_2 structure are RuB_2 , OsB_2 , and AgB_2 [12]. The results for RuB_2 are fairly typical of an extreme case. The boron calculated valence was an impossible 5.9, while $V(est) = 3.64$, even though $\delta = 0.53$ for Ru instead of a normal $\delta = 0.50$. Boron deficiency ameliorates this situation and if these compounds exist as an AlB_2 type, their stoichiometry deviates significantly from the ideal; thus for $RuB_2(1-x)$, $x > 0.4$. For RuB_2 and OsB_2 , this composition had been previously questioned by Przybylska, Reddoch and Ritter for other reasons [13].

Structural Variation of Hybridization: Although Pauling's metallic radii method does not depend per se on coordination, we have found that the resultant hybridization changes away from his normal values are usually in agreement with what a chemist is led to by simple valence bond considerations. For example, in our treatment of compounds having the WC structure [12], we found that without reducing the $R(1)$ value of P in MoP, self-consistency was not obtainable for P; thus $V(calc) = 4.95$ while $V(est) = 3.11$. However, by introducing a small amount of phosphorous d-character, 4-8%, the $R(1)$ value is reduced, so that self-consistency is readily obtainable. Thus, at $\delta(p) = 0.04$, self-consistency occurs with $V(calc) = V(est) = 4.16$. In the WC structure, the non-metal is in trigonal prismatic coordination, for which d-character is required if a valence bond construction is employed. One valence bond method which discusses the trigonal prismatic coordination at low d-character is that employing the Bidirectional Orbital Approximation (BOA), wherein a single orbital forms half-bonds with two (not one) near neighbors [14]. Three such bidirectional orbitals of mostly p-character but 7-8% d-character can bond six atoms in a trigonal prismatic coordination like that of P in MoP. In short, this is approximately the same amount of d-character suggested by the metallic radii approach.

Another example where the metallic radii agree with valence bond arguments is represented by the V_3Sn -type superconducting intermetallic compounds having the A-15 structure. In this structure, the V site atom has an unusual bond situation in that it has two very strong V-V bonds ($n_{VV} = \approx 0.6$ to ≈ 1.5) to form a linear chain

while it bonds twelve other atoms in a much weaker manner ($n_{vj} = 0.05$ to ≈ 0.35). A valence bond estimate of the d-character required in such a situation is 48.6% (an average of five bonding models) [15].

In order to obtain self-consistency in the metallic radii calculations for some forty of these intermetallic compounds having the Al₅ structure, it was found necessary to increase the d-character (δ_i) of the V site atom by the following amounts: Ti, from 0.27 to 0.37; V, from 0.35 to 0.39; Cr, good at 0.39; Nb, from 0.39 to 0.43; and Mo, from 0.43 to 0.44. In each case, we note that the required d-character is high and that any change in d-character is to increase it toward the valence bond estimate of 48.6%. Thus, while the metallic radii approach is certainly empirical in nature, it contributes to and reinforces our chemical interpretation.

Non-existent Compounds: For some compounds reported in the literature, the results of the metallic radii approach are so unreasonable that the stated existence of the compound should be seriously questioned. Such an example is AuB₂, where the metallic d-character had to be decreased from $\delta = 0.36$ to $\delta = 0.30$ [12]. This is a very unusual and unlikely circumstance. In addition, the valence of boron was 2.64, significantly below a minimum boron valence of 3.0. There is, therefore, good evidence that this compound does not exist as reported.

Another example is W₂B₅, in which both a large charge transfer occurs to the boron atoms and the tungsten d-character must be increased to unlikely levels before self-consistency is obtainable. This result confirms the earlier suspicions of Lundstrom [16]. The situation for the analogous compound, Ru₂B₅, is even more suspect based on the metallic radii approach [17].

In summary of this section, then, we see that the Pauling metallic radii not only constitute a useful test for phase existence but also provide information on valence, effective charge, bond strengths, composition, and hybridization.

Future Directions:

In order to maximize the utility of Pauling's metallic radii approach beyond the mere testing for the validity of a phase and toward a capacity for prediction, it is desirable that energy terms be added. Thus one could seek a least squares fit to the observed distances (or between $V(\text{calc})$ and $V(\text{est})$) and minimize an "energy of formation" at the same time. The energy terms to be included should depend on bond orders, n_{ij} , electronegativity differences, promotion energies for unusual hybridization, charge transfer energies, and a Madelung constant term. The Madelung term might be dependent upon coordination number in a manner

related perhaps to Templeton's suggestion [18] for a "reduced Madelung constant." Such terms should be initialized, of course, to give the known results for the elemental structures and other well-characterized compounds. Such an approach in the application of the metallic radii method would eliminate the current uncertainties (e.g., does one achieve self-consistency by charge transfer or by increased d-character hybridization?). More important, it would extend the approach toward the predictability required by the cost-effectiveness orientation of modern research managers.

Restatement

We have, it is to be hoped, argued the general soundness of the following two assumptions for this work and have demonstrated therein convincingly the forcefulness of the conclusion (3, below).

1. The existence and stability criteria for compounds are reflected primarily in their composition and crystal structure (i.e., bond distances).

2. This information can be most universally interpreted for semi-conducting and metallic materials via application of Pauling's metallic radii.

3. If Pauling's semi-empirical approach cannot be readily adjusted to a crystal's stated structure, the crystal structure and/or composition should be questioned.

References

1. L. Pauling, "Nature of the Chemical Bond," 3rd ed., Cornell University Press, Ithaca, N.Y., 1960, p. 400 ff.
2. F. L. Carter, J. Less-Common Metals, 47, 157 (1976).
3. F. L. Carter, "Valence Bond Formation in the Rare Earth Compounds Having the CaCu_5 Structure," Proceedings of the 9th Rare Earth Research Conference, Virginia Polytechnic Institute and State University, 10-14 Oct 1971, Vol. II, p. 617.
4. F. L. Carter, submitted for publication, Acta Cryst.
5. F. L. Carter and G. C. Carter, Proc. of 10th Rare Earth Research Conference, Carefree, Ariz., 30 April - 3 May, 1973, Vol. II, p. 1044.
6. Prof. L. Pauling has recently written a note indicating that a suggested high density form of Si "must be wrong, because of poor values of the bond lengths." Private communication.
7. Almin, K. E., Acta Chem. Scand. 2, 400 (1945).
8. F. L. Carter and R. Mazelsky, J. Phys. Chem. Solids, 25, 571 (1964).
9. W. B. Pearson, in G. V. Raynor (ed.), A Handbook of Lattice Spacings and Structures of Metals and Alloys-2, Vol. 8, Pergamon Press, Oxford, 1967.
10. F. L. Carter, "A Mechanism for the High Temperature Transformation and the Resultant Premartensitic TiNi(II) ," Symposium on TiNi and Associated Compounds, F. E. Wang, ed., 20 Feb 1968, NOLTR 68-16.
11. F. J. A. Den Broeder and K. H. J. Buschow, J. Less-Common Metals, 29, 65 (1972).
12. F. L. Carter, in R. S. Roth and S. J. Schneider (eds.), Solid State Chemistry, Nat. Bureau Stand. Spec. Publ. No. 364, 1972, p. 515.
13. M. Przybylska, A. H. Reddoch, and G. J. Ritter, J.A.C.S., 85, 407 (1963).
14. F. L. Carter, in L. Bennett (ed.), Electron Density of States, Nat. Bureau Stand. Spec. Publ. No. 323, 1971, p. 385.
15. F. L. Carter, "Valence Bonding in Alloys Having the β -Tungsten Structure," Westinghouse Paper 64-929-442-P3, 23 March 1964 (copy available from author).
16. T. Lundstrom, Ask. Kemi., 30, 115 (1968).
17. See discussion, ref. [2].
18. D. H. Templeton, J. Chem. Phys., 23, 1826 (1955).



Computation of the Component Activities from Ternary
Miscibility Gap Data: the Cu-Ag-S and Cu-Ag-Se Systems

U. V. CHOUDARY and Y. A. CHANG
Materials Department
College of Engineering and Applied Science
University of Wisconsin-Milwaukee
Milwaukee, Wisconsin 53201

ABSTRACT

The high temperature phase relations in the ternary Cu-Ag-S and Cu-Ag-Se systems at 1473 K have been analyzed in light of the recently developed thermodynamic method by the authors. From a knowledge of the experimental tie-line distribution data in the ternary miscibility gap, the boundary binary thermodynamics and the limiting activity coefficients of sulfur in the copper-silver melts, a consistent set of thermodynamic activities is derived in the Cu-Ag-S system. A similar analysis of the Cu-Ag-Se phase relations yields the metal activities and the relative selenium potentials; the absolute activities of selenium could not be determined due to lack of reliable Gibbs energies of mixing data in the Cu-Se and Ag-Se boundary binaries. An extension of the present method to obtain precise values of thermodynamic stabilities of binary and ternary carbides from the ternary metal-metal-carbon phase relations is pointed out.

INTRODUCTION

Phase equilibria and thermodynamic properties of alloy systems are closely interrelated. For instance, if the Gibbs energies of all the competing phases in any binary or ternary system are known as a function of composition and temperature, the phase diagram of the system can be computed. Conversely, from the experimentally determined phase diagrams, useful thermodynamic data of the alloy phases can often be extracted. This approach becomes extremely useful when it is experimentally difficult if not impossible to determine the appropriate thermodynamic properties.

Recently, Choudary and Chang¹ developed a thermodynamic method to calculate the thermodynamic activities (or the chemical potentials) of the component elements A, B, and C from a knowledge of the tie-line distribution data in the ternary miscibility gap (see Fig. 1), the thermodynamics of the boundary binary systems, and the limiting activity coefficients of C in solutions of A and B. This method is particularly applicable to ternary systems where the third component C is a non-metal such as O, S, Se, B, C. Many of these systems are of extractive metallurgical interest and are characterized by a ternary miscibility gap in the melt with one of the boundaries lying close to the A-B binary. Although experimental phase relations in the ternary miscibility gap are known for some of these systems, the chemical potentials of the components A, B, and C have not been determined and are usually difficult to derive experimentally. Yet, a basic knowledge of the thermodynamics of ternary systems such as A-B-O and A-B-S is essential for assessing the complex interactions in the multi-component solutions of metal-matte-slugs encountered in extractive metallurgical operations.

In order to derive such basic data of importance in the smelting and refining processes of copper and lead, the present thermodynamic method has been used successfully to compute the chemical potentials of the component elements in the Cu-Pb-O¹ and Cu-Pb-S² systems at 1473 K. In the Cu-Pb-S²

system, the activity values of lead determined experimentally and those derived from this method are in good accord. For the Cu-Pb-O system, no experimental activity data are available. Since the method was developed from classical thermodynamics, the derived chemical potentials of the components should be exact if the phase equilibria data are correct.

To further our understanding of the metal-matte chemistry in copper extraction, the high temperature phase relations of the Cu-Ag-S system are analyzed to derive the activities of the components. Furthermore, a knowledge of the thermodynamic properties of the Cu-Ag-S system is of significant interest to mineralogists. In view of the importance of the quantitative knowledge of Cu, Ag and Se interactions in the recovery of Ag and Se from copper anode slimes, the phase relations in the Cu-Ag-Se ternary system are also analyzed.

THERMODYNAMIC TREATMENT

Since the thermodynamic method has been presented in detail elsewhere¹, only a brief description of the method is given here. From a knowledge of the tie-line distribution within the two liquid-phase field (see Fig. 1), the limiting activity coefficients of component C, γ_C^0 , in the A-B solutions, and the thermodynamic properties of the boundary binaries, the chemical potentials of the component elements along the miscibility gap can be calculated from the relations developed in this section.

The Wagner's relation^{1,3}

$$\left(\frac{\partial \ln (\gamma_B/\gamma_A)}{\partial y_C} \right)_{y_B} = \left(\frac{\partial \ln \gamma_C}{\partial y_B} \right)_{y_C} \equiv \theta \quad [1]$$

can be integrated from $y_C = 0$ to $y_C = y_C^*$ at constant y_B to obtain the following equation for the ratio of activity coefficients of B and A along the metal-rich miscibility gap as:

$$\left(\ln \frac{\gamma_B}{\gamma_A} \right)_{y_B}^{y_C = y_C^*} = \left(\ln \frac{\gamma_B}{\gamma_A} \right)_{y_B}^{y_C = 0} + (\theta y_C^*)_{y_B} \quad [2]$$

In the above equation, θ is assumed to be constant in the compositional range $0 < y_C < y_C^*$ which is a valid approximation for $y_C^* \approx 0$. Thus the value of $(\theta)_{y_B}^{y_C^*}$ can be evaluated from the experimentally determined limiting activity coefficient of C in the A-B solutions. Even if the values of γ_C^0 are not available as a function of y_B , they may be estimated either from one of the several formulations of the quasichemical solutions models⁴⁻¹⁰, the Wagner model¹¹ or the extended Wagner model by Chiang and Chang¹². The parameters for the Wagner model as well as the extended Wagner model may be predicted from correlations proposed by Chiang and Chang¹² and Kuo and Chang¹². Knowing the ratios of the activity coefficients of B and A as a function of y_B from Eq. [2], it is possible to

calculate the activities of all three components by integrating the following equations between the appropriate compositional limits along the miscibility gap boundary:

$$d \left(\ln a_i \right)_{y_B^* \text{ or } y_B'} = Z_i d\psi^* \quad [3]$$

where ψ^* denotes $\ln \left(\frac{a_B}{a_A} \right)_{y_B^*}$ which is equal to $\ln \frac{\gamma_B}{\gamma_A} \bigg|_{y_B^*} + \ln \frac{y_B}{y_A} \bigg|_{y_B^*}$, and the sub-

script i stands for A, B, or C. The integration functions — Z_A , Z_B , and Z_C — defined as

$$Z_A = \frac{y_B' y_C^* - y_B^* y_C'}{y_C' - y_C^*} \quad [4]$$

$$Z_B = 1 + Z_A \quad [5]$$

$$Z_C = \frac{y_B^* - y_B'}{y_C' - y_C^*} \quad [6]$$

are calculable from the tie-line distribution data in the ternary miscibility gap.

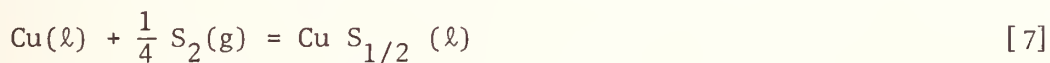
APPLICATION TO THE CU-AG-S SYSTEM

Since the calculation of the chemical potentials of the components along the miscibility gap depends on a knowledge of the phase relationships and the thermodynamic properties of the boundary binary and the ternary systems, they will be briefly reviewed. The thermodynamic values to be discussed hereafter refer to the temperature of 1473 K unless stated otherwise.

Cu-S

Kellogg¹³ has critically evaluated the high temperature phase relations and the thermodynamic properties of the Cu-S system; the selected values employed in the present analysis are taken from his evaluation. The atom fraction of sulfur at saturation, x_S^* , is taken to be $0.0226 \pm .001$. The values of the limiting activity coefficient of sulfur in liquid copper, $\gamma_{S(Cu)}^o$, and the Gibbs energy self interaction parameter, $\epsilon_{S(Cu)}^S = (\partial \ln \gamma_S / \partial x_S)$, are derived as $3.97 (\pm 0.4) \times 10^{-3}$ and -14 ± 2 , respectively. Thus, the values of a_{Cu} , a_S , and p_{S_2} in the miscibility gap are found to be $0.981 \pm .002$, 6.53×10^{-5} and $9.37 (\pm 1.5) \times 10^{-7}$ atm., respectively. The standard states are Cu(l) and S(l). The change of standard states for sulfur from $\frac{1}{2} S_2(g)$ to S(l) is made using the data from JANAF¹⁴.

The equilibrium constant, $K_{CuS_{1/2}}$, for the reaction



is found to be 32.3, while the values of a_{Cu} , a_S , and p_{S_2} at the stoichiometric composition Cu_2S are 0.437 ± 0.02 , 3.36×10^{-4} , and $2.53 (\pm 2) \times 10^{-5}$ atm., respectively.

Ag-S

Recent thermodynamic investigations of the Ag-Ag₂S system over the temperature interval 1273-1473 K by Yazawa and Schnalek¹⁵ are in excellent accord with the earlier extensive phase equilibria and thermodynamic determinations of Rosenqvist¹⁶ in the temperature range 773-1523 K. Mills¹⁷ has reviewed and critically assessed the various thermodynamic studies of the Ag-S system; his suggested high temperature thermodynamic properties at 1373 and 1523 K are mainly based on the investigations of Rosenqvist, and Yazawa and Schnalek.

At 1473 K, the Ag-S system does not exhibit a miscibility gap; the critical point lies at approximately 24 at.% S and 1400 K. In conjunction with appropriate JANAF data, $\gamma_{S(Ag)}^O$ is derived as $0.045 \pm .004$ from the investigations of Rosenqvist¹⁶ and Yazawa and Schnalek¹⁵. Since none of the above authors' investigations extend up to the composition corresponding to Ag_2S at 1473 K, the activities of silver and sulfur can be extrapolated from Rosenqvist's values of a_{Ag} , a_S , and $\Delta\bar{H}_S$ values at 1398 K. Also, the extrapolated values have to be consistent with the derived values of activities in the Ag-rich region of the miscibility gap. From these considerations, the values of a_{Ag} , a_S , and p_{S_2} at $x_S = 0.333$ and $T = 1473$ K are selected to be 0.691 ± 0.004 , 8.2×10^{-3} , and $1.5(\pm 0.6) \times 10^{-2}$ atm, respectively. The standard states are pure liquid silver and sulfur. From the above selected values, the equilibrium constant, $K_{AgS_{1/2}}$, for the reaction



is found to be $4.13 \pm .4$ from the above selected values.

Cu-Ag

The thermodynamic properties of Cu-Ag solutions pertinent to the present analysis are taken from Hultgren, et al.¹⁸

Cu-Ag-S

The high temperature phase relations in the ternary Cu-Ag-S system have been investigated by Gerlach, et al.¹⁹, and Kristovnikov, et al.²⁰ The tie-line distributions at 1473 K, depicted in Fig. 2, are taken from Gerlach, et al. The silver-rich portion of the miscibility gap, shown as dashed line in Fig. 2, is drawn to be consistent with the fact that Ag and S are completely miscible at this temperature¹⁶. No thermodynamic properties have been reported along the miscibility gap. Kristovnikov, et al.²⁰, have studied the Cu_2S - Ag_2S system and found it to be pseudo-eutectic; Cu_2S and Ag_2S are completely miscible in the liquid state at 1473 K.

Solid solutions of $\text{Cu}_2\text{S}-\text{Ag}_2\text{S}$ have been investigated in the temperature range 703-980 K by Perrot and Jeannot;²¹ the activities of $\text{CuS}_{1/2}$ and $\text{AgS}_{1/2}$ exhibit small positive deviations from ideality at 980 K.

The limiting activity coefficient of S in Cu-Ag solutions has been determined by Cheng;²² his experimental values for $y_{\text{Ag}} = 0$ to 1 at 1358 K are also available in a paper by Fruehan and Richardson.²³ Jacob and Jeffes⁹ have reported that the experimental values of Cheng are in good accord with the predicted values from their quasichemical model. Hence, in the present analysis, the values of $\ln \gamma_{\text{S}}^{\text{O}}$ in Cu-Ag solutions at 1473 K are computed from the following quasi-chemical relation of Jacob and Jeffes:⁹

$$\ln \gamma_{\text{S}(\text{Cu-Ag})}^{\text{O}} = y_{\text{Cu}} \ln \gamma_{\text{S}(\text{Cu})}^{\text{O}} + y_{\text{Ag}} \ln \gamma_{\text{S}(\text{Ag})}^{\text{O}} - 2 \frac{\Delta H}{RT} \quad [9]$$

where ΔH is the enthalpy of mixing for the Cu-Ag solution and R is the universal gas constant.

Computation of the Activities of Cu, Ag and S in the Miscibility Gap

From Eqs. [2] and [9], and the standard thermodynamic relationship between the integral and partial quantities, an expression for calculating the ratio of activities of silver and copper along the metal-rich miscibility gap can be written as:

$$\begin{aligned} \psi^* &= \left(\ln \frac{a_{\text{Ag}}}{a_{\text{Cu}}} \right)_{y_{\text{Ag}}} \\ &\quad y_{\text{S}} = y_{\text{S}}^* \\ &= \left(\ln \frac{\gamma_{\text{Ag}}}{\gamma_{\text{Cu}}} \right)_{y_{\text{Ag}}} + \left(\ln \frac{y_{\text{Ag}}}{y_{\text{Cu}}} \right) + y_{\text{S}}^* \left\{ \ln \frac{\gamma_{\text{S}(\text{Ag})}^{\text{O}}}{\gamma_{\text{S}(\text{Cu})}^{\text{O}}} + \frac{2}{RT} \left(\frac{\Delta H - \Delta \bar{H}_{\text{Ag}}}{1 - y_{\text{Ag}}} \right) \right\} \quad [10] \\ &\quad y_{\text{S}} = 0 \end{aligned}$$

where $\Delta\bar{H}_{\text{Ag}}$ represents the relative partial molar enthalpy of silver in the Cu-Ag solutions.

Utilizing the calculated values of ψ^* from the above expression and integrating Eq. [3] with $y_{\text{Ag}}^* = 0$ as the lower limit, activities of the components can be derived as:

$$\left(\ln a_i\right)_{y_{\text{Ag}}^*} = \left(\ln a_i\right)_{y_{\text{Ag}}^*=0} + \int_0^{y_{\text{Ag}}^*} Z_i d\psi^* \quad [11]$$

where the subscript i stands for Cu, Ag, or S, and Z_{Cu} , Z_{Ag} , and Z_{S} represent the integration functions calculable from Eqs. [4] to [6].

The pertinent integration plots are presented in Figs. 3 and 4 while the derived activities of Cu, Ag and S are shown in Figs. 5, 6, and 7. The activities of Cu and Ag are also presented in Fig. 8 for sulfur-free ($y_{\text{S}}=0$) and sulfur-saturated ($y_{\text{S}} = y_{\text{S}}^*$) solutions as a function of the metal atom ratio. The positive deviations from ideality are less pronounced for the sulfur-saturated melts. The maximum uncertainty in the activities from all the sources is estimated to be $\pm 8\%$.

Computation of the Sulfur Potential in the Cu_2S - Ag_2S Psuedo-Binary

The sulfur potentials along the Cu_2S - Ag_2S join are not known experimentally, but may be computed using the method described below. However, the computed values must be consistent with (i) the known values of p_{S_2} at the stoichiometric compositions Cu_2S - Ag_2S ; (ii) Wagner's relation represented by Eq. [2]; (iii) derived values of p_{S_2} in the miscibility gap. From Eqs. [7] and [8], the ratio of activity coefficients of the sulfides, $\text{CuS}_{1/2}$ and $\text{AgS}_{1/2}$, can be related to the ratio of activity coefficients of the metals, and that of the respective equilibrium constants as:

$$\ln \frac{\gamma_{\text{AgS}_{1/2}}}{\gamma_{\text{CuS}_{1/2}}} = \ln \frac{\gamma_{\text{Ag}}}{\gamma_{\text{Cu}}} - \ln \frac{K_{\text{AgS}_{1/2}}}{K_{\text{CuS}_{1/2}}} = \ln \frac{\gamma_{\text{Ag}}}{\gamma_{\text{Cu}}} - 2.06 \quad [12]$$

For the mid-range composition, where the miscibility gap lies close to the $\text{CuS}_{1/2} - \text{AgS}_{1/2}$ join, the value of $\ln \frac{\gamma_{\text{Ag}}}{\gamma_{\text{Cu}}}$ on the join may be calculated from the value at the S-rich side of the miscibility gap at constant γ_{Ag} from Wagner's relation expressed in Eq. [2]. From these considerations, slight positive deviations from ideality are inferred in the $\text{CuS}_{1/2} - \text{AgS}_{1/2}$ quasi-binary. The estimated sulfur potentials along the pseudo-binary join and the derived values along the miscibility gap are shown in Fig. 9. The maximum uncertainties in $\ln p_{\text{S}_2}$ values are ± 0.3 and ± 0.7 along the miscibility gap and $\text{CuS}_{1/2} - \text{AgS}_{1/2}$ join, respectively.

APPLICATION TO THE CU-AG-SE SYSTEM

The phase relations in the $\text{Cu-Cu}_2\text{Se-Ag}_2\text{Se-Ag}$ section have been well established by the determinations of Asano, et al.,²⁴ over the temperature interval 873-1473 K. At 1473 K, the miscibility gap in the Cu-Se system extends all the way to the Ag-Se system. Based on the chemical analysis of nearly twenty melts in the miscibility gap, Asano, et al.,²⁴ have determined the tie-line distribution at 1473 K; it is in essential agreement with that of Emicke²⁵ for the silver-rich portion at 1223 K. The $\text{Cu}_2\text{Se-Ag}_2\text{Se}$ quasi-binary has been found to be of the pseudo-eutectic type by Asano, et al.; a single liquid exists throughout the compositional range at 1473 K.

Reliable high temperature thermodynamic data are not available for the boundary binaries Cu-Se, Ag-Se and the ternary system. However, a thermodynamic analysis of the phase relations at 1473 K may be carried out assuming the variation of the limiting activity coefficient of Se with atom ratio of Ag is approximately the same as that of S in the Cu-Ag melts. The pertinent integration plots based on the tie-line

distribution data of Asano, et al., are presented in Figs. 10 and 11. The derived metal activities with an estimated overall maximum uncertainty of $\pm 10\%$ are shown in Figs. 12 and 13. Since the activity of Se is not known at either of the boundary binaries, only the relative activity is presented in Fig. 14. Once the high temperature thermodynamic properties of either Cu-Se or Ag-Se melts are known, absolute selenium activity can be readily obtained from the derived relative selenium activity.

ANALYTICAL APPROACH TO THE PRESENT THERMODYNAMIC METHOD

The thermodynamic properties of the boundary binary solutions (A-B) as well as the limiting activity coefficient of C in solutions of A and B can often be expressed as a simple function of the metal atom ratio. In such cases, thermodynamic activities along the miscibility gap can be represented analytically at least in a limited compositional range. Further, if the tie-line distribution data is extensive, the integration function Z and the \ln (activity ratio) may be fitted to a suitable function of y_B and the pertinent integrations may be performed analytically to derive the activities.

To facilitate discussion in this section, the following nomenclature is adopted:

$$\begin{aligned} \xi &= y_{Ag}; & \eta &= y_S; & \psi &= \ln \frac{a_{Ag}}{a_{Cu}} \\ \phi &= \ln \frac{\gamma_{Ag}}{\gamma_{Cu}}; & Y &= \ln \frac{y_{Ag}}{y_{Cu}}; & \theta &= \frac{\partial \ln \gamma_S}{\partial \xi} = \frac{\partial \phi}{\partial \eta} \end{aligned}$$

The superscript 'o' is used to designate the values in C-free A-B binary.

The thermodynamic properties of Cu-Ag solutions at 1473 K can be adequately described by the regular solution model. Thus, the ratio of the activity coefficients of Ag and Cu may be expressed as a linear function of the metal atom ratio

$$\phi^o = \frac{\epsilon}{RT} (1 - 2\xi) \quad [13]$$

where the regular solution parameter, ϵ , for Cu-Ag system is taken to be 3366 cal, based on the selected thermodynamic properties by Hultgren, et al.¹⁸

Also, the variation of the limiting activity coefficient of sulfur in Cu-Ag melts is a simple linear function of ξ :

$$\theta^* \approx \theta^0 = -0.5 + 5.8 \xi \quad [14]$$

Since $\eta^* = 0.02 \pm .004$, the activity ratio along the miscibility gap can be expressed from Eqs. [2], [13] and [14] as:

$$\psi^* = \psi^0 + \theta^0 \eta^* = (1.14 - 2.184 \xi) + \ln \frac{\xi}{1-\xi} \quad [15]$$

Also, the integration functions Z_{Cu} , Z_{Ag} and Z_{S} have been found to vary linearly for $0 < \xi^* < 0.7$, i.e., $Z_{\text{Cu}} = -1.11 \xi^*$ and $Z_{\text{S}} = 1.68 \xi^*$. Thus, analytical integration of Eqs. [3] to [5] yield the following expressions for the activities of components in the compositional range $0 < \xi < 0.7$ along the miscibility gap.

$$\ln a_{\text{Cu}} = -.02 + 1.212 \xi^2 + 1.11 \ln (1-\xi) \quad [16]$$

$$\ln a_{\text{Ag}} = 1.14 - 2.184 \xi + 1.212 \xi^2 + \ln \xi + 0.11 \ln (1-\xi) \quad [17]$$

$$\ln a_{\text{S}} = -9.64 - 1.84 \xi^2 - 1.68 \ln (1-\xi) \quad [18]$$

$$\ln p_{\text{S}_2} = -13.88 - 3.68 \xi^2 - 3.36 \ln (1-\xi) \quad [19]$$

Noting that $Z_{\text{Cu}} = -1.033 \xi^*$ and $Z_{\text{Se}} \approx 1.231 \xi^*$ for $0 < \xi^* < 0.7$, metal activities and the relative selenium activities can be similarly represented along the miscibility gap in the Cu-Ag-Se system.

$$\ln a_{\text{Cu}} = -.02 + 1.28 \xi^2 + 1.033 \ln (1-\xi) \quad [20]$$

$$\ln a_{\text{Ag}} = 1.12 - 2.184 \xi + 1.128 \xi^2 + \ln \xi + 0.033 \ln (1-\xi) \quad [21]$$

$$\left(\ln a_{\text{Se}} \right)_{\xi^*} - \left(\ln a_{\text{Se}} \right)_{\xi^*=0} = -1.834 \xi^2 - 1.68 \ln (1-\xi) \quad [22]$$

EXTENSION OF THE PRESENT THERMODYNAMIC

METHOD TO OTHER SYSTEMS

The present method can be extended to ternary systems where all the components A, B and C are metals, provided the miscibility gap lies close to one of the boundary binaries. Even in the absence of limiting experimental activity coefficients of C in A-B alloys, activities in the miscibility gap can be computed from the boundary binary thermodynamics by assuming a linear variation of $\ln \gamma_C^0$ with metal atom ratio. Even if the ternary systems are not characterized by a miscibility gap, Wagner's relation given by Eq. [2] is highly valuable to check the internal consistency of experimental or derived thermodynamic properties from various solution models.

Recent analysis of ternary phase relations in metal-metal-carbon systems such as Fe-Mn-C,²⁶ Fe-Cr-C in solid²⁶ as well as liquid²⁷ state up to graphite saturation, shows that highly reliable Gibbs energies of formation for the binary and ternary carbides can be derived utilizing the present method. Since phase relations are well established for many of the ternary carbon systems, analysis of them in light of the present method will be useful for obtaining hitherto unavailable precise thermodynamic properties of transition metal carbides. Similar analysis of solid state phase relations in other ternary systems such as A-B-O, A-B-S will also be valuable for assessing the stabilities of oxides, sulfides, silicates and spinels.

ACKNOWLEDGMENTS

The authors wish to acknowledge partial support of this research from the International Copper Research Association.

REFERENCES

1. U. V. Choudary and Y. A. Chang: Met. Trans., 1976, vol. 7B, pp. 655-660.
2. U. V. Choudary, Y. E. Lee and Y. A. Chang: Met. Trans., in review.
3. C. Wagner: Met. Trans., 1975, vol. 6B, pp. 395-398.
4. C. B. Alcock and F. D. Richardson: Acta Met., 1958, vol. 6, pp. 385-95;
1960, vol. 8, pp. 882-87.
5. G. R. Belton and E. S. Tankins: Trans. TMS-AIME, 1965, vol. 233, pp. 1892-98.
6. U. Block and H. P. Stüwe: Z. Metallkunde, 1969, vol. 60, pp. 766-71.
7. N. A. Gokcen: Scripta Met., 1969, vol. 3, pp. 157-60.
8. R. J. Fruehan and F. D. Richardson: Trans. TMS-AIME, 1969, vol. 245,
pp. 1721-26.
9. K. T. Jacob and J.H.E. Jeffes: Trans. Inst. Min. Met., 1971, vol. C80,
pp. 32-41.
10. K. T. Jacob and C. B. Alcock: Acta Met., 1972, vol. 20, pp. 221-32.
11. C. Wagner: Acta Met., 1973, vol. 21, pp. 1297-1303.
12. T. Chiang and Y. A. Chang: Met. Trans., 1976, vol. 7B, pp. 453-67; S. Kuo and
Y. A. Chang: Met. Trans. in review.
13. H. H. Kellogg: Can. Met. Quart., 1969, vol. 8, pp. 3-23.
14. JANAF Thermochemical Tables, 2nd edn., National Bureau of Standards, 1971.
15. A. Yazawa and F. Schnalek: Freiberger Forschrift, 1967, vol. 118B, pp. 7-24.
16. T. Rosenqvist: Trans. AIME, 1949, vol. 185, pp. 451-60.
17. K. C. Mills: Thermodynamic Data for the Inorganic Sulfides, Selenides, and
Tellurides, Butterworths, London, 1974, pp. 102-8.
18. R. Hultgren, P. D. Desai, D. T. Hawkins, M. Gleiser, and K. K. Kelley:
Selected Values of the Thermodynamic Properties of Binary Alloys, ASM,
Metals Park, 1973.

19. J. Gerlach, U. Hennig, and K. Trettin: Erzmetall, 1966, vol. 19, pp. 458-63.
20. A. N. Kristovnikov, A. Yu. Mendelevich, and V. M. Glazov: R. J. Inorg. Chem., 1968, vol. 4, pp. 1047-8.
21. P. Perrot and C. Jeannot: Rev. Chim. Miner., 1971, vol. 8, pp. 87-97.
22. L. L. Cheng: Ph.D. Thesis, University of London, 1959.
23. R. J. Fruehan and F. D. Richardson: Trans. TMS-AIME, 1969, vol. 245, pp. 1721-60.
24. N. Asano, K. Wase, and T. Nomura: Nippon Kogyo Kaishi, 1971, vol. 87, pp. 485-90.
25. K. Emicke: Erzmetall, 1962, 15, pp. 15-20.
26. U. V. Choudary and Y. A. Chang: unpublished research, 1976, to be submitted to Met. Trans.
27. U. V. Choudary and G. R. Belton: unpublished research, 1976, to be submitted to Met. Trans.

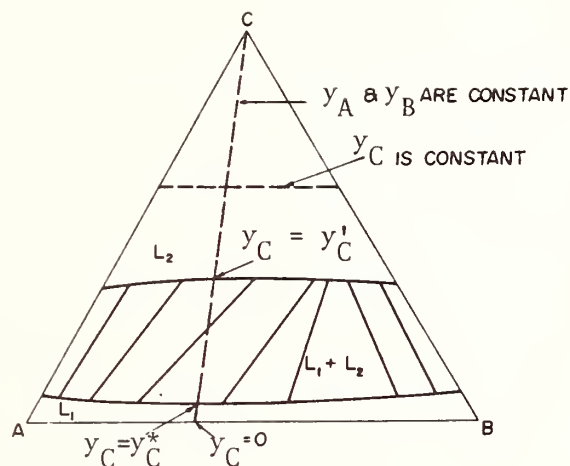


Fig. 1. A schematic of an isothermal section showing a miscibility gap in a ternary system A-B-C.

$$\text{Atom Ratio of } i = y_i \equiv \frac{n_i}{n_A + n_B} \equiv \frac{x_i}{1-x_C}; y_B \equiv \xi; y_C = \eta$$

n_i - No. of atoms of the i th component; x_i - atom fraction.

'*' - Denotes the value at the metal-rich boundary

'\prime' - Denotes the value at the metal-deficient boundary

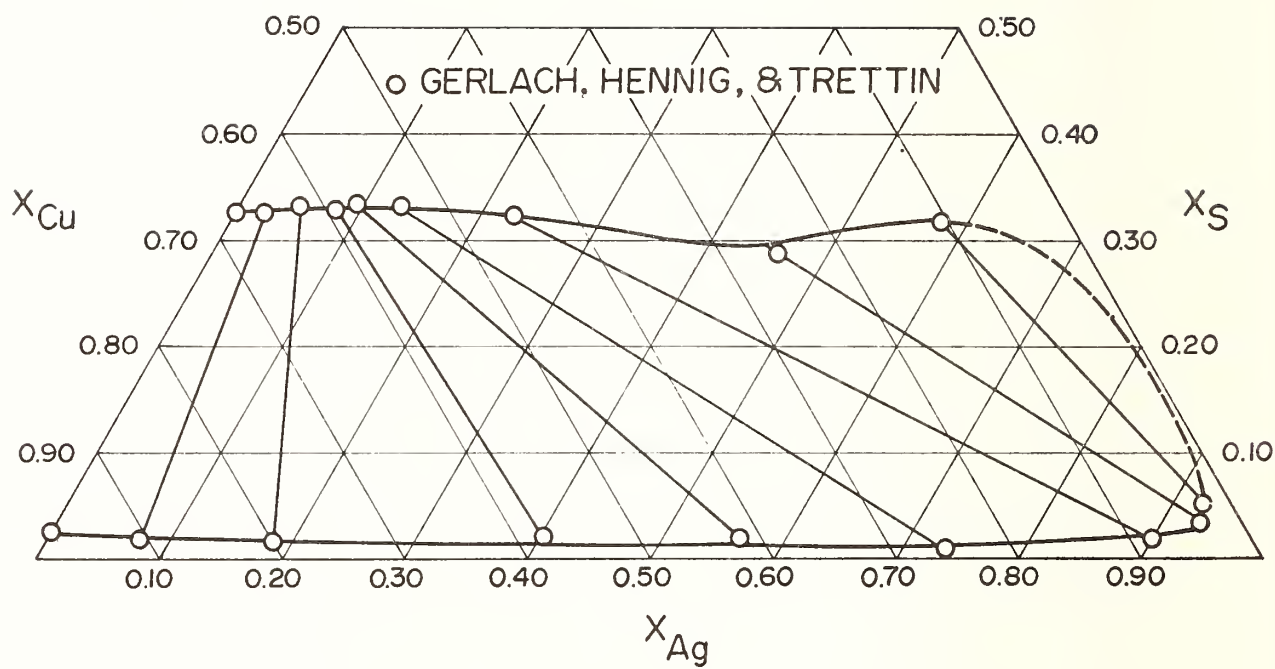


FIGURE 2. Experimental tie-line distributions along the ternary miscibility gap of the Cu-Ag-S system at 1473 K.

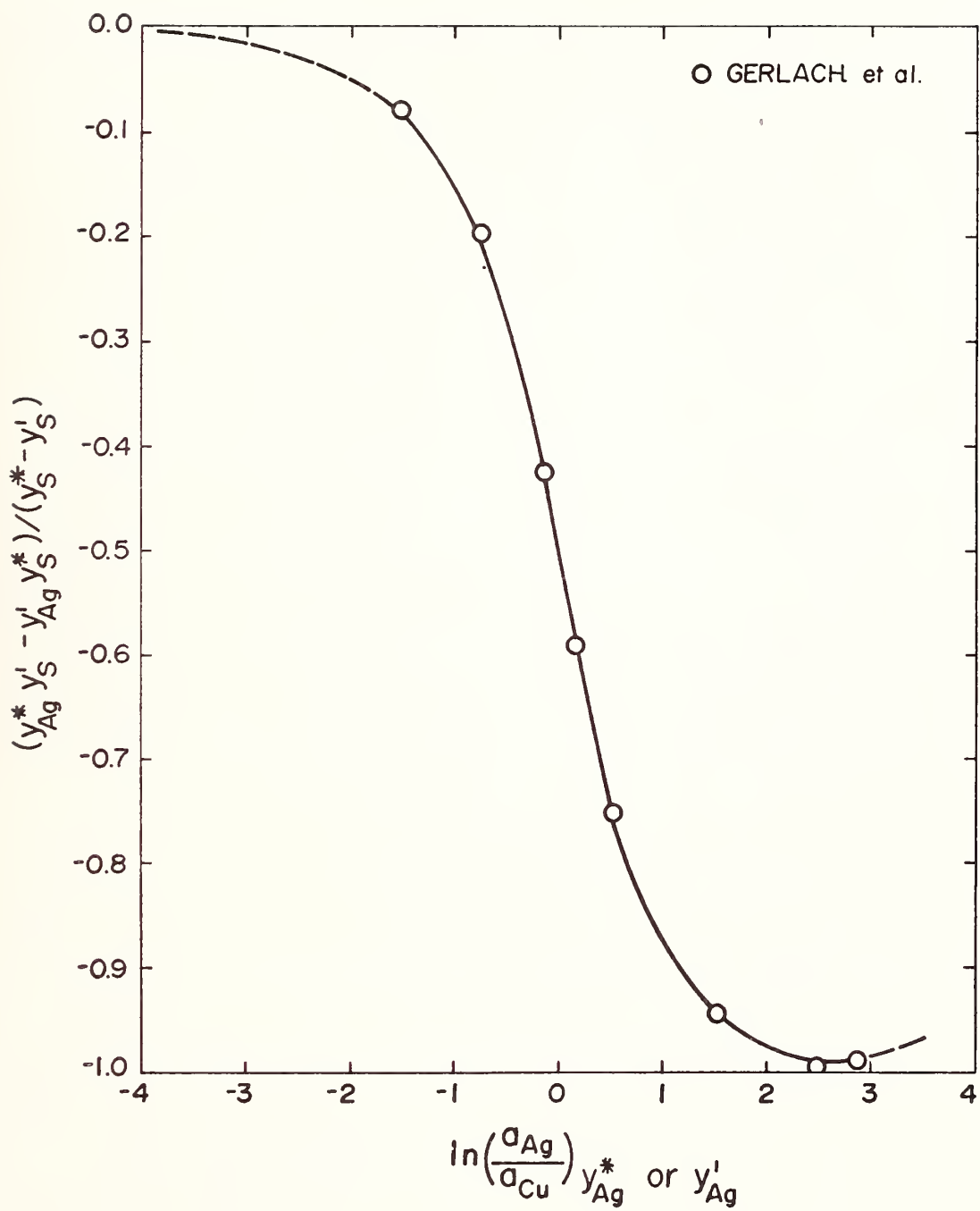


FIGURE 3. Integration plot for deriving the activities of copper and silver at 1473 K in the ternary miscibility gap of the Cu-Ag-S system.

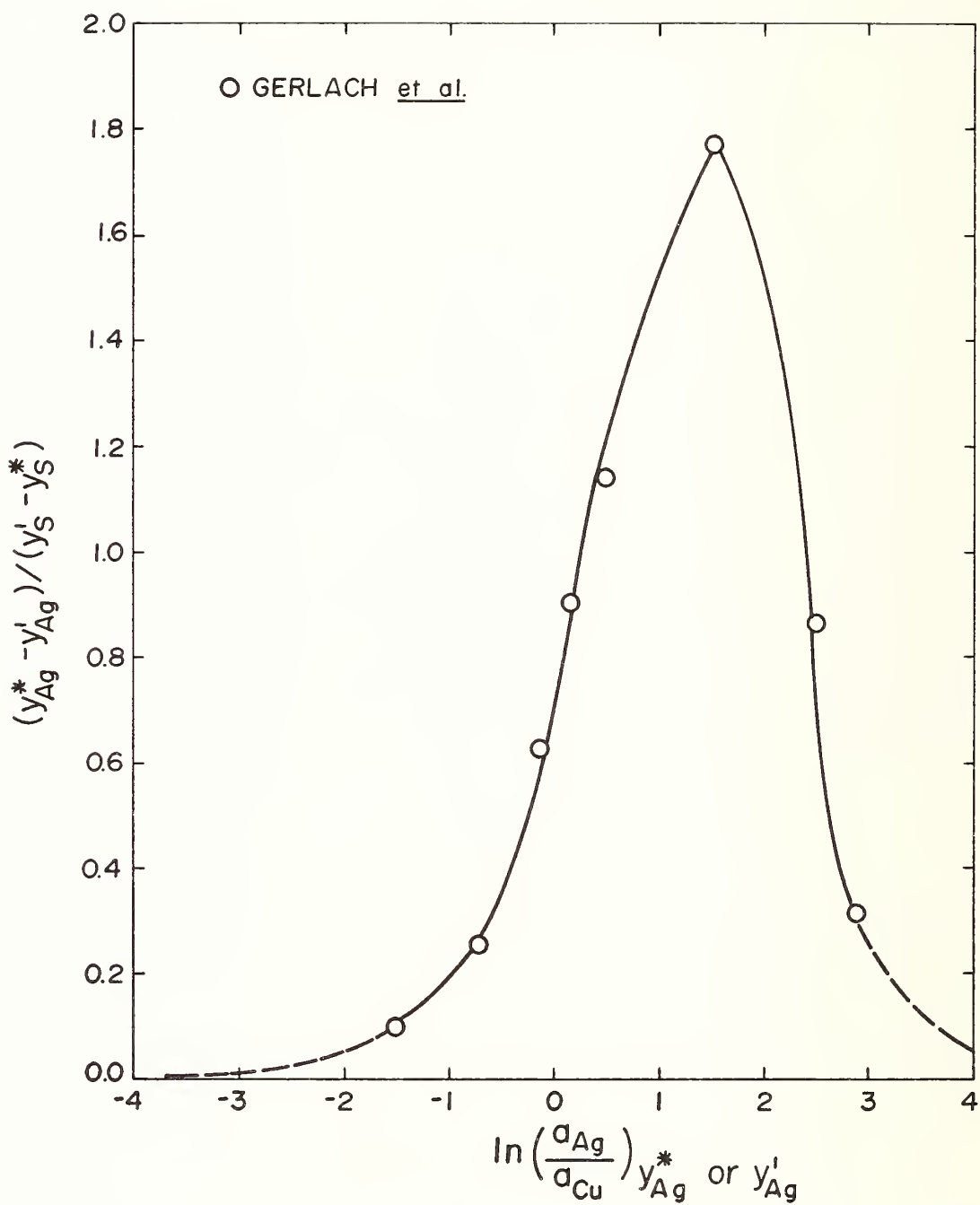


FIGURE 4. Integration plot for deriving the activities of sulfur at 1473 K in the ternary miscibility gap of the Cu-Ag-S system.

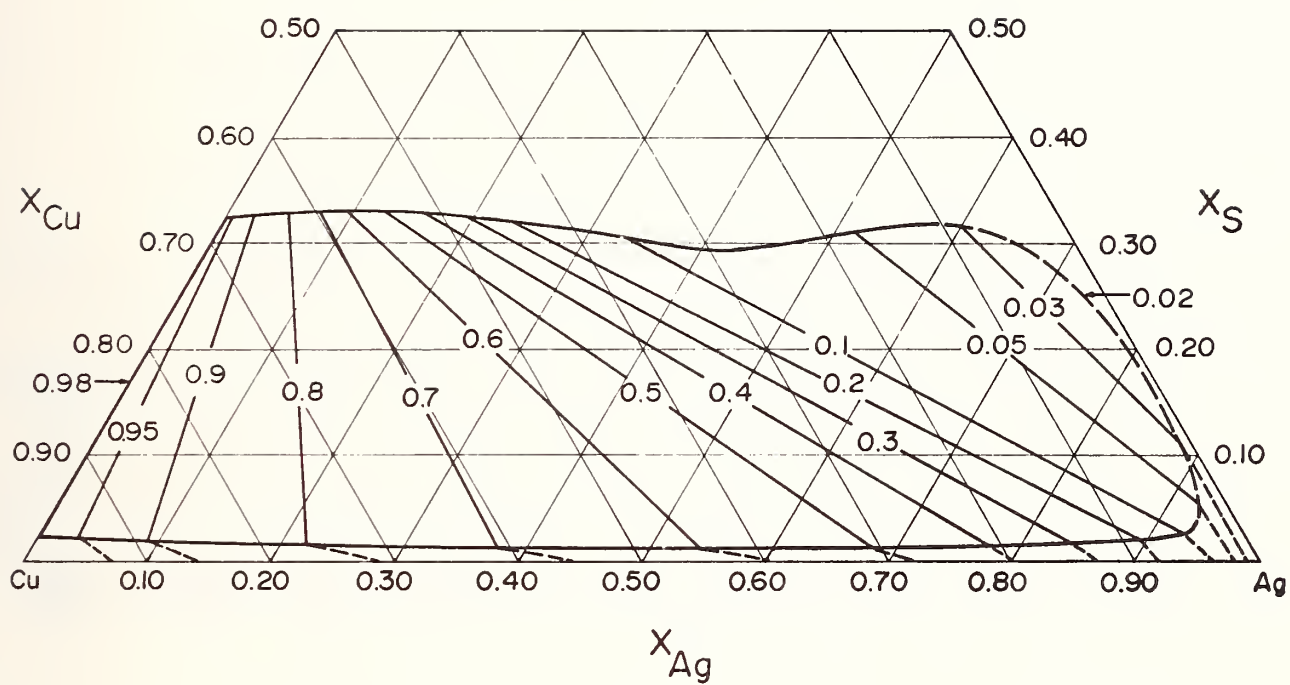


FIGURE 5. Isoactivities of copper in Cu-Ag-S melts at 1473 K (standard state: pure liquid copper).

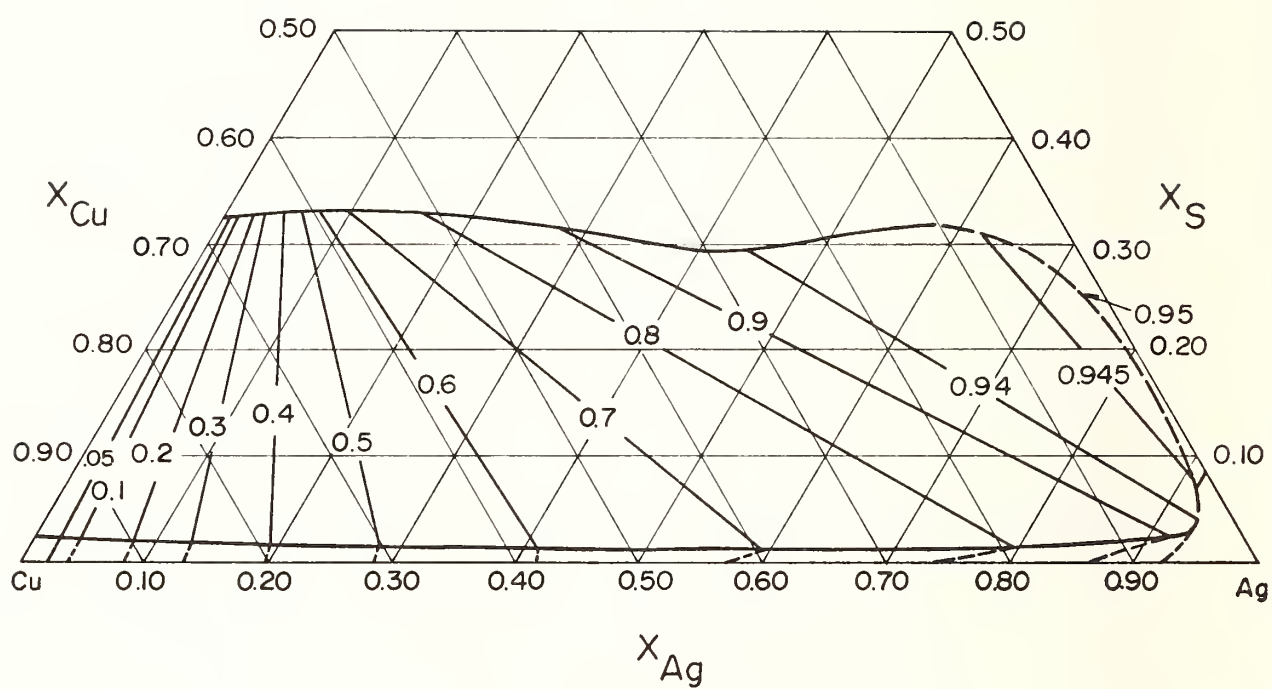


FIGURE 6. Isoactivities of silver in Cu-Ag-S melts at 1473 K (standard state: pure liquid lead).

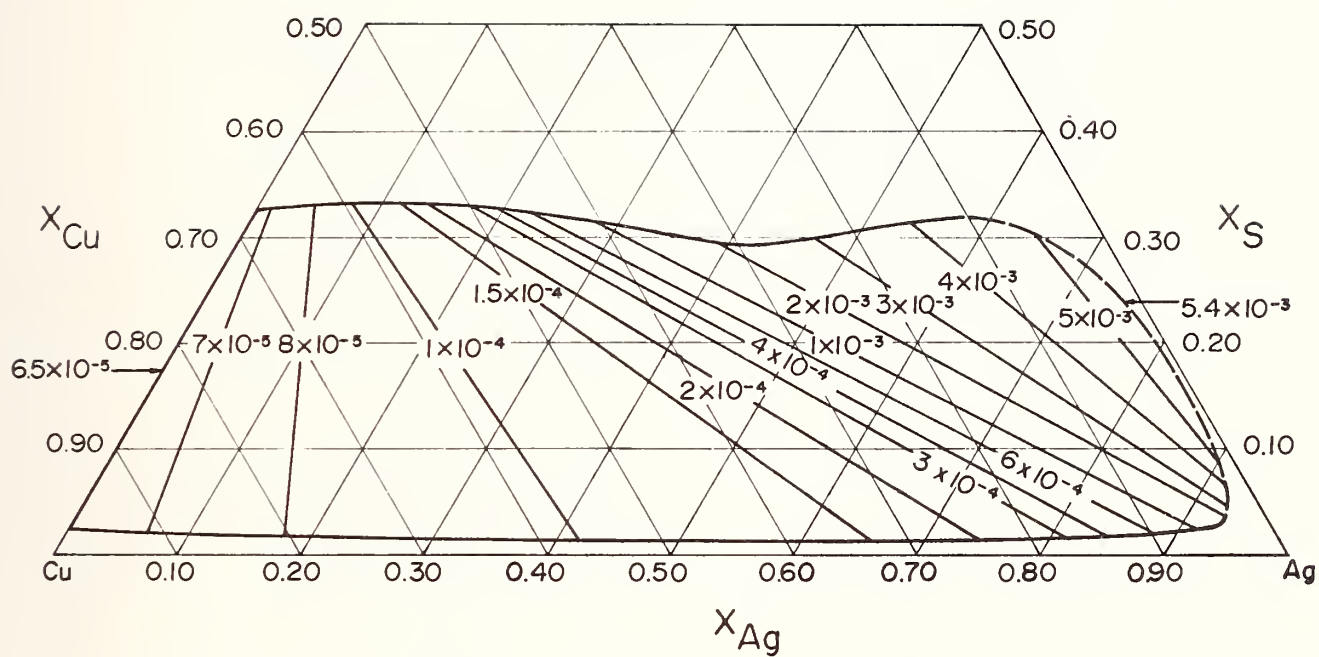


FIGURE 7. Isoactivities of sulfur in Cu-Ag-S melts at 1473 K (standard state: pure liquid sulfur).

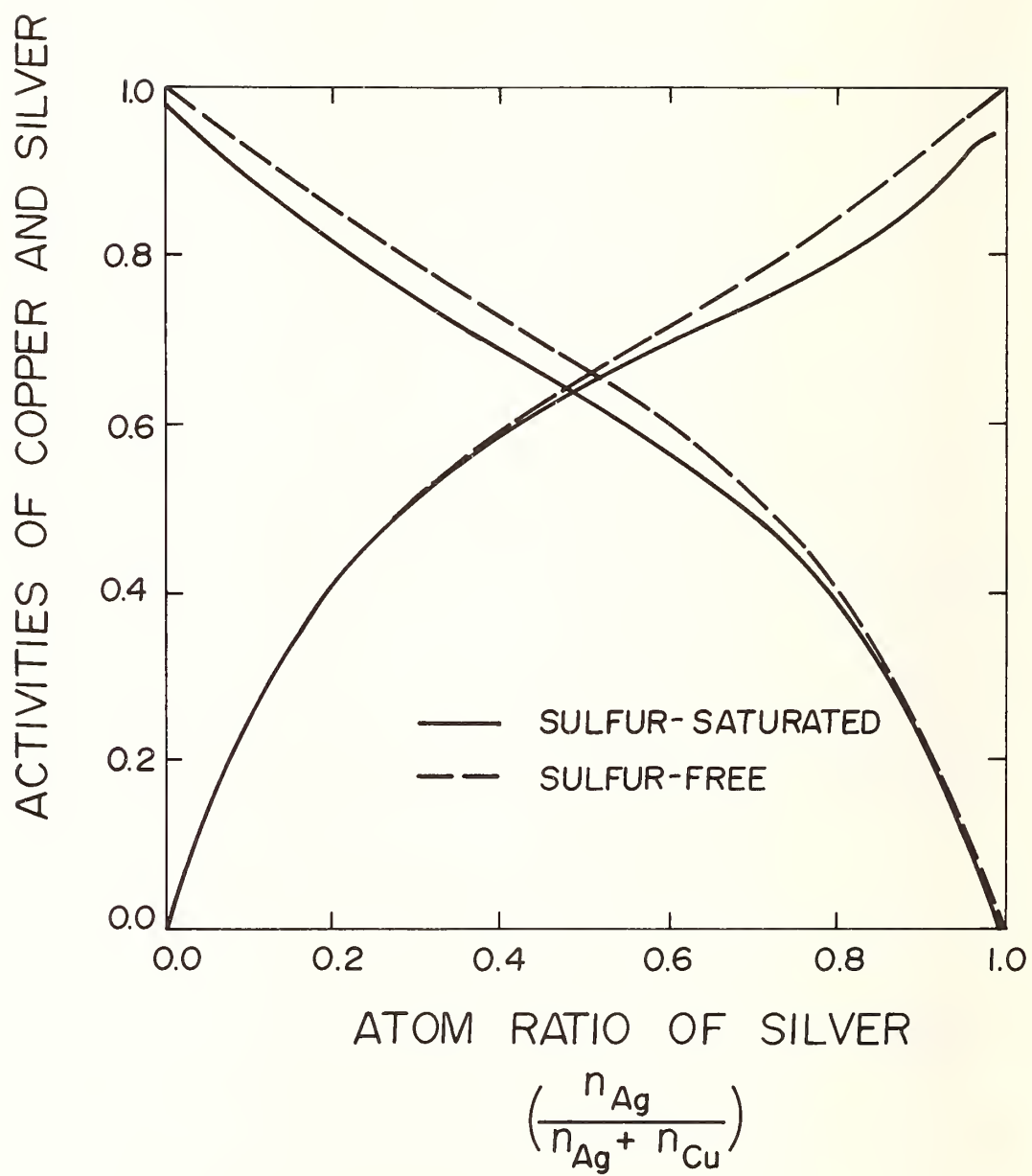


FIGURE 8. Activities of Cu and Ag in sulfur-free and sulfur-saturated copper-silver melts at 1473 K.

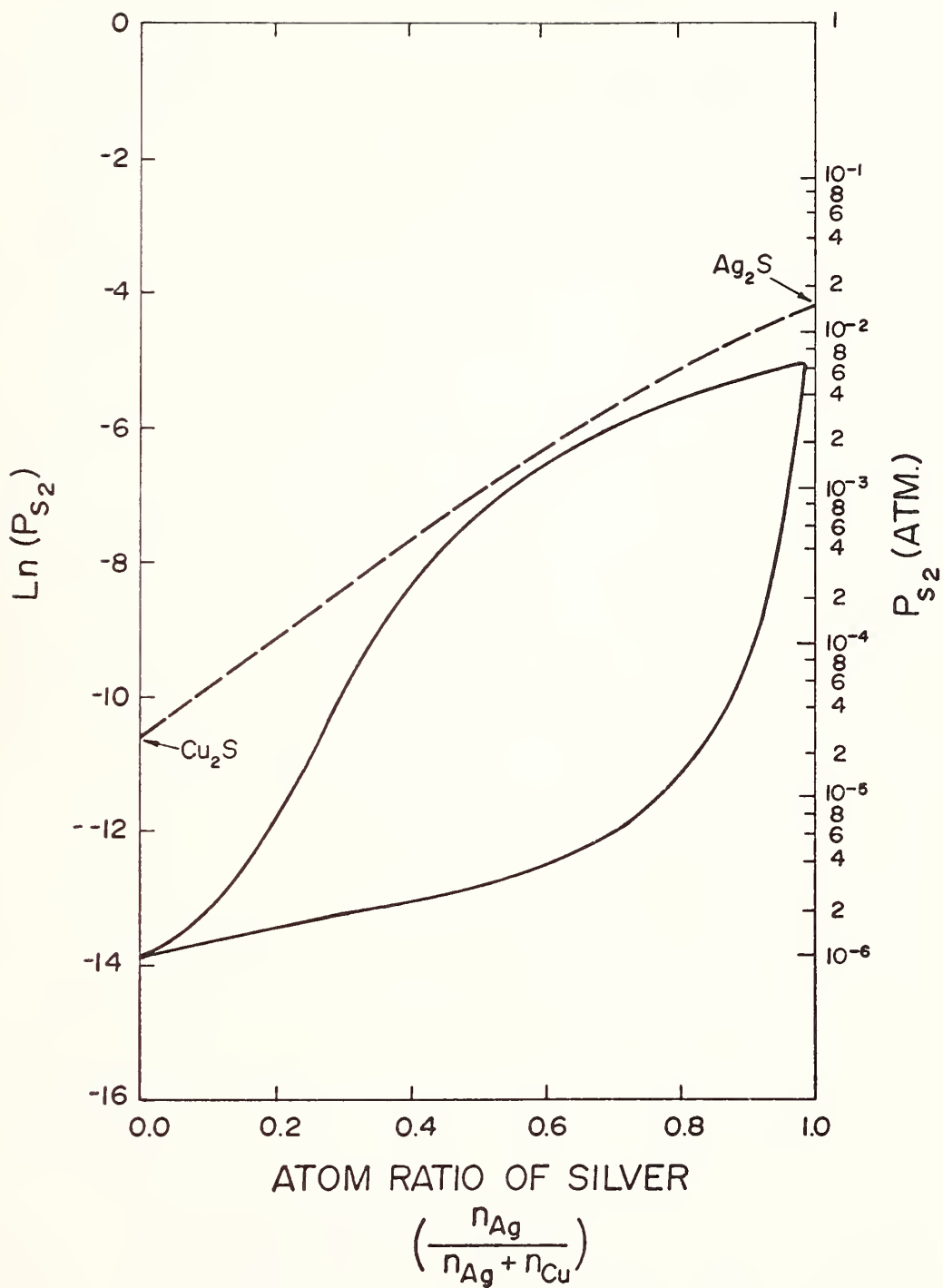


FIGURE 9. Sulfur potential as a function of atom ratio of silver along the ternary miscibility gap and the pseudo-binary section $CuS_{\frac{1}{2}}-AgS_{\frac{1}{2}}$ in the Cu-Pb-S system at 1473 K.

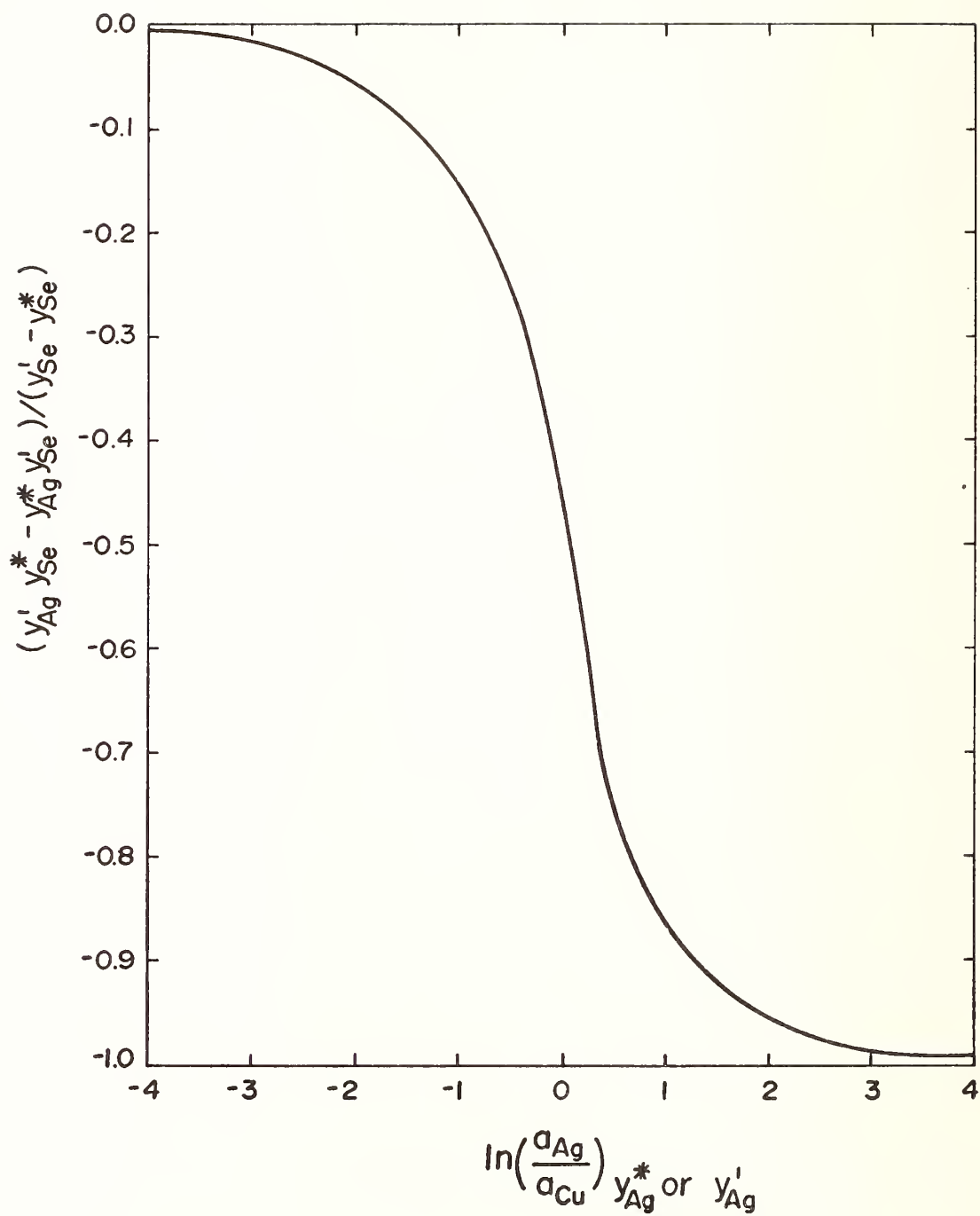


FIGURE 10. Integration plot for deriving the activities of copper and silver at 1473 K in the ternary miscibility gap of the Cu-Ag-Se system.

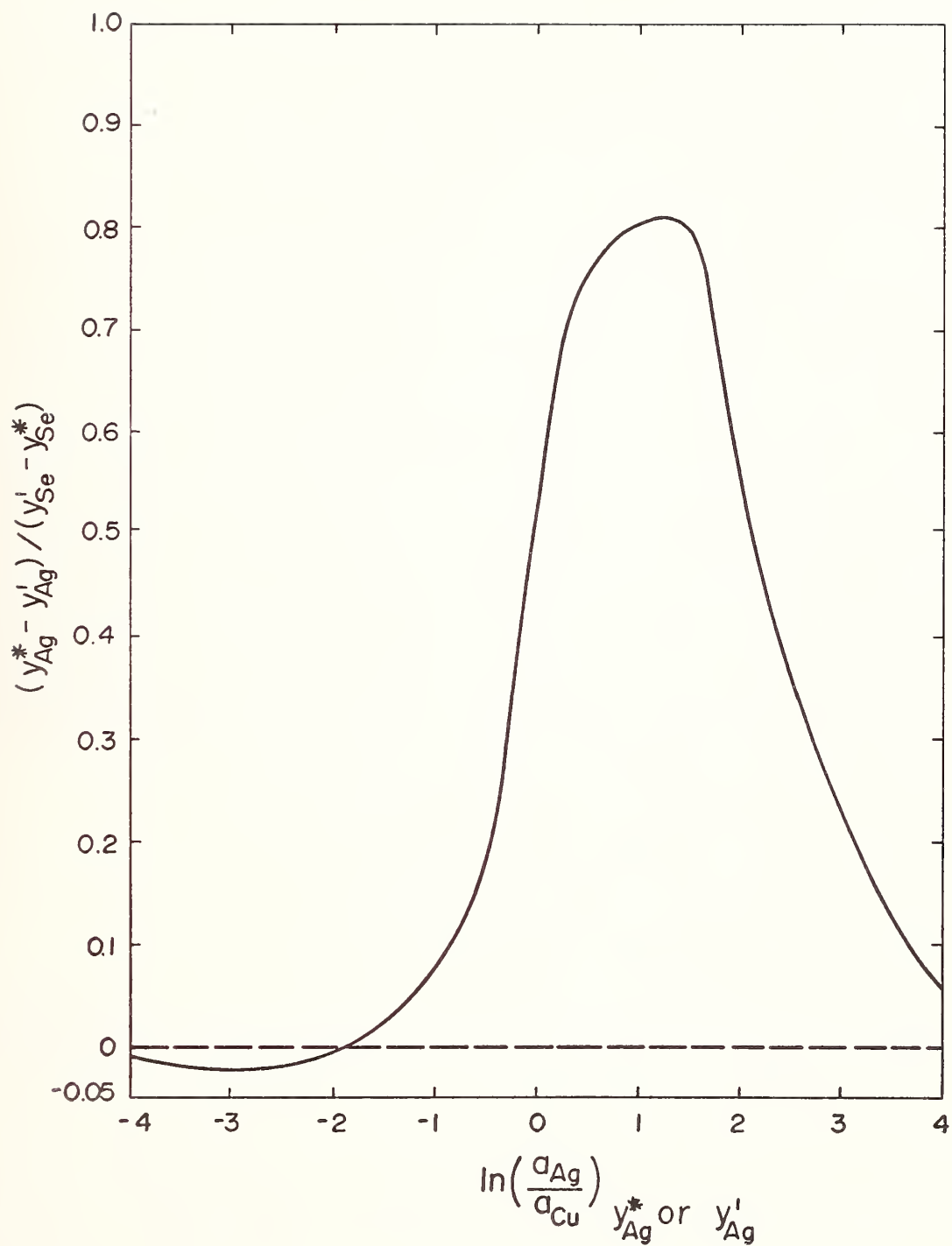


FIGURE 11. Integration plot for deriving the relative activities of selenium at 1473 K in the ternary miscibility gap of the Cu-Ag-Se system.

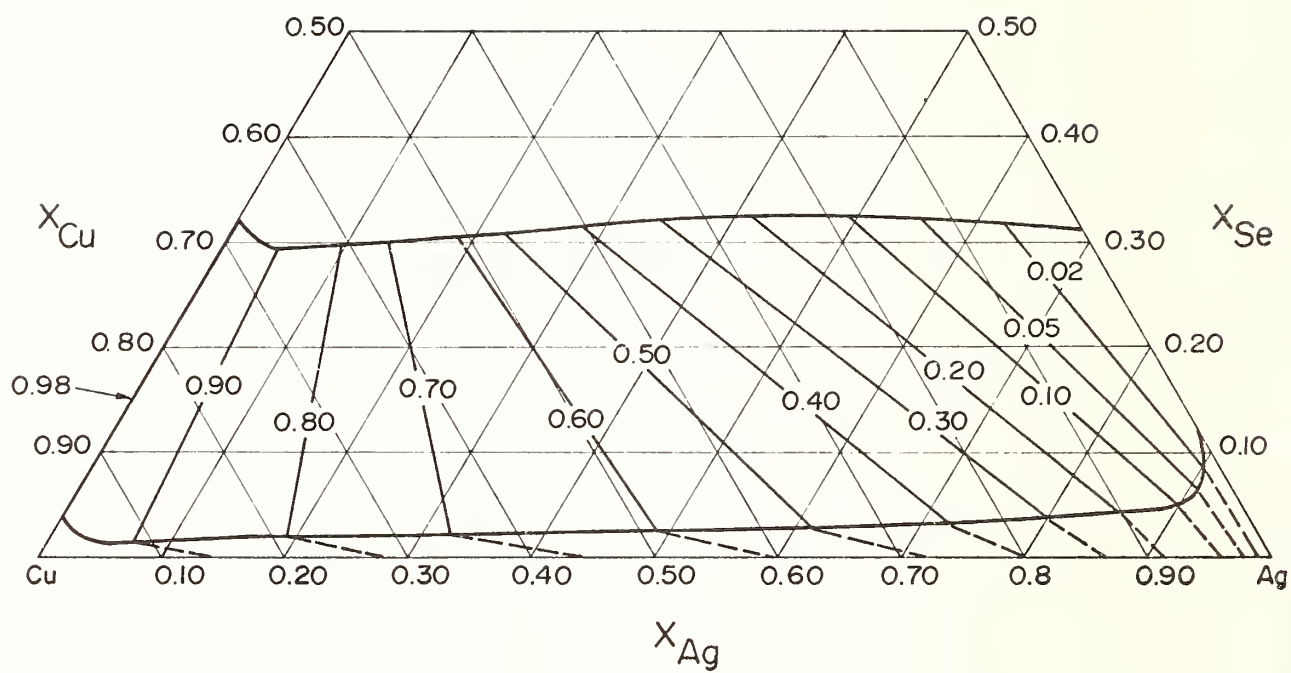


FIGURE 12. Isoactivities of copper in Cu-Ag-Se melts at 1473 K (standard state: pure liquid copper).

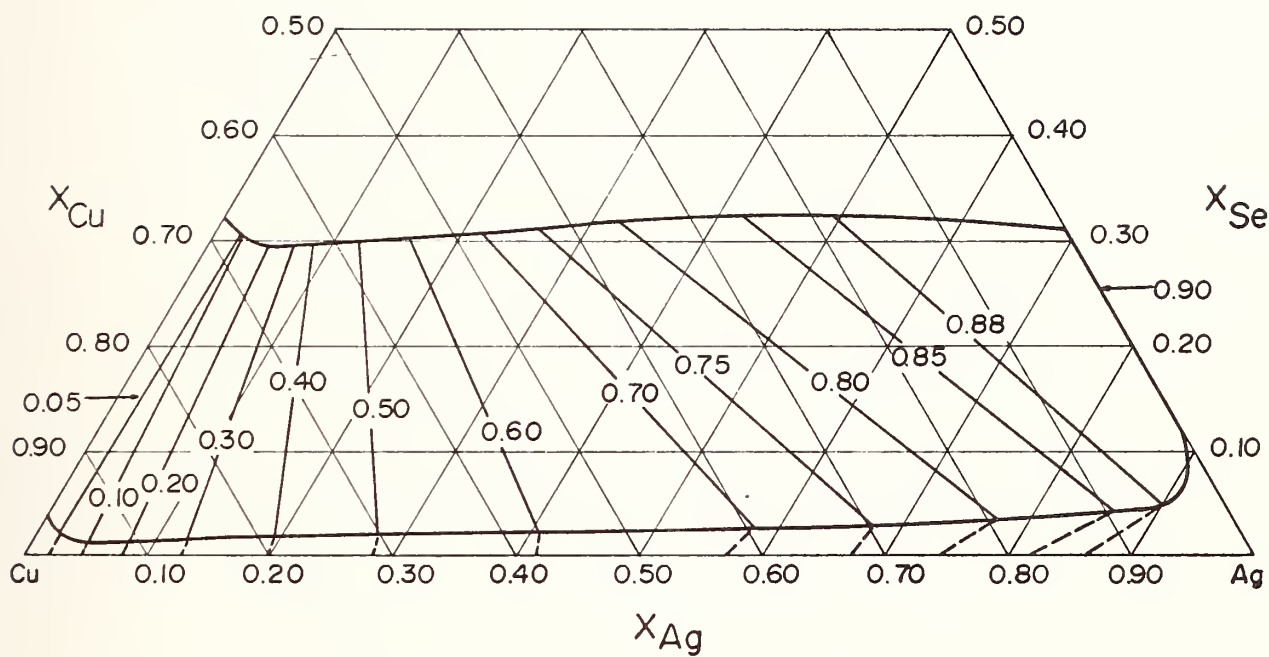


FIGURE 13. Isoactivities of silver in Cu-Ag-Se melts at 1473 K (standard state: pure liquid silver).

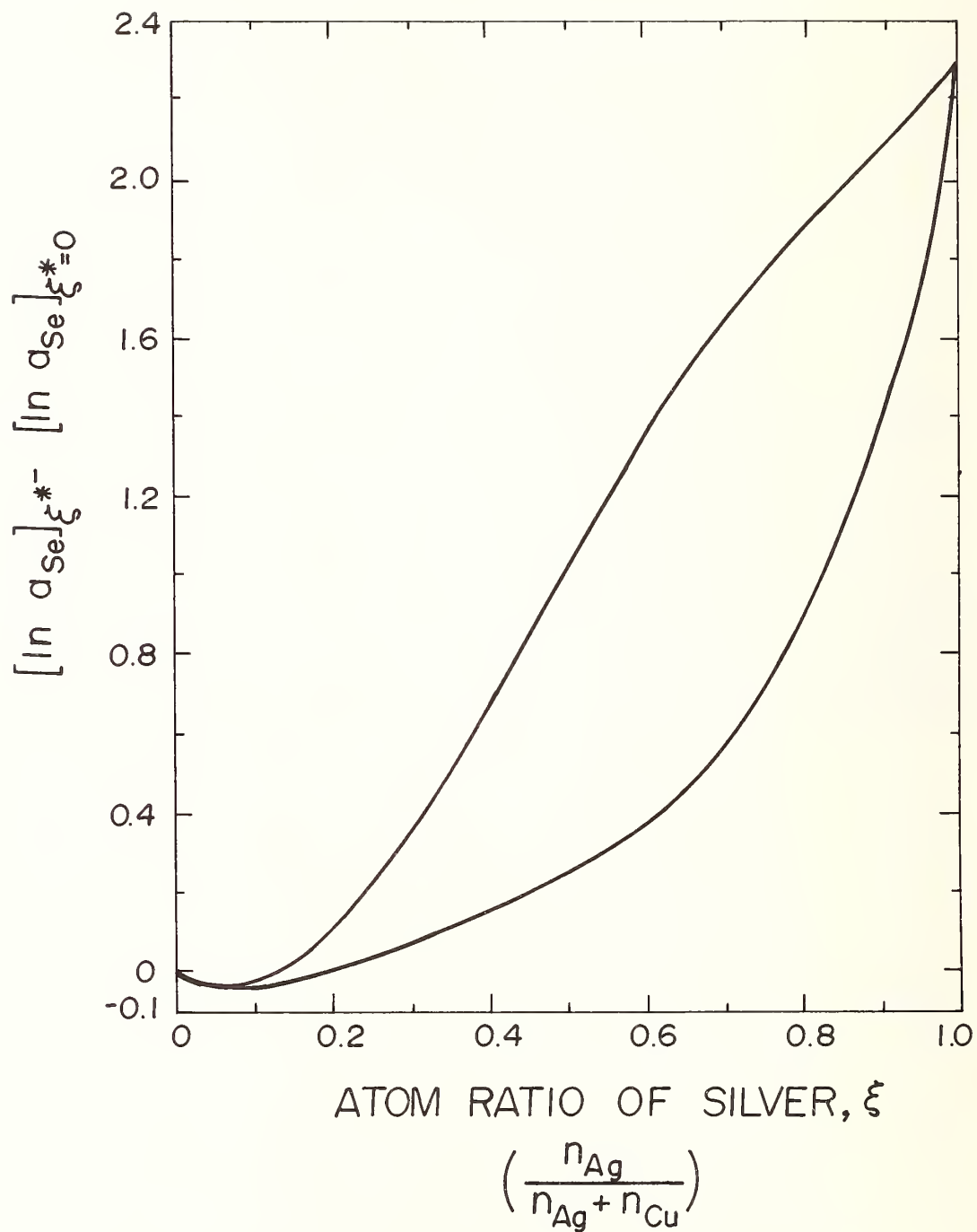


FIGURE 14. Relative activities of selenium in Cu-Ag-Se melts at 1473 K.



THE MATHEMATICAL REPRESENTATION OF ACTIVITY DATA IN THREE COMPONENT SYSTEMS

Issac Eliezer and Reed A. Howald

Chemistry Department of Montana State
University, Bozeman, Montana 59715

The activity coefficient of each species in a three component system (and other thermodynamic properties as well) can be expressed as a Redlich-Kister expansion in the sum of the other two mole fractions,

$$T = X_j + X_k.$$

$$\log \gamma_i = T^2 \left[A_i + B_i(-3+4T) + C_i(-5+6T)(-1+2T) + D_i(-7+8T)(-1+2T^2 + \dots) \right]$$

The coefficients in this equation are functions of S defined as $X_j/(X_j+X_k)$, the Redlich-Kister coefficients for the three binary subsystems, and an additional set of parameters describing interactions of all three components at once (B_3^a , C_3^a , C_3^b , etc.).

Typical equations for the calculation of the coefficients A_i through H_i are shown. We have derived these equations, and programmed them for computer calculation. The operation of our computer program is described. By transforming the parameter matrix, activity coefficients and activities can be calculated and printed for each of the three components.

The terms which are required beyond those for the binary systems, B_3^a etc., correspond to equations for the excess quantities of mixing of the form:

$$Y^e = N_3^i X_1 X_2 X_3 T^{n-2} (-1+2S)^{i-1}$$

An alternative form with orthogonal functions is considered briefly.

The equations and programming have been checked by application to the solid and liquid phases in the iron-nickel-carbon system. Parameters are shown for several three component systems, and calculations of phase equilibria in three component systems are outlined and compared to the original experimental data.

As an example of the use a large quantity of data for a ternary system to determine the parameters in the equations, the system benzene - carbon tetrachloride - acetonitrile is analyzed.

INTRODUCTION --- The thermodynamic properties of solutions can be expressed as power series in the mole fractions. A variety of different power series have been proposed for binary systems, and an even wider range of choices is possible for three component systems. The selection among these choices will ultimately be made on the basis of convenience, assuming they all represent the thermodynamic properties to the same degree of accuracy. In this paper we wish to present a system of equations which makes full use of the expressions obtained for the three binary pairs making up the three component system, which is easily extended to include additional parameters for higher powers of mole fractions, and which is well adapted to computer calculation.

The Augmented Redlich-Kister Formalism. --- For reasons outlined in an accompanying paper¹ we have selected the Redlich-Kister equations² to express data for two component systems. These equations have the advantage that the same coefficients (the Redlich-Kister coefficients A, B, C, etc.) appear in expressions for each of the partial molal properties and for the excess functions of mixing, Y^e :

$$\bar{Y}_1 = X_2^2 \left[A_{12} + B_{12}(-1+4X_1) + C_{12}(-1+6X_1)(-1+2X_1) + D_{12}(-1+8X_1)(-1+2X_1)^2 \dots \right]^{(1)}$$

$$\bar{Y}_2 = X_1^2 \left[A_{12} + B_{12}(-3+4X_1) + C_{12}(-5+6X_1)(-1+2X_1) + D_{12}(-1+8X_1)(-1+2X_1)^2 \dots \right]^{(2)}$$

$$Y^e = X_1 X_2 \left[A_{12} + B_{12}(-1+2X_1) + C_{12}(-1+2X_1)^2 + D_{12}(-1+2X_1)^3 \dots \right] \quad (3)$$

The quantity Y^e is defined as:

$$Y^e = X_1 \bar{Y}_1 + X_2 \bar{Y}_2 \quad (4)$$

These equations satisfy the Gibbs-Duhem relationship. They can be written in a variety of forms. For example: $-1+2X_1$ can be written in a variety of ways:

$$-1+2X_1 = X_1 - X_2 = 1-2X_2 \text{ etc.} \quad (5)$$

which are entirely equivalent in binary systems but are no longer equal when a third material is present. The proper expressions to use for three component solutions are the main concern of this paper, but for a start we can pick any two of the three mole fractions as independent variables, with the third determined from:

$$X_1 + X_2 + X_3 = 1 \quad (6)$$

The lowest power of mole fraction appearing in any of the expressions is 2, and there are three and only three independent quadratic terms in X_1 and X_2 :

$$\bar{Y}_1 = AX_1^2 + A'X_1X_2 + A''X_2^2 + \dots \quad (7)$$

Similarly there are only four independent cubic terms:

$$\bar{Y}_1 = \dots + BX_1^3 + B'X_1^2X_2 + B''X_1X_2^2 + B'''X_2^3 + \dots \quad (8)$$

five quartics etc. Thus the Redlich-Kister "A" values for the three binary systems are the only quadratic terms required, and the expression for Y^e to this degree of approximation can be written as:

$$Y^e = A_{12}X_1X_2 + A_{13}X_1X_3 + A_{23}X_2X_3 \quad (9)$$

It is desirable that three of the four cubic coefficients be B_{12} , B_{13} , and B_{23} , however one additional B coefficient is required. Similarly there will be two C's and three D's etc. beyond the values which are determined for the three binary subsystems. Thus we are led to consider an augmented Redlich-Kister formalism for three component systems.

The Redlich-Kister form for the B_{12} contribution to the activity coefficients in the two-component system is:

$$\log \gamma_1 = B_{12}X_2^2 (3-4X_2) + \dots \quad (10)$$

and our initial expectation was to find an expression for $\log \gamma_1$ in the three-component system which was similarly a product of three terms. There is, however, nothing which factors this far and still satisfies the Gibbs-Duhem relationship. After a long period of trial and error we found a correct expression:

$$\log \gamma_1 = B_{12}X_2(2X_1-X_2-2X_1^2+2X_1X_2) \dots \quad (11)$$

This equation has a somewhat neater appearance when written as a function of X_2 and X_3 :

$$\log \gamma_1 = B_{12} \left[X_2^2 (3-4X_2) + X_2 X_3 (2-6X_2-2X_3) \right] + \dots \quad (12)$$

The corresponding equation for $\log \gamma_2$ and $\log \gamma_3$ are:

$$\log \gamma_2 = B_{12} \left[X_1^2 (-3+4X_1) + X_1 X_3 (-2+6X_1+2X_3) \right] \quad (13)$$

$$\log \gamma_3 = B_{12} X_1 X_2 (-2X_1+2X_2) \quad (14)$$

Equations 12 - 14 can be combined to give the contribution of B_{12} to G^e , the excess free energy of mixing:

$$G^e = X_1 \log \gamma_1 + X_2 \log \gamma_2 + X_3 \log \gamma_3 \quad (15)$$

$$G^e = B_{12} X_1 X_2 (X_1 - X_2) + \dots \quad (16)$$

Similar expressions are valid for B_{13} and B_{23}

$$G^e = B_{13} X_1 X_3 (X_1 - X_3) + \dots \quad (17)$$

$$G^e = B_{23} X_2 X_3 (X_2 - X_3) + \dots \quad (18)$$

These expressions are simple enough to permit extrapolation to higher Redlich-Kister terms:

$$G^e = C_{12} X_1 X_2 (X_1 - X_2)^2 + D_{12} X_1 X_2 (X_1 - X_2)^3 + \dots \quad (19)$$

Similarly, the extra terms give reasonably simple expressions for Y^e . For example, the extra B term which we can write as B_3^a , corresponds to an excess free energy of mixing which must go to zero when any one of the three mole fractions goes to zero. The simplest function with this behavior is $X_1X_2X_3$, so we may attempt:

$$G^e = B_3^a X_1X_2X_3 + \dots \quad (20)$$

Expression for \bar{Y}_i for the Redlich-Kister terms. --- From the definition for a partial molal quantity:

$$\bar{Y}_3 = \left. \frac{\partial Y}{\partial n_3} \right|_{n_1, n_2} \quad (21)$$

and the expression for Y in terms of Y^e :

$$Y = n_1 Y_1^0 + n_2 Y_2^0 + n_3 Y_3^0 + (n_1 + n_2 + n_3) Y^e \quad (22)$$

where Y^0 is the molar value of the pure material, we can readily derive the relation between \bar{Y}_3 and Y^e :

$$\bar{Y}_3 = Y_3^0 + Y^e + (n_1 + n_2 + n_3) \left. \frac{\partial Y^e}{\partial n_3} \right|_{n_1, n_2} \quad (23)$$

The only complication is in taking the partial derivative. This is easiest if we write Y^e as a function of $S = X_1 / (X_1 + X_2)$ and

(24)

$T \equiv 1 - X_3 = X_1 + X_2$. The choice of these independent variables is dictated by the advisability of having one variable closely related to n_3 , and one which is unchanged as n_3 varies holding n_1 and n_2 constant. Then one can rewrite the partial derivative:

$$\left. \frac{\partial Y^e}{\partial n_3} \right|_{n_1, n_2} = \left. \frac{\partial Y^e}{\partial T} \right|_S \left. \frac{\partial T}{\partial n_3} \right|_{n_1, n_2} \quad (26)$$

$$= (dY^e/dT) \frac{-(n_1 + n_2)}{(n_1 + n_2 + n_3)^2} \quad (27)$$

$$= (dY^e/dT) (-T) (1/(n_1 + n_2 + n_3)) \quad (28)$$

The expression for $\bar{Y}_3 - Y_3^0$ is then :

$$\bar{Y}_3 - Y_3^0 = Y^e - T(dY^e/dT) \quad (29)$$

The general expressions for Y^e from equation 19 are :

$$Y^e = N_{12} X_1 X_2 (X_1 - X_2)^n + \dots \quad (30)$$

$$Y^e = N_{13} X_1 X_3 (X_1 - X_3)^n + \dots \quad (31)$$

$$Y^e = N_{23} X_2 X_3 (X_2 - X_3)^n + \dots \quad (32)$$

which can be rewritten using:

$$X_1 = ST \quad (33)$$

$$X_2 = (1-S)T = T-ST \quad (34)$$

$$X_3 = 1-T \quad (35)$$

as:

$$Y^e = N_{12} T^{n+2} S(1-S)(-1+2S)^n + \dots \quad (36)$$

$$Y^e = N_{13} T(1-T)(-1+T+ST)^n S + \dots \quad (37)$$

$$Y^e = N_{23} T(1-T)(-1+2T-ST)^n (1-S) + \dots \quad (38)$$

Equation 36 is easy to differentiate, giving:

$$\bar{Y}_3 - Y_3^o = N_{12} (S)(1-S)(-1+2S)^n (T^{n+2} - T(n+2)T^{n+1}) + \dots \quad (39)$$

$$\bar{Y}_3 - Y_3^o = N_{12} (S)(1-S)(-1+2S)^n (n+1)(-1) T^{n+2} + \dots \quad (40)$$

The other two derivations are somewhat more involved, but eventually lead to the equations:

$$\bar{Y}_3 - Y_3^o = N_{13} S T^2 (-1+T+ST)^{n-1} (-1-n-nS+T+ST+nST) + \dots \quad (41)$$

$$\bar{Y}_3 - Y_3^o = N_{23} (1-S) T^2 (-1+2T-ST)^{n-1} (-1+2n+nS+2T+2nT-ST-nST) \quad (42)$$

It is useful to convert these power series in T to the Redlich-Kister form:

$$\bar{Y}_3 - Y_3^0 = T^2 \left[A_3' + B_3' (-3+4T) + C_3' (-5+6T)(-1+2T) + \dots \right] \quad (43)$$

and each of the Redlich-Kister coefficients from the binary systems will make a contribution to the "pseudobinary" Redlich-Kister coefficient, A_3' , B_3' , etc. The transformation from power series into Redlich-Kister coefficients can be accomplished by multiplying by the upper triangular matrix \mathbb{L}^{-1} shown in Table 1. The denominators of the fractions in Table 1 are simply $n2^{(n-1)}$ and come directly from the Redlich-Kister equations. The numerators can be calculated by starting with 1 along the diagonal and adding successive binomial coefficients, $n!/i!(n-i)!$.

Thus the T^{n+2} appearing in equation 40 transforms into columns of Table 1 multiplied by appropriate factors. These results are shown in Table 2.

Equations 41 and 42 contain numerous powers of T with complex coefficients and the transformation is more difficult. This transformation has not yet been accomplished for the general n^{th} term, but the first eight terms transform to the simple expressions shown in Tables 3 and 4 and these relations can probably be extrapolated indefinitely.

The extra terms of the augmented Redlich-Kister formalism. --

Just as one has a choice for binary systems between using the Margules, Redlich-Kister, and Bale-Pelton equations, one has a choice between power series in mole fractions, simple powers of T and S, or orthogonal power series in expressing the experimental data on three component system. The extra terms beyond those which can be evaluated for the three binary subsystems can all be represented by terms for the excess quantity of mixing which can be written as:

$$Y^e = NX_1 X_2 X_3 F(a, b) + \dots \quad (44)$$

where F is a function of two concentration variables. The first term, for which we have used the coefficient B_3^a , has simply $F=1$:

$$Y^e = B_3^a X_1 X_2 X_3 + \dots \quad (45)$$

The simplest symmetrical first power term is $X_1 - X_2 = T(-1+2S)$, giving:

$$Y^e = C_3^b X_1 X_2 X_3 (X_1 - X_2) = C_3^b X_1 X_2 X_3 T(-1+2S) \quad (46)$$

The function $X_1 - X_2$, is part of an E pair of functions in the C_{3v} symmetry of this problem. The other part, orthogonal to this, is $-\frac{1}{3} + X_3$, possibly multiplied by a suitable normalization constant. Our initial treatment of a three component system using C terms³ gave equations which correspond to:

$$Y^e = C_{321} X_1 X_2 X_3 \left(-\frac{1}{3} + X_3\right) + \dots \quad (47)$$

However, when this is converted to showing F as a function of S and T, one gets:

$$Y^e = C_{321} X_1 X_2 X_3 \left(\frac{2}{3} - T\right) + \dots \quad (48)$$

and it is considerably more convenient to use a linear combination of equations 45 and 48, which eliminates the constant, $\frac{2}{3}$.

$$Y^e = C_3^a X_1 X_2 X_3 T + \dots \quad (49)$$

The relations between our older³ and new terminology can be written as:

$$C_{123} = C_3^b \quad (50)$$

$$B_{123} = B_3^a - \left(\frac{2}{3}\right)C_3^a \quad (51)$$

$$C_{321} = \left(\frac{1}{3}\right)C_3^a \quad (52)$$

The D terms can all be written with T^2 :

$$Y^e = D_3^a X_1 X_2 X_3 T^2 + \dots \quad (53)$$

$$Y^e = D_3^b X_1 X_2 X_3 T^2(-1+2S) + \dots \quad (54)$$

$$Y^e = D_3^c X_1 X_2 X_3 T^2(-1+2S)^2 + \dots \quad (55)$$

Here the alphabetical superscript (i in D_3^i) corresponds to the power of $-1+2S$ appearing in the equation. This form and notation can be extended indefinitely:

$$Y^e = E_3^d X_1 X_2 X_3 T^3(-1+2S)^3 + \dots \quad (56)$$

$$Y^e = H_3^d X_1 X_2 X_3 T^6(-1+2S)^3 + \dots \quad (57)$$

The sacrifice of orthogonality and even correct C_{3v} symmetry in this formulation is more than compensated by the ease of manipulation of the equations in these relatively simple forms. For example; the second orthogonal function of A symmetry is:

$$F(a, b) = X_1^2 + X_2^2 + X_3^2 - \frac{1}{2} \quad (58)$$

$$F(a, b) = \frac{1}{6} \left[(2-3T)^2 + 3T^2(-1+2S)^2 - 1 \right] \quad (59)$$

This not only involves all three powers of T, which is a nuisance in converting to the pseudobinary Redlich-Kister form, but it cannot be

factored into a function of S times a function of T. If this form is used, the various pseudobinary Redlich-Kister terms will be different and complex functions of S. On the other hand, expressions of the form:

$$Y^e = N_3^m X_1 X_2 X_3 T^n (-1+2S)^m + \dots \quad (60)$$

are readily converted into the pseudobinary form. First they are rewritten as a function of S and T only:

$$Y^e = N_3^m S(1-S)(1-T)T^{n+2}(-1+2S)^m + \dots \quad (61)$$

This equation can be differentiated and equation 29 then gives:

$$\bar{Y}_3 - Y_3^o = N_3^m S(1-S)(-1+2S)^m \left[(n+2)T^{(n+2)} - (n+1)T^{(n+1)} \right] \quad (62)$$

This expression is easily converted into the pseudobinary form using Table 1. The functions of S carry through unchanged, being simply multiplied by the binomial coefficient divided by 2^n . Table 5 shows the values for the first eight extra terms, and the extension to further terms is clear.

Tables 2 through 5 outline a method for calculation $\log \gamma_3$ for a particular composition of the ternary system. $\log \gamma_1$ and $\log \gamma_2$ can be calculated using the same equations and the same computer program if one firsts rennumbers the components as:

$$\begin{array}{lcl}
1 & \longrightarrow & 2 \\
2 & \longrightarrow & 3 \\
3 & \longrightarrow & 1
\end{array}
\tag{63}$$

As a result of this renumbering A_{12} becomes A_{23} , A_{13} becomes $A_{21} = A_{12}$ and A_{23} becomes $A_{31} = A_{13}$. The transformations of the B_{ij} 's are:

$$\begin{array}{lcl}
B_{12} & \longrightarrow & B_{23} \\
B_{13} & \longrightarrow & B_{21} = -B_{12} \\
B_{23} & \longrightarrow & B_{31} = -B_{13}
\end{array}
\tag{64}$$

The same kinds of transformations occur for all the N_{ij} with sign changes for the even numbered ones, B, D, F, H, etc.

The transformation of the extra, N_1^m , terms is somewhat more complicated. In choosing powers of $(1-X_3)$ and $(X_1 - X_2)$ to express Y^e , we have picked one material as special, and a substantial transformation is required to change to $(1-X_2)$ and $(X_3 - X_1)$ for the independent variables. Even if we chose symmetry adapted expressions for Y^e , we would need a transformation of this type for the terms of E symmetry since they are neither symmetric nor antisymmetric with respect to the rotations of 120° . The transformation matrix \mathbb{M} to convert the N_3^m coefficients to N_2^m (ready to calculate $\log Y_2$) is the matrix specified by the equation:

$$\left| \begin{matrix} B_2^a & C_2^a & C_2^b & D_2^a & D_2^b & D_2^c & E_2^a & \dots \end{matrix} \right\rangle = \mathbb{M} \left| \begin{matrix} B_3^a & C_3^a & C_3^b & D_3^a & D_3^b & \dots \end{matrix} \right\rangle \quad (65)$$

The first 10 x 10 portion of the matrix \mathbb{M} is shown in Table 6. The individual columns are not difficult to evaluate. One must multiply out $(1 - \frac{1}{2}T - \frac{1}{2}ZT)^m$ $(-1 + \frac{3}{2}T - \frac{1}{2}ZT)^h$ and collect powers of Z and T.

It is not likely that more than 10 of these extra coefficients will be required in practice. Our current computer program will handle 28 of these coefficients together with up to 24 Redlich-Kister coefficients for the three binary subsystems (8 each).

The section of this computer program for the calculation of Redlich-Kister coefficients (BETA (IK, I, I2)) for pseudobinary systems is shown in Table 7. The parameters used for the calculation are stored in the matrix form shown in Table 8.

Evaluation of constants. --- There are two ways to approach the problem of finding values for the coefficients in an augmented Redlich-Kister treatment of a ternary system. For systems close to ideal or which otherwise involve only a small number of coefficients, one can best start with data for the binary subsystems, and then evaluate B_3^a , C_3^a , and C_3^b from a few experiments with all three materials present. This approach will break down if there are many extra coefficients to determine. When a lot of experimental data is required, the best way to organize it is probably to consider the data for a particular ratio of two mole fractions at one time, and obtain pseudobinary Redlich-Kister coefficients for a whole series of values of S. We will illustrate these two approaches with appropriate examples.

The solid gamma Fe-Ni system is close enough to ideal that the enthalpy and activity coefficient data can be well represented by two Redlich-Kister coefficients.³ The Fe-C and Ni-C systems are very far from ideal, but the limited solubility of graphite in these metals⁴ means that all the data is over a small concentration range. For this reason the data requires at the most, three Redlich-Kister coefficients for a fit within experimental error. We have recently reexamined³ the data on these three subsystems to obtain the N_{ij} values shown in Table 9. Then the values of B_3^a and C_3^b were obtained by selecting two compositions for which the activity coefficient of carbon was known. Using

$B_3^a = 0$ and $C_3^b = 0$, we calculated $\log \gamma_3$ for carbon from the values for Redlich-Kister coefficients for all the binary subsystems. The difference between the experimental⁵ and calculated values for $\log \gamma_3$ then gives an equation for B_3^a and C_3^b .

$$\log \gamma_{\text{exp}} - \log \gamma_{\text{calc}} = B_3^a(1-X_3)^2(S)(1-S)(-5-.5(-1+4X_3)) + C_3^b(1-X_3)^2 \quad (66)$$

$$(S)(1-S)(-1+2S)(.25+.50(-1+4X_3)+.25(-1+6X_3)(-1+2X_3))$$

B_3^a and C_3^b can be calculated from two equations of this type, giving the values $B_3^a = -3.75$ and $C_3^b = -.40$.

The liquid Fe-Ni-C system was treated similarly, however in this case there is additional data on the activity of iron in solutions saturated with carbon,⁶ and it is possible to estimate \bar{C}_3^a in addition. These values are shown in Table 10.

If one needs only three extra coefficients and there are measurements of all three activities at $X_1 = X_2 = X_3 = 1/3$, then one can evaluate them from the three equations:

$$\log \gamma_3 - \log \gamma'_3 = -(1/27)(B_3^a) \quad (67)$$

$$\log \gamma_2 - \log \gamma'_2 = -(1/27)(B_3^a + C_3^a - C_3^b) \quad (68)$$

$$\log \gamma_1 - \log \gamma'_1 = -(1/27)(B_3^a + C_3^a + C_3^b) \quad (69)$$

We can illustrate the systematic treatment of a large quantity of data on the activity of one material in a three component system by a consideration of the system benzene - carbon tetrachloride - acetonitrile. This system was chosen because there is a substantial amount of good data available⁷, and also because there are statements in the literature^{7, 8} that the coefficients for the binary subsystems in this case adequately represent the ternary data. For liquids in this system it is easy to measure the total vapor pressure and the composition of the equilibrium vapor. Hence, one can calculate partial pressures for each component, but we will consider here only the information on the activity of acetonitrile since in many systems, one activity can be measured more accurately than the others. It is customary to correct for non-ideality of the vapor using the equation:

$$\log \gamma_3 = \log(Y_3 P / X_3 P_3^0) + (1/2.303 RT) (B_{33} - V_3^0)(P - P_3^0) + P(S_{13} Y_1 (1 - Y_3) + S_{23} Y_2 (1 - Y_3) - S_{12} Y_1 Y_2) \quad (70)$$

developed by Scatchard⁸ where Y_i stands for mole fractions in the vapor and X_3 is the mole fraction of acetonitrile in the liquid. Values for B_{33} and S_{ij} are given in reference 7, and the calculation of $\log \gamma_3$ at each experimental composition in Table II of reference 7 is quite straightforward. For each composition one must also calculate $S = X_{\text{benzene}} / (X_{\text{benzene}} + X_{\text{carbon tetrachloride}})$. The data points are grouped around certain S values, however to bring them to exactly constant values of S as in Table 11, one must interpolate. The interpolation was performed

linearly between two experimental points or between an experimental point and a calculated value for $\log \gamma_3$ at $S = 0$ or $S = 1.0$. The corrected data in Table 11 were then fitted to a Redlich-Kister expansion:

$$\log \gamma_3 = (1-X_3)^2 (A'_3 + B'_3(1-4X_3) + C'_3(1-6X_3)(1-2X_3) + \dots) \quad (7)$$

using four terms at each S value. The values of A'_3 , B'_3 , C'_3 , and D'_3 obtained are plotted against S in figures 1 through 4. The extreme scatter for D'_3 in figure 4 suggests that the fourth term is not really necessary to fit the data for most S values. The data at $S = .59$ is clearly less accurate than that at other values, and these points are omitted from the graphs and from the fitting procedure.

The A'_3 values have contributions from every parameter used as indicated in Tables 2 through 5. Fortunately, the S dependencies are all quite simple except for the N_{13} and N_{23} terms which should be well known from data on these two binary mixtures. We can thus calculate A'_3 (corrected) by subtracting contributions from A_{13} , B_{13} , C_{13} , D_{13} , A_{23} , B_{23} , C_{23} , and D_{23} :

$$\begin{aligned} A'_3(\text{corrected}) = & A'_3 - A_{13}(S) + B_{13}(1/2)(S)(1-S) - C_{13}(1/4)(S)(1-S)^2 \\ & + D_{13}(1/8)(S)(1-S)^3 - A_{23}(1-S) + B_{23}(1/2)(1-S)(S) \\ & - C_{23}(1/4)(1-S)(S)^2 + D_{23}(1/8)(1-S)(S)^3 \end{aligned} \quad (72)$$

The extension of equation 72 to cases where E and F terms are needed for the binary subsystem is quite straightforward.

The values obtained for $A_3^{\text{I}}(\text{corrected})$ are then fitted to a Redlich-Kister type expansion in powers of $(-1+2S)$

$$A_3^{\text{I}}(\text{corrected}) = (S)(1-S) \left[A_a + B_a(-1+2S) + C_a(-1+2S)^2 + \dots \right] \quad (73)$$

and the coefficients in this expansion are simple functions of the remaining parameters:

$$A_a = -A_{12} + (1/2)B_3^a + (1/4)C_3^a + (1/8)D_3^a \quad (74)$$

$$B_a = -(3/2)B_{12} + (1/4)C_3^b + (1/8)D_3^b \quad (75)$$

$$C_a = -(7/4)C_{12} + (1/8)D_3^c \quad (76)$$

etc. The coefficients in these equations come from Tables 2 and 5. In this particular case, $A_3^{\text{I}}(\text{corrected})$ is well fitted by $A_a = -.2418$ and $B_a = -.2125$. No C_a term is needed, and so $D_3^c = 0$. This is a further indication (beyond the scatter in figure 4) that D_3^n terms are not required in this ternary system. Since A_{12} and B_{12} are known, only one additional equation is required:

$$A_b = .0158 = (1/2)B_3^a + (1/2)C_3^a \quad (77)$$

to evaluate:

$$B_3^a = -.7904 \quad (78)$$

$$C_3^a = .8220$$

$$C_3^b = -.8464$$

completing the full set of coefficients for the ternary system benzene-carbon tetrachloride - acetonitrile listed in Table 12. The solid lines in Figures 1-4 are values for A_3^1 , B_3^1 , etc., calculated from the constants in Table 12. One is likely to encounter more complex systems where equations 74 through 76 have 9 unknowns, and the full set of additional equations 81-87 may be needed. These equations come from similar corrections of B_3^1 , C_3^1 etc., for contributions from N_{13} and N_{23} :

$$\begin{aligned} B_3^1(\text{corrected}) = B_3^1 - (1/2)B_{13}(S)(1+S) + (1/2)C_{13}(S)(1+S)(1-S) - (3/8)D_{13} \\ (S)(1+S)(1-S)^2 - B_{23}(1/2)(1-S)(2-S) + C_{23}(1/2)(1-S)(2-S)(S) \\ - D_{23}(3/8)(1-S)(2-S)(S)^2 \end{aligned} \quad (79)$$

$$\begin{aligned} C_3^1(\text{corrected}) = C_3^1 - C_{13}(1/4)(S)(1+S)^2 + D_{13}(3/8)(S)(1+S)(1-S) \\ - C_{23}(1/4)(1-S)(2-S)^2 + D_{23}(3/8)(1-S)(2-S)^2(S) \end{aligned} \quad (80)$$

The coefficients and functions of S in equations 79 and 80, are taken from tables 3 and 4. The corrected values B_3^1 , C_3^1 etc., are then fitted to power series like:

$$B_3^1(\text{corrected}) = S(1-S) \left[A_b + B_b(-1+2S) + C_b(-1+2S)^2 + \dots \right] \quad (81)$$

and the equations for A_b , B_b , and A_c etc., are obtained from Tables 2 and 5:

$$A_b = (1/2)B_3^a + (1/2)C_3^a + (3/8)D_3^a \quad (82)$$

$$B_b = -(1/2)B_{12} + (1/2)C_3^b + (3/8)D_3^b \quad (83)$$

$$C_b = -(4/4)C_{12} + (3/8)D_3^c \quad (84)$$

$$A_c = (1/4)C_3^a + (3/8)D_3^a \quad (85)$$

$$B_c = (1/4)C_3^b + (3/8)D_3^b \quad (86)$$

$$C_c = -(1/4)C_{12} + (3/8)D_3^c \quad (87)$$

References

1. I. Eliezer and R. A. Howald, "A Program for Binary Phase Equilibria Using the Redlich-Kister Equations", this volume, paper TPSI-6.
2. O. Redlich, A. T. Kister, and C. E. Turnquist, Chem. Eng. Progr., Symposium Series, 48 (2), 49 (1952)
3. I. Eliezer and R. A. Howald, J. Chem. Phys., submitted
4. J. F. Elliott, M. Gleiser, and V. Ramakrishna, Thermochemistry for Steelmaking, Addison-Wesley Pub. Co., Reading, Mass. (1963)
5. T. Wada, H. Wada, J. F. Elliott and J. Chipman, Metal. Trans., 2, 2199 (1971)
6. C. Petot and E. Bonnier, Bull. Soc. Chim. France, 1967, 836 (1967)
7. H. A. Clarke and R. W. Missen, J. Chem. Eng. Data, 19, 343 (1974)
8. G. Scatchard, L. B. Ticknor, J. R. Goates, and E. R. McCartney, J. Am. Chem. Soc., 74, 3721 (1952)

TABLE 1

The transformation matrix, \mathbb{L}^{-1} , to obtain Redlich-Kister coefficients from a power series in T.

$$|A, B, C, \dots\rangle = \mathbb{L}^{-1} |C_1, C_2, C_3, \dots\rangle$$

1	3/4	7/12	15/32	31/80	63/192	127/448	255/1024
0	1/4	4/12	11/32	26/80	57/192	120 /448	247/1024
0	0	1 /12	5/32	16/80	42/192	99/448	219/1024
0	0	0	1/32	6/80	22/192	64/448	163/1024
0	0	0	0	1/80	7/192	29/448	93/1024
0	0	0	0	0	1/192	8/448	37/1024
0	0	0	0	0	0	1/448	9/1024
0	0	0	0	0	0	0	1/1024
0	0	0	0	0	0	0	0

Table 2

Contributions to terms in the pseudobinary equation for $\log \gamma_3$
 $\log \gamma_3 = T^2 \left[A'_3 + B'_3 (-3+4T) + C'_3 (-5+6T)(-1+2T) \dots \right]$
 from Redlich-Kister coefficients for components 1 and 2.

CONTRIBUTION

to	from A_{12}	B_{12}	C_{12}	D_{12}	E_{12}
A'_3	$-S(1-S)$	$-\frac{3}{2}S(1-S)(1-2S)$	$-\frac{7}{4}S(1-S)(1-2S)^2$	$-(\frac{15}{8})S(1-S)(1-2S)^3$	$-(\frac{31}{16})S(1-S)(1-2S)^4$
B'_3	0	$-\frac{1}{2}S(1-S)(1-2S)$	$-(\frac{4}{4})S(1-S)(1-2S)^2$	$-(\frac{11}{8})S(1-S)(1-2S)^3$	$-(\frac{26}{16})S(1-S)(1-2S)^4$
C'_3	0	0	$-(\frac{1}{4})S(1-S)(1-2S)^2$	$-(\frac{5}{8})S(1-S)(1-2S)^3$	$-(\frac{16}{16})S(1-S)(1-2S)^4$
D'_3	0	0	0	$-(\frac{1}{8})S(1-S)(1-2S)^3$	$-(\frac{6}{16})S(1-S)(1-2S)^4$
E'_3	0	0	0	0	$-(\frac{1}{16})S(1-S)(1-2S)^4$

Table 3

Contributions to terms in the pseudobinary equation for $\log v_3$

$$\log v_3 = T^2 \left[A'_3 + B'_3 (-3+4T) + C'_3 (-5+6T)(-1+2T) \dots \right]$$

from Redlich-Kister coefficients for components 1 and 3

CONTRIBUTION

to	from A_{13}	B_{13}	C_{13}	D_{13}	E_{13}
A'_3	S	$-(\frac{1}{2})S(1-S)$	$\frac{1}{4}S(1-S)^2$	$-\frac{1}{8}S(1-S)^3$	$\frac{1}{16}S(1-S)^4$
B'_3	0	$(\frac{1}{2})S(1+S)$	$-\frac{1}{2}S(1-S)(1+S)$	$\frac{3}{8}S(1-S)^2(1+S)$	$\frac{4}{16}S(1-S)^3(1+S)$
C'_3	0	0	$\frac{1}{4}S(1+S)^2$	$-\frac{3}{8}S(1-S)(1+S)^2$	$\frac{6}{16}S(1-S)^2(1+S)^2$
D'_3	0	0	0	$\frac{1}{8}S(1+S)^3$	$-\frac{4}{16}S(1-S)(1+S)^3$
E'_3	0	0	0	0	$\frac{1}{16}S(1+S)^4$

Table 4

Contributions to terms in the pseudobinary equation for $\log \gamma_3$

$$\log \gamma_3 = T^2 \left[A'_3 + B'_3 (-3+4T) + C'_3 (-5+6T)(-1+2T) \dots \right]$$

from Redlich-Kister coefficients for components 2 and 3

CONTRIBUTION

to	from A_{23}	B_{23}	C_{23}	D_{23}	E_{23}
A'_3	$(1-S)$	$-\frac{1}{2}S(1-S)$	$(\frac{1}{4})(S)^2(1-S)$	$-(\frac{1}{8})(S)^3(1-S)$	$(\frac{1}{16})(S)^4(1-S)$
B'_3	0	$(\frac{1}{2})(2-S)(1-S)$	$-(\frac{1}{2})(S)(2-S)(1-S)$	$(\frac{3}{8})(S)^2(2-S)(1-S)$	$-(\frac{4}{16})(S)^3(2-S)(1-S)$
C'_3	0	0	$(\frac{1}{4})(2-S)^2(1-S)$	$-(\frac{3}{8})S(2-S)^2(1-S)$	$(\frac{6}{16})(S)^2(2-S)^2(1-S)$
	0	0	0	$(\frac{1}{8})(2-S)^3(1-S)$	$-(\frac{4}{16})(S)(2-S)^3(1-S)$
E'_3	0	0	0	0	$(\frac{1}{16})(2-S)^4(1-S)$

Table 5

Contributions to terms in the pseudobinary equation for $\log \gamma_3$

$$\log \gamma_3 = T^2 \left[A'_3 + B'_3(-3+4T) + C'_3(-5+6T)(-1+2T) \right] + \dots$$

from the extra terms in the ternary system.

CONTRIBUTION					
	from	B_3^a	C_3^b	C_3^a	D_3^c
to					
A'_3		$(1/2)(S)(1-S)$	$(1/4)(S)(1-S)(-1+2S)$	$(1/4)(S)(1-S)$	$(1/8)(S)(1-S)(-1+2S)^2$
B'_3		$(1/2)(S)(1-S)$	$(1/2)(S)(1-S)(-1+2S)$	$(1/2)(S)(1-S)$	$(3/8)(S)(1-S)(-1+2S)^2$
C'_3	0	0	$(1/4)(S)(1-S)(-1+2S)$	$(1/4)(S)(1-S)$	$(3/8)(S)(1-S)(-1+2S)^2$
D'_3	0	0	0	0	$(1/8)(S)(1-S)(-1+2S)^2$

Table 5 (continued)

CONTRIBUTION		E_3^c		
from	D_3^b	D_3^a	E_3^d	E_3^c
to				
A'_3	$(1/8)(S)(1-S)(-1+2S)$	$(1/8)(S)(1-S)$	$(1/16)(S)(1-S)(-1+2S)^3$	$(1/16)(S)(1-S)(-1+2S)^2$
B'_3	$(3/8)(S)(1-S)(-1+2S)$	$(3/8)(S)(1-S)$	$(4/16)(S)(1-S)(-1+2S)^3$	$(4/16)(S)(1-S)(-1+2S)^2$
C'_3	$(3/8)(S)(1-S)(-1+2S)$	$(3/8)(S)(1-S)$	$(6/16)(S)(1-S)(-1+2S)^3$	$(6/16)(S)(1-S)(-1+2S)^2$
D'_3	$(1/8)(S)(1-S)(-1+2S)$	$(1/8)(S)(1-S)$	$(4/16)(S)(1-S)(-1+2S)^3$	$(4/16)(S)(1-S)(-1+2S)^2$
E'_3	0	0	$(1/16)(S)(1-S)(-1+2S)^3$	$(1/16)(S)(1-S)(-1+2S)^2$

Table 6

The transformation matrix from the N_3^i to the N_2^i coefficients.

$$\begin{vmatrix} B_2^a & C_2^a & C_2^b & D_2^a & D_2^b & D_2^c & E_2^a & \dots \end{vmatrix} = \mathbb{M} \begin{vmatrix} B_3^a & C_3^a & C_3^b & D_3^a & D_3^b & D_3^c & E_3^a & \dots \end{vmatrix}$$

$$\mathbb{M} = \begin{matrix} & 1 & 1 & -1 & 1 & -1 & 1 & 1 & -1 & 1 & -1 \\ 0 & -(1/2) & (3/2) & -1 & 2 & -3 & -(3/2) & (5/2) & -(7/2) & (9/2) \\ 0 & -(1/2) & -(1/2) & -1 & 0 & 1 & -(3/2) & (1/2) & (1/2) & -(3/2) \\ 0 & 0 & 0 & (1/4) & -(3/4) & (9/4) & (3/4) & -(7/4) & (15/4) & -(27/4) \\ 0 & 0 & 0 & (1/2) & -(1/2) & -(3/2) & (3/2) & -(3/2) & -(1/2) & (9/2) \\ 0 & 0 & 0 & (1/4) & (1/4) & (1/4) & (3/4) & (1/4) & -(1/4) & -(3/4) \\ 0 & 0 & 0 & 0 & 0 & 0 & -(1/8) & (3/8) & -(9/8) & (27/8) \\ 0 & 0 & 0 & 0 & 0 & 0 & -(3/8) & (5/8) & -(3/8) & -(27/8) \\ 0 & 0 & 0 & 0 & 0 & 0 & -(3/8) & (1/8) & (5/8) & (9/8) \\ 0 & 0 & 0 & 0 & 0 & 0 & -(1/8) & -(1/8) & -(1/8) & -(1/8) \end{matrix}$$

Table 7

Listings of sections of a computer program for ternary systems.

1. Calculation of pseudobinary coefficients (A_3^I , B_3^I , C_3^I , etc.).

The values are stored in BETA(KI, I, I2). FC(I) stores I!.

113.	160	CONTINUE	1793
114.		D9 230 I=1,8	1794
115.	230	BETA(KI,I,I2)=0,	1795
116.		S=X1/(X1+X2)	1796
117.		IF (S.EQ.0) S=1.0E+50	1797
118.		Q=1-S	
119.		IF (Q.EQ.0) Q=1.0E+50	
120.		XK=X1+X2	1798
121.		Z=1+2*S	1799
122.		IF (Z.EQ.0,0) Z=1.0E+50	1800
123.		D9 220 I=2,8	1801
124.		D9 220 K=1,I	1802
125.		C2=FC(I-1)/(FC(K=1)*FC(I=K)*2**(I-1))	1803
126.		ITM=I+2	
127.		D9 220 J=4,ITM	
128.		BETA(KI,K,I2)=BETA(KI,K,I2)+C2*S*(1-S)*((Z)**(J=4))*RT(I,J)	1805
129.	220	CONTINUE	1806
130.		D9 232 I=1,8	1807
131.		C1=2./(-2**I)	1808
132.		C4=-C1*(-1)**I	1809
133.		C3=1.	1810
134.		D9 232 J=1,8	1811
135.		BETA(KI,I,I2)=BETA(KI,I,I2)+C4*S*(1-S)*((-Z)**(J=1))*RT(J,1)	1812
136.		C2=(-C1)*FC(J-1)/(FC(I-1)*FC(J=I)*(-2)**(J=I))	1813
137.		BETA(KI,I,I2)=BETA(KI,I,I2)+C2*S*(Q**(J=I))*((1+S)**(I=1))	
138.		2 *RT(J,2)	1815
139.		BETA(KI,I,I2)=BETA(KI,I,I2)+C2*(S**(J=I))*(1-S)*((2-S)**(I=1))	1816
140.		2 *RT(J,3)	1817
141.		C3=C3*2+FC(J)/(FC(I=1)*FC(J+1=I))	1818
142.		C4=-C3*(-.5)**J	1819
143.	232	CONTINUE	1820
144.		I=KI	1821
145.		IF (I0PT(6)=8) 181,181,200	
146.	181	WRITE(108,703) TEMP(I),(BETA(I,J,I2),J=1,4)	1823
147.	182	WRITE(108,703) TEMP(I),(BETA(I,J,I2),J=5,8)	1824
148.	703	FORMAT('T=',F9.3,4F13.8)	1825
149.	200	CONTINUE	1826
150.		TPK=TP	1827

Table 7 (continued)

2. Rearrangement of the coefficients stored in RT so that pseudobinary coefficients can be calculated for the other components. CMM stores the elements of the matrix MI shown in Table 6.

168.	IF (IOP(6)=9) 250,251,251	
169.	250 WRITE(108,710) I1,X3,GF(JJ,I2),AF(JJ,I2),AF(JJ,I2),GL	1845
170.	710 F9RMAT('X',I1,' ',F10.8,F11.5,E13.7,'ACT.',3F11.5)	1846
171.	251 IC=IC+1	
172.	KZZ(1)=KZK	1848
173.	IF (IC=4) 69,61,999	1849
174.	69 CONTINUE	1850
175.	DO 301 J=1,8	1851
176.	X=RT(J,1)	1852
177.	RT(J,1)=RT(J,2)*(-1)**(J-1)	1853
178.	RT(J,2)=RT(J,3)*(-1)**(J-1)	1854
179.	301 RT(J,3)=X	1855
180.	L=L+1	1856
181.	DO 328 I=2,10	1857
182.	ITM=I+2	
183.	DO 328 J=4,ITM	
184.	L=L+1	1859
185.	328 RKK(L)=RT(I,J)	1860
186.	DO 329 I=1,28	1861
187.	RKL(I)=0.	1862
188.	DO 329 J=1,28	1863
189.	329 RKL(I)=RKL(I)+CMM(J,I)*RKK(J)	1864
190.	L=L+1	1865
191.	ITM=I+2	
192.	DO 332 I=2,8	1866
193.	DO 332 J=4,ITM	
194.	L=L+1	1868
195.	332 RT(I,J)=RKL(L)	1869
196.	X=X1	1870
197.	X1=X3	1871
198.	X3=X2	1872
199.	X2=X	1873
200.	KZZ(1)=1	1874
201.	KI=1	1875
202.	GO TO 160	1876

Table 8

A useful matrix form for augmented Redlich-Kister coefficients
for a ternary system.

A_{12}	A_{13}	A_{23}	0	0	0	0	0
B_{12}	B_{13}	B_{23}	B_3^a	0	0	0	0
C_{12}	C_{13}	C_{23}	C_3^a	C_3^b	0	0	0
D_{12}	D_{13}	D_{23}	D_3^a	D_3^b	D_3^c	0	0
E_{12}	E_{13}	E_{23}	E_3^a	E_3^b	E_3^c	E_3^d	0
F_{12}	F_{13}	F_{23}	F_3^a	F_3^b	F_3^c	F_3^d	F_3^e

Table 9

Redlich-Kister Coefficients for the Binary Subsystems of the
Fe - Ni - C gamma phase.

Components	Coefficient	$\log \gamma$ at 1000 K	Enthalpy (cal mol ⁻¹)
Fe - Ni	A ₁₂	-.64667	-3904.
	B ₁₂	.42750	2533.
Fe - C	A ₁₃	5.1823	28971.
	B ₁₃	-5.7708	-27380.
	C ₁₃	1.9685	8933.
Ni - C	A ₂₃	5.5121	13328.
	B ₂₃	-3.0	0.

Table 10.

Coefficients found for the Fe - Ni - C liquid system.

Enthalpy (cal mol^{-1})

	subscripts and superscripts				
N	12	13	23	3a	3b
A	-4545	-24280	-17705	0	0
B	2482	4696	0	0	0
C	0	0	0	0	0

 $\log \gamma_{1000}$

	subscripts and superscripts				
N	12	13	23	3a	3b
A	-.75554	-.37940	-2.7448	0.0	0.0
B	.41473	-.65530	.0162	3.5	0.0
C	0.0	.62925	0.0	6.0	0.80

Table 11

Data for $\log \gamma$ for acetonitrile from Clarke and Missen⁷ corrected for non-ideality of the vapor and interpolated to selected values of $S = X_{\text{benzene}} / (X_{\text{benzene}} + X_{\text{carbon tetrachloride}})$

S = .13		S = .23		S = .375	
<u>X₃</u>	<u>log γ_3</u>	<u>X₃</u>	<u>log γ_3</u>	<u>X₃</u>	<u>log γ_3</u>
.4036	.2304	.1833	.4418	.3147	.2717
.4960	.1672	.3044	.3063	.4194	.1969
.5897	.1194	.4221	.1899	.5101	.1461
.6602	.08297	.4918	.1534	.5778	.1109
.7310	.05382	.5633	.1122	.6460	.07579
.7824	.03643	.6401	.07578	.7131	.05393
.8170	.03252	.7460	.03941	.7550	.03442
.8560	.01618	.7884	.02461	.7966	.02509
.8780	.00827			.8144	.01916
.9030	.01099				

Table 11 (continued)

S = .59		S = .65		S = .73		S = .92	
<u>X₃</u>	<u>log γ_3</u>	<u>X₃</u>	<u>log γ_3</u>	<u>X₃</u>	<u>log γ_3</u>	<u>X₃</u>	<u>log γ_3</u>
.3827	.2001	.1671	.3345	.1516	.3178	.1560	.3331
.5138	.1273	.2990	.2484	.2881	.2461	.2811	.2316
.6032	.05829	.4026	.1791	.3959	.1683	.3952	.1663
.6585	.06402	.4926	.1261	.4794	.1231	.5047	.1135
.7118	.04430	.5748	.09271	.5540	.08942	.5699	.09026
.7680	.03512	.6452	.06666	.6312	.06304	.6397	.06670
.8180	.02023	.7081	.04369	.6670	.05736	.7061	.04900
		.7623	.03428	.7167	.03737	.7575	.03201
		.8121	.02068	.7588	.02583	.7958	.02096
				.7786	.02038	.8294	.01760

Table 12

A set of augmented Redlich-Kister parameters for the ternary system benzene - carbon tetrachloride - acetonitrile.

A	.0521	.4419	.7792	0	0	0
B	.00058	.0056	.0817	-.7904	0	0
C	0	.04815	.1114	.8220	-.8464	0
D	0	0	.06835	0	0	0

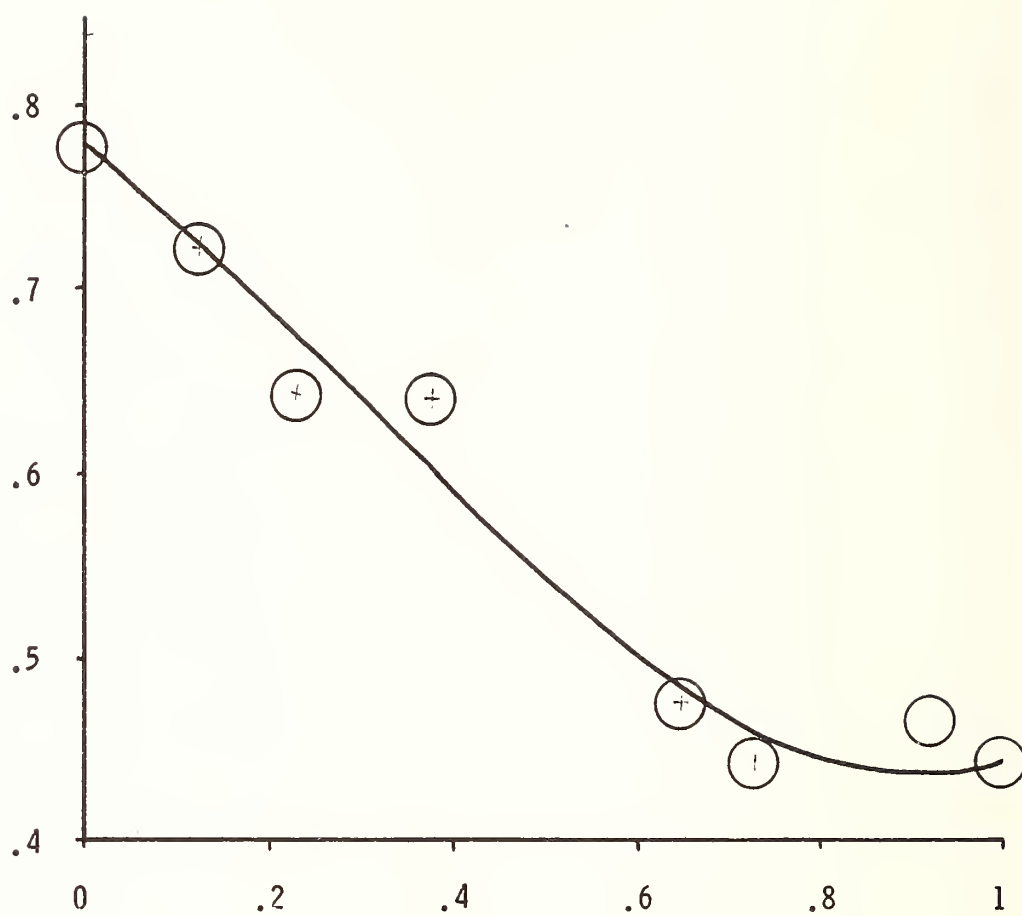


Figure 1

Plot of A_3' vs. $S = X_1 / (X_1 + X_2)$ for the system benzene-carbon tetrachloride-acetonitrile. The solid line is calculated from the values in Table 12.

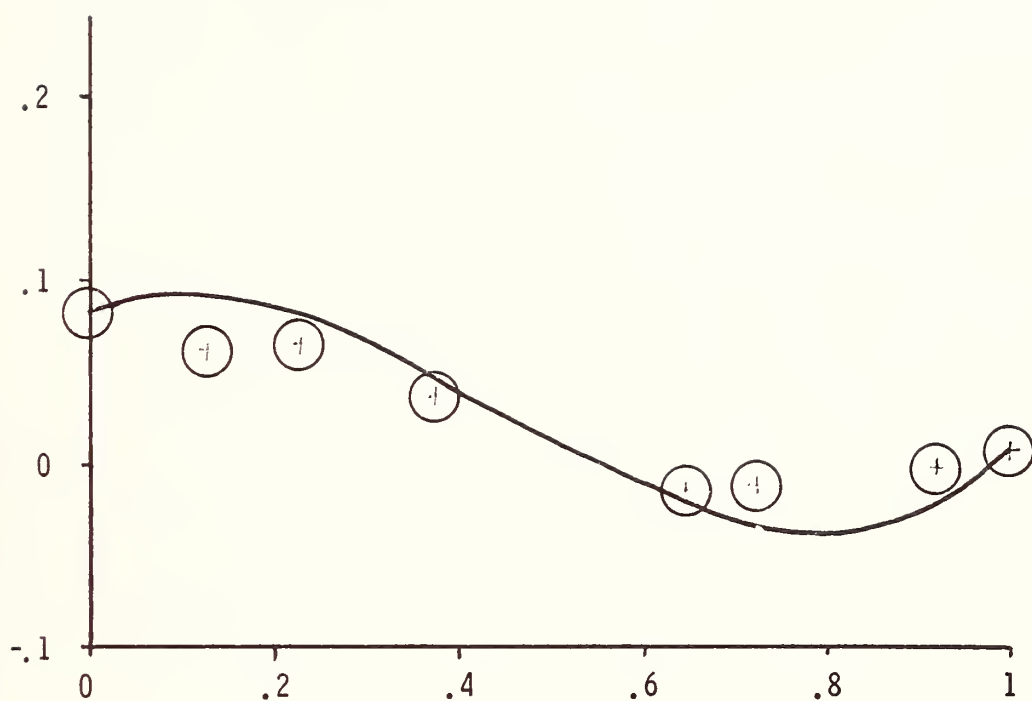


Figure 2

Plot of B'_3 vs. $S = X_1 / (X_1 + X_2)$ for the system benzene-carbon tetrachloride-acetonitrile. The solid line is calculated from the values in Table 12.

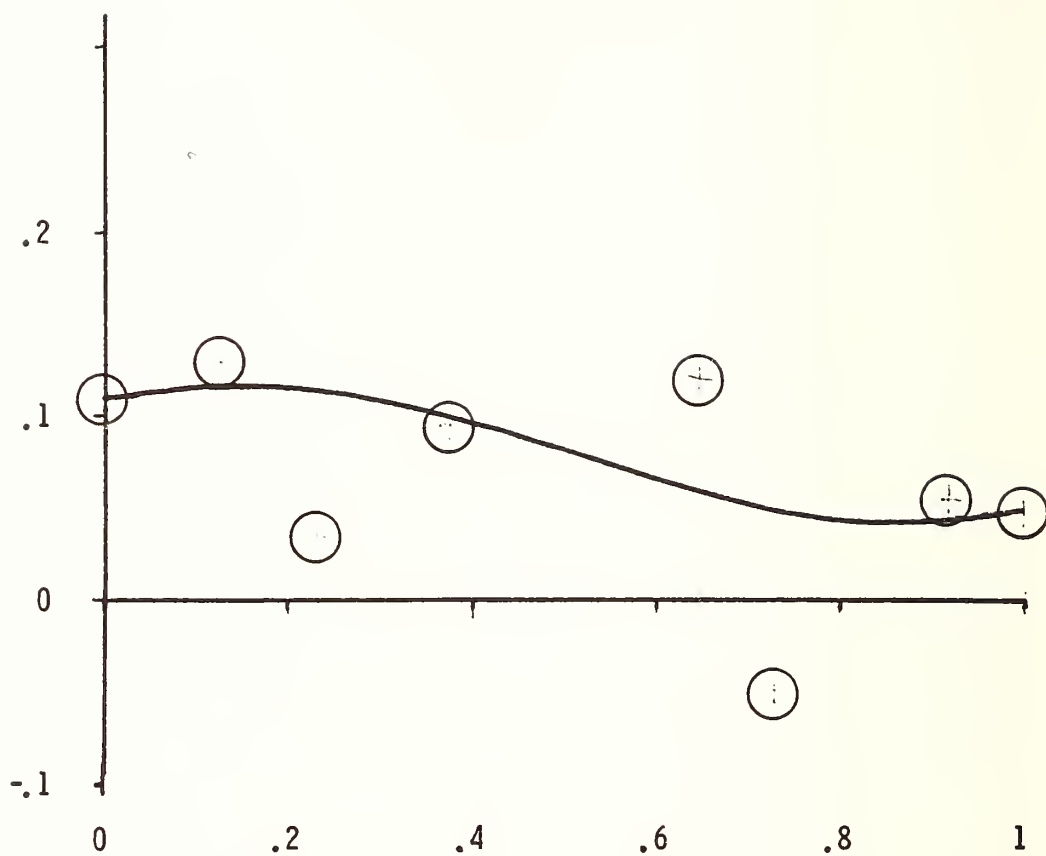


Figure 3

Plot of C_3^I vs. $S = X_1/(X_1 + X_2)$ for the system benzene-carbon tetrachloride-acetonitrile. The solid line is calculated from the values in Table 12.

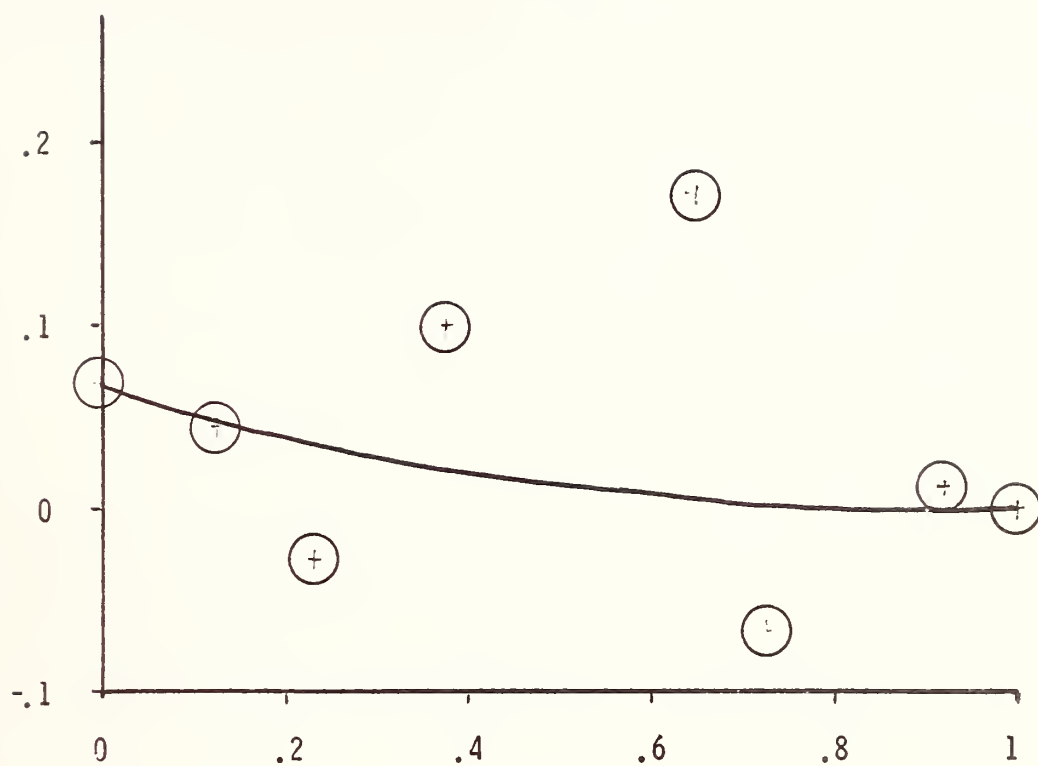


Figure 4

Plot of D_3' vs. $S = X_1 / (X_1 + X_2)$ for the system benzene-carbon tetrachloride-acetonitrile. The solid line is calculated from the values in Table 12.



A PROGRAM FOR BINARY PHASE EQUILIBRIA USING THE REDLICH-KISTER EQUATIONS

Isaac Eliezer and Reed A. Howald

Chemistry Department of Montana State University,
Bozeman, Montana, 59715

Abstract

Several mathematical forms have been proposed and used to describe the relationship between thermodynamic properties and composition in binary systems. No consensus has been reached on what are the best forms, primarily because there is a basic conflict between the requirement of convenience and the requirement of satisfying the Gibbs-Duhem relationship. The subject is currently of special importance because the availability of large high speed computers permits the application of the equations to a wide range of materials problems encountered in many engineering applications.

Power series in mole fraction are well adapted to the general representation of data and to computer calculation of phase diagrams. At least two series in mole fraction have now been programmed for computers: a simple power series and the modified Legendre polynomials of Bale and Pelton.

We have chosen to program the Redlich-Kister equations

$$\log \gamma_1 = (1-X_1)^2 \left[A+B(-1+4X_1)+C(-1+6X_1)(-1+2X_1)+D(-1+8X_1)(-1+2X_1)^2 + \dots \right]$$

$$\log \gamma_2 = X_1^2 \left[A+B(-3+4X_1)+C(-5+6X_1)(-1+2X_1)+D(-7+8X_1)(-1+2X_1)^2 + \dots \right]$$

primarily because the same set of coefficients appears in the equation for both components. These coefficients are the coefficients in a simple power series expansion of the excess free energy of mixing in the variable $(-1+2X)$. Other advantages and disadvantages of the three polynomial forms are discussed, along with the conversion matrices used to convert from one polynomial form to another. It is suggested that both Redlich-Kister and Bale-Pelton coefficients should be reported when experimental data are fitted.

The capabilities of our program are described in terms of the subroutines currently available. Applications to multiphase binary systems of engineering importance are shown, including calculated phase diagrams.

INTRODUCTION --- The earliest generalized power series expansion for thermodynamic properties of binary systems was provided by the Margules equations¹:

$$\bar{Y}_1 = (1-X_1)^2 (A_1 + B_1 X_1 + C_1 X_1^2 \dots) \quad (1)$$

$$Y^e = X_1 (1-X_1) (A_e + B_e X_1 + C_e X_1^2 \dots) \quad (2)$$

$$\bar{Y}_2 = X_1^2 (A_2 + B_2 X_1 + C_2 X_1^2 \dots) \quad (3)$$

The Margules equations are still widely used. However they have two major drawbacks which have led to many efforts to develop alternative formulations. The first difficulty is that different coefficients appear in all three equations, and there are another three sets of coefficients if the expansions are written as power series in X_2 instead of X_1 . Conversions from one set of coefficients to another are not too difficult (they involve multiplication by an upper triangular matrix as illustrated in Table 1), But it is still confusing and tedious to have three or more similar but distinct sets of coefficients.

The second drawback concerns the extreme non-orthogonality of power series over the range from 0 to 1. In this region, X_1^5 and X_1^6 are very similar. We can define the degree of non-orthogonality of two functions by a parameter P , defined as:

$$P = \left[\int_0^1 f g dx \right]^2 / \int_0^1 f^2 dx \int_0^1 g^2 dx \quad (4)$$

In this particular case, we have:

$$P = \left[\int_0^1 X^5 X^6 dX \right]^2 / \int_0^1 X^{10} dX \int_0^1 X^{12} dX = .9931 \quad (5)$$

Orthogonality, $P = 0$, is useful² because then the values of the first coefficients do not depend strongly on the number of coefficients selected to represent the data. At the other extreme, P values greater than 0.99 require that the coefficients be determined and recorded with more significant figures than are present in the original data. Bale and Pelton have shown that even DOUBLE PRECISION computer calculation is inadequate for a 19 term Margules expansion².

The Legendre polynomials are exactly orthogonal over the interval from -1 to 1, and an expansion in Bale-Pelton coefficients, q_i ,^{2,3} works very well:

$$Y^e = X_1 X_2 (q_0 + q_1(X_1 - X_2) + q_2 P_2(X_1 - X_2) + q_3 P_3(X_1 - X_2) \dots) \quad (6)$$

In this equation the first two Legendre polynomials, $P_0 = 1$, and $P_1(X_1 - X_2) = X_1 - X_2$, have been written explicitly.

Unfortunately, derivatives of the Legendre polynomials can get quite complicated, and the easiest way to apply the Gibbs-Duhem relation to Y^e in this form is to define two new sets of coefficients, a_i and b_i :

$$\bar{Y}_1 = X_2^2 \sum_i a_i P_i(X_1 - X_2) \quad (7)$$

$$\bar{Y}_2 = X_1^2 \sum_i b_i P_i(X_1 - X_2) \quad (8)$$

It is impossible to keep exactly orthogonal polynomials in all three equations without having three different sets of coefficients.

The Redlich-Kister equations⁴ provide a reasonable compromise between the conflicting requirements of simplicity, convenience, and

orthogonality. The Redlich-Kister coefficients appear in the expansion of Y^e as $X_1 X_2$ times a power series in $X_1 - X_2$.⁵

$$Y^e = X_1 X_2 (A + B(X_1 - X_2) + C(X_1 - X_2)^2 + D(X_1 - X_2)^3 \dots) \quad (9)$$

It might appear that non-orthogonality might be as serious a problem here as with the Margules equations, but since the interval of integration is changed to -1 to +1, one has exact orthogonality between odd and even powers. For seven Redlich-Kister coefficients the largest value one encounters for the non-orthogonality parameter P is:

$$P = \left[\int_{-1}^{+1} X^4 X^6 dX \right]^2 / \int_{-1}^{+1} X^8 dX \int_{-1}^{+1} X^{12} dX = .9669$$

This is a substantial improvement over $P = .9931$. This same conclusion can be substantiated by an examination of Tables 2 and 3, the conversion matrices from Bale-Pelton coefficients to Margules and Redlich-Kister coefficients respectively. The largest entry in absolute value in Table 3 is $-(693/16) = -43.3125$, so that at worst only two additional significant figures are required for eight Redlich-Kister terms beyond the best orthogonal formulation. On the other hand the Margules coefficients would need 4 additional significant figures for the same accuracy, corresponding to an entry of 16632 in the eighth column.

The major advantage of the Redlich-Kister coefficients is the existence of relatively simple expressions for \bar{Y}_1 and \bar{Y}_2 using the same coefficients:

$$\bar{Y}_1 = X_2^2 \left[A + B(-1 + 4X_1) + C(-1 + 6X_1)(-1 + 2X_1) + D(-1 + 8X_1)(-1 + 2X_1)^2 + E(-1 + 10X_1)(-1 + 2X_1)^3 \dots \right] \quad (10)$$

$$\bar{Y}_2 = X_1^2 \left[A + B(-3+4X_1) + C(-5+6X_1)(-1+2X_1) + D(-7+8X_1)(-1+2X_1)^2 + E(-9+10X_1)(-1+2X_1)^3 \dots \right] \quad (11)$$

The earliest publication of these equations was by Scatchard⁵. However the coefficients were used in an earlier paper of Redlich and Kister⁶, and they are responsible for popularizing the method⁴. Thus, referring to equations 9-11 as the Redlich-Kister equations is well justified as well as standard practice⁷⁻⁸.

Conversions between various sets of coefficients. --- The Redlich-Kister polynomials are simple and easy to use, but they are not orthogonal. For comparisons of independent determinations using different numbers of coefficients it will often be best to convert to Bale-Pelton coefficients. We suggest that, in reporting calculations on binary systems, both Redlich-Kister and Bale-Pelton coefficients be tabulated. Conversions to and comparisons with power series in X_1 and X_2 will also continue to be important. There are many significant interconversions (at least 91), and some way of keeping them straight is important. Figure 1 illustrates how any conversion of coefficients can be accomplished going through the Redlich-Kister coefficients with seven conversion matrices (\mathbb{J} through \mathbb{P}) and their inverse matrices. A few of the easier conversions along the circumference are also shown.

One can go back and forth between Redlich-Kister and Bale-Pelton coefficients with the matrices \mathbb{N} and \mathbb{N}^{-1} shown in Table 3. The columns in \mathbb{N}^{-1} are the coefficients of the Legendre polynomials, so these matrices can be extended indefinitely. Table 4 shows \mathbb{K} and \mathbb{K}^{-1} for conversions between Redlich-Kister coefficients and the

Margules constants of eqn. 2. The columns of \mathbb{K} are the constants in an expansion of $(-1+2X)^n$. These two matrices are especially significant because all the conversion matrices can be written as products of \mathbb{K} and \mathbb{N} with the two simple matrices \mathbb{D} and \mathbb{P} shown in Table 5. This is illustrated in Table 6 for all the matrices shown explicitly in Figure 1. A number of these equations show products of the form $\mathbb{P} \mathbb{X} \mathbb{P}$; however, these triple products are very easy to evaluate since one needs only to change the sign of certain of the off diagonal matrix elements (along diagonals). For example, $\mathbb{P} \mathbb{K} \mathbb{P}$ is just like \mathbb{K} except that all the signs are positive, and $\mathbb{F} = \mathbb{P} \mathbb{D} \mathbb{P}$.

Overview of the BPHD Program --- The BPHD program is designed primarily for the calculation of equilibrium constants and activities as a function of composition in binary systems. Equilibrium constants are calculated by interpolation of stored free energy function data, and activity calculations are based upon the Redlich-Kister equations⁴:

$$\log \gamma_1 = (1-X)^2 \left[A + B(-1+4X) + C(-1+6X)(-1+2X) . . . \right] \quad (12)$$

$$\log \gamma_2 = X^2 \left[A + B(-3+4X) + C(-5+6X)(-1+2X) . . . \right] \quad (13)$$

The program includes provisions for calculating the free energy function and the Redlich-Kister coefficients as a function of temperature. However, this requires known expressions for the heat capacities as a function of temperatures, known enthalpies, and a full set of Redlich-Kister coefficients at one standard temperature. Since much of the development was undertaken for high temperature equilibria, the

standard temperature is usually 1000 K, but much of the program will operate with a standard temperature of 298.15 K as well.

Since the program is meant to be very general, applicable to any binary system, the data for particular components and systems are not included in the program. Such data must be provided from the terminal or from a data file before the calculations will proceed. It is expected that most of the use of this program will involve entering new data files, for new systems or for more accurate representation of old systems. The separation of data files from the program is designed to facilitate such updating of old files and the development of new data files.

Data files are normally read under a 12G.4 format. The card

700 FORMAT (12G.4)

appears in almost all subroutines. It allows for the reading of up to twelve numbers on a single line. Successive numbers must be separated by one or more spaces, but this format does not require that numbers occupy any set locations on a line. It allows for the entry of both integers and decimal fractions. Decimal fractions can be entered in either decimal or exponential notation: 0.00435 or .435E-2. The decimal point must be included in all numbers which are not read as integers, or there is likely to be a mistake in reading the numbers. We have found the 12G.4 format convenient since when such errors occur, a factor of 10^4 error is usually evident. For example all temperature data should be entered with a decimal point as in 1400., while the value 1400 will be interpreted as 0.14. For computers which do not accept a widthless format, we suggest the use of 700 FORMAT (6G10.4) cards instead.

Obtaining Coefficients by Least Squares

Redlich-Kister coefficients and power series expressions for heat capacities which appear in the data files are often obtained by least squares procedures. We have not included a least squares fitting procedure in the BPHD program primarily because most users and computer centers have their own least squares and multiple regression programs with which they are already familiar. There are however, certain features of the particular power series we have chosen to use which need to be explained.

We have chosen to express heat capacities as a power series in $T - T_0$, where T_0 is a standard temperature usually 1000 K. In this form, the first term is a heat capacity at T_0 , which is usually an experimentally accessible temperature. Thus, the value used is quite easy to check in contrast to the value A in the series.

$$C_p = A + BT + CT^2. \dots \quad (14)$$

The series we have chosen as standard is:

$$C_p = A + B(T - T_0) + C(T - T_0)^2 + D(T - T_0)^3 + E(T - T_0)^4 \quad (15)$$

When using a heat capacity expression in BPHD for the first time, it is advisable to print out the full results of the calculation and compare the heat capacity values calculated at different temperatures with the original heat capacity data you are trying to fit. If these agree reasonably well, then the calculated values for the enthalpy and the free

energy function are presumably correct as well.

Equations of the Redlich-Kister form can also be set up for enthalpy, heat capacity, etc. For instance, for the total enthalpy of a binary system, we can write:

$$H/(n_1+n_2) = H_2^{\circ} + (H_1^{\circ}-H_2^{\circ})X + X(1-X) \left[A + B(-1+2X) + C(-1+2X)^2 \dots \right] \quad (16)$$

where n=number of moles, X = mole fraction, H° = enthalpy of standard state. Alternatively the excess enthalpy, ΔH_m can be defined:

$$\Delta H_m = H/(n_1 + n_2) - H_2^{\circ} - (H_1^{\circ} - H_2^{\circ})X \quad (17)$$

and so, using (5):

$$\Delta H_m = X(1-X) \left[A + B(-1+2X) + C(-1+2X)^2 + D(-1+2X)^3 \dots \right] \quad (18)$$

A similar expression can be used for the activity coefficients:

$$X_1 \log \gamma_1 + X_2 \log \gamma_2 = X(1-X) \left[A + B(-1+2X) + C(-1+2X)^2 \dots \right] \quad (19)$$

Sometimes this will give better values for the Redlich-Kister coefficients than either of the separate equations for the individual activity coefficients:

$$\log \gamma_1 = (1-X)^2 \left[A + B(-1+4X) + C(-1+6X)(-1+2X) + D(-1+8X)(-1+2X)^2 \dots \right] \quad (20)$$

and:

$$\log \gamma_2 = X^2 \left[A + B(-3+4X) + C(-5+6X)(-1+2X) + D(-7+8X)(-1+2X)^2 \dots \right] \quad (21)$$

We have chosen to use base 10 logarithms in the equations for the activity coefficients. However, one could use natural logarithms instead, if all the coefficients are multiplied by $\ln 10 = 2.30259$.

Calculation of the Free Energy Function

The standard equilibrium expression:

$$K_T = 10^{\frac{-\Delta H_T}{2.303RT}} 10^{\frac{\Delta S_T}{2.303R}} \quad (22)$$

can be rewritten as:

$$K_T = 10^{\frac{-\Delta H_{298.15}^{\circ}}{2.303RT}} 10^{\frac{\Delta \bar{\Phi}_T}{2.303R}} \quad (23)$$

where the temperature dependence of both ΔH and ΔS is put into the free energy function, $\bar{\Phi}$, defined by $\bar{\Phi} = - \frac{G_T^{\circ} - H_{298.15}^{\circ}}{T}$. It is then possible to calculate equilibrium constants at any temperature from values of $H_{298.15}^{\circ}$ for each compound and from tables of $\bar{\Phi}$ as a function of temperature like the JANAF tables.⁹ For phase equilibria calculations it is often necessary to know K to four significant figures. In most cases, one can obtain this accuracy to interpolating from tables of $\bar{\Phi}$, provided the interval in the table is as small as 20 to 30 K. The program BPHD can be used to create tables of the free energy function at any set of temperatures that one chooses.

The free energy function can be calculated at any temperature if its value is known at some standard temperature and if a heat capacity expression valid over the temperature range of interest including the

standard temperature is known. For the temperature range from 1000 K to 2000 K, we have picked 1000 K as a standard temperature, T_o , and most heat capacity data can be accurately represented over this temperature range by power series of the form:

$$C_p = A + B(T-1000) + C(T-1000)^2 + D(T-1000)^3 + E(T-1000)^4 \quad (24)$$

This information for a particular species such as graphite can be provided to the computer in three lines of an input file:

```
C          (S, GRAPHITE)

10         4         1         3.020         2324.         2824.

2         5.15465         .00159627         -.13423E-5         .45542E-9
```

The first line is just an identifying label and can say anything. The second line starts with three integers. The first two numbers serve as an identifying label for the computer, specifying the component and the phase. In the example shown above, carbon (graphite) is component 10 of phase 4. The program is currently dimensioned to handle up to 10 components in up to 4 phases.

The free energy function can be calculated from the formula:

$$(\Phi_T) = (\Phi_{T_o}) - H(T_o) - H(298.15) \left(\frac{1}{T} - \frac{1}{T_o} \right) - \frac{1}{T} \int_{T_o}^T C_p dT + \int_{T_o}^T (C_p/T) dT \quad (25)$$

The two integrals can be evaluated analytically for the heat capacity expressions used here. There is substantial cancellation between the two integrals and this is recognized in the programming of this computation in subroutine PPI.

The third integer is normally given the value 1. This number identifies the position used for the standard temperature. It is followed by the value of the free energy function at 1000 K, H_{1000}^O - $H_{298.15}^O$, and finally by the enthalpy at 1000 K defined as $\Delta H_{f,298.15}^O + (H_{1000}^O - H_{298.15}^O)$. In the particular case of graphite, since it is the reference state for carbon, $\Delta H_{f,298.15}^O = 0.0$ and the last two numbers are the same. Note that the enthalpies are given in calories mol^{-1} , and not kcal mol^{-1} .

When the third line starts with the integer 2, the next five numbers in the line are coefficients in the power series expansion of the heat capacity. Thus the expression used here for the heat capacity of graphite is:

$$C_p = 5.15465 + .00159627(T-1000) - .13423 \times 10^{-5}(T-1000)^2 + .45542 \times 10^{-9}(T-1000)^3 + 0(T-1000)^4 \quad (26)$$

When the third line starts with 1, the computer will read three lines of heat capacity data, with several options available as to the form of the heat capacity expression.

The program will read in data for up to 40 materials (10 components of 4 phases) in any order from the input file. However, it is necessary

for the file to identify the last material. The computer will continue until it finds component zero of phase zero. Thus the last two lines in the file should be:

```
END (or any other arbitrary name)
```

```
0 0 1
```

A sample file is shown in Table 7.

Once the data file is ready, it is assigned a number to identify it and the program is run. The instructions required to assign an identifying number to a file, to compile a Fortran program and to run it will vary from one computer installation to another. Each individual using this program should find out the directions for these three operations at his own computing center. For the Sigma 7 at Montana State University, an example of control commands is:

```
!FORT SPHD OVER BPHD  
BC  
!SET F:12 DC/CRIS; IN  
! LINK BPHD OVER LMPD  
!LMPD.
```

The program starts by typing the key, OPTIONS. At this point if you wish to calculate and tabulate values for the free energy function, you should type in 1792. This series of four integers with no spaces controls a series of IF statements in the main program and in subroutine GNN to call the subroutines TPIN (for entering the temperatures) and PHIC (for calculating the free energy functions). The program then proceeds to type the key, ENTER NUMBER OF TEMPERATURES AND N TEMP VALUES. The example shown in Table 8, uses three tem-

perature values, but any number up to 20 can be used. The first temperature entered must be the standard temperature chosen in building the input files. If some of the later temperatures are left blank, the program will continue the series of equally spaced temperatures suggested by the last two values entered.

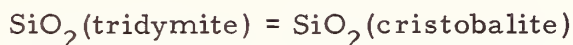
Typing a substantial table from a terminal can be quite tedious. In most cases where we want a full table, we operate this part of the program in BATCH so that the output is printed on a high speed line printer. From the terminal we usually suppress part or all of the printing by entering a value for IOPT(6). The value 4 entered in 17920004 or 9 2 0 0 0 4 suppresses printing completely. 9 2 0 0 0 2 is a useful compromise which prints only part of the output. If you want to decide for each species in a file whether to print the results or not, you should use 17920006 or 9 2 0 0 0 6. The options for printing and skipping in this case, are 1 and 4 respectively.

The Calculation of Equilibrium Constants

It is easy to calculate equilibrium constants by hand from a table of H_{298}° and free energy function values, but the calculation is also programmed in subroutine EPHI. This subroutine is called by the value 7 for IOPT(1), the first of the 9 IOPT values called for at the beginning of subroutine GNN. You can type in the free energy function and H_{298}° values that you need for the calculation, but this is not necessary if you have been through subroutine PHIC. All that is usually needed is to enter the number of phases and then enter the coefficients of the balanced chemical equation following the keys:

ENTER THE COEFFICIENTS AND THEN THE H_{298}° VALUES, PHASE N

Table 9 shows calculations of K's for the melting of tridymite and for the:



equilibrium. Where a lone question mark appears on a line, a line of zeros has been entered by hitting the return key.

A table of equilibrium constant values at the set of temperatures last used in PHIC is automatically typed, and further temperatures can be used by interpolation if desired.

Following the KEQ value, the program prints the values for ΔH and ΔG at each temperature. It is often desirable to correct the entries for one or more of the species to get better values for K or for ΔH .

Changing Φ_{1000}° will raise or lower all the K values by a particular factor, and ΔH can be changed by changing values for H_{1000}° . If you want to change ΔG without changing H_{298}° , the values of $H_{1000}^{\circ} - H_{298}^{\circ}$ and H_{1000}° should both be adjusted by the same amount.

The Calculation of Activities Given X_1

Like the free energy function, Redlich-Kister coefficients are functions of the temperature and values for a particular temperature can be obtained by interpolation in a table. The program allows for reading a table of values at nine successive temperatures or for calculating such a table (with or without printing it) from the values at 1000 K, Redlich-Kister coefficients for enthalpy at 1000 K and heat capacity power series coefficients.

$$A(T) = A(T_0) - AH(T_0) \left[(1/T) - (1/T_0) \right] / 4.5756 \quad (27)$$

$$B(T) = B(T_0) - BH(T_0) \left[(1/T) - (1/T_0) \right] / 4.5756 \quad (28)$$

etc. There are additional terms required if there is a substantial change in the heat capacity on mixing the components, and these integrals are included in the program. However in most cases, values of zero can be used for the heat capacity coefficients. We will discuss first the procedure for calculating a set of Redlich-Kister coefficients from the values at 1000 K and enthalpy and heat capacity coefficients. This part of the program uses a data file which usually has the form:

A	B	C	D . . .
A(H)	B (H)	C(H)	D(H) . . .
0.			
0.			
0.			
0.			

The particular file for carbon in liquid iron is:

-3.79398	-.655295	.629251
-24280.	4696.	0.
0.		
0.		
0.		
0.		

The four lines after the enthalpy coefficients represent coefficients in a power series in temperature for the excess heat capacity of mixing. However, there are almost no high temperature systems where the heat capacity is known accurately as a function of composition and one ordinarily assumes that the excess heat capacity of mixing is negligibly small at all temperatures, so that there are zeroes in all four of these lines. In this case, the Redlich-Kister coefficients are linear in $1/T$ as in the equation:

$$A = A_{1000} + (A(H)/4.5756)(1/T - 1/1000) \quad (29)$$

When there is a zero in the second line as well, i. e. the enthalpy coefficients are also zero, the Redlich-Kister coefficients used do not vary with the temperature. Large enthalpy terms (like $-25280.$ cal mol⁻¹ for $A(H)$ in the above example) give Redlich-Kister coefficients with a large temperature dependence, and here it is necessary to calculate the Redlich-Kister coefficients at the exact temperatures to be used or else to interpolate over very short temperature intervals, no larger than 25 degrees.

This calculation is easily performed once a file of the input data has been prepared. The file is assigned an identifying number and the program is run with either 1791 as the initial input or the values 9 and 1 for IOPT(1) and IOPT(2) in subroutine GNN. The same subroutine as above (TPIN) is used for the selection of the temperatures to be used in the calculation, and the first temperature in the file must be that for which the first line of the input file is valid, normally 1000 K.

If the temperatures you want have already been entered, you may keep the same set by simply hitting the return key.

The computer will then type the key: IDENTIFY THE PHASE AND THEN THE INPUT FILE. You should answer this by entering two integers: A number from 1 to 4 to identify the phase you are using and then the value for IDATA needed to read the input file. The computer will then calculate and print eight Redlich-Kister coefficients for each temperature you have specified and store them under the phase number you used.

If you wish to do this same calculation without printing the results, use the commands 17910002 or 9 1 0 0 0 2. The value IOPT(6) = 2 suppresses the printing step.

The calculated Redlich-Kister coefficients are stored in the file BETA. The dimensions of BETA are BETA (12, 20, 4) allowing for 12 Redlich-Kister coefficients (although the program now uses only 8), 20 temperatures, and 4 phases.

Once the beta values are in, the calculation of $\log \gamma$ and activity proceeds using subroutines GOM and GOMM. There are many ways to call these subroutines, but the one which we use most is with the IOPT values 8 5. This way one starts with the key:

IOP(7) = 0 ENTER TEMP. AND MOLE FRACTION

Then if you type in a temperature in the range covered by the values you have entered and a mole fraction, the activities of each of the components will be calculated and printed. An example of a Redlich-

Kister coefficient calculation is given in Table 10.

Finding a Mole Fraction Given an Activity

Quite often you will have a value for the activity of one of the components and want to know what mole fraction gives that activity. Our program for this calculation is called automatically after using GOM with the IOPT values 8 and 5, or it can be entered directly with 8 and 6. This subroutine, CLM, starts with the key, 5 YOU ARE IN CLM, ENTER KZZ VALUES TO CONTROL ACTIONS. You will ordinarily follow this command by entering a single integer, 1, 3, or 4. The value 3 specifies that you are going to enter a value for the activity of component 1. The value 4 similarly specifies component 2. The value 1 will let you choose. It prints the key WHICH COMPONENT? ENTER HC(J), J = 1, 4, NOW: followed by 4 values. HC(J) are the coefficients in the balanced equilibrium equations and the program is set up to look for the value of $a_1^{HC(1)} * a_2^{HC(2)} * a_3^{HC(3)} * a_4^{HC(4)}$ which you have chosen by setting the HC(J) values. Of course the most common entries are 1.0, 0. and 0., 1.0 for activities of components 1 and 2 respectively. However for an equilibrium like $KAlO_2(s) = KO_{.5}(in \beta-AlO_{1.5}) + AlO_{1.5}(\beta)$, you will be looking for a composition of the beta phase where $a_{KO.5}^{1.0} * a_{AlO1.5}^{1.0}$ is equal to the equilibrium constant, and you would want to enter the values 1.0 1.0. Table 8 show several examples of the use of CLM. The key ENTER TEMPERATURE, ACTIVITY, AND INTEGERS is preceded by two integers, the first of which is I1 and the second of which is I2, the number identifying the phase. If you have the wrong phase,

I2 can be changed by returning to GNN and using the value IOPT(1) = 16. This results in an unkeyed input request line which should be two integers, 1 for I1 and then the value for I2.

There are several interesting features in CLM. It ordinarily starts with $X_1 = 1.0 \times 10^{-28}$ and increases X_1 by steps of 0.01 until it passes the correct value, and then searches for the exact root. It will ordinarily note any maxima or minima found along the way. Some times when there are maxima or minima, the root found will not be the one you really want. When this happens, you will want to start the search for roots at a different value of X_1 . This is accomplished by entering the temperature, the activity, and then the integer 1 following the key ENTER TEMPERATURE, ACTIVITY, AND INTEGERS. The starting value for X_1 is then entered on the next line.

If no roots are found before $X_1 = 1.0$, the program will not print the ROOT BETWEEN line, but it will ordinarily go back and print the values of mole fractions and activities for your starting value of X_1 , so you can perhaps see where the problem lies.

Many of the subroutines, including GOM and CLM, will return to the beginning so that the same calculation can be repeated for a different temperature or for some change in mole fraction or activity. This feature is needed to get enough values to plot activity vs. mole fraction or a solubility line on a phase diagram. The ordinary way to get out of these repeating subroutines is to hit return, entering a line of zeroes.

Equilibrium Between Two Phases of Variable Composition

The last major type of calculation required for two component

phase diagrams is to search for the values of activities and mole fractions at equilibrium between two phases, both of which have variable composition. In this case, you need two equilibrium constants:

$$K_1 = \frac{a_1 \text{ in phase 2}}{a_1 \text{ in phase 1}}$$

and:

$$K_2 = \frac{a_2 \text{ in phase 2}}{a_2 \text{ in phase 1}}$$

The calculation normally proceeds by assuming a value for one of the activities in one phase, calculates the activity for the other component in the other phase, and searches for suitable mole fractions for this other phase. If you make the right choice of components and phases, the calculation will usually converge after 4 to 16 steps of alternating between the phases. Subroutine ALTNT has been written to do the activity calculations and the alternating of phases automatically. It is written to start with an activity of .98 for component 2 in phase 2, so phase 2 is ordinarily selected as the phase which is richest in component 2. Subroutine ALTNT is called from GNN with the IOPT values 0 7. The IOPT values 0 7 1 and 0 7 9 will give more and less printed output respectively. It is necessary to have the Redlich-Kister coefficients available in the storage locations BETA and to have the equilibrium constants K_1 and K_2 ready to enter. However, the values $1/K_1$ and $1/K_2$ are equally acceptable.

The first key in ALTNT is ENTER TEMPERATURE AND A CONTROL INTEGER. For the calculation described here no control integer is necessary and one merely enters a temperature value, with

a decimal point. The computer then asks you to ENTER TWO EQUILIBRIUM CONSTANTS, and you type in the values for K_1 and K_2 .

If you have values for $1/K_1$ and $1/K_2$ instead, type them in but type 1 after the two values. This calculates K_1 and K_2 and uses them in the computation. Table 12 shows examples of these two entries. The program starts with the value 0.98 for a_2 in phase 2 and prints the successive values for a_1 in phase 1 that it obtains at each iteration. When the computer is satisfied that the calculation has converged, it will print the results for each phase, but more often it will ask :

SHALL WE CONTINUE. The integer 1 means yes, but 0 and -1 will both take you back to the beginning to enter a new temperature, to reenter the old temperature, or to leave the subroutine (by pressing the RETURN key). Sometimes convergence is very slow, and you can improve this by guessing at a better starting value for the activity of component 2 in phase 2. If you want to do this, you need a fourth entry, the value 1, in the line following the key ENTER TWO EQUILIBRIUM CONSTANTS. Then on the next line, you type in the value you want to try for a_2 in phase 2.

This is sufficient instruction in the program to repeat a calculation of a phase diagram using a copy of our input files. Tables 13 - 19 show a calculation of the Ni-C phase diagram shown in Figure 2. The thermodynamic data for solid and liquid Ni and C are shown in Table 13. The values for Ni and for graphite are those selected to agree with the JANAF tables. The values for liquid C are selected to fit the equation $K = 1.33 - 5460/T$ for the equilibrium constant for the melting of carbon. This means that $\Delta C_p = 0$ for this reaction, and ΔH

is independent of temperature.

We have used two Redlich-Kister coefficients for carbon in solid Ni, the values $A = 5.5121 + (13328/4.5756)(1/T - 1/1000)$ and $B = -3.6$. Similarly, two coefficients are used for the liquid phase. Table 13 and 14 are listings of the input files including the thermodynamic data for the calculation of equilibrium constants and of Redlich-Kister coefficients. The calculation of Redlich-Kister coefficients at three temperatures is shown in Table 15. The calculations of equilibrium constants for the melting of Ni and C are shown in Table 16. Table 17 shows the calculation of the solubility of graphite in solid Ni, and the corresponding calculation for the liquid phase is in Table 18. The last 2 lines of the phase diagram, describing the equilibrium between the solid and liquid Ni rich phases, are calculated using ALTNT as in Table 19. The activities of liquid carbon are always very small, and this is a case where the initial estimate a_2 in phase 2 = 0.98 made in ALTNT will not work at all.

It is possible to use ALTNT for cases where a single phase separates into two different compositions, as in cases of two immiscible liquids. It is quite possible to represent such phases by a single set of Redlich-Kister coefficients. To use such a set in a phase equilibrium calculation it is necessary to read the values twice, once for phase 1 and once for phase 2.

Figure 3 is a flow chart showing the main sequences in which the subroutines are called.

Every new system to which the program is applied, is likely to bring up new problems. Some of these will be ones which we have already dealt with, and the modifications of BPHD needed may already be present. BPHD has developed by the continuous incorporation of

new features, always attempting to keep the older calculations in working order. This makes the program versatile, but somewhat complex. This kind of complete discussion of the program is available in a manual written for users of the program.¹⁰

Figure 4 shows a portion of the $\text{SiO}_2\text{-KO}_{0.5}$ phase diagram calculated with the coefficients listed in Table 20. This system is chosen here as an example of listing and using a large number of parameters. The values shown are of little more than historic interest because at the time they were selected there was insufficient accurate data on this binary system to fix seven parameters.

References

1. M. Margules, Sitzungsber. Wien. Akad., (2), 104, 1243 (1895)
2. C. W. Bale and A. W. Pelton, Metal. Trans., 6A, 1963 (1975)
3. R. A. Howald and I. Eliezer, Metal. Trans., in press
4. O. Redlich, A. T. Kister, and C. E. Turnquist, Chem. Eng. Progr., Symposium Series, 48(2), 49 (1952)
5. G. Scatchard, Chem. Revs., 44, 7 (1949)
6. O. Redlich and A. T. Kister, Ind. Engng. Chem., 40, 345 (1948)
7. E. A. Guggenheim, Thermodynamics, North Holland Pub. Co., Amsterdam, pp. 249-250 (1957)
8. J. M. Smith and H. C. Van Ness, Introduction to Chemical Engineering Thermodynamics, McGraw-Hill Book Co., New York, pp. 332-3 (1975)
9. JANAF Thermochemical Tables, Nat. Stand. Ref. Data Ser. 37 (1971)
10. R. A. Howald and I. Eliezer, BPHD: a Computer Program for the Calculation of Multiphase Equilibria (1976)

Table 1..

Typical conversion matrices for the Margules equations.

From eqn. 1 to eqn. 2:

$$\begin{bmatrix} A_e & B_e & C_e & D_e \dots \end{bmatrix} > = \mathbb{F} \begin{bmatrix} A_1 & B_1 & C_1 & D_1 \dots \end{bmatrix} >$$

$\mathbb{F} =$	1	0	0	0	0	0	$\mathbb{F}^{-1} =$	1	0	0	0	0
	0	(1/2)	0	0	0	0		0	2	0	0	0
	0	0	(1/3)	0	0	0		0	0	3	0	0
	0	0	0	(1/4)	0	0		0	0	0	4	0
	0	0	0	0	0	(1/5)		0	0	0	0	5

From eqn. 2 to eqn. 3:

$$\begin{bmatrix} A_2 & B_2 & C_2 & D_2 \dots \end{bmatrix} > = \mathbb{F} \begin{bmatrix} A_e & B_e & C_e & D_e \dots \end{bmatrix} >$$

$\mathbb{F} =$	1	-1	0	0	0	0	$\mathbb{F}^{-1} =$	1	(1/2)	(1/3)	(1/4)	(1/5)
	0	2	-2	0	0	0		0	(1/2)	(1/3)	(1/4)	(1/5)
	0	0	3	-3	0	0		0	0	(1/3)	(1/4)	(1/5)
	0	0	0	4	-4	0		0	0	0	(1/4)	(1/5)
	0	0	0	0	5	0		0	0	0	0	(1/5)

Table 1 (continued)

From eqn. 1 to eqn. 3:

$$|A_2 B_2 C_2 D_2 \dots\rangle = \mathbb{G} |A_1 B_1 C_1 D_1 \dots\rangle$$

$\mathbb{G} = \mathbb{H}\mathbb{F}$	1	$-(1/2)$	0	0	0	$\mathbb{G}^{-1} =$	1	$(1/2)$	$(1/3)$	$(1/4)$	$(1/5)$
	0	1	$-(2/3)$	0	0		0	1	$(2/3)$	$(2/4)$	$(2/5)$
	0	0	1	$-(3/4)$	0		0	0	1	$(3/4)$	$(3/5)$
	0	0	0	1	$-(4/5)$		0	0	0	1	$(4/5)$
	0	0	0	0	1		0	0	0	0	1

Table 2.

Conversion matrices from Bale-Pelton to Margules coefficients.

From eqn. 6 to eqn. 2:

$$|A_e B_e C_e D_e \dots\rangle = \mathbb{H} |q_0 q_1 q_2 q_3 \dots\rangle$$

$\mathbb{H} =$	1	-1	1	-1	1	-1	1	-1
	0	2	-6	12	-20	30	-42	56
	0	0	6	-30	90	-210	420	-756
	0	0	0	20	-140	560	-1680	4200
	0	0	0	0	70	-630	3150	-11550
	0	0	0	0	0	252	-2772	16632
	0	0	0	0	0	0	924	-12012
	0	0	0	0	0	0	0	3432

$\mathbb{H}^{-1} =$	1	(1/2)	(1/3)	(1/4)	(1/5)	(1/6)	(1/7)	(1/8)
	0	(1/2)	(3/6)	(9/20)	(28/70)	(90/252)	(297/924)	(1001/3432)
	0	0	(1/6)	(5/20)	(20/70)	(75/252)	(275/924)	(1001/3432)
	0	0	0	(1/20)	(7/70)	(35/252)	(154/924)	(637/3432)
	0	0	0	0	(1/70)	(9/252)	(54/924)	(273/3432)
	0	0	0	0	0	(1/252)	(11/924)	(77/3432)
	0	0	0	0	0	0	(1/924)	(13/3432)
	0	0	0	0	0	0	0	(1/3432)

Table 3.

The conversion matrix from Redlich-Kister to Bale-Pelton coefficients.

From equations 9-11 to eqn. 6:

$$|q_0 \ q_1 \ q_2 \ q_3 \ \dots\rangle = \mathbb{N} |A \ B \ C \ D \ \dots\rangle$$

$$\mathbb{N} = \begin{array}{cccccccc} 1 & 0 & (1/3) & 0 & (1/5) & 0 & (1/7) & 0 \\ 0 & 1 & 0 & (3/5) & 0 & (27/63) & 0 & (143/429) \\ 0 & 0 & (2/3) & 0 & (20/35) & 0 & (110/231) & 0 \\ 0 & 0 & 0 & (2/5) & 0 & (28/63) & 0 & (182/429) \\ 0 & 0 & 0 & 0 & (8/35) & 0 & (72/231) & 0 \\ 0 & 0 & 0 & 0 & 0 & (8/63) & 0 & (88/429) \\ 0 & 0 & 0 & 0 & 0 & 0 & (16/231) & 0 \\ 0 & 0 & 0 & 0 & 0 & 0 & 0 & (16/429) \end{array}$$

$$\mathbb{N}^{-1} = \begin{array}{cccccccc} 1 & 0 & -(1/2) & 0 & (3/8) & 0 & -(5/16) & 0 \\ 0 & 1 & 0 & -(3/2) & 0 & (15/8) & 0 & -(35/16) \\ 0 & 0 & (3/2) & 0 & -(30/8) & 0 & (105/16) & 0 \\ 0 & 0 & 0 & (5/2) & 0 & -(70/8) & 0 & (315/16) \\ 0 & 0 & 0 & 0 & (35/8) & 0 & -(315/16) & 0 \\ 0 & 0 & 0 & 0 & 0 & (63/8) & 0 & -(693/16) \\ 0 & 0 & 0 & 0 & 0 & 0 & (321/16) & 0 \\ 0 & 0 & 0 & 0 & 0 & 0 & 0 & (429/16) \end{array}$$

Table 4.

One of the conversion matrices from Redlich-Kister to Margules coefficients.

From equations 9-11 to eqn. 2:

$$|A_e B_e C_e D_e \dots\rangle = \mathbb{K} |A B C D \dots\rangle$$

$\mathbb{K} =$	1	-1	1	-1	1	-1	1	-1
	0	2	-4	6	-8	10	-12	14
	0	0	4	-12	24	-40	60	-84
	0	0	0	8	-32	80	-160	280
	0	0	0	0	16	-80	240	-560
	0	0	0	0	0	32	-192	672
	0	0	0	0	0	0	64	-448
	0	0	0	0	0	0	0	128

$\mathbb{K}^{-1} =$	1	(1/2)	(1/4)	(1/8)	(1/16)	(1/32)	(1/64)	(1/128)
	0	(1/2)	(2/4)	(3/8)	(4/16)	(5/32)	(6/64)	(7/128)
	0	0	(1/4)	(3/8)	(6/16)	(10/32)	(15/64)	(21/128)
	0	0	0	(1/8)	(4/16)	(10/32)	(20/64)	(35/128)
	0	0	0	0	(1/16)	(5/32)	(15/64)	(35/128)
	0	0	0	0	0	(1/32)	(6/64)	(21/128)
	0	0	0	0	0	0	(1/64)	(7/128)
	0	0	0	0	0	0	0	(1/128)

Table 5.

Two simple conversion matrices which combine with \mathbb{N} and \mathbb{K} from Tables 3 and 4.

$\mathbb{D} = 1$	1	0	0	0	$\mathbb{D}^{-1} = 1$	$-(1/2)$	$(1/3)$	$-(1/4)$	$(1/5)$
0	2	2	0	0	0	$(1/2)$	$-(1/3)$	$(1/4)$	$-(1/5)$
0	0	3	3	0	0	0	$(1/3)$	$-(1/4)$	$(1/5)$
0	0	0	4	4	0	0	0	$(1/4)$	$-(1/5)$
0	0	0	0	5	0	0	0	0	$(1/5)$

$\mathbb{P} = \mathbb{P}^{-1}$	=	1	0	0	0	0
		0	-1	0	0	0
		0	0	1	0	0
		0	0	0	-1	0
		0	0	0	0	1

Table 6.

Summary of conversion matrices shown in Figure 1.

$$\mathbb{E} = \mathbb{K} \mathbb{D}^{-1} \mathbb{K}^{-1} \quad \text{see Table 1}$$

$$\mathbb{F} = \mathbb{P} \mathbb{D} \mathbb{P} \quad \text{see Table 1}$$

$$\mathbb{G} = \mathbb{K} \mathbb{F} \mathbb{D}^{-1} \mathbb{K}^{-1} = \mathbb{K} \mathbb{P} \mathbb{D} \mathbb{P} \mathbb{D}^{-1} \mathbb{K}^{-1} \quad \text{see Table 1}$$

$$\mathbb{H} = \mathbb{K} \mathbb{N}^{-1} \quad \text{see Table 2}$$

$$\begin{array}{ccccc} \mathbb{J} = \mathbb{K} \mathbb{D} = & 1 & -1 & 1 & -1 & 1 & \mathbb{J}^{-1} = & 1 & (1/4) & (1/12) & (1/32) & (1/80) \\ & 0 & 4 & -8 & 12 & -16 & & 0 & (1/4) & (2/12) & (3/32) & (4/80) \\ & 0 & 0 & 12 & -36 & 72 & & 0 & 0 & (1/12) & (3/32) & (6/80) \\ & 0 & 0 & 0 & 32 & -128 & & 0 & 0 & 0 & (1/32) & (4/80) \\ & 0 & 0 & 0 & 0 & 80 & & 0 & 0 & 0 & 0 & (1/80) \end{array}$$

$$\begin{array}{ccccc} \mathbb{L} = \mathbb{K} \mathbb{F} = & 1 & -3 & 5 & -7 & 9 & \mathbb{L}^{-1} = & 1 & (3/4) & (7/12) & (15/32) & (31/80) \\ & 0 & 4 & -16 & 36 & -64 & & 0 & (1/4) & (4/12) & (11/32) & (26/80) \\ & 0 & 0 & 12 & -60 & 168 & & 0 & 0 & (1/12) & (5/32) & (16/80) \\ & 0 & 0 & 0 & 32 & -192 & & 0 & 0 & 0 & (1/32) & (6/80) \\ & 0 & 0 & 0 & 0 & 80 & & 0 & 0 & 0 & 0 & (1/80) \end{array}$$

$$\begin{array}{ccccc} \mathbb{M} = \mathbb{N} \mathbb{F} = & 1 & -1 & 1 & -1 & 1 & \mathbb{M}^{-1} = & 1 & (1/2) & 0 & -(2/16) & 0 \\ & 0 & 2 & -2 & 2.4 & -2.4 & & 0 & (1/2) & (1/2) & -(2/16) & -(3/8) \\ & 0 & 0 & 2 & -2 & (18/7) & & 0 & 0 & (1/2) & (1/16) & -(3/8) \\ & 0 & 0 & 0 & 1.6 & -1.6 & & 0 & 0 & 0 & (1/16) & (7/8) \\ & 0 & 0 & 0 & 0 & (8/7) & & 0 & 0 & 0 & 0 & (7/8) \end{array}$$

$$\begin{array}{ccccc} \mathbb{O} = \mathbb{N} \mathbb{D} = & 1 & 1 & 1 & 1 & 1 & \mathbb{O}^{-1} = & 1 & -(1/2) & 0 & (2/16) & 0 \\ & 0 & 2 & 2 & 2.4 & 2.4 & & 0 & (1/2) & -(1/2) & -(2/16) & (3/8) \\ & 0 & 0 & 2 & 2 & (18/7) & & 0 & 0 & (1/2) & -(1/16) & -(3/8) \\ & 0 & 0 & 0 & 1.6 & 1.6 & & 0 & 0 & 0 & (1/16) & -(7/8) \\ & 0 & 0 & 0 & 0 & (8/7) & & 0 & 0 & 0 & 0 & (7/8) \end{array}$$

Table 6 (continued)

$$\begin{aligned}
 \mathbb{R} = \mathbb{N} \mathbb{F} \mathbb{N}^{-1} = & \begin{array}{ccccc} 1 & -1 & 1 & -1 & 1 \\ 0 & 2 & -3 & 3 & -3 \\ 0 & 0 & 3 & -5 & 5 \\ 0 & 0 & 0 & 4 & -7 \\ 0 & 0 & 0 & 0 & 5 \end{array} & \mathbb{R}^{-1} = & \begin{array}{ccccc} 1 & (1/2) & (1/6) & (1/12) & (1/20) \\ 0 & (1/2) & (3/6) & (3/12) & (3/20) \\ 0 & 0 & (1/3) & (5/12) & (5/20) \\ 0 & 0 & 0 & (1/4) & (7/20) \\ 0 & 0 & 0 & 0 & (1/5) \end{array}
 \end{aligned}$$

$$\begin{aligned}
 \mathbb{S} = \mathbb{N} \mathbb{D} \mathbb{N}^{-1} = & \begin{array}{ccccc} 1 & 1 & 1 & 1 & 1 \\ 0 & 2 & 3 & 3 & 3 \\ 0 & 0 & 3 & 5 & 5 \\ 0 & 0 & 0 & 4 & 7 \\ 0 & 0 & 0 & 0 & 5 \end{array} & \mathbb{S}^{-1} = & \begin{array}{ccccc} 1 & -(1/2) & (1/6) & -(1/12) & (1/20) \\ 0 & (1/2) & -(3/6) & (3/12) & -(3/20) \\ 0 & 0 & (1/3) & -(5/12) & (5/20) \\ 0 & 0 & 0 & (1/4) & -(7/20) \\ 0 & 0 & 0 & 0 & (1/5) \end{array}
 \end{aligned}$$

$$\begin{aligned}
 \mathbb{T} = \mathbb{N} \mathbb{F} \mathbb{D}^{-1} \mathbb{N}^{-1} = & \begin{array}{ccccc} 1 & -1 & 1 & -1 & 1 \\ 0 & 1 & -2 & 2.5 & -2.7 \\ 0 & 0 & 1 & -2.5 & 3.5 \\ 0 & 0 & 0 & 1 & -2.8 \\ 0 & 0 & 0 & 0 & 1 \end{array} & \mathbb{T}^{-1} = \mathbb{P} \mathbb{T} \mathbb{P}
 \end{aligned}$$

$$\begin{aligned}
 \mathbb{W} = \mathbb{W}^{-1} = \mathbb{L} \mathbb{P} \mathbb{L}^{-1} = \mathbb{K} \mathbb{F} \mathbb{P} \mathbb{F}^{-1} \mathbb{K}^{-1} = & \begin{array}{ccccc} 1 & (3/2) & 2 & (5/2) & 3 \\ 0 & -1 & -(8/3) & -5 & -8 \\ 0 & 0 & 1 & (15/4) & 9 \\ 0 & 0 & 0 & -1 & -(24/5) \\ 0 & 0 & 0 & 0 & 1 \end{array}
 \end{aligned}$$

Table 7

K20 (G)	7	3	1	71.11	10462.6	-23537.4
	2	14.904				
FE (G)	9	3	1	46.141	4033.	103533.
	2	5.36152		-.41359E-3	.75550E-6	-.1603E-9
FE (C, GAMMA)	9	2	1	10.026	6789.	6789.
	2	7.73018		.0020027	-.4161E-8	
K2C03 (L)	4	4	1	57.546	27309.	-242911.
	2	50.0				
ALO1.5 (C, BETA, 6-77)	8	4	1	13.0705	9317.	-188988.
	2	14.908		.0023471	-.12717E-5	.34615E-9
LI(C03).5 (S)	10	2	1	18.522	12540.5	-132779.5
	2	23.109		.01551	-.0000200	
LI(C03).5 (L)	10	1	1	23.0615	13036.	-127779.
	2	22.16				
KALO2(S)	10	3	1	31.3415	16317.	-256645.8
	2	24.005		.0033071	-.12717E-5	.34615E-9
KALO2 (L)	10	4	1	32.779	16706.	-249320.5
	2	28.762		.0018		
KO.5 (G)	8	3	1	61.358	6287.	21887.
	2	9.12996		.27908E-3	-.2310E-7	
KALS1308 (L, GLASS)	9	1	1	94.72	47988.	-886596.
	2	77.049		.014243	.3525E-4	
ALO1.5 (C, GAMMA)	7	4	1	13.000	9317.	-188283.
	2	14.908		.0023471	-.1272E-5	.3462E-9
K2S04 (S, BETA)	1	4	1	61.69	31630.	-311030.
	2	46.90		.0201		
K2S04 (LIQUID)	2	4	1	69.2907	31630.	-300924.5
	2	47.28				
NEXT TO LAST CARD	0	0	1			

Table 8

!SET F:12 DC/TCBT;IN

!SET F:13 DC/TECT;IN

!SET F:14 DC/CRIS;IN

!LINK BPHD OVER LMPD

LINKING BPHD

'P1' ASSOCIATED.

LINKING SYSTEM LIB

!LMPD.

OPTIONS?

?1792

0 ENTER NUMBER OF TEMPERATURES, AND N TEMP VALUES

?3 1000. 1073. 1473.

IDENTIFY THE INPUT FILE

?14

K0.5 IN LIQUID SiO2

COMPONENT 1 OF PHASE 1 H0298 IS -89562.1875

AT1000.000 H0 = -81000.18750 AND PHI IS 25.476303 CP= 11.45000

AT1073.000 H0 = -80159.50000 AND PHI IS 23.086655 CP= 11.58140

AT1473.000 H0 = -75382.93750 AND PHI IS 29.001068 CP= 12.30140

SiO2 (LIQUID)

COMPONENT 2 OF PHASE 1 H0298 IS -215010.0000

AT1000.000 H0 = -205669.00000 AND PHI IS 18.202774 CP= 16.61000

AT1073.000 H0 = -204447.68750 AND PHI IS 18.946747 CP= 16.85214

AT1473.000 H0 = -197407.81250 AND PHI IS 22.656967 CP= 18.41333

K0.5 (C, IN TRIDYMITE

COMPONENT 1 OF PHASE 2 H0298 IS -80000.0000

AT1000.000 H0 = -71655.00000 AND PHI IS 18.000000 CP= 9.09700

AT1073.000 H0 = -70938.31250 AND PHI IS 18.589844 CP= 9.16708

AT1473.000 H0 = -67244.68750 AND PHI IS 21.291153 CP= 9.55108

SiO2 (C, TRIDYMITE)

COMPONENT 2 OF PHASE 2 H0298 IS -217270.0000

AT1000.000 H0 = -206702.62500 AND PHI IS 17.559998 CP= 16.72176

AT1073.000 H0 = -205476.56250 AND PHI IS 18.319580 CP= 16.86310

AT1473.000 H0 = -193613.62500 AND PHI IS 22.076843 CP= 17.39197

SiO2 (C, CRISTOBALITE

COMPONENT 4 OF PHASE 2 H0298 IS -215687.0000

AT1000.000 H0 = -206670.00000 AND PHI IS 18.136993 CP= 16.72176

AT1073.000 H0 = -205443.93750 AND PHI IS 18.859131 CP= 16.86310

AT1473.000 H0 = -193581.00000 AND PHI IS 22.477097 CP= 17.39197

SiO2 (C, QUARTZ)

COMPONENT 5 OF PHASE 2 H0298 IS -217970.0000

AT1000.000 H0 = -207130.00000 AND PHI IS 16.973007 CP= 16.48000

AT1073.000 H0 = -205920.56250 AND PHI IS 17.750580 CP= 16.65518

AT1473.000 H0 = -199066.43750 AND PHI IS 21.568054 CP= 17.61519

ENTER IDATA FOR FILE TO BE REWOUND, IT IS NOW -2

?14

IN GNN, ENTER 9 IOPT VALUES 9 2 0 0 0 0 0 0 0

?7

ENTER THE NUMBER OF PHASES AND IOPT(9)

?2

ENTER ICOMP, IPHASE, AND THEN 2 VALUES FOR PHI

Table 9

Calculation of some equilibrium constants for reactions of SiO_2 .

CP-V CIB AT YOUR SERVICE
ON AT 16:48 SEP 13, '76
LOGON PLEASE: 156, ELIEZER,

CIB IN ... NORMAL CHARGES AGAIN...DOWN AT MIDNIGHT FOR
TYPE NEWS FOR USER INFO, ENTER FOR SUGGESTIONS

```
!C CRIS TO ME
K0.5 IN LIQUID SiO2
1 1 1 25.4763 8562. -81000.2
2 11.45 .00180
SiO2 (LIQUID)
2 1 1 18.20277 10341. -205669.
2 16.61 .0032268 .12384E-5
K0.5 (C, IN TRIDYMIT)
1 2 1 18.000 8345. -71655.
2 9.097 .00096
SiO2 (C, TRIDYMIT)
2 2 1 17.560 10567.4 -206702.6
2 16.72175 .00205366 -.00000165179 .64630E-9
SiO2 (C, CRISTOBALITE)
4 2 1 18.137 10017. -206670.
2 16.72175 .00205366 -.00000165179 .6463E-9
SiO2 (C, QUARTZ)
5 2 1 16.973 10840. -207130.
2 16.480 .0024
END
0 0 1
```

!SET F:14 DC/CRIS:IN

!LMPD.

OPTIONS?

?17920006

0 ENTER NUMBER OF TEMPERATURES, AND N TEMP VALUES

?3 1000. 1073. 1473.

IDENTIFY THE INPUT FILE

?14

K0.5 IN LIQUID SiO2

?4

SiO2 (LIQUID)

?

COMPONENT 2 OF PHASE 1 H0298 IS -216010.0000

AT1000.000 H0 =-205669.00000 AND PHI IS 18.202774 CP= 16.61000

AT1073.000 H0 =-204447.68750 AND PHI IS 18.946747 CP= 16.95214

AT1473.000 H0 =-197407.81250 AND PHI IS 22.656967 CP= 18.41333

Table 9 (continued)

K0.5 (C,IN TRIDYMITE

?4

SI02 (C,TRIDYMITE)

?

COMPONENT 2 OF PHASE 2 H0298 IS -217270.0000

AT1000.000 H0 =-206702.62500 AND PHI IS 17.559993 CP= 16.72176

AT1073.000 H0 =-205476.56250 AND PHI IS 18.319530 CP= 16.36310

AT1473.000 H0 =-198613.62500 AND PHI IS 22.076343 CP= 17.39197

SI02 (C,CRISTOBALITE

?

COMPONENT 4 OF PHASE 2 H0298 IS -216637.0000

AT1000.000 H0 =-206670.00000 AND PHI IS 18.136993 CP= 16.72176

AT1073.000 H0 =-205443.93750 AND PHI IS 18.859131 CP= 16.36310

AT1473.000 H0 =-198581.00000 AND PHI IS 22.477097 CP= 17.39197

SI02 (C,QUARTZ)

?4

ENTER IDATA FOR FILE TO BE REWOUND, IT IS NOW ###

?14

IN GVN, ENTER 9 IOPT VALUES 9 2 0 0 0 4 0 6 0

?7

ENTER THE NUMBER OF PHASES AND IOPT(9)

?2

ENTER ICOMP, IPHASE, AND THEN 2 VALUES FOR PHI

?

ENTER THE COEFFICIENTS AND THEN THE H0298 VALUES, PHASE 1

?0. 1.

ENTER THE COEFFICIENTS AND THEN THE H0298 VALUES, PHASE 2

?0. -1.

AT 1073.00K, KEQ = .759327E 00 .102387E 04 .537050E 03

AT 1473.00K, KEQ = .370642E 00 .120531E 04 .405473E 03

O DO YOU WANT TO CALCULATE KEQ AT OTHER TEMPERATURES?

?

IN GVN, ENTER 9 IOPT VALUES 7 0 0 0 0 0 0 0 5

?7

ENTER THE NUMBER OF PHASES AND IOPT(9)

?2

ENTER ICOMP, IPHASE, AND THEN 2 VALUES FOR PHI

?

ENTER THE COEFFICIENTS AND THEN THE H0298 VALUES, PHASE 1

?

ENTER THE COEFFICIENTS AND THEN THE H0298 VALUES, PHASE 2

?0. -1. 0. 1.

AT 1073.00K, KEQ = .998097E 00 .326250E 02 .406201E 01

AT 1473.00K, KEQ = .100225E 01 .326250E 02-.657300E 01

O DO YOU WANT TO CALCULATE KEQ AT OTHER TEMPERATURES?

?3

ENTER THE COEFFICIENTS AND THEN THE H0298 VALUES, PHASE 1

?0. 1.

ENTER THE COEFFICIENTS AND THEN THE H0298 VALUES, PHASE 2

?0. 0. 0. -1.

AT 1073.00K, KEQ = .760775E 00 .996250E 03 .532938E 03

AT 1473.00K, KEQ = .363639E 00 .117319E 04 .412051E 03

O DO YOU WANT TO CALCULATE KEQ AT OTHER TEMPERATURES?

?

IN GVN, ENTER 9 IOPT VALUES 7 0 0 0 0 0 0 0 5

?

SORRY, NO OTHER SYSTEMS ARE AVAILABLE YET

DO YOU WANT TO CONTINUE? USE 1 FOR YES

?

STOP 0

Table 10

Calculation of Redlich-Kister coefficients at 1300K in the $\text{K}_2\text{O}-\text{Al}_2\text{O}_3$ system.

!C CLUM

-13.155 -4.587

-71352. -25971.

0.

0.

0.

0.

-.546255 7.34730 14.4529 7.56354

3298.85 20269.3 36991.3 20376.3

0.

0.

0.

0.

-97.484095 -129.7985 14.4529 7.56354 0. 170.

3298.85 20269.3 36991.3 20376.3

0.

0.

0.

0.

!SET F:12 DC/CLUM;IN

!LMPD.

OPTIENS?

?1791

0 ENTER NUMBER OF TEMPERATURES, AND N TEMP VALUES

?2 1000. 1300.

IDENTIFY THE PHASE BY 1,2, OR 3, AND THEN THE INPUT FILE

?1 12

T= 1000.000	-13.15499973	-4.58699989	.00000000	.00000000
	.00000000	.00000000	.00000000	.00000000

T= 1300.000	-9.55640316	-3.27716827	.00000000	.00000000
	.00000000	.00000000	.00000000	.00000000

ENTER THE NUMBER FOR ANOTHER PHASE IF THERE IS ONE

?2

T= 1000.000	-.54625499	7.34729958	14.45289993	7.56354046
	.00000000	.00000000	.00000000	.00000000

T= 1300.000	-.71263057	6.32502937	12.58726501	6.53587532
	.00000000	.00000000	.00000000	.00000000

ENTER THE NUMBER FOR ANOTHER PHASE IF THERE IS ONE

?1

T= 1000.000	-97.48410034	-129.79849243	14.45289993	7.56354046
	.00000000	170.00000000	.00000000	.00000000

T= 1300.000	-97.65046692	-130.82075500	12.58726501	6.53587532
	.00000000	170.00000000	.00000000	.00000000

ENTER THE NUMBER FOR ANOTHER PHASE IF THERE IS ONE

?

IN GNN, ENTER 9 OPT VALUES 9 1 0 0 0 0 0 0 0

?8 5

IOP(7)= 0 ENTER TEMP. AND MOLE FRACTION

?1300. .08

.000000	-8.239993	-578.357178	-6.974330	-3.701484
.08000?	.00000=ACTIVITY OF	.00000	.84872E-08	-.18585E 02
.92000?	.00020=ACTIVITY OF	.00018	.18294E-03	

Table 11

Use of subroutine CLM

A. Redlich-Kister coefficients for the Fe-C liquid system.

!EDIT BSTEEL

EDIT HERE

*TY 1-6

1.000 -3.79379 -.655295 .629251

2.000 -24280. 4696. 0.

3.000 0.

4.000 0.

5.000 0.

6.000 0.

*END

!SET F:13 DC/BSTEEL;IN

!LMPD.

OPTIONS?

?1791

0 ENTER NUMBER OF TEMPERATURES, AND N TEMP VALUES

?4 1000. 1573. 1773.

IDENTIFY THE PHASE BY 1,2, OR 3, AND THEN THE INPUT FILE

?1 13

T=	1000.000	-3.79378986	-.65529501	.62925100	.00000000
		.00000000	.00000000	.00000000	.00000000

T=	1573.000	-1.86082745	-1.02914905	.62925100	.00000000
		.00000000	.00000000	.00000000	.00000000

T=	1773.000	-1.48029613	-1.10274792	.62925100	.00000000
		.00000000	.00000000	.00000000	.00000000

T=	1973.000	-1.17591231	-1.16142464	.62925100	.00000000
		.00000000	.00000000	.00000000	.00000000

ENTER THE NUMBER FOR ANOTHER PHASE IF THERE IS ONE

?

Table 11 B

Use of CLM to find the solubility of carbon in liquid iron

```

IN GNN, ENTER 9 I0PT VALUES   9   1   0   0   0   0   0   0   0
?8 5
I0P(7)= 0 ENTER TEMP. AND MOLE FRACTION
?1773. .8
      .000000   -2.471651   -1.776355   -.098866   -1.136867
      .80000?   .79640=ACTIVITY 0F   .63712   .63712E 00   -.45079E 00
      .20000?   .07297=ACTIVITY 0F   .01459   .14594E-01
?
5 YOU ARE IN CLM, ENTER KZZ VALUES TO CONTROL ACTIONS
?4
1 ENTER TEMPERATURE, ACTIVITY, AND INTEGERS
?1773. .01781\011
      .954902E 00 MINIMUM AT X =   .06324393   .97270316
      .978954E 00 MAXIMUM AT X =   .18828118   .99675554
ROOT BETWEEN
      .78665538   .78665686 AT T =   1773.000
      .000000   -2.505487   -1.743021   -.114038   -1.078630
      .78666?   .76906=ACTIVITY 0F   .60499   .60499E 00   -.50255E 00
      .21334?   .08344=ACTIVITY 0F   .01780   .17801E-01
1 ENTER TEMPERATURE, ACTIVITY, AND INTEGERS
?1573. .00722598 1
?.7
ROOT BETWEEN
      .81015253   .81015301 AT T =   1573.000
      .000000   -2.659728   -2.162739   -.095862   -1.419507
      .81015?   .80193=ACTIVITY 0F   .64969   .64969E 00   -.43126E 00
      .18985?   .03806=ACTIVITY 0F   .00723   .72260E-02
1 ENTER TEMPERATURE, ACTIVITY, AND INTEGERS

```

Table 12

Examples using subroutine ALTNT

```

!C BETA
-.3966 2.4039 5.5772 -.5137 -1.76 1.76 4.4
0 0 14458.3 -23002.6 0 0 0
0.
0.
0.
0.
-3.25
-9151.2
0.
0.
0.
0.
END
0 0 1

!SET F:13 DC/BETA;IN

!LMPD.
OPTIONS?
?17910002
  0 ENTER NUMBER OF TEMPERATURES, AND N TEMP VALUES
?15 1000. 1840. 1860.
?
IDENTIFY THE PHASE BY 1,2, OR 3, AND THEN THE INPUT FILE
?1 13
ENTER THE NUMBER FOR ANOTHER PHASE IF THERE IS ONE
?2
ENTER THE NUMBER FOR ANOTHER PHASE IF THERE IS ONE
?
IN GVN, ENTER 9 IOPT VALUES   9   1   0   0   0   2   0   2   0
?0 7
ENTER TEMPERATURE AND A CONTROL INTEGER
?1900.
ENTER TWO EQUILIBRIUM CONSTANTS
?709.655 .977530 1
  .957980
WILL YOU ACCEPT GAMMA OF   .498214E-02 .812682E-05 .116097E-04
?1
  .975949
  .976290
  .000000   -1.303731   4.500839   -1.145223   .017726
  .000000   -2.302638   -2.302638   -2.296866   -.000004
  .062757   .071577 GIVES ACTIVITY IN PHASE 1 OF   .004492   .44919
4E-02
  .937243   1.041660 GIVES ACTIVITY IN PHASE 1 OF   .976289   .97628
9E 00
  .001254   .005043 GIVES ACTIVITY IN PHASE 2 OF   .000006   .63297
5E-05
  .998746   .999992 GIVES ACTIVITY IN PHASE 2 OF   .998738   .99873
3E 00

```


Table 12 (continued)

ENTER TEMPERATURE AND A CONTROL INTEGER

?1920.

ENTER TWO EQUILIBRIUM CONSTANTS

?696.351 .983015 1

.963355

.981640

.981971

.000000 -1.287062 5.572361 -1.152577 .016062

.000000 -2.291673 -2.291673 -2.286860 -.000003

.053685 .070376 GIVES ACTIVITY IN PHASE 1 OF .003778 .37781

5E-02

.946315 1.037675 GIVES ACTIVITY IN PHASE 1 OF .981967 .98196

7E 00

.001050 .005166 GIVES ACTIVITY IN PHASE 2 OF .000005 .54256

5E-05

.998950 .999994 GIVES ACTIVITY IN PHASE 2 OF .998944 .99894

4E 00

ENTER TEMPERATURE AND A CONTROL INTEGER

?1920.

ENTER TWO EQUILIBRIUM CONSTANTS

?696.351 .983015 1 '1

? .9989

.981934

.981977

.053677 .070379 GIVES ACTIVITY IN PHASE 1 OF .003778 .37777

6E-02

.946323 1.037672 GIVES ACTIVITY IN PHASE 1 OF .981972 .98197

2E 00

.001050 .005166 GIVES ACTIVITY IN PHASE 2 OF .000005 .54250

8E-05

.998950 .999994 GIVES ACTIVITY IN PHASE 2 OF .998944 .99894

4E 00

ENTER TEMPERATURE AND A CONTROL INTEGER

?1920.

ENTER TWO EQUILIBRIUM CONSTANTS

? .00143606 1.017278

.963355

.981640

.981971

.000000 -1.287062 5.572361 -1.152577 .016062

.000000 -2.291673 -2.291673 -2.286860 -.000003

.053685 .070376 GIVES ACTIVITY IN PHASE 1 OF .003778 .37781

5E-02

.946315 1.037675 GIVES ACTIVITY IN PHASE 1 OF .981967 .98196

7E 00

.001050 .005166 GIVES ACTIVITY IN PHASE 2 OF .000005 .54256

Table 12 (continued)

6E-05

.998950 .999994 GIVES ACTIVITY IN PHASE 2 OF .998944 .99894

4E 00

ENTER TEMPERATURE AND A CONTROL INTEGER

?1960.

ENTER TWO EQUILIBRIUM CONSTANTS

?671.606 .994233 1

.974349

.993223

.993653

.000000 -.665728 14.465683 -.653675 .001196

.000000 -2.270414 -2.270414 -2.267885 -.000001

.99367 8

.990966 COMP. 2 AT T = 1960.0000.1002725E 01.9936778E 00

.000000 -.664044 14.482361 -.652101 .001182

.00903? .22279=ACTIVITY OF .00201 .20126E-02 -.62083E 01

.99097? 1.00272=ACTIVITY OF .99367 .99367E 00

.000555 COMP. 1 AT T = 1960.0000.5396448E-02.2996723E-05

.000000 -2.270414 -2.270414 -2.267893 -.000001

.00056? .00540=ACTIVITY OF .00000 .29967E-05 -.12718E 02

.99944? 1.00000=ACTIVITY OF .99944 .99944E 00

.0053964SHALL WE CONTINUE?

?1

.993679

.009013 .223068 GIVES ACTIVITY IN PHASE 1 OF .002011 .20105

4E-02

.990987 1.002713 GIVES ACTIVITY IN PHASE 1 OF .993676 .99367

6E 00

.000555 .005396 GIVES ACTIVITY IN PHASE 2 OF .000003 .29936

3E-05

.999445 .999998 GIVES ACTIVITY IN PHASE 2 OF .999444 .99944

4E 00

ENTER TEMPERATURE AND A CONTROL INTEGER

?

Table 13

Input thermodynamic data for iron, nickel, and carbon.

```

!C FENIC
C(GRAPHITE)
5 1 1 3.03 2824. 2824.
2 5.18396 .00122208 -.529846E-6
NI(S)
2 1 1 10.77 5215. 5215.
2 7.86096 .00314322 -.35278E-5 .890841E-9
FE(GAMMA)
3 1 1 10.025 6789. 6789.
2 7.73018 .0020027 -.416124E-8
FE(ALPHA)
4 1 1 10.123 5820. 5928.
2 13.2341 -.0253213 .486523E-4 -.272654E-7
FE(L)(JANAF)
3 2 1 11.7639 6134. 9272.
2 10.1877 .37823E-3 .139724E-7
C IN FE GAMMA
1 1 1 7.274 2824. 13376.
2 5.18396 .00122208 -.529846E-6
C IN FE(L)
1 2 1 7.03 2824. 8245.
2 5.18396 .00122208 -.529846E-6
NI(L)
2 2 1 12.1700 5215. 8060.5
2 10.30
C,GRAPHITE,JANAF
6 1 1 3.020 2824. 2824.
2 5.15465 .00159627 -.13423E-5 .45542E-9
C(L) IN FE(L) XC=1
5 2 1 -23.0722 2824. 12457.7
2 5.15465 .00159627 -.13423E-5 .45542E-9
C(L) IN FE(L) X=0
4 2 1 7.001 2824. 8224.
2 5.15465 .00159627 -.13423E-5 .45542E-9
END
0 0 1

```

Table 14

Input file for the calculation of Redlich-Kister coefficients for the nickel-carbon system.

!QUIT

!BUILD BENIC

1.000	5.5121	-3.
2.000	13323.	0.
3.000	0.	
4.000	0.	
5.000	0.	
6.000	0.	
7.000	-2.7448	.0162
8.000	-17705.	0.
9.000	0.	
10.000	0.	
11.000	0.	
12.000	0.	
13.000		

!SET F:12 DC/BENIC;IN

Table 15

Calculation of Redlich-Kister coefficients for the liquid Ni-C system.

!LMPD.

ØPTIONS?

?1791

0 ENTER NUMBER ØF TEMPERATURES, AND N TEMP VALUES

?4 1000. 1773. 1573. 1973.

IDENTIFY THE PHASE BY 1,2, ØR 3, AND THEN THE INPUT FILE

?1 12

T=	1000.000	5.51210022	-3.00000000	.00000000	.00000000
		.00000000	.00000000	.00000000	.00000000
T=	1773.000	4.24215603	-3.00000000	.00000000	.00000000
		.00000000	.00000000	.00000000	.00000000
T=	1573.000	4.45104122	-3.00000000	.00000000	.00000000
		.00000000	.00000000	.00000000	.00000000
T=	1973.000	4.07561970	-3.00000000	.00000000	.00000000
		.00000000	.00000000	.00000000	.00000000

ENTER THE NUMBER FØR ANØTHER PHASE IF THERE IS ØNE

?2

T=	1000.000	-2.74479961	.01620000	.00000000	.00000000
		.00000000	.00000000	.00000000	.00000000
T=	1773.000	-1.05779743	.01620000	.00000000	.00000000
		.00000000	.00000000	.00000000	.00000000
T=	1573.000	-1.33528137	.01620000	.00000000	.00000000
		.00000000	.00000000	.00000000	.00000000
T=	1973.000	-.83656979	.01620000	.00000000	.00000000
		.00000000	.00000000	.00000000	.00000000

ENTER THE NUMBER FØR ANØTHER PHASE IF THERE IS ØNE

?

Table 16

Calculation of equilibrium constants for the melting of C and Ni

!SET F:13 /FENIC;IN

!LMPD.

OPTIONS?

?17920004

0 ENTER NUMBER OF TEMPERATURES, AND N TEMP VALUES

?11 1000. 1600. 1620.

IDENTIFY THE INPUT FILE

?13

ENTER IDATA FOR FILE TO BE REWOUND, IT IS NOW ###

?13

IN GNN, ENTER 9 IPT VALUES 9 2 0 0 0 4 0 4 0

?7
ENTER THE NUMBER OF PHASES AND IPT(9)

?2 5

ENTER ICOMP, IPHASE, AND THEN 10 VALUES FOR PHI

?

ENTER THE COEFFICIENTS AND THEN THE H0298 VALUES, PHASE 1

?0. 0. 0. 0. 0. -1.

ENTER THE COEFFICIENTS AND THEN THE H0298 VALUES, PHASE 2

?0. 0. 0. 0. 1.

AT 1600.00K, KEQ = .826935E-02 .249830E 05 .152462E 05

AT 1620.00K, KEQ = .911174E-02 .249830E 05 .151245E 05

AT 1640.00K, KEQ = .100162E-01 .249830E 05 .150028E 05

AT 1660.00K, KEQ = .109854E-01 .249830E 05 .148811E 05

AT 1680.00K, KEQ = .120219E-01 .249830E 05 .147594E 05

AT 1700.00K, KEQ = .131283E-01 .249830E 05 .146377E 05

AT 1720.00K, KEQ = .143072E-01 .249830E 05 .145159E 05

AT 1740.00K, KEQ = .155611E-01 .249830E 05 .143942E 05

AT 1760.00K, KEQ = .168927E-01 .249830E 05 .142725E 05

AT 1780.00K, KEQ = .183045E-01 .249830E 05 .141508E 05

0 DO YOU WANT TO CALCULATE KEQ AT OTHER TEMPERATURES?

?

IN GNN, ENTER 9 IPT VALUES 7 0 0 0 0 0 0 0 5

?9 2 C 0 0 4

0 ENTER NUMBER OF TEMPERATURES, AND N TEMP VALUES

?11 1000. 1600. 1620.

IDENTIFY THE INPUT FILE

?13

ENTER IDATA FOR FILE TO BE REWOUND, IT IS NOW 13

?13

IN GNN, ENTER 9 IPT VALUES 9 2 0 0 0 4 0 0 0

?7
ENTER THE NUMBER OF PHASES AND IPT(9)

?2 5

ENTER ICOMP, IPHASE, AND THEN 10 VALUES FOR PHI

?

ENTER THE COEFFICIENTS AND THEN THE H0298 VALUES, PHASE 1

?0. -1.

ENTER THE COEFFICIENTS AND THEN THE H0298 VALUES, PHASE 2

?0. 1.

AT 1600.00K, KEQ = .910820E 00 .396829E 04 .296995E 03

AT 1620.00K, KEQ = .925022E 00 .400093E 04 .250899E 03

AT 1640.00K, KEQ = .939206E 00 .403366E 04 .204405E 03

AT 1660.00K, KEQ = .953375E 00 .406650E 04 .157505E 03

Table 16 (continued)

```

AT 1630.00K, KEQ = .967525E 00 .409948E 04 .110216E 03
AT 1700.00K, KEQ = .931663E 00 .413262E 04 .625222E 02
AT 1720.00K, KEQ = .995782E 00 .416596E 04 .144458E 02
AT 1740.00K, KEQ = .100989E 01 .419952E 04-.340234E 02
AT 1760.00K, KEQ = .102398E 01 .423332E 04-.828755E 02
AT 1780.00K, KEQ = .103806E 01 .426740E 04-.132121E 03
O DO YOU WANT TO CALCULATE KEQ AT OTHER TEMPERATURES?
?
IN GVV, ENTER 9 IOPT VALUES 9 2 0 0 0 3 0 5 0
?7
ENTER THE NUMBER OF PHASES AND IOPT(9)
?2
ENTER ICOMP, IPHASE, AND THEN 7 VALUES FOR PHI
?
ENTER THE COEFFICIENTS AND THEN THE H0293 VALUES, PHASE 1
?0 -1.
ENTER THE COEFFICIENTS AND THEN THE H0293 VALUES, PHASE 2
?0 1.
AT 1560.00K, KEQ = .882366E 00 .390312E 04 .387957E 03
AT 1600.00K, KEQ = .910820E 00 .396829E 04 .296295E 03
AT 1640.00K, KEQ = .939206E 00 .403366E 04 .204405E 03
AT 1680.00K, KEQ = .967525E 00 .409948E 04 .110216E 03
AT 1720.00K, KEQ = .995782E 00 .416596E 04 .144458E 02
AT 1760.00K, KEQ = .102398E 01 .423332E 04-.828755E 02
AT 1800.00K, KEQ = .105212E 01 .430177E 04-.181745E 03
O DO YOU WANT TO CALCULATE KEQ AT OTHER TEMPERATURES?
?1
ENTER ONE OR MORE TEMPERATURE
?1730. 1740. -100.
AT 1730.00K, KEQ = .100234E 01 .418280E 04-.975000E 01
AT 1740.00K, KEQ = .100989E 01 .419964E 04-.340352E 02
ENTER ONE OR MORE TEMPERATURE
?1726. 1727. 1728. 1728. -10.
AT 1726.00K, KEQ = .100002E 01 .417606E 04-.585937E-01
AT 1727.00K, KEQ = .100072E 01 .417775E 04-.247974E 01
AT 1728.00K, KEQ = .100143E 01 .417943E 04-.490161E 01
AT 1728.00K, KEQ = .100143E 01 .417943E 04-.490161E 01
ENTER ONE OR MORE TEMPERATURE
?1725. -10.
AT 1725.00K, KEQ = .999312E 00 .417438E 04 .236011E 01
ENTER ONE OR MORE TEMPERATURE
?1725.8 1725.9 1726. -10.
AT 1725.80K, KEQ = .999876E 00 .417573E 04 .424072E 00
AT 1725.90K, KEQ = .999946E 00 .417589E 04 .133838E 00
AT 1726.00K, KEQ = .100002E 01 .417606E 04-.585937E-01
ENTER ONE OR MORE TEMPERATURE
?1725.97
AT 1725.97K, KEQ = .999996E 00 .417601E 04 .124512E-01
IN GVV, ENTER 9 IOPT VALUES 7 0 0 0 0 0 3 0 5
?
SORRY, NO OTHER SYSTEMS ARE AVAILABLE YET
DO YOU WANT TO CONTINUE? USE 1 FOR YES
?
*STOP* 0

!BYE
PLEASE HANG UP PHONE- CONNECT TIME WILL BE CHARGED!!

CPU = .0599 CON = :15 INT = 33 CHG = $.61

```

Table 17

Solubility of graphite in solid nickel.

```

!SET F:12 DC/BENIC;IN

!LMPD.
OPTIØNS?
?17910002
  0 ENTER NUMBER ØF TEMPERATURES, AND N TEMP VALUES
?8 1000. 1300. 1350.
IDENTIFY THE PHASE BY 1,2, ØR 3, AND THEN THE INPUT FILE
?1 12
ENTER THE NUMBER FØR ANØTHER PHASE IF THERE IS ØNE
?
IN GNN, ENTER 9 IØPT VALUES   9   1   0   0   0   2   0   2   0
?8 6
  2 YØU ARE IN CLM, ENTER KZZ VALUES TØ CØNTRØL ACTIØNS
?1
WHICH CØMPØNENT? ENTER HC(J),J=1,4, NØW:##### .00
?0. 1.
  1 ENTER TEMPERATURE, ACTIVITY, AND INTEGERS
?1550. 1. 1
?.9
RØØT BETWEEN
.97832537 .97832584 AT T = 1550.000
.000000 -4.261386 1.738614 -.002002 1.664063
.97833? .99540=ACTIVITY ØF .97383 .97383E 00 -.26523E-01
.02167? 46.13832=ACTIVITY ØF 1.00003 .10000E 01
  1 ENTER TEMPERATURE, ACTIVITY, AND INTEGERS
?1500. 1. 1
?.9
RØØT BETWEEN
.98038864 .98038912 AT T = 1500.000
.000000 -4.223504 1.776496 -.001624 1.707500
.98039? .99627=ACTIVITY ØF .97573 .97573E 00 -.23546E-01
.01961? 50.99162=ACTIVITY ØF 1.00001 .10000E 01
  1 ENTER TEMPERATURE, ACTIVITY, AND INTEGERS
?1450. 1. 1
?.9
RØØT BETWEEN
.98244143 .98244190 AT T = 1450.000
.000000 -4.181175 1.818824 -.001289 1.755512
.98244? .99704=ACTIVITY ØF .97953 .97953E 00 -.20683E-01
.01756? 56.95239=ACTIVITY ØF 1.00000 .10000E 01
  1 ENTER TEMPERATURE, ACTIVITY, AND INTEGERS
?

```

Table 18

Solubility of graphite in liquid nickel.

!LMPD.

2PTIONS?

?17910002

C ENTER NUMBER OF TEMPERATURES, AND N TEMP VALUES

?11 1000. 1530. 1530.

IDENTIFY THE PHASE BY 1, 2, OR 3, AND THEN THE INPUT FILE

?1 12

ENTER THE NUMBER FOR ANOTHER PHASE IF THERE IS ONE

?2

ENTER THE NUMBER FOR ANOTHER PHASE IF THERE IS ONE

?

IN GNN, ENTER 9, 10PT VALUES 9 1 0 0 0 2 0 2 0

?1\8 6

2 YOU ARE IN CLM, ENTER KZZ VALUES TO CONTROL ACTIONS

?4

1 2ENTER TEMPERATURE, ACTIVITY, AND INTEGERS

?1600. .00826935

ROOT BETWEEN

.906287 .906287 AT T = 1600.000

.000000 -1.251243 -1.283643 -.010989 -1.054327

.90629? .97502=ACTIVITY OF .88364 .88364E 00 -.12370E 00

.09371? .08824=ACTIVITY OF .00827 .82694E-02

1 2ENTER TEMPERATURE, ACTIVITY, AND INTEGERS

?1620. .00911174

ROOT BETWEEN

.903693 .903694 AT T = 1620.000

.000000 -1.221555 -1.253954 -.011330 -1.024055

.90369? .97425=ACTIVITY OF .88042 .88042E 00 -.12735E 00

.09631? .09461=ACTIVITY OF .00911 .91117E-02

1 2ENTER TEMPERATURE, ACTIVITY, AND INTEGERS

?1640. .0100162

ROOT BETWEEN

.901073 .901073 AT T = 1640.000

.000000 -1.192596 -1.224997 -.011672 -.994613

.90107? .97348=ACTIVITY OF .87718 .87718E 00 -.13104E 00

.09893? .10125=ACTIVITY OF .01002 .10016E-01

1 2ENTER TEMPERATURE, ACTIVITY, AND INTEGERS

?1700. .0131283

ROOT BETWEEN

.893048 .893049 AT T = 1700.000

.000000 -1.109843 -1.142243 -.012695 -.910979

.89305? .97119=ACTIVITY OF .86732 .86732E 00 -.14235E 00

.10695? .12275=ACTIVITY OF .01313 .13128E-01

1 2ENTER TEMPERATURE, ACTIVITY, AND INTEGERS

?1740. .0155611

ROOT BETWEEN

.887560 .887561 AT T = 1740.000

.000000 -1.057874 -1.090274 -.013374 -.858878

.88756? .96967=ACTIVITY OF .86064 .86064E 00 -.15007E 00

.11244? .13840=ACTIVITY OF .01556 .15561E-01

1 2ENTER TEMPERATURE, ACTIVITY, AND INTEGERS

?1573. .00722598

ROOT BETWEEN

.909737 .909737 AT T = 1573.000

.000000 -1.292620 -1.325020 -.010532 -1.096613

Table 18 (continued)

```

.90974?      .97604=ACTIVITY 0F      .88794      .88794E 00 - .11885E 00
.09026?      .08005=ACTIVITY 0F      .00723      .72260E-02
1 2ENTER TEMPERATURE, ACTIVITY, AND INTEGERS
?
IN GNN, ENTER 9 10PT VALUES      8 6 0 0 0 2 0 3 0
79 2 0 0 0 4
0 ENTER NUMBER OF TEMPERATURES, AND N TEMP VALUES
?
IDENTIFY THE INPUT FILE
?13
78 5
10P(7)= 0 ENTER TEMP. AND MOLE FRACTION
?1773. .9
.000000      -1.015677      -1.048077      -.010157      -.848942
.90000?      .97688=ACTIVITY 0F      .87920      .87920E 00 - .12875E 00
.10000?      .14160=ACTIVITY 0F      .01416      .14160E-01
?
5 YOU ARE IN CLM, ENTER KZZ VALUES TO CONTROL ACTIONS
?4
1 1ENTER TEMPERATURE, ACTIVITY, AND INTEGERS
?1773. .0173011 1
?.7
ROOT BETWEEN
.882946 .882947 AT T = 1773.000
.000000      -1.016782      -1.049182      -.013931      -.817936
.88295?      .96843=ACTIVITY 0F      .85507      .85507E 00 - .15657E 00
.11705?      .15208=ACTIVITY 0F      .01780      .17801E-01
1 1ENTER TEMPERATURE, ACTIVITY, AND INTEGERS
?1573. .00722598 1
?.7
ROOT BETWEEN
.909747 .909748 AT T = 1573.000
.000000      -1.292529      -1.324929      -.010528      -1.096563
.90975?      .97605=ACTIVITY 0F      .88796      .88796E 00 - .11883E 00
.09025?      .08006=ACTIVITY 0F      .00723      .72260E-02
1 1ENTER TEMPERATURE, ACTIVITY, AND INTEGERS
?1773. .0365270 1
?.7
ROOT BETWEEN
.816176 .816176 AT T = 1773.000
.000000      -1.021109      -1.053509      -.034505      -.701788
.81618?      .92362=ACTIVITY 0F      .75384      .75384E 00 - .28257E 00
.18382?      .19871=ACTIVITY 0F      .03653      .36527E-01
1 1ENTER TEMPERATURE, ACTIVITY, AND INTEGERS
?
IN GNN, ENTER 9 10PT VALUES      8 5 0 0 0 2 0 3 0
ENTER THE COEFFICIENTS AND THEN THE H0298 VALUES, PHASE 1
?0 0 0 0 0 -1.
ENTER THE COEFFICIENTS AND THEN THE H0298 VALUES, PHASE 2
?0 0 0 0 1.
AT 1560.00K, KEQ = .676038E-02 .249830E 05 .154896E 05
AT 1580.00K, KEQ = .748111E-02 .249830E 05 .153679E 05
AT 1600.00K, KEQ = .826935E-02 .249830E 05 .152462E 05
AT 1620.00K, KEQ = .911174E-02 .249830E 05 .151245E 05
AT 1640.00K, KEQ = .100162E-01 .249830E 05 .150028E 05
AT 1660.00K, KEQ = .109854E-01 .249830E 05 .148811E 05
AT 1680.00K, KEQ = .120219E-01 .249830E 05 .147594E 05

```

Table 19

Finding equilibrium compositions for solid and liquid phases in equilibrium with each other in the Ni-C system using subroutine ALTNT.

```

!SET F:12 /BNIC;IN

!SET F:13 DC/FENIC;IN

.LMPD.
OPTI0NS?
?17910002
  0 ENTER NUMBER 0F TEMPERATURES, AND N TEMP VALUES
?1000. 1973. 1580.-
  11 1000. 1973. 1580. 1600.
IDENTIFY THE PHASE BY 1,2, 0R 3, AND THEN THE INPUT FILE
?1 12
ENTER THE NUMBER FOR AN0THER PHASE IF THERE IS 0NE
?2
ENTER THE NUMBER FOR AN0THER PHASE IF THERE IS 0NE
?
IN GNN, ENTER 9 I0PT VALUES   9   1   0   0   0   2   0   2   0
?8 5
I0P(7)= 0 ENTER TEMP. AND M0LE FRACTI0N
?1600. .9
      .000000   -1.251651   -1.284050   -.012517   -1.040080
      .90000?   .97159=ACTIVITY 0F   .87443   .87443E 00   -.13418E 00
      .10000?   .09118=ACTIVITY 0F   .00912   .91184E-02
?
  5 YOU ARE IN CLM, ENTER KZZ VALUES T0 C0NTR0L ACTI0NS
?4
  1 2ENTER TEMPERATURE, ACTIVITY, AND INTEGERS
?1973. .0365270
R00T BETWEEN
.853199 .853200 AT T = 1973.000
      .000000   -.797482   -.829882   -.017186   -.604112
      .85320?   .96120=ACTIVITY 0F   .82010   .82010E 00   -.19833E 00
      .14680?   .24882=ACTIVITY 0F   .03653   .36527E-01
  1 2ENTER TEMPERATURE, ACTIVITY, AND INTEGERS
?
IN GNN, ENTER 9 I0PT VALUES   8   5   0   0   0   2   0   3   0
?0 7 9
ENTER TEMPERATURE AND A C0NTR0L INTEGER
?1600.
ENTER TW0 EQUILIBRIUM C0NSTANTS
?.91082 .00826935 0 1
?..011

F0RTRAN RUN-TIME ERR0R IN '9BCDREAD' CALLED AT L2C X'17445'.
..011
\
ILLEGAL NUMERIC INPUT CHARACTER. FIELD TERMINATED.

      .000000
      .718277
      .924686
      .975248
      .9754385SHALL WE C0NTINUE?

```


Table 19 (continued)

?1

.937241
 .990061
 .990845
 .991025
 .9753107 SHALL WE CONTINUE?

?1

.991100
 .991130
 .976413 .994510 GIVES ACTIVITY IN PHASE 1 OF .971053 .97105

3E 00

.023537 42.019943 GIVES ACTIVITY IN PHASE 1 OF .991126 .99112

6E 00

.906845 .975309 GIVES ACTIVITY IN PHASE 2 OF .884454 .88445

4E 00

.093155 .087984 GIVES ACTIVITY IN PHASE 2 OF .008196 .81961

0E-02

ENTER TEMPERATURE AND A CONTROL INTEGER

?1520.

ENTER TWO EQUILIBRIUM CONSTANTS

?.925022 .00911174 0 1

?.008

.877988
 .801761
 .783949
 .779757
 .9816904 SHALL WE CONTINUE?

?1

.778661
 .778413
 .778322
 .778289
 .9817030 SHALL WE CONTINUE?

?1

.778277
 .979407 .995756 GIVES ACTIVITY IN PHASE 1 OF .975250 .97525

0E 00

.020593 37.792480 GIVES ACTIVITY IN PHASE 1 OF .778276 .77827

6E 00

.918941 .981703 GIVES ACTIVITY IN PHASE 2 OF .902127 .90212

7E 00

.081059 .087484 GIVES ACTIVITY IN PHASE 2 OF .007091 .70914

1E-02

ENTER TEMPERATURE AND A CONTROL INTEGER

?1540.

ENTER TWO EQUILIBRIUM CONSTANTS

?.939206 .0100162 0 1

?.006

.599030
 .592666
 .591113
 .590761
 .9873246 SHALL WE CONTINUE?

?1

.590643
 .590603

Table 19 (continued)

	.590590						
2E 00	.982564	.996914	GIVES ACTIVITY IN PHASE	1 0F		.979532	.97953
2E 00	.017436	33.872269	GIVES ACTIVITY IN PHASE	1 0F		.590592	.59059
2E 00	.931791	.937327	GIVES ACTIVITY IN PHASE	2 0F		.919982	.91993
2E-02	.068209	.086725	GIVES ACTIVITY IN PHASE	2 0F		.005915	.59154
ENTER TEMPERATURE AND A CONTROL INTEGER							
?1660.							
ENTER TWO EQUILIBRIUM CONSTANTS							
?.953375 .0109354 0 1							
?.005							
	.455149						
	.432325						
	.426674						
	.425355						
?1	.9920924	SHALL WE CONTINUE?					
	.424953						
	.424832						
	.424793						
	.424782						
?1	.9920975	SHALL WE CONTINUE?					
	.424778						
3E 00	.935940	.997964	GIVES ACTIVITY IN PHASE	1 0F		.983933	.98393
0E 00	.014060	30.212734	GIVES ACTIVITY IN PHASE	1 0F		.424780	.42478
7E 00	.945529	.992097	GIVES ACTIVITY IN PHASE	2 0F		.938057	.93805
	.054471	.085667	GIVES ACTIVITY IN PHASE	2 0F		.004666	.46663
5E-02							
ENTER TEMPERATURE AND A CONTROL INTEGER							
?1680.							
ENTER TWO EQUILIBRIUM CONSTANTS							
?.967525 .0120219 0 1							
?.0035							
	.291135						
	.281376						
	.278996						
	.278322						
?1	.9959022	SHALL WE CONTINUE?					
	.278131						
	.278075						
	.278060						
6E 00	.989612	.998872	GIVES ACTIVITY IN PHASE	1 0F		.988496	.98849
8E 00	.010388	26.768448	GIVES ACTIVITY IN PHASE	1 0F		.278058	.27805
5E 00	.960328	.995904	GIVES ACTIVITY IN PHASE	2 0F		.956395	.95639
6E-02	.039672	.084260	GIVES ACTIVITY IN PHASE	2 0F		.003343	.33427

Table 19 (continued)

ENTER TEMPERATURE AND A CONTROL INTEGER

?1700.

ENTER TWO EQUILIBRIUM CONSTANTS

? .981663 .0131283 0 1

? .002

.152343

.149076

.148203

.147965

.9985899 SHALL WE CONTINUE?

?1

.147900

.147883

.147873

.993704

.999579 GIVES ACTIVITY IN PHASE 1 OF

.993286

.99328

6E 00

.006296

23.487122 GIVES ACTIVITY IN PHASE 1 OF

.147877

.14787

7E 00

.976443

.993590 GIVES ACTIVITY IN PHASE 2 OF

.975072

.97507

2E 00

.023552

.082429 GIVES ACTIVITY IN PHASE 2 OF

.001941

.19413

7E-02

ENTER TEMPERATURE AND A CONTROL INTEGER

?1720.

ENTER TWO EQUILIBRIUM CONSTANTS

? .995782 .0143072 0 1

? .001

.069395

.042338

.034918

.032833

.9999173 SHALL WE CONTINUE?

?1

.032329

.032175

.032133

.032121

.9999182 SHALL WE CONTINUE?

?1

.032118

.998418

.999973 GIVES ACTIVITY IN PHASE 1 OF

.998391

.99839

1E 00

.001532

20.305603 GIVES ACTIVITY IN PHASE 1 OF

.032118

.32117

9E-01

.994261

.999918 GIVES ACTIVITY IN PHASE 2 OF

.994180

.99418

0E 00

.005739

.080072 GIVES ACTIVITY IN PHASE 2 OF

.000460

.45951

9E-03

ENTER TEMPERATURE AND A CONTROL INTEGER

?

SORRY, NO OTHER SYSTEMS ARE AVAILABLE YET

DO YOU WANT TO CONTINUE? USE 1 FOR YES

?1

OPTIONS?

?17

IN GNN, ENTER 9. 12PT VALUES 1 7 0 0 0 0 0 0 0

?16

?1 2

Table 20.

Preliminary estimates of constants for the liquid $\text{KO}_{0.5} - \text{SiO}_2$ system.

Redlich-Kister coefficients			Bale-Pelton coefficients		
	$\log \gamma_{1000}$	enthalpy		$\log \gamma_{1000}$	enthalpy
A	-.3966	0	q_0	1.7391	1053
B	2.4089	0	q_1	2.8550	-3672
C	5.5772	3160	q_2	4.8077	2107
D	-.5137	-6120	q_3	.5767	-2448
E	-1.76	0	q_4	.9691	0
F	1.76	0	q_5	.2235	0
G	4.4	0	q_6	.3048	0

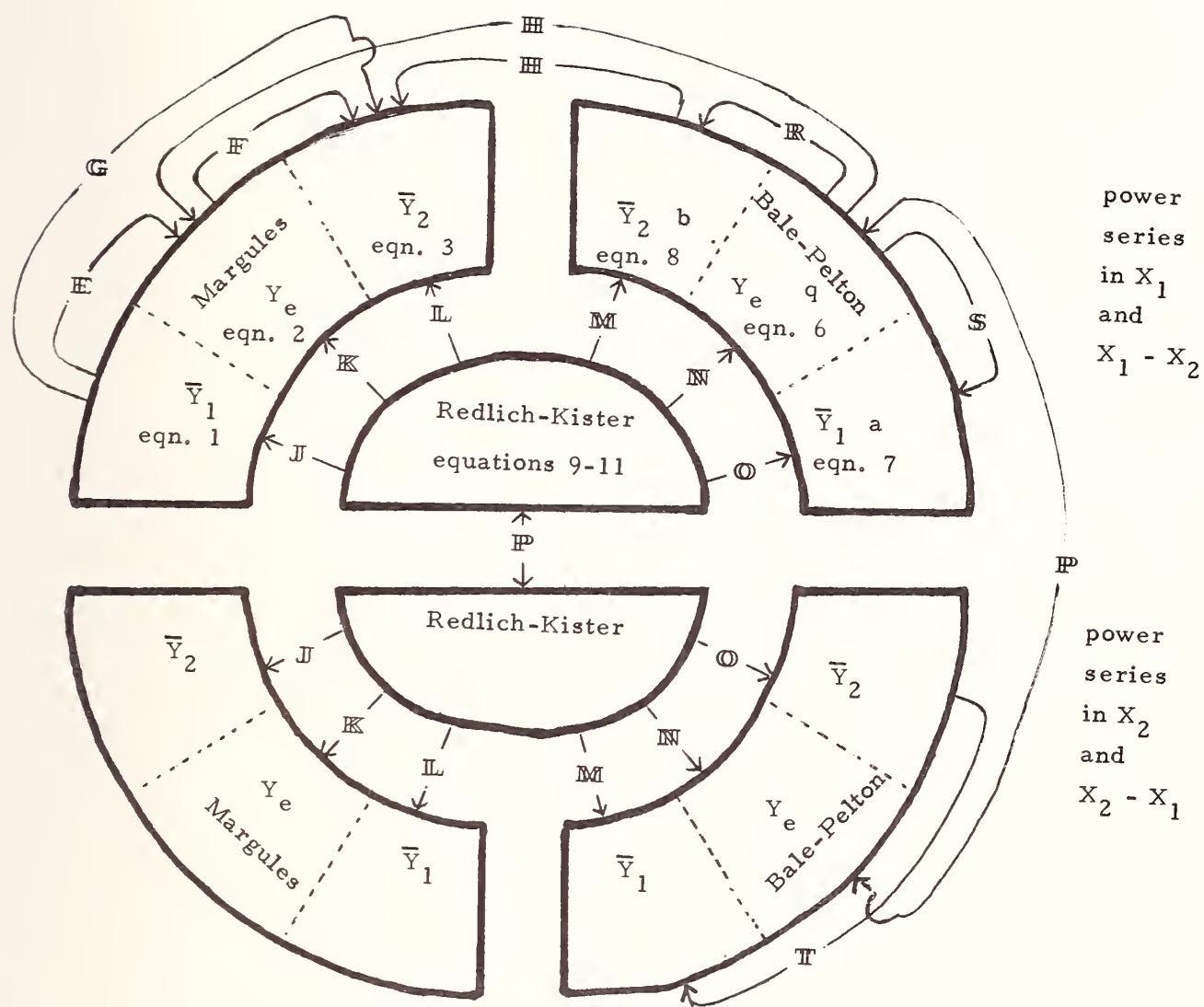


Figure 1

Diagram illustrating the relationships of conversion matrices between various sets of coefficients.

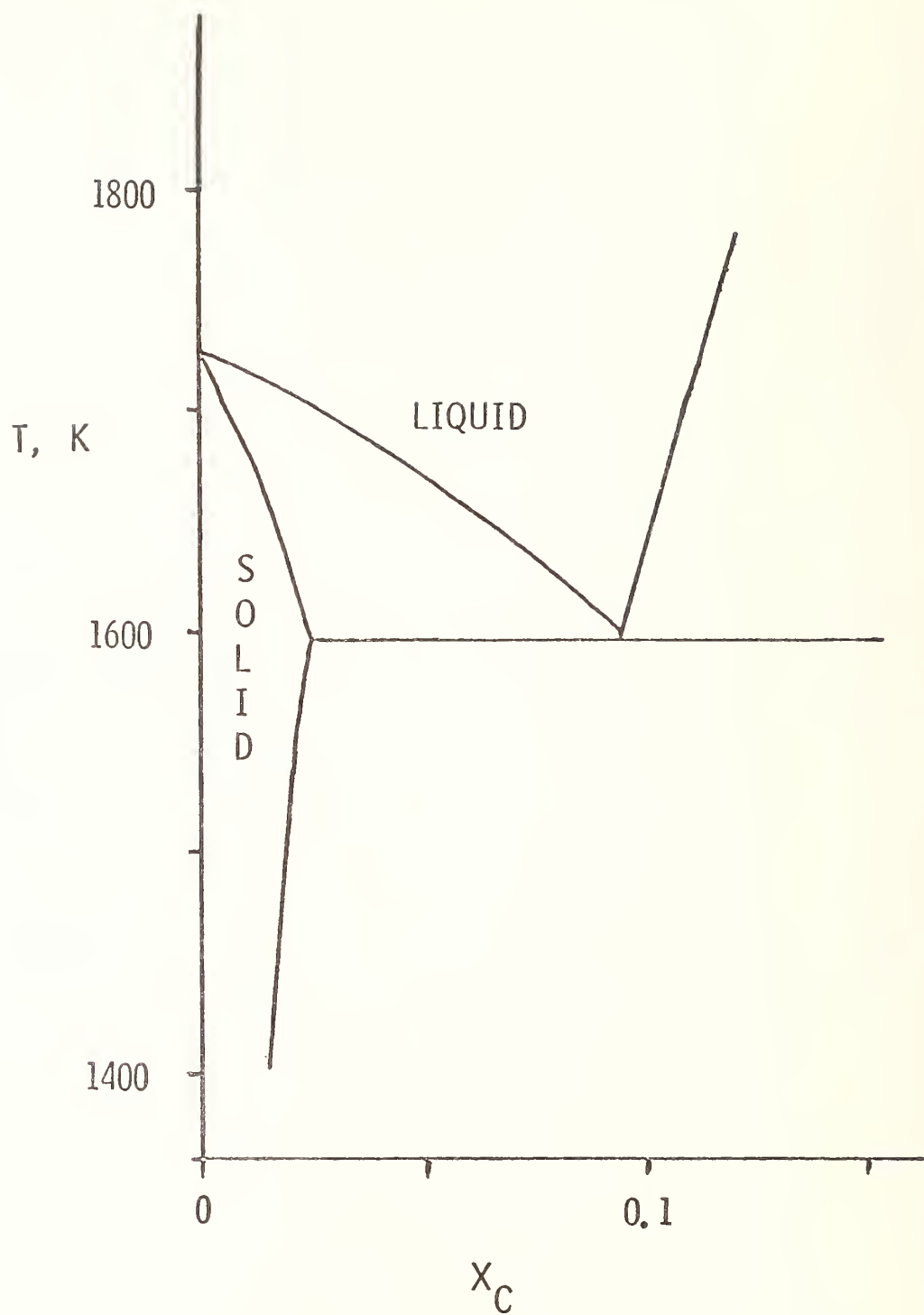


Figure 2

The nickel - carbon phase diagram

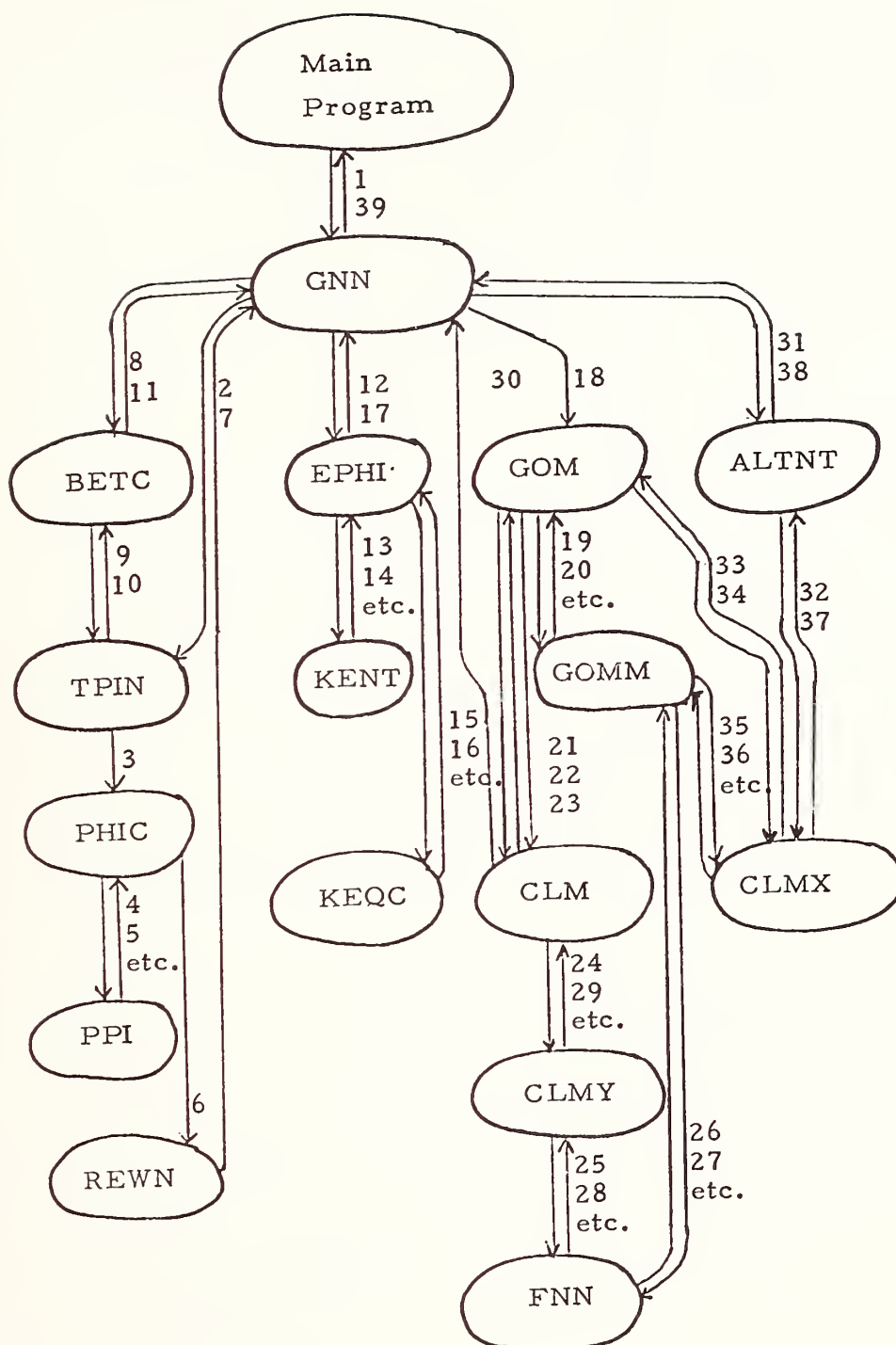


Figure 3

Flow chart of BPHD for some major calculations.

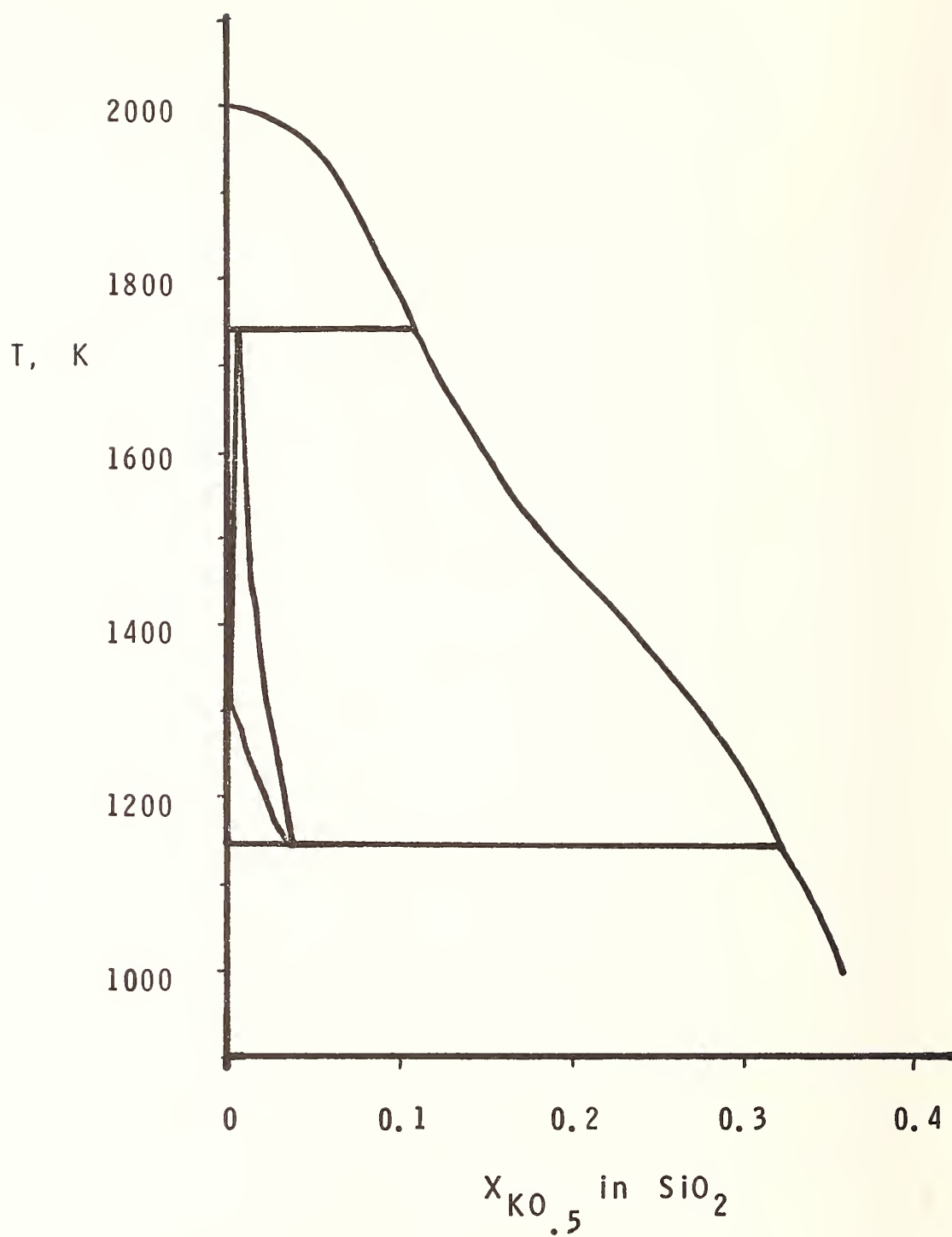


Figure 4. Calculated phase diagram for $\text{SiO}_2 - \text{KO}_{.5}$.



Polynomial Representation of the Excess Free Energy of Multicomponent Systems and their Use in Phase Diagram Calculations

H. Gaye
IRSID - PCM 57
Maizières - les - Metz
France

and

C. H. P. Lupis
Department of Metallurgy and Materials Science
Carnegie - Mellon University
Schenley Park, Pittsburgh, Pa. 15213

Various polynomial formalisms can be proposed for the representation of the excess free energy of multicomponent solutions:

- for the partial molar properties, the "interaction coefficients" approach provides polynomials in terms of solute mole fractions;
- for the integral excess free energy, symmetric expressions in terms of all mole fractions can be used.

An advantage of polynomial formalisms is that the coefficients can be mapped into one-dimensional arrays, so that the number of components and the order of the polynomials can easily remain unrestricted.

Several applications of these formalisms to the integration of the Gibbs-Duhem equation will be presented. To that effect, a new method of integration was derived. It is based upon the expressions:

$$\ln \gamma_1 = \frac{G^E}{RT} - \sum_{j=2}^m x_j \frac{\partial (G^E/RT)}{\partial x_j}$$
$$\ln \gamma_i = \ln \gamma_1 + \frac{\partial (G^E/RT)}{\partial x_i} \quad (\text{for } i = 2, 3, \dots, m)$$

The flexibility of polynomials has also been useful in the compilation and exploitation of the phase diagrams of oxide systems. Because many of the solid phases are stoichiometric, a relatively good picture of the diagrams can be derived from the knowledge of the liquidus surfaces. Representing them as polynomials:

$$T_{\text{liq}} = P(\text{composition})$$

allows simple interpolations and extrapolations and the calculation of crystallization paths. The example of blast furnace slags (in the system $\text{CaO-SiO}_2\text{-Al}_2\text{O}_3\text{-MgO}$) will be presented.



Thermodynamic Data for the Fe-O System
Evaluated Using a New Computer-Aided Strategy

John L. Haas, Jr. and James R. Fisher
National Center for the Thermodynamic Data of Minerals
U. S. Geological Survey
National Center, Stop 959
Reston, Virginia 22092

*This paper will describe the computational techniques
employed in evaluating the example given in this abstract*

Tables of thermodynamic properties and their confidence limits from 0 to 1800 K at one atm were obtained for the oxides wustite $\text{Fe}_{0.947}\text{O}$, magnetite Fe_3O_4 , and hematite Fe_2O_3 . In addition to reflecting the calorimetry accurately, the set is in better agreement with the known phase equilibria than previous sets. We evaluated the published experimental data for the phases and their interactions using the program PHAS20. PHAS20 is a weighted multiple regression routine which combines an empirical equation for the heat capacity with the functional relations among heat capacity, entropy, enthalpy, free energy, equilibrium constants, and electrochemical potentials for a group of chemically related phases. Confidence limits for the tabulated data were obtained from the program RECKON, using the same relations, the refined constants, the variances, and covariances, and statistical theory.

The results show that the thermodynamic tables for wustite cannot be significantly improved except by better data for the reported second-order composition- and temperature-dependent structural effects within the solid solution. The thermodynamic tables for hematite can be improved by better data on the solid solution limits for both hematite and magnetite as well as the effect of composition on the activity of the Fe_2O_3 and Fe_3O_4 components in the solid solutions. The thermodynamics of magnetite below 1000 K cannot be significantly improved through existing experimental techniques. There are no indications that magnetite and hematite have a residual entropy at the zero of absolute temperature due to internal disorder.



Analysis and Synthesis of Phase Diagrams of the Fe-Cr-Ni, Fe-Cu-Mn and Fe-Cu-Ni Systems.

Mitsuhiro Hasebe and Taiji Nishizawa

Department of Materials Science,
Faculty of Engineering,
Tohoku University, Sendai, Japan

Synopsis

The phase equilibria in the Fe-Cr-Ni, Fe-Cu-Mn and Fe-Cu-Ni systems were examined by microprobe analysis of ternary diffusion couples consisting of their components. The experimental data were analyzed thermodynamically using an extended regular solution model and the thermodynamic data on the binary systems concerned, and the thermodynamic parameters were evaluated by linear programming. The phase diagrams over a wide temperature range were synthesized by computer calculation on the basis of these parameters.

I. Introduction

Most of the previously published phase diagrams for alloy systems have been determined on the basis of the metallographic information alone. The way of constructing phase diagrams, however, requires a great deal of time, labor and materials, particularly in the case of multi-component systems. For this reason, the vacuum deposition of three kinds of metals from three corners⁽¹⁾ and the multi-component diffusion couple technique^{(2)~(4)} have been designed to obtain necessary data over a wide range of composition from one specimen.

Besides, remarkable progress has been made for the analysis and synthesis of the phase diagrams in recent years by means of computer calculation^{(5)~(7)}. It should be noted that this method permits the synthesis of the phase diagrams of real alloys over a wide range of temperature and composition by computation combined with thermodynamic analysis of the experimental data.

Following these lines of both experimental and theoretical approaches, we have made extensive work to establish the phase diagrams of the alloy systems composed of iron and first-row transition elements in the periodic table. In this paper, the phase diagrams of the Fe-Cr-

Ni, Fe-Cu-Mn and Fe-Cu-Ni systems are presented.

II. Experimental Procedure

The experiments were carried out mainly for the ternary phase equilibria. The binary Fe-Cu system was also examined to confirm the composition of the γ phase (γ -Fe-Cu solid solution) in equilibrium with the ϵ phase (Cu-Fe solid solution) or the liquid phase.

II-1. Preparation of specimens

The specimens used in the present work were prepared from pure materials listed in Table 1 by induction-melting and casting in vacuum or under argon atmosphere. After a homogenization-anneal, they were cut into pieces of 5 \times 10 mm cube and then heated in wet hydrogen flow at about 1100 K for 1 \sim 2 days in order to remove carbon and nitrogen.

The multi-layer diffusion couples were used for determining the equilibrium compositions of the γ phase and the ϵ phase in the Fe-Cu system. The couples were made by alternatively laminating about ten sheets of pure iron and copper foils of 80 \sim 100 μ m thickness, both of which had been thinned by rolling and electrolytic polishing.

In the experiments on the ternary systems, a ternary diffusion couple technique was employed for obtaining sufficient data over a wide range of composition from one specimen. As illustrated in Fig. 1, a binary diffusion couple was first prepared from a pair of metals or alloys by joining in a dry hydrogen atmosphere at 1073 K, sealed in a transparent quartz capsule under vacuum or an argon of 1/3 atmospheric pressure, and fully annealed at a high temperature for the moderation of the concentration gradient. Then, a ternary couple was made by joining a third metal piece onto one side of the binary couple. The diffusion couple was sealed again in a quartz capsule and finally equilibrated at fixed temperatures.

In the Fe-Cu-Mn and Fe-Cu-Ni systems, Fe:Fe-50wt%Mn and Fe:Fe-50wt%Ni were chosen as the first couples and pure copper was used as the third metal because it has a lower melting point than the others. In preparing the Fe-Cr-Ni couple, chromium was used as the third metal and the Fe-Ni binary couple was vacuum sealed in a capsule with several pellets of high purity chromium. The ternary couple was spontaneously built up owing to the vaporization and deposition of chromium during

heating at the equilibration temperature.

II-2. Microanalysis of equilibrium composition

The binary and ternary diffusion couples prepared by the method mentioned above were heated at the fixed temperatures between 1123 and 1473 K for 5~33 days. After quenching in ice brine, they were cut in parallel to the direction of diffusion of the third component, and the concentration profile of each component across the interphase boundary was obtained by microanalysis. The equilibrium compositions were determined by extrapolating the profiles to the position of the interphase boundary. Figure 2 illustrates the microstructure of the cross-section and the concentration profile for a ternary Fe-Cu-Ni couple.

It has been pointed out that the interphase boundary composition in diffusion couples deviates to some extent from the equilibrium value⁽⁸⁾⁽⁹⁾. In the present work, however, this may be neglected because the deviations are less than 1% at the most after heating for a long time.

In the investigation of the liquid/solid equilibria, the two-phase alloy specimens were used instead of the diffusion couples. These specimens were quenched from the equilibration temperatures between 1223 and 1523 K for microanalysis of each phase. The determination of composition of the liquid phase was made by counting the average intensity of radiation from an area swept with a width of 40 μm so as to eliminate due to dendritic segregation.

The microanalysis was carried out by Shimadzu ARL-EMX microanalyzer using LiF and quartz crystals for K_α radiation and RAP crystal for L_α radiation. The accelerating voltage and the sample current of the electron beam was kept at 20 kV, 3×10^{-8} A or 30 kV, 10^{-8} A. The take-off angle of the spectrometer was 52.5°.

The relative intensities of radiation K_i in the binary system were converted to the weight fractions C_i according to the next equation proposed by Ziebold and Ogilvie⁽¹⁰⁾:

$$\frac{1-K_i}{K_i} = \alpha_{ij} \frac{1-C_i}{C_i} . \quad (1)$$

The conversion parameters α_{ij} for the i -th component in the binary i - j systems were determined by a calibration experiment as presented in

Table 2.

The conversion of the ternary data was made according to the equation of the form

$$\frac{1-K_i}{K_i} = \bar{\alpha}_i \frac{1-C_i}{C_i}, \quad (2)$$

where $\bar{\alpha}_i$ is a conversion parameter for the i -th component in the ternary i - j - k system and is approximated by a weighted average of the binary parameters as follows :

$$\bar{\alpha}_i = \frac{\alpha_{ij}C_j + \alpha_{ik}C_k}{C_j + C_k}. \quad (3)$$

The validity of equations (2) and (3) has been confirmed by a preliminary experiment on several ternary specimens.

III. Thermodynamic Analysis

III-1. Expression of the free energy of solid solution

The free energy of multi-component solid solutions was described by an extended regular solution approximation as follows :

$$G = \sum_{i=1}^N x_i (\circ G_i + RT \ln x_i) + \sum_{i=1}^{N-1} \sum_{j=i+1}^N x_i x_j \Omega_{ij} + \sum_{i=1}^{N-2} \sum_{j=i+1}^{N-1} \sum_{k=j+1}^N x_i x_j x_k \Omega_{ijk}, \quad (4)$$

where x_i is the atomic fraction, $\circ G_i$ is the free energy of the i -th component at T K. Ω_{ij} and Ω_{ijk} are the interaction parameters in the binary i - j system and the ternary i - j - k system, respectively. These parameters generally depend upon both temperature and composition, and many studies have been made on the way of describing their dependency⁽¹¹⁾. Here, the empirical expressions of the following form were employed :

$$\begin{aligned} \Omega_{ij} &= \Omega_{ij}^0 + \Omega_{ij}^1 (x_j - x_i) + \Omega_{ij}^2 (x_j - x_i)^2 + \cdots + \Omega_{ij}^n (x_j - x_i)^n, \\ \Omega_{ijk} &= \Omega_{ijk}^i x_i + \Omega_{ijk}^j x_j + \Omega_{ijk}^k x_k, \\ \Omega_{ij}^n &= A_{ij}^n + B_{ij}^n T + C_{ij}^n T \ln T, \\ \Omega_{ijk}^i &= A_{ijk}^i + B_{ijk}^i T + C_{ijk}^i T \ln T. \end{aligned} \quad (5)$$

III-2. Analysis by linear programming

The thermodynamic parameters in equations (4) and (5) were evaluated by linear programming on the basis of the experimental results on the ternary systems as well as thermodynamic data on the binary systems.

The phase equilibrium can be described by an equality of chemical potentials, which are related to the free energy of each phase. The activity data can also be described by equations associated with the free energy of each phase. These are rearranged into linear equations concerning the thermodynamic parameters X as follows :

$$a_{i1}X_1 + a_{i2}X_2 + \dots + a_{in}X_n + e_i = R_i . \quad (6)$$

The coefficient a_{ij} and the right-hand side value R_i are known quantities, and e_i is the corresponding error. Then the parameter X_j is evaluated in such a way as to minimize the objective function :

$$Z = \sum_i |e_i| . \quad (7)$$

Such a linear programming technique has been successfully applied by Rao et al.⁽¹²⁾ to the thermodynamic analysis of the binary Pb-Sb system.

Besides an equality like equation (6), the constraint of an inequality was used in this work. For example, the free energy of the liquid phase must be lower than that of the solid phase at the liquidus. This fact is described in the following form and is also of use in linear programming for the evaluation of the parameter X_j :

$$a'_{i1}X_1 + a'_{i2}X_2 + \dots + a'_{in}X_n < R'_i . \quad (8)$$

III-3. Computation of phase boundaries

The computer calculation of the phase boundary compositions can in principle be divided into two ways. One is to solve the simultaneous equations concerning the chemical potentials of the components in each phase. The other is to search for a set of phases having the best composition to minimize the free energy of the entire alloy system. The former was carried out by Kaufman and Bernstein⁽¹³⁾, and the latter by Counsell et al.⁽¹⁴⁾ In this work, the latter was employed because it is simpler in operation and faster to find the equilibrium composition of each phase. The "Simplex" method, the steepest descent method developed by Nelder and Mead⁽¹⁵⁾, was used in performing the calculation.

IV. Results

IV-1. Evaluation of parameters

Experimental results on the equilibrium composition of each phase are given in Tables 3~8. On the basis of these results, the thermodynamic parameters in equations (4) and (5) were evaluated as listed in Tables 9 and 10. The phase diagrams and thermodynamic data on the binary Fe-Cr^{(9)(16)~(32)}, Fe-Mn^{(18)(33)~(43)}, Fe-Ni^{(18)(22)(34)(44)~(59)}, Fe-Cu^{(60)~(70)}, Cr-Ni^{(22)(29)(32)(46)(71)~(77)}, Cu-Mn^{(18)(78)~(83)} and Cu-Ni^{(78)(84)~(95)} systems and the ternary Fe-Cr-Ni^{(46)(96)~(99)} and Fe-Cu-Ni⁽¹⁴⁾ systems were also employed for the evaluations. The free energy of the component $^{\circ}G_i$ used was the literature value^{(100)~(103)}. The parameters concerning the σ phase were estimated from the data on the Fe-Cr⁽²²⁾ and Cr-Co-Ni⁽¹⁰⁴⁾ systems.

IV-2. Calculation of phase diagram

The phase diagrams are constructed by computation using the above-mentioned parameters. Figures 3~9 and 10~20 are the computed diagrams of the binary and ternary systems, respectively. The calculation of the phase equilibria relating to the α Fe phase was limited to temperatures above 1073 K, because it has been pointed out by Zener⁽¹⁰⁷⁾, Weiss and Tauer⁽¹⁰⁸⁾, and Hillert et al.⁽⁵⁾⁽²¹⁾⁽³⁴⁾ that the thermodynamic functions of α Fe solid solution show an anomaly due to the magnetic transition. The phase diagrams over a temperature range below the Curie point will be presented elsewhere.

Comparisons of the accepted diagrams with those obtained in the present work are given in Figs. 13 and 20. There are some discrepancies due to the fact that the accepted diagrams were synthesized by calculation using the binary data alone⁽¹⁴⁾⁽¹⁰¹⁾ or constructed experimentally in a conventional way⁽¹⁰⁹⁾.

The thermodynamic properties can be calculated by computation as in the case of the phase diagrams. As examples, the activities in the binary Fe-Cr system and the iso-activity lines for chromium in the ternary Fe-Cr-Ni system are shown in Figs. 21 and 22, respectively.

Acknowledgments

The authors wish to express their gratitude to Mr. Y.Kohsaka, now at Technical Research Center, Nippon Kokan K.K., Kawasaki, Japan, for his invaluable assistance throughout the present experiments. Thanks are also due to Prof. H.Takeyama and his staff at the Computer Center, Tohoku University, for their kind help in computer calculation. One of the authors (M.H.) wishes to thank for the financial support of the Sakkokai Foundation.

References

- (1) K.Kennedy, T.Stefansky, G.Davy, V.F.Zackay and E.R.Parker : J. Appl. Phys., 36(1965), 3808.
- (2) A.Boettcher, G.Haase and R.Thun : Z. Metallk., 46(1955), 386.
- (3) G.Kirchner, G.Larbo and B.Uhrenius : Pract. Metallogr., 8(1971), 641.
- (4) J.S.Kirkaldy, G.M.Bolze, D.McCutcheon and J.Young : Met. Trans., 4(1973), 1519.
- (5) M.Hillert : Phase Transformations, Ed. by M.Cohen, ASM, Cleveland, Ohio, (1969), 181.
- (6) International Symposium on Metallurgical Chemistry, England, (1971); International Symposium on Thermodynamics of Alloys, Munster, (1972).
- (7) A.D.Pelton and W.T.Thomson : Prog. Solid State Chem., 10(1975), 119.
- (8) J.R.Eifert, D.A.Chatfield, G.W.Powell and J.W.Spretnak : Trans. Met. Soc. AIME, 242(1968), 66.
- (9) T.Nishizawa and A.Chiba : Trans. Japan Inst. Metals, 16(1975), 767.
- (10) T.O.Ziebold and R.E.Ogilvie : Anal. Chem., 35(1963), 621; 36(1964), 322.
- (11) I.Ansara : Metallurgical Chemistry, Ed. by O.Kubaschewski, HSMO, London, (1972), 403.
- (12) M.V.Rao, R.Hiskes and W.A.Tiller : Acta Met., 21(1973), 733.
- (13) L.Kaufman and H.Bernstein : Computer Calculation of Phase Diagrams, Academic Press, New York, (1970).
- (14) J.F.Counsell, E.B.Lees and J.Spencer : Metallurgical Chemistry, Ed. by O.Kubaschewski, HSMO, London, (1972), 451.
- (15) J.A.Nelder and R.Mead : Computer J., 7(1964/5), 308.
- (16) F.Adcock : J. Iron Steel Inst., 124(1931), 99.
- (17) J.W.Putman, R.D.Potter and N.J.Grant : Trans. ASM, 43(1951), 824.
- (18) A.Hellawell and W.Hume-Rothery : Phil. Trans. Roy. Soc. London, Ser.A, 249(1957), 417.
- (19) K.Bungardt, E.Kunze and E.Horn : Arch. Eisenhüttenw., 29(1958), 193.
- (20) E.Baerlecken, W.A.Fisher and K.Lorentz : Stahl Eisen, 81(1961), 768.
- (21) G.Kirchner, T.Nishizawa and B.Uhrenius : Met. Trans., 4(1973), 167.
- (22) W.A.Dench : Trans. Faraday Soc., 59(1963), 1279.
- (23) C.L.McCabe, R.G.Hudson and H.W.Paxton : Trans. Met. Soc. AIME, 212(1958), 102.
- (24) E.Z.Vintaikin : Dokl. Akad. Nauk SSSR, 118(1958), 977.
- (25) O.Kubaschewski and G.Heymer : Acta Met., 8(1960), 416.
- (26) Y.Jeannin, C.Mannerkantz and F.D.Richardson : Trans. Met. Soc. AIME, 227(1963), 300.
- (27) P.B.Reese, R.A.Rapp and G.Pierre : Trans. Met. Soc. AIME, 242(1968), 1719.
- (28) D.C.Lidster and H.B.Bell : Trans. Met. Soc. AIME, 245(1969), 2273.

- (29) F.N.Mazandarany and R.D.Pehlke : Met. Trans., 4(1973), 2067.
- (30) M.Onillon and M.Olette : Compt. Rend. Acad. Sci., C, 264(1967), 46.
- (31) R.J.Fruehan : Trans. Met. Soc. AIME, 245(1969), 1215.
- (32) S.W.Gilby and G.R.Pierre : Trans. Met. Soc. AIME, 245(1969), 1749.
- (33) A.R.Troiano and F.T.McGuire : Trans. ASM, 31(1943), 340.
- (34) M.Hillert, T.Wada and H.Wada : J. Iron Steel Inst., 205(1967), 539.
- (35) B.Predel and W.Gust : Arch. Eisenhuttenw., 43(1972), 721.
- (36) K.Ishida : Thesis, Tohoku University, Sendai, (1974).
- (37) W.B.Kendall and R.Hultgren : Trans. ASM, 53(1961), 199.
- (38) K.Sanbongi and M.Ohtani : Sci. Rept. Res. Inst. Tohoku Univ. Ser.A, 7(1955), 204.
- (39) J.F.Butler, C.L.McCabe and H.W.Paxton : Trans. Met. Soc. AIME, 221(1961), 479.
- (40) R.Smith and R.Shuttleworth : Acta Met., 13(1965), 623.
- (41) P.Roy and R.Hultgren : Trans. Met. Soc. AIME, 233(1965), 1811.
- (42) R.J.Hawkins : Chemical Metallurgy of Iron and Steel, Iron and Steel Inst., London, (1973), 310.
- (43) V.N.Eremenko, G.M.Lukashenko and V.R.Sidorko : Izvest. Akad. Nauk SSSR, 11(1969), 170.
- (44) D.Hanson and J.R.Freeman : J. Iron Steel Inst., 107(1923), 301.
- (45) T.Kase : Sci. Rept. Tohoku Univ., 16(1927), 491.
- (46) C.H.M.Jenkins, E.H.Bucknall, C.R.Austin and G.A.Mellor : J. Iron Steel Inst., 86(1937), 187.
- (47) E.A.Owen and Y.H.Liu : J. Iron Steel Inst., 163(1949), 132.
- (48) J.I.Goldstein and R.E.Ogilvie : Trans. Met. Soc. AIME, 233(1965), 2083.
- (49) W.Steiner and O.Krisement : Arch. Eisenhuttenw., 32(1961), 701.
- (50) O.Kubaschewski and L.E.Stuart : J. Chem. Eng. Data, 12(1967), 418.
- (51) B.Predel and R.Mohs : Arch. Eisenhuttenw., 41(1970), 143.
- (52) K.Ono, Y.Ueda, A.Yamaguchi and J.Moriyama : J. Japan Inst. Metals, 36(1972), 188.
- (53) O.Kubaschewski and O.Goldbeck : Trans. Faraday Soc., 45(1948), 948.
- (54) R.A.Oriani : Acta Met., 1(1953), 448.
- (55) C.Gatellier, D.Henriet and M.Olette : Compt. Rend. Acad. Sci., 271(1970), 453.
- (56) R.Speiser, A.J.Jacobs and J.W.Spretnak : Trans. Met. Soc. AIME, 215(1959), 185.
- (57) G.R.Zellars, S.L.Payne, J.P.Morris and R.L.Kipp : Trans. Met. Soc. AIME, 215(1959), 181.
- (58) G.R.Belton and R.J.Fruehan : J. Phys. Chem., 71(1967), 1403.
- (59) K.C.Mills, K.Kinoshita and P.Grieverson : J. Chem. Thermody., 4(1972), 581.

- (60) G.Tammann and W.Oelsen : Z. anorg. Chem., 186(1930), 257.
- (61) A.G.H.Andersen and A.W.Kingsbury : Trans. AIME, 152(1943), 38.
- (62) H.A.Wriedt and L.S.Darken : Trans. Met. Soc. AIME, 218(1960), 30.
- (63) A.H.Qureshi : Z. Metallk., 52(1961), 799.
- (64) G.R.Speich, J.A.Gula and R.M.Fisher : The Electron Microprobe, Ed. by T.D.Mckinley, K.F.J.Heinrich and D.B.Witty, New York, (1966), 525.
- (65) Y.Nakagawa : Acta Met., 6(1958), 704.
- (66) W.Oelsen, E.Schurmann and C.Florin : Arch. Eisenhuttenw., 32(1961), 719.
- (67) Y.Tozaki, Y.Iguchi, S.Ban-ya and T.Fuwa : Metallurgical Chemistry, Ed. by O.Kubaschewski, HSMO, London, (1972), 130.
- (68) J.P.Morris and G.R.Zellars : J. Metals, 8(1956), 1086.
- (69) A.D.Kulkarni : Met. Trans., 4(1973), 1713.
- (70) B.B.Argent : Chemical Metallurgy of Iron and Steel, Iron and Steel Inst., London, (1973), 301.
- (71) M.Matsunaga : Japan Nickel Review, 1(1933), 347.
- (72) C.J.Bechtoldt and H.C.Vacher : Trans. Met. Soc. AIME, 221(1960), 14.
- (73) A.Chiba : Thesis, Tohoku University, (1971).
- (74) G.Grube and M.Flad : Z. Elektrochem., 48(1942), 377.
- (75) O.Kubaschewski and W.A.Dench : Z. Elektrochem., 64(1960), 801.
- (76) M.G.Panish, R.F.Newton, W.R.Grimes and F.F.Blankenship : J. Phys. Chem., 62(1958), 980.
- (77) L.A.Pugliese and G.R.Fitterer : Met. Trans., 1(1970), 1997.
- (78) E.Schurmann and E.Schultz : Z. Metallk., 62(1971), 758.
- (79) R.Hultgren, P.D.Desai, D.T.Hawkins, M.Gleiser and K.K.Kelley : Selected Values of the Thermodynamic Properties of Binary Alloys, ASM, Metals Park, Ohio, (1973).
- (80) B.F.Peters and D.R.Wiles : Can.J. Chem., 41(1963), 2591.
- (81) V.N.Eremenko, G.M.Lukashenko and V.R.Sidorko : Izvest. Akad. Nauk SSSR, 6(1964), 151.
- (82) R.W.Krenzer and M.J.Pool : Trans. Met. Soc. AIME, 245(1969), 91.
- (83) P.J.Spencer and J.N.Pratt : Trans. Faraday Soc., 64(1968), 1470.
- (84) E.A.Feest and R.D.Doherty : J. Inst. Metals, 99(1971), 102.
- (85) K.Tanaka and T.Nishizawa : unpublished work
- (86) B.D.Bastow and D.H.Kirkwood : J. Inst. Metals, 99(1971), 277.
- (87) B.Predel and R.Mohs : Arch. Eisenhuttenw., 42(1971), 575.
- (88) O.Kubaschewski, W.A.Dench and V.Genta : Symposium on Physical Chemistry of Metallic Solutions and Intermetallic Compounds, National Physical Laboratory, Teddington, (1958), Vol.I, paper 1G.
- (89) R.A.Oriani and W.K.Murphy : Acta Met., 8(1960), 23.

- (90) L.Elford, F.Muller and O.Kubaschewski : Ber. Bunsenges. Physik. Chem., 73(1969), 601.
- (91) M.G.Benz and J.F.Elliott : Trans. Met. Soc. AIME, 230(1964), 706.
- (92) R.N.Dokken and J.F.Elliott : Trans. Met. Soc. AIME, 233(1965), 1351.
- (93) R.A.Rapp and F.Maak : Acta Met., 10(1962), 63.
- (94) I.Katayama, H.Shimatani and Z.Kozuka : J. Japan Inst. Metals, 37(1973), 509.
- (95) A.D.Kulkarni and R.E.Johnson : Met. Trans., 4(1973), 1723.
- (96) J.W.Schultz and H.F.Merrick : Met. Trans., 3(1972), 2479.
- (97) O.Kubaschewski and L.E.H.Stuart : J. Chem. Eng. Data, 12(1967), 418.
- (98) W.Slough, J.Spencer and O.Kubaschewski : J. Chem. Thermody., 2(1970), 117.
- (99) S.W.Gilby and G.R.Pierre : Trans. Met. Soc. AIME, 245(1969), 1749.
- (100) L.Kaufman : Phase Stability in Metals and Alloys, Ed. by P.S.Rudman, J.Stringer and R.I.Jaffee, McGraw-Hill, New York, (1967), 125.
- (101) L.Kaufman and H.Nesor : Z. Metallk., 64(1973), 249.
- (102) R.J.Orr and J.Chipman : Trans. Met. Soc. AIME, 239(1967), 630.
- (103) R.Hultgren, P.D.Desai, D.T.Hawkins, M.Gleiser, K.K.Kelley and D.D.Wagman : Selected Values of the Thermodynamic Properties of Elements, ASM, Metals Park, Ohio, (1973).
- (104) M.Hasebe and T.Nishizawa : to be published.
- (105) P.Schafmeister and R.Ergang : Arch. Eisenhüttenw., 12(1939), 459.
- (106) A.J.Cook and B.R.Brown : J. Iron Steel Inst., 171(1952), 345.
- (107) C.Zener : J. Metals, 7(1955), 619.
- (108) R.J.Weiss and K.J.Tauer : Phys. Rev., 102(1956), 1490.
- (109) A.J.Bradley, W.F.Cox and H.J.Goldschmidt : J. Inst. Metals, 67(1941), 189.

Table 1 Chemical composition of materials.

Materials	Impurities (wt. ppm)
Electrolytic iron (99.95)	C40, Si40, P30, S40, Cu40, Mn40
Electrolytic chromium (99.28)	C200, Si80, P10, S260, Al40, Cu5, Pb20, Fe1400
High purity chromium (99.999)	Fe3, Pb2, Mg<1
Electrolytic manganese (99.9)	C100, Si100, P100, Fe100, S100, Al Tr.
Mond cobalt (>99.5)	S60, C100, Fe1200, Ni1200, Si230, Mn60
Electrolytic nickel (Ni+Co>99.5)	Co<300, Fe<50, Cu<50, Pb<10, Mn<20, S<10, Si<50, C<200
High purity copper (99.999)	Ag4.0, Au0.1, Fe1.0, Pb0.5, S3.2, Ni, Sn, Zn n.d.

Table 2 Empirical conversion parameters α_{ij} for microanalysis (at 20kV and 30kV).

	$\begin{matrix} j \\ i \end{matrix}$	Fe	Cr	Mn	Ni	Cu
K_{α}	Fe		1.140	(0.902)	0.760 (0.786)	0.706 (0.725)
	Cr	0.778		-	0.790	-
	Mn	(0.928)	-		-	(0.760)
	Ni	1.100 (1.180)	1.290	-		0.913 (0.858)
	Cu	1.220 (1.180)	-	-	1.010 (1.000)	
L_{α}	Ni	2.650	2.400	-		-
	Cu	3.620 (5.800)	-	(4.980)	3.650 (5.700)	

values in bracket for 30kV

Table 3 Experimental results of the γ/ϵ and the γ /liquid equilibrium in the binary Fe-Cu system.

T(K)	x_{Cu}^{γ}	x_{Fe}^{ϵ}	x_{Fe}^{l}
1173	0.034	0.018	-
1223	0.039	0.022	-
1273	0.064	0.029	-
1323	0.066	0.033	-
1373	0.106	-	0.047
1423	0.103	-	0.031
1473	0.114	-	0.036
1523	0.116	-	0.047
1573	0.129	-	-
1623	0.139	-	-

Table 4 Experimental results of the α/γ equilibria in the ternary Fe-Cr-Ni system.

	α		γ	
	x_{Cr}	x_{Ni}	x_{Cr}	x_{Ni}
1473 K	0.199	0.036	0.177	0.045
	0.233	0.043	0.198	0.069
	0.282	0.070	0.232	0.105
	0.368	0.110	0.285	0.179
	0.390	0.122	0.295	0.200
1373 K	0.420	0.116	0.300	0.200
	0.365	0.085	0.255	0.160
	0.314	0.064	-	-
	0.264	0.055	0.190	0.090
	0.207	0.025	0.158	0.037
	0.560*	0.133*	0.339*	0.309*
1273 K	0.347	0.051	0.230	0.120
	0.365	0.066	-	-
	0.465	0.080	0.285	0.200
	0.523	0.098	0.290	0.275
	0.502	0.105	0.304	0.258
	0.525	0.100	0.313	0.250
	0.497	0.098	0.298	0.260
	0.222	0.017	0.175	0.033
	0.272	0.032	0.210	0.050
	0.320	0.045	0.220	0.100
	0.385	0.062	0.255	0.140
	0.433	0.082	0.271	0.185
	0.668	0.097	0.346	0.361
	0.675	0.092	0.345	0.380
	0.611*	0.099*	0.326*	0.305*
1193 K	0.444	0.060	-	-
	0.465	0.060	0.265	0.215
	0.462	0.069	0.275	0.225
	0.404	0.048	0.250	0.160
	0.350	0.035	0.225	0.110
	0.265	0.025	0.175	0.055
	0.215	0.008	0.150	0.015
	0.380*	0.046*	0.256*	0.122*
	0.678*	0.060*	0.325*	0.292*

* taken from two-phase alloys

Table 5 Experimental results of miscibility gap in the ternary Fe-Cu-Mn system.

	γ		$\gamma'(\epsilon)$	
	x_{Cu}	x_{Mn}	x_{Cu}	x_{Mn}
1173 K	0.103	0.044	0.923	0.051
	0.129	0.061	0.938	0.059
	0.113	0.077	0.908	0.079
	0.105	0.105	0.916	0.084
	0.109	0.111	0.894	0.105
	0.092	0.109	0.887	0.107
1123 K	0.106	0.025	0.889	0.034
	0.109	0.059	0.913	0.063
	0.108	0.093	0.895	0.094
	0.108	0.122	0.880	0.114
	0.099	0.156	0.850	0.139
	0.095	0.176	0.832	0.149
	0.113*	0.221*	0.767*	0.189*
	0.121*	0.320*	0.722*	0.248*
	0.120*	0.440*	0.609*	0.353*
	0.133*	0.589*	0.413*	0.511*

* taken from two-phase alloys

Table 6 Experimental results of the γ /liquid equilibria in the ternary Fe-Cu-Mn system.

	γ		liquid	
	x_{Cu}	x_{Mn}	x_{Cu}	x_{Mn}
1323 K	0.121	0.062	0.868	0.114
	0.078	0.184	0.762	0.220
	0.075	0.296	0.648	0.295
	0.141	0.503	0.563	0.407
	0.202	0.621	0.456	0.513
1223 K	0.104	0.201	0.782	0.206
	0.090	0.240	0.762	0.226
	0.076	0.266	0.731	0.254
	0.100	0.396	0.674	0.313
	0.127	0.509	0.620	0.368
	0.190	0.546	0.600	0.388
	0.089	0.375	0.669	0.314
1173 K	0.105	0.165	0.770	0.186
	0.147	0.303	0.726	0.248
	0.093	0.354	0.705	0.268
	0.149	0.520	0.624	0.366

Table 7 Experimental results of miscibility gap in the ternary Fe-Cu-Ni system.

	γ		$\gamma'(\epsilon)$	
	x_{Cu}	x_{Ni}	x_{Cu}	x_{Ni}
1323 K	0.184	0.236	0.868	0.083
	0.214	0.256	0.841	0.103
	0.227	0.242	0.879	0.073
	0.299	0.286	0.778	0.144
	0.283	0.258	0.804	0.114
	0.441	0.265	0.661	0.204
	0.403	0.269	0.693	0.183
	0.151	0.097	0.941	0.035
	0.126	0.089	0.927	0.027
	0.158	0.157	0.909	0.052
	0.186	0.198	0.829	0.067
	0.245	0.250	0.822	0.103
	0.297	0.282	0.761	0.136
1223 K	0.181	0.281	0.881	0.093
	0.188	0.263	0.922	0.062
	0.188	0.299	0.862	0.107
	0.195	0.274	0.882	0.088
	0.243	0.313	0.809	0.130
	0.231	0.305	0.869	0.101
	0.197	0.350	0.776	0.157
	0.304	0.314	0.801	0.147
	0.277	0.352	0.714	0.187
	0.267	0.331	0.751	0.153
	0.342	0.365	0.745	0.198
	0.334	0.343	0.791	0.146
	0.465	0.328	0.713	0.216
	0.138	0.018	0.974	0.018
	0.151	0.108	0.943	0.047
1123 K	0.111	0.079	0.970	0.002
	0.083	0.106	0.946	0.027
	0.103	0.158	0.911	0.040
	0.110	0.189	0.934	0.042
	0.219	0.411	0.799	0.147
	0.205	0.422	0.836	0.131
	0.236	0.434	0.789	0.166
	0.261	0.428	0.819	0.142
	0.241	0.427	0.795	0.162
	0.406	0.383	0.724	0.218
	0.140	0.348	0.873	0.092

Table 8 Experimental results of the γ /liquid equilibria in the ternary Fe-Cu-Ni system.

	γ		liquid	
	x_{Cu}	x_{Ni}	x_{Cu}	x_{Ni}
1523 K	0.180	0.153	0.896	0.054
	0.227	0.220	0.817	0.085
	0.279	0.283	0.792	0.115
	0.374	0.377	0.722	0.190
1423 K	0.209	0.173	0.915	0.039
	0.701	0.170	0.881	0.079
	0.338	0.215	0.908	0.050

Table 9 Evaluated interaction parameters in the binary systems.
(J/mol)

system i-j	phase	n	0	1	2
Fe-Cr	l	A_{ij}^n	19310	13360	-
		B_{ij}^n	-11.20	-5.343	-
	α	A_{ij}^n	24710	664	-
		B_{ij}^n	-11.76	1.736	-
	γ	A_{ij}^n	13840	6276	-
		B_{ij}^n	-13.61	-3.310	-
Fe-Mn	l	A_{ij}^n	-26520	-10870	-
		B_{ij}^n	17.10	7.263	-
	α	A_{ij}^n	-10830	-280	-
		B_{ij}^n	8.581	0.533	-
	γ	A_{ij}^n	-19760	-440	-
		B_{ij}^n	13.58	1.127	-
Fe-Ni	l	A_{ij}^n	-16690	-10750	-
		B_{ij}^n	3.592	2.401	-
	α	A_{ij}^n	-10270	-12150	-
		B_{ij}^n	0.306	3.902	-
	γ	A_{ij}^n	-26170	-15140	-
		B_{ij}^n	81.59	33.26	-
		C_{ij}^n	-9.602	-3.807	-

Table 9 (continued)

system i-j	phase	n	0	1	2
Fe-Cu	l	A_{ij}^n	36440	-400	11560
		B_{ij}^n	-2.730	0.738	-4.153
	α	A_{ij}^n	43390	-	-
		B_{ij}^n	-6.197	-	-
	γ	A_{ij}^n	31010	5410	14930
		B_{ij}^n	0	-2.618	-5.627
Cr-Ni	l	A_{ij}^n	-15270	-36170	-
		B_{ij}^n	4.197	15.25	-
	α	A_{ij}^n	23370	-26030	-
		B_{ij}^n	-17.22	4.665	-
	γ	A_{ij}^n	4268	-31080	-
		B_{ij}^n	-15.80	19.23	-
Mn-Cu	l	A_{ij}^n	-2131	-24090	6360
		B_{ij}^n	-0.323	13.89	-6.004
	α	A_{ij}^n	23960	-	-
		B_{ij}^n	-13.64	-	-
	γ	A_{ij}^n	12790	-9837	9749
		B_{ij}^n	-3.893	4.192	-9.816
Ni-Cu	l	A_{ij}^n	10460	-1451	-
		B_{ij}^n	2.087	0.394	-
	γ	A_{ij}^n	8138	-2537	-
		B_{ij}^n	3.009	0.828	-

Table 10 Evaluated interaction parameters in the ternary systems.
(J/mol)

system i-j-k	phase	p i j k	i	j	k
Fe-Cr-Ni	l, α , γ	A_{ijk}^p	0	0	0
Fe-Cu-Mn	l	A_{ijk}^p	0	0	0
	γ	A_{ijk}^p	10460	10460	10460
Fe-Cu-Ni	l	A_{ijk}^p	0	0	0
	γ	A_{ijk}^p	-77400	-111300	-49000
		B_{ijk}^p	72.8	73.2	41.8

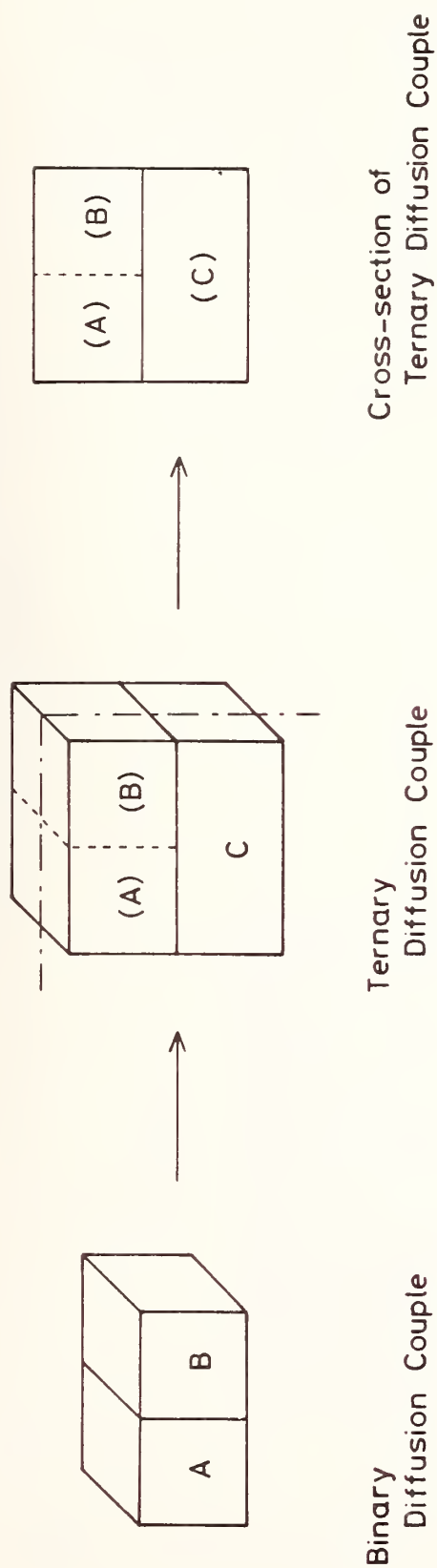


Fig. 1 Construction of a ternary diffusion couple.

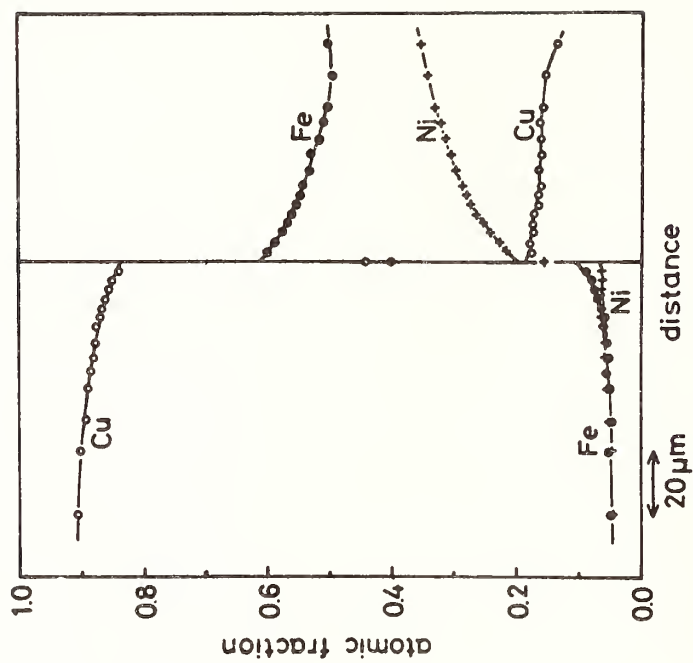
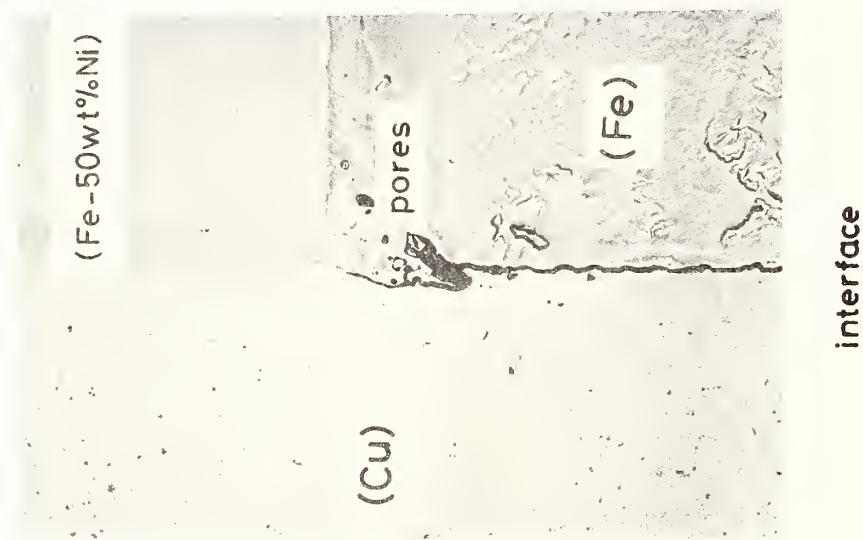


Fig. 2 The cross-section and the concentration profile for a ternary Fe-Cu-Ni diffusion couple heated at 1323 K for 7 days.

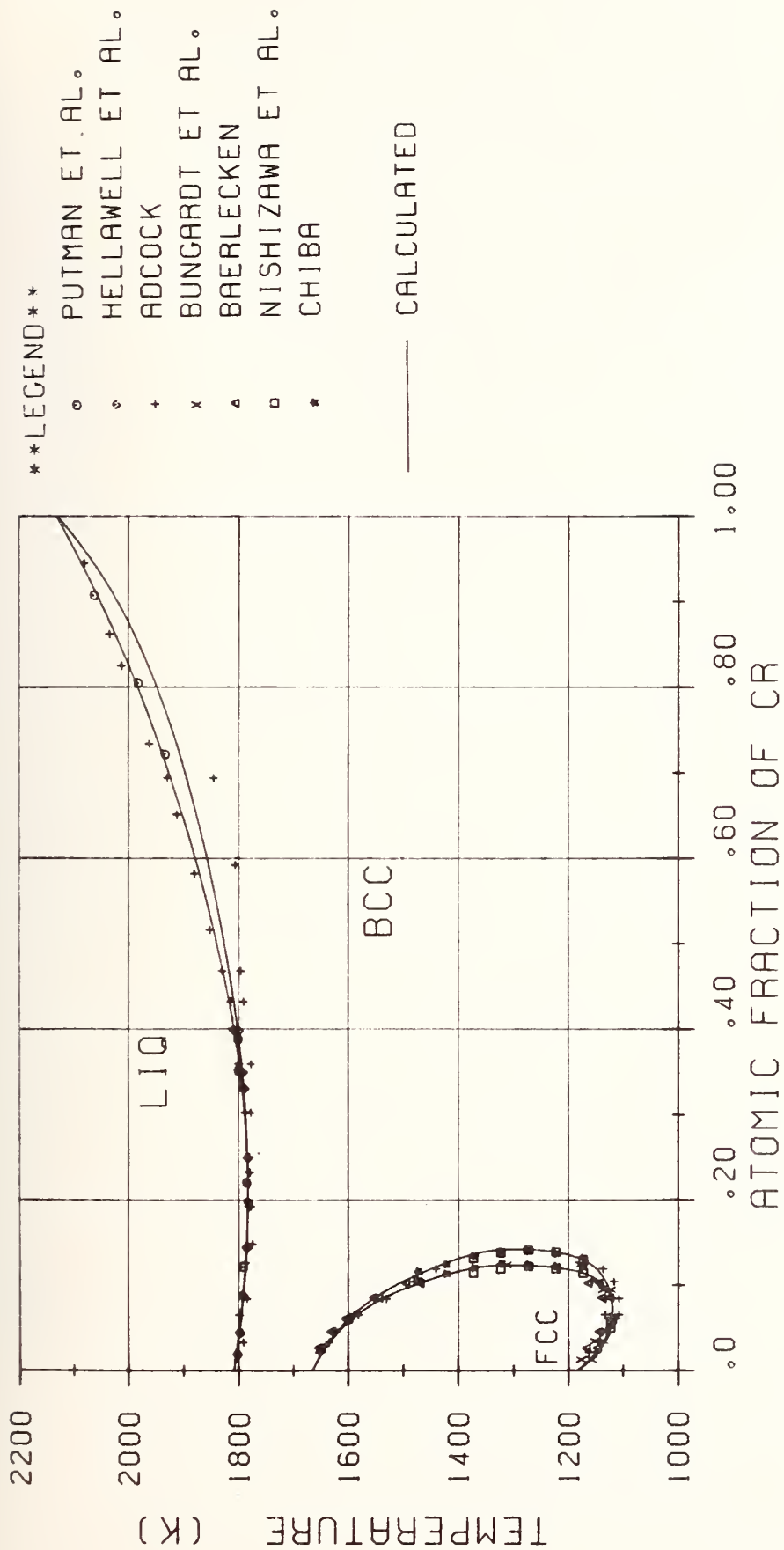


Fig. 3 Computer generated phase diagram in the binary Fe-Cr system.

LEGEND

○ HELLAWELL ET AL.

— CALCULATED

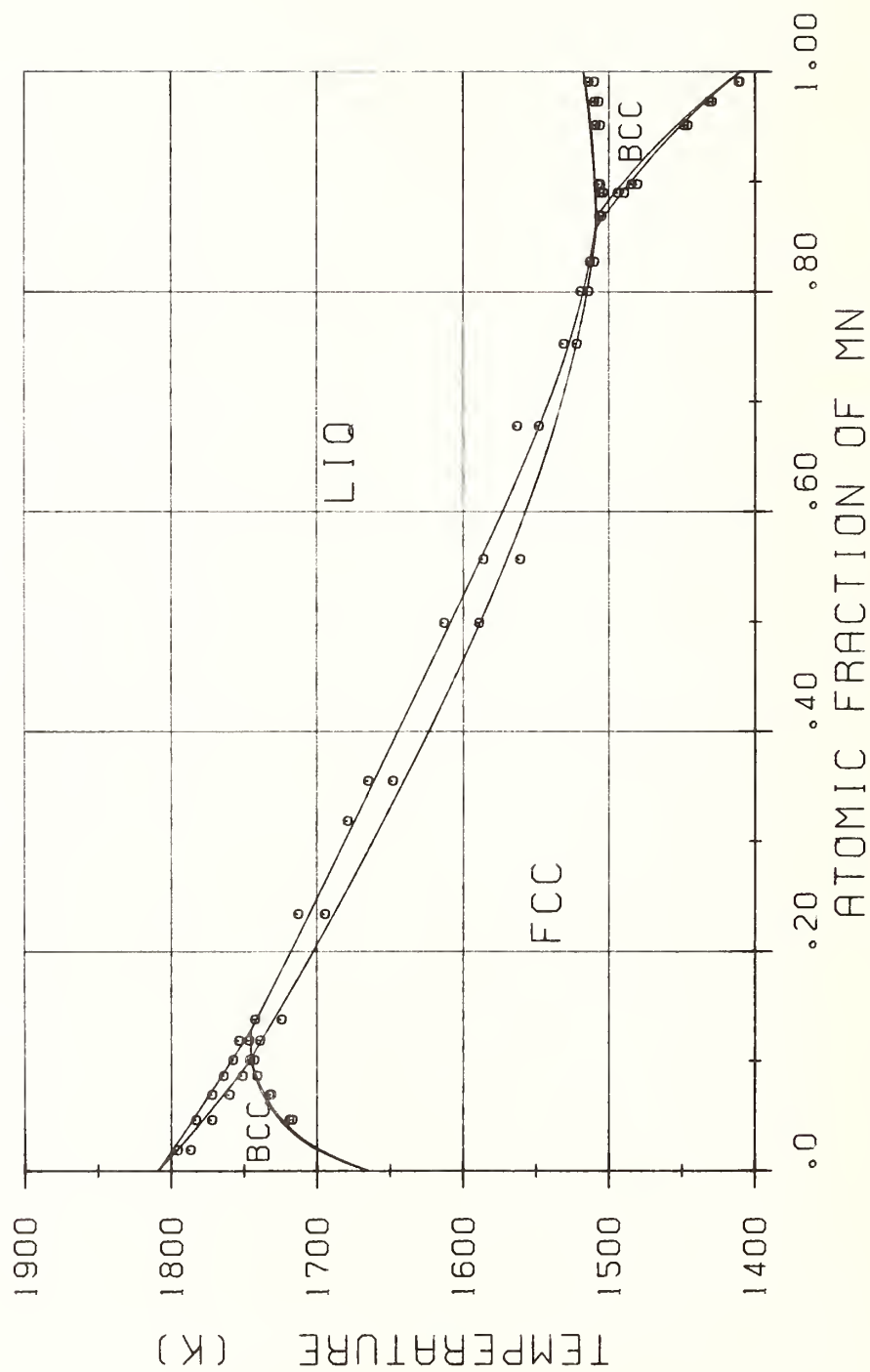


Fig. 4 Computer generated phase diagram in the binary Fe-Mn system.

LEGEND

○ HANSON ET AL.

□ KASE

◇ HELLAWEELL ET AL.

— CALCULATED

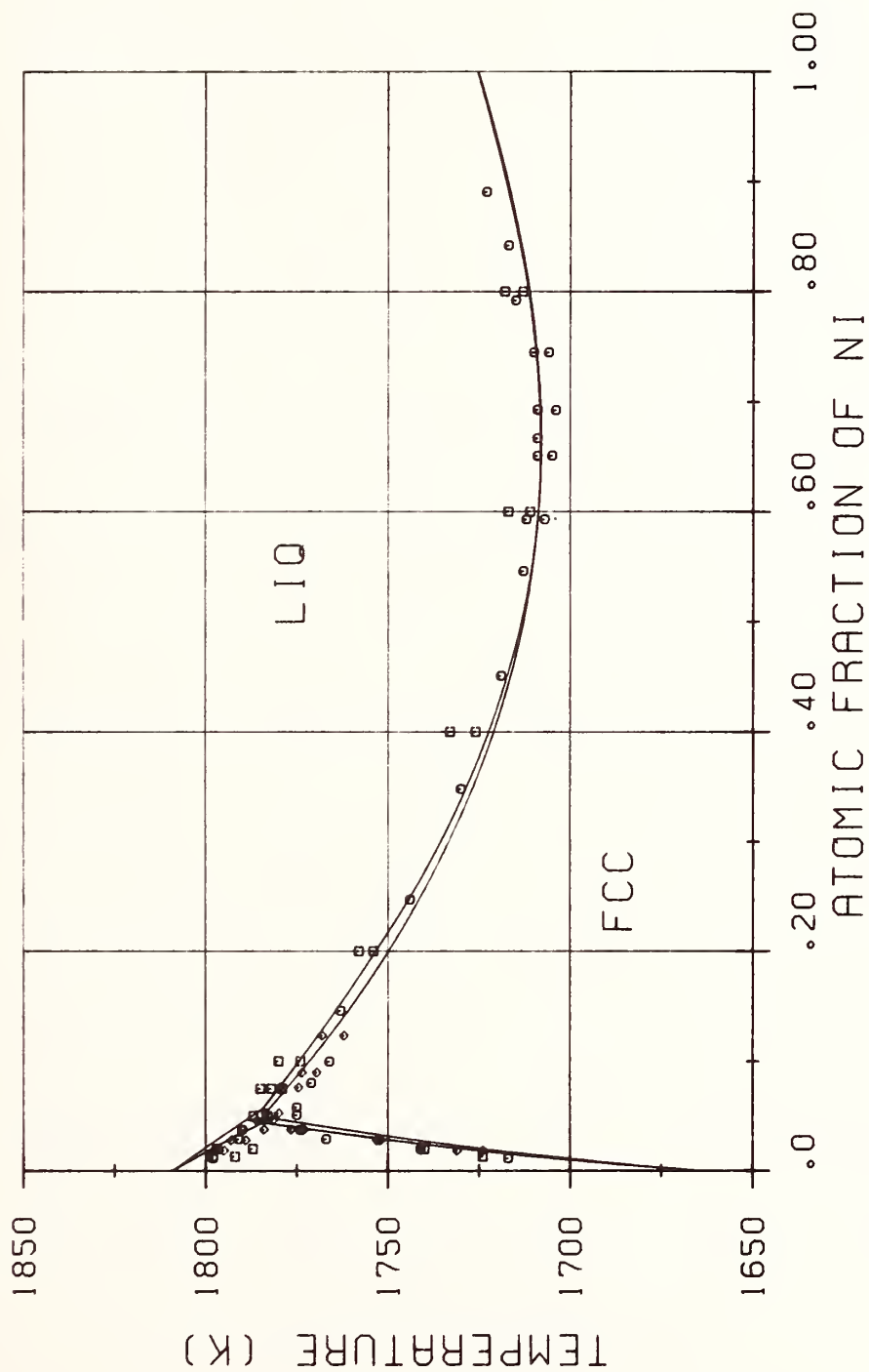


Fig. 5 Computer generated phase diagram in the binary Fe-Ni system.

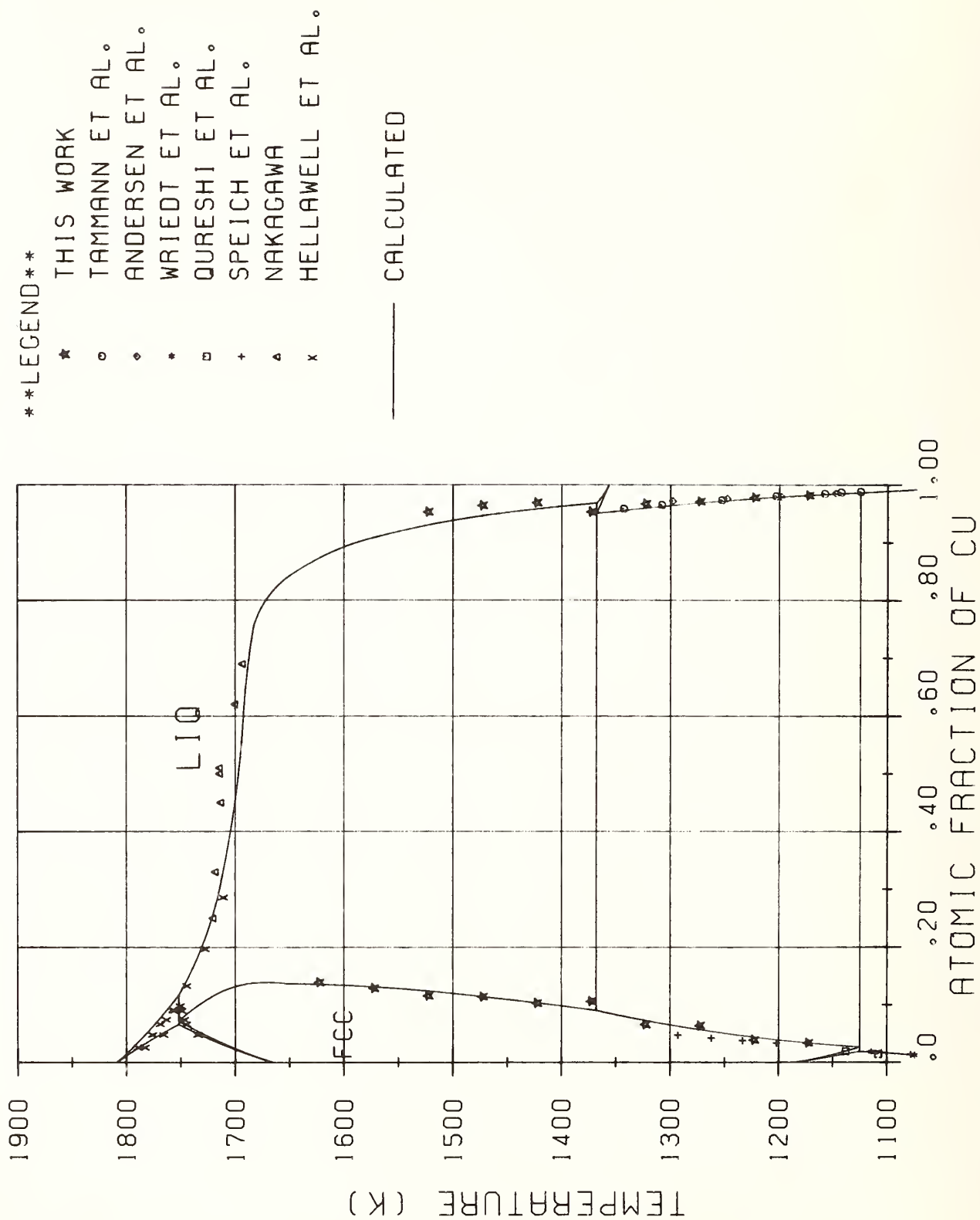


Fig. 6 Computer generated phase diagram in the binary Fe-Cu system.

LEGEND

◊ HELLAWELL ET AL.

○ SCHURMANN ET AL.

----- SHUNK

----- CALCULATED

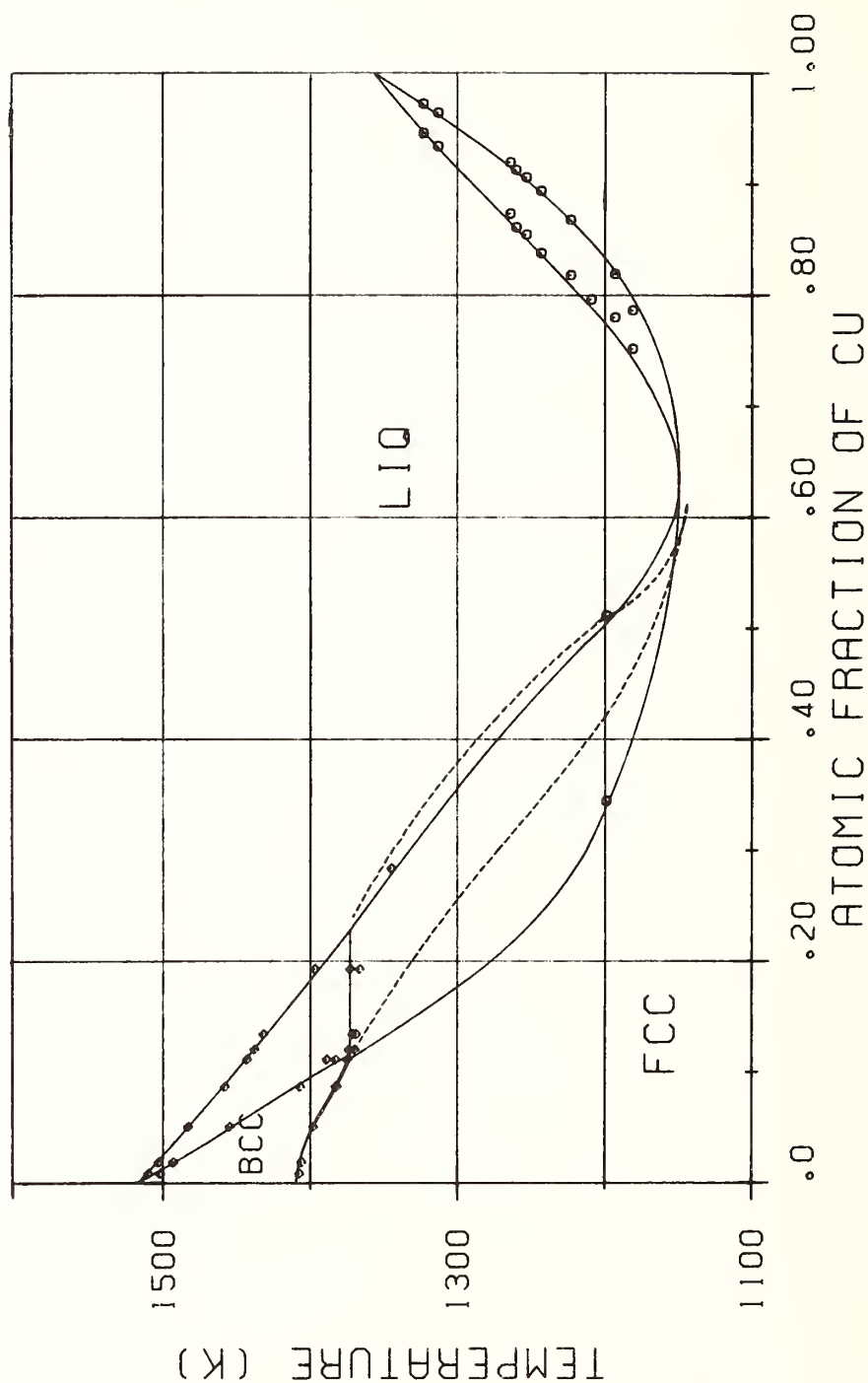


Fig. 8 Computer generated phase diagram in the binary Cu-Mn system.

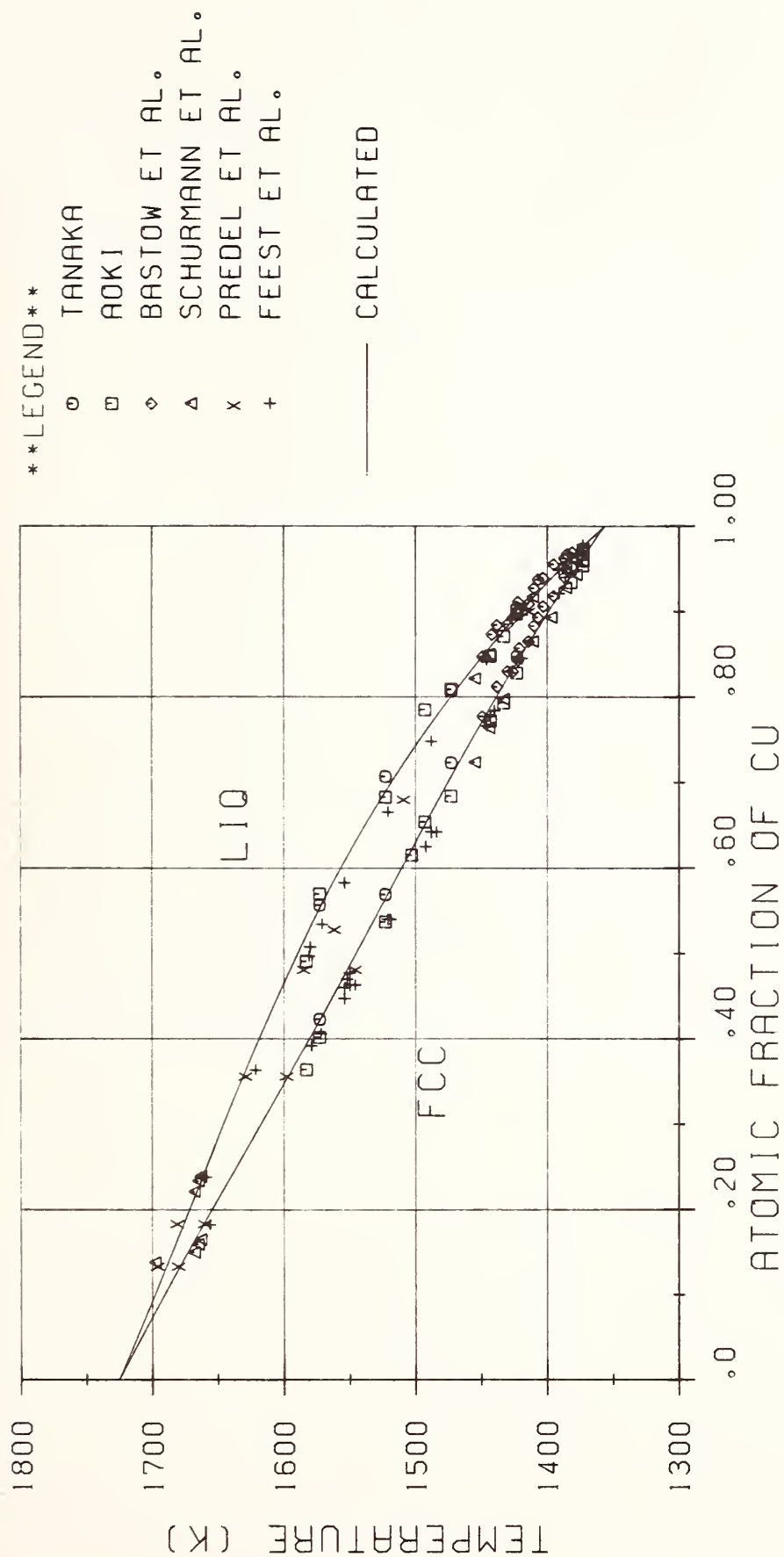


Fig. 9 Computer generated phase diagram in the binary Cu-Ni system.

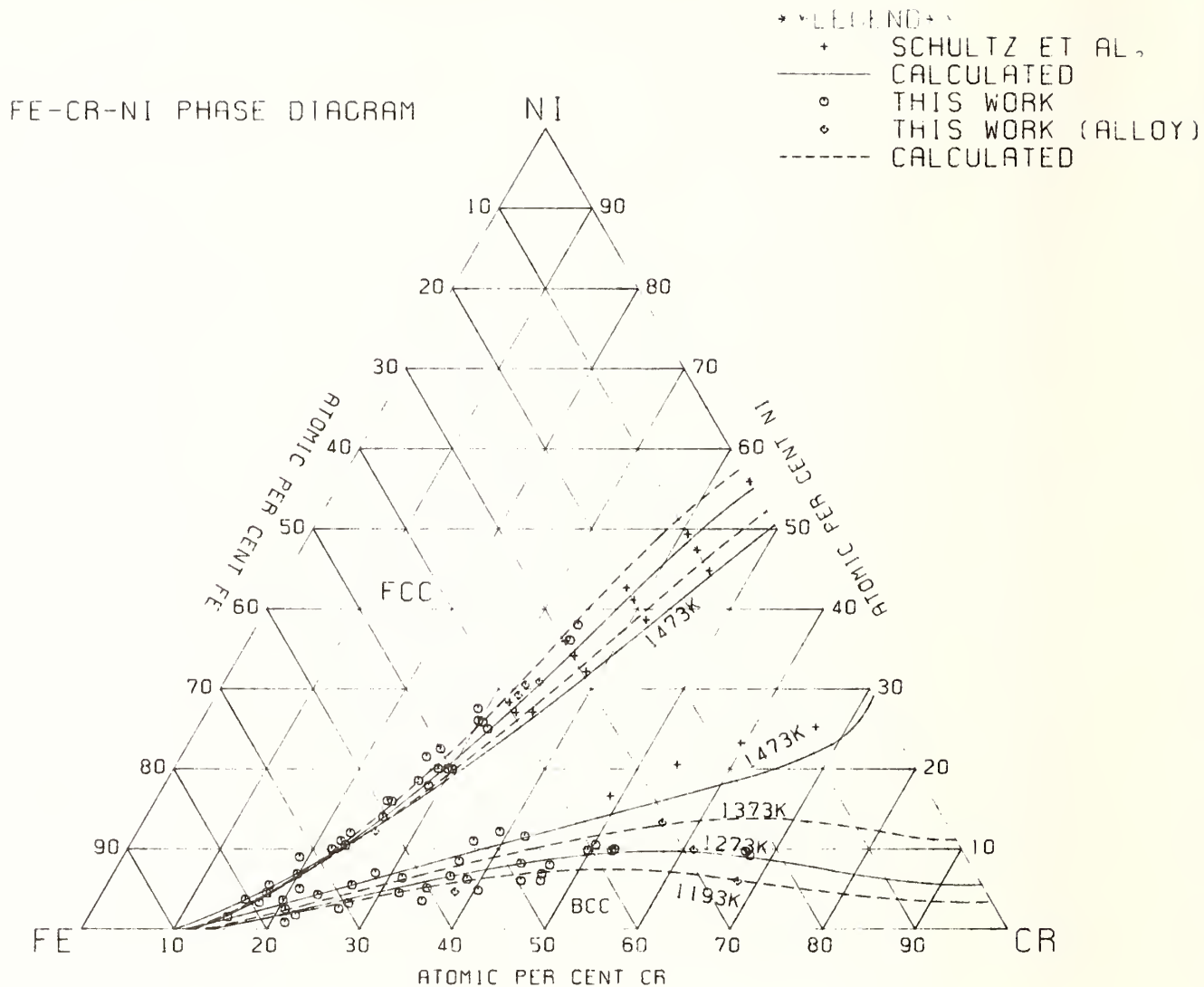


Fig. 10 The α/γ phase equilibria in the ternary Fe-Cr-Ni system between 1193 and 1473 K.

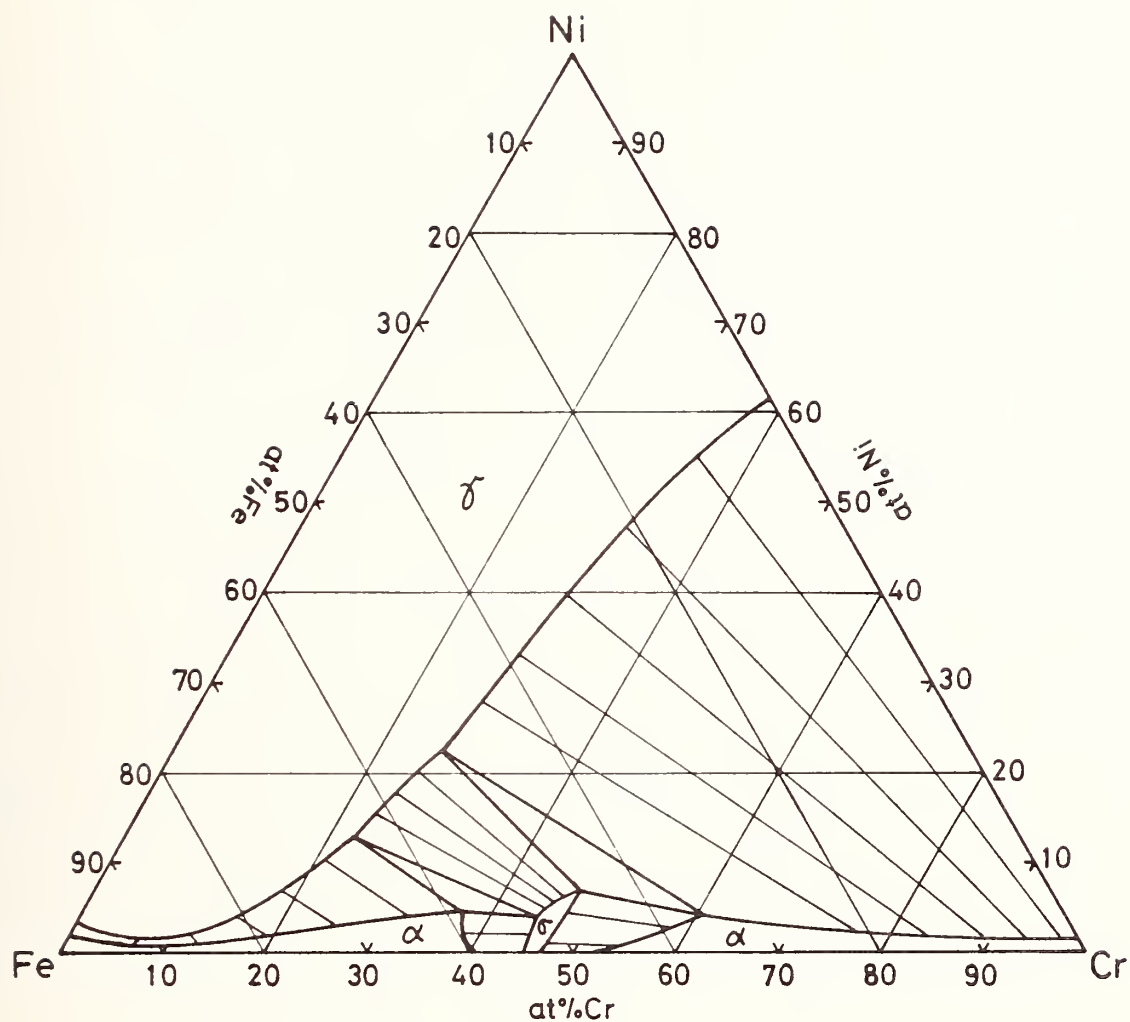


Fig. 12 Isothermal sections of the ternary Fe-Cr-Ni system at 1073 K. (a) Computer calculated.

Fe-Cr-Ni Phase Diagram

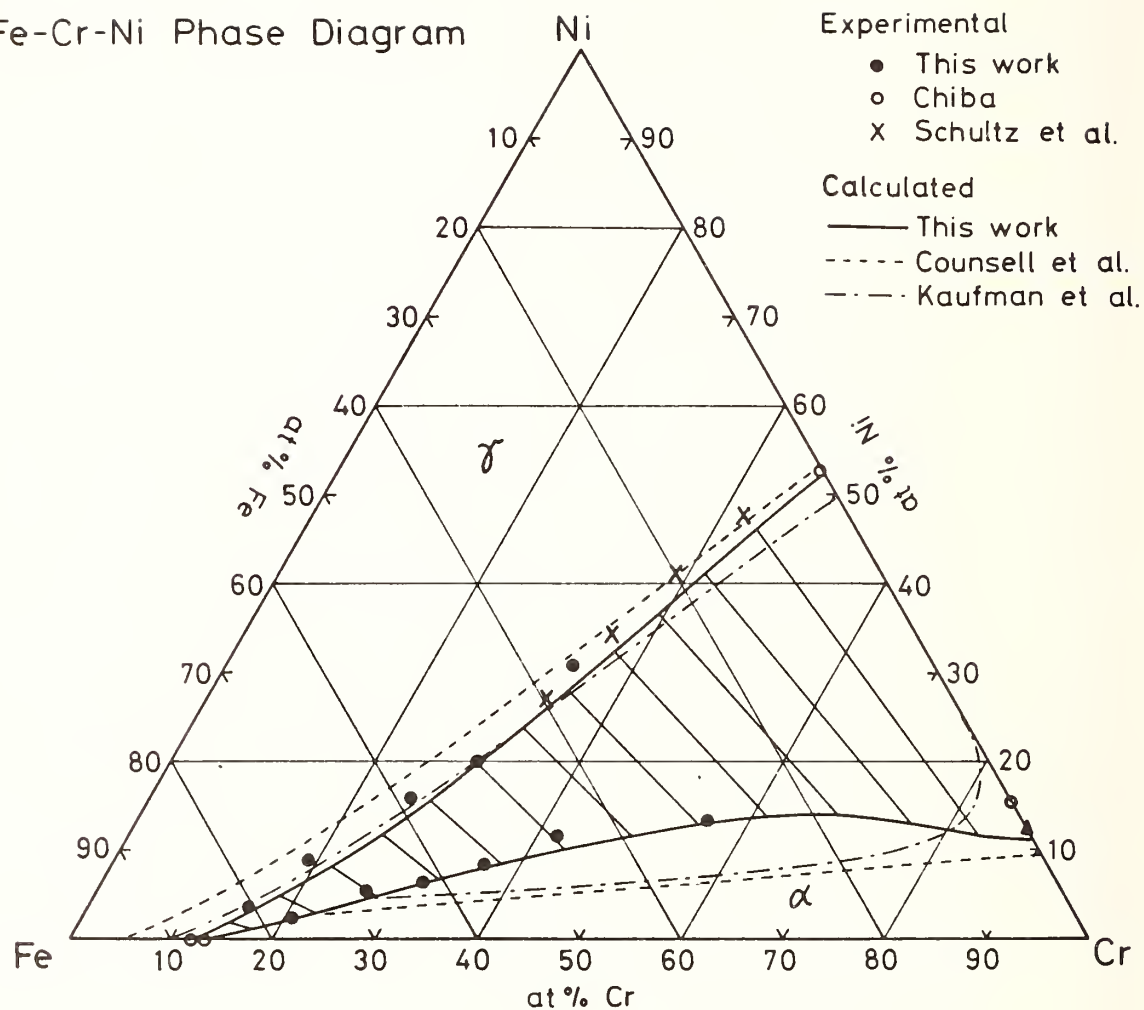


Fig. 13 Comparison between calculated and experimentally determined phase boundaries in the Fe-Cr-Ni system at 1373 K.

FE-MN-CU PHASE DIAGRAM

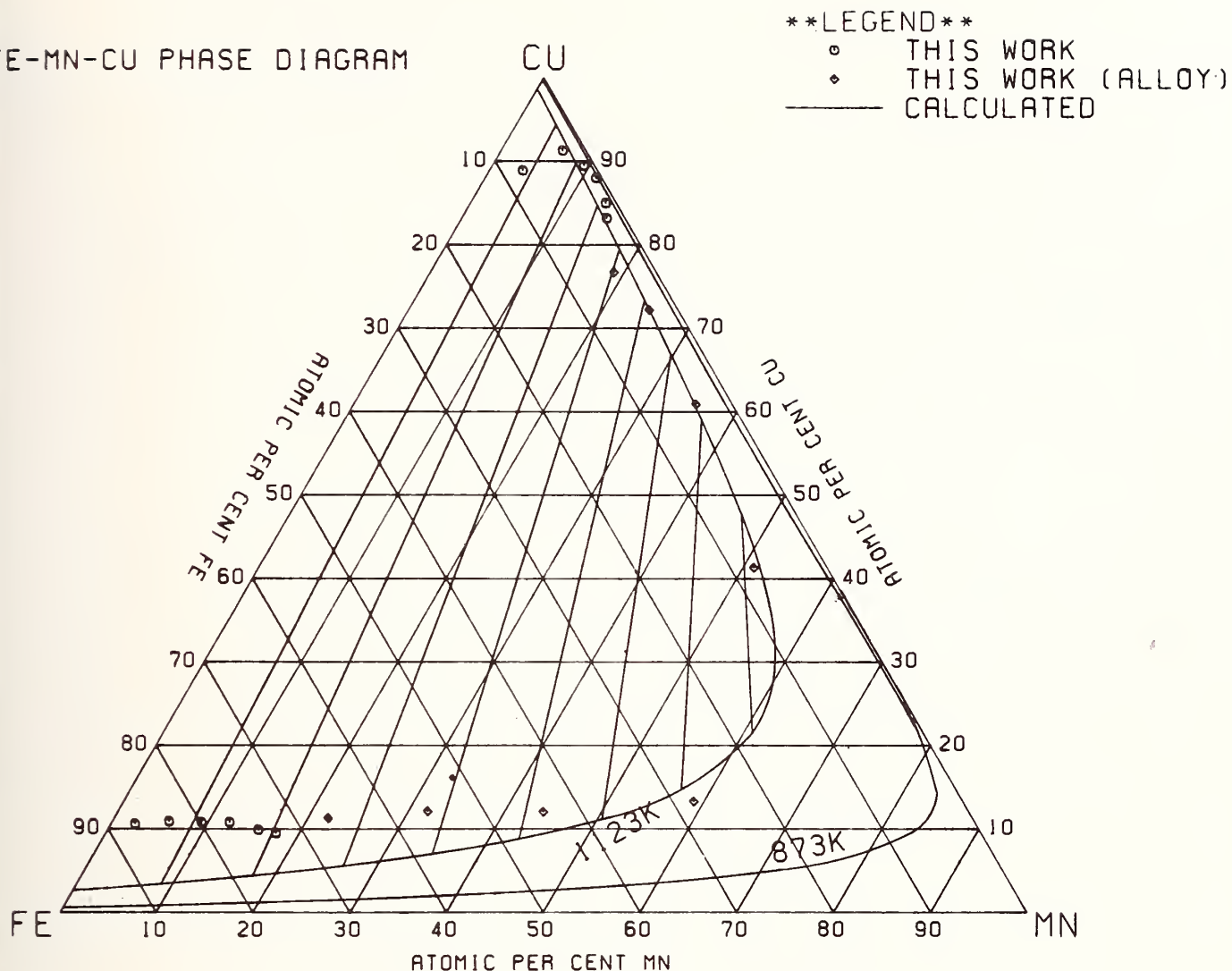


Fig. 14 Miscibility gap in the ternary Fe-Cu-Mn system between 873 and 1123 K.

FE-CR-NI PHASE DIAGRAM

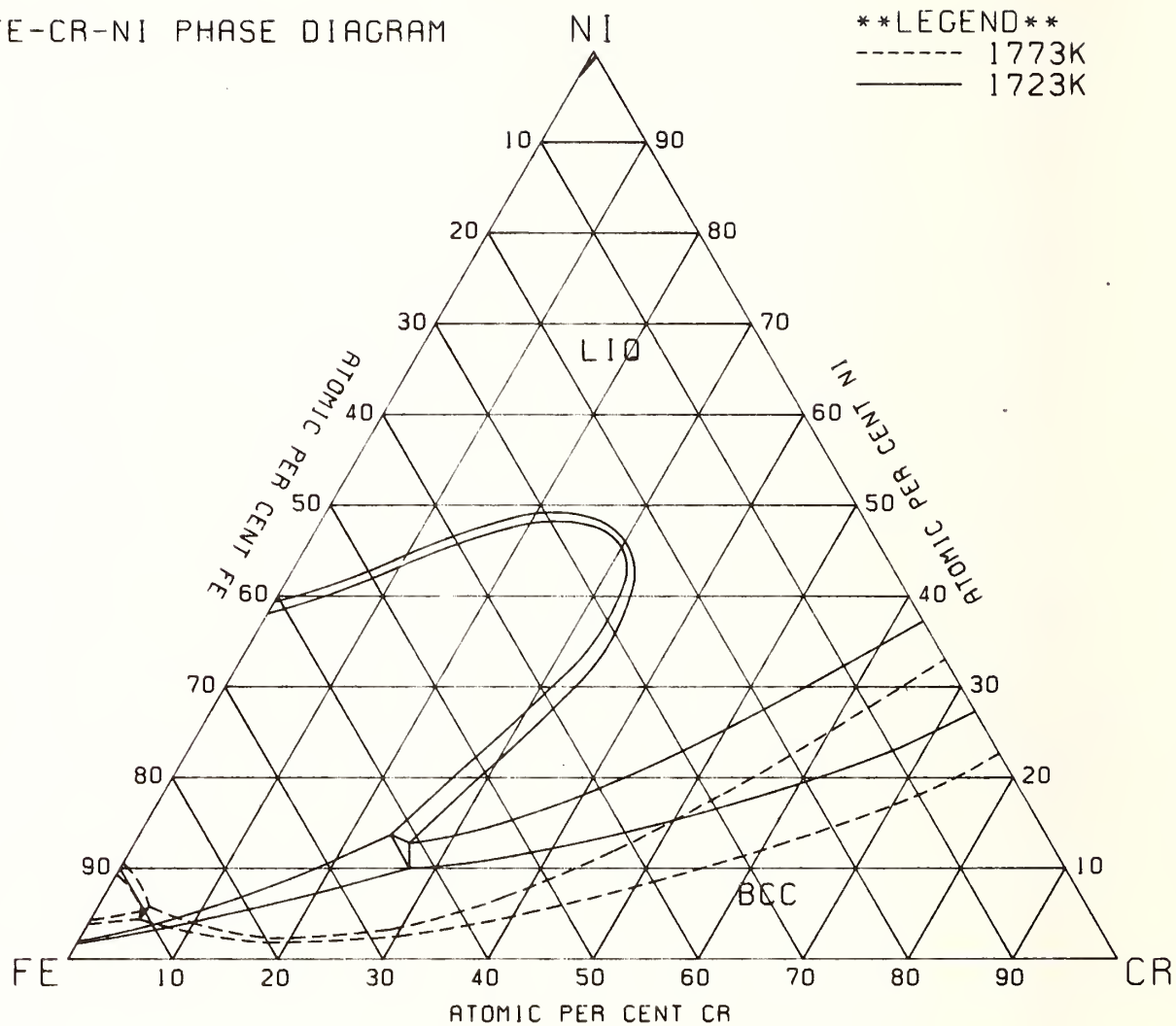


Fig. 11 The solid/liquid phase equilibria in the Fe-Cr-Ni system between 1723 and 1773 K.

FE-MN-CU PHASE DIAGRAM

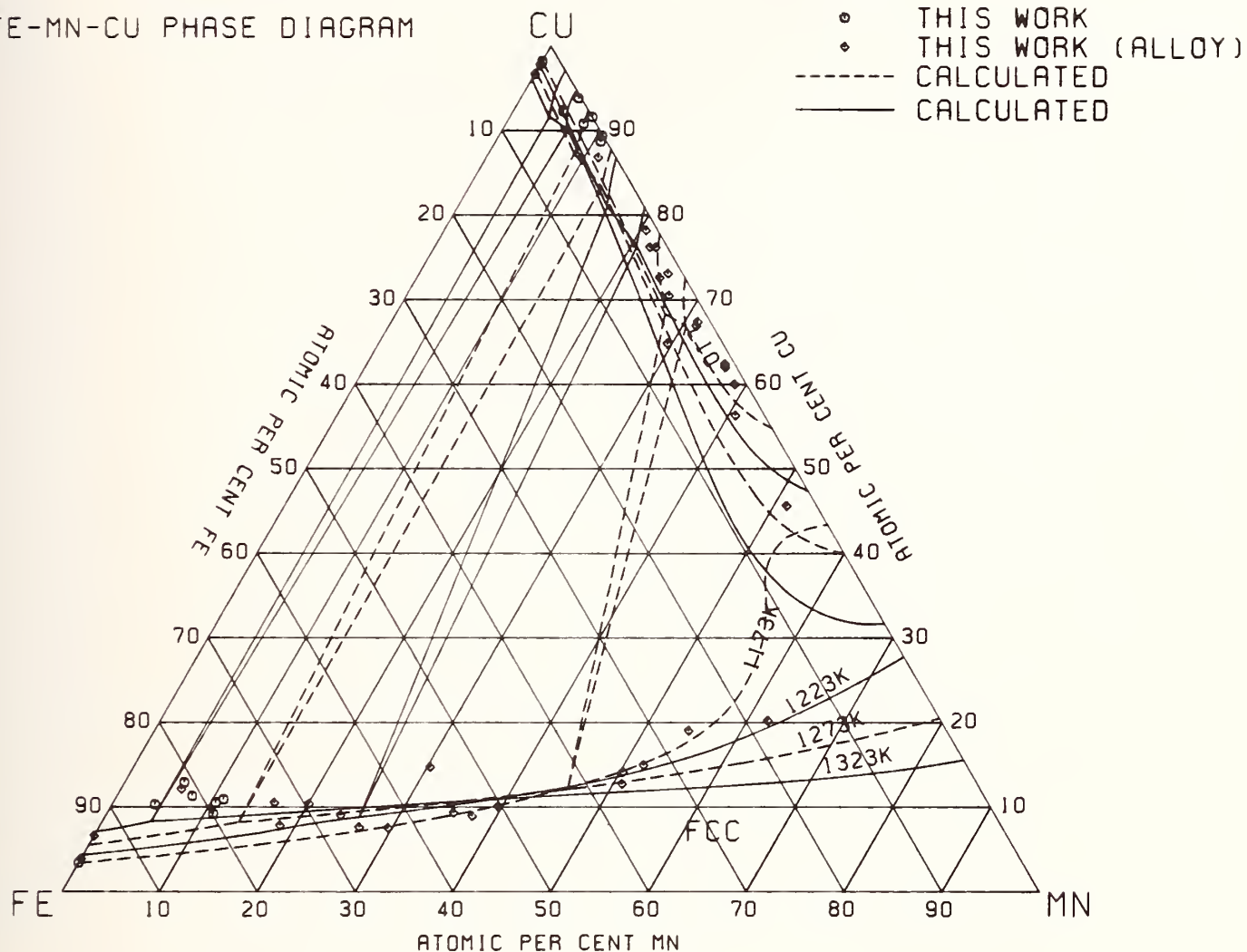


Fig. 15 The γ /liquid phase equilibria in the ternary Fe-Cu-Mn system between 1173 and 1323 K.

FE-MN-CU PHASE DIAGRAM

****LEGEND****

———— 1573K

----- 1423K

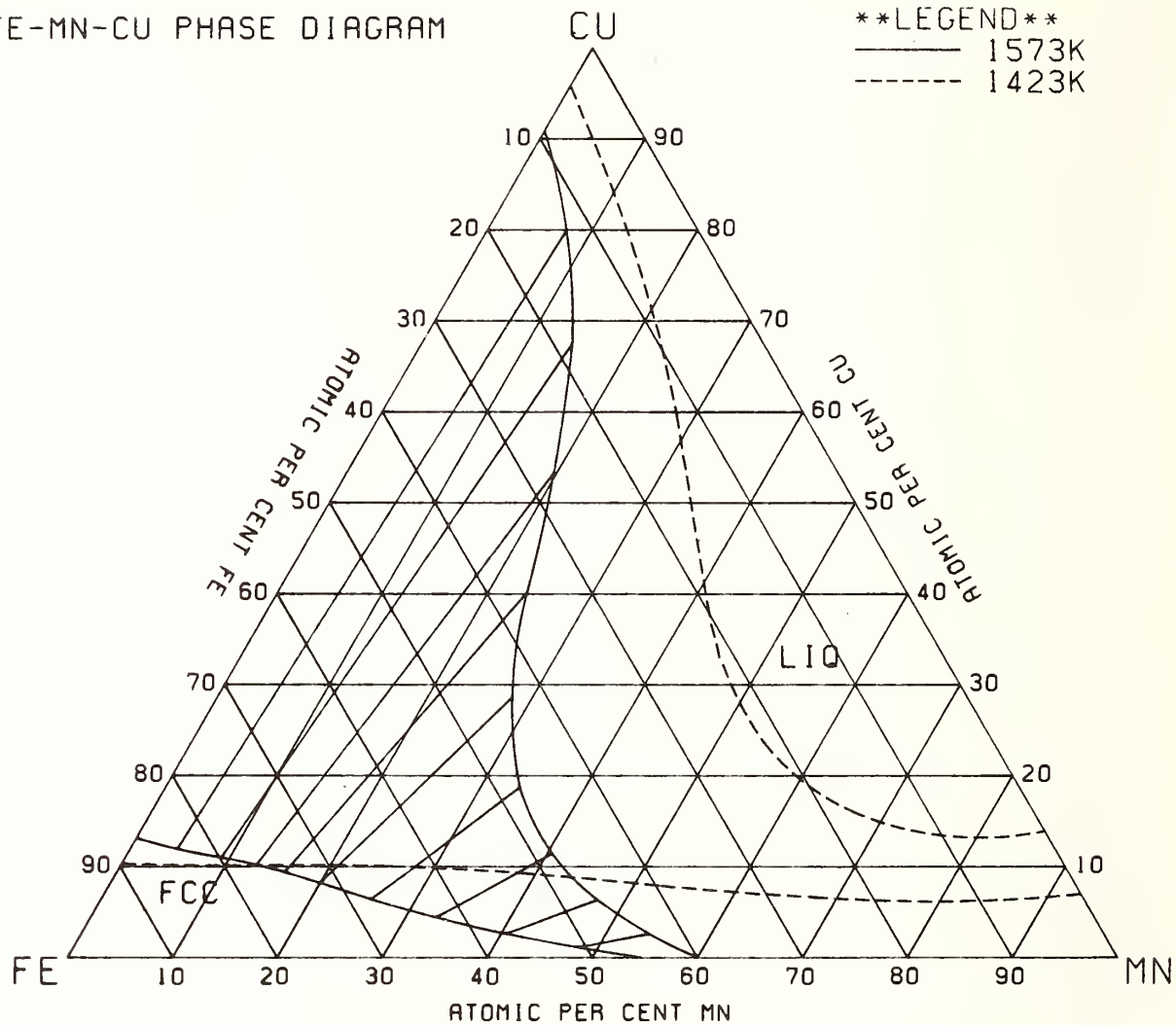


Fig. 16 The γ /liquid phase equilibria in the ternary Fe-Cu-Mn system between 1423 and 1573 K.

FE-NI-CU PHASE DIAGRAM

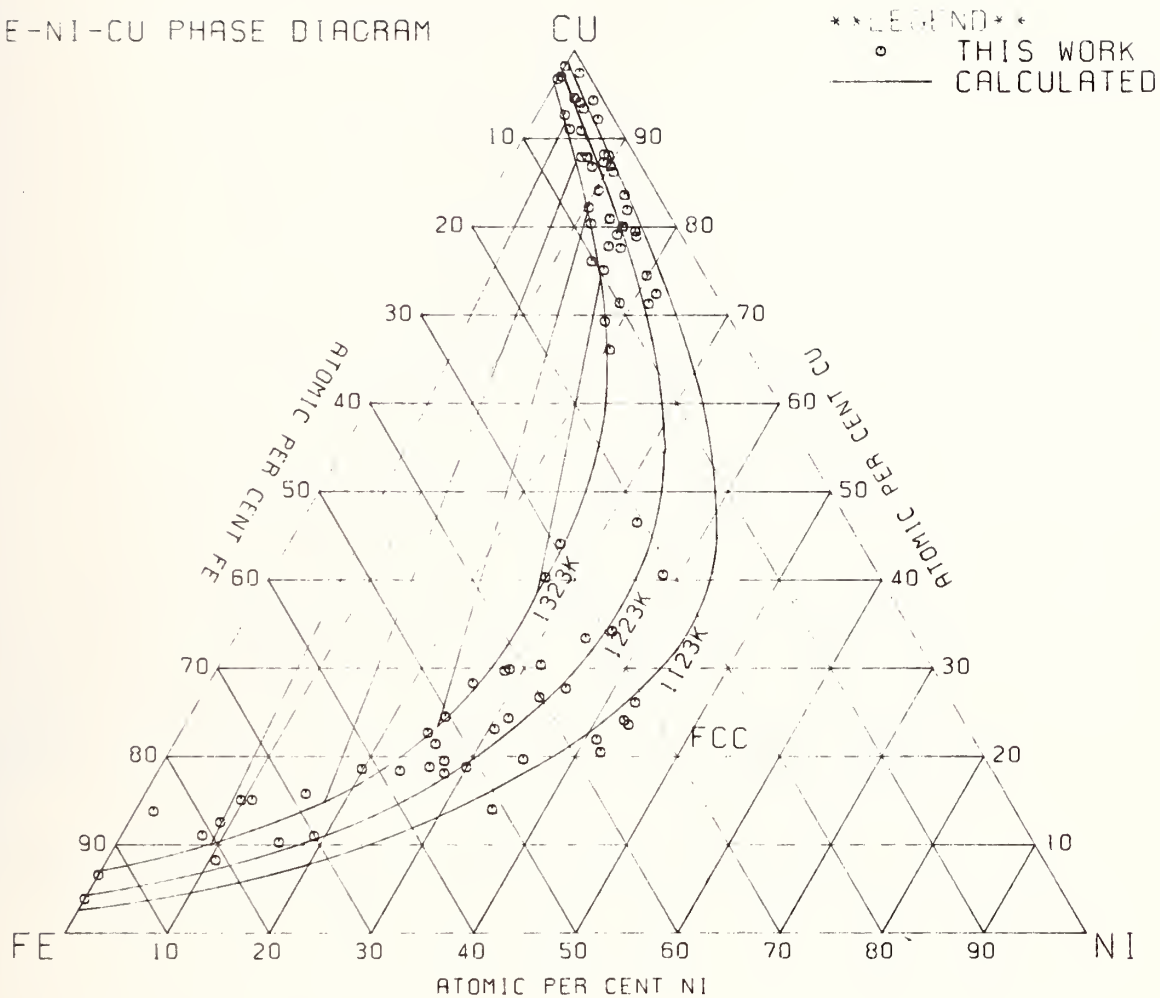


Fig. 17 Miscibility gap in the ternary Fe-Cu-Ni system between 1123 and 1323 K.

FE-NI-CU PHASE DIAGRAM

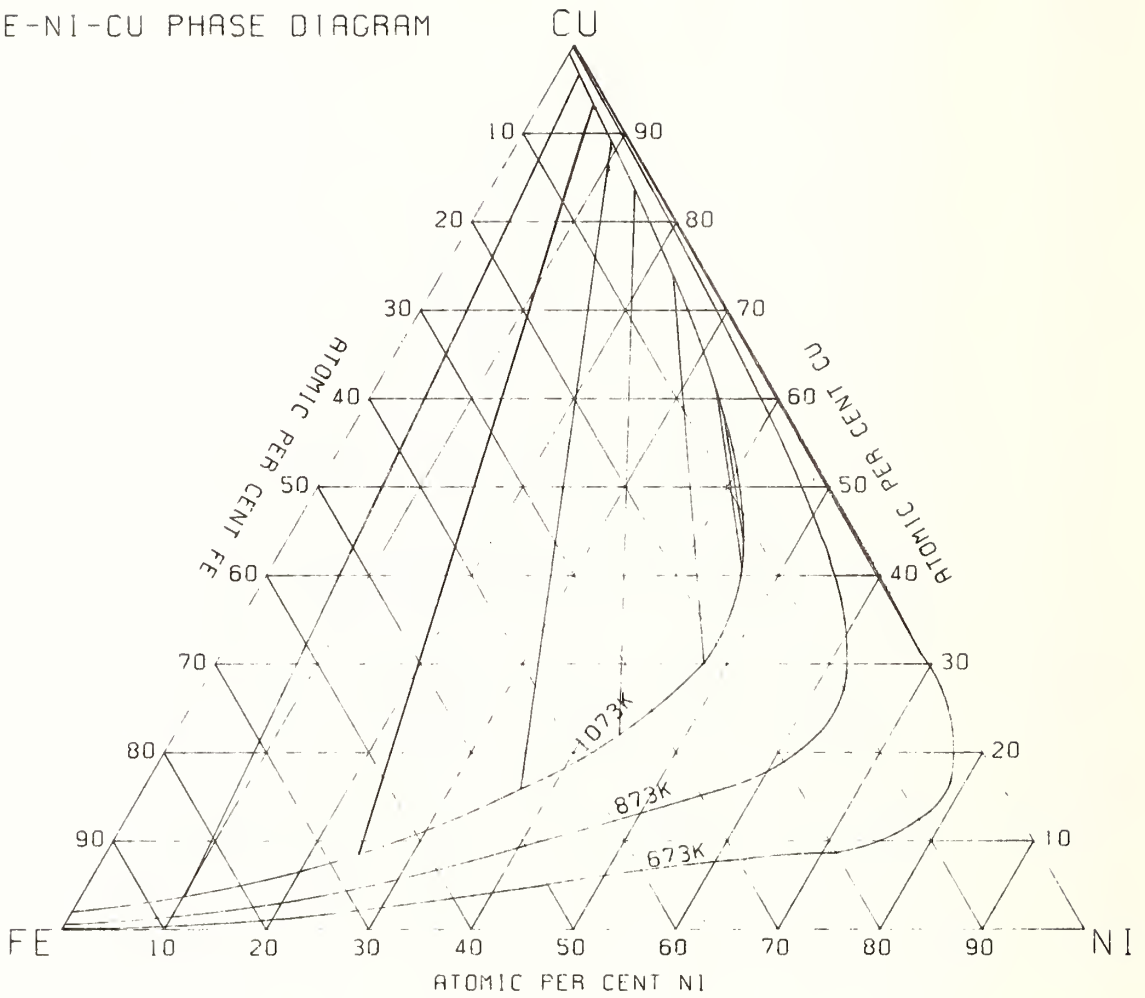


Fig. 18 Miscibility gap in the ternary Fe-Cu-Ni system between 673 and 1073 K.

FE-NI-CU PHASE DIAGRAM

LEGEND

— CALCULATED
 ◊ THIS WORK (ALLOY)
 - - - CALCULATED

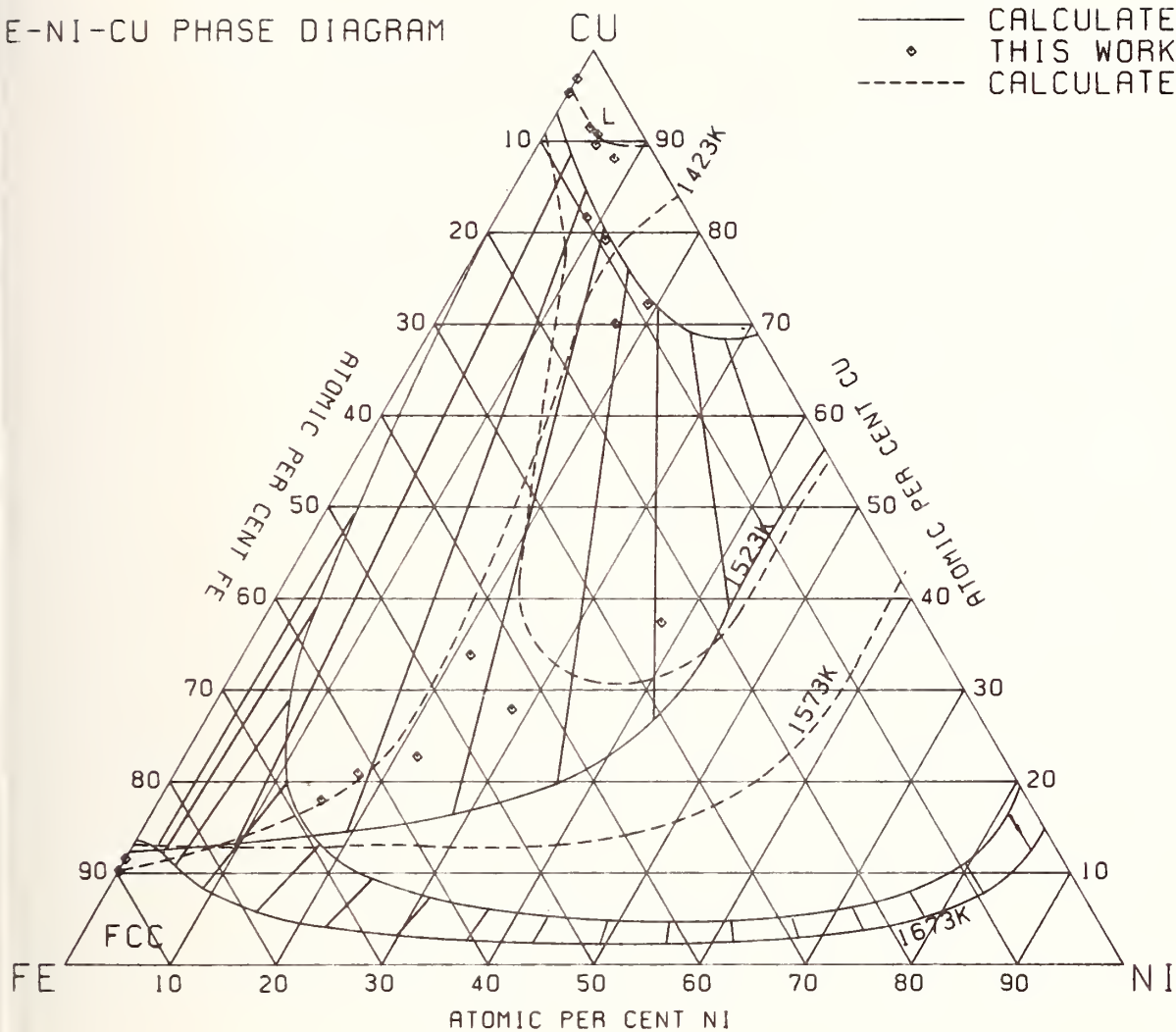


Fig. 19 The γ /liquid phase equilibria in the ternary Fe-Cu-Ni system between 1423 and 1673 K.

Fe-Cu-Ni Phase Diagram

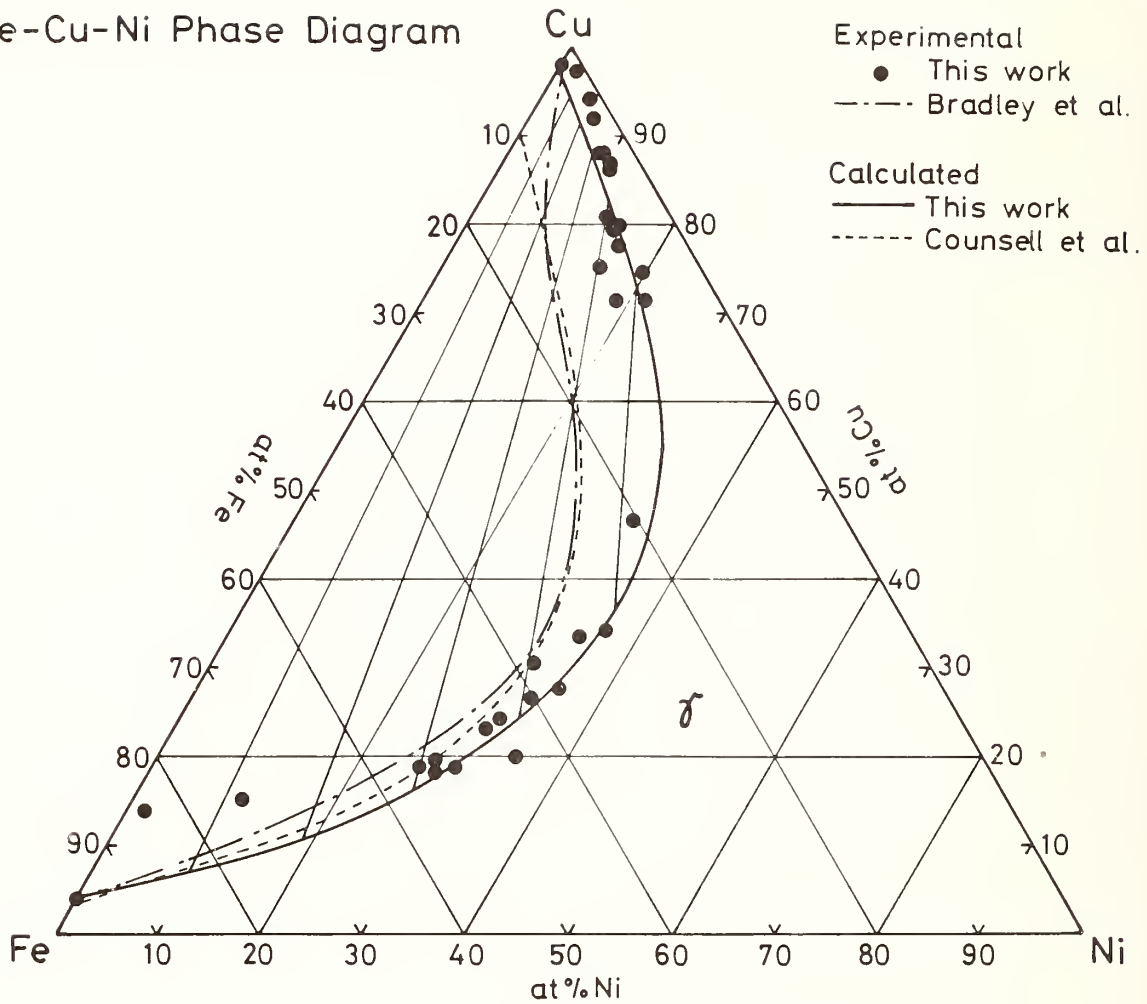


Fig. 20 Comparison between calculated and experimentally determined phase boundaries in the Fe-Cu-Ni system at 1223 K.

LEGEND
 ○ 1273K MAZANDARANY
 △ 1313K JEANNIN ET AL.
 — CALCULATED

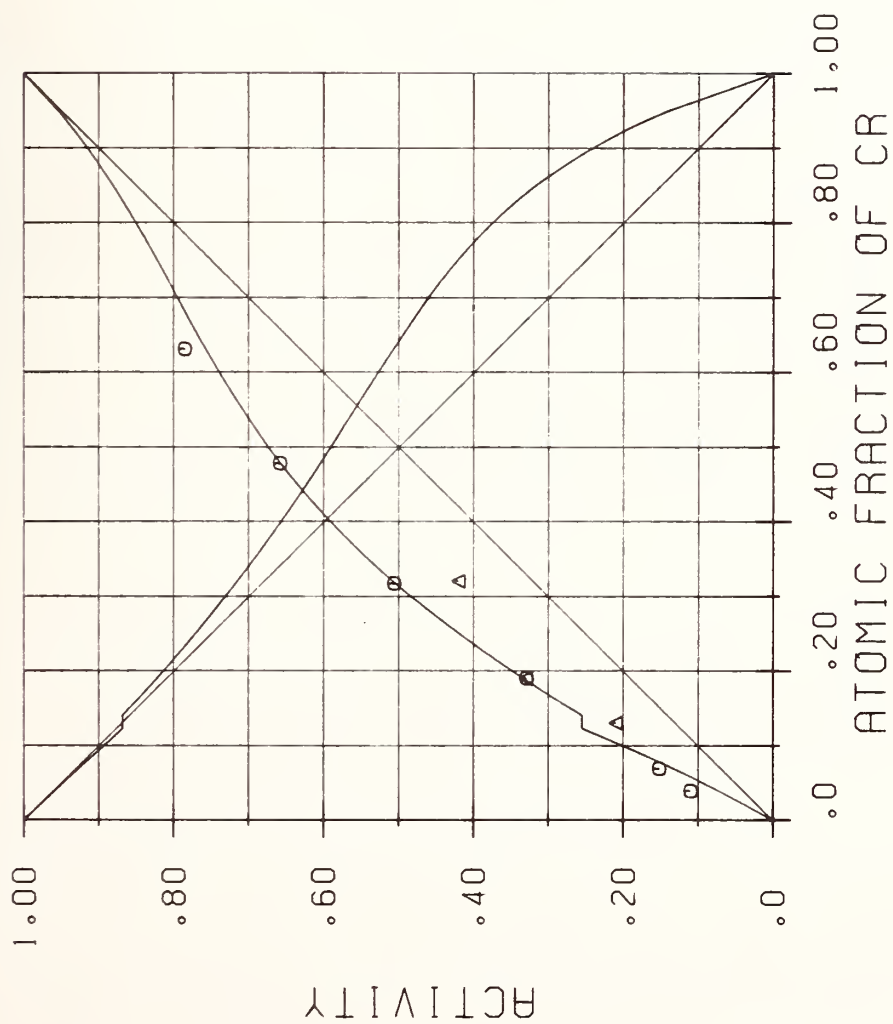


Fig. 21 Activities in the binary Fe-Cr system at 1273 K.

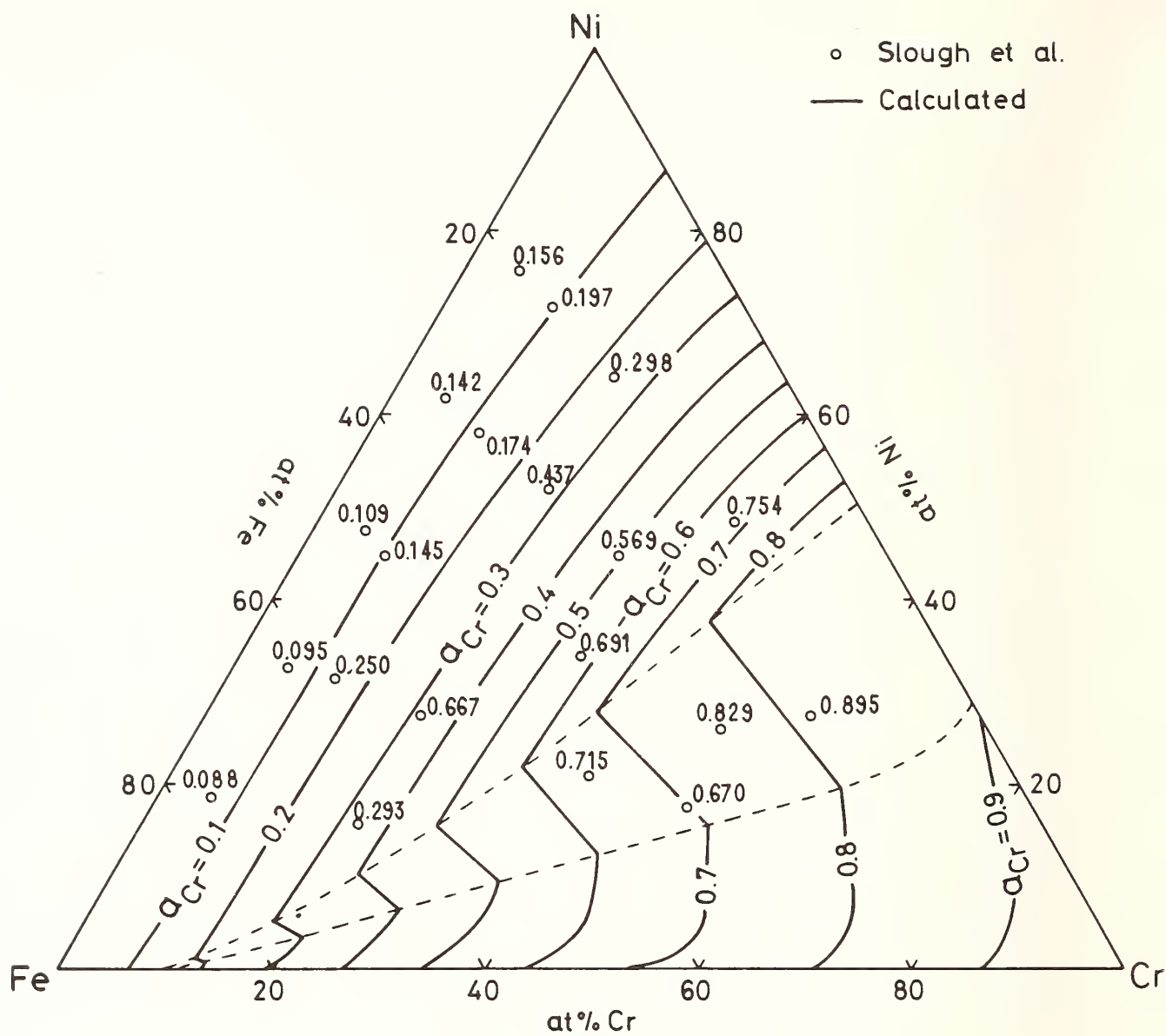


Fig. 22 Iso-activity lines for chromium in the ternary Fe-Cr-Ni system at 1473 K.



Optimization of Phase Diagrams by a Least Squares Method Using Simultaneously Different Types of Data.

E.-Th. Henig, H.L. Lukas, B. Zimmermann and G. Petzow
Max-Planck-Institut für Metallforschung, Institut für
Werkstoffwissenschaften, Büsnauerstr. 175, 7000 Stuttgart-80,
FRG.

Introduction

There are three main problems in constitutional research:

1. Using the existing experimental data the phase diagrams should be as accurate as possible,
2. A powerful tool is necessary to evaluate the enormous number of still unknown multicomponente systems,
3. The information should be storable in a compact form.

The optimal accuracy is obtained if all experimental data are taken into account and if thermodynamic consistency exists between all thermodynamic functions of the different phases and the phase diagram. If these functions are presented analytically they can be extrapolated for systems with one additional component. If the analytical representation uses always the same, standardised pattern, all the information of a system is contained in a set of coefficients and easily stored.

The optimization of a system based on different types of data usually is done by a trial and error method. With increasing number of components and/or increasing number of different types of data, this method becomes more and more cumbersome. Therefore a straight forward method is desirable. As straight forward method the Least Squares method of GAUSS is adapted here ¹⁾. This method is well known for optimization of single functions and also for the determination of the partial free enthalpy (Gibbs energy) from binary phase diagrams ²⁾ or from two phase tie lines of a ternary system ³⁾.

Analytical representation

The goal of the least squares method is the simultaneous calculation of the different thermodynamic functions. Therefore, an analytical formalism is necessary which describes the different functions with coefficients taken from one common set of coefficients. In this way also the thermodynamic consistency is expressed, which is given by the well known and used thermodynamic relations.

We used a combination of the matrix representation of Wiederkehr ⁴⁾ and the description of binary excess functions by Legendre-polynomials after Bale and Pelton ⁵⁾.

The formalism is extended by the Kohler ⁶⁾ extrapolations of the binary excess functions to describe the excess functions of ternary phases. An additional homogeneous polynomial (ternary correction) with the common factor $x_1x_2x_3$, which disappears in the binaries, is also introduced. The coefficients of this polynomial are determined by a few measurements in the ternary. The formulas are shown in appendix 1.

Instead of Kohler's extrapolation we used also the extrapolations of Bonnier and Caboz ⁷⁾, Toop ⁸⁾ and Hillert ⁹⁾. Those yield different functions and phase diagrams. But after adding the appropriate ternary correction function to each extrapolated function the differences decrease and become smaller than the accuracy of the measurements.

The matrices of different phases of one system are easily combined into one large matrix of coefficients of the whole system ⁴⁾. This is shown in figure 1 where the matrix belongs to the hypothetical system of figure 2.

Not all the coefficients are unknown. Normally the coefficients of the stable phases of the pure elements are known, they are designated with K in figure 1. The coefficients belonging to the ideal solution R in the second column and zero in all

other columns. Coefficients denoted by a dot are not significant, they are taken zero and treated as known coefficients. Only the coefficients quoted U are unknown and subject of the GAUSSian calculation.

Calculation

In the GAUSSian calculation one equation of error belongs to each experimental value. It describes the difference between the calculated and the measured value of one quantity.

Many thermodynamic statements are composed of a set of two or more independent measured values. For example a tie line in a binary system is defined by two independently measured concentration/temperature pairs. These equations are constructed in a form in which one equation is strongly dependent on one and weakly dependent on the other variables. In this way the different accuracy of the measured values affect mainly the related equation of error.

The different types of values (calorimetric, emf or vapor-pressure, phase diagram measurements) have their special equation of error. Also for one type of measurement special equations exist for different number of phases. They are compiled in appendix 2.

By these equations all measurable thermodynamic values can be treated, specially also values, which cannot be treated easily by trial and error methods. For example the change of enthalpy during mixing of two melts of alloys of slightly different composition. Measurements of this kind can be used advantageously for establishing the curvature of the enthalpy concentration curves.

In order to compare the errors of all measurements, they must be weighted and have the same dimension. In our method each error is compared with the accuracy of the corresponding measurement (as given by an author or estimated). If the error is divided by this accuracy, a dimensionless relative error is defined which is expressed in % of the accuracy. In

addition to the measured value itself also the variables temperature and concentration have limited accuracies. To take account of this they are transformed to the dependent variable by multiplying them with the derivative of the dependent variable with respect to the variable in question. Combining all this the weight of the square of the error is:

$$P = 1/(\Delta v)^2 + \left(\frac{\partial v}{\partial T} \Delta T\right)^2 + \left(\frac{\partial v}{\partial x} \Delta x\right)^2$$

Δv is the accuracy of dependent variable, ΔT of the temperature and Δx of the concentration. If there is more than one concentration involved in a set of measurements there are additional terms of the type $\left(\frac{\partial v}{\partial x} \Delta x\right)^2$.

The method described here is applied in the following way:

- (i) Optimization of the binary systems.
- (ii) Extrapolation of the optimized thermodynamic functions of the binary phases into the ternary.
- (iii) Optimization of the correction function using only a few ternary data.
- (iv) Extrapolation and optimization for the quaternary system, and so on.

The result of this procedure is a set of coefficients which contains the entire information of the systems in a thermodynamically consistent form. This set of coefficients provides the basis for the calculation of any thermodynamic diagram, in particular the phase diagram.

The method has been used successfully for the calculation of the ternary systems Ag-Bi-Pb ¹⁰⁾, Ag-Bi-Tl ¹¹⁾ and Ag-Pb-Tl ¹²⁾.

The financial support by the Deutsche Forschungsgemeinschaft is greatly acknowledged.

References

1. B. Zimmermann, Thesis, Uni Stuttgart 1976.
2. R. Hiskes and W.A. Tiller, Mater.Sci.Eng., 2 (1968) 320, 4 (1969) 163 and 4 (1969) 173.
3. G. Kirchner and B. Uhrenius, Acta met., 22 (1974) 523.
4. R.R.V. Wiederkehr, J.Chem.Phys., 37 (1962) 1192.
5. C.W. Bale and A.D. Pelton, Metall.Trans., 5 (1974) 2323.
6. F. Kohler, Monatsh. Chemie, 91 (1960) 738.
7. E. Bonnier and R. Caboz, C.R. Acad.Sci., 250 (1960) 527.
8. G.W. Toop, Trans.Met.Soc.AIME, 233 (1965) 850.
9. M. Hillert, Project Meeting CALPHAD V, 21.-25.6.1976, Düsseldorf.
10. H.L. Lukas, E.-Th. Henig and B. Zimmermann, to be published Z. Metallkde.
11. B. Zimmermann, E.-Th. Henig and H.L. Lukas, Z.Metallkde. 67 (1976) 815.
12. E.-Th. Henig and H.L. Lukas, to be published Z.Metallkde.

Appendix 1

MATRIX REPRESENTATION of Thermodynamic Functions after Wiederkehr ⁴⁾

$$((T_i)) \cdot ((C_{ij})) \cdot ((X_j)) = \text{value}$$

$((T_i))$ = line vector temperature and type of function
(enthalpy, entropy, Gibbs free
energy, specific heat)

$((C_{ij}))$ = matrix coefficients of individual system

$((X_j))$ = column vector concentration(s) and type of
function (integral, partial,....
sum of functions of two phases)

T_i Matrices of Different Functions

H	(1 0 T	$T^2/2$	$-T^{-1}$	$T^3/3$...)
S	(0 1 $\log(T)$	T	$-T^{-2}/2$	$T^2/2$...)
G	(1 -T $T(1-\log(T))$	$-T^2/2$	$-T^{-1}/2$	$-T^3/6$...)
C_p	(0 0 1	T	T^{-2}	T^2 ...)

X_j Matrices of Different Functions after Bale and Pelton ⁵⁾ Binary Phases

(P may be any of the functions H, S, G or C_p)

P	(1-x x	$(1-x)\log(1-x)$...	$x(1-x)P_1(1-2x)$...) + x $\log(x)$
P_1	(1 0	$\log(1-x)$...	$x^2 P_1(1-2x)$...) + $2x^2(1-x) \partial P_1 / \partial (1-2x)$
P_2	(0 1	$\log(x)$...	$(1-x)^2 P_1(1-2x)$...) - $2x(1-x)^2 \partial P_1 / \partial (1-2x)$

phase
stability
terms

ideal
solution
term

excess terms

Excess Terms of X_j Matrix of a Ternary Phase

Integral function

$$\dots x_1 x_2 P_1 \left(\frac{x_1 - x_2}{x_1 + x_2} \right) \dots x_2 x_3 P_1 \left(\frac{x_2 - x_3}{x_2 + x_3} \right) \dots x_3 x_1 P_1 \left(\frac{x_3 - x_1}{x_3 + x_1} \right) \dots$$

$$x_1^{n-p-q} x_2^p x_3^q \dots \text{ for } n \geq 3 \quad \begin{array}{l} \text{ternary correction} \\ p = 1 \dots n-2 \\ q = 1 \dots n-1-p \end{array}$$

(homogeneous polynomial)

$$P_1 \left(\frac{x_i - x_j}{x_i + x_j} \right) \quad \text{Kohler extrapolation of above formulas}$$

Partial functions are derived from the integral functions by the formula

$$P_i = P + \frac{\partial P}{\partial x_i} - \sum_{j=1}^3 x_j \frac{\partial P}{\partial x_j}$$

Appendix 2

EQUATIONS of ERROR

Calorimetric Measurements

Nr. of phases	equation
1	$H - (1-x)^{\circ}H_1 - x^{\circ}H_2 - \text{value} = \text{error}$
2	$H'(T_1) - H''(T_2) - \text{value} = \text{error}$
3	$H'(T_1) - \frac{x''' - x'}{x''' - x''} H''(T_2) - \frac{x' - x''}{x''' - x''} H'''(T_2) - \text{value} = \text{error}$

4 (ternary systems only)

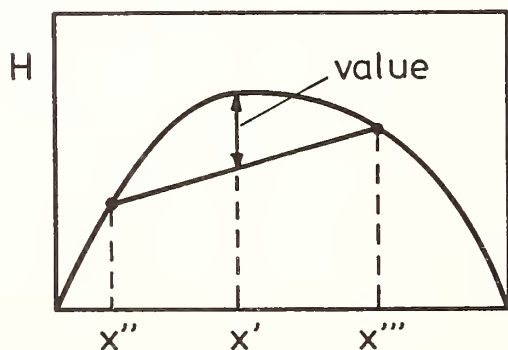
$$H'(T_1) - \frac{|Det''|}{|Det'|} H''(T_2) - \frac{|Det''''|}{|Det'|} H'''(T_2) - \frac{|Det''''|}{|Det'|} H''''(T_2) - \text{value} = \text{error}$$

or

$$\frac{|Det'|}{D} H'(T_1) + \frac{|Det''|}{D} H''(T_1) - \frac{|Det''''|}{D} H'''(T_2) - \frac{|Det''''|}{D} H''''(T_2) - \text{value} = \text{error}$$

$$\text{where } D = |Det'| + |Det''|$$

$$|Det'| = \begin{vmatrix} x_3'' & x_2'' & 1 \\ x_3''' & x_2''' & 1 \\ x_3'''' & x_2'''' & 1 \end{vmatrix}$$



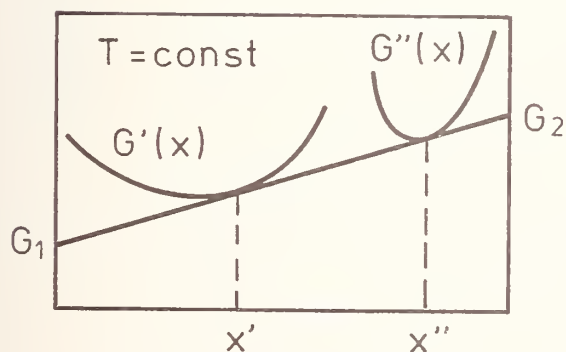
EMF and Vapor Pressure Measurements

Nr. of phases	equation
1	$G_i(x, T) - {}^0G_i^r(T) - \text{value} = \text{error}$
2	$G_i'(x, T) - {}^0G_i^r(T) - \text{value} = \text{error}$
	$G_i''(x, T) - {}^0G_i^r(T) - \text{value} = \text{error}$
	$G' - x' \frac{G'' - G'}{x'' - x'} - {}^0G_1^r(T) - \text{value} = \text{error} \quad (i=1)$

Symmetrical form of last equation:

$$i=1 \quad \frac{G' x''}{x'' - x'} + \frac{G'' x'}{x' - x''} - {}^0G_1^r - \text{value} = \text{error}$$

$$i=2 \quad \frac{G'(1-x'')}{x' - x''} + \frac{G''(1-x')}{x'' - x'} - {}^0G_2^r - \text{value} = \text{error}$$



Phase Diagrams

Binary:

2 phases:

$$G'(x') + (x'' - x')(\partial G'/\partial x)_{x'} - G''(x'') = \text{error}$$

point on tangent at x'' as point on
function of x' curve

$$G''(x'') + (x' - x'')(\partial G''/\partial x)_{x''} - G'(x') = \text{error}$$

See the last picture

3 phases:

2 equations of the type above, weighted by 1/2
(referred to square of error)

$$G'(x''' - x'') + G''(x' - x''') + G'''(x'' - x') = \text{error}$$

Ternary:

2 phases:

$$G' + (x_2'' - x_2')\left(\frac{\partial G'}{\partial x_2}\right)_{x_2', x_3'} + (x_3'' - x_3')\left(\frac{\partial G'}{\partial x_3}\right)_{x_2', x_3'} - G''(x_2'', x_3'') = \text{error}$$

$$G'' + (x_2' - x_2'')\left(\frac{\partial G''}{\partial x_2}\right)_{x_2'', x_3''} + (x_3' - x_3'')\left(\frac{\partial G''}{\partial x_3}\right)_{x_2'', x_3''} - G'(x_2', x_3') = \text{error}$$

$$\left(a\frac{\partial G'}{\partial x_2} + b\frac{\partial G'}{\partial x_3}\right)_{x_2', x_3'} - \left(a\frac{\partial G''}{\partial x_2} + b\frac{\partial G''}{\partial x_3}\right)_{x_2'', x_3''} = \text{error}$$

3 phases:

6 equations of type of equation 1 and 2 above

4 phases:

12 equations of type of equation 1 and 2 above, weighted by 2/3 (referred to square of error) and

$$|Det'| G' - |Det''| G'' + |Det'''| G''' - |Det''''| G'''' = \text{error}$$

$$\text{where } Det' = \begin{vmatrix} x_3'' & x_2'' & 1 \\ x_3''' & x_2''' & 1 \\ x_3'''' & x_2'''' & 1 \end{vmatrix}$$

other determinants are formed by cyclic replacement of phase indices in $|Det'|$

Three Phase Equilibrium, where one phase is stoichiometric in one direction

$$G'(x_2', x_3') + (x_1^* - x_1') (\partial G' / \partial x_1)_{x_2', x_3'} - G^*(x^*) = \text{error}$$

$$\text{where } x_1^* = \frac{x_j''' - x_j'}{x_j''' - x_j''} x_1'' + \frac{x_j'' - x_j'}{x_j'' - x_j'''} x_1'''$$

$$G^*(x^*) = \frac{x_j''' - x_j'}{x_j''' - x_j''} G''(x_2'', x_3'') + \frac{x_j'' - x_j'}{x_j'' - x_j'''} G'''(x_2''', x_3''')$$

x_j is the concentration to which the phase is stoichiometric (either $1 - x_2 - x_3$ or x_2 or x_3)

x_1 is the difference of the two other concentrations.

phase 1							2	3	4			
K	K	O	U	U	U	U	K	K	O	U	K	U
K	K	-R	U	U	U	U	K	K	-R	U	K	U
K	K	O	U	.	.	.	K	K	O	.	K	U
K	K	O	K	K	O	.	K	.

Fig. 1 Matrix of coefficients of a hypothetical binary system containing 4 phases, shown in fig. 2.

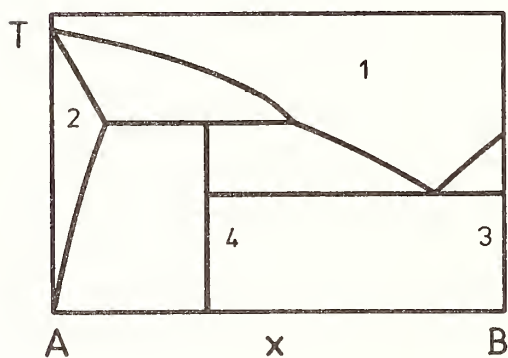


Fig. 2 Hypothetical system of the matrix shown in fig. 1.



Theoretical Calculation of Phase Diagrams Using the Cluster Variation Method

Ryoichi Kikuchi*[†] and Didier de Fontaine[†]

Abstract

The paper explains how the cluster variation (CV) method and the natural iteration (NI) technique can be used together in calculating phase diagrams. The grand potential Ω (rather than the free energy) is minimized, with temperature and chemical potential μ_i 's (rather than composition) kept fixed. The crossing point of Ω vs μ_i curves determines the coexisting phases. The NI technique solves the non-linear simultaneous equations which result from the CV formulation. Unlike the conventional Newton-Raphson iteration method, the NI method always converges and, at each iteration step, the grand potential Ω decreases step by step. The paper discusses the tetrahedron approximation for the fcc lattice, an extrapolation method for making the NI series converge faster, and orthogonality relations in connection with the chemical potential diagram.

*Hughes Research Laboratories, Malibu, CA 90265

[†]Materials Department, School of Engineering and Applied Science,
University of California, Los Angeles, CA 90024

1. Introduction

The companion article ("Fundamental Calculations of Coherent Phase Diagrams")¹ in this volume discusses the background to and the need for using the cluster variation (CV) method in combination with the natural iteration (NI) technique for phase diagram calculations. The application of the CV method in this field has progressed greatly since Golosov et al.² and van Baal³ independently used the tetrahedron approximation of the fcc lattice in calculating diagrams of Cu_3Au and CuAu-type ordered phases.

The NI technique,⁴ which was discovered nearly simultaneously with the activities in Refs. 2 and 3, has greatly simplified the calculations required for the CV method. Application of CV-NI methods to ternary systems has been reported recently.^{5,6} In this paper, we report detailed computational steps for calculating phase diagrams.

2. Pair Approximation

In this section, we explain the CV method, taking a pair of nearest neighbors as the basic cluster. We discuss the phase-separating case; each lattice point is equivalent and no superlattices are needed.

All the possible configurations of a nearest-neighbor pair are listed in Table I for the example of a binary alloy. As shown in the table, a distribution variable of y_{ij} is assigned to each configuration, with $i = 1$ used to designate an A atom and $i = 2$ for a B atom. The

variable y_{12} , for example, is the probability that a certain pair takes the A-B configuration. The y 's are normalized to unity:

$$\sum_i \sum_j y_{ij} = 1 \quad . \quad (2.1)$$

Table I. Configurations of a Pair

Configuration	Distribution Variable
A-A	y_{11}
A-B	y_{12}
B-A	y_{21}
B-B	y_{22}

When we formulate the CV method using the notation i and j as in (2.1), it is applicable to the binary case and also to cases with more components. For a ternary system with vacancies, for example, we can choose $i = 3$ for a C atom and $i = 4$ for a vacancy.

In addition to the pair variables, the y_{ij} 's, in Table I, we need distribution variables, x_i 's, for the configuration of a lattice point. These are listed in Table II. When the number of lattice points in a system is N , and the number of A atoms is N_A , and of B atoms is N_B , then the meaning of x_i is given by the relations:

$$N_A = x_1 N \quad \text{and} \quad N_B = x_2 N \quad , \quad (2.2)$$

where the variables x_i and y_{ij} are related by the geometric relation:

$$x_i = \sum_j y_{ij} \quad . \quad (2.3)$$

We will write the free energy (actually the grand potential Ω) in terms of the x 's and y 's and then minimize Ω with respect to the y 's to derive the y values which correspond to the equilibrium state.

Table II. Configurations of a Point

Configuration	Distribution Variable
A	x_1
B	x_2

Energy is the first quantity we examine. For a system with N lattice points and a coordination number 2ω , the total number of nearest-neighbor bonds will be ωN . Since this paper treats only the nearest-neighbor interaction case, the total energy E_N of the system is

$$E_N = \omega N \sum_i \sum_j \epsilon_{ij} y_{ij} \quad , \quad (2.4)$$

where ϵ_{ij} is the nearest-neighbor interaction potential between the i^{th} and j^{th} species. The ϵ_{ij} 's for the binary alloy case are ϵ_{11} for an A-A pair, $\epsilon_{12} = \epsilon_{21}$ for an A-B pair, and ϵ_{22} for a B-B pair.

The entropy for the pair approximation of the CV method for a system of N lattice points is^{7,8}

$$S_N = k \ln \frac{\left[\prod_i (x_i N)! \right]^{2\omega-1}}{\left[\prod_i \prod_j (y_{ij} N)! \right]^\omega N!^{\omega-1}} . \quad (2.5a)$$

Stirling's approximation allows us to rewrite (2.5a) as

$$S_N = kN \left[(2\omega - 1) \sum_i x_i \ln x_i - \omega \sum_i \sum_j y_{ij} \ln y_{ij} \right] . \quad (2.5b)$$

Using S_N in (2.5b) and E_N in (2.4), the Helmholtz free energy F_N , expressed as a function of the y_{ij} 's, is

$$F_N = E_N - TS_N . \quad (2.6)$$

One method of deriving the equilibrium state is to minimize F_N in (2.6) with respect to the y_{ij} 's, holding the composition $x_1 = 1 - x_2$ fixed. This method yields the equilibrium free energy for the assigned value of x_1 .

When the system phase separates, the plot of F_N vs x_1 will be as shown in Fig. 1. In Fig. 1, the coexisting two phases are B and F,

which share the common tangent to the curve. Written mathematically, the coexistence condition is

$$\frac{F_N(F) - F_N(B)}{x_1(F) - x_1(B)} = F'_N(F) = F'_N(B) \quad , \quad (2.7)$$

where F'_N is the derivative of the F_N versus x_1 curve in Fig. 1 and (F) and (B) refer to points in Fig. 1. If we write the common tangent as μN (i. e. , $F'_N(F) = F'_N(B) = \mu N$), then (2.7) can be rewritten as

$$F_N(F) - \mu N x_1(F) = F_N(B) - \mu N x_1(B) \quad . \quad (2.8)$$

This means that if we define a new function

$$\Omega_N = F_N - \mu x_1 N \quad , \quad (2.9)$$

the value of this function will be the same at points B and F. The requirement that μ is the tangent, dF_N/dx_1 , leads to the condition

$$\left. \frac{\partial \Omega_N}{\partial x_1} \right|_{\mu} = \frac{dF_N}{dx_1} - \mu N = 0 \quad , \quad (2.10)$$

which means that the function Ω_N is a minimum with respect to x_1 in equilibrium state for a fixed value of μ .

Taking into account the symmetry of the A and B components, we redefine Ω_N from (2.9) as

$$\Omega_N \equiv F_N - \sum_i \mu_i x_i N \quad , \quad (2.11)$$

which we will call the grand potential. In this expression, μ_1 is the chemical potential for A atoms and μ_2 that for B atoms:

$$\mu_1 = \left(\frac{\partial F_N}{\partial N_A} \right)_{N_B}, \quad \mu_2 = \left(\frac{\partial F_N}{\partial N_B} \right)_{N_A}. \quad (2.12)$$

Our program is to find the equilibrium state of the system as a minimum of Ω_N with respect to the y_{ij} 's keeping the μ_i 's (rather than the x_i 's) fixed, and then to plot Ω_N against μ_1 (rather than x_1 , as was done in Fig. 1). For the example of a binary alloy for which vacancies are neglected, we can impose a subsidiary condition:

$$\mu_1 + \mu_2 = 0. \quad (2.12)$$

When the equilibrium state is found for a fixed value $\mu_1 (= -\mu_2)$, the grand potential Ω_N is a function of μ_1 . For the system of Fig. 1, the Ω_N vs μ_1 curve looks as shown in Fig. 2. In Fig. 2, the points designated by A, B, ..., G, H correspond to those with the same letters in Fig. 1. As expected, the common tangent B-F in Fig. 1 shrinks to a point in Fig. 2. In determining the coexisting phases, it is easier and more accurate to find where two curves cross, as in Fig. 2, than to locate two points of a common tangent, as in Fig. 1. For this reason, we will work with Ω_N in this paper.

In passing, we may comment that a spinodal is represented by an inflexion point, $d^2 F_N / dx_1^2 = 0$, in Fig. 1, and by a cusp or spinode in Fig. 2 (points C and G); this indicates the origin of the word spinodal.

3. The Natural Iteration Calculation

In carrying out the computation described in the previous section, it is convenient to use the NI method,⁴ a mathematical approach which was designed specifically for solving the equations needed in the CV formulation. Using (2.6), (2.5b), and (2.4), we write the grand potential Ω_N in (2.11) as

$$\begin{aligned} \Phi \equiv \frac{\beta \Omega_N}{N} = & \beta \omega \sum_{i,j} \epsilon_{ij} \mu_{ij} - \frac{2\omega - 1}{2} \left[\sum_i \mathcal{L}(x_i) + \sum_j \mathcal{L}(x_j) \right] \\ & + \omega \sum_{i,j} \mathcal{L}(y_{ij}) - (\omega - 1) - \frac{\beta}{2} \sum_{i,j} (\mu_i + \mu_j) y_{ij} \\ & + \beta \lambda \left(1 - \sum_{i,j} y_{ij} \right) , \end{aligned} \quad (3.1)$$

where

$$\beta \equiv \frac{1}{kT} \quad (3.2b)$$

and the \mathcal{L} -operator is defined as

$$\mathcal{L}(x) \equiv x \ln x - x . \quad (3.2b)$$

This operator originates in the Stirling approximation of the factorial.

In the expression Φ , the first term comes from E_N in (2.4). The

two terms $\mathcal{L}(x_i)$ and $\mathcal{L}(x_j)$ are equal and come from the x -term in S_N of (2.5b). In the two $\mathcal{L}(x)$ terms in (3.1), we use the expressions

$$x_i = \sum_j y_{ij} \quad \text{and} \quad x_j = \sum_i y_{ij} \quad (3.3)$$

to make the treatment symmetric. Also for symmetry, the $\mu_i + \mu_j$ sum is written as in (3.1) because

$$\frac{1}{2} \sum_{i,j} (\mu_i + \mu_j) y_{ij} = \frac{1}{2} \sum_i \mu_i x_i + \frac{1}{2} \sum_j \mu_j x_j = \sum_i \mu_i x_i, \quad (3.4)$$

which is the second term in expression (2.11) for Ω_N . The λ terms in (3.1) take care of normalizing the y 's as in (2.1).

When we minimize Φ in (3.1), the y_{ij} 's are regarded as independent and x_i and x_j as dependent through (3.3). Differentiation then leads to

$$\begin{aligned} \frac{\partial \Phi}{\partial y_{ij}} &\equiv \beta \omega \epsilon_{ij} - \frac{2\omega - 1}{2} \ln(x_i x_j) + \omega \ln y_{ij} \\ &\quad - \frac{\beta}{2} (\mu_i + \mu_j) - \beta \lambda = 0 \end{aligned} \quad (3.5)$$

or

$$y_{ij} = \exp \left[\frac{\beta \lambda}{\omega} - \beta \epsilon_{ij} + \frac{\beta}{2\omega} (\mu_i + \mu_j) \right] (x_i x_j)^{(2\omega-1)/(2\omega)}. \quad (3.6)$$

The NI method works as follows. We fix the values of $\beta = 1/kT$ and $\mu_1 (= -\mu_2)$ and then begin with the first input value of x_1 , which is guessed.

(i) For the input value x_1 (and hence $x_2 = 1 - x_1$), we calculate

$$y_{ij}^{(0)} \equiv \exp \left[-\beta \epsilon_{ij} + \frac{\beta}{2\omega} (\mu_i + \mu_j) \right] (x_i x_j)^{(2\omega-1)/(2\omega)} \quad (3.7)$$

for all values of i and j . Then we determine the normalization factor $\exp(\beta\lambda/\omega)$ using the normalization relation (2.1) as

$$\exp(\beta\lambda/\omega) = \left[\sum_i \sum_j y_{ij}^{(0)} \right]^{-1} \quad (3.8)$$

Multiplying $y_{ij}^{(0)}$ in (3.7) and $\exp(\beta\lambda/\omega)$ yields the output y_{ij} . In short, step (i) is to calculate the left-hand side of (3.6), y_{ij} , as the output when the inputs x_i and x_j are used on the right-hand side. This output is written as \hat{y}_{ij} .

(ii) The next step is to use the output values \hat{y}_{ij} to calculate the next inputs, \hat{x}_i and \hat{x}_j , from (3.3). Then we return to step (i) above and repeat the cycle.

This process of going back and forth between steps (i) and (ii) is the NI method. It differs from the well-known Newton method (or the Newton-Raphson method when the number of independent variables is more than one), in that NI has the unique feature that the function being minimized (in the present example, the grand potential Ω_N) always

decreases step by step at each iteration. This property of a monotonic decrease, which can be proved analytically,⁴ has the important consequence that the NI procedure converges from whatever initial guess we start with (except for pathological cases).

An example is shown in Fig. 3, which is for bcc ($\omega = 4$) and $\mu_1 = \mu_2 = 0$ for the phase-separating case. Each dot represents output of one iteration cycle. The figure shows two iteration series (one from the right and the other from the left). The point marked $n = \infty$ is the convergence point. In one calculation, the initial guessed value of x_1 was taken as $x_1 = 0.4$, near the top of the right-hand series of dots. If the Newton-Raphson method had been used, the initial guess $x_1 = 0.4$ would have led to the metastable solution at $x_1 = 0.5$, which does not correspond to the phase-separation. The NI method seeks, as illustrated in Fig. 3, the stable solution at $x_1 = 0.02456$. If we start from an initial value x_1 larger than 0.5, NI leads to the other stable solution at $x_1 = 0.97544$. Since the grand potentials for these two points are equal, as are the chemical potentials, they are the two coexisting phases.

As a measure of convergence, we can use

$$\Delta_n \equiv \left| x_1^{(n)} - x_1^{(n-1)} \right|, \quad (3.9)$$

where n is the number of iterations. The quantity Δ_n decreases exponentially as the iteration proceeds, as shown in Fig. 4. Along with Δ_n , the difference $\left| \Omega^{(n)} - \Omega^{(n-1)} \right|$ also decreases exponentially as

n increases. For the iteration calculation, we can safely regard the iteration as converged when Δ_n becomes less than 10^{-6} . When the iteration has converged, we can prove from (3.1) and (3.5) that

$$\Phi = \Phi - \sum y_{ij} \frac{\partial \Phi}{\partial y_{ij}} = \beta \lambda \quad , \quad (3.10a)$$

which means that the Lagrange multiplier λ , which appears in the normalization factor in (3.8), is the value of the grand potential Ω_N per lattice point:

$$\lambda = \Omega_N / N \quad . \quad (3.10b)$$

4. Tetrahedron Approximation for fcc

The decisive difference between the CV method and the widely used Bragg-Williams method involves the treatment of the ordered phases in the fcc structure. For this structure, the basic cluster of the CV formulation is the tetrahedron made of four nearest-neighbor lattice points.^{2,3}

First, we formulate the clustering case. In this case, all lattice points can be treated as equivalent, and superlattices are not needed. As the distribution variables, we use y_{ij} and x_i (defined in Tables I and II) together with the variables z_{ijkl} . A z_{ijkl} is defined as the distribution variable for the configuration i-j-k-l of the tetrahedron. In a ternary system, for example, each i, j, k, and l takes a value 1, 2, or 3 corresponding to an A, B, or C atom.

The energy for a system of N lattice points is written, in place of (2.4), as

$$E_N = 2N \sum_{i,j,k,l} \epsilon_{ijkl} z_{ijkl} \quad , \quad (4.1)$$

where $2N$ is the total number of tetrahedra in the system and the energy per tetrahedron is written as ϵ_{ijkl} . When we write the energy in this form, ϵ_{ijkl} can contain four-body interactions in a tetrahedron. As an example, in the binary system the general expression for the energy parameters are

$$\begin{aligned} \epsilon_{1111} &= 0 \\ \epsilon_{1112} &= \frac{3}{2} \epsilon_{12}(1 + \alpha) \\ \epsilon_{1122} &= 2\epsilon_{12} \\ \epsilon_{1222} &= \frac{3}{2} \epsilon_{12}(1 + \beta) \\ \epsilon_{2222} &= 0 \end{aligned} \quad (4.2)$$

In this example, there are three relevant parameters in the binary case: the parameter ϵ_{12} takes care of the nearest-neighbor interaction and α and β are for four-body interactions.³

The entropy expression in the tetrahedron approximation for a system of N lattice points is^{7,8}

$$S_N = k \ln \frac{\left[\prod_{i,j} (y_{ij} N)! \right]^6 N!}{\left[\prod_{i,j,k,l} (z_{ijkl} N)! \right]^2 \left[\prod_i (x_i N)! \right]^5} \quad (4.3)$$

This may be compared with S_N of the pair approximation in (2.5a).

The grand potential Ω_N is written, corresponding to (3.1), in a symmetric form as

$$\begin{aligned} \Phi \equiv \frac{\beta \Omega_N}{N} = & 2\beta \sum \epsilon_{ijkl} z_{ijkl} + 2 \sum \mathcal{L}(z_{ijkl}) \\ & + \frac{5}{4} \sum \left[\mathcal{L}(x_i) + \mathcal{L}(x_j) + \mathcal{L}(x_k) + \mathcal{L}(x_l) \right] + 1 \\ & - \sum \left[\mathcal{L}(y_{ij}) + \mathcal{L}(y_{ik}) + \mathcal{L}(y_{il}) + \mathcal{L}(y_{jk}) + \mathcal{L}(y_{jl}) + \mathcal{L}(y_{kl}) \right] \\ & - \frac{1}{8} \beta \sum (\mu_i + \mu_j + \mu_k + \mu_l) z_{ijkl} \\ & + \beta \lambda \left(1 - \sum z_{ijkl} \right) \quad (4.4) \end{aligned}$$

Summations are done over the indices in each summand. The last terms multiplied by $\beta\lambda$ takes care of the normalization of z 's:

$$1 = \sum_{i,j,k,l} z_{ijkl} \quad . \quad (4.5)$$

For x_i 's and y_{ij} 's in the \mathcal{L} terms, we use the geometrical reduction relations:

$$x_i = \sum_{j,k,l} z_{ijkl} \quad , \quad \text{etc.} \quad (4.6)$$

$$y_{ij} = \sum_{k,l} z_{ijkl} \quad , \quad \text{etc.}$$

Comparing Φ in (4.4) with Φ in (3.1) shows the change made as we go from the pair approximation to the tetrahedron approximation.

In deriving the equilibrium state, we minimize Φ in (4.4) with respect to the z_{ijkl} 's while holding $\beta = 1/kT$ and the μ_i 's fixed. Differentiation leads to

$$z_{ijkl} = e^{\beta\lambda/2} z_{ijkl}^{(0)} \quad (4.7a)$$

$$z_{ijkl}^{(0)} = \exp \left[-\beta \epsilon_{ijkl} + \frac{\beta}{8} (\mu_i + \mu_j + \mu_k + \mu_l) \right] Y^{1/2} X^{-5/8} \quad , \quad (4.7b)$$

where

$$Y \equiv y_{ij} y_{ik} y_{il} y_{jk} y_{jl} y_{kl}$$

$$X \equiv x_i x_j x_k x_l \quad . \quad (4.7c)$$

The NI procedure consists of two steps, as in the pair case in Section 3. To start the iteration calculations, we guess initial values of the x_i 's and y_{ij} 's. For most calculations, we may specify only the x_i 's and then write the y_{ij} 's of the initial guess as

$$y_{ij} = x_i x_j \quad . \quad (4.8)$$

For the iteration calculation, we fix the values of β and of the μ_i 's.

The two steps in the calculation are given below.

- (i) Use the input values x_i and y_{ij} to calculate $z_{ijkl}^{(0)}$ in (4.7b).

Then the normalization factor $\exp(\beta\lambda/2)$, as obtained from the normalization relation (4.5), is

$$\exp(\beta\lambda/2) = \left[\sum z_{ijkl}^{(0)} \right]^{-1} \quad (4.9)$$

Multiplying this by $z_{ijkl}^{(0)}$ yields the output \hat{z}_{ijkl} from (4.7a).

In calculating $z_{ijkl}^{(0)}$ of (4.7b), sometimes the product of six y 's causes underflow. To avoid this, it is safer to take the logarithm of both sides of (4.7b) and to first calculate $\ln z_{ijkl}^{(0)}$ and then derive $z_{ijkl}^{(0)}$ by exponentiation.

(ii) Using the output values \hat{z}_{ijkl} , we derive the output values \hat{x}_i and \hat{y}_{ij} from the geometric reduction relations (4.6). These \hat{x}_i and \hat{y}_{ij} are then used as the input for the next iteration cycle.

Using the same argument as in (3.10a), we can prove that λ in the normalization factor in (4.9) is the grand potential after the iteration has converged:

$$\Phi = \Phi - \sum z_{ijkl} \frac{\partial \Phi}{\partial z_{ijkl}} = \beta \lambda \quad , \quad (4.10a)$$

so that

$$\lambda = \Omega_N / N \quad . \quad (4.10b)$$

In the NI scheme, the iteration proceeds by fixing T and μ_i 's. In drawing the isothermal phase diagram of the conventional three-component triangular type, it is convenient to use the diagram in the chemical potential space as a guide. Since the zero point of the μ_i 's can, without loss of generality, be chosen arbitrarily, we can impose the relation:

$$\mu_1 + \mu_2 + \mu_3 = 0 \quad . \quad (4.11)$$

Thus, the μ -diagram can be drawn using three μ_i axes 120° apart from each other with the origin as $\mu_i = 0$. An example is shown in Fig. 5(b), which accompanies the composition diagram in Fig. 5(a). A tie line in Fig. 5(a) corresponds to a point in (b). The letters A, B, C, ... in (a) and (b) indicate the same coexisting phases. We will comment more on this figure in Section 7.

5. Ordered Phases in fcc

The treatment in Section 4 applies to the case where all lattice points are equivalent. Therefore, it applies to the analysis of the system where the interaction between different species is repulsive and the system phase-separates, and also to the case where the different species attract but the temperature is high so that the system is in the disordered phase.

For the ordered phases of the fcc structure, we consider the A_3B -type and the $\dot{A}B$ -type, both of which can be treated based on nearest-neighbor interactions. For these structures, we need sublattices, as shown in Fig. 6, in which the four s. c. sublattices are named α , β , γ , and δ . The amazing feature of the NI formulation is that practically the same formulation in (4.7) can be used for both the ordered and disordered phases.

The only refinement we need on (4.7) in treating the ordered phase is that the sublattice information is used explicitly in the Y and X expressions. When the species i , j , k , and l are located on the α , β , γ , and δ sublattices of Fig. 6, the expressions in (4.7c) are modified as

$$Y = y_{ij}^{(\alpha\beta)} y_{ik}^{(\alpha\gamma)} y_{il}^{(\alpha\delta)} y_{jk}^{(\beta\gamma)} y_{jl}^{(\beta\delta)} y_{kl}^{(\gamma\delta)}$$

$$X = x_i^{(\alpha)} x_j^{(\beta)} x_k^{(\gamma)} x_l^{(\delta)} .$$
(5.1)

Corresponding to these, the four subscripts i, j, k , and l on z and $z^{(0)}$ in (4.7a) are on lattice points α, β, γ , and δ in this order.

Although we used the general designations α, β, γ , and δ in Fig. 6 and in (5.1), actually some of these are grouped together. In the A_3B -type order ($L1_2$), lattice points α, β , and γ are equivalent; in the AB -type order ($L1_0$), α and β are equivalent, and γ and δ are equivalent.

Being able to use practically the same formulation for different phases greatly reduces the potential for human error in computation. This is another advantage of the NI method.

6. Extrapolation Formulation

In Fig. 4, $\left| x_1^{(n)} - x_1^{(n-1)} \right|$ decreases exponentially as NI proceeds. In that expression, n is the number of iterations.

We can prove in general that any variable appearing in the NI formulation approaches its convergence value exponentially for a sufficiently large number of iterations. Each z , y , and x obeys this general property. Using this property, we can extrapolate the iteration calculation from a finite step n to $n \rightarrow \infty$. It is done as follows.

To simplify the notation, we will drop subscripts and let x represent any $x_i, y_{ij}, z_{ijkl}, y_{ij}^{(\alpha\beta)}$, etc. Since x behaves exponentially, we can write

$$x(n) = x(\infty) + ae^{-bn} \quad . \quad (6.1)$$

Since the right-hand side contains three unknown constants $x(\infty)$, a , and b , we can solve $x(\infty)$ when we know three values: $x(n)$, $x(n + m)$, and $x(n + 2m)$. Simple arithmetic leads to

$$x(\infty) = x(n) + \frac{x(n + m) - x(n)}{1 - e^{-bm}}, \quad (6.2a)$$

where

$$e^{-bm} = \frac{x(n + 2m) - x(n + m)}{x(n + m) - x(n)}. \quad (6.2b)$$

When we use the extrapolation scheme, the extrapolated value $x(\infty)$ is used as the starting input for the second iteration series. Since $x(\infty)$ is already close to the convergence value, the second iteration series usually converges rapidly. When the convergence is slow, we may need the second extrapolation and the third iteration series.

For this extrapolation to be effective, the exponential convergence of (6.1) must be approximately valid. Since (6.1) is usually not obeyed early in the iteration, we may have to wait until $n = 30$, 50, or 100 before applying the (6.2) extrapolation. Used with sufficient care, this extrapolation scheme is really helpful. As an extreme example we may quote a certain combination of T and μ , for which $n = 100$ and $m = 50$ were used and (6.2) was applied with z_{ijkl} for x . The iteration with the extrapolation converged at 283 total iterations. Starting from the same initial values, the iteration without extrapolation took 5603 iterations before convergence.

7. Orthogonality Relations

When a point in a phase diagram has been determined, to know roughly where the nearby point lies assists in the computation. Such information is provided by the orthogonality theorem.

The binary case is discussed first. The phase diagram is usually drawn in T versus x space, where x is the composition variable. The orthogonality relation, however, holds in T versus μ space. The theorem is derived using a technique similar to the proof of the Clapeyron-Clausius relation. The Helmholtz free energy F satisfies

$$dF = -S dT + N\mu dx \quad . \quad (7.1)$$

In this expression, μ is the chemical potential corresponding to x and N is the number of lattice points in a system. The grand potential Ω is derived from F as $\Omega = F - N\mu x$ so that from (7.1)

$$d\Omega = -S dT - Nx d\mu \quad . \quad (7.2)$$

This relation holds for one phase. Along the phase boundary curve on which two phases (I) and (II) coexist in the T vs μ plane, we have two relations:

$$\begin{aligned} d\Omega^{(I)} &= -S^{(I)} dT - Nx^{(I)} d\mu \\ d\Omega^{(II)} &= -S^{(II)} dT - Nx^{(II)} d\mu \end{aligned} \quad (7.3)$$

in which dT and $d\mu$ are the same. Along the phase boundary curve,

$$d\Omega^{(I)} = d\Omega^{(II)} \quad . \quad (7.4)$$

Substituting (7.3) into (7.4) yields

$$(S^{(I)} - S^{(II)}) dT + N(x^{(I)} - x^{(II)}) d\mu = 0 \quad . \quad (7.5)$$

In this expression, $S^{(I)} - S^{(II)}$ and $x^{(I)} - x^{(II)}$ are the differences between the two coexisting phases. The relation (7.5) shows that the vectors $(S^{(I)} - S^{(II)}, N(x^{(I)} - x^{(II)}))$ and $(dT, d\mu)$ are orthogonal. We may also write from (7.5)

$$\frac{d\mu}{dT} = - \frac{S^{(I)} - S^{(II)}}{N(x^{(I)} - x^{(II)})} \quad . \quad (7.6)$$

This relation is used in guessing a nearby point in the T - μ diagram when one point on the phase diagram has been determined.

In Fig. 7 we show the T - μ diagram⁹ of the Cu-Au system calculated using the tetrahedron approximation of Section 5. Figure 7 corresponds to the T vs composition diagram, Fig. 5, of the companion paper in this volume.¹ Figure 8 is the entropy vs composition diagram corresponding to Fig. 7. We can see that a tie line in Fig. 8 is orthogonal to the tangent on the T - μ curve of Fig. 7 at the corresponding point after the abscissa scales are adjusted. In the actual computation program, we do not draw the S vs x diagram but let the computer calculate $d\mu/dT$ from (7.6).

We next discuss the orthogonality relation in the ternary case.

In this case we are usually interested in the isothermal diagram.

Thus, corresponding to (7.3), we have

$$d\Omega^{(I)}/N = - \sum_{i=1}^3 x_i^{(I)} d\mu_i \quad (7.7)$$

$$d\Omega^{(II)}/N = - \sum_{i=1}^3 x_i^{(II)} d\mu_i \quad .$$

From the difference between the two relations in (7.7) and the equality $d\Omega^{(I)} = d\Omega^{(II)}$ on the coexisting curve, we derive

$$\sum_{i=1}^3 \left(x_i^{(I)} - x_i^{(II)} \right) d\mu_i = 0 \quad . \quad (7.8)$$

This suggests that the vectors $x_i^{(I)} - x_i^{(II)}$ and $d\mu_i$ are orthogonal.

This can actually be proved⁶ by transforming the coordinate axes from those coplanar and 120° apart to the regular cartesian ones.

We can verify the validity of the orthogonality that a tie line in

Fig. 5(a) is perpendicular to the tangent on the μ -curve at the corresponding point in Fig. 5(b). When a point in the μ -diagram has been calculated, a nearby point on the curve can be roughly estimated using (7.8).

8. Further Comments on the CV-NI Method

When the second-neighbor interaction is to be taken into account in the fcc structure, we need as the basic cluster a double-tetrahedron¹⁰ made of six points. In working with the double-tetrahedron, subsidiary conditions on the distribution variables are needed for symmetry. The method of dealing with such subsidiary conditions within the framework of NI has been worked out.¹¹

For the bcc structure, the CV method which is one step better than the pair approximation uses a non-regular tetrahedron. The result was reported previously,¹⁰ and the details will be published shortly.¹²

In addition to the extrapolation formulation of Section 6, other methods have been devised for making the NI approach converge more quickly, and some of these have been tested successfully.¹³

References

1. D. de Fontaine and R. Kikuchi, "Fundamental Calculations of Coherent Phase Diagrams," (this volume).
2. N. S. Golosov, L. Ya. Pudan, G. S. Golosova, and L. E. Popov, Soviet Phys. - Solid State 14, 1280 (1972).
3. C. M. van Baal, Physica (Utr.) 64, 571 (1973).
4. R. Kikuchi, J. Chem. Phys. 60, 1071 (1974).
5. R. Kikuchi, "Ternary Phase Diagram Calculations - I General Theory," Acta Metall. (Dec. 1976).
6. R. Kikuchi, D. de Fontaine, M. Murakami, and T. Nakamura, "Ternary Phase Diagram Calculations - II Examples of Clustering and Ordering Systems," Acta Metall. (1976).
7. R. Kikuchi, Phys. Rev. 81, 988 (1951).
8. D. M. Burley, Phase Transition and Critical Phenomena, Vol. 2, C. Domb and M. S. Green, eds. (Academic Press, New York, 1972) Chapter 9.
9. R. Kikuchi and D. de Fontaine, Scripta Met. 10, 995 (1976).
10. R. Kikuchi and C. M. van Baal, Scripta Met. 8, 425 (1974).
11. R. Kikuchi, "Natural Iteration Method and Boundary Free Energy," J. Chem. Phys. (Dec. 1976).
12. R. Kikuchi, "Structure of Phase Boundaries" (to be published).
13. J.M. Sanchez, Ph.D. Dissertation, School of Engineering and Applied Sciences, UCLA (1977).

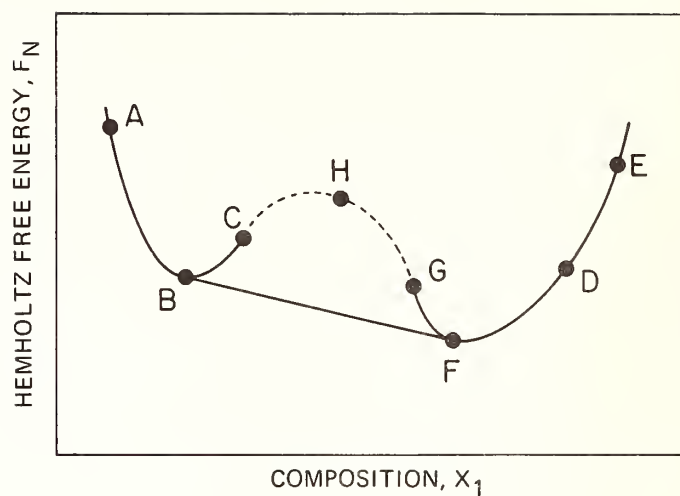


Fig. 1 Schematic diagram of the Helmholtz free energy F_N of a binary alloy plotted against x_1 , the density of A atoms.

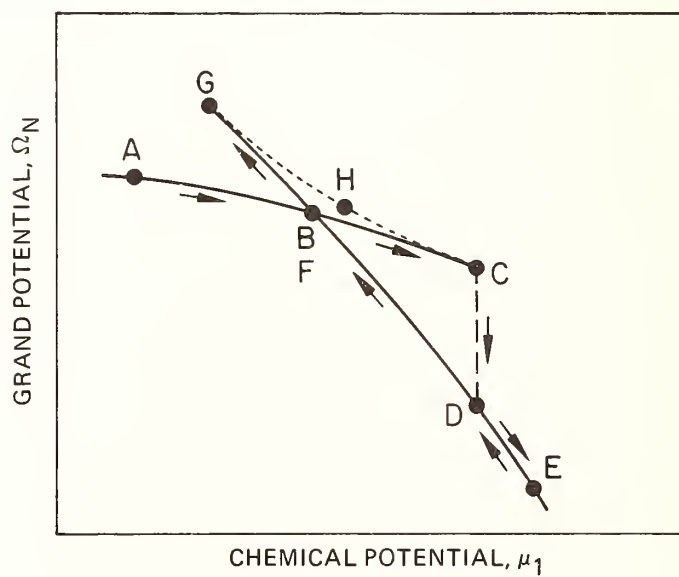


Fig. 2 Schematic diagram of the grand potential Ω_N plotted against μ_1 , the chemical potential of the A atom. Letters correspond to those of Fig. 1.

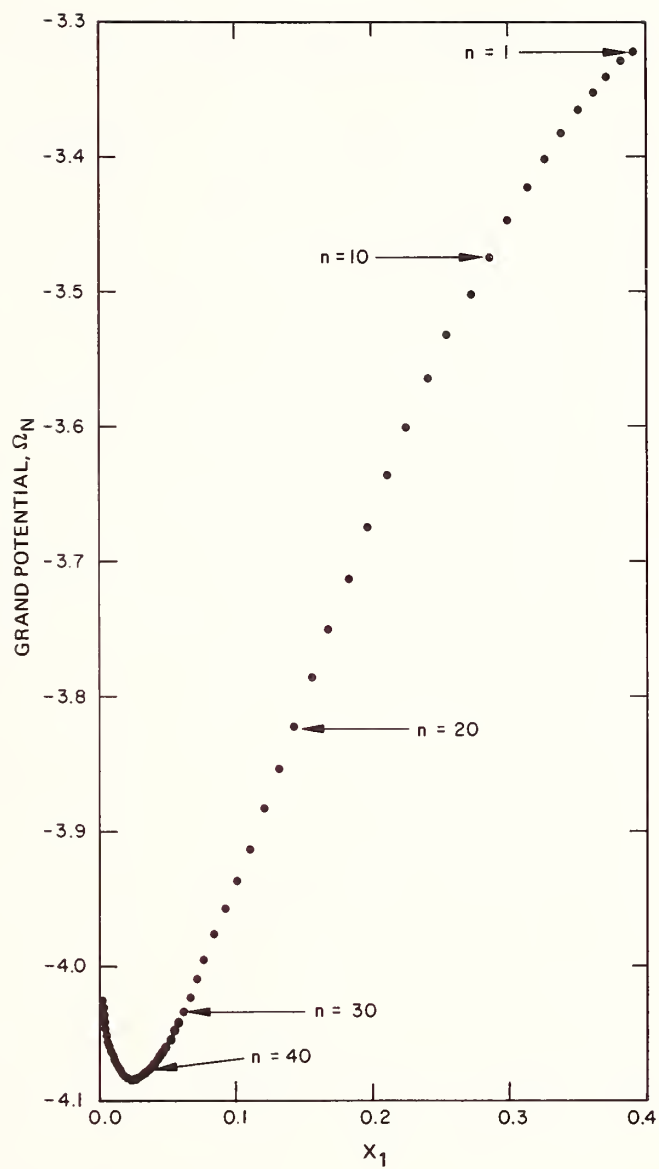


Fig. 3 Behavior of the grand potential Ω_N as the NI proceeds. The number of iterations is indicated by n .

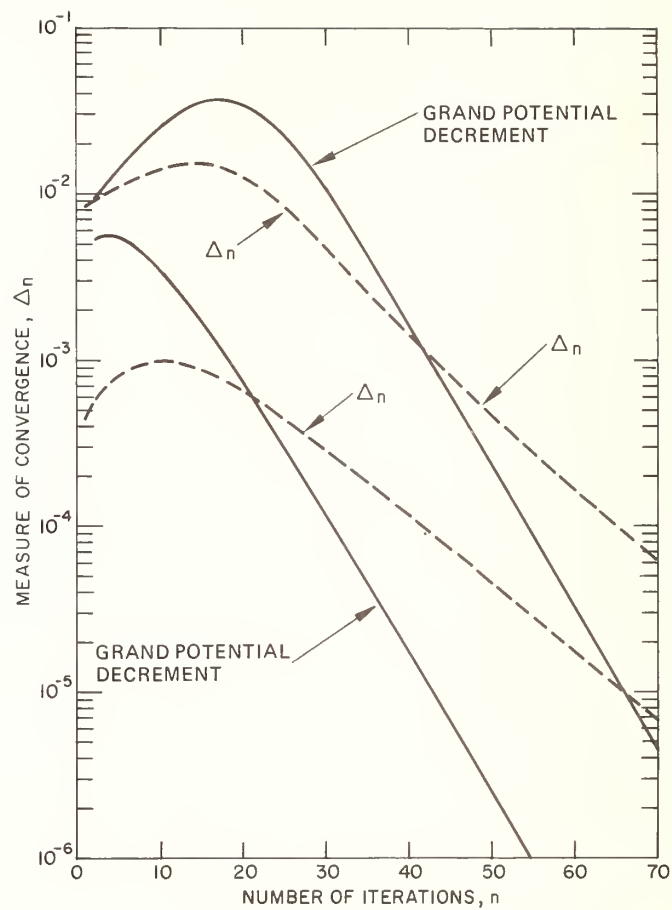


Fig. 4 The number of convergence Δ_n defined in (3.9) plotted against the number of iterations n . The figure also shows $|\Omega(n) - \Omega(n-1)|$.

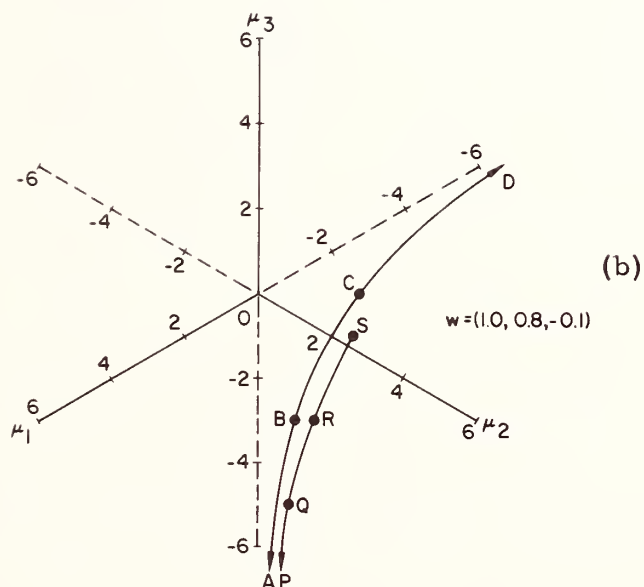
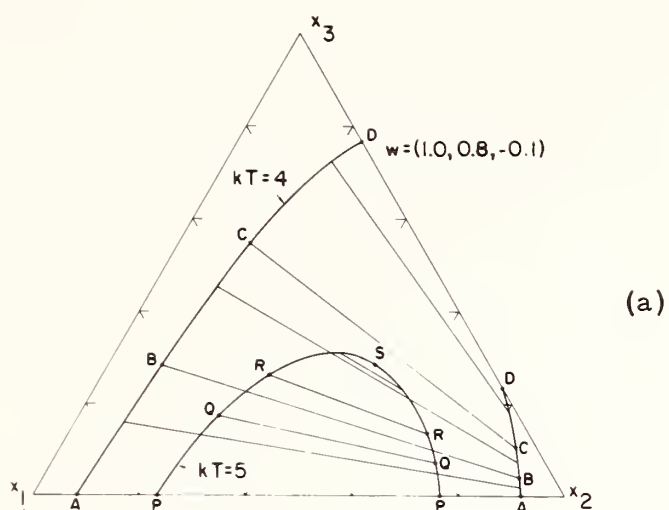


Fig. 5 Phase separation diagrams of a ternary system. A tie line in (a) corresponds to a point on the chemical potential diagram in (b).

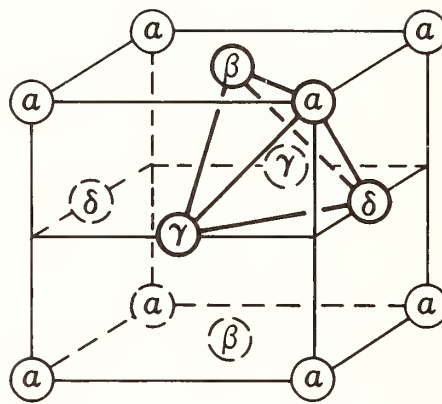


Fig. 6 The basic cluster tetrahedron for an ordered fcc phase.

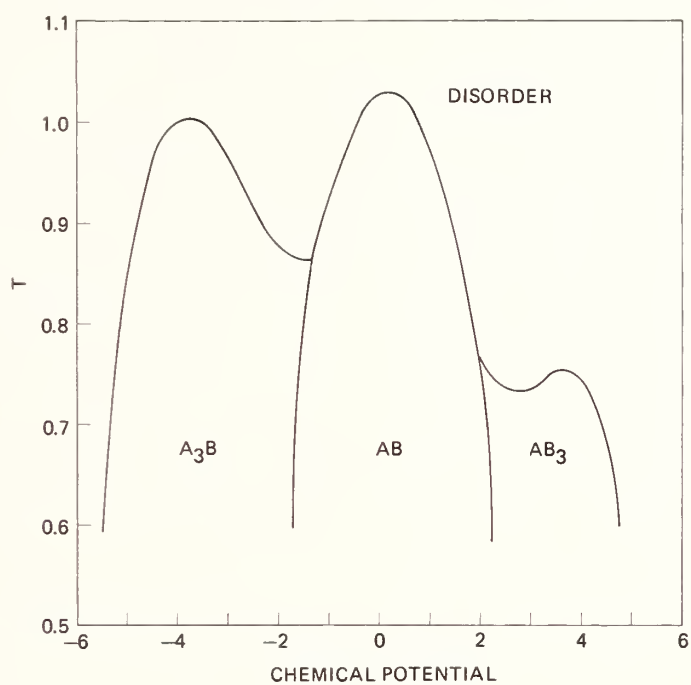


Fig. 7 The calculated T vs μ diagram of the Cu-Au system.

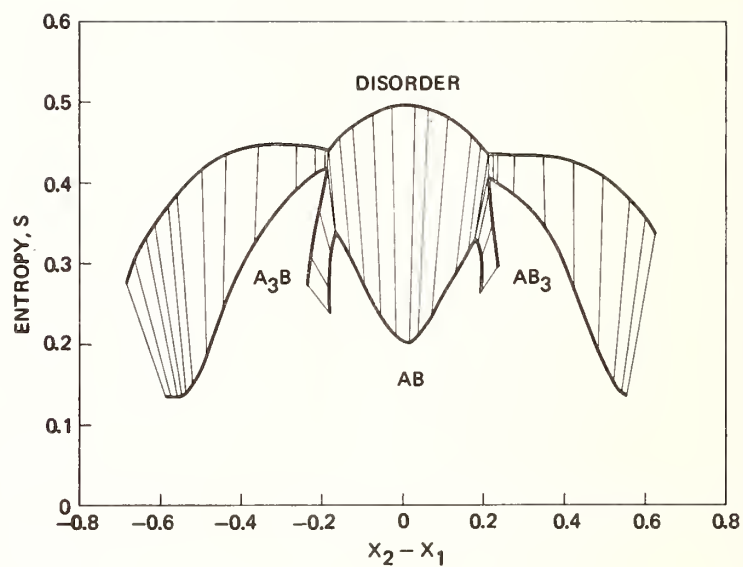


Fig. 8 The calculated diagram of S vs composition x corresponding to Fig. 7.



FUNDAMENTAL CALCULATIONS OF COHERENT PHASE DIAGRAMS

Didier de Fontaine and Ryoichi Kikuchi*

Department of Engineering and Applied Science
University of California, Los Angeles

Abstract

By "coherent phase diagram" is meant a temperature-concentration diagram indicating thermodynamic relationships between ordered and disordered solid phases which can all be derived from the same parent lattice. Incoherent phase diagrams cannot, at present, be computed from first principles, but they can be determined experimentally. By contrast, many coherent phase diagrams cannot be readily constructed experimentally, hence a reliable theoretical model yielding useful prototype phase diagrams is highly desirable. Such a model is provided by the Cluster Variation method first developed in 1951. In this method, the configurational entropy is treated in a very accurate manner, in contrast to the regular solution or Bragg-Williams entropy which in many cases can be 100% in error, or lead to phase diagrams which are not even topologically correct. This is illustrated in the case of the Cu-Au system, for which an excellent fit to the experimental phase diagram has recently been obtained, following the ideas of van Baal. The problem of predicting ordered ground states from a knowledge of pair interaction parameters and that of estimating these parameters themselves from band structure calculations is briefly covered.

* Permanent Address: Hughes Research Labs, Malibu, California, 90265

1. Introduction

Most computations of temperature-composition phase diagrams to date are semi-empirical, in the sense that separate free energy functions are constructed for the phases which are known to appear in the system⁽¹⁾. The free energy functions used are usually based on the regular, sub-regular or Bragg-Williams mean-field models, with parameters adjusted to the empirically known portions of the phase diagram or to experimentally determined bulk thermodynamic data. It is of course of considerable interest to inquire whether it is presently possible to perform more fundamental phase diagram calculations which, in some way, can be derived from "first principles". It can be immediately stated that such fundamental calculations of phase diagrams of systems presenting intermediate phases of arbitrary crystal structure, say intermetallic compounds, is presently out of the question. However, for certain classes of binary and ternary systems, namely *coherent* systems, fundamental phase diagram calculations having real predictive power are becoming feasible. The purpose of this communication is to review current progress in this specialized field.

First a definition: by coherent system is meant one in which all phases derive from a unique lattice framework (for instance fcc or bcc) simply by rearranging A, B, C... atoms on the lattice sites in various ordered or clustered configurations. In these systems, when a new ordered phase appears, it must be completely coherent with the parent phase, so that no lattice *discontinuities* are tolerated. Elastic *distortions* may be present, however. Examples of fully coherent systems are Cu-Au (to be examined in detail below), Cu-Pt, Cu-Ag-Au, etc... . Of course, equilibrium phases must generally be separated by incoherent *interfaces*, but in these simple systems, the incoherent phase

diagram may be regarded as deriving directly from the corresponding, more fundamental, *coherent (metastable) phase diagram*, the only one under consideration here.

It may appear that fully coherent phase diagrams form such a restricted class as to be of little practical interest. This is not the case: most useful materials, alloys in particular, are prepared under conditions which are far removed from thermodynamic equilibrium. Hence, observed microstructures are primarily governed by kinetic effects, and it is known that, for these reasons, coherent products are the first to form in a great many cases. Coherency is often subsequently lost, but the final microstructure then retains essential features which were imparted by the fully coherent early stages of the phase transformations. Hence, some knowledge of underlying coherent phase equilibria is essential for gaining an understanding of microstructure, and hence of properties, even in "incoherent" systems.

Coherent phase diagrams, being generally of a metastable nature, are not easy to determine experimentally. Therefore, it is particularly fortunate that it is precisely these phase equilibria which are amenable to "fundamental" calculations. Conversely, stable incoherent phase equilibria cannot be calculated at present from "first principles", but incoherent diagrams can in principle be determined experimentally. The theorist's task is then to superimpose the calculated coherent diagram on the experimental incoherent one.

What is needed for a coherent phase diagram calculation? Basically, a reliable configurational free energy function from which one may deduce all coherent ordered phases and their domain of existence in temperature-concentration space. The two contributions to the free energy can be calculated separately, these are: the internal energy (practically equal to the enthalpy in condensed systems) which contains the physics of the problem, and the configurational entropy which is determined from the ways in which

certain sets of symbols can be distributed on lattice sites. The vibrational entropy makes a sizable contribution to the total free energy but its *change* on ordering is regarded as small and shall therefore be neglected. Regular, sub-regular and Bragg-Williams models (referred to collectively in what follows as BW models) are unacceptable for both enthalpy and entropy contributions, as will be shown in the Cu-Au case in Sect. 3. The reason for the failure of mean-field models to predict phase diagrams which, in certain cases, are even topologically correct is twofold: (A) the BW models make the very poor *zeroth or decoupling approximation*

$$\langle \sigma_p \sigma_{p'} \rangle \rightarrow \langle \sigma_p \rangle \langle \sigma_{p'} \rangle \quad (1)$$

consisting of replacing the average (denoted by brackets) of two-site (and three-site, etc.) occupation by a product of single-site occupation. The symbols σ_p denote occupation parameters with value 1 or 0 depending upon whether lattice site p is or is not occupied by an atom of given type;

(B) the BW entropy, of type

$$-k \sum_p \langle \sigma_p \rangle \ln \langle \sigma_p \rangle, \quad (2)$$

where k is Boltzmann's constant, neglects pair (and higher) correlations.

An exact closed-form free energy is not available even under the simplifying assumption that the internal energy consists of a sum of nearest neighbor pair interactions. This would be equivalent to solving the Ising problem in three dimensions, which no one has succeeded in doing to date. One must therefore resort to approximate methods, one of the most successful being the Cluster Variation method (CV) developed in 1951⁽²⁾. The basic idea of this method, which constitutes a hierarchy of increasingly accurate approximations, will be presented briefly in Sect. 2, and in more detail in a companion paper⁽³⁾.

As an illustration, the CV method will be used to calculate the solid-state portion of the Cu-Au phase diagram. This application is presented in Sect. 3, along with a brief historical survey of Cu-Au phase diagram calculations.

The CV method assumes that the phases which appear in the coherent phase diagram are known *a priori*: these are the phases which must be present at absolute zero, the so-called *ordered ground states*. Fortunately, elegant methods⁽⁴⁻⁷⁾ are now available for predicting ordered ground states in substitutional solutions: the problem is completely solved for ordered structures, based on the fcc and bcc lattices, which are stable for pair interactions limited to second coordination shell. Most commonly occurring ordered structures are thereby predicted. Recent work by Kanamori⁽⁸⁾ has extended this to cover the very complicated structures which are stable under the action of up to 4th - neighbor pair interactions.

In both CV and ordered ground state calculations, the pair (or triplet, etc.) interaction parameters are assumed to be given. Of course, for a complete first-principle phase diagram determination, these parameters would have to be obtained from electronic band structure calculations. Reliable numerical values from quantum mechanical calculations appear to be a long way off, however, although significant progress has been made with the advent of pseudopotentials^(9,10) and of the Coherent Potential Approximation⁽¹¹⁾. Ordered ground states and the problem of calculating pair potentials are very briefly commented upon in Sect. 4.

The topics presented in this article are treated in more detail in a forthcoming review article⁽¹²⁾.

2. The Cluster Variation Method

For given crystal lattice, a *basic figure*, or small group of lattice

points is selected. This basic figure may be the nearest-neighbor (n.n) pair, the n.n. tetrahedron (in fcc), the bcc cube, etc... A *cluster* is defined as a particular distribution of A, B, C... atoms on the lattice sites of the basic figure selected. To each distribution is assigned a cluster variable whose value at equilibrium is the frequency of occurrence of that particular cluster in the solid solution. Let us designate all cluster variables collectively by the set $[\alpha]$. Then the free energy of the system in a state characterized by particular values of $[\alpha]$ is defined by the *free energy function*

$$F[\alpha] = E[\alpha] - TS[\alpha] , \quad (3)$$

where T is the absolute temperature and E and S are respectively the internal energy and configurational entropy for which explicit expressions will presently be given. The *equilibrium free energy* F_e is obtained by finding the particular set of cluster variables $[\alpha]$ which minimizes the free energy function (3):

$$F_e = \min_{[\alpha]} F[\alpha] . \quad (4)$$

In general, the larger is the basic figure used in the calculations, the more accurate will be the derived free energy.

The energy $E[\alpha]$ is written as a sum of pair and cluster interactions, while the entropy is calculated from appropriate combinatorial factors, the derivation of which constitutes one of the main features (and difficulties) of the CV method. Consider a specific example, that of an fcc substitutional solution in the n.n. tetrahedron approximation. Let z_{ijkl} be the tetrahedron cluster variables, with i, j, k, l denoting the atomic species occupying the four vertices of the tetrahedron.

The internal energy $E[\alpha]$ is assumed to be given by the sum of the energies of all clusters present in the system. Only the largest clusters need be used explicitly, in the present case the n.n. tetrahedron. Hence,

the energy function is

$$E \equiv E[\alpha] = 2N \sum_{i,j,k,l} \epsilon_{ijkl} z_{ijkl} \quad (5)$$

where ϵ_{ijkl} denotes the energy of that particular tetrahedron cluster, and where N is the total number of lattice points. The cluster energies ϵ can be calculated on the basis of a sum of pair interactions, or distinct clusters may be given distinct energies different from the direct sum of constituent pairs. In this way, many-body interactions can easily be introduced in the internal energy, as will be seen in the next section. The quadruple sum in Eq.(5) runs over the subscript values (1,2) for binary systems, (1,2,3) for ternary systems, etc...

The configurational entropy is obtained from the Boltzmann formula

$$S[\alpha] = k \ln W[\alpha] \quad (6)$$

where W is the total number of ways of distributing the various clusters over the lattice sites in such a way that the cluster frequencies $[\alpha]$, in the present case the tetrahedron frequencies z_{ijkl} , pair frequencies y_{ij} and point frequencies x_i (concentrations); have specified values. An exact expression for W cannot be found for three-dimensional lattices because of the difficulty of eliminating inconsistencies of site occupation which arise inevitably when different clusters are distributed statistically over the lattice sites. The philosophy of the CV method is to correct systematically and optimally (but approximately) for these overlaps by means of familiar combinatorial factors. In the present case, the weight factor W of the distribution $\{\alpha\}$ for the fcc lattice in the n.n. tetrahedron approximation is⁽²⁾

$$W = \frac{\{\text{---}\}^6 N!}{\{\text{---}\}^2 \{\text{---}\}^5} \quad (7)$$

where the standard CV combinatorial notation has been used:

$$\{\cdot\} \equiv \prod_i (x_i N)! \quad (8)$$

which, for binary systems containing N_A A atoms and N_B B atoms, reads

$$\{\cdot\} \equiv N_A! N_B! .$$

The pair and tetrahedron symbols in Eq. (7) are given by appropriate generalizations of Eq. (8).

The free energy function $F[\alpha]$ is now obtained by putting (7) into (6), by using Stirling's formula to approximate the logarithms of factorials, and by inserting (6) and (5) into (3). The result in the fcc n.n. tetrahedron approximation is

$$\begin{aligned} F = N \sum_{ijkl} W_{ijkl} z_{ijkl} &+ NkT \left[5 \sum_i x_i \ln x_i - 6 \sum_{i,j} y_{ij} \ln y_{ij} \right. \\ &\left. + 2 \sum_{ijkl} z_{ijkl} \ln z_{ijkl} \right]. \end{aligned} \quad (9)$$

This formula is appropriate for the disordered phase. For ordered structures, sublattices must be defined, and Eq. (9) takes on a more complex appearance since now different cluster variables must be defined according to the manner in which clusters straddle the sublattices.

The equilibrium state is found by minimizing equations such as (9) with respect to cluster variables subject to various constraints which are present because of the interdependence of the variables. The practical difficulty here is that the total numbers (ν) of variables and of equal number of (non-linear) equations resulting from the minimization rises rapidly with the number n of components in the system and number m of cluster points, the formula being

$$\nu = n^m. \quad (10)$$

For binary and ternary systems in the tetrahedron approximation, Eq. (10) gives the reasonably tractable numbers 16 and 81, respectively. Recently, the CV method has been applied to the omega displacive transformation⁽¹³⁾

in the eight-point primitive bcc unit cell cluster approximation, with point variables +1, 0, -1; the total number of variables was then $3^8 = 6561$. Such impressively large systems of non-linear simultaneous equations can now be handled successfully through the powerful Natural Iteration algorithm described elsewhere^(3,14).

Conditions for phase equilibria are obtained by determining the concentrations for which the equality of chemical potentials hold. The procedure for calculating phase diagrams is thus to minimize the grand potential

$$\Omega = F - N \sum_i \mu_i x_i \quad (11)$$

rather than F itself as in Eq.(4). The method is explained in more detail in a companion paper⁽³⁾. For second-order phase transitions, the critical point is obtained by the standard method of setting equal to zero the determinant of the second derivatives of F with respect to independent configuration variables.

It is important to note that the CV method not only can produce phase diagrams, but also equilibrium values of the cluster variables at any temperature and average concentration. Hence, unlike BW models, the CV method can provide short-range (SRO) as well as long-range order (LRO) information, which may be tested against experimental evidence, such as x-ray or neutron diffraction SRO intensity data.

3. The Cu-Au System

Some of the foregoing considerations will now be applied to the problem of calculating the solid-state portion of the Cu-Au phase diagram. The experimentally determined diagram is shown in Fig. 1⁽¹⁵⁾. One notes the existence of three ordered regions: two ordered phases have well-

defined transition points where the fcc solid solution (α) transforms by a first-order reaction to the $L1_2$ structure at the Cu_3Au composition and to a long-period modification (II) of the $L1_0$ structure at the CuAu composition. This long-period structure itself transforms at a slightly lower temperature to the true $L1_0$ structure (CuAuI). The structure of Au_3Cu is also $L1_2$ but apparently presents no well-defined common maximum⁽¹⁶⁾ in the order and disorder curves⁽¹⁷⁾.

Shockley used a Bragg-Williams n.n. interaction model in 1938⁽¹⁸⁾ to calculate the Cu-Au phase relations, but the resulting phase diagram, shown in Fig. (2), is not even topologically correct. The ordered phase fields are nested, instead of separated, and culminate in a unique second-order transition temperature at the center of the diagram. One must conclude from this disappointing attempt that there is something inherently wrong with the BW approximation which cannot be remedied by more elaborate polynomial expansions of some "excess" free energy.

If one is to discard mean-field theories, then perhaps the Bethe approximation will work better. Unfortunately, this approximation, which is identical to the CV method in the n.n. pair approximation (in the entropy) gives no phase transition at all!⁽¹⁹⁾ The next successful attempt was that of Li⁽²⁰⁾ in 1949 who used the Guggenheim quasi-chemical theory in the tetrahedron approximation. Li's phase diagram is shown in Fig. 3. Marked improvements over Shockley's diagram are apparent, namely the existence of three distinct phase regions. However, all three ordered phase fields have the same shape, and eutectoid and peritectoid reactions are absent.

The tetrahedron-based configurational entropy formula used by Li is now known to be defective, which led van Baal to try CV method in 1973⁽²¹⁾; the configurational entropy was that of the tetrahedron approximation, Eq. (7), and the internal energy was written as a sum of n.n. pair

interactions. The resulting phase diagram is shown in Fig. 4, as recalculated by one of the present authors⁽¹⁴⁾. Many essential features of the experimental diagram are present: three separate ordered phase fields, eutectoids, and good qualitative agreement with at least the left (Cu-rich) side of the actual phase diagram. This important calculation by van Baal is very encouraging, particularly when it is recognized that the diagram as drawn in Fig. 4 is based on a *unique free energy function which contains no adjustable parameters*. It follows that Fig. 4 represents a universal phase diagram for all fcc ordering systems with internal energy obtained from n.n. pair interactions alone. Obviously, this is an oversimplification, but the fact that the diagram is by and large topologically correct provides support for the CV method.

The Shockley BW diagram (Fig. 2) also contains no adjustable parameters. Hence a very honest comparison can be made between the BW and CV models: good and bad features of the resulting phase diagrams must reflect the essential qualities of the underlying free energy function, not of any numerical fitting. The conclusion is inescapable: the BW approximation is quite unacceptable, at least for the fcc lattice, while the CV tetrahedron approximation is qualitatively correct, though in need of quantitative improvement.

Van Baal⁽²¹⁾ noted that all phase diagrams constructed from an internal energy based on pair interactions with concentration - independent parameters must be completely symmetric about the 50/50 composition. To break the symmetry, either many-body interactions must be introduced or concentration-dependent pair interaction parameters must be used. The former scheme was suggested by van Baal who showed that the energy equation (5) could be written explicitly as

$$E = 12 N \epsilon_{12} [(1+\alpha) z_{1112} + 2z_{1122} + (1+\beta) z_{1222}] \quad (12)$$

where ϵ_{12} is the effective pair interaction parameter

$$\epsilon_{12} = V_{AB} - \frac{V_{AA} + V_{BB}}{2} \quad (13)$$

in which V_{ij} denotes the interaction energy of a n.n. ($i, j = A, B$) pair.

In Eq. (12), $\epsilon_{12}(1+\alpha)$ and $\epsilon_{12}(1+\beta)$ are the energies of n.n. tetrahedra occupied by three A and one B atom, and three B and one A atom, respectively. With $\alpha=\beta=0$, Eq. (12) is the correct energy expression in a purely pairwise scheme. Hence the parameters α and β represent here the fractional deviation of the tetrahedron energy from that which would be calculated from summing its constituent pairs. These parameters therefore represent essential many-body interactions. Equation (12) with $\alpha=0$, $\beta \neq 0$ was used by van Baal⁽²¹⁾ to show the resulting asymmetry in the transition temperature vs. concentration curves. Corresponding phase diagram calculations were not reported.

The authors recently followed up on van Baal's suggestion and calculated a phase diagram based on the free energy function (9) with internal energy given by Eq. (12). The values $\alpha=0.01$ and $\beta=-0.08$ were chosen, resulting in the phase diagram shown in Fig. 5. Although further refinements are possible, this diagram is remarkably close to the experimental one. The shallow maximum of the Au_3Cu phase field is an unsatisfactory feature, but could be eliminated by fine tuning of the α and β parameters. Of course, the existence of the CuAuII phase cannot be predicted: higher-neighbor interactions would be required.

The dashed line in both Fig. 5 and 2 indicate the *ordering spinodal*, i.e. the locus along which the solution becomes inherently unstable to a $\langle 100 \rangle$ composition plane wave of infinitesimal amplitude^(12,22). The fact that, in the CV diagram (Fig. 5), the ordering spinodal does not touch the ordus or disordus lines indicates that the ordering reactions are first order, even at the CuAu stoichiometric composition. This is in accordance

with experimental findings, and with the Landau rules⁽²³⁾. By the same token, note that the BW diagram (Fig. 2) incorrectly predicts a double second-order transition at the 50/50 composition.

Several points may be emphasized in connection with the diagram of Fig. 5:

- a reasonably correct coherent phase diagram has been calculated from a single free energy function in an fcc-based system,
- an ordering spinodal has been constructed,
- the need for many-body (tetrahedron) interactions has been clearly demonstrated, and is seen to play an essential role,
- the calculation yields much more than merely the phase diagram: SRO information is automatically provided in the form of 3 y_{ij} n.n. frequencies and 5 n.n. tetrahedron cluster frequencies at any required concentration and temperature. The pair frequencies can be tested against SRO diffuse intensity data, as mentioned above.

Other fcc and bcc-based phase diagrams may be computed in a similar manner. However, in order to obtain ordered phases other than the $L1_2$ and $L1_0$, it is necessary to include at least next-nearest-neighbor pair interactions. This, in turn, requires the use of a larger basic figure, such as the double tetrahedron for which the CV entropy formula has been derived⁽²⁴⁾. A research program aimed at computing prototype coherent phase diagrams for all possible fcc and bcc - based ordered structures is currently underway⁽²⁵⁾.

4. Ground States and Potentials

In the CV method, ordered phases are simply handled by defining appropriate sublattices. Thus a knowledge of which ordered structures to expect is a separate problem. It may be assumed that candidate ordered

phases of coherent type are those which will be found at absolute zero in the system of interest. By definition, these are the (coherent) *ordered ground states*. Under certain restrictive (but realistic) assumptions, it is now possible to *predict* which ordered structures will be absolutely stable for given ranges of pair interaction parameters and concentrations. The ground state problem is completely solved for fcc and bcc binary substitutional solutions with internal energy given by a sum of first and second neighbor pair interactions, for all ranges of concentrations and pair interaction parameter ratios^(4,6,7,26). Considerable progress is also being made in extending the range of pair interactions to third and fourth neighbors^(4,5,8).

The problem is to find that distribution of A, B atom on lattice sites which minimizes the energy E , given the average concentration x of B atoms and the pair interaction parameters ϵ_s , the latter being given by Eq. (13), extended here to arbitrary coordination shell $s=1,2,3,4,\dots$. The energy to be minimized can be written

$$E = N \sum_s z_s \epsilon_s y_s \quad (14)$$

where y_s is the pair frequency and z_s the coordination number for shell s . The minimization of E in Eq. 14 need not be accomplished by trial and error: indeed Kanamori already devised in 1965⁽²⁶⁾ a set of inequalities which must hold between linear combinations of pair frequencies y_s and concentrations x , and which allows for the unambiguous determination of ordered ground states. A systematic method for deriving the inequalities was discovered by Kaburagi and Kanamori in 1975⁽⁴⁾; it makes use of clusters of lattice points as does the method of Allen and Cahn⁽⁷⁾, developed independently. Linear programming is featured in the latter method and also in that of Kudō and Katsura⁽⁵⁾.

It is interesting to note that all the commonly observed binary alloy ordered structures based on the bcc and fcc lattices can be predicted theoretically by the above mentioned methods when only first and second-neighbor interactions are considered. This is not to say that actual interactions do not extend beyond the second coordination shells, nor that many-body forces are unimportant; simply, this means that the stability of ordered structures can, by and large, be rationalized by use of a single parameter: the ratio of first to second neighbor pair interaction, along with the sign of the first-neighbor interaction. In addition, theoretical ground state calculations predict the existence (and stability) of ordered structures which have apparently not yet been observed: examples are the A_2B and A_5B monoclinic structures of space group $B2/m$ ^(6,7).

Certain known structures owe their stability (at 0°K) to higher-neighbor interactions. An example is the Au_5Mn_2 structure which Kanamori⁽⁸⁾ was able to predict on the basis of extremely complex analysis of ordering in the fcc lattice with up to fourth-neighbor interactions. The structure is shown in projection at the top portion of Fig. 6⁽⁸⁾. The Kanamori "S" symbols have arguments

$$S(p_1, p_2, p_3, p_4; x)$$

where the (modified) pair frequencies are

$$p_s = y_s z_s / x,$$

x being the stoichiometric composition. Figure 6 also shows two A_2B structures, illustrating the fact that unit cells may become very large and atomic arrangements very complex when higher-neighbor interactions are taken into account. Figure 7⁽⁸⁾ gives an example of two other A_2B structures which are "degenerate", meaning that their pair count up to fourth neighbor is identical. The top structure has space group $B2/m$, the lower one $Immm$ ⁽²⁷⁾,

which is the Pt_2Mo (or Ni_2V or metastable Ni_2Mo) structure. Fifth neighbor interactions would be required to lift the degeneracy.

To conclude this survey of the possibility of "first-principle" coherent phase diagram calculations, let us briefly mention the problem of theoretically estimating values of the pair interaction parameters ϵ , which have thus far been regarded as known entities. The problem is an extremely difficult one which formally necessitates the solution of the Schrödinger equation for a solid solution of arbitrary atomic configuration. It appears that accurate solutions are a long way off.

Certain recently developed approximate techniques are quite promising, however. The central problem often consists in finding suitable perturbation expansions which converge sufficiently rapidly so that the expansion may be limited to second order. For pure *simple metals*, it is possible to construct a *pseudopotential*, so that the Schrödinger equation may be solved to second order in this small energy-dependent potential^(9,10). It then follows that the band structure energy may be written conveniently as a sum of pairwise effective interactions. Unfortunately, the list of "simple metals" for which pseudopotentials can be tabulated is not as extensive as one would like. For other metals, particularly the transition elements, i.e. the majority of technologically important materials, the Fermi surfaces have complicated shapes deviating very significantly from the spherical one, and there is considerable overlap of the d-bands in the crystalline state. Hence, the pseudopotential formulation is impractical, and the cohesive energy cannot be written as a sum of pair (or even cluster) interactions⁽²⁸⁾.

For alloys (solid solutions), the problem is compounded by the fact that ionic potentials differ from site to site so that the crystal potential loses the translation symmetry of the lattice. The customary

way out of that difficulty was to assume an average potential V of the form

$$V = (1-x)V_A + xV_B \quad (15)$$

where V_A and V_B are the potentials of the constituents. However, this *virtual crystal* method has been shown to give rather poor account of itself in the case of concentrated solutions. Its application to the Hg-Mg system made by Inglesfield⁽²⁹⁾ in the pseudopotential framework can therefore certainly not be generalized with confidence.

When the difference of the constituent ionic potentials is large with respect to the width of the d-band, a completely different approach must be used. Currently, the most satisfactory method is that of the *Coherent Potential Approximation* (CPA): for the disordered case, one must seek an average single-site potential to be obtained self-consistently, rather than by the simple weighted sum of Eq. (15)⁽¹¹⁾. The calculation of cohesive energies then proceeds by standard techniques. It is impractical to obtain (small) ordering energies by taking the difference of two large cohesive energies in the ordered and disordered states. Rather, a way was recently discovered⁽³⁰⁾ of expanding the concentration fluctuation term, usually neglected in single-site CPA energy calculations, in a convergent generalized perturbation expansion. It is then possible to obtain LRO⁽³¹⁾ and SRO⁽³⁰⁾ configurational energies, though not the total cohesive energy, as sums of effective pairwise interactions, just as in the usual phenomenological theories. This is an important result, as it is clearly desirable to justify, and if possible to calculate, pair interaction parameters which play such a basic role in alloy theory, as shown for example by the considerations set forth in Sect. 2 and 3. It remains to be seen whether truly predictive results can be obtained by this extension of the CPA.

5. Conclusion

Ab initio calculations of *coherent* phase diagrams are becoming feasible thanks to recent theoretical developments. The three basic elements of the calculations are: (a) the estimation of pair (and many-body) interaction parameters, (b) the prediction of ordered ground states of ordering from a knowledge of pair parameter ratios, and (c) the determination of (coherent) phase equilibria and resulting phase diagrams. Corresponding advances in theoretical methods are: (a) recent extensions of the coherent potential approximation to cover LRO and SRO^(30,31), (b) the solution of the ground state problem in increasingly general situations⁽⁴⁻⁸⁾, and (c) the development of rapidly convergent algorithms for the Cluster Variation method^(13,14).

We have described the application of the CV method in the tetrahedron approximation to the Cu-Au phase diagram. By the same token, we have demonstrated the inapplicability of the BW model to fcc-based coherent phase diagrams. Despite the very obvious and serious deficiencies of mean-field (BW-like) models, the latter are being consistently used in nearly all current phase diagram calculations. Notable exceptions may be found in recent work carried out in France⁽³²⁾, Germany⁽³³⁾, Holland⁽³⁴⁾ and the Soviet Union⁽³⁵⁾. It is not likely that increasingly elaborate polynomial expansions will remedy the ills of mean-field models; even in those cases for which good fits are obtained numerically (always possible when enough adjustable parameters are used), the fitted parameters may have little physical meaning. In fact, it is not often appreciated that, since the BW models tend to overestimate the configurational entropy by as much as a 100%, the fitted pair interaction parameters and resulting internal energy will be estimated incorrectly in the same proportion.

Investigators have perhaps been put off by the apparent complexity of CV calculations as opposed to BW ones. Actually, as shown elsewhere⁽³⁶⁾, the CV method in the Natural Iteration scheme turns out to be rather

simpler to handle than the traditional regular solution model in the Newton-Raphson scheme. Furthermore, certain ternary equilibria which are easily missed in the latter method are found without difficulty in the former⁽³⁶⁾.

It is hoped that the present communication has contributed to bringing new theoretical techniques to the attention of investigators interested in phase diagram calculations; if so, the primary objective of the authors will have been reached.

ACKNOWLEDGEMENTS

The authors thank Professor J. Kanamori of the University of Osaka for having supplied us with copies of Figs. 6 and 7. The calculation of the Cu-Au phase diagram is part of an NSF-funded study of the Ag-Au-Cu ternary system.

DISCUSSION

O. Kleppa - The Au-Ag system has a strong negative enthalpy of mixing in the solid state, so it should form an ordered phase at low temperatures. This has not yet been observed as far as I know.

D. de Fontaine - Yes, we can predict this, but we have to be given the pair interaction parameters. But whether it will be seen or not depends on the kinetics of the system. Maybe it is too low.

M. Hoch - In your Cu-Au system, ordering is parallel to the 100 plane. Now Cu-Pt has complete solid solubility at high temperatures, and a very similar solidus-liquidus. If you cool that, it orders on the 111 plane and you get (Cu, Pt) compounds. My question is, where does your calculation take into effect that in the Cu-Au system we don't get 111 ordering, and in Cu-Pt we don't get 100 ordering?

D. de Fontaine - We haven't done that kind of calculation yet, but it is planned. The difference between these two types of ordering is the following. If you allow both 1st and 2nd neighbor pair interactions in the system, you can differentiate between these and other types of ordering. This has been shown by John Cahn and coworkers and by Kanamori in Japan. You can plot diagrams of ratios of 2nd nn to 1st nn pair interaction parameters, and develop maps this way and stay with absolute

certainty (at $T = 0$ K), that a certain phase like the (Cu, Pt) or like the (Cu, Au), given the stoichiometry, should be stable in a given range. In order to make our calculation predictive, or useful, for those situations as well, we have to include 2nd nn pair interactions. In the framework of the cluster variation method this can only be done if the cluster size is increased from the single tetrahedron, which contains only first neighbor bonds, to the double tetrahedra or to even large clusters. Recently, at UCLA, one of our students has done a calculation, for a ternary, with an 8-point cluster, which contains up to the fourth neighbor interactions. It is a little bit rough, because the number of simultaneous nonlinear equations you have to solve is 6561. It can be done and it will be done very shortly, I hope.

References

1. L. Kaufman and H. Bernstein, Computer Calculations of Phase Diagrams, Acad. Press, N.Y. (1970)
2. R. Kikuchi, Phys. Rev. 81, 988 (1951).
3. R. Kikuchi and D. de Fontaine (this symposium, preceding paper, TPSI-12a)
4. M. Kaburagi and J. Kanamori, Progress of Theor. Phys. 54, 30 (1975).
5. T. Kudō and S. Katsura, Progress of Theor. Phys. 56, 435 (1976).
6. M. J. Richards and J. W. Cahn, Acta Met. 19, 1263 (1971).
7. S. M. Allen and J. W. Cahn, Acta Met. 20, 423 (1972).
8. J. Kanamori, J. Met. Soc. Japan 15, 35 (1976) [in Japanese].
9. W. A. Harrison, Pseudopotentials in the Theory of Metals, W. A. Benjamin, N.Y. (1966).
10. V. Heine and D. Weaire, Solid State Physics, H. Ehrenreich, F. Seitz, D. Turnbull, Eds., Acad. Press, N.Y. (1970), pg 249-463.
11. H. Ehrenreich and L. M. Schwartz, Solid State Physics, H. Ehrenreich, F. Seitz, D. Turnbull, Eds., Acad. Press, N.Y. (1976), pg. 149-286.
12. D. de Fontaine Solid State Physics, H. Ehrenreich, F. Seitz, D. Turnbull, Eds., Acad. Press, N.Y. (in preparation).
13. J. M. Sanchez, Ph.D. Dissertation, School of Engineering and Applied Sciences, UCLA (1977).
14. R. Kikuchi, J. Chem. Phys. 60, 1071 (1974).

15. M. Hansen, Constitution of Binary Alloys, McGraw-Hill Book Co., N.Y. (1958).
16. D. Gratias, private communication to D.F.
17. Terms coined by P. Bardhan; J. B. Cohen, private communication to D.F.
18. W. Shockley, J. Chem. Phys. 6, 130 (1938).
19. R. Kikuchi and H. Sato, Acta Met., 22, 1099 (1974).
20. Y.Y. Li, J. Chem. Phys. 17, 447 (1949).
21. C.M. van Baal, Physica 64, 571 (1973).
22. D. de Fontaine, Acta Met. 23, 553 (1975).
23. L. D. Landau and E. M. Lifshitz, Statistical Physics, Addison-Wesley, Reading, Mass. (1958).
24. R. Kikuchi and C.M. van Baal, Scripta Met. 8, 425 (1974).
25. Research supported by Army Research Office (Durham), D. de Fontaine principal investigator, UCLA.
26. J. Kanamori, Progress of Theor. Phys. 35, 16 (1966).
27. International Tables for X-Ray Crystallography, edited by N.F.H. Henry and K. Lonsdale, Vol. I, Kynoch Press, Birmingham (1952).
28. J. Friedel, The Physics of Metals, I - Electrons, edited by J.M. Ziman, Cambridge, The University Press (1969), pg 340-408.
29. J. E. Inglesfield, Acta Met. 17, 1395 (1969).
30. F. Ducastelle and F. Gautier, J. Phys. F. Metal Phys. 6, 2039 (1976).
31. F. Gautier, F. Ducastelle and J. Giner, Phil. Mag. 31, 1373 (1975).
32. J. L. Boquet, private communication to R.K.
33. G. Inden, private communication.
34. E. Van Royen and S. Radelaar, private communication.
35. N.S. Golosov, L. E. Popov and L. Ya. Pudan, J. Phys. Chem. Solids, 34, 1149 and 1157 (1973).
36. R. Kikuchi, D. de Fontaine, M. Murakami and T. Nakamura, Acta Met. (in press).

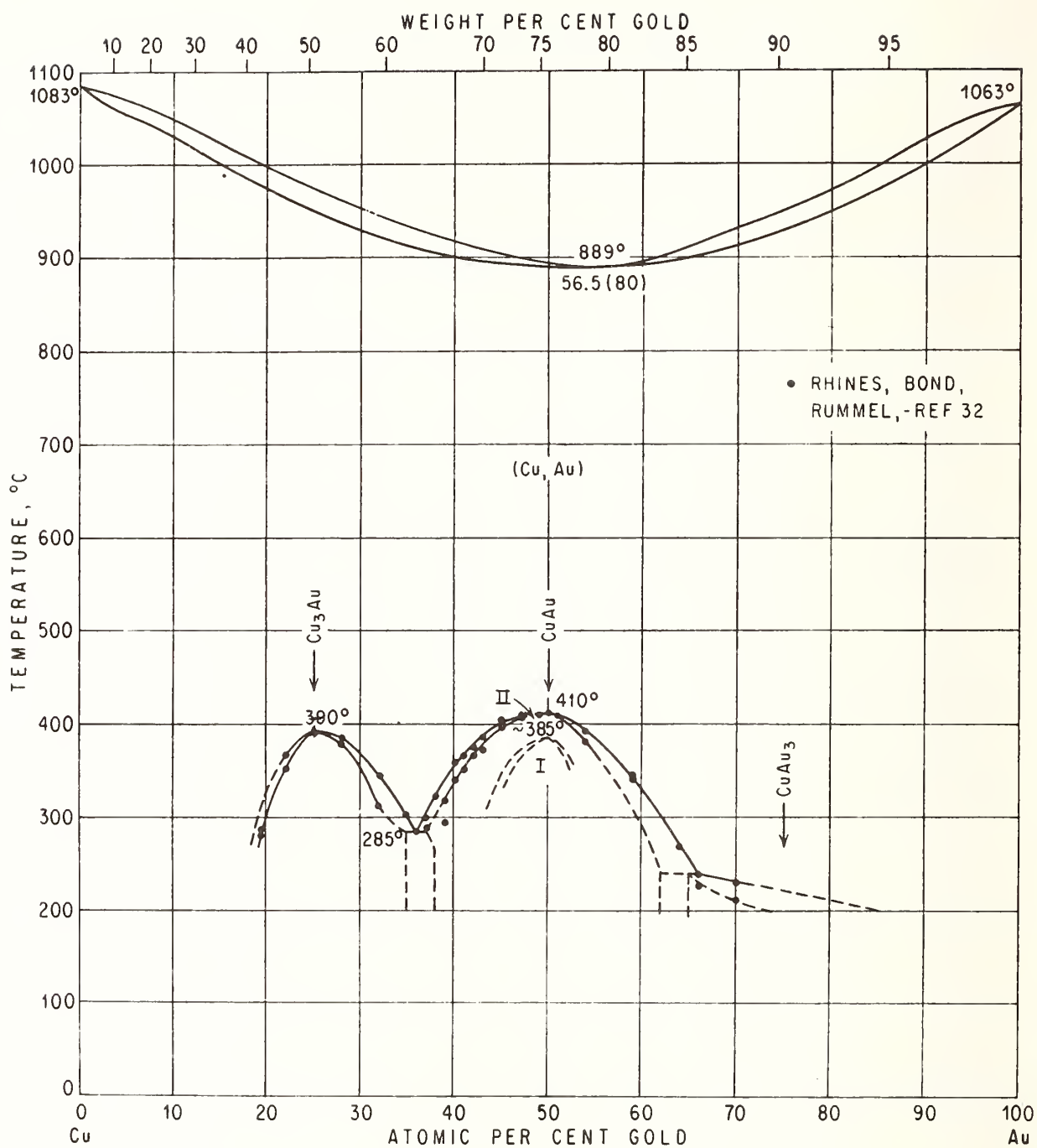


Fig. 1. Experimentally determined Cu-Au phase diagram⁽¹⁵⁾.

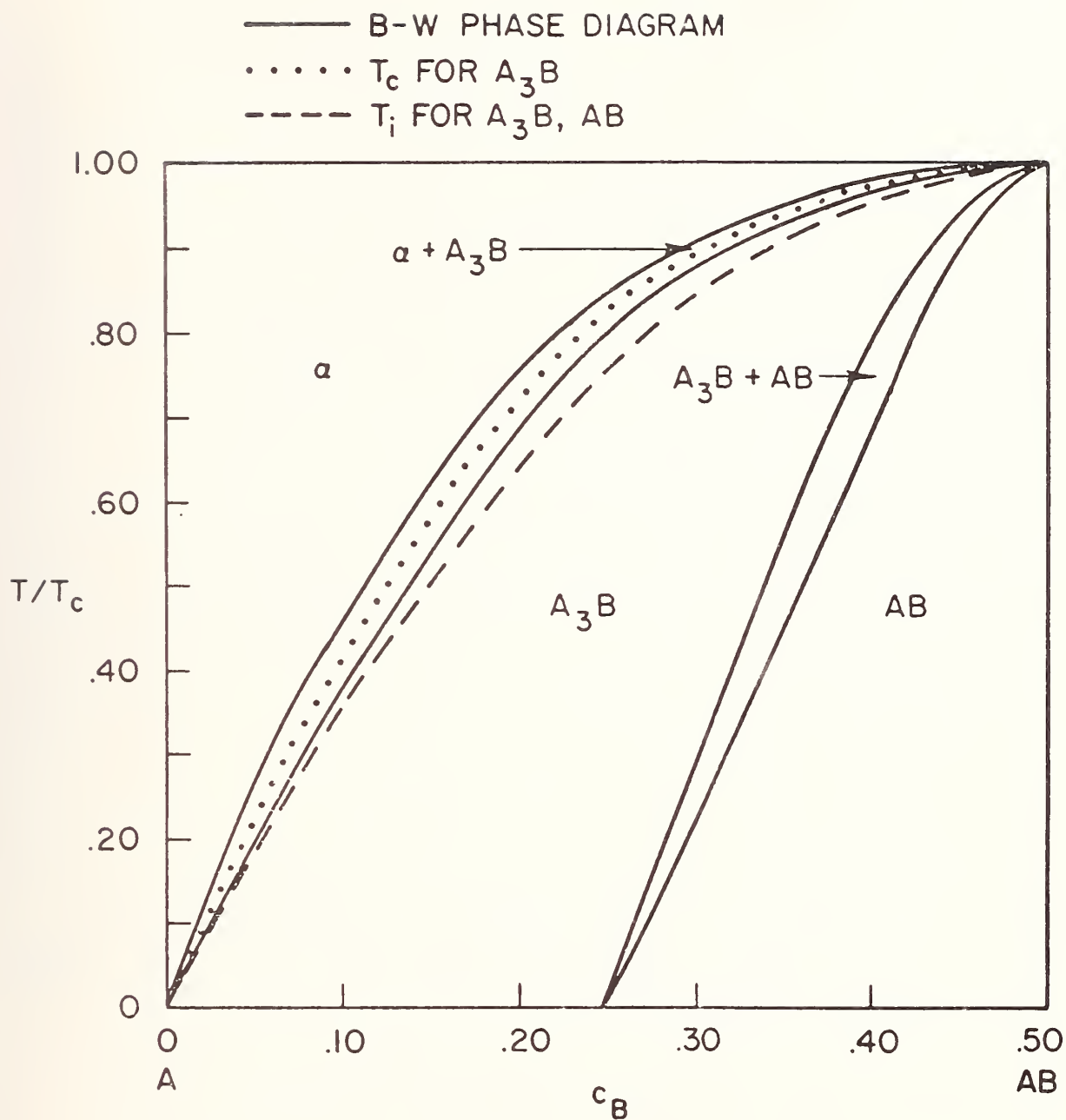


Fig. 2. Cu-Au phase diagram calculated according to the Bragg-Williams model. After Shockely⁽¹⁸⁾.

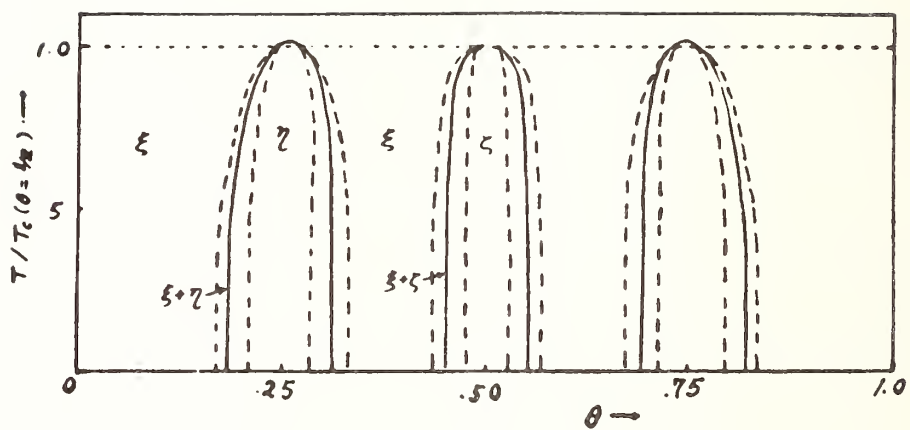


Fig. 3. Cu-Au phase diagram calculated by Li⁽²⁰⁾ according to the quasi-Chemical theory of Guggenheim (dotted lines). Full lines indicate locus of transition points.

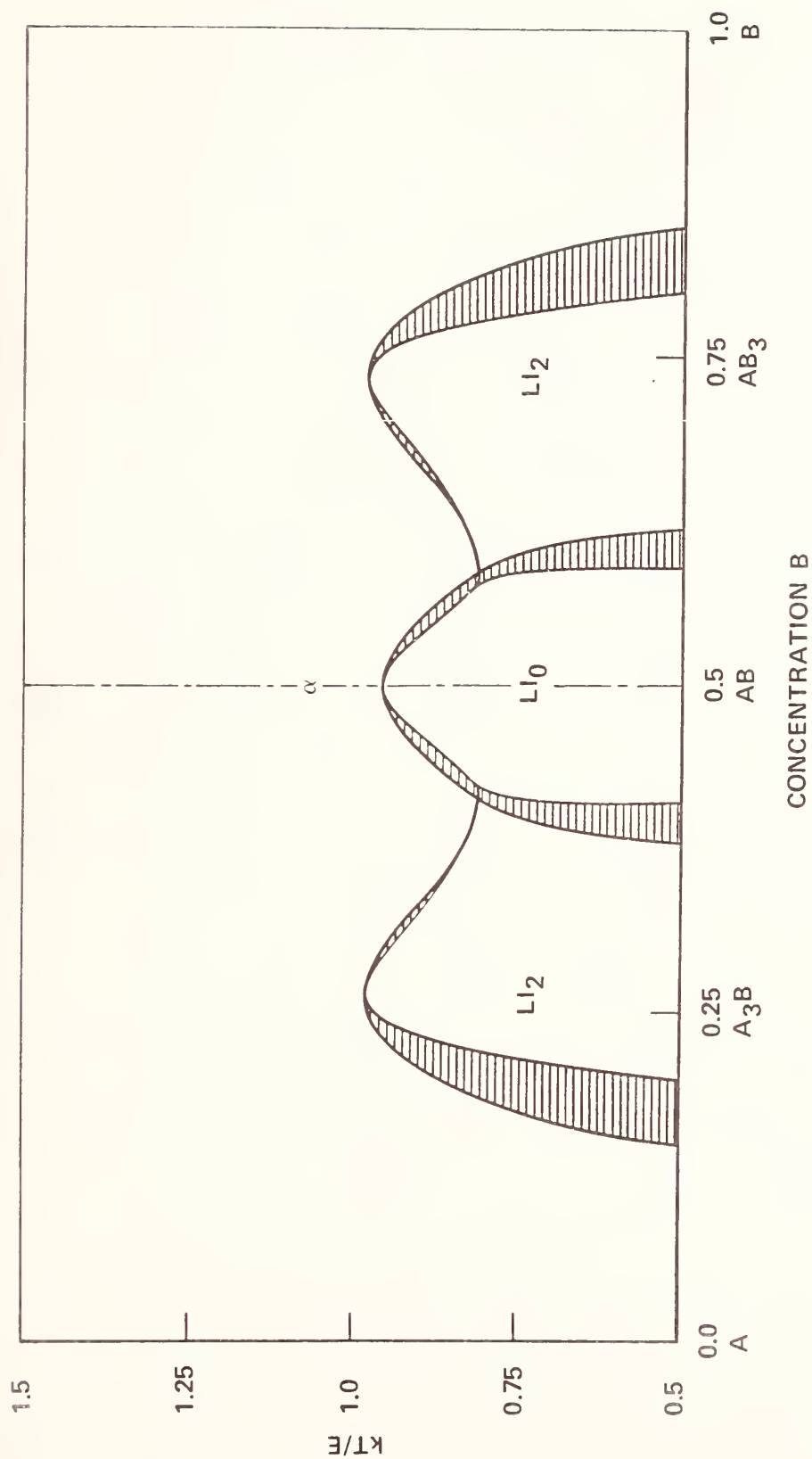


Fig. 4. Cu-Au phase diagram calculated according to the CV model in the tetrahedron approximation with n.n. pair interaction. After van Baa1(21) and Kikuchi(14).

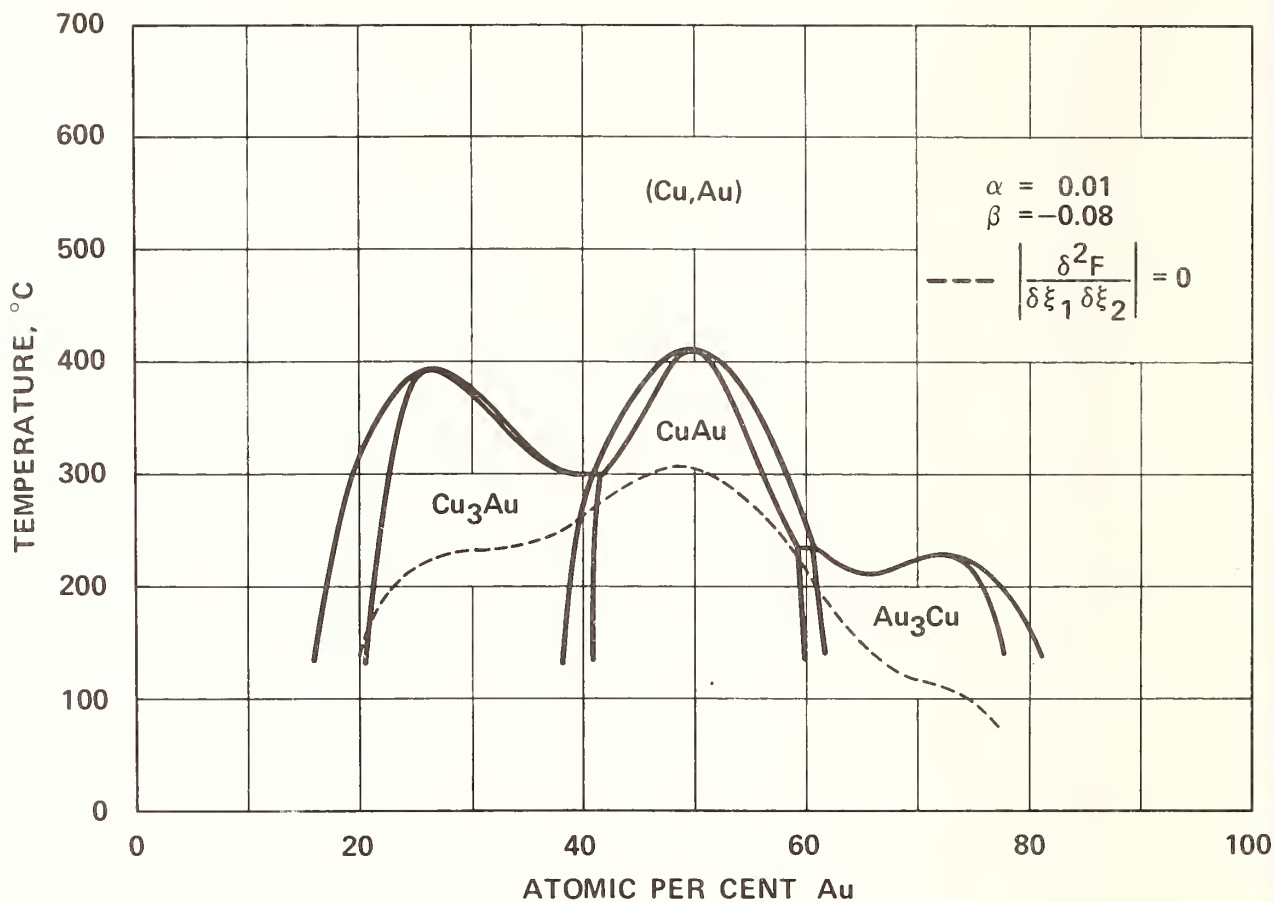


Fig. 5. Cu-Au phase diagram according to the CV model in the tetrahedron approximation with CuCuCuAu and CuAuAuAu many-body interactions.

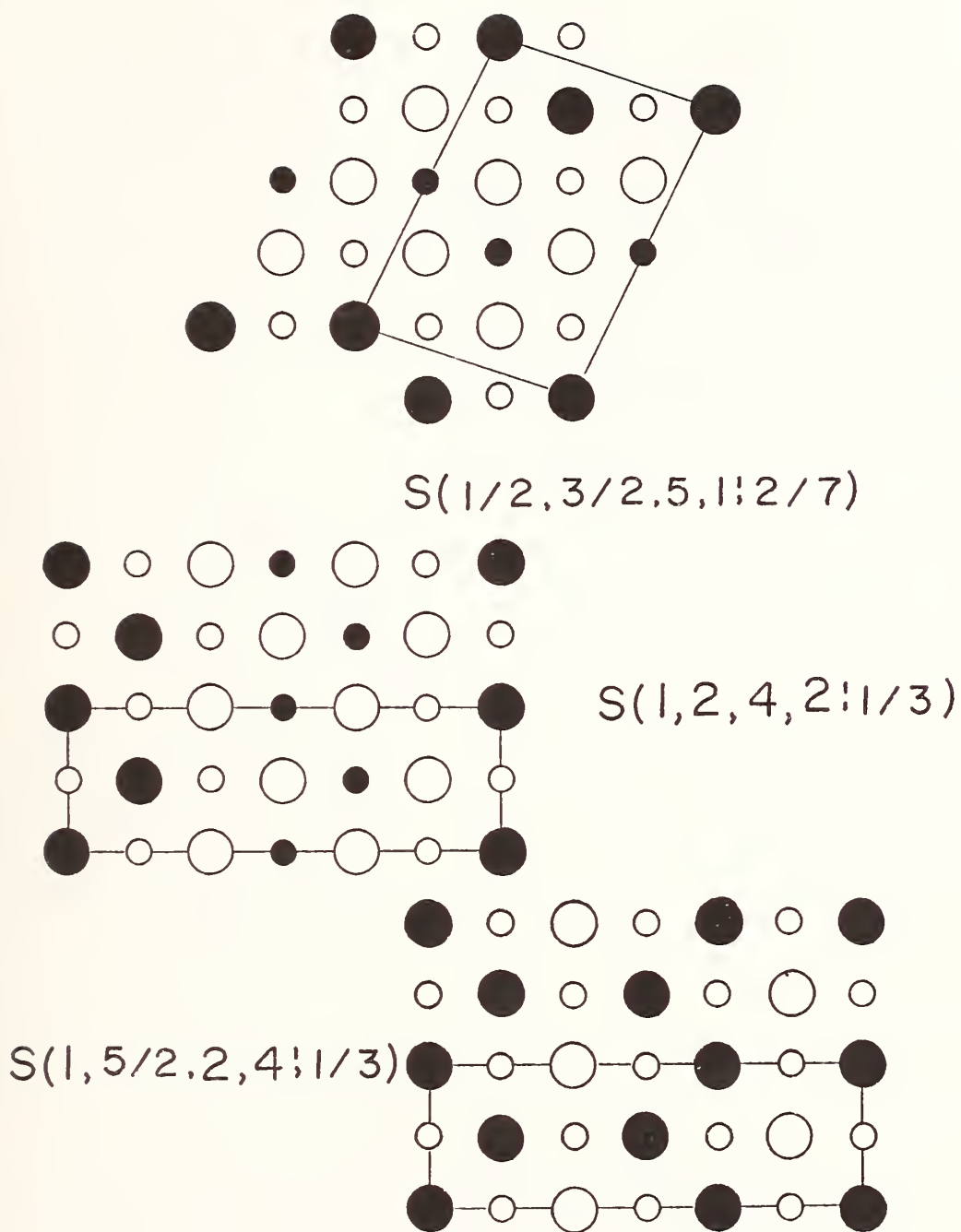


Fig. 6. Projection of the Au_5Mn_2 ordered structure (top) and A_2B structures predicted by Kanamori from a pair interaction model up to fourth coordination shell in the fcc lattice⁽⁸⁾. Open circles: majority component; atoms in planes at integral values of z-coordinate; small circles: atoms at half-integral values of z-coordinate.

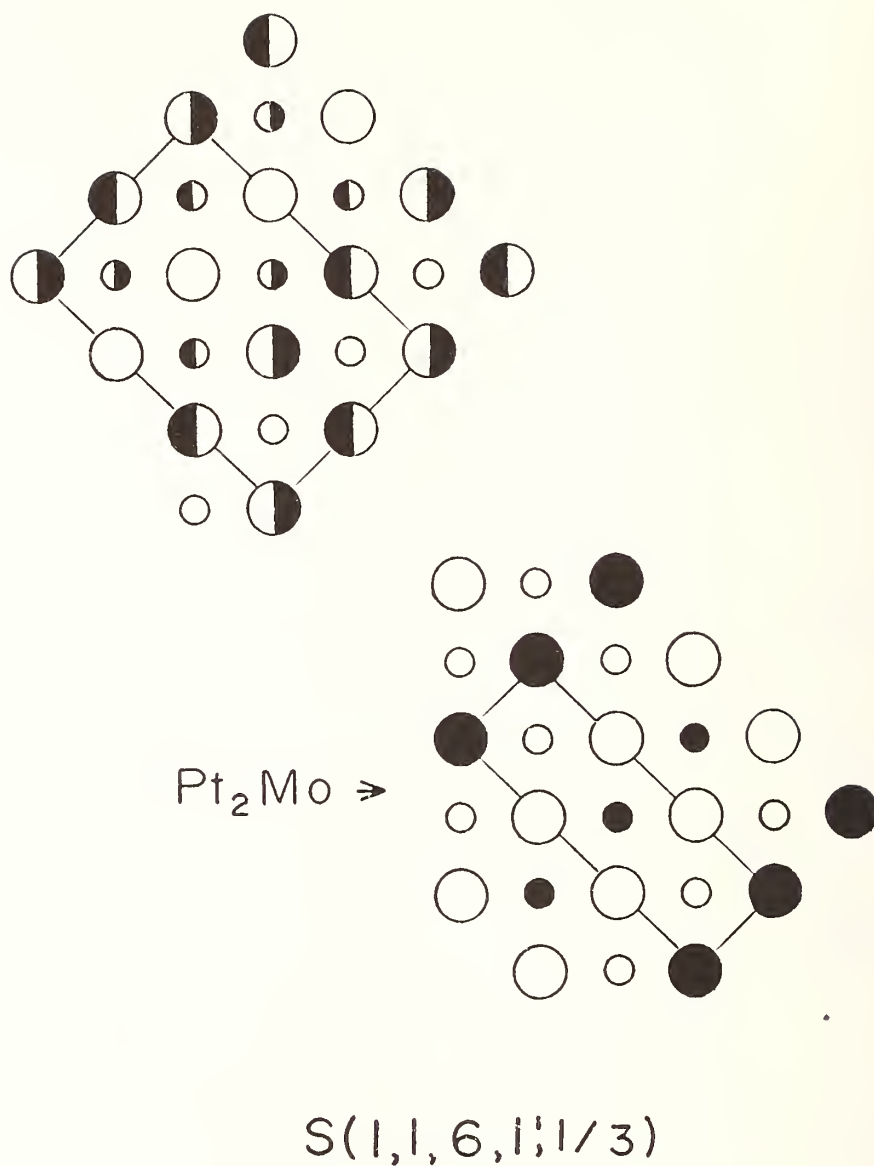


Fig. 7. Projection of two degenerate A_2B ordered structures which have same internal energy in a pairwise model with up to fourth-neighbor interactions⁽⁸⁾. Black-white circles: A-B-A...chains along z axis; white-black circles: B-A-B...chains along z axis.



GENERATION OF SELF-CONSISTENT GIBBS ENERGY FUNCTIONS FOR BINARY SYSTEMS: THE Fe-Cu SYSTEM AS AN EXAMPLE*

by J. F. Smith and D. M. Bailey

Ames Laboratory USERDA and Department of Materials Science and
Engineering, Iowa State University, Ames, Iowa 50011 U.S.A.

O. Kubaschewski

Lehrstuhl für Metallurgie der Kernbrennstoffe und Theoretische
Hüttenkunde der Rheinisch-Westfälischen Technischen Hochschule

5100 Aachen, Germany

Abstract

At present a high level of interest exists concerning the prediction of multicomponent phase equilibria by extrapolation of binary Gibbs energy data. The basic problem is the development of good, self-consistent analytical descriptions of the temperature and composition dependences of the Gibbs energies of formation of the phases in the contributory binary systems. The general process for developing such Gibbs energy functions through combination of experimental thermodynamic data with experimental data concerning binary phase equilibria is illustrated by an analysis of a representative binary system, in this case the Fe-Cu system.

*Work was performed in part at the Lehrstuhl für Metallurgie der Kernbrennstoffe und Theoretische Hüttenkunde der Rheinisch-Westfälischen Technischen Hochschule and in part at the Ames Laboratory, for the U.S. Energy Research and Development Administration under Contract No. W-7405-eng-82.

INTRODUCTION

An estimation of the phase equilibria in a multicomponent system can be made if Gibbs energy functions are available for describing the formation of the competitive phases in the system. Such functions can be most simply generated by combination of functions which describe the Gibbs energies of formation of the phases in the contributory binary systems. A number of surveys¹⁻⁴ are available which illustrate the various procedures which have been suggested for combination of binary data. The level of interest in the combination of binary data for extrapolation into multicomponent systems is evidenced by the broad-based participation, including scientists in France, Germany, Great Britain, Sweden, and the U.S.A., in the CALPHAD project⁵ (CALculation of PHase Diagrams). However, no combination procedure will produce reliable estimates of multicomponent phase equilibria without good input data. Thus the most basic problem is the development of good analytical descriptions of the temperature and composition dependences of the Gibbs energies of formation of the phases in the contributory binary systems.

The present paper utilizes an analysis of the Fe-Cu system to illustrate what Kaufman⁶ has called the ABC procedure. In essence step A is the utilization of the best available thermodynamic data to generate an initial set of Gibbs energy functions. Step B is the input of experimental data pertaining to the phase equilibria to facilitate smoothing and parameter adjustment in the

Gibbs energy functions. Step C is the calculation of an equilibrium temperature-composition diagram from the final set of smoothed and adjusted Gibbs energy functions and the comparison of this calculated diagram with the experimental phase diagram. It may be noted that Gibbs energy functions which are developed in this manner implicitly contain good approximations for the binary interaction parameters. Further, it should be emphasized that the strengths, and thereby the importance, of the interactions decrease with the order of the interactions so that the estimation of multicomponent phase equilibria on the basis of binary interaction parameters includes the dominant interactions. Of course, small additional terms may be added to the Gibbs energy functions of multicomponent phases to include ternary interactions if appropriate thermodynamic and/or phase equilibria data are available. However, the general absence³ of quarternary and higher order data is not likely to be a serious hindrance to this general approach for the estimation of multicomponent phase equilibria.

In selecting the more reliable from among a number of independent thermodynamic data for any given binary system, two 'thumb' rules may be invoked. First, high-temperature data are normally preferable to low-temperature data because kinetic inhibition of equilibrium is less likely at higher temperatures. Second, enthalpy data tend to be more reliable, albeit not always more precise, than Gibbs energy data. On the basis of this latter observation, the most uncertain terms in experimental data tend to be the excess entropy terms, and these terms therefore have

the most latitude for adjustment when fitting analytical expressions for Gibbs energies to the phase boundaries in experimental temperature-composition diagrams.

Other secondary factors such as the reproducibility of experimental values, comparative reputations of different experimental techniques, etc., may also be invoked to select between discordant data. The ultimate criterion is, however, that the Gibbs energy functions which are generated should closely reproduce the phase boundaries of the experimental temperature-composition diagram. When this situation is obtained, the Gibbs energy functions, although they may be less than completely accurate, are at least internally consistent.

REPRESENTATIVE PROCEDURE

Fe-Cu System: The development of Gibbs energy functions for the formation of the competing phases in the Fe-Cu system is here outlined as an example of the generation of self-consistent analytical expressions for a binary system. More specific details are available elsewhere.⁷ The present paper is meant to serve only as an illustration of the type of computation and the nature of the successive steps that lead to a satisfactory match between analytical Gibbs energy functions and the experimental phase fields of a temperature-composition diagram. While a portion of the present work was done from a computer terminal interacting with an IBM 360/65 computer, this was done primarily for the convenience arising from the output facility of an associated on-line incremental

plotter. Most of the initial analysis was done with a simple desk calculator in combination with manual graphing, and it is to be emphasized that all of the work, with the possible exception of one item which is later noted, could have been done with almost any of the current generation of programmable desk calculators. This has been verified by repeating representative computations on SR-52 and HP-55 calculators.

In the Fe-Cu system⁸ there is an fcc terminal solid solution, the ϵ -phase, on the Cu-rich side of the system. This phase decomposes peritectically at 1367 K into a Cu-rich liquid plus γ -phase. The γ -phase is the fcc terminal solid solution on the Fe-rich side of the system at intermediate temperatures. On cooling to 1123 K the γ -phase decomposes eutectoidally into ϵ -phase plus α -phase and on heating to 1751 K the γ -phase decomposes peritectically into δ -phase plus liquid. The α and δ -phases are respectively the low and high temperature terminal bcc solid solutions on the Fe-rich side of the system.

The Liquid Phase: Extensive thermodynamic data are available only for liquid alloys. These data result from independent investigations, five each, of the enthalpies⁹⁻¹³ and Gibbs energies¹⁴⁻¹⁸ of liquid alloy formation in the temperature range 1700-1900 K. The composite data span the full composition range of the system, and the enthalpy data show reproducibility to ~5% while the reproducibility of the Gibbs energy data is ~15%.

In conformity with the previously noted selection criteria these data were taken to be of good reliability, and a preliminary

Gibbs energy function for the formation of liquid alloys, ΔG_L , was generated from the values selected from these data by Hultgren et al.¹⁹ This was done by first converting the selected values for enthalpies and excess entropies of liquid alloy formation from tabular form to analytical form,

$$J(N_{Fe}, N_{Cu}) = N_{Fe} N_{Cu} [a_0 + a_1(N_{Fe} - N_{Cu}) + a_2(N_{Fe} - N_{Cu})^2 + a_3(N_{Fe} - N_{Cu})^3]. \quad (1)$$

For the conversion it was found convenient to apply the constraint that for a binary system $N_{Fe} = 1 - N_{Cu}$ where N_i represent the mole fraction of the i th component. This constraint allows representation in simple power series

$$J(N_{Fe}, N_{Cu}) = J(N_{Fe}) = \sum b_n N_{Fe}^n. \quad (2)$$

A least-squares program, such as is commonly available, was then utilized for evaluating the coefficients, b_n , from the tabulated values. The requirements that the enthalpies and excess entropies of alloy formation equal zero at $N_{Fe} = 0$ and $N_{Fe} = 1$ were met by requiring, respectively, $b_0 = 0$ and $\sum b_n = 0$. After fitting, the functions were inverted to the form of Eq. 1. Liquid Cu and γ -Fe were arbitrarily chosen as the standard states for the Gibbs energy functions for the formation of all phases in the system, and values for the elemental phase transformations²⁰ were combined with the enthalpy and excess entropy functions in a regular solution approximation to produce the preliminary expression for $\Delta G_L(N_{Fe}, N_{Cu}, T)$.

The fcc Phases: No experimental thermodynamic measurements for the solid phases in the binary Fe-Cu system were found. However, Counsell et al.²¹ had made some calorimetric measurements of the enthalpies of formation of a few solid alloys in the Fe-Cu-Ni ternary system. Through combination of these enthalpy values with thermodynamic data for Fe-Ni and Ni-Cu alloys plus some knowledge of the phase equilibria in certain sections of the ternary system, Counsell et al. developed a set of functions for describing the thermodynamics of formation of the fcc phase in the ternary system. In the present work these functions were extrapolated to the binary limit by setting $N_{Ni} = 0$.

After conversion to the standard states of the present work, graphical representations of the Gibbs energy function vs. composition showed that the fcc phase at intermediate alloy compositions tended to decompose to the ϵ -phase and γ -phase terminal solutions and at 1367 K the projected equilibrium between liquid and γ -phase showed compositions in reasonable accord with the phase diagram. However, at 1367 K the Gibbs energy of formation of the ϵ -phase was much too negative to be consistent with peritectic decomposition. This disparity prompted a modification of the excess entropy term, $\Delta S_{\gamma,\epsilon}^E$, from a value of $2.9805 N_{Fe} N_{Cu}$ from Counsell et al.²¹ to

$$\Delta S_{\gamma,\epsilon}^E = 2.9805 \alpha N_{Fe} N_{Cu} + 3.308(1-\alpha) N_{Fe}^2 N_{Cu} \quad (3)$$

where $2.9805 N_{Fe} N_{Cu} = 3.308 N_{Fe}^2 N_{Cu}$ at $N_{Fe} = 0.9$ so that $\Delta S_{\gamma,\epsilon}^E$ is

invariant with respect to α at that composition. Thus $\Delta S_{\gamma,\epsilon}^E$ was made insensitive to the parameter α in the Fe-rich region but highly sensitive in the Cu-rich region so that α could be adjusted to equilibrate the ϵ -phase with liquid and γ -phase at 1367 K. This is illustrated in Fig. 1.

After adjustment of α , the Gibbs energy function for the formation of fcc alloys indicated equilibrium compositions for the ϵ and γ -phases over the temperature range 1123-1367 K in acceptable accord with the experimental terminal solubilities.^{8,22} Above 1367 K evaluation of the equilibria between liquid and γ -phase predicted a liquidus line in good agreement with the phase diagram for $N_{Fe} < 0.15$ but was slightly below the experimental liquidus in the region $0.15 < N_{Fe} < 0.4$ and beyond $N_{Fe} = 0.4$ drifted significantly above the experimental liquidus. To achieve agreement, the coefficients in the expression for ΔG_L were refined through successive approximations. This refinement was restricted to terms involving higher powers of N_{Fe} so that the refinement did not perturb the agreement already existing in the Cu-rich region. Since the experimental spread among determinations⁸ of the liquidus line is about ± 15 K in the composition range $0.3 < N_{Fe} < 0.7$, refinement was terminated when the predicted and experimental liquidus lines agreed within this spread. It is worth noting that the refined parameters produce no inconsistency with input thermodynamic data. The refined parameters indicate enthalpies and Gibbs energies of liquid alloy formation agreeing on the average within 3.3% and 5.4%, respectively,

with values tabulated by Hultgren et al.,¹⁹ and this is well below the scatter in the composite of the input experimental data.

The computer program for evaluating the equilibrium compositions at fixed temperature conformed to the following logic sequence. First, at an arbitrarily selected composition, the slope and intercept of the ΔG vs. composition curve were evaluated for the first phase. Second, the slope of the ΔG vs. composition curve for the second phase was evaluated at some selected starting composition. The slopes for the two phases were then compared and, on the basis of the comparison, a new composition was selected for the second phase and the calculation was repeated. Iteration continued with bracketing convergence until the slopes for the two phases matched within a 'good enough' factor. Third, the intercept for the second phase was calculated and compared with the intercept from the first phase. On the basis of the intercept comparison, the composition for the first phase was adjusted and the whole process was repeated until agreement was obtained within 'good enough' limits for both the slopes and intercepts of the two phases being tested for equilibration; such agreement defines a common tangent to the Gibbs energy functions for the two phases. The compositions at the points of tangency were then taken as the calculated phase boundaries.

The bcc Phases: No thermodynamic data were found for the bcc Fe-Cu alloys, but Zener²³ has suggested that for Fe and Fe alloys the greater stability of the bcc structure relative to the fcc structure at low temperatures is due to differences in magnetic

contributions to the Gibbs energies. This suggestion has been pursued by a number of investigators; these include Hillert et al.²⁴ who have developed a simple formulation for approximating the magnetic contribution to the Gibbs energy of formation of bcc Fe alloys. This approximation requires knowledge of two quantities: first, the change in Curie temperature per mole fraction of alloying component which for Cu alloys was obtained from the phase diagram,⁸ and, second, the magnetic contribution to the entropy of bcc Fe which was obtained in analytical form by a least-squares fit to the tabular data developed by Weiss and Tauer.²⁵

With this input, the general formulation of Hillert et al.²⁴ leads to an expression for the Gibbs energy of formation of bcc Fe-Cu alloys from bcc Fe and bcc Cu. The expression contains four adjustable parameters which specify the magnitudes and composition dependences of the non-magnetic contributions to the enthalpies and excess entropies associated with the formation reaction. Conversion of standard state to liquid Cu was accomplished by adding terms for fusion²⁰ and for the bcc→fcc transformation;²⁶ conversion of standard state to fcc Fe was accomplished by adding a term for the bcc→fcc transformation which was taken from the critical evaluation of data for pure Fe by Orr and Chipman.²⁷ This term was evaluated by a least-squares fit to their tabulated data, and satisfactory fitting required powers of temperature ranging from zero through six. The fitting of this term is probably beyond the capability of most desk calculators.

After conversion to the standard states of the present work, the Gibbs energy function for the formation of the bcc phases still contained four adjustable parameters and was in a form suitable for comparison with the Gibbs energy functions for the liquid and fcc phases. The adjustable parameters were then evaluated on the bases of the peritectic reaction at 1751 K which involves the liquid, γ , and δ -phases and the eutectoid reaction at 1123 K which involves the ϵ , γ , and α -phases. At each of these two temperatures both the magnitude and slope of the bcc Gibbs energy function are constrained at the equilibrium composition of the participating bcc phase, and the constraining limitations are derivable from the Gibbs energy functions already generated for the liquid and fcc phases. Thus there are only four constraints to fix four adjustable parameters plus two additional variables which are the composition of the δ -phase at 1751 K and the composition of the α -phase at 1123 K. This problem was approached by first solving for the magnitudes of the non-magnetic enthalpy and excess entropy of bcc alloy formation without allowing for compositional dependence. The constraints are then sufficient to fix the two magnitudes and the two compositions. The resulting composition for the δ -phase in the peritectic reaction at 1751 K differed by more than an atom per cent from the experimental value of Hellawell and Hume-Rothery,²⁸ and, in view of the limited terminal solubility, this was considered unacceptable. Parameters defining the compositional dependences were then freed within the limitation that the sums of

the new composition independent and composition dependent terms were not allowed to vary appreciably from the initial composition independent values. Then, in an iterative procedure the calculated composition of the δ -phase at 1751 K was moved into near accord with the Hellawell and Hume-Rothery value and the numerical values of the adjustable parameters were fixed.

RESULTS AND DISCUSSION

The Gibbs energies of formation of the Fe-Cu phases from liquid Cu and fcc Fe which were generated by the foregoing procedure are, in cal/gm-atom, for the liquid,

$$\begin{aligned} \Delta G_L = & 3500 N_{Fe} + N_{Fe}N_{Cu}[8203+433.3(N_{Fe}-N_{Cu}) + 1808(N_{Fe}-N_{Cu})^2 \\ & + 578(N_{Fe}-N_{Cu})^3] - T\{-1.987N_{Fe}\ln N_{Fe}-1.987N_{Cu}\ln N_{Cu} \\ & + 1.944N_{Fe} + N_{Fe}N_{Cu}[0.44438+0.39238(N_{Fe}-N_{Cu}) \\ & + 0.61813(N_{Fe}-N_{Cu})^2 + 0.56113(N_{Fe}-N_{Cu})^3]\}, \end{aligned} \quad (4)$$

for the fcc phases,

$$\begin{aligned} \Delta G_{\gamma, \epsilon} = & -3120N_{Cu} + 10107 N_{Fe}N_{Cu}^2 + 12936N_{Fe}^2N_{Cu} - T\{-1.987 \\ & N_{Fe}\ln N_{Fe}-1.987N_{Cu}\ln N_{Cu}-2.30N_{Cu}+0.8196N_{Fe}N_{Cu} \\ & +2.3983N_{Fe}^2N_{Cu}\}, \end{aligned} \quad (5)$$

and for the bcc phases,

$$\begin{aligned}\Delta G_{\alpha,\delta} = & N_{\text{Fe}}N_{\text{Cu}}\{13000+494.7(N_{\text{Fe}}-N_{\text{Cu}})+1084S_{\text{mag},\alpha}-T[2.500 \\ & +2.542(N_{\text{Fe}}-N_{\text{Cu}})]\} + T(1.987N_{\text{Fe}}\ln N_{\text{Fe}}+1.987N_{\text{Cu}}\ln N_{\text{Cu}}) \\ & + N_{\text{Cu}}(-1620+1.5T) + \Delta G_{\text{Fe,tr}}.\end{aligned}\quad (6)$$

In the last expression, $S_{\text{mag},\alpha}$ represents the magnetic entropy of bcc Fe and $\Delta G_{\text{Fe,tr}}$ represents the Gibbs energy for the fcc→bcc transformation in pure Fe, and these are:

$$\begin{aligned}S_{\text{mag},\alpha} = & -19.930 + 5.2602 \times 10^{-2}T - 4.7618 \times 10^{-5}T^2 \\ & + 1.9274 \times 10^{-8}T^3 - 2.9356 \times 10^{-12}T^4\end{aligned}\quad (7)$$

and

$$\begin{aligned}\Delta G_{\text{Fe,tr}} = & -40027.7 + 158.219T - 0.261351T^2 + 2.30512 \times 10^{-4}T^3 \\ & - 1.14285 \times 10^{-7}T^4 + 3.01614 \times 10^{-11}T^5 - 3.30930 \times 10^{-15}T^6\end{aligned}\quad (8)$$

Because of the rapid change in the thermodynamic functions of Fe in the vicinity of the Curie temperature, all fitting of data^{25,27} was done for values above this temperature so Eqs. 6, 7, and 8 are valid only for temperatures above ~1050 K. Fig. 2 shows the calculated phase diagram (solid lines) together with representative points from the experimental phase diagram with the error bars on the experimental liquidus points in the composition range $0.3 < N_{\text{Fe}} < 0.7$ showing the previously noted ± 15 K tolerance. Table I shows a comparison of calculated and observed compositions for the two peritectic and one eutectoid reaction.

Obviously the calculation of one binary diagram is by itself a useless endeavor since the experimental diagram is already available. However, the combination of Gibbs energy functions from related phase diagrams to predict multicomponent equilibria is quite worthwhile since the experimental difficulty becomes orders of magnitude more complex, tedious, time-consuming, and expensive when expanding from binary to ternary to quaternary, etc., systems. Thus, even though high precision is not expected in extrapolating binary data to estimate multicomponent equilibria, considerable experimental effort may be saved if one can localize a region of interest. A number of possibilities come readily to mind as examples. If high temperature strength is the desired property, regions of maximal melting might be sought. If oriented eutectics are to be grown, regions of eutectic solidification may be sought. If deleterious phases (e.g. σ -phases) or desirable phases (e.g. age hardening precipitates) are important, their true thermodynamic stability independent of kinetic factors may be tested. If high-temperature superconductors are desired, phase compositions with appropriate electron/atom ratios may be examined for marginal stability or metastability. In short, the possible applications are limited by the ingenuity of the investigator, and the present paper illustrates that the generation of appropriate Gibbs energy functions for reproducing compositions of experimental phase equilibria for a representative binary system to within ~1 at. % is not particularly difficult nor excessively time-consuming. The primary limitation of this ABC approach is that it will not predict the existence of phases which are not functionally represented.

REFERENCES

1. L. Kaufman and H. Bernstein, Computer Calculation of Phase Diagrams, Chaps. 9-13 (Academic Press, New York, 1970).
2. P. J. Spencer, F. H. Hayes, and O. Kubaschewski, *Rev. Chim. minerale* 9, 13-29 (1972).
3. I. Ansara, in Metallurgical Chemistry Symposium 1971, ed. by O. Kubaschewski, pp. 403-430 (Her Majesty's Stationery Office, London, 1972).
4. O. Kubaschewski and I. Barin, *Pure and Appl. Chem.* 38, 469-494 (1974).
5. For information contact L. Kaufman, Manlabs, Inc., Cambridge, Mass. 02139, U.S.A.
6. L. Kaufman, in Metallurgical Chemistry Symposium 1971, ed. by O. Kubaschewski, pp. 373-402 (Her Majesty's Stationery Office, London, 1972).
7. O. Kubaschewski, J. F. Smith and D. M. Bailey, *Z. Metallk.*, in process.
8. M. Hansen and K. Anderko, Constitution of Binary Alloys, 2nd ed., pp. 580-582 (McGraw-Hill, New York, 1958).
9. F. Woolley and J. F. Elliott, *Trans. Met. Soc. AIME* 239, 1872-1873 (1967).
10. W. Oelsen, E. Schürmann, and C. Florin, *Arch. Eisenhüttenw.* 32, 719-728 (1961).
11. A. Podgornik, quoted by Oelsen et al., ref. 10.
12. Y. Tozaki, Y. Iguchi, S. Ban-ya, and T. Fuwa, in Chemical Metallurgy of Iron and Steel, Proc. of the Int. Symp. on Met. Chem. - Applications of Ferrous Met. held Univ. of

Sheffield, 19-21 July 1971, pp. 130-132 (Iron and Steel Inst., London, 1973).

13. A. El'-Khasan, K. Abdel-Aziz, A. A. Vertman, and A. M. Samerin, *Izvest, Akad. Nauk SSSR, Met.* 3, 19-30 (1966).
14. J. P. Morris and G. R. Zellars, *J. Metals* 8, 1086-1090 (1956).
15. M. Olette and M. Onillon, *Comptes Rendus Acad. Sc. Paris* 261, 3597-3600 (1965).
16. P. J. Koros and J. Chipman, *J. Metals* 8, 1102-1104 (1956).
17. F. C. Langenberg, *J. Metals* 8, 1024-1025 (1956).
18. U. V. Choudary, J. A. Serkin, and G. R. Belton, *Met. Trans.* 6B, 399-403 (1975).
19. R. Hultgren, P. D. Desai, D. T. Hawkins, M. Gleiser, and K. K. Kelley, Selected Values of the Thermodynamic Properties of Binary Alloys, pp. 737-741 (Am. Soc. for Metals, Metals Park, Ohio 44073, 1973).
20. R. Hultgren, R. L. Orr, P. D. Anderson, and K. K. Kelley, Selected Values of Thermodynamic Properties of Metals and Alloys, pp. 89-95 and 103-112 (John Wiley and Sons, Inc., New York, 1965).
21. J. F. Counsell, E. B. Lees, and P. J. Spencer, in Metallurgical Chemistry Symposium 1971, ed. by O. Kubaschewski, pp. 451-458 (Her Majesty's Stationery Office, London, 1972).
22. G. R. Speich, J. A. Gula, and R. M. Fisher, in The Electron Microprobe, ed. by T. D. McKinely, K. F. J. Heinrich and D. B. Witty, pp. 525-541 (John Wiley and Sons, New York, 1966).
23. C. Zener, *Trans. AIME* 203, 619-630 (1955).

24. M. Hillert, T. Wada, and H. Wada, J. Iron Steel Inst. 205, 539-546 (1967).
25. R. J. Weiss and K. J. Tauer, Phys. Rev. 102, 1490-1495 (1956).
26. L. Kaufman, Report PB 144220, Office of Technical Services, Cambridge, Mass., 1959.
27. R. L. Orr and J. Chipman, Trans. Met. Soc. AIME 239, 630-633 (1967).
28. A. Hellawell and W. Hume-Rothery, Phil. Trans. Roy. Soc. London A249, 432-433 (1957).

Table I. Comparison of calculated and observed equilibrium compositions (N_{Fe}) for the phases involved in the two peritectic and one eutectoid reaction in the Fe-Cu system.

	<u>Liq.</u>	<u>γ-phase</u>	<u>δ-phase</u>	
Peritectic reaction	0.873	0.920	0.934	(calc.)
at 1751 K	0.897	0.917	0.933	(ref. 28)
	<u>Liq.</u>	<u>ϵ-phase</u>	<u>γ-phase</u>	
Peritectic reaction	0.039	0.048	0.942	(calc.)
at 1367	0.032	0.045	~0.925	(ref. 8)
	-----	-----	0.940	(ref. 22)
	<u>ϵ-phase</u>	<u>γ-phase</u>	<u>α-phase</u>	
Eutectoid reaction	0.016	0.982	0.990	(calc.)
at 1123 K	0.012	~0.97	~0.99	(ref. 8)
	-----	0.977	0.981	(ref. 22)

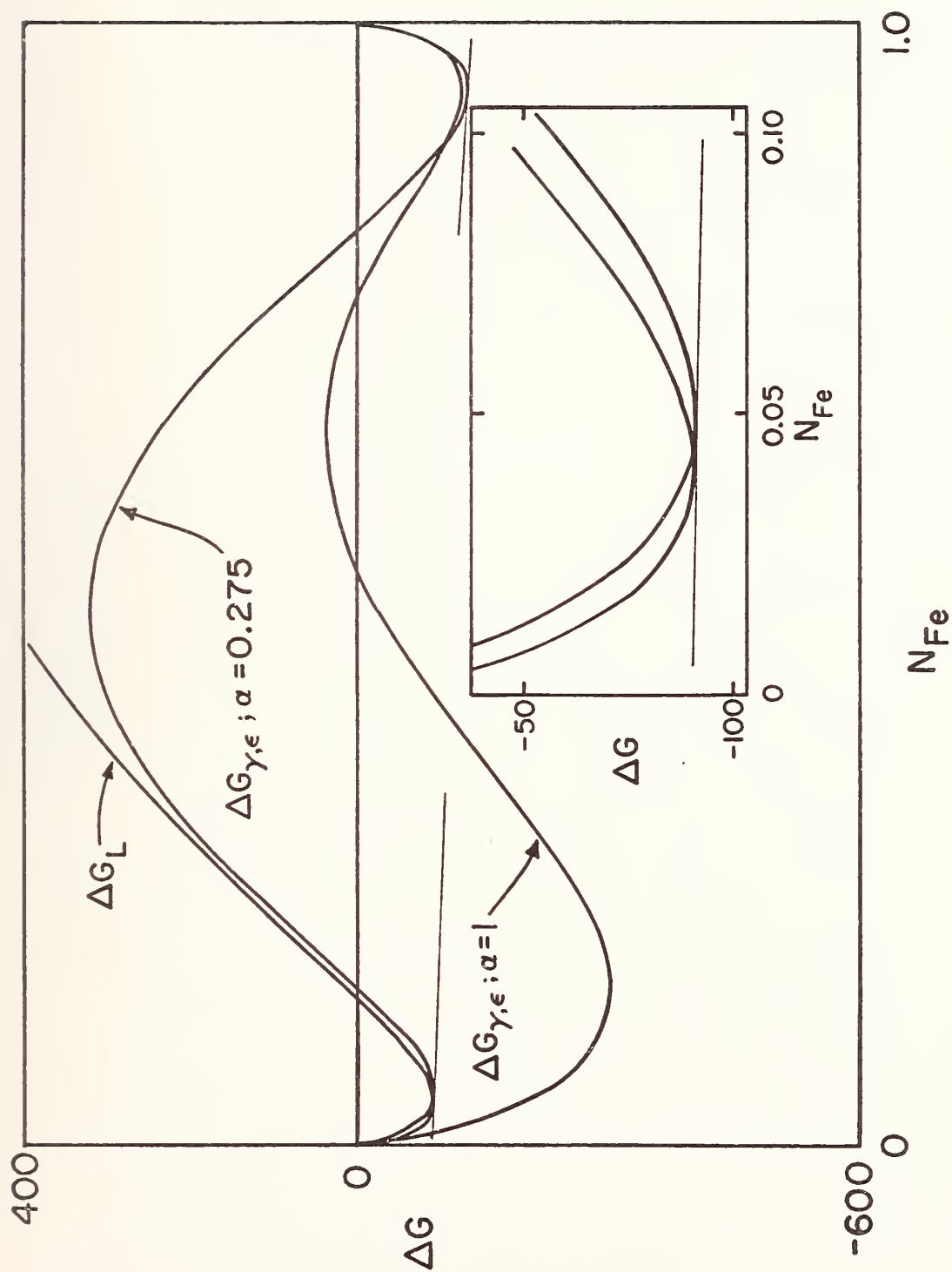


Fig. 1. Adjustment of the parameter α in $G_{\gamma,\epsilon}$ to effect peritectic equilibrium at 1367 K.

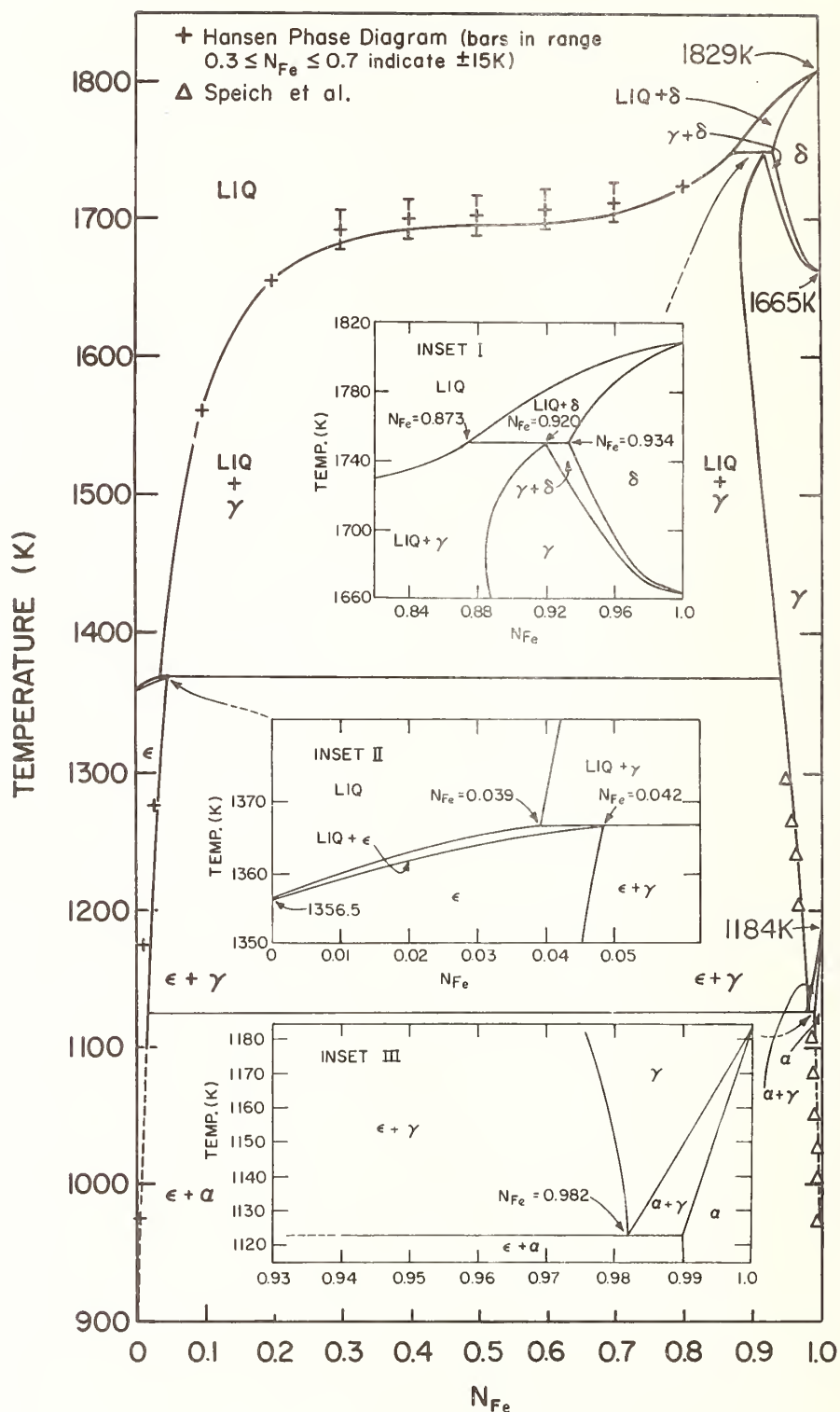


Fig. 2. Comparison of representative points from the experimental Fe-Cu phase diagram with the calculated diagram (solid lines).



CHARACTERISTICS AND CALCULATION OF STABILITY DIAGRAMS

Scott McCormick

Metallurgical and Materials Engineering Department
Illinois Institute of Technology
Chicago, Illinois 60616

Yaz Bilimoria

Inland Steel Research Laboratories
East Chicago, Indiana 46312

ABSTRACT

Stability diagrams are equilibrium diagrams that map phase equilibria in systems containing both metallic and non-metallic components as a function of temperature, non-metal chemical potential or activity, and X_M , the ratio of M atoms to metal atoms. They offer an alternative perspective on phase equilibria and reaction paths in these systems. The characteristics and calculation of two forms of stability diagrams for systems containing non-metallic and metallic components will be discussed. In these two types of diagrams phase equilibria are mapped as a function of (1) non-metal activity and X_M at constant temperature, and (2) temperature and X_M at constant or continuously varying non-metal activity.

These diagrams are similar in form to conventional temperature-composition diagrams with horizontal tie lines and eutectic and peritectic-like features. The lever law can be used to calculate the distribution of metal atoms between phases in equilibrium. Non-metal activity- X_M plots are ideal for carrying out ternary Gibbs-Duhem integrations with Schuhmann's method.

These types of diagrams can be calculated from plots of Gibbs free energy versus X_M at constant temperature and non-metal activity. One mole of metal is chosen as the basis for the calculation. The two free energy ordinates are the molar free energies of the two metals. Temperature and non-metal activity are fixed, so that the condensed phases, stable and unstable, have the same non-metal chemical potential. The free energy of the system is therefore minimized when the combined free energies of the two metals are at a minimum. The curves are of the form

$$G^\eta = X_A {}^0G_A^\eta + X_B {}^0G_B^\eta + RT (X_A \ln a_A^\eta + X_B \ln a_B^\eta)$$

The $^{\circ}G_M^{\eta}$ terms are the molar free energies of component M in η -phase standard states at fixed temperature and non-metal activity. The a_M^{η} terms are the metal activities in solution with respect to the $^{\circ}G_M^{\eta}$ standard states. To calculate the free energy curves, the thermodynamics of each stable solid or liquid solution must be known.

The Fe-Cr-O-C system is used to illustrate these principles.

CHARACTERISTICS AND CALCULATION OF STABILITY DIAGRAMS

Equilibrium diagrams are maps of the regions of stability of solid, liquid, and gaseous phases as a function of two or more independent thermodynamic variables. The most common choices of independent variables are temperature and composition. Alternative choices of variables allow systems to be examined from different perspectives and can yield different insights into system behavior.

In systems containing both non-metallic and metallic components, it is interesting to map phase equilibria on stability diagrams in which the independent variables are temperature, the chemical potentials or activities of the non-metals, and metal composition as measured by X_i , the ratio of moles of metal i to moles of metal, so that

$$X_i = n_i / (n_i + n_j + \dots)$$

where n_i , n_j , ... represent moles of metallic components.

Several representative stability diagrams are shown in figures 1-5 for systems containing iron and chromium. The characteristics of these types of diagrams have been discussed by Pelton, Schmalzried, et al.⁽¹⁻⁵⁾. Briefly, figures 1-5 are structurally similar to conventional binary and ternary temperature-composition diagrams. The rules of construction are identical. All n -phase regions must be bounded by regions containing $(n + 1)$ phases or $(n + 1)$ -phase invariant equilibria. In systems with two metal components, boundaries of one-phase regions must meet with curvatures such that the boundaries extrapolate into the adjacent two-phase regions.

In Figures 1-5 a horizontal line in a two-phase region represents a condition of constant temperature and non-metal activity, a tie line. The metallic compositions can be read at the ends of the tie lines. The distribution of metal between two equilibrium phases can be calculated from the lever law.

It can be seen in Figures 1-3 that on isothermal diagrams of systems containing two metallic components, any variables that fix the non-metal activities can be chosen as independent variables. When the non-metal is oxygen, these could include $\text{H}_2\text{O}/\text{H}_2$, CO_2/CO , and SO_3/SO_2 pressure ratios or $h_{\underline{\text{O}}}$, the Henrian activity of monatomic oxygen in a liquid or solid solution. For carbon one could use $\text{CH}_4/(\text{H}_2)^2$ or $(\text{CO})^2/\text{CO}_2$ pressure ratios or $h_{\underline{\text{C}}}$, the Henrian activity of carbon in a liquid or solid solution. When temperature is chosen as an independent variable the non-metal activities can be fixed or allowed to vary continuously with temperature as shown in Figure 4.

Phase equilibria in systems containing three metallic components can be mapped as a function of metal composition at fixed temperature and non-metal potential as shown in Figure 5.

Calculation of Stability Diagrams

Stability diagrams can be calculated from plots of Gibbs free energy versus metal composition at constant temperature, pressure, and non-metal chemical potential. This will be demonstrated for the hypothetical A-B-O system with the aid of Figure 6.

One mole of metal is chosen as the basis for the calculation. The curves in Figure 6b represent the free energies of one mole of metal in each of three phases as a function of X_B at constant T , P , and μ_{O_2} . The condensed phases, stable and unstable, have the same oxygen potential so that the free energy of the system is minimized at any X_B when the combined free energies of A and B are at a minimum. The free energy curves are of the form

$$G^\eta = X_A^\eta \circ G_A^\eta + X_B^\eta \circ G_B^\eta + RT (X_A^\eta \ln a_A^\eta + X_B^\eta \ln a_B^\eta) \quad (2a)$$

or, alternatively,

$$G^\eta = X_A^\eta \circ G_A^\eta + X_B^\eta \circ G_B^\eta + RT (X_A^\eta \ln X_A^\eta + X_B^\eta \ln X_B^\eta) \\ + RT (X_A^\eta \ln \gamma_A^\eta + X_B^\eta \ln \gamma_B^\eta) \quad (2b)$$

$\circ G_A^\eta$ and $\circ G_B^\eta$ are the molar free energies of A and B in η -phase standard states at the specified temperature and oxygen potential in the binary A-O and B-O systems, respectively. For example, $\circ G_A^{AO_x}$ represents the molar free energy of A in binary AO_x at the given T and P_{O_2} . The value of $\circ G_A^{AO_x} - \circ G_A^a$ can be calculated from the Gibbs-Duhem equation since it is equal to the difference in the molar free energy of A in AO_x at P_{O_2} and in AO_x at $P_{O_2}^{A/AO_x}$, the partial pressure of oxygen in equilibrium with A and AO_x .

$$dG_A^{AO_x} = -x dG_O^{AO_x} \quad (3a)$$

$$\int_{\circ G_A^a}^{\circ G_A^{AO_x}} dG_A^{AO_x} = -\frac{RT}{2} \int_{\ln P_{O_2}^{A/AO_x}}^{\ln P_{O_2}} x d \ln P_{O_2} \quad (3b)$$

$$^{\circ}G_A^{AO_x} - ^{\circ}G_A^a = - \frac{XRT}{2} (\ln P_{O_2} - \ln P_{O_2}^{A/AO_x}) \quad (3c)$$

Note that the standard states for A and B are defined so that $^{\circ}G_A^{\eta}$ and $^{\circ}G_B^{\eta}$ are functions of both temperature and oxygen potential. If the oxygen/metal atom ratio is a function of oxygen pressure, the ratio must be expressed as a function of P_{O_2} and included within the integral in Equation 3b.

The last term in Equation 2a is the free energy of mixing, the free energy change accompanying the formation of an η -phase solution from A and B in their η -phase standard states. Activities are defined conventionally.

$$\ln a_A^{\eta} = (G_A^{\eta} - ^{\circ}G_A^{\eta})/RT \quad (4)$$

G_A^{η} is the partial molar free energy of A in an η -phase solution. As shown in Figure 6b it is the intercept with the G_A^{η} ordinate of a line tangent to the G^{η} curve at a given composition.

At constant temperature and oxygen pressure the activity of A or B in an (A, B) O_x solution referred to the Raoultian standard state defined above ($a_A^{AO_x}$, for example) is equal to the Raoultian activity of the binary oxide (a_{AO_x}) in the solution. This is shown as follows:

$$RT \ln a_{AO_x} = (G_{AO_x} - ^{\circ}G_{AO_x}) \quad (5a)$$

$$RT \ln a_{AO_x} = (G_A^{(A,B)O_x} - ^{\circ}G_A^{AO_x}) + x (G_O^{(A,B)O_x} - ^{\circ}G_O^{AO_x}) \quad (5b)$$

But since P_{O_2} is constant, $G_O^{(A,B)O_x} = ^{\circ}G_O^{AO_x}$, and

$$RT \ln a_{AO_x} = (G_A^{(A,B)O_x} - ^{\circ}G_A^{AO_x}) = ^{\circ}G_O^{AO_x} = RT \ln a_A^{(A,B)O_x} \quad (5c)$$

$$a_{AO_x} = a_A^{(A,B)O_x} \quad (5d)$$

Activity coefficients are defined conventionally:

$$\gamma_A^\eta = a_A^\eta / X_A^\eta \quad (6)$$

It follows from Equations 5d and 6 that

$$\gamma_A^{(A,B)O_x} = \gamma_{AO_x} \quad (7)$$

These activities and activity coefficients can be assumed to be independent of oxygen potential unless the oxygen/metal atom ratio varies with oxygen potential. Even for this case the activities will not vary with oxygen potential if the oxygen/metal ratio in solution is a weighted average of the ratios in the binary AO_x and BO_x phases.

For equilibrium between two condensed phases $(A,B)O_x$ and $(A,B)O_y$,

$$G_A^{(A,B)O_x} = G_A^{(A,B)O_y} \quad (8a)$$

$$G_B^{(A,B)O_x} = G_B^{(A,B)O_y} \quad (8b)$$

so that

$$\begin{aligned} & \circ G_A^{(A,B)O_x} + RT (\ln X_A^{(A,B)O_x} + \ln \gamma_{AO_x}) \\ & = \circ G_A^{(A,B)O_y} + RT (\ln X_A^{(A,B)O_y} + \ln \gamma_{AO_y}) \end{aligned} \quad (9a)$$

and

$$\begin{aligned} & \circ G_B^{(A,B)O_x} + RT (X_B^{(A,B)O_x} + \ln \gamma_{BO_x}) \\ & = \circ G_B^{(A,B)O_y} + RT (\ln X_B^{(A,B)O_y} + \ln \gamma_{BO_y}) \end{aligned} \quad (9b)$$

From Equations 3 and 9a,

$$\begin{aligned}
 & -\frac{xRT}{2} (\ln P_{O_2} - \ln P_{O_2}^{A/AO_x}) + RT (\ln X_A^{(A,B)O_x} + \ln \gamma_{AO_x}) \\
 & = -\frac{yRT}{2} (\ln P_{O_2} - \ln P_{O_2}^{B/BO_x}) + RT (\ln X_B^{(A,B)O_x} + \ln \gamma_{BO_x}) \quad (10)
 \end{aligned}$$

$$\begin{aligned}
 \ln \left(\frac{X_A^{(A,B)O_x}}{X_A^{(A,B)O_y}} \right) &= \ln \left(\frac{\gamma_{AO_y}}{\gamma_{AO_x}} \right) + \left(\frac{x-y}{2} \right) \ln P_{O_2} \\
 &+ \frac{y}{2} \ln P_{O_2}^{A/AO_y} - \frac{x}{2} \ln P_{O_2}^{A/AO_x} \quad (11a)
 \end{aligned}$$

Similarly, for component B,

$$\begin{aligned}
 \ln \left(\frac{X_B^{(A,B)O_x}}{X_B^{(A,B)O_y}} \right) &= \ln \left(\frac{\gamma_{BO_y}}{\gamma_{BO_x}} \right) + \left(\frac{x-y}{2} \right) \ln P_{O_2} \\
 &+ \frac{y}{2} \ln P_{O_2}^{A/AO_y} - \frac{x}{2} \ln P_{O_2}^{A/AO_x} \quad (11b)
 \end{aligned}$$

Equations 11 are similar to those derived by Sticker and Schmalzried⁽⁵⁾ for equilibrium between metal (A,B) and oxide (A,B)O phases. Similar equations can be derived for systems with three or more metallic components.

To construct stability diagrams, sets of equations similar to 9 or 11 must be solved for pairs of stable phases over the temperature and oxygen potential ranges of interest. A number of computer techniques have been developed to solve equations of this type. The real problem is not computational but thermodynamic. For each phase, ${}^{\circ}G_{A,B}^{\eta}$ must be known as a function of temperature and non-metal

potential and $\ln \gamma_{A,B,\dots}^{\eta}$ or $\Delta G^{\eta, xs}$ must be known as a function of composition and temperature.

This is a difficult but not insoluble problem. Data is available for many metallic solutions. Less work has been done on the thermodynamics of oxide, sulfide, nitride, and carbide phases. Although there exists a large body of phase equilibrium measurements at known non-metal chemical potentials. A judicious correlation of this data can yield a large amount of thermodynamic information.

For example, if the non-metal activities and phase boundaries are known on a ternary A-B-O isotherm, metal activities can be calculated from ternary Gibbs-Duhem integrations using Schuhmann's method.⁽⁶⁾

Schuhmann's Equation 6 can be rewritten

$$\left(\frac{\delta G_A}{\delta G_O} \right)_{n_A, n_B} = - \left(\frac{\delta n_O}{\delta n_A} \right)_{G_O, n_B} \quad (12)$$

The integration is carried out along a path of constant n_A and n_B , vertically in Figure 6, so that in any phase

$$G'_A - G''_A = - \frac{RT}{2} \int_{\ln P'_{O_2}}^{\ln P''_{O_2}} \left(\frac{\delta n_O}{\delta n_A} \right)_{G_O, n_B} d \ln P_{O_2} \quad (13)$$

For phases with a fixed oxygen/metal atom ratio, the partial derivative within the integral is equal to that ratio. If the ratio varies with oxygen pressure, the integration is more complex.

UTILITY OF STABILITY DIAGRAMS

The limited use of stability diagrams to date in systems containing two or more metallic components is probably due to their limited availability and that few people have thought about what to do with them even if they were available.

These diagrams should be most useful for analyzing phase equilibria and reaction paths in systems open with respect to the non-metallic components. This would involve such systems as the oxidation, sulfidation, or carburization of alloys and the reduction of ores.

Figure 7 shows a reaction path and accompanying microstructure for the oxidation of a hypothetical binary alloy. If continuous protective scale layers are formed and local equilibrium assumed at all interfaces, the oxide-gas interface can be represented by a point somewhere along an oxygen isobar. The value of X_B at this point will depend on the original alloy composition, solid state diffusion rates in the underlying oxide and metal phases, and the reaction kinetics at the oxide-gas interface early in the process. A planar two phase boundary is represented by a path along a two-phase tie line. A two phase scale or internal oxidation is represented by a reaction path that crosses tie lines. If the metallic components are conserved (no volatile metal bearing species formed), any deviation of the reaction path to one side of the vertical X_B line representing the original alloy must be balanced by having part of the path lie on the other side as well. For an oxidation process controlled by solid state diffusion for all $t > 0$, the reaction path will be constant. If surface reaction kinetics were rate-limiting at early stages of the reaction, the path could be time-dependent.

SUMMARY

Stability diagrams are an attractive alternative representation of phase equilibria in systems containing both metallic and non-metallic components. They can be calculated from plots of Gibbs free energy versus metal composition at constant temperature and non-metal chemical potential. Their utility should increase as more diagrams become available.

REFERENCES

1. A. D. Pelton and H. Schmalzried: Met. Trans., 1973, Vol. 4, p. 1395.
2. H. Schmalzried and A. D. Pelton: Ber. Bunsenges Phys. Chem., 1973, Vol. 77, p. 90.
3. A. D. Pelton and W. T. Thompson: Progress in Solid State Chemistry, 1975, Vol. 10, p. 119.
4. J. Sticher and H. Schmalzried: Report to the Institut für Theoretische Huttenkunde und Angewandte Physikalische Chemie der Technischen Universität Clausthal, May 1975.
5. J. Sticher and H. Schmalzried: Arch. Eisenhüttenw., 1976, Vol. 47, p. 261.
6. R. Schuhmann: Acta Met., 1955, Vol. 3, p. 219.
7. T. Wada, H. Wada, J. F. Elliott, and J. Chipman: Met. Trans., 1972, Vol. 3, p. 2865.
8. R. Benz, J. F. Elliott, and J. Chipman: Met. Trans., 1974, Vol. 5, p. 2235.
9. C. T. Fujii and R. A. Muessner: Trans. Met. Soc. AIME, 1968, Vol. 242, p. 1259.
10. K. T. Jacob and C. B. Alcock: Met. Trans. B, 1975, Vol. 68, p. 215.
11. T. Katsura and A. Muan: Trans. Met. Soc. AIME, 1964, Vol. 230, p. 77.
12. P. Riband and A. Muan: Trans. Met. Soc. AIME, 1964, Vol. 230, p. 88.

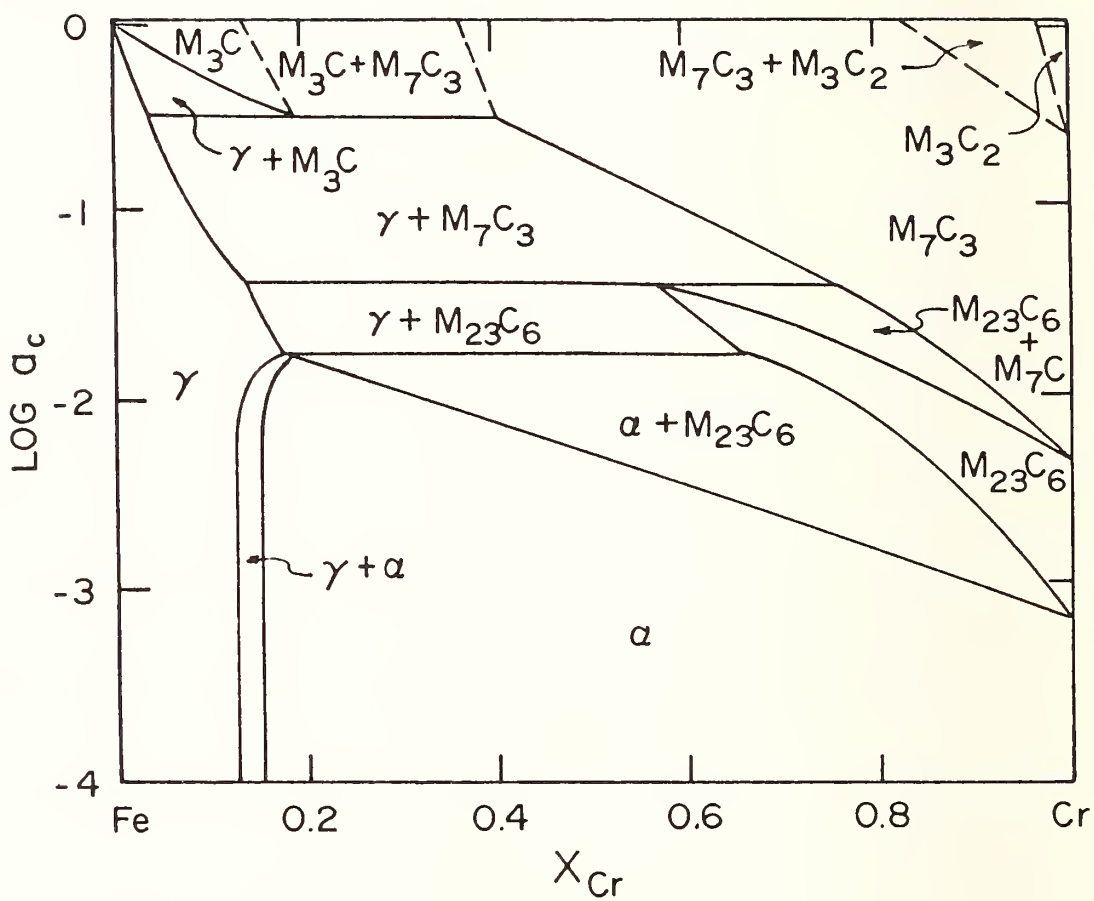


Figure 1. Stability diagram for the Fe-Cr-C system at 1273°K adjusted to match measured phase equilibria^(7,8).

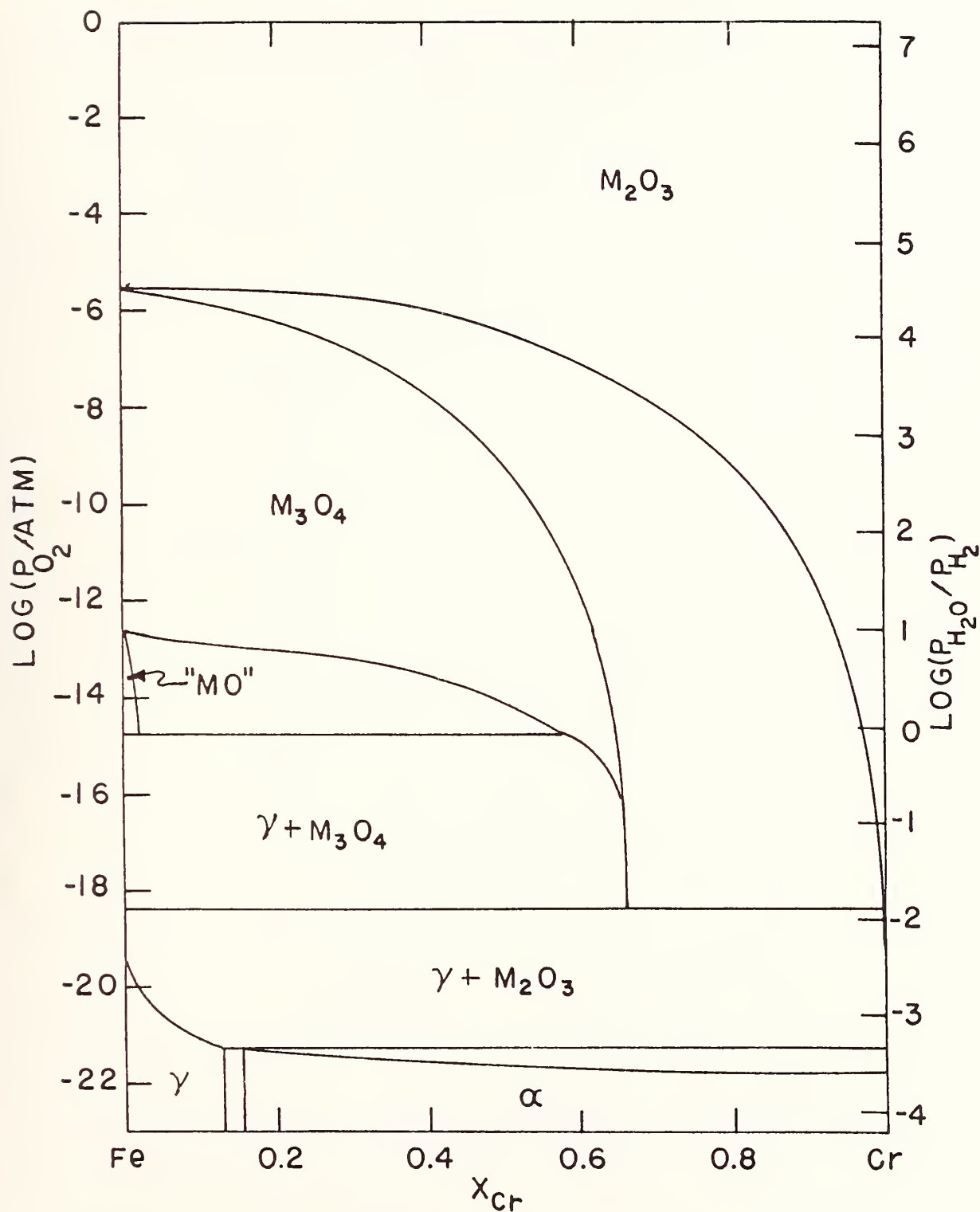


Figure 2. Stability diagram for the Fe-Cr-O system at 1273°K adjusted to match measured phase equilibria (9,10).

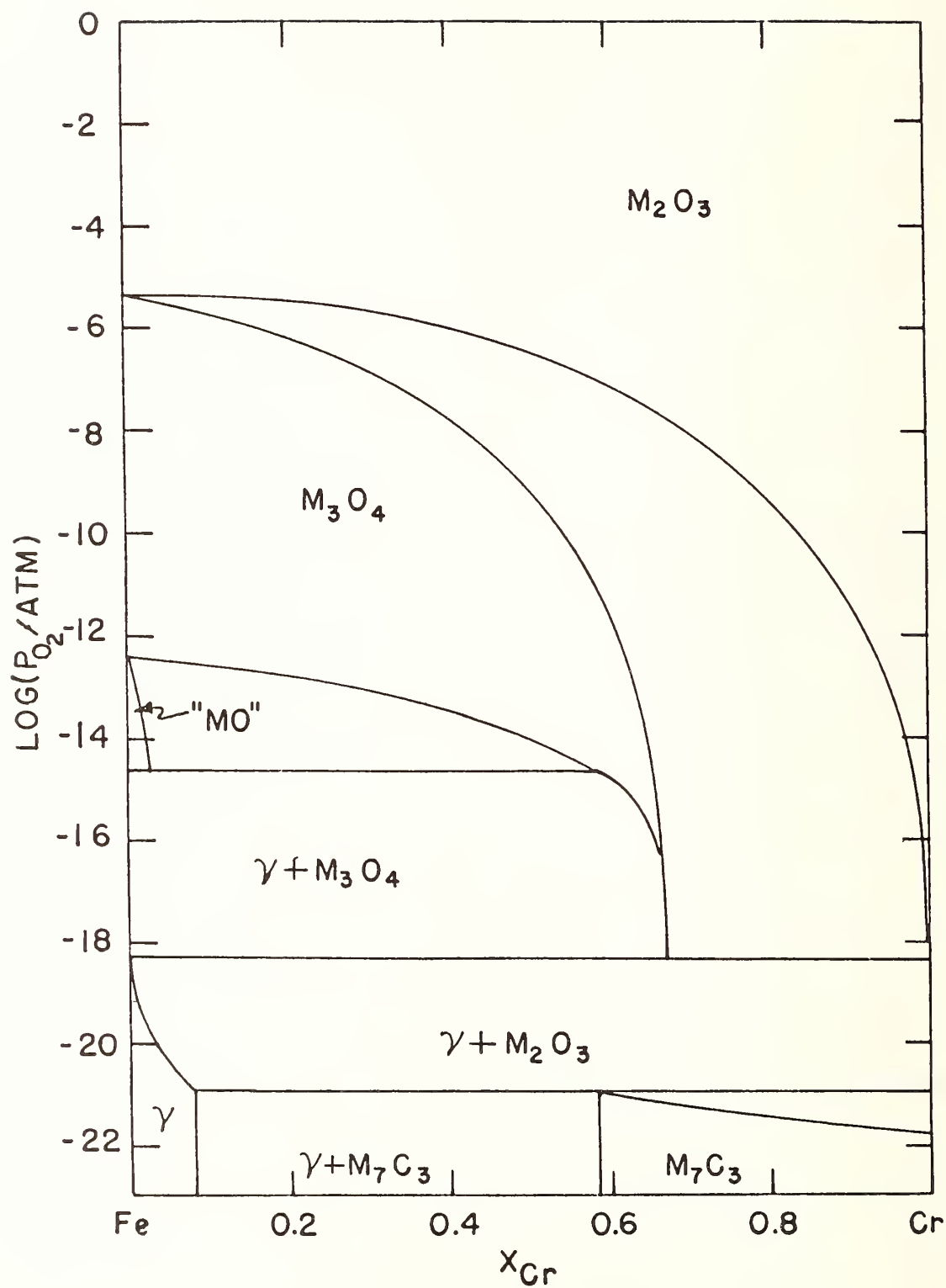


Figure 3. Stability diagram for the Fe-Cr-O-C system at 1273°K at $a_c = 0.1$.

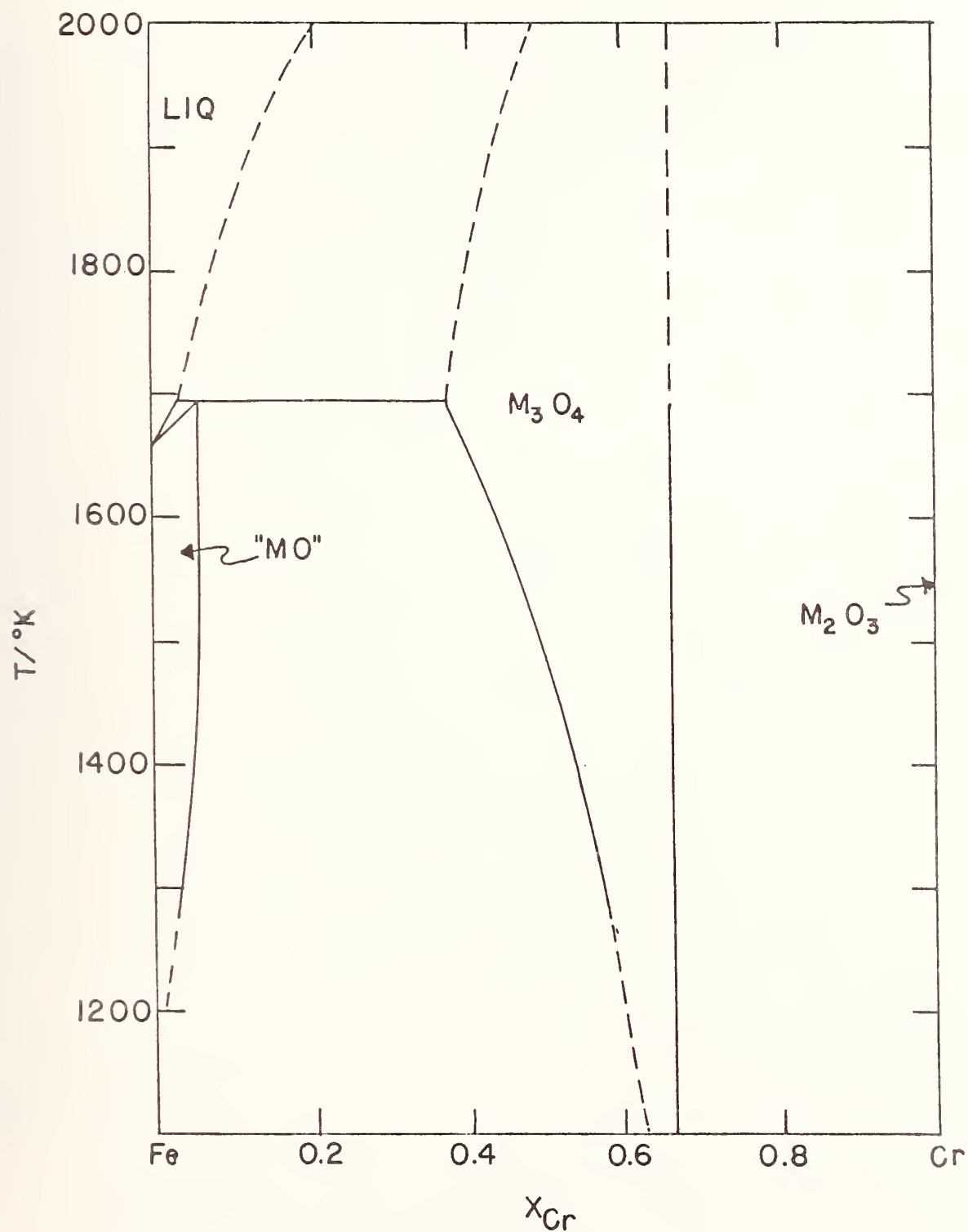


Figure 4. Stability diagram for the Fe-Cr-O system for CO_2/H_2 pressure ratio of 1.0 adjusted to match measured phase equilibria^(9, 12)

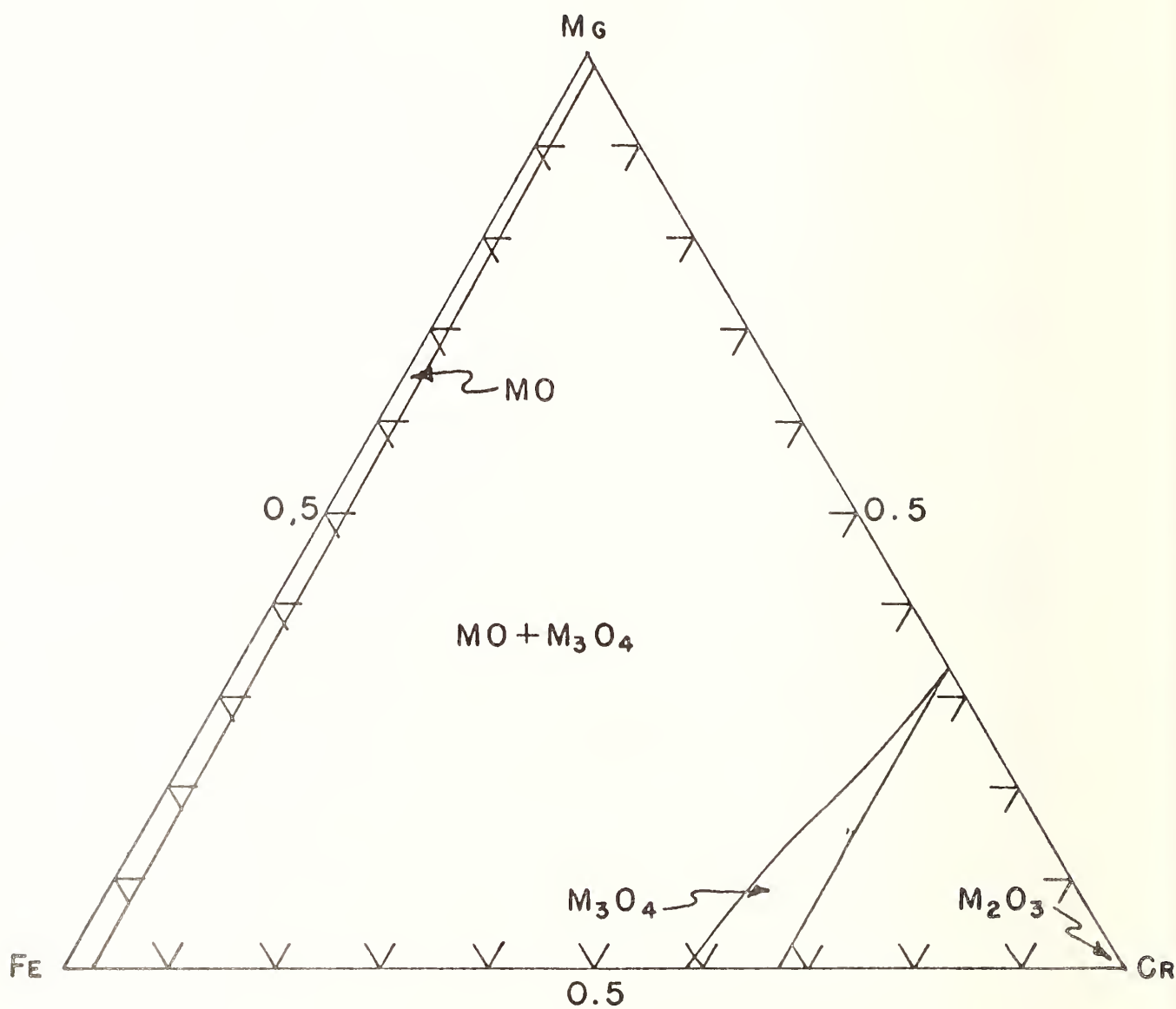


Figure 5. Stability diagram for the Fe-Cr-Mg-O system at 1273°K and $P_{O_2} = CO_2/H_2$ pressure ratio of 1.0.

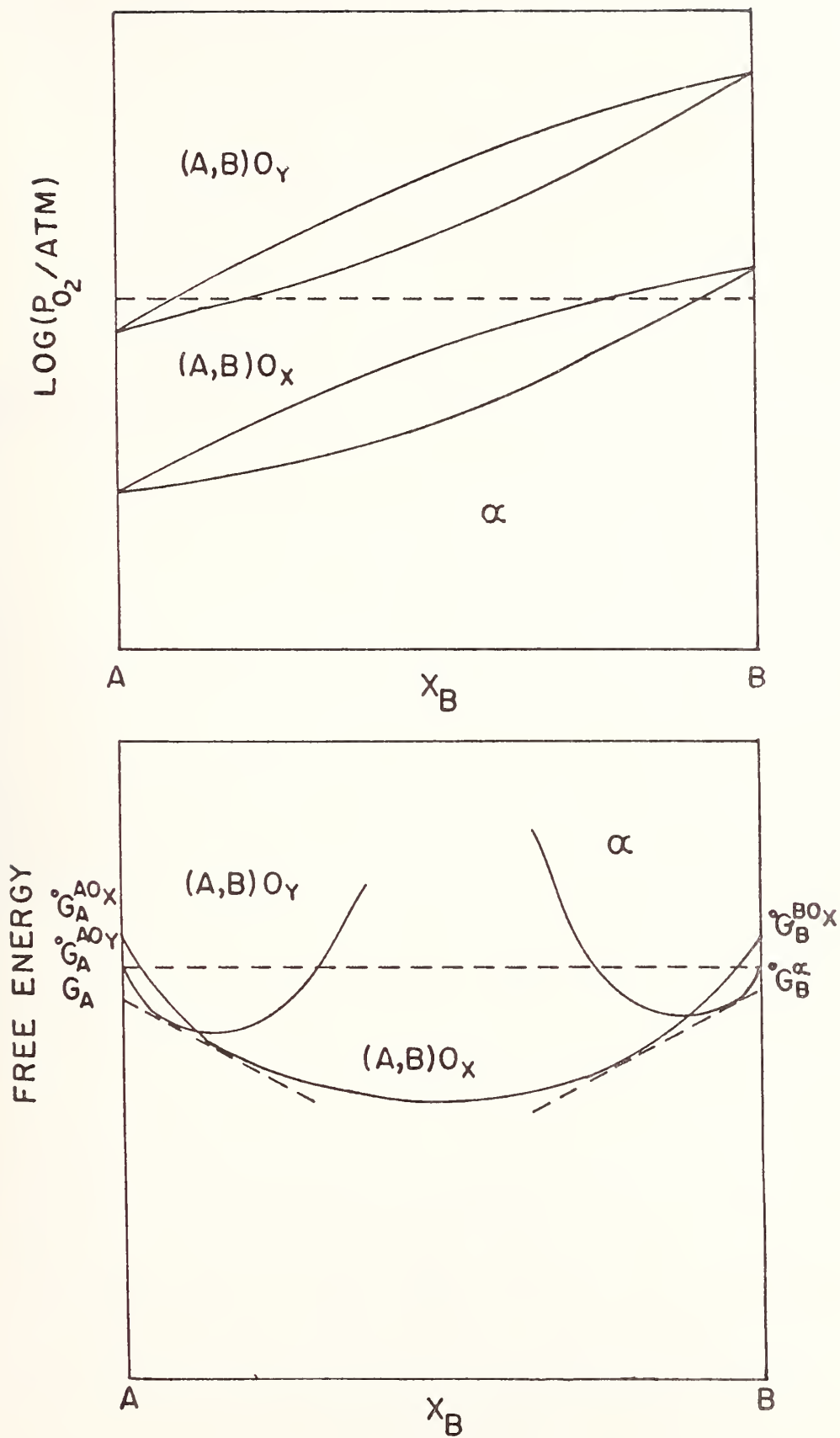


Figure 6. Isothermal stability diagram for a hypothetical A-B-O system.

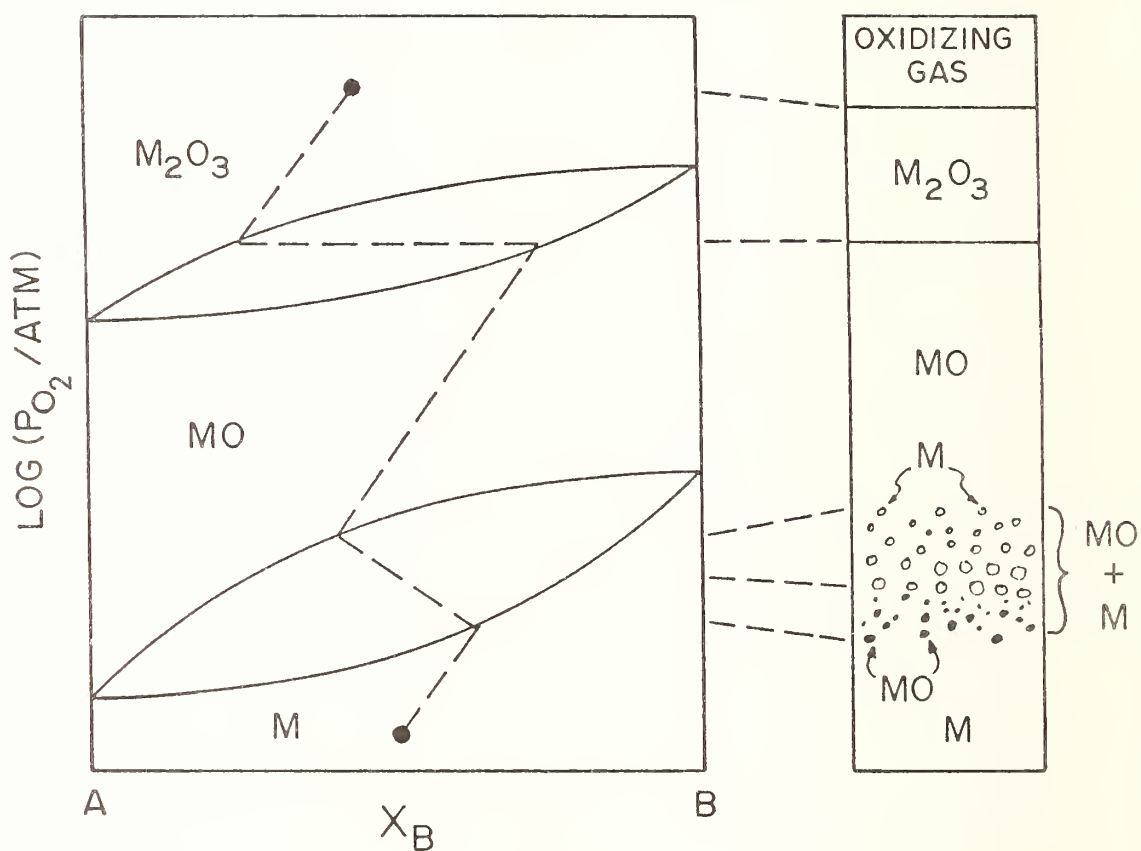


Figure 7. Reaction path and microstructure for oxidation of a hypothetical A-B alloy.



UNITED KINGDOM ATOMIC ENERGY AUTHORITY
REACTOR FUEL ELEMENT LABORATORIES SPRINGFIELDS

THE EFFECT OF IRRADIATION ON PHASE STABILITY

L Kaufman,* J S Watkin,† J H Gittus† and A P Miodownik‡

(*MANLABS USA; †UKAEA, RFL Springfields; ‡University of Surrey, UK)

INTRODUCTION

In a recent paper Watkin⁽¹⁾ has noted large variations in the neutron induced void swelling behaviour of a range of annealed austenitic alloys, irradiated to 30 dpa at 600°C in the Dounreay Fast Reactor. These data were analysed in terms of the calculated fraction of sigma phase expected to be present under isothermal conditions from which it was concluded that swelling tended to increase with sigma content. [Fig. 1]

An increasing amount of evidence has now accumulated showing that this assumption may not be tenable. Brown⁽⁴⁾ has been unable to detect the presence of sigma-phase in M316** fuel pin cladding irradiated in the Dounreay Fast Reactor at any temperature up to 973 K although this is a temperature range where sigma phase formation is both regularly observed in this alloy, in the absence of irradiation, and predicted by calculated phase diagrams. Instead an ordered fcc phase has been discovered⁽⁵⁾ in specimens irradiated at temperatures less than 823 K. At the time of writing some doubt exists as to the precise composition of the phase. Initially it was thought to be $\text{Ni}_3(\text{Fe}, \text{Mn})$ but more recently it is thought more likely to be based on Ni_3Si . A similar phase is predicted to occur on the calculated ternary diagrams at temperatures below 823 K but not in the 316 composition range. Bilsby⁽⁶⁾ has observed an ordered phase in an M316 specimen irradiated by Watkin to 25 atomic displacements per atom at 773 K and has noted the absence of sigma-phase in the same specimen. It is also significant that under normal circumstances 316-type stainless steel is non-magnetic but many reports exist to suggest that after irradiation alloys of this type are slightly magnetic. Cawthorne and Brown⁽⁵⁾ suggest that the ordered phase which is magnetic, may be in part responsible for some of the magnetism exhibited by M316 after irradiation, although they have commented that irradiated specimens not containing that phase are also magnetic. Baron, Cadalbert and Delaplace⁽⁷⁾ found abnormal magnetism in a 316L (low carbon version of AISI-316 type

**M316 is a UKAEA specification for 316-type stainless steel in which tighter control is kept on the major alloying constituents.

stainless steel) hexagonal tube irradiated in the Rapsodie Fast Reactor, and have tentatively suggested the magnetic behaviour may be due to the formation of a bcc-phase caused by the presence of hydrogen formed from (n,p) transmutations with the major alloying constituents, without however giving direct evidence for their suggestion.

There are therefore three unequivocal facts which must be taken into consideration in the case of irradiated stainless steel:

- (a) the non-appearance of sigma-phase at temperatures and durations where this would be observed without irradiation.
- (b) the appearance of an ordered phase in a composition range and at temperatures where it would normally not be observed without irradiation.
- (c) the appearance of magnetism after irradiation both in the presence and absence of the ordered phase.

An almost parallel situation has been observed in W-Re binary alloys irradiated by Williams, Steigler and Wiffen⁽⁸⁾ in EBR II to neutron exposures in the range 6.1 to 37.10^{21} n/cm² (> 0.1 MeV). They reported that after irradiation at temperatures equal to or greater than 1373 K, electron diffraction patterns showed the presence of cubic WRe₃ precipitates in an alloy (W-25 at.% Re). Published phase diagrams however predict the alloy to be single phase (bcc) at this temperature. Sigma-phase precipitation could be expected at (> 25 at.%) but WRe₃ would only be expected at Re contents greater than 60 at.%.

Irradiation therefore has a marked effect on the relative stability of certain phases in Fe-Cr-Ni ternary alloys and W-Re alloys. There are three possible reasons for these effects:

- (1) That irradiation brings about the true equilibrium structure of these alloys by enhancing diffusion which under normal circumstances would be too slow (at the temperatures in question).
- (2) That irradiation changes the relative free energy of various phases by differentially increasing the concentration of defects. This is analogous to the Wigner energy phenomenon in graphite irradiations.
- (3) That irradiation inhibits the formation of some phases by bombardment processes which physically knock precipitate atoms back into solution.

In this paper we confine ourselves to determine the changes in the free energy of sigma-phase and Ni₃Fe that are required firstly, to suppress the formation of sigma-phase at the 316 composition for temperatures between 673 - 873 K and secondly to enhance the stability of Ni₃Fe to encompass the 316 composition for temperatures below 823 K.

THE EFFECT OF VARYING THE FREE ENERGY OF SIGMA-PHASE

The free energy of sigma phase has been formulated by Kaufman and Bernstein⁽²⁾ and Kaufman and Nesor⁽³⁾ assuming the phase to be a line compound which runs between Ni_{0.38}Cr_{0.62} and Cr_{0.47}Fe_{0.53}. The general composition of sigma (σ) (Ni_{z σ} , Cr_{x σ} , Fe_{y σ}) is defined by:

$$x_{\sigma} = 0.62 - 0.283 y_{\sigma} \quad \dots (1a)$$

$$y_{\sigma} = 1 - x_{\sigma} - z_{\sigma} \quad \dots (1b)$$

$$z_{\sigma} = 1 - 0.62 - 0.717 y_{\sigma} \quad \dots (1c)$$

The free energy of sigma (G_{σ}) can be expressed in terms of four components:

$$G_{\sigma} = \Delta G_1 + \Delta G_2 + \Delta G_3 + \Delta G_4 \quad \dots (2)$$

where $\Delta G_1 = (z_{\sigma} G_{Ni}^{bcc} + x_{\sigma} G_{Cr}^{bcc} + y_{\sigma} G_{Fe}^{bcc}) \quad \dots (3)$

$$\Delta G_2 = [1 - (y_{\sigma}/x_{\sigma})] \Delta G_A + [y_{\sigma}/(1 - x_{\sigma})] \Delta G_B \quad \dots (4)$$

$$\Delta G_3 = RT [y_{\sigma} \ln y_{\sigma} + z_{\sigma} \ln z_{\sigma} - (1 - x_{\sigma}) \ln(1 - x_{\sigma})] \quad \dots (5)$$

$$\Delta G_4 = C^* y_{\sigma} (0.38 - 0.717 y_{\sigma}) / (0.38 + 0.283 y_{\sigma}) \quad \dots (6)$$

These four terms can be identified with the characteristics of bcc phase from which sigma derives (ΔG_1); compound parameters specifically associated with the binary sigma phases (ΔG_2); a mixing term (ΔG_3); and finally a ternary excess free energy term (ΔG_4). For the purpose of the current exercise, the free energy of the sigma phase has been varied by altering C^* , leaving all other parameters in equation (2 ~ 6) the same. Table 1 shows the effect of changing C^* on the relative stability of sigma-phase at 873 K as measured by its intrusion into the ternary section: the values being obtained from figures 2a to 2d.

Because changes in G_{σ} caused by varying C^* depend upon the precise composition of sigma-phase in equilibrium with the matrix, the free energy increases in Table 1 refer to the composition of sigma-phase at the point of maximum intrusion into the ternary in the reference unirradiated state.

TABLE 1

The effect of changing C^* on the relative stability of sigma phase in the Fe-Cr-Ni system at 873 K

Ternary excess parameter C^* cal/g.at	Increase in G_{σ} cal/g.at (J/g.at)	Relative intrusion. of sigma phase into the ternary	Comments
- 1000	0	1	Reference state corresponding to normal conditions.
+ 1500	233 (975)	$\frac{1}{3}$	Arbitrary increase in C^* until sigma tends to zero.
+ 4000	475 (1987)	1/10	

This exercise was repeated at 673 K, which revealed that sigma-phase was suppressed when C^* was set at 1500 cal/g.at i.e. only ~ 200 cal/g.at (~ 1000 J/g at) is required at this lower temperature compared to about 500 cal/g.at (~ 2000 J/g.at) at 873 K.

THE EFFECT OF VARYING THE FREE ENERGY OF FeNi_3

The description of the free energy of Ni_3Fe is similar to that employed for sigma phase except in this case the compound is described as running across the nickel corner of the ternary at constant nickel (that is Ni_3Fe to Ni_3Cr). Firstly, because some doubt exists as to the precise composition of the ordered phase found on irradiation, and the distinct possibility that silicon and/or manganese could be present, it was thought prudent to investigate the influence of such an addition on the stability of Ni_3Fe before determining the energy change needed to expand the stability of Ni_3Fe to the 316 composition range. Thus preliminary calculations were carried out at 673, 723 and 773 K to estimate the effect of replacing 1.5 at.% Mn for chromium in $(\text{Ni}_{0.75}\text{Mn}_{0.25})$. (The level of 1.5 at.% Mn was chosen because such an addition is made to 316 stainless steel.) These calculations revealed an almost constant stabilising effect of Mn at 175 cal/g.at [~ 730 J/g.at] for all temperatures between 673 and 773 K. This value was translated into an equivalent change in C^* (12000 cal/g.at) for $\text{Ni}_{0.75}(\text{Fe,Cr})_{0.25}$. The effect of this change on the fcc/ Ni_3Fe interaction at 673 and 723 K is shown in Figs 3(a) and 3(b). By comparing these figures with 3(c) and 3(d) [the relevant diagrams without a Mn addition], it can be seen that Mn has a potent stabilising effect on Ni_3Fe .

In figure 3(b) further fcc/ Ni_3Fe interactions have been calculated with C^* set at - 20000, - 22500 and - 25000 which yield a critical C^* of - 23700 for the appearance of $\text{Ni}_{0.75}(\text{FeMn})$ at the 316 composition. This value translates back to a required energy change of - 350 cal/g.at [- 1460 J/g.at].

As yet we have been unable to determine the effect of silicon (0.5 to 1.2 at.% being usual in 316-type steels), because equivalent thermodynamic data are not available, but the principles used here will be extended to include Si additions when suitable data become available.

CONSIDERATION OF ANALOGOUS CHANGES IN THE W-Re SYSTEM

The free energy curves for the body centred cubic (bcc) and the close packed hexagonal phases (cph) have been calculated for the W-Re system at 1373 K using parameters taken from reference (2), Fig. 4. The free energy of sigma-phase has also been positioned at - 6500 cal/g.at (- 27200 J/g.at) by using the 'tangent rule' in reverse i.e. taking the intersection of the tangent to the G^{bcc} curve at the upper limit of its stability range (26 at.% Re) with the lower compositional extreme of the single sigma-phase field (44 at.% Re). Similarly the free energy of X-phase (WRe_3) has been determined from the intersection of the tangent to the G^{cph} curve at 90 at.% Re with the composition WRe_3 (W-75 at.% Re) assuming the phase to be a line compound.

For WRe_3 to form at the composition W-25 at.% Re, as occurred in Williams experiments, (8) the free energy of sigma-phase must have increased relative to the other phases. The minimum increase is 1500 cal/g.at (6250 J/g.at) and is given by the construction AB in Fig. 4. An alternative view would be that the free energy of WRe_3 has been reduced by about 3500 cal/g.at (14650 J/g.at) as shown by the construction CD.

These figures are much higher than the values deduced for the effect of irradiation in the Fe-Cr-Ni system. However further inspection of Fig. 4 shows that the free energy of WRe_3 is very sensitive to the slope of the G^{cph} curve where the tangent is drawn (90 at.% Re) and any variation here could have a marked effect on the figures quoted above.

Fuller details of these and other similar calculations will be published in due course.

SUMMARY AND CONCLUSIONS

The aim of this paper has been to determine changes in the free energy of sigma-phase and Ni_3Fe that are required firstly, to suppress the formation of sigma-phase at the AISI 316 composition for temperatures between 673 and 873 K and secondly, to enhance the stability of Ni_3Fe to encompass the 316 composition for temperatures below 823 K; that is, to tailor the Fe-Cr-Ni ternary equilibrium diagram to fit the observations made after irradiation in a fast reactor.

It has been calculated that an increase in free energy of 250-500 cal/g.at (1000-2000 J/g.at) is required to suppress the appearance of sigma-phase in the temperature range 673-873 K. Similarly Ni_3Fe requires a reduction in free energy of 350-500 cal/g.at (1500-2000 J/g.at) to account for its appearance in the range 673-773 K.

In the analogous W-Re binary system, energy changes of somewhat higher values are required 1500-3500 cal/g.at (6500-14500 J/g.at) to account for the observed structural changes on irradiation at 1373 K.

It is envisaged that the establishment of the order of magnitude for such changes will aid the determination of an appropriate mechanism for the required energy change, and the design of alloys with maximum resistance to phase transformations under irradiation.

REFERENCES

1. WATKIN J S. Dependence of void swelling on the electron vacancy concentration. ASTM STP611 1976.
2. KAUFMAN L and BERNSTEIN H. Computer calculation of phase diagrams. Academic Press 1970.
3. KAUFMAN L and NESOR H. Relation of thermochemistry and phase diagrams of condensed systems. Treatise on solid state chemistry. Vol. 5 Changes of State, Plenum Press 1975.
4. BROWN C (private communication).
5. BROWN C and CATHORNE C. Journal of Nuclear Materials (to be published).
6. BILSBY C F (private communication).
7. BARON J L, CADALBERT R and DELAPLACE J. J. Nuclear Materials 1974. 51 p266.
8. WILLIAMS R K, STEIGLER J O and WIFFEN F W. Irradiation effects in tungsten-rhenium alloys. ORNL-TM-4500, 1974.

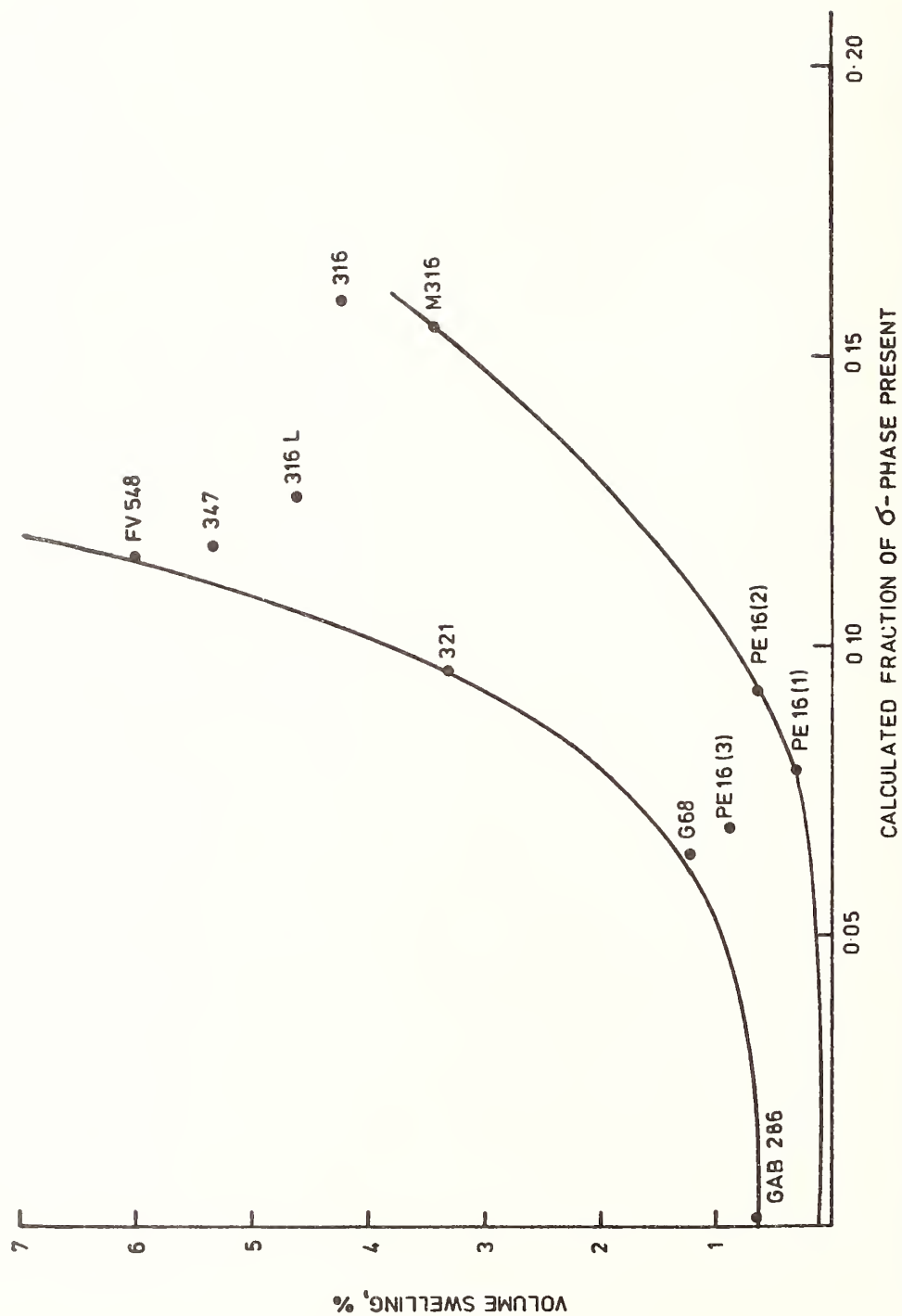
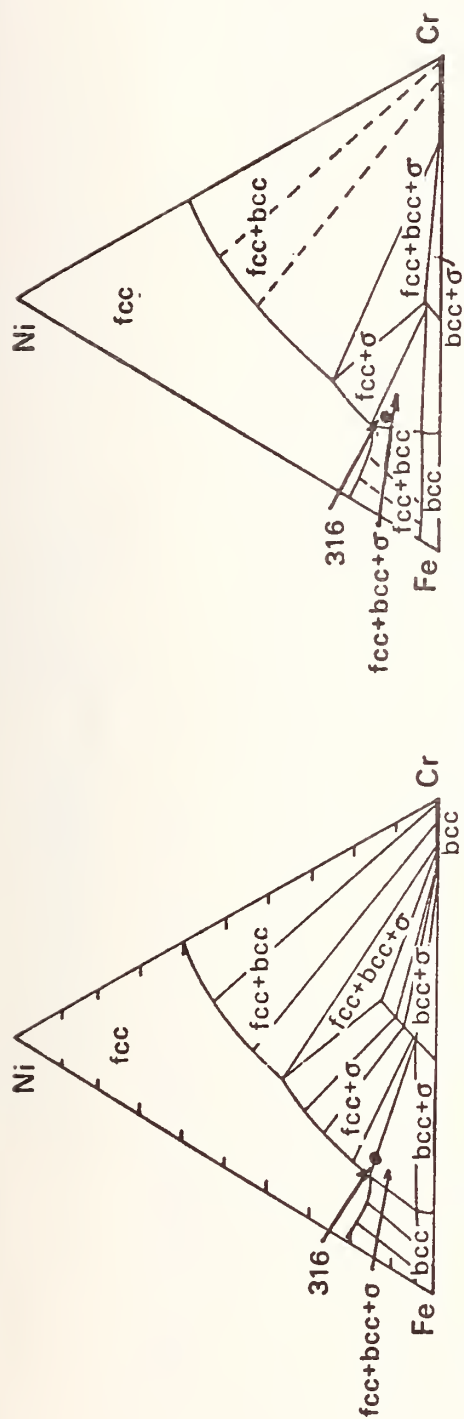
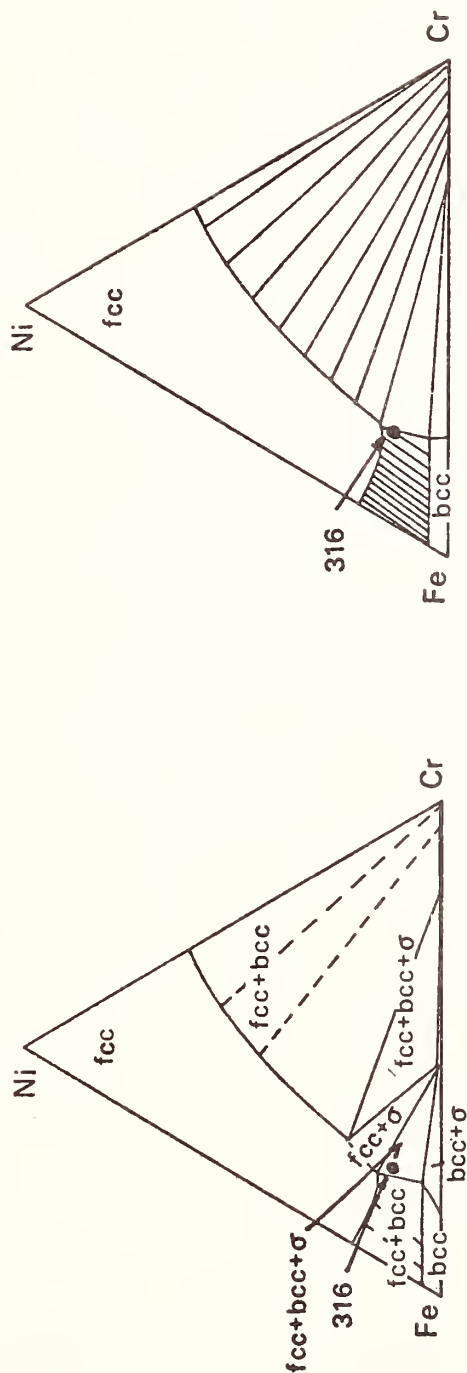


FIG.1. SWELLING AT 30 dpa AND 600°C AS A FUNCTION OF CALCULATED SIGMA CONTENT



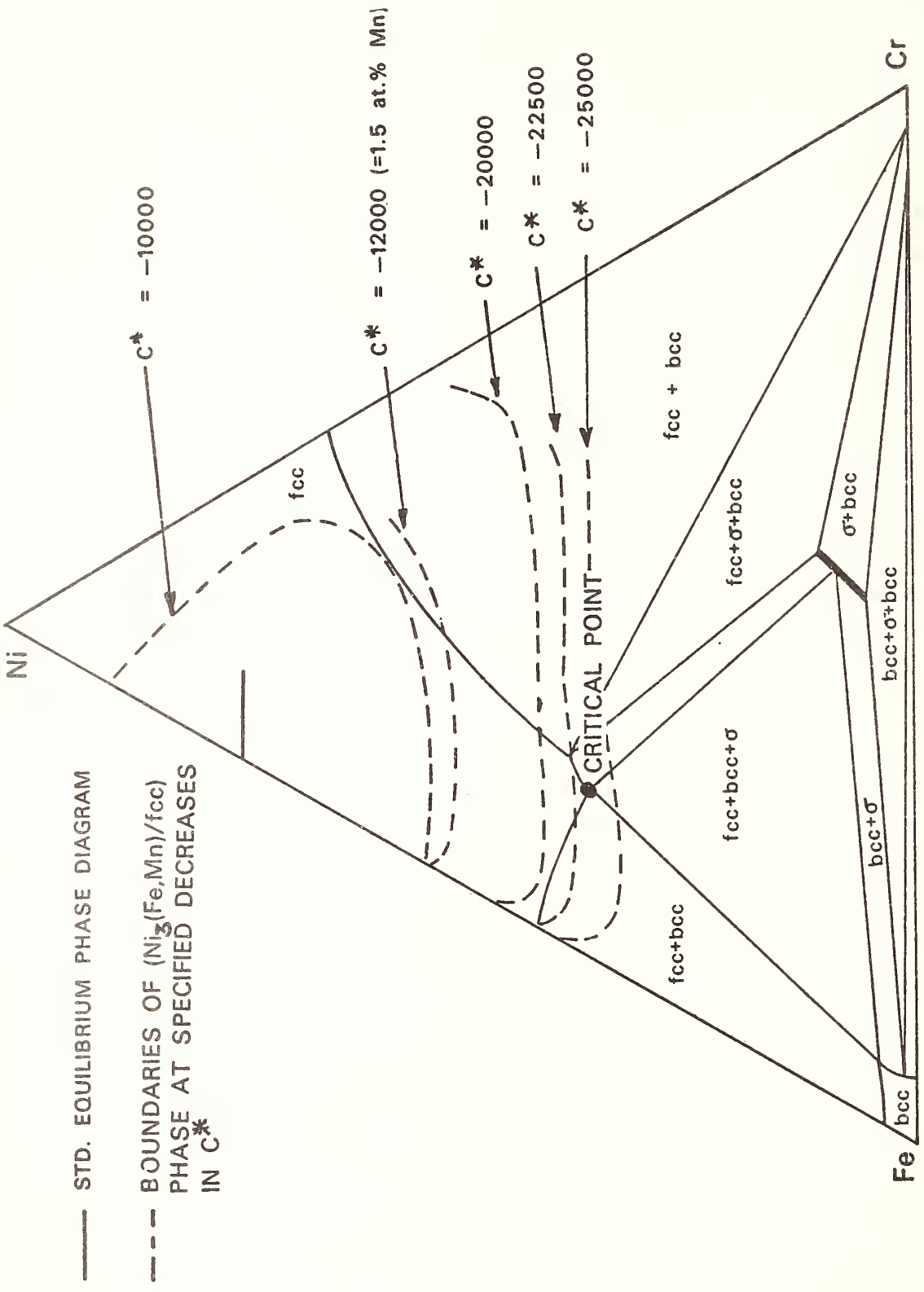
(a) STANDARD TERNARY SECTION ($C^* = -1000$) (b) WHEN C^* IS INCREASED TO 1500



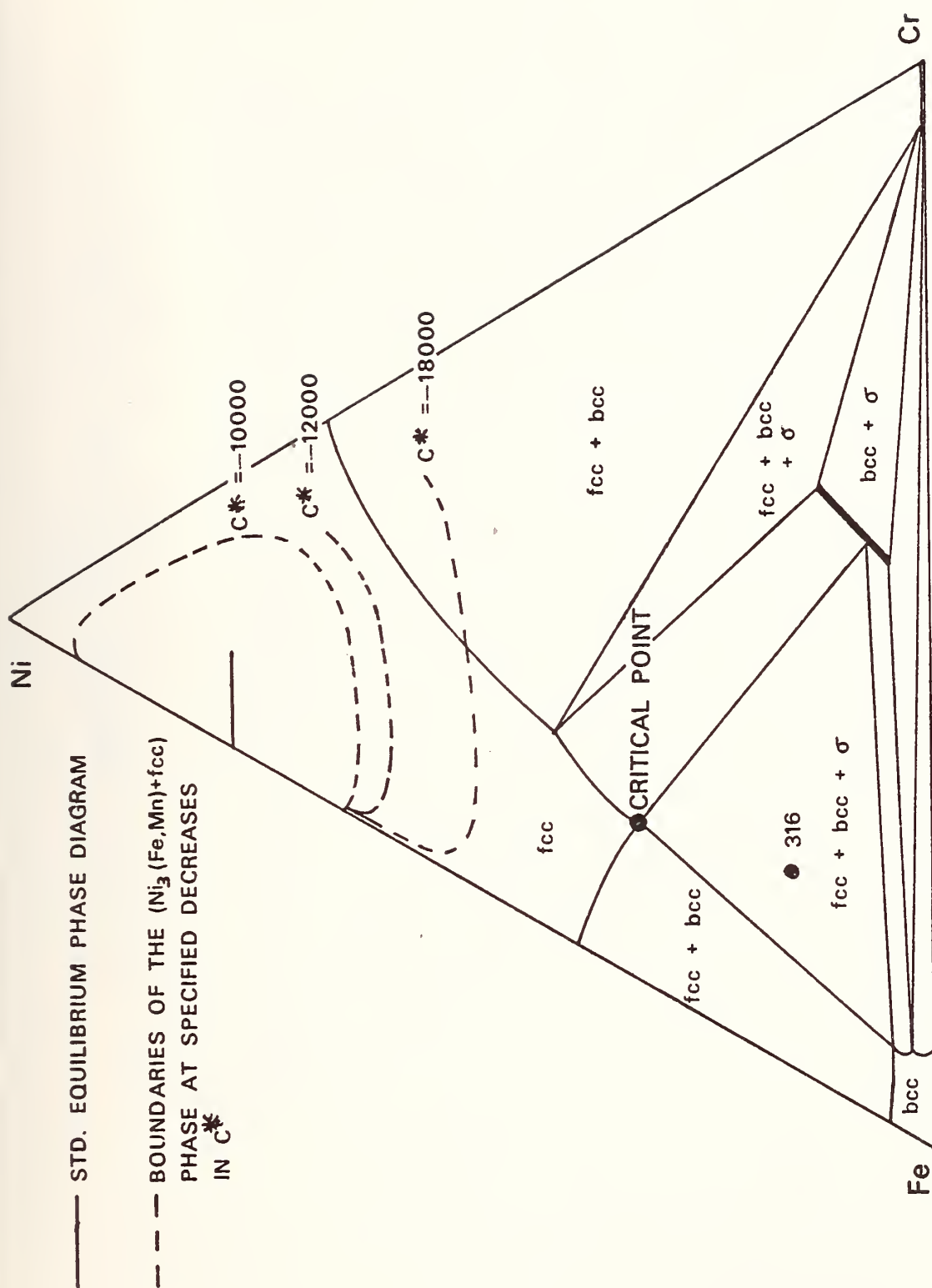
(c) WHEN C^* IS INCREASED TO 4000

(d) WHEN C^* IS INCREASED TO > 4000

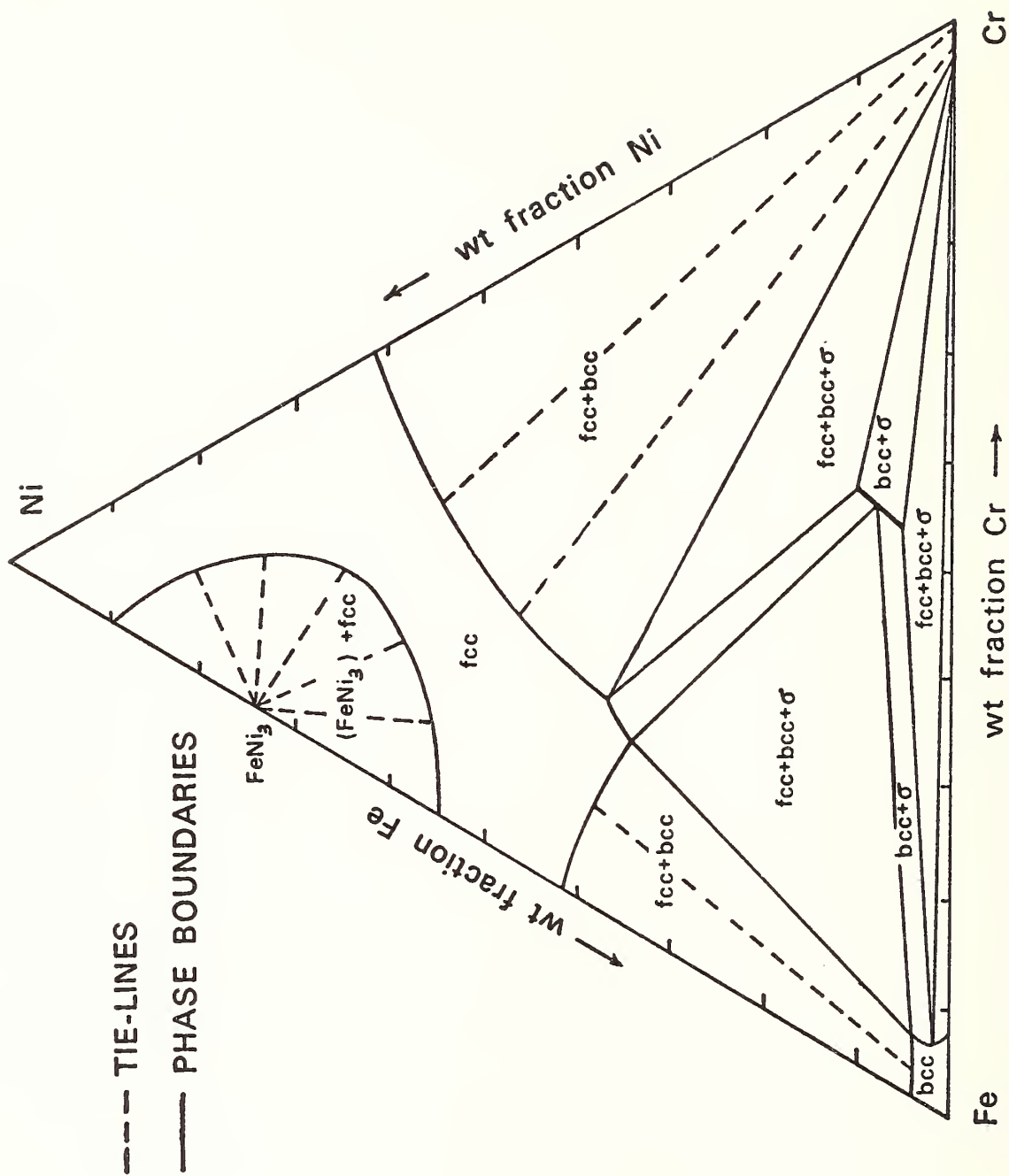
FIG2. THE EFFECT OF DECREASING THE STABILITY OF SIGMA PHASE ON THE Fe-Cr-Ni TERNARY AT 600°C (873K)



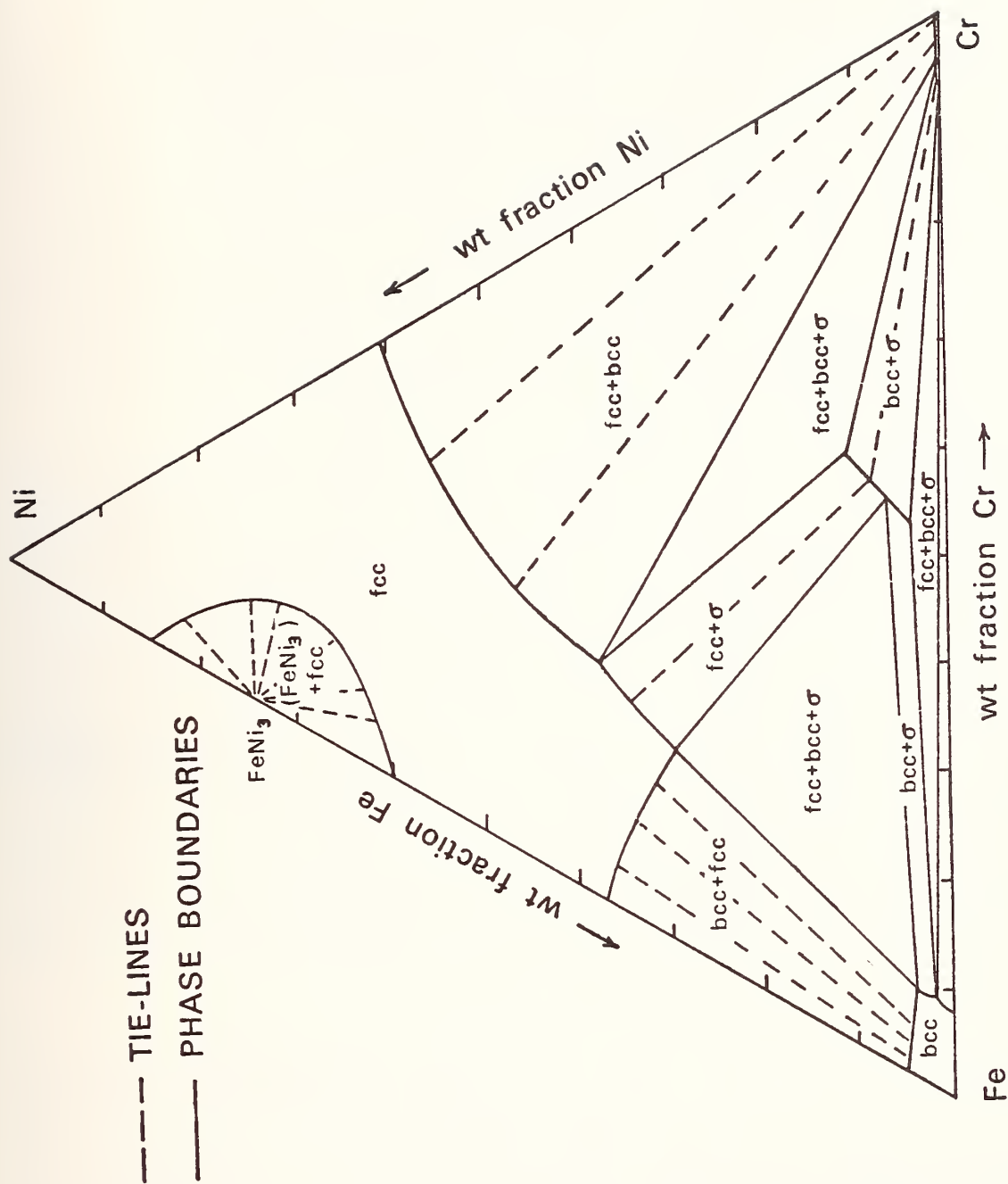
3(a) THE EFFECT OF 1.5 at % Mn ADDITION ($C^* = -12000$)
 ON THE fcc/ $\text{Ni}_3(\text{Fe,Mn})$ INTERACTION AT 400°C (673 K)



3(b) THE EFFECT OF 1.5 at % Mn ADDITION ($C^* = -1200$) ON THE fcc/ $\text{Ni}_3(\text{Fe, Mn})$ INTERACTION AT 450°C (723K)



3(c) CALCULATED ISOTHERMAL SECTION OF
Fe-Cr-Ni TERNARY DIAGRAM AT 400°C (673K)



3(d) CALCULATED ISOTHERMAL SECTION OF
 Fe-Cr-Ni TERNARY DIAGRAM AT 450°C (723 K)

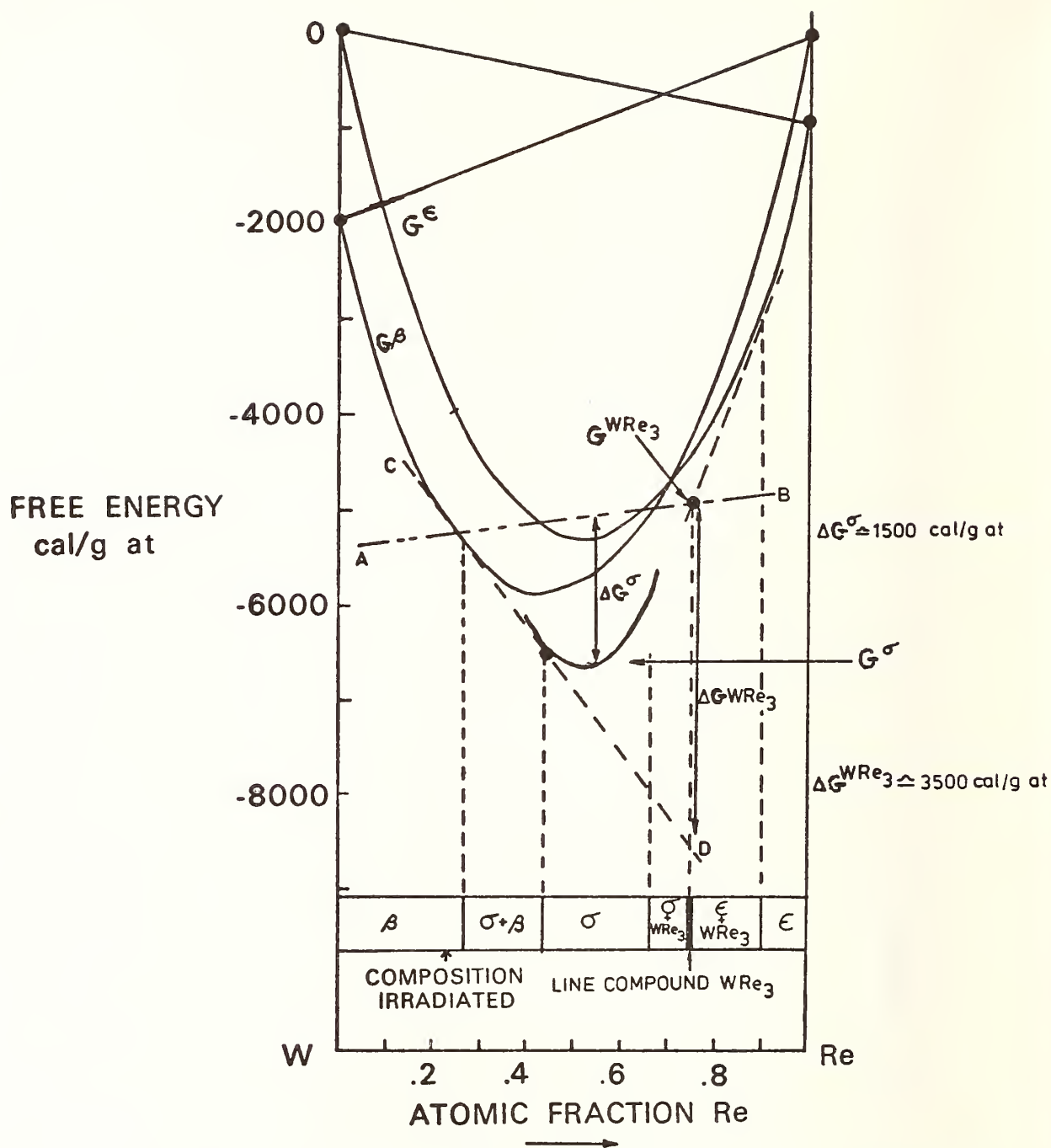


FIG 4 CALCULATED FREE ENERGY - COMPOSITION RELATIONS FOR bcc (β), hcp (ϵ), SIGMA (σ) AND $W-Re_3$ FOR THE THE W-Re BINARY SYSTEM AT 1100°C (1373 K)



F*A*C*T

(FACILITY FOR THE ANALYSIS OF CHEMICAL THERMODYNAMICS)

- A COMPUTERIZED CANADIAN THERMODYNAMIC DATA TREATMENT CENTRE -

A.D. Pelton, C.W. Bale,

Département de génie métallurgique,
Ecole Polytechnique (Université de Montréal),
Montréal, Québec, Canada

W.T. Thompson

Department of Mining and Metallurgical Engineering,
McGill University,
Montréal, Québec, Canada

ABSTRACT

The present state of development of F*A*C*T (Facility for the Analysis of Chemical Thermodynamics), a thermodynamic data treatment centre based in Canada, is described. Users at remote terminals, contacting the system via telephone hook-up, will be able to perform many different thermodynamic calculations using the computer in full conversational mode. The calculations will employ a system data base and/or user-supplied data. A major part of F*A*C*T is devoted to the calculation of phase diagrams with the resulting output printed on the user's terminal. These programs are briefly discussed in this article. These calculate (a) potential-potential phase diagrams for 2-, 3-, 4- and 5-component systems (such as predominance area, Ellingham, stability, combination, and Pourbaix diagrams, etc.); (b) potential-composition diagrams for 2-, 3-, and 4-component systems (such as temperature-composition and chemical potential-composition phase diagrams); and (c) chemical reaction paths (calculations of isothermal, adiabatic, isentropic, etc. chemical reaction paths as well as of the conditions for chemical equilibria). The use of these programs has been illustrated by the calculation of various phase diagrams and reaction paths in the Fe-Ni-S-O system. It is planned to have F*A*C*T on-line with these three programs, with a limited data base, by the end of 1977.

INTRODUCTION

Although the principles of thermodynamic analysis are well-established and its importance is unchallenged, the vast body of thermodynamic data now available is not being put to its best use because the calculations involved are tedious and very time-consuming, usually requiring the knowledge of a specialist.

This article describes the present state of development of F*A*C*T (Facility for the Analysis of Chemical Thermodynamics) - a thermodynamic data treatment centre based in Canada. Users at remote terminals, contacting the system via telephone, will be able to perform many different thermodynamic calculations in conversational mode. All input and output (including graphical output) will be on the remote terminals. The user will not need a CALCOMP or other plotter in order to generate a phase diagram. Calculation will be performed with the use of the system's data base and/or with user-supplied data.

At present, three calculating/plotting programs are in an advanced stage of

development. It is expected that these will be available on-line with a limited data base by the end of 1977. Two of these programs are for the computation and subsequent graphical representation of potential-potential phase diagrams and potential-composition phase diagrams. The third program calculates changes in all of the thermodynamic properties associated with a chemical reaction.

The use of F*A*C*T will now be illustrated for the analysis of heterogeneous and homogeneous equilibria in the Fe-Ni-S-O system.

Consider the four independent variables temperature, T ; relative chemical potential of oxygen, $RT \ln p_{O_2}$; relative chemical potential of sulfur, $RT \ln p_{S_2}$; and molar metal ratio, $\xi = n_{Ni}/(n_{Ni} + n_{Fe})$ (where n_i = number of moles). If one of these four variables is held constant, a space diagram with the other three as axes can be drawn. (Strictly speaking, the total hydrostatic pressure must also be held constant.) For example, in Fig. 1a is the space diagram T - $RT \ln p_{O_2}$ - ξ at a very low constant p_{S_2} . On the left

face of this figure would appear the Ellingham diagram for the Fe-O system (Fig. 4). On the right face would appear the Ellingham diagram for the Ni-O system. These are potential-potential phase diagrams (thermal potential versus chemical potential) in which areas represent one-phase equilibria, lines represent two-phase equilibria, and points represent three-phase equilibria. On the front face, at a constant p_{O_2} sufficiently low that no oxide phases

occur, would appear the binary temperature-composition phase diagram for the Fe-Ni system (Fig. 8). This is a potential-composition phase diagram (the potential, in this case, being the thermal potential) in which two-phase equilibria are represented by horizontal tie-lines. In Fig. 1b is the space diagram $RT \ln p_{O_2}$ - $RT \ln p_{S_2}$ - ξ

at constant T . On the right and left faces of this diagram would appear the "predominance area phase diagrams" for the Ni-S-O (Fig. 2) and the Fe-S-O systems. These are potential-potential phase diagrams (chemical potential versus chemical potential). On the front face (at very low constant p_{S_2}) would appear the $RT \ln p_{O_2}$ - ξ phase diagram for the Fe-Ni-O system at constant T (Fig. 10). This diagram is a potential-composition phase diagram and obeys the rules of construction of this type of phase diagram.

An infinite number of other space diagrams for this quaternary system could be drawn. The traces of two-dimensional sections through these space diagrams often yield phase diagrams of the potential-potential or potential-composition type. We may, for example, be interested in a vertical section through Fig. 1a but at a sufficiently high partial pressure of oxygen that oxide phases also appear (Fig. 9). Slices through Fig. 1b at constant p_{SO_2} would also be of interest (Fig. 5). Useful diagrams also result if the independent variables are redefined. We may, for example, be interested in a potential-potential phase diagram of $RT \ln p_{SO_2}$ versus $RT \ln p_{O_2}$ at constant T (Fig. 3).

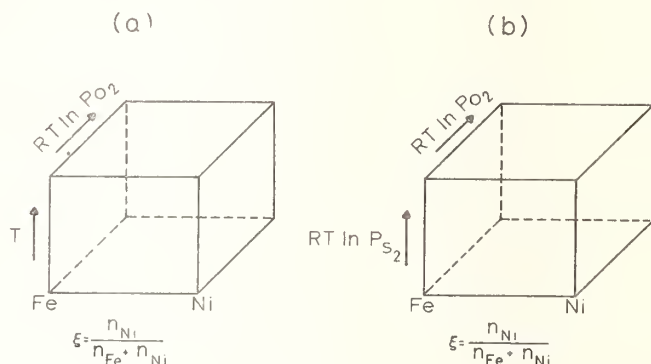


FIG. 1. Space diagrams for the Fe-Ni-S-O system (a) $RT \ln p_{S_2} = \text{constant} \ll 0$ (b) $T = \text{constant}$.

The theory of the geometry of various types of phase diagram representations and the detailed procedures involved in calculating these diagrams from thermodynamic data have been discussed previously (1,2).

It can be seen from Table I that, having called the program, the user has indicated the column width of his terminal, and that he wishes to generate potential-potential diagrams of the three component system, Ni-S-O. The computer has replied that such diagrams for this system can be computed if the user identifies and defines a vertical axis, a horizontal axis, and one independent constant. From the phase rule for a three-component system under a total (theoretical) hydrostatic pressure of 1 atm, the most stable phase can be calculated from a definition of any three independent variables. In Table I, up to and including line 600, the user has identified, and defined the limits of, the vertical axis, $\log_{10} p_{S_2}$, and the horizontal axis, $\log_{10} p_{O_2}$. In line 700, the constant temperature is entered. It is to be noted that the variable T is always specified as either a horizontal axis or a constant.

In F*A*C*T, precautions have been taken to guard against typing or logical errors that might be entered inadvertently by the user. Thus, in line 500, we see that the user has entered P(CL2) as a variable, which clearly cannot be part of the Ni-S-O system. This has been pointed out by the computer. Subsequently, the user has made a correction to the more logical P(O2). Also, we note that after line 700 the user is given the option to check and change any numbered line(s) before obtaining the graphical output.

In the graphical output generated at the terminal (Fig. 2), the phases of the predominance area diagram have, where possible, been labelled by the computer. The most stable phase at any position was calculated by comparing the free energies of all condensed phases. The thermodynamic data necessary for this calculation was taken from a data base stored in the computer memory. The actual positions of the two-phase boundary lines were determined by a scanning of the system by a "divided differences technique" within the limits of the axes.

A more useful predominance area phase diagram for the Ni-S-O system is illustrated in Fig. 3. Here, the vertical axis of Fig. 2, $\log_{10} p_{S_2}$, has been replaced by $\log_{10} p_{SO_2}$. This diagram was readily obtained as can be seen from the bottom of Table I where the user has merely indicated that he wishes to continue calculations for the Ni-S-O system and has redefined line 500.

Other types of potential-potential phase diagrams can be computed with this program. In Fig. 4 is the Ellingham diagram for the Fe-O system (relative chemical potential of oxygen, $RT \ln p_{O_2}$, versus temperature). In Fig. 5 is the Ellingham diagram for the Fe-S-O system at constant $p_{SO_2} = 10^{-4}$ atm.

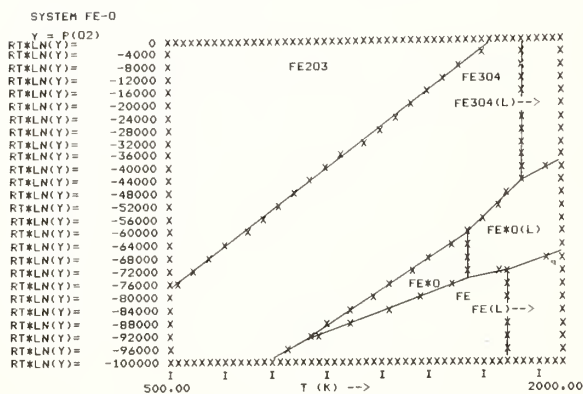


FIG. 4 Ellingham diagram for Fe-O (Solid lines have been added by hand).

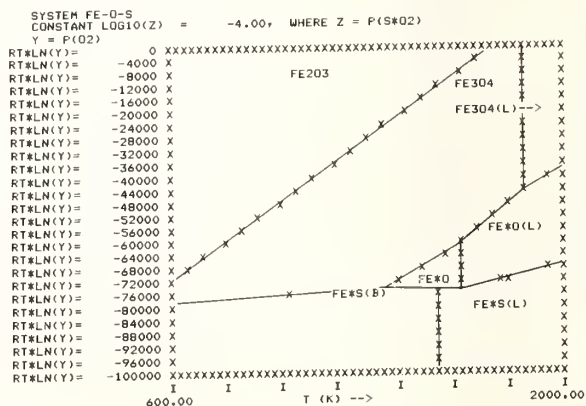


FIG. 5 Ellingham diagram for Fe-O-S at constant p_{SO_2} (Solid lines have been added by hand).

The program can handle systems containing up to five components with complex gas mixtures as variables. We note that, from the phase rule, a potential-potential phase diagram of a five-component system can be calculated from a definition of the horizontal axis, the vertical axis, and three independent constants. For example in Fig. 6 is the predominance area diagram for the Fe-C-O-S-H quinary system at 900 K.

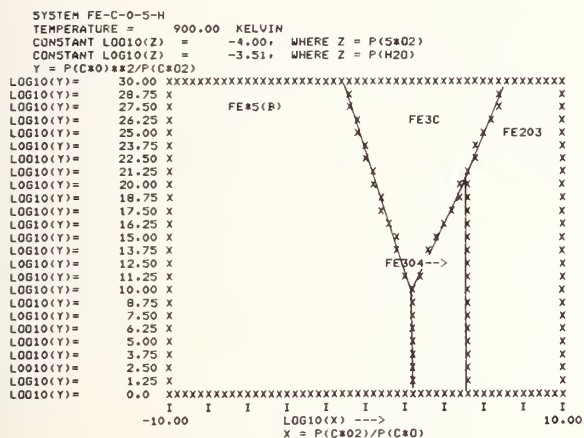


FIG. 6 Combination potential-potential phase diagram for the Fe-C-O-S-H system (Solid lines have been added by hand).

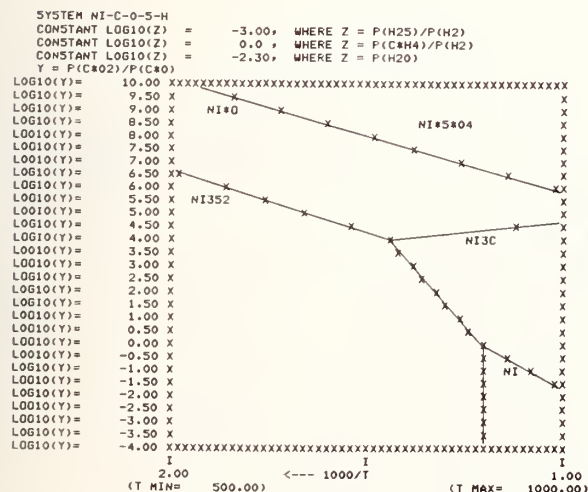


FIG. 7 Combination potential-potential phase diagram for the Ni-C-O-S-H system (Solid lines have been added by hand).

TABLE II

```

*** POTENTIAL - POTENTIAL DIAGRAMS ***

YOUR TERMINAL (1) CAN, OR (2) CAN NOT PRINT 130 COLUMNS PER LINE
(ENTER 1 OR 2)
2

DEFINE TOTAL NUMBER OF COMPONENTS (ENTER 2,3,4 OR 5)
5

SYSTEM M-A-B-C-D

ENTER H (FOR EXAMPLE CU)
FE
ENTER A (FOR EXAMPLE S)
C
ENTER B (FOR EXAMPLE O)
O
ENTER C
S
ENTER D
H

AT 1 ATMOS (THEORETICAL) PRESSURE, PREDOMINANCE AREA (OR STABILITY)
DIAGRAM FOR THE SYSTEM FE-C-O-S-H CAN BE COMPUTED BY DEFINING:
(I) A VERTICAL AXIS, (II) A HORIZONTAL AXIS, AND
(III) 3 CONSTANT(S)

***** IDENTIFY VERTICAL AXIS: (1) LOG10(Y), (2) LN(Y) OR (3) RT*LN(Y) ?
1

***200*** ENTER VERTICAL VARIABLE Y (FOR EXAMPLE P(S2)**(0.5) ETC)
P(C*00)**2/P(C*02)

***300*** DEFINE LOWER AND UPPER LIMITS OF VERTICAL AXIS AND INCREMENTAL STEP
(IF INCREMENTAL STEP IS UNDEFINED GRAPHICAL OUTPUT WILL BE 25 LINES)
0 30

***** IDENTIFY HORIZONTAL AXIS: (1) LOG10(X), (2) LN(X) OR (3) 1/T Y
1

***500*** ENTER HORIZONTAL VARIABLE X (FOR EXAMPLE P(S*03)/P(S*02) ETC)
P(C*02)/P(C*00)
ERROR ENCOUNTERED IN COLUMN 8
'/' MUST BE FOLLOWED BY '/' OR '*'
-PLEASE RE-ENTER
P(C*02)/P(C*00) UNMATCHED PARENTHESES, -PLEASE RE-ENTER
P(C*02)/P(C*00)

***600*** DEFINE LOWER AND UPPER LIMITS OF HORIZONTAL AXIS

***700*** ENTER CONSTANT TEMPERATURE (KELVINS)
-20
ERROR, MINIMUM PERMISSIBLE TEMPERATURE IS 298

***700*** ENTER CONSTANT TEMPERATURE (KELVINS)
900

*****IDENTIFY THE TYPE OF CONSTANT(S) C = (1) LOG10(Z), (2) LN(Z) OR (3) RT*LN(Z)
1

***900*** DEFINITION OF CONSTANT(S)
ENTER THE VARIABLE Z (FOR EXAMPLE P(S*02) ETC)
P(S*02)
ENTER VALUE OF 'C' (NOTE, 'C' NOT 'Z')
-4

ENTER THE NEXT VARIABLE Z
P(H20)
ENTER VALUE OF 'C' (NOTE, 'C' NOT 'Z')
-3.51

IF YOU WISH TO CHANGE ONE OR MORE OF THE LINES, LIST, IN ORDER, THE LINE
NUMBER(S), IF NOT PRESS 'RETURN'.

PRESS 'RETURN' WHEN READY FOR GRAPHICAL OUTPUT
  
```

Conversational input used to generate Fig. 6.

The vertical axis is $\log_{10}(P_{CO_2}/P_{CO})$, the horizontal axis is $\log_{10}(P_{CO_2}/P_{CO})$, and the constants are $p_{SO_2} = 10^{-4}$ atm, $p_{H_2O} = 10^{-3.51}$ atm, and $T = 900$ K. In Fig. 7 is the phase diagram for the Ni-C-O-S-H quinary system. The vertical axis is $\log_{10}(P_{CO_2}/P_{CO})$ and the horizontal axis is $1/T$ corresponding to a temperature range of 500 - 1000 K. The constants are $p_{H_2S}/p_{H_2} = 10^{-3}$, $p_{CH_4}/p_{H_2} = 1.0$, and $p_{H_2O} = 10^{-2.3}$ atm. The listing of the interactive conversation which generated Fig. 6 is given in Table II. This particular system has been chosen in order to show how gas mixtures may be employed as either axes or constants, and how typing or logical errors may be readily corrected by the user. (See lines 500 and 700 in Table II).

The usefulness of Figs 6 & 7 for the Fe-Ni-S-O system is apparent when one considers that, experimentally, sulfur potentials are often defined by H_2S/H_2 or SO_2/O_2 mixtures and oxygen potentials by CO_2/CO or H_2/H_2O mixtures. Thus, the possible formation of carbides, carbonates, hydrides, etc. must be considered.

Present developments in F*AC*T concerned with the calculation of potential-potential phase diagrams include the addition of isobaric (or isoactivity) lines and P_{total} curves on the diagrams, as well as the calculation of Pourbaix (electrical potential, E , versus pH) diagrams. Other developments include the ability to accept user-supplied data and the calculation of metastable phase boundaries.

POTENTIAL-COMPOSITION PHASE DIAGRAMS

A computer-generated T-composition phase diagram for the Fe-Ni binary system is shown in Fig. 8. The calculation is based upon the thermodynamic properties of the phases as given in the critical compilations of the "CALPHAD" group (3).

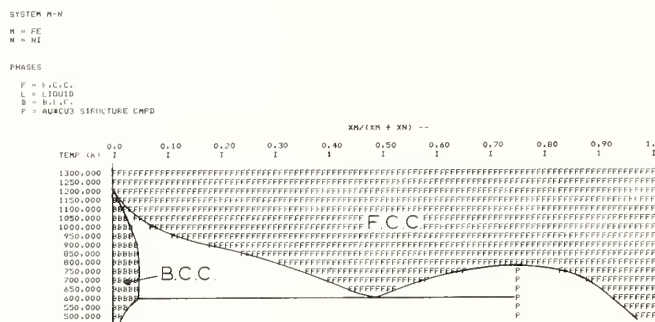


FIG. 8 Temperature-composition phase diagram for the Fe-Ni binary system

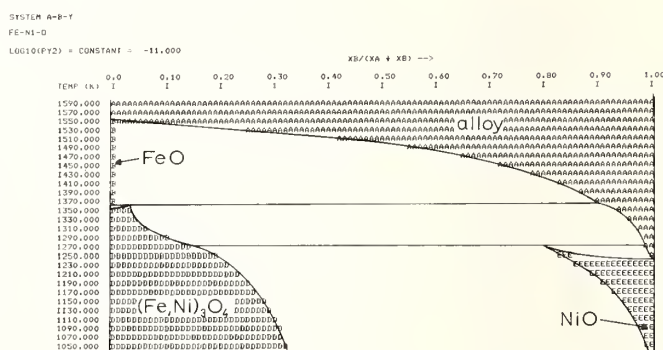


FIG. 9 Temperature-composition phase diagram at constant $p_{O_2} = 10^{-11}$ atm for the Fe-Ni-O system.

For the three-component system Fe-Ni-O, a potential-composition phase diagram can be drawn if another potential is held constant. In Fig. 9 is the computer-generated T- ξ diagram for the Fe-Ni-O system at constant $p_{O_2} = 10^{-11}$ atm. In Fig. 10 is the

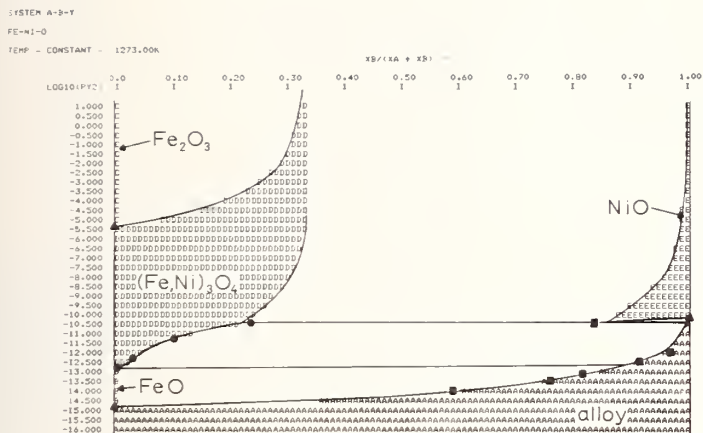


FIG. 10 $\log_{10}P_{O_2}$ - composition phase diagram at constant T for the Fe-Ni-O system
 ●(ref. 4); ■(ref. 5); ▲(points from standard thermodynamic tables).

computer-generated $\log_{10}P_{O_2}$ - ξ diagram at constant $T = 1273$ K.

In all these computer-generated diagrams, one-phase regions are indicated by a code letter, and two-phase regions by blank areas. The solid lines on Figs 8-16 have been added by hand in order to improve the clarity of the reproduction. Similarly, the labelling of the one-phase fields has also been added. In Table III is a listing of the conversational input which generated the diagram in Fig. 10. After signing on, the user indicates the width of his terminal. (Phase diagrams 50 columns in width can also be generated if the user has only a 72-column wide terminal.) The next few lines in Table III are self-explanatory. At line 1000, the user enters a code number for the system which is taken from a list of systems which have been analyzed and stored in the system's data base. Alternatively, the user may decide to enter all the data himself. In the present example, he chooses the Fe-Ni-O system. The computer then lists the phases for which stored data are available along with the temperature limits for which these data are applicable, and the user indicates which phases he wishes to consider. (One may, for example, choose to ignore certain phases in order to generate metastable phase boundaries.) The user may also choose to add some data sets of his own. The computer then lists the chosen phases along with the code letter to be used in the output for each phase. The user has the

TABLE III

```
IS YOUR TERMINAL (1)CAPABLE, (2)NOT CAPABLE OF 121 COLUMNS OF OUTPUT
1
ENTER UNITS OF ENERGY, (1)CAL, (2)JDOULES
1
ENTER UNITS OF TEMP, (1)K, (2)C, (3)F
1
DO YOU (1)WANT (2)NOT WANT PROMPTING?
1

*****1000***** ENTER CODE NUMBER OF SYSTEM.
OR PRESS RETURN IF YOU ARE SUPPLYING ALL DATA YOURSELF.
2

SYSTEM FE-NI-O

PHASE CODE

1 F.C.C. (GAMMA) ALLOY 300 - 1800 K
2 WUSTITE (FEO) (LINE COMPOUND) 800 - 1700 K
3 FE2O3 SOLID (LINE COMPOUND) 800 - 2400 K
4 SPINEL 800 - 2300 K
5 NI#O-FE#O SOLID 800 - 2333 K

REFERENCE PHASES (G = 0) ARE NUMBERS 1 FOR A AND 1 FOR B

FREE ENERGIES TO BE ENTERED AS
DELTA G = A + B*T + C*(T**2) + D*(T**3) + E*(T**4) + F*T*ALOG(T) + G/T
WHERE T IS KELVINS AND ALOG IS NATURAL LOG

*****1100***** ENTER CODE NUMBERS OF PHASES TO BE CONSIDERED
1 2 3 4 5
ENTER NUMBER OF ADDITIONAL USER-SUPPLIED PHASES
0

*****1105***** PHASE A PHASE CODE NUMBER 1
DO YOU (1) WANT (2) NOT WANT A LISTING OF DATA SET CONTENTS?
1
ENTER PHASE TYPE CODE
1
ENTER STOICHIOMETRIC FACTORS 1,J,N OF COMPOUND A(1)B(J)Y(N) AT THE LEFT
1.00 0.0 0.0
ENTER COEFFTS A,B,C,D,E,F,G OF FREE ENERGY OF A( 1.00)B( 0.0 )Y( 0.0 )
0.0 0.0 0.0 0.0 0.0
ENTER STOICHIOMETRIC FACTORS II,J,N,N OF COMPOUND A(II)B(J)Y(N) AT THE
RIGHT
0.0 1.00 0.0
ENTER COEFFTS A,B,C,D,E,F,G OF FREE ENERGY OF A( 0.0 )B( 1.00)Y( 0.0 )
0.0 0.0 0.0 0.0 0.0
ENTER COEFFICIENTS (MAX OF 7 TERMS) OF THE SERIES FOR ENTHALPY OF MIXING
DELTA H = X1*X2*(D0 + D1*X2 + D2*(X2**2) + D3*(X2**3) + ....)
-0.40000E 03 -0.10000E 04 0.0 0.0
0.0 0.0 0.0
ENTER COEFFTS (MAX OF 7 TERMS) OF SERIES FOR EXCESS ENTROPY OF MIXING
SEXCESS = X1*X2*(D0 + D1*X2 + D2*(X2**2) + D3*(X2**3) + ....)
0.0 0.0 0.0 0.0
0.0 0.0 0.0 0.0

*****1110***** PHASE B PHASE CODE NUMBER 2
DO YOU (1) WANT (2) NOT WANT A LISTING OF DATA SET CONTENTS?
2

*****1115***** PHASE C PHASE CODE NUMBER 3
DO YOU (1) WANT (2) NOT WANT A LISTING OF DATA SET CONTENTS?
2

*****1120***** PHASE D PHASE CODE NUMBER 4
DO YOU (1) WANT (2) NOT WANT A LISTING OF DATA SET CONTENTS?
2

*****1125***** PHASE E PHASE CODE NUMBER 5
DO YOU (1) WANT (2) NOT WANT A LISTING OF DATA SET CONTENTS?
2

*****1200***** IS WIDTH OF X-AXIS IN MOLE PERCENT, (1) 10 (2) 100
10
INPUT CANNOT BE INTERPRETED. REENTER
2

*****1300***** IS Y-AXIS (1)T, (2)LOG10(ACTIVITY(Y)), (3)LOG10(PY2)?
3
ENTER, IN ORDER, LOWER LIMIT, INCREMENT, AND UPPER LIMIT OF Y-AXIS
-22 -10 0.25
UPPER LIMIT MUST BE GREATER THAN OR EQUAL TO LOWER LIMIT AND INCREMENT
MUST BE POSITIVE. REENTER
-22 0.25 -10

*****1310***** ENTER THE CONSTANT TEMPERATURE
1000

IF YOU WISH TO CHANGE A LINE, ENTER ITS NUMBER. IF NOT, PRESS RETURN KEY
TO START CALCULATION
1310
DO YOU (1)WANT (2)NOT WANT PROMPTING?
2
*****1310*****
1273

IF YOU WISH TO CHANGE A LINE, ENTER ITS NUMBER. IF NOT, PRESS RETURN KEY
TO START CALCULATION
```

Conversational input used to generate Fig. 10

option of inspecting the stored data for any phase. In Table III he has chosen to do this for phase A, and the computer has listed out the stored thermodynamic data for this phase in the same format, with the same questions asked, as it would if this were a user-supplied data set. In line 1200 the width of the x-axis is specified. In line 1300 the scale of the y-axis (in this case $\log_{10} p_{O_2}$), and the limits and increment of this axis are chosen. Finally, in line 1310 the constant potential (in this case, T) is specified. As was pointed out in the previous section, attempts have been made to make F*A*C*T as error-proof as possible by the incorporation of a large number of error messages which appear if the user makes a logical or typing error. Examples are given at lines 1200 and 1300. The user is now given the chance to go back, if he wishes, to change any section of input by entering its number. In the example in Table III, he has chosen to reenter line 1310 in order to change the temperature from 1000 to 1273 K. At this point, by entering one of the line numbers 1105 to 1125, he would be able to modify the stored data for one of the phases if he so desired. The same opportunity to change some input lines is also offered after the diagram has been printed. The user is thereby permitted to quickly recalculate the diagram for different limits of the axes, for example.

Space does not permit a complete description of the programming techniques to be given here. A detailed discussion will be published shortly. The method used is essentially that of calculating the lowest common tangent to the free energy-composition curves. The thermodynamic data required are the stoichiometry of the phases as well as the free energies of formation (expressed as functions of T) of all compounds as well as expressions for the thermodynamic properties of solution (g^E , Δh , s^E) of all phases. In Table III, Δh and s^E for the Fe-Ni alloy phase (line number 1105) are expressed as simple power series of the mole fractions. However, several other mathematical descriptions can be used (each with its own "phase type code"). Thus, Henrian solutions, spinel solutions, etc. can be treated. This will be the subject of a series of forthcoming articles. In the case of the Fe-Ni-O system, for example, the solution properties of the Fe-Ni alloy phase are expressed as power series in the mole fractions; the FeO and NiO phases are taken to be Henrian solutions; the $(Fe,Ni)_3O_4$ phase is considered to be an ideal mixture of the two inverse spinels Fe_3O_4 and $NiFe_2O_4$; while Fe_2O_3 and $FeNi_3$ are taken to be "line compounds" of fixed composition.

Other computer-generated potential-composition phase diagrams for the Fe-Ni-O system are shown in Figs 11-12. These are T- ξ diagrams at constant ratios of p_{CO}/p_{CO_2} and p_{H_2}/p_{H_2O} . (Such constant ratios fix a constant p_{O_2} at any constant T, but this is not the same p_{O_2} at all temperatures).

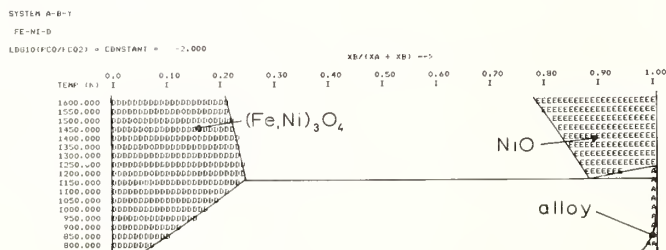


FIG. 11 Temperature-composition phase diagram for Fe-Ni-O at constant $p_{CO}/p_{CO_2} = 10^{-2}$.

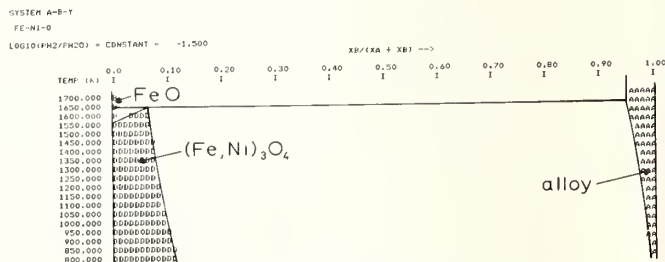


FIG. 12 Temperature-composition phase diagram for Fe-Ni-O at constant $p_{H_2}/p_{H_2O} = 10^{-1.5}$.

For the quaternary Fe-Ni-S-O system, a potential-composition phase diagram can be drawn if two other potentials are held constant. In Fig. 13 is the diagram of $\log_{10} p_{O_2} - \xi$ for this quaternary system at constant $T = 1173$ K and $p_{SO_2} = 10^{-10}$ atm. Since, at constant p_{SO_2} , $\log p_{O_2}$ varies inversely as $\log p_{S_2}$, Fig. 13 is also a plot of $-\log p_{S_2}$ versus ξ . Thus, Fig. 13 is made up of the $\log p_{O_2} - \xi$ diagram for the Fe-Ni-O system (as in Fig. 10) at the top, with the $\log p_{S_2} - \xi$ diagram for the Fe-Ni-S system inverted at the bottom. As p_{SO_2} is raised, the two halves of Fig. 13 move together until they intersect as is illustrated in Figs 14-15.

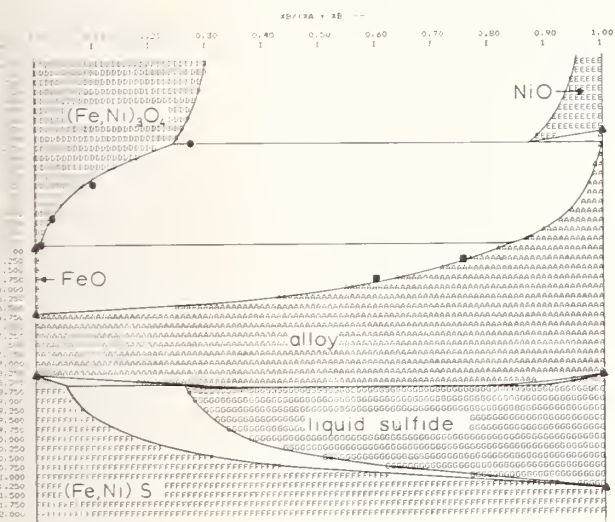


FIG. 13 $\log_{10} p_{O_2}$ versus $\xi = x_{Ni} / (x_{Ni} + x_{Fe})$ for the Fe-Ni-O system at $T = 1173$ K and $p_{SO_2} = 10^{-10}$ atm. ●(ref. 4); ■(ref. 5); ▲(points from standard thermodynamic tables).

In Fig. 16 is an example of a diagram with an expanded x-axis with an attendant resolution of 0.1 mole %. Fig. 16 is a blow-up of a portion of Fig. 13.

Some experimental points (4,5) are shown on Figs 10 & 13 in order to indicate the typical agreement obtained between the calculated diagrams and the experimental diagrams for the limited ranges of T , composition, and partial pressure for which experimental phase diagrams are available.

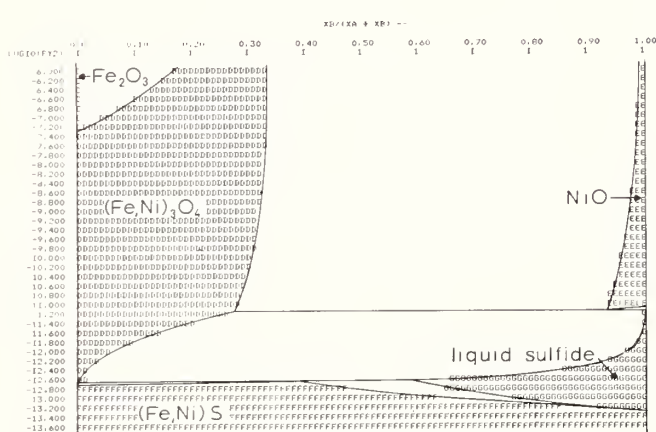


FIG. 14 $\log_{10} p_{O_2}$ versus $\xi = x_{Ni} / (x_{Ni} + x_{Fe})$ for the Fe-Ni-S-O system at $T = 1173$ K and $p_{SO_2} = 10^{-2.0}$ atm.

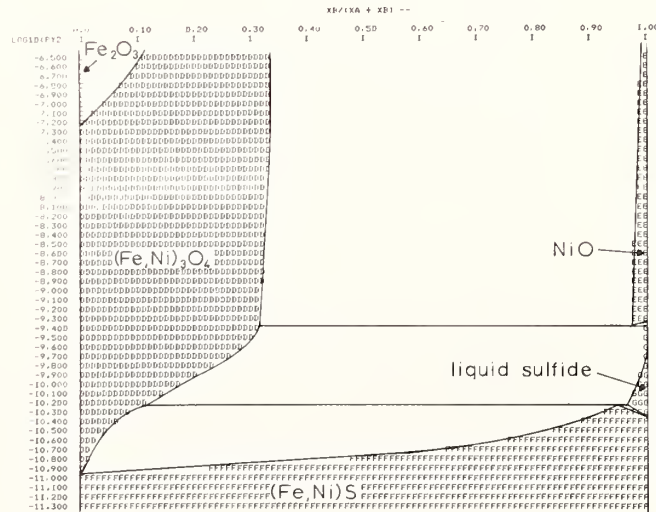


FIG. 15 $\log_{10} p_{O_2}$ versus $\xi = x_{Ni} / (x_{Ni} + x_{Fe})$ for the Fe-Ni-S-O system at $T = 1173$ K and $p_{SO_2} = 10^{1.0}$ atm.

Present work on this program is concerned mainly with the preparation of a data base for a number of systems of the type A-B-Y where A and B are metals and Y is a non-metal (O,S,C,Cl, etc.). The data base is being obtained from experimental thermodynamic data (curve-fitting), from comparison of calculated and experimental phase diagrams (where available), by interpolation and extrapolation with the aid of statistical models where data are not available, or by a combination of the above.

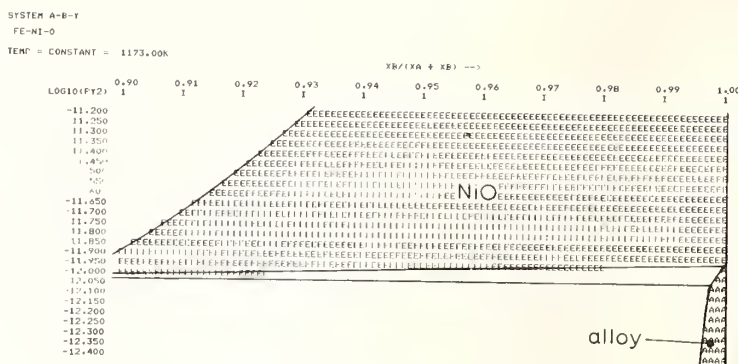


FIG. 16 $\log_{10}P_{O_2}$ versus ξ for the range $0.9 \leq \xi \leq 1.0$ for the Fe-Ni-O system at 1173 K (a blow-up of a portion of Fig. 13)

REACTION PATH CALCULATIONS

This feature of F*A*C*T is intended to complement the phase diagram programs by permitting users to conduct calculations other than those related directly to phase stability. This program computes the changes in the thermodynamic properties H, S, V, U, A, and G between specified or implied initial and final states of a system. Since this routine embraces calculations as elementary as determining the change in G associated with isothermal isobaric chemical reactions to the calculation of ΔH for reactions with many reactants and products at different temperatures and pressures, it is useful not only for important practical problems, but also for educational purposes to give the users a better insight into the significance of the phase diagram programs.

Consider, as an initial example related to the sulfur-oxygen gas equilibrium, the reaction shown in Table IV. The user has entered the balanced chemical equation. Considerable freedom in the style of input is permitted, as long as elements within each compound are separated by a stoichiometric number or by a *(equivalent to a stoichiometric number of 1). In this way,

TABLE IV

ENTER THE CHEMICAL EQUATION

S#02 + 1/2 O2 = S#03

(T+P+GAS) (T+P+GAS) (T+P+GAS)

CALCULATIONS ARE BASED ON THE NUMBER OF GRAM MOLES OF REACTANTS AND PRODUCTS INDICATED IN THE CHEMICAL EQUATION

TEMPERATURE	PRESSURE	DELTH	DELTS	DELTU	DELTU	DELTA	DELTG
(K)	(ATM)	(CAL)	(CAL/K)	(LIT)	(CAL)	(CAL)	(CAL)
298.15	1.00	-23450.	-22.55	-12.2	-23154.	-16431.	-16727.
400.0	1.0	-23484.	-22.66	-16.4	-23067.	-14024.	-14422.
500.0	1.00	-23433.	-22.55	-20.5	-22937.	-11664.	-12160.
600.0	1.0	-23323.	-22.35	-24.6	-22728.	-9320.	-9915.
700.0	1.00	-23165.	-22.10	-28.7	-22470.	-6997.	-7692.
700.0	10.0	-23165.	-19.82	-2.87	-22470.	-8599.	-9294.
700.0	100.0	-23165.	-17.53	-.287	-22470.	-10200.	-10895.
700.0	1000.0	-23165.	-15.24	-.287E+01	-22470.	-11801.	-12496.

RETURN

it is possible, for example, to distinguish Co from CO when all alphabetical characters are upper-case. The subscripts are used to identify the states. Algebraic symbols, T and P, for temperature and pressure indicate that the numerical values of these properties are unspecified and will either be entered or calculated later. With the depression of the 'return' key, the information following the equation up to the first row in the tabular output is generated. The changes in the six basic extensive thermodynamic functions are calculated in the indicated units for the system-generated temperature of 298.15 K and pressure of 1.0 atm. In subsequent lines, following each system-generated '!', the user enters in free format two numbers which become the temperature and pressure

Conversational input and output using the reaction path program illustrating calculations for isothermal isobaric paths.

defining a new set of property changes which are calculated and printed on the next line after depression of the 'return' key. At no point does the user enter data, since F*A*C*T has its own data base. If data are not in storage, appropriate messages are issued. Table IV shows, for example, that the isothermal standard enthalpy change is virtually constant and that the Gibbs free energy change tends to favour SO_2 at higher temperatures. At 700 K the user has also entered progressively higher values for the pressure. The effect is instructive. ΔH is not altered (gases are presently regarded as ideal) and ΔV diminishes.

It is not necessary that the pressures and temperatures for each compound be assigned values in the tabular output. (n-1) compounds in an n compound reaction may have (possibly different) numerical values set into the subscripts for the temperature and pressure. Furthermore, the same compound may appear on both sides of the reaction. This provides considerable power in solving many problems of practical importance as illustrated in Table V. Hot SO_2 is reacting with an excess of warm air to produce SO_3 . The user, by varying the temperature of the products, is examining ΔH . On the fourth entry he has neglected to specify the pressure and so a thermodynamic error message is generated. From the magnitude of the enthalpy changes at 600 and 700 K, it appears that ΔH will be zero near 800 K. The temperature corresponding to $\Delta H = 0$ is the adiabatic reaction product temperature for the isobaric process. This temperature can be directly determined by specifying $P = 1.0$ atm and $\Delta H = 0$ by entering these values in the appropriate columns. This the user has subsequently done. Asterisks are used in F*A*C*T to indicate those columns left unspecified on entry. The required T has been calculated directly to be 770.8 K. In the next line the user has inadvertently specified three properties. This impossible situation causes F*A*C*T to generate the error message following this line. In the final two lines, the user has entered a zero in the ΔV column and has found that $\Delta V = 0$ when $T = 479.8$ K. (In a flowing process, reactant and product flow would be the same). This finding is shown to be independent of the pressure.

In Table VI the user has employed the reaction path program to study the reaction involving Fe, Fe_3O_4 and FeO involved in Fig. 4. In the last line, by setting ΔG to zero (by entering a zero in the ΔG column) the user has determined the precise value of the temperature at the Fe/ Fe_3O_4 /FeO triple point. The equations entered in Table VII then

TABLE V

ENTER THE CHEMICAL EQUATION

S#02 + 2 O2 + 7.52 N2 =
(1000*P+GAS) (400*P+GAS) (400*P+GAS)

CONTINUE

S#03 + 3/2 O2 + 7.52 N2
(T+P+GAS) (T+P+GAS) (T+P+GAS)

CALCULATIONS ARE BASED ON THE NUMBER OF GRAM MOLES OF REACTANTS AND PRODUCTS INDICATED IN THE CHEMICAL EQUATION

TEMPERATURE (K)	PRESSURE (ATM)	DELTH (CAL)	DELTS (CAL/K)	DELTU (LIT)	DELTU (CAL)	DELTA (CAL)	DELTA (CAL)	DELTA (CAL)
298.1	1.00	-38393.	-55.08	-149.	-34778.	80068.	76453.	
400.0	1.0	-30566.	-33.32	-65.6	-28977.	28070.	26481.	
500.0	1.00	-22598.	-15.55	16.6	-22999.	-24981.	-24580.	
600.0	1.00	-14412.	-0.63	98.8	-16803.	-79658.	-77267.	
700.0								
TWO COLUMNS MUST RECEIVE ENTRIES								
700.0	1.0	-6035.	12.28	181.	-10416.	-135721.	-131341.	
700.0	1.00							
770.8	1.0	0	20.49	239.	-5788.	176127.	-170339.	
770.8	1.00							
ONLY TWO COLUMNS MAY RECEIVE ENTRIES								
479.8	1.0			0				
479.8	1.00	-24223.	-10.07	0	-24223.	-14146.	-14146.	
479.8	100.0			0				
479.8	100.	-24223.	-14.29	0	-24223.	-14146.	-14146.	

- RETURN

Conversational input and output using the reaction path program illustrating calculations for adiabatic and isovolumetric paths.

TABLE VI

ENTER THE CHEMICAL EQUATION

FE + FE3O4 = 4 FE4O
(T+P+S1) (T+P+S1) (T+P+S1)

CALCULATIONS ARE BASED ON THE NUMBER OF GRAM MOLES OF REACTANTS AND PRODUCTS INDICATED IN THE CHEMICAL EQUATION

TEMPERATURE (K)	PRESSURE (ATM)	DELTH (CAL)	DELTS (CAL/K)	DELTU (LIT)	DELTU (CAL)	DELTA (CAL)	DELTA (CAL)	DELTA (CAL)
298.1	1.00	12100.	13.51	-137E-02	12100.	8072.	8072.	
400.0	1.0	12666.	15.17	-137E-02	12666.	6597.	6597.	
500.0	1.00	12792.	15.47	-137E-02	12792.	5056.	5056.	
600.0	1.0	12467.	14.89	-137E-02	12467.	3532.	3532.	
700.0	1.00	11680.	13.69	-137E-02	11680.	2099.	2099.	
800.0	1.0	10426.	12.02	-137E-02	10426.	810.	809.	
871.5	1.00	9242.	10.60	-137E-02	9242.	0.	0.	

Conversational input and output using the reaction path program illustrating the calculation of the temperature of the Fe/ Fe_3O_4 /FeO triple point ($\Delta G = 0$).

permit the determination of the partial pressure of oxygen at that triple point since the temperature has been previously established. The number of moles of reactants involved in the equation does not, of course, affect the equilibrium oxygen pressure as illustrated in Table VII by the tabular output for the second equation.

Table VIII illustrates the consequence of not specifying the phase state for one of the compounds. F*A*C*T assumes that the most stable state at the temperature and pressure is desired. In this mode, all of the reactant and product states appear in columns on the extreme right in the order determined by the input equation. It is not possible, when operating in this mode, to set values into columns other than the temperature and pressure columns.

Future developments to this program include the ability to employ user-supplied data, and the ability to indicate that groups of reactants and products exist in solutions. Furthermore, a plotting routine is to be developed to supplement the tabular output.

CONCLUSIONS

A brief description has been presented of the present state of development of F*A*C*T (Facility for the Analysis of Chemical Thermodynamics) - a thermodynamic data treatment centre and data bank based in Canada. Users, at standard remote terminals, will be able to 'carry on a conversation' with the computer by means of a telephone connection. F*A*C*T will be able to perform many different thermodynamic calculations in full conversational mode by employing a data base and/or user-supplied data. All resulting outputs, whether they are tables of figures or phase diagrams, will be printed out on the user's terminal. Three main programs have been presented in this article. The use of these programs has been illustrated by the calculation of various phase diagrams and reaction paths in the Fe-Ni-S-O quaternary system and its sub-systems. The diagrams presented include predominance area phase diagrams, Ellingham diagrams, stability diagrams, combination diagrams, and temperature-composition and chemical potential-composition phase diagrams. The chemical reaction paths include adiabatic, isothermal, isovolumetric, and isentropic paths. Work in progress involves the incorporation of an extensive

TABLE VII

ENTER THE CHEMICAL EQUATION

$$\text{FE} + \frac{1}{2} \text{O}_2 = \text{FE}_2\text{O}_3$$

(T,P,S1) (T,P,G) (T,P,S1)

CALCULATIONS ARE BASED ON THE NUMBER OF GRAM MOLES OF REACTANTS AND PRODUCTS INDICATED IN THE CHEMICAL EQUATION

TEMPERATURE (K)	PRESSURE (ATM)	DELTH (CAL)	DELTS (CAL/K)	DELTV (LIT)	DELTU (CAL)	DELTA (CAL)	DELTO (CAL)
298.1	1.00	-63790.	-16.94	-12.2	-63404.	-58353.	-58649.
871.5	*	*****	0				
871.5	.107E-24	-62790.	-71.95	-.333E+27	-61835.	865.	0.

RETURN

ENTER THE CHEMICAL EQUATION

$$2 \text{FE} + \text{O}_2 = 2 \text{FE}_2\text{O}_3$$

(T,P,S1) (T,P,G) (T,P,S1)

CALCULATIONS ARE BASED ON THE NUMBER OF GRAM MOLES OF REACTANTS AND PRODUCTS INDICATED IN THE CHEMICAL EQUATION

TEMPERATURE (K)	PRESSURE (ATM)	DELTH (CAL)	DELTS (CAL/K)	DELTV (LIT)	DELTU (CAL)	DELTA (CAL)	DELTO (CAL)
298.1	1.00	-127400.	-33.88	-24.5	-126808.	-116706.	-117298.
871.5	*	*****	0				
871.5	.107E-24	-125401.	-143.89	-.666E+27	-123670.	1730.	0.

RETURN

Conversational input and output using the reaction path program illustrating the calculation of equilibrium partial pressure of oxygen.

TABLE VIII

ENTER THE CHEMICAL EQUATION

$$4 \text{H}_2 + \text{Fe}_3\text{O}_4 = 4 \text{H}_2\text{O} + 3 \text{FE}$$

(T,P,GAS) (T,P,S1) (T,P) (T,P,S1)

CALCULATIONS ARE BASED ON THE NUMBER OF GRAM MOLES OF REACTANTS AND PRODUCTS INDICATED IN THE CHEMICAL EQUATION

TEMPERATURE (K)	PRESSURE (ATM)	DELTH (CAL)	DELTS (CAL/K)	DELTV (LIT)	DELTU (CAL)	DELTA (CAL)	DELTO (CAL)	PHASES REACTANTS PRODUCTS
298.1	1.00	-6379.	-74.57	-97.8	-4012.	18221.	15854.	G S1 = L S1
372.0	1.0	-4531.	-69.02	-122.	-1578.	24100.	21146.	G S1 = L S1
372.0	1.00	-4531.	-69.02	-122.	-1578.	24100.	21146.	G S1 = L S1
373.0	1.0	-4508.	-68.96	-122.	-1546.	24176.	21215.	G S1 = L S1
373.0	1.00	-4508.	-68.96	-122.	-1546.	24176.	21215.	G S1 = L S1
373.5	1.0	34592.	35.82	-.234E-01	34592.	21213.	21212.	G S1 = G S1
373.5	1.00	34592.	35.82	-.234E-01	34592.	21213.	21212.	G S1 = G S1
400.0	1.0	34212.	34.84	-.234E-01	34213.	20276.	20276.	G S1 = G S1
400.0	1.00	34212.	34.84	-.234E-01	34213.	20276.	20276.	G S1 = G S1
490.0	100.0	-3759.	-30.72	-1.26	-699.	11589.	8530.	G S1 = L S1
490.0	100.	-3759.	-30.72	-1.26	-699.	11589.	8530.	G S1 = L S1
500.0	100.0	-1623.	-25.94	-1.59	2231.	15202.	11348.	G S1 = L S1
500.0	100.	-1623.	-25.94	-1.59	2231.	15202.	11348.	G S1 = L S1
600.0	100.0	185.	-22.64	-1.92	4833.	18415.	13767.	G S1 = L S1
600.0	100.	185.	-22.64	-1.92	4833.	18415.	13767.	G S1 = L S1
700.0	100.0	28930.	25.24	-.234E-01	28986.	11318.	11261.	G S1 = G S1
700.0	100.	28930.	25.24	-.234E-01	28986.	11318.	11261.	G S1 = G S1
298	0.01	35602.	38.84	-.234E-01	35602.	24029.	24029.	G S1 = G S1
298.0	.100E-01	35602.	38.84	-.234E-01	35602.	24029.	24029.	G S1 = G S1

Conversational input and output using the reaction path program illustrating the calculation of the stable phase for a given set of conditions.

data base. Other work in progress is concerned with increasing the scope of the system. Under development are programs involved with the calculation of Pourbaix diagrams, the calculation of ternary composition-composition diagrams with special emphasis on fused salt systems, and the graphical representation of the thermodynamic parameters for various chemical reaction paths, among others.

F*A*C*T is expected to be on-line with the three programs described in this article and a limited data base by the end of 1977. A series of detailed articles describing each of the programs is to be published shortly.

REFERENCES

1. A.D. Pelton and H. Schmalzried, Met. Trans., 4, 1395 (1973).
2. A.D. Pelton and W.T. Thompson, Prog. Sol. State Chem., 10, 119 (1975)
3. "A Sampler of Coupled Thermodynamical and Phase Diagram Data for Metallic Systems", Calphad Project 1975.
4. A. Dalvi and R. Sridhar, to be published.
5. H. Davies and W.W. Smeltzer, J. Electrochem. Soc., 119, 1362 (1972).

ACKNOWLEDGMENTS

The authors are indebted to the National Research Council of Canada for a COOP grant, and to the Canadian department of Energy Mines and Resources for financial support of the project concerned with the calculation of potential-composition diagrams in ternary system. Thanks are due to the computer centres of Ecole Polytechnique and McGill Universities for their help and cooperation.



THE CALCULATION OF POURBAIX DIAGRAMS USING A MODIFIED LINEAR PROGRAMMING TECHNIQUE

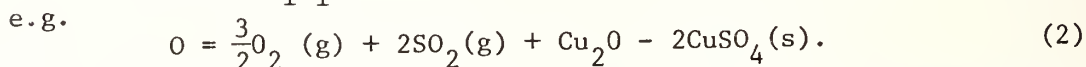
Barry H. Rosof

Technology Division, Cabot Corporation, Kokomo, Indiana 46901

An algorithm for calculating Pourbaix Diagrams (both partial pressure diagrams and potential pH diagrams) that is particularly suitable for use on a digital computer is presented. The algorithm consists of two principal parts. In the first part, the thermodynamic conditions under which a given phase is stable with respect to all other phases is formulated as a set of linear inequalities. In the second part, the set of linear inequalities is solved by a modified linear programming technique to yield the region in which the subject phase is the stable phase.

Any chemical reaction can be written as

$$0 = \sum v_i A_i, \quad (1)$$



By convention Species 3 and 4 are taken as the metal bearing species. The condition that Species 3 is stable wrt Species 4 ($\Delta G_R \leq 0$) can be written after rearranging and after fixing the activities of all species except Species 1 and 2 as

$$a_1 \xi_1 + a_2 \xi_2 \leq B, \quad (3)$$

where

$$-B = \Delta G_R^\circ + \sum_{i=3}^n v_i RT \xi_i, \quad (4)$$

$$\xi_i = \ln a_i \text{ or } \ln P_i \quad (5)$$

and

$$a_i = v_i RT. \quad (6)$$

In the present case

$$\frac{3}{2} RT \ln P_{O_2} + 2RT \ln P_{SO_2} \leq \Delta G_R^\circ, \quad (7)$$

where the activities of the solid phases have been set equal to unity.

For Species 3 to be stable it must not only be stable wrt Species 4 but also stable wrt all other possible metal bearing species, e.g. Cu_2O must be stable wrt CuS , Cu_2S , Cu , CuO , etc., as well as wrt $CuSO_4$. If there are n metal bearing species there are $n-1$ stability conditions, each of the form given in Equation 3. The $n-1$ stability conditions, or constraints, define the region where Species 3 (Cu_2O) is stable as a function of ξ_1 and ξ_2 ($\ln P_{O_2}$ and $\ln P_{SO_2}$). The constraints delimit a polygon in ξ_1 - ξ_2 space.

The problem of finding the region (of stability) that satisfies the $n-1$ constraints can be solved by a modified version of the linear programming technique known as the two phase simplex process.

In Phase 1 the standard tableau is set up, but the cost row is omitted. (The "cost" row for Phase 1 is retained.) The conventional Phase 1 algorithm is executed leading to a basic feasible solution.

A basic feasible solution corresponds to one corner of the polygon delimiting the region of stability. The corner where Cu, Cu₂S and Cu₂O coexist (Fig. 1) is a basic feasible solution for Cu₂O. The object in Phase 2 is to find all basic feasible solutions.

The algorithm for selecting the vector to enter the base in Phase 2 is modified as follows: The two vectors not in the base are labeled A and B. Vector A is chosen to enter the base, Vector B becomes Vector A, and the vector leaving the base becomes Vector B. The vector leaving the base is chosen in the standard fashion so that the new solution is also a basic feasible solution. This procedure is repeated until the original basic feasible solution is obtained, yielding all corners of the polygon.

A new species is then chosen as the subject species and the entire procedure repeated to yield the polygon delimiting its region of stability. This procedure is continued until the region of stability is found for all metal bearing species to yield the complete diagram.

Electrochemical as well as high temperature systems can be treated. Additional non-metal bearing chemical species can be included at fixed activities. For example, the Cu-O₂-SO₂ diagram changes markedly if chlorine is introduced into the system at a fixed partial pressure of 10⁻¹⁰ atm.

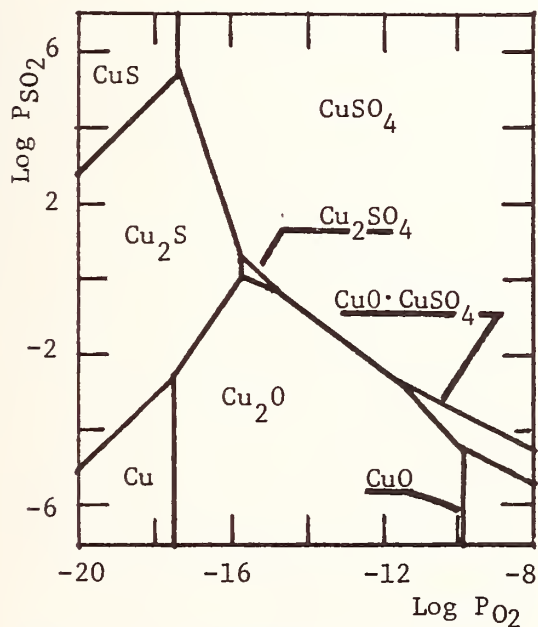


Fig. 1 Cu-O₂-SO₂ System
T = 700°K.

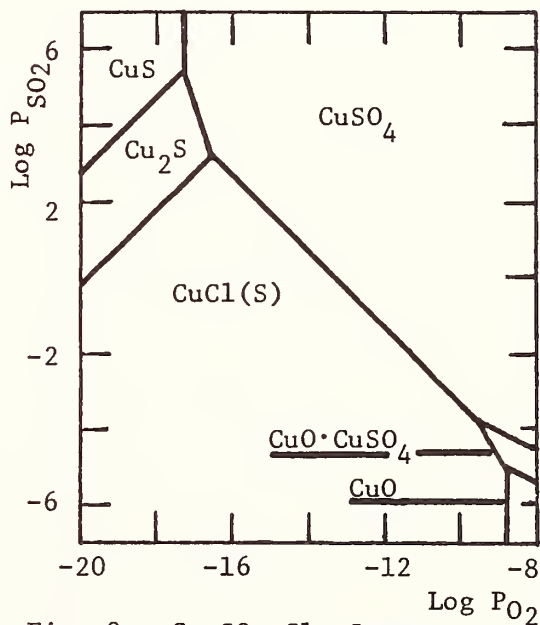


Fig. 2. Cu-SO₂-Cl₂ System
T = 700°K P_{Cl₂} = 10⁻¹⁰ atm
P_{CuCl(g)} < 10⁻² atm.
P_{Cu₃Cl_{3(g)}} < 10⁻² atm.

Computer software (Fortran IV) has been developed. Calculation of
of Pourbaix Diagrams using this software has proved to be very inexpensive
and efficient. Copies of the computer software can be obtained by writing
to:

Dr. Barry H. Rosof
Technology Division
Cabot Corp.
1020 W. Park Avenue
Kokomo, Indiana 46901



THEORETICAL CONCEPTS USEFUL IN THE CALCULATION OR STORAGE OF PHASE DIAGRAMS OF IONIC SYSTEMS*

Marie-Louise Saboungi and Milton Blander
Chemical Engineering Division, Argonne National Laboratory, Argonne, Illinois 60439

Introduction

Solution theories which provide a reasonable representation of the thermodynamic behavior of multicomponent ionic solutions can prove to be important in a variety of applications. One can use theoretical equations:

1. to calculate phase diagrams a priori from the subsidiary binaries,
2. to construct and complete phase diagrams from very few measured points,
3. to check the self consistency of published phase diagrams and consequently to provide a logical basis for the selection of reliable diagrams, and
4. to efficiently store phase diagrams with very few parameters.

We will focus on the conformal ionic solution theory for ternary systems¹⁻⁵ since it is the only theory which accounts for coulombic interactions between ions in a rigorous way. The calculations based on a statistical mechanical perturbation method have only been made for simple systems containing ions of the same charge. We will also present empirical extensions for cases where the cations and/or the anions have different charges.

Ternary ionic systems contain four kinds of ions. Those having two kinds of cations and two kinds of anions are ternary reciprocal systems, and those with three kinds of cations (or anions) and one kind of anion (or cation) are additive ternary systems. In the following sections, we will discuss the theory for these two classes of systems.

1. Reciprocal Systems

The calculation for reciprocal systems has been carried out only to second order for the simplest member of the class of reciprocal systems, i.e., the $A^+, B^+/X^-, Y^-$ system. In such a system, there are four constituents, AX, AY, BX and BY, and only three components which can be chosen in

four different ways. If AY, BX and BY are chosen as the three components, then the total molar Gibbs free energy of mixing is given by

$$\begin{aligned} \Delta G^m = RT[& X_A \ln X_A + X_B \ln X_B + X_X \ln X_X + X_Y \ln X_Y] \\ & + X_A X_X \Delta G^\circ + \lambda_{AXAX} X_A X_X X_Y + \lambda_{BAXX} X_B X_A X_X X_Y + \lambda_{XAXX} X_X X_A X_X X_B \\ & + \lambda_{YXAX} X_Y X_X X_A X_B + X_A X_B X_X X_Y \Lambda \end{aligned} \quad (1)$$

where ΔG° is the standard Gibbs free energy change for the metathetical reaction $AX + BY \rightleftharpoons AY + BX$, the X_i 's are ion fractions of the i th ion, the λ 's are coefficients deduced from the four subsidiary binaries (e.g., in the binary AX-BX, the excess Gibbs free energy of mixing, $\Delta G_X^E = \lambda_{AXAX} X_A X_X$) and Λ is calculated to be $\frac{-(\Delta G^\circ)^2}{2ZRT}$ where Z is a parameter taken to be 6.

Reciprocal systems generally have a complex topology which is largely related to the terms containing ΔG° . In the simplest case where no compounds or solid solutions exist, the phase diagram is characterized by two ternary eutectics or one ternary eutectic and one ternary peritectic. If $|\Delta G^\circ|$ is large, the isothermal contours are complex curves which reflect the large deviations from ideality, positive deviations for one pair of constituents (e.g., AX and BY when ΔG° is positive) and negative deviations for the other pair of constituents (e.g., AY and BX).

Equation (1) has been used to calculate liquidus phase diagrams of simple reciprocal systems a priori from data on lower order systems.^{6,7} To do this, expressions for activity coefficients of the four constituents are derived from Eq. (1). For the component BY, for example, one can define an activity coefficient by the relation

$$a_{BY} = X_B X_Y \gamma_{BY} \quad (2)$$

where a_{BY} and γ_{BY} are the activity and the activity coefficient of component BY, respectively. The activity coefficients are given by

$$\begin{aligned}
 RT \ln \gamma_{BY} = & X_A X_X \Delta G^\circ + X_A X_X (X_X - X_Y) \lambda_A + X_X (X_A X_Y + X_B X_X) \lambda_B \\
 & + X_A (X_A X_Y + X_B X_X) \lambda_Y + X_A X_X (X_A - X_B) \lambda_X \\
 & - X_A X_X (X_A X_Y + X_B X_X - X_B X_Y) \frac{(\Delta G^\circ)^2}{2ZRT}
 \end{aligned} \quad (3)$$

For those simple systems where neither compounds nor solid solutions are present, liquidus temperatures may be calculated by properly combining Eqs. (2) and (3) with the Schröder-van Laar equation. A comparison between the measured and calculated liquidus phase diagrams for the Li,Na/F,Cl and Li,K/F,Cl systems is illustrated in Figs. 1 and 2, respectively. Even though the phase diagrams for these two systems have rather complex topologies, it can be seen that the relatively simple Eqs. (1)-(3) lead to a reasonably good representation of both systems. However, differences do exist between the measured and calculated phase diagrams. On the one hand, some of these differences arise because of uncertainties in constructing such a complex phase diagram from a limited number of measurements. There were not enough measured points to fully define the shape of most of the liquidus isotherms and it is probable that the shapes calculated from theory are thermodynamically more self-consistent than the reported phase diagrams constructed from a limited amount of data. For example, the 700 and 750°C isotherms in the NaCl phase field of the calculated diagram are probably more reliable than the reported isotherms.

On the other hand, some of the differences between the measured and calculated phase diagrams are related to inadequacies of Eq. (1) which has been derived only to second order. Measurements of enthalpies of mixing

of many binary systems indicate that higher order terms are necessary in order to describe the results accurately. For binary systems having relatively large deviations from ideality, even fourth order terms are needed. Liquidus temperatures are generally fairly insensitive to these higher order terms so that, although necessary, highly precise values of these terms are not needed to improve calculated phase diagrams. Equation (1) can be written to include some of the higher order terms of the binary systems as follows:

$$\begin{aligned} \Delta G^m = & RT[X_A \ln X_A + X_B \ln X_B + X_X \ln X_X + X_Y \ln X_Y] \\ & + X_A X_X \Delta G^\circ + X_A \Delta G_A^E + X_B \Delta G_B^E + X_X \Delta G_X^E + X_Y \Delta G_Y^E \\ & - X_A X_B X_X X_Y \frac{(\Delta G^\circ)^2}{2ZRT} \end{aligned} \quad (4)$$

where ΔG_i^E is the excess Gibbs free energy of mixing of the binary system having the common ion, i . For example, ΔG_A^E is the excess free energy of mixing of the mixture AX-AY at an ion fraction X_X (and X_Y) for which the calculation is made. The functions ΔG_i^E can be constructed to describe the binary systems as accurately as desired. As a result, the binary edges of the phase diagram can be made as close to measurements as desired. By thus constraining the edges of the diagrams to be much more precise, the remainder of the diagram, especially the areas near the edges, can be significantly improved. A common form which might be used for ΔG_A^E , for example, is

$$\Delta G_A^E = a \frac{X_X X_Y}{X_X X_Y} + b \frac{X_X X_Y (X_X - X_Y)}{X_X X_Y} + c \frac{X_X^2 X_Y^2}{X_X X_Y} \quad (5)$$

Another modification of Eq. (1) involves a different approximation for Λ :

$$\Lambda = -(\Delta G^\circ + \sum \lambda_i/2)^2 / 2ZRT \quad (6)$$

or even a more general form such as

$$\Lambda = -\left(\Delta G^\circ + 2\sum_i \Delta G_i^E(50-50 \text{ mixture})\right)^2/2ZRT \quad (7)$$

The form in Eq. (6) has been found to be necessary in order to calculate miscibility gaps in reciprocal systems. In systems where the binary systems exhibit relatively large deviations from ideality, corrections as in Eqs. (6) and (7) compensate, at least in part, for some of the mathematical peculiarities inherent in a series expansion truncated beyond the second order terms.

Thus far we have considered simple systems. To our knowledge, no rigorous theory exists for charge asymmetric systems with cations and/or anions of different charge types. An empirical extension of equations derived from the CIS theory has been tried. The Gibbs free energy of mixing would read as

$$\begin{aligned} \Delta G^m = & RT[X_A \ln X_A + X_B \ln X_B + X_X \ln X_X + X_Y \ln X_Y] \\ & + X'_A X'_X \Delta G^\circ + X'_A \Delta G_A^E + X'_B \Delta G_B^E + X'_X \Delta G_X^E + X'_Y \Delta G_Y^E \\ & - X'_A X'_B X'_X X'_Y \frac{(\Delta G^\circ)^2}{2ZRT} \end{aligned} \quad (8)$$

where ΔG° is now the standard Gibbs free energy change per equivalent in the metathetical reaction and X' represents equivalent fractions. For a number of asymmetric binary systems, as, e.g., the $AX-BX_2$ system, the excess Gibbs free energies of mixing are reasonably well represented by an expression such as

$$\Delta G_X^E = X'_A X'_B \lambda_X \quad (9)$$

A test of expressions such as Eqs. (8) and (9) has demonstrated that reasonably representative phase diagrams of asymmetric systems may be calculated a priori from minimal information on the binary systems and from data on the free energies of formation of the four constituents.⁹ Where equations such as Eq. (9) do not represent the deviations from ideality of the binaries very well, other more accurate forms may be substituted for ΔG_1^E .

The equations described have been used to calculate a number of liquidus phase diagrams of simple and asymmetric reciprocal systems a priori.⁵⁻⁹ The correspondence between measured and calculated phase diagrams has generally been good. Consequently, the techniques can be used to reliably predict phase diagrams as illustrated in Fig. 3, which shows the calculated liquidus phase diagram for the $\text{Li}^+, \text{Na}^+ / \text{OH}^-, \text{CO}_3^{=}$ system. Knowledge of the phase relations in this system is of special interest for fuel cell technology. Again, this computation has been indeed simplified since neither solid solutions nor compounds have been considered. A more accurate calculation should include the two reported binary compounds; this can be done in a relatively simple and standard manner so that the total Gibbs free energy of the system is minimized. (In the particular case of Fig. 3, the binary compounds undoubtedly subtend a very small fraction of the composition field.)

2. Additive Ternary Systems

The conformal ionic solution theory has also been derived for additive ternary systems up to fourth order terms.⁴ If we designate an additive ternary system as AX-BX-CX, for example, the theory leads to the expression

$$\Delta G^E = \sum_{i < j} \sum \lambda_{ij} X_i X_j + \sum_{i \neq j} \sum b_{ij} X_i^2 X_j + \sum_{i < j} \sum c_{ij} X_i^2 X_j^2 \quad (10)$$

$$+ AX_1 X_2 X_3 + \sum_i B_i X_i^2 X_j X_k$$

$i \neq j < k$

where 1, 2 and 3 represent the salts AX, BX and CX, respectively. All of the coefficients in Eq. (10) can be evaluated from data on the three subsidiary binary systems. The coefficients λ_{ij} , b_{ij} and c_{ij} are directly related to the second, third and fourth order terms which describe the three binary systems. The coefficient B_i is given exactly by the relation

$$B_i = 2(c_{ij}c_{ik})^{1/2} \text{ with } i \neq j \neq k \quad (11)$$

and to a good approximation A is given by

$$A = -(b_{12}^{1/3} + b_{13}^{1/3})(b_{21}^{1/3} + b_{23}^{1/3})(b_{31}^{1/3} + b_{32}^{1/3}) \quad (12)$$

where $b_{ij} = -b_{ji}$ ($i \neq j$). Equation (12) is exact when fourth order terms are not included (e.g., $c_{ij} = 0$ and $B_i = 0$). Up to the second order, the equations derived from the CIS theory appear to be adequate for representing phase diagrams of simple systems containing only monovalent ions and having relatively small deviations from ideality.³ No systems with binary or ternary compounds, solid solutions, or with cations or anions of different charge type have been yet investigated. Similar to what has been done for reciprocal systems, an extension of Eqs. (10)-(12) can be made to represent the thermodynamics of solutions containing ions of different valences.

Another possible empirical form is

$$\Delta G^E = \sum_{k \neq i < j} X'_k \Delta G^E_{ij} + CX'_1 X'_2 X'_3 + \sum D_i X_i'^2 X'_j X'_k \quad (13)$$

where X' represents equivalent ion fractions, C and D_i are empirical constants and ΔG^E_{ij} is the total excess Gibbs free energy of mixing of the

binary systems i-j at mole fractions such that the ratio (X_i/X_j) in the binary is the same as in the ternary.

Storage of Phase Diagrams

Thus far, theoretical equations and empirical extensions have been only applied to calculate phase diagrams a priori. They can also be used to construct reliable phase diagrams from a relatively small number of experimental points at key compositions. One potential use which has been considered very little is for the computer storage of complex phase diagrams. Such storage, if techniques for accurately representing ternary phase diagrams can be developed, would provide ready and remote access to large collections of phase diagrams stored in central data banks.

For the storage of phase diagrams, one requires equations which can accurately represent known phase diagrams. The accuracy of the equations in representing phase diagrams can be improved if one relaxes the constraints on the coefficients of all the equations considered. The theory defines these parameters within the limitations inherent in the models used. For example, the parameter Z in Eq. (8) is constrained by the theory to be the same for an entire class of conformal solutions. If Z could be considered as a parameter which can have one of several (let us say 10) possible values, the fit of a calculated phase diagram to any given reliable measurements can be improved. Such an adjustment probably would compensate for higher order terms which are not included in the equations.

In order to utilize Eqs. (8) and (9) combined with the Schröder-van Laar equation to calculate phase diagrams, one requires data on enthalpies of fusion and free energies of formation of the four constituents as well as the four binary parameters, λ_1 , and Z . If ΔH_m , ΔG° and λ_1 can be considered to be independent of temperature, a minimum of 13 parameters is necessary for one system. If the temperature dependence of the parameters needs to be taken into account, more than 13 are required. However, if one considers a large collection of similar phase diagrams, the number of parameters per phase diagram is reduced considerably because some of the parameters are common to several systems. For example, if one considers all the possible phase diagrams one can make from ten different cations and ten different anions, there are 2025 ternary reciprocal systems, 2400 additive ternary systems, 900 binary systems and 100 different constituent compounds.

To store the ternary reciprocal systems separately without considering the commonality of any of the parameters would require at least 26,000 parameters. By considering all the systems together, one can store all the phase diagrams with a minimum of 900 binary parameters, 100 values of the free energies of formation, 100 values of enthalpies of fusion at a standard temperature, and perhaps 10 values of Z . In order to include binary or ternary compounds or solid solutions, at least one more parameter is necessary per compound or solid solution.

Similarly, for additive ternary systems, if only second order equations are required, each phase diagram would require three parameters λ_{ij} plus three enthalpies of fusion giving a minimum of six parameters for one diagram. For a collection of ten cations and ten anions, the 2400 possible additive ternary systems, if considered separately, would require a minimum of over 10^4 parameters. When considered together, there are a minimum of

only 900 binary parameters λ_{ij} , and 100 parameters for the enthalpies of fusion. For all ternary systems, additive and reciprocal, the minimum number required is 900 binary parameters, 100 enthalpies of fusion, 100 values of the free energies of formation at a standard temperature, and 10 values of Z .

Thus far, we have considered only a minimal set of parameters. More complex expressions for the excess free energies of mixing of the binary systems would require more. Consideration of the temperature coefficients of any of the parameters would also increase the number. For example, the free energies of formation are functions of temperature. However, taking this into account is not as large an improvement as it might seem since the values of ΔG° which are calculated from these are generally relatively independent of temperature, and ΔG° calculated at one standard temperature for all systems may prove to be reasonable at all temperatures. The temperature coefficients of ΔH_m are usually not important unless liquidus temperatures are much lower than the melting points. Further parameters are required if compounds and solid solutions are accounted for. Even when all these (including temperature coefficients) are considered, the number of parameters needed to describe the large number (4425) of ternary systems one can make from ten cations and ten anions is still relatively small (probably less than 9000 parameters). Consequently, if one considers the complexity of ternary phase diagrams, especially of ternary reciprocal systems, theoretical equations hold the promise of being used for the economical storage of phase diagrams in data banks.

Conclusions

Theories of ternary ionic systems permit one to calculate phase diagrams a priori. Such calculations also support their utility in the construction of reliable phase diagrams from a small number of well-chosen experimental measurements. One unexplored use is for the computer storage of complex phase diagrams. If calculational techniques and thermodynamically self-consistent extensions of theory can be developed, the economical storage of accurate phase information in large data banks can be effected.

REFERENCES

*Work performed under the auspices of the U. S. Energy Research and Development Administration.

1. H. Reiss, J. L. Katz and O. Kleppa, J. Chem. Phys. 36, 144 (1962).
2. M. Blander and S. J. Yosim, J. Chem. Phys. 39, 2610 (1963).
3. M. L. Saboungi and P. Cerisier, J. Electrochem. Soc. 121, 1258 (1974).
4. M. L. Saboungi and M. Blander, J. Chem. Phys. 63, 212 (1975).
5. M. Blander and M. L. Saboungi, "Fundamental Aspects of Molten Salt Solutions and Their Applications in Technology," in Proceedings of the International Symposium on Molten Salts, ed., Pemsler et al., The Electrochemical Society, Princeton, N. J. (1976) pp. 93-110.
6. M. L. Saboungi and M. Blander, High Temp. Sci. 6, 37 (1974).
7. M. Blander and L. E. Topol, Inorg. Chem. 5, 1641 (1966).
8. M. L. Saboungi, H. Schnyders, M. S. Foster and M. Blander, J. Phys. Chem. 78, 1091 (1974).
9. M. L. Saboungi and M. Blander, J. Am. Ceram. Soc. 58, 1 (1975).

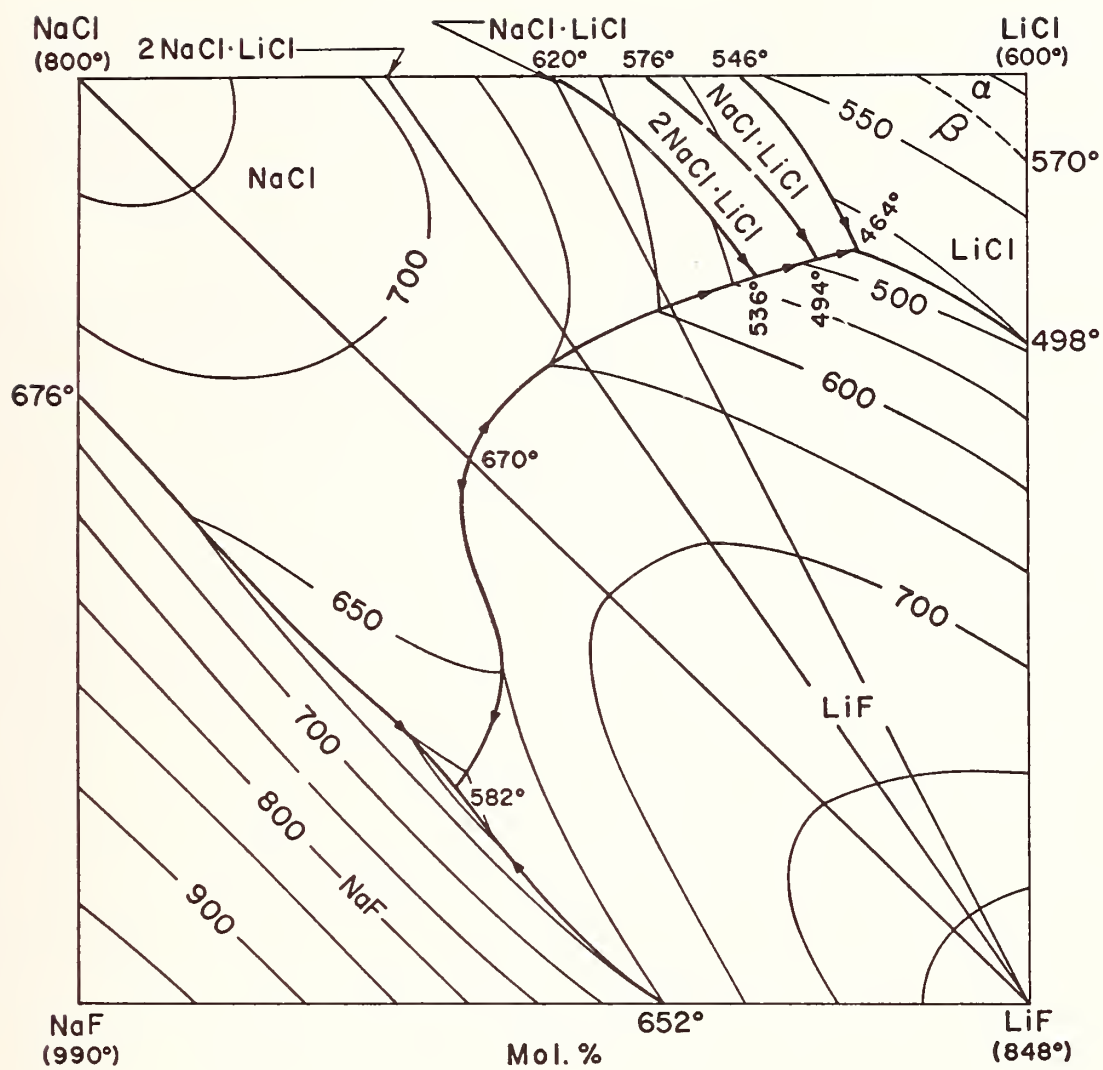


FIGURE 1a. THE MEASURED PHASE DIAGRAM OF $\text{Li}^+, \text{Na}^+/\text{F}^-, \text{Cl}^-$

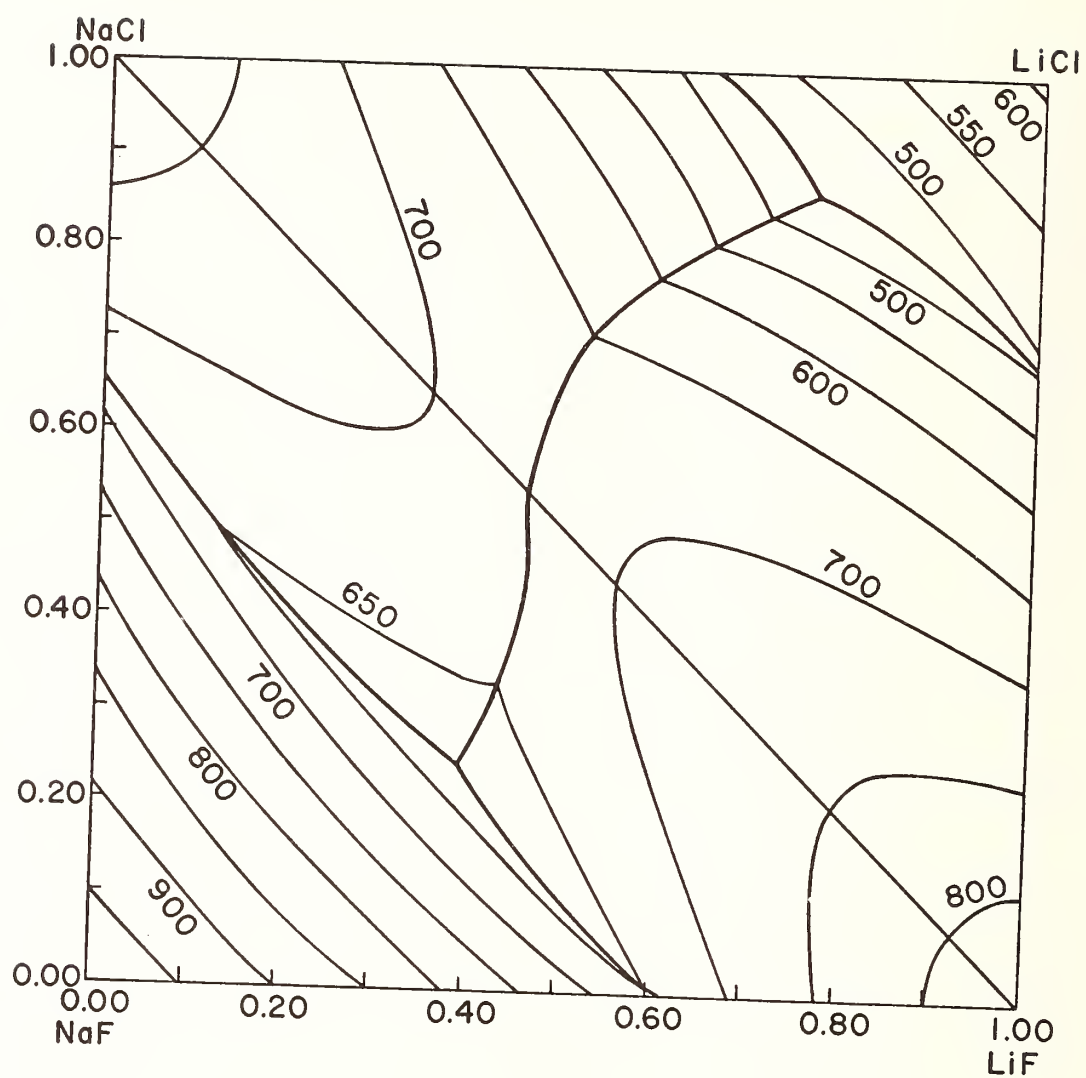


FIGURE 1b. THE CALCULATED PHASE DIAGRAM OF $\text{Li}^+, \text{Na}^+/\text{F}^-, \text{Cl}^-$

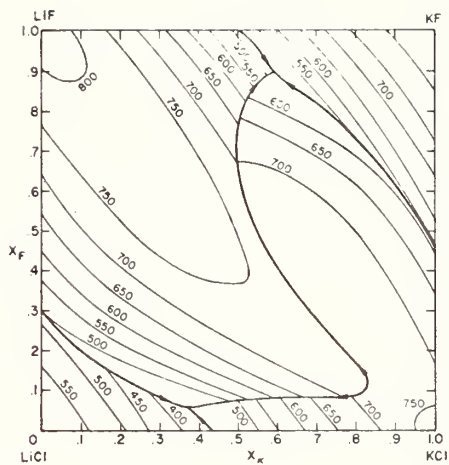
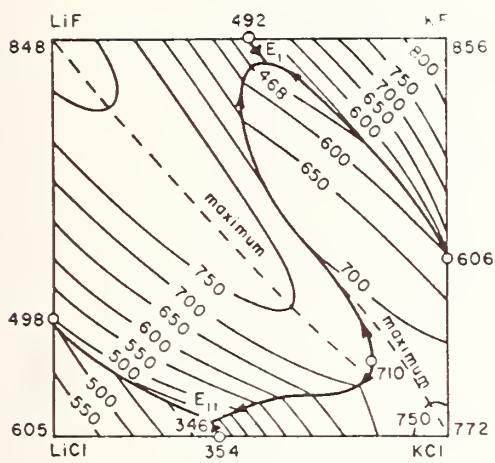


FIGURE 2. THE Li,K/F,Cl PHASE DIAGRAM

a. MEASURED

b. CALCULATED

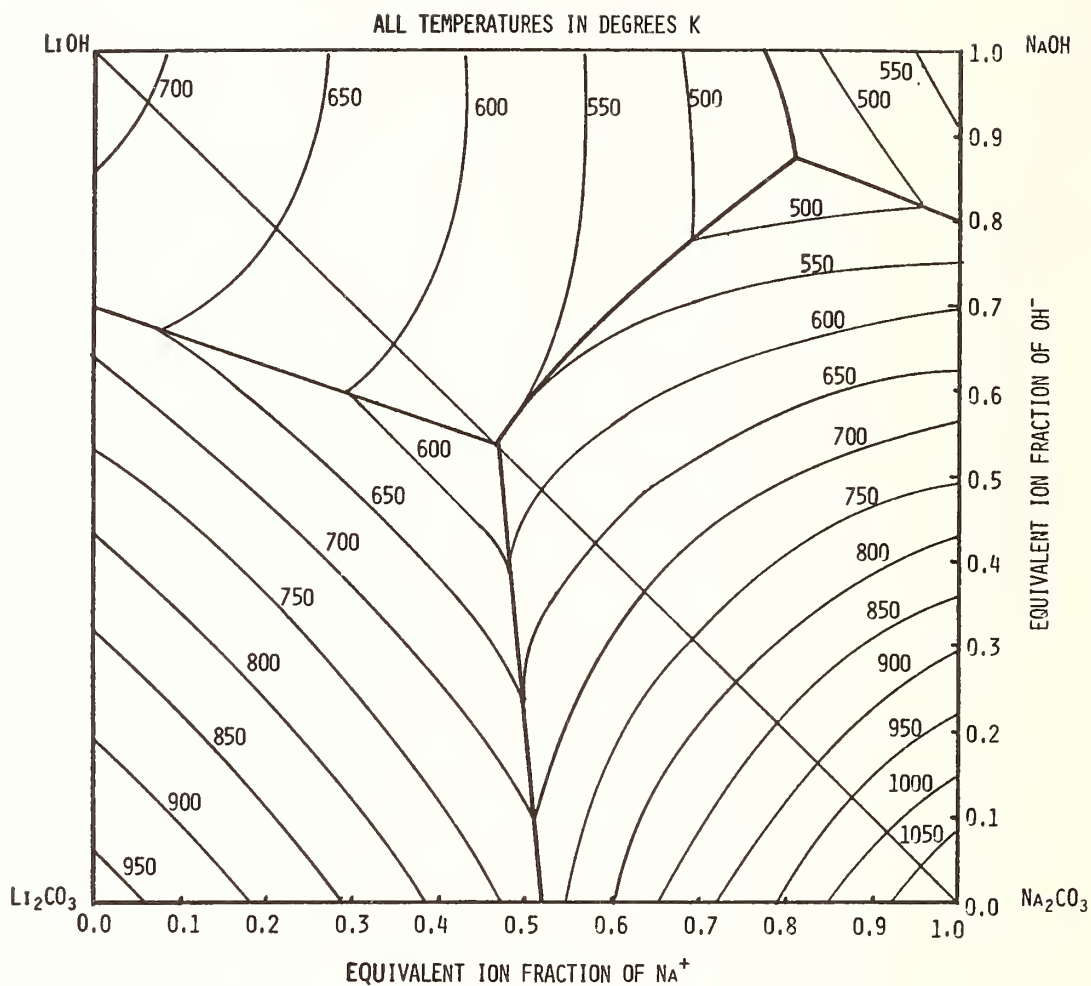


FIGURE 3. COMPUTER GENERATED PHASE DIAGRAM OF THE Li,Na/OH,CO_3 SYSTEM



ESTIMATION OF ISOTHERMAL SECTIONS OF TERNARY PHASE DIAGRAMS OF LITHIUM CONTAINING SYSTEMS: THE Al-Li-Mg SYSTEM*

Marie-Louise Saboungi and Chen C. Hsu

Chemical Engineering Division, Argonne National Laboratory, Argonne, Illinois 60439

INTRODUCTION

Currently, in the development of high-temperature batteries at the Argonne National Laboratory, solid Li-Al alloys appear to be the leading candidates for the negative electrode.¹ Despite the overall good performance of the cells, some problems were encountered; after repeated cycling, a loss of capacity accompanied by a change in the morphology of Li-Al alloys was observed.² In an effort to overcome these limitations and improve the Li diffusivity in the α -Al, modifications either in the design or in the constituents are being examined. One approach consists of adding an appropriate third element (e.g., Mg) to the Li-Al alloys. Consequently, a knowledge of the phases present in the Al-Li-Mg system and their boundaries at the temperatures of operation of the battery (T ranging from 673 K to 773 K) is vital. In the literature, there are very few and often irreconcilable experimental data related to the phase diagram of the Al-Li-Mg system.³⁻⁶

These considerations led us to calculate isothermal sections of Al-Li-Mg using a computer-program^{7a} developed by Kaufman and Nesor.^{7b} In this particular practical case, the numerical method of generating phase diagrams presents several advantages. First, for the subsidiary binary systems, we can check the self-consistency of the measured phase diagrams and the published thermodynamic data and consequently select the most reliable phase diagrams. Second, we can obtain additional information such as the free energy of formation at different temperatures of the reported binary compounds. Third, we can define, to a good approximation, the topological features of the ternary Al-Li-Mg system and therefore minimize the number of measurements necessary to obtain a reliable phase diagram. One needs only few measurements at well-defined compositions to check the accuracy of such calculations.

We report on the calculations of isothermal sections ($T = 673$ K, 723 K and 773 K) of the Al-Li-Mg. An additional temperature ($T = 648$ K) was investigated to allow for a direct comparison between the calculated phase diagram and earlier data limited to the magnesium-rich corner.

I. Method of Calculations

The numerical method used in this investigation has been extensively described by Kaufman and coworkers. For the sake of brevity, we will only outline the equations used for the solution phase interactions and for the compound-solution interactions in the binary and ternary systems.

1. Solution Phase Interactions

a. Binary Mixtures

In these calculations, an extension of the regular solution model is used to describe the behavior of the mixture. In the i - j system, $G_{ij}(\Phi)$, the Gibbs free energy of a solution phase, Φ , is defined as:

$$G_{i,j}(\Phi) = x_i G_i^\circ(\Phi) + x_j G_j^\circ(\Phi) + RT[x_i \ln x_i + x_j \ln x_j] + \Delta G_{i,j}^E(\Phi) \quad (1)$$

where $G_i^\circ(\Phi)$ is the Gibbs free energy of the pure i th element in the Φ phase, x_i is the atomic fraction of the i th element, and $\Delta G_{i,j}^E(\Phi)$ refers to the excess Gibbs free energy of the solution in the Φ phase. In what follows, this latter function is assumed to vary with composition according to the equation:

$$\Delta G_{i,j}^E(\Phi) = x_i x_j [x_i \Phi(i,j) + x_j \Phi(j,i)] \quad (2)$$

where $\Phi(i,j)$ and $\Phi(j,i)$ can be temperature dependent functions. This formulation presents the advantage of taking the asymmetry of the solution into account since $\Phi(i,j)$ could differ from $\Phi(j,i)$. If $\Phi(i,j) = \Phi(j,i)$, the

solution is symmetrical. If $\Phi(i,j) = \Phi(j,i) = \text{constant}$, the solution is regular according to the Hildebrand definition. If $\Phi(i,j) = \Phi(j,i) = 0$, the solution is ideal. In these calculations, $\Phi(i,j)$ and $\Phi(j,i)$ are expressed as

$$\Phi(i,j) = a + bT \quad (3)$$

and

$$\Phi(j,i) = a' + b'T \quad (4)$$

where a , a' , b and b' are constants calculated either from reliable thermodynamic data (electromotive force data, calorimetric data, etc.) or from the measured phase diagram using the Schröder-van-Laar equations. Finally, a liquid interaction coefficient can be defined as:

$$L_{i,j}(x_i, x_j) = x_i L(i,j) + x_j L(j,i) \quad (5)$$

b. Ternary Mixtures

In the ternary system, i-j-k, the Kohler equations⁸ are used to describe the solution interactions. The Gibbs free energy of mixing of a solution phase, Φ , is given by:

$$\begin{aligned} \Delta G_{i,j,k}(\Phi) &= G_{i,j,k}(\Phi) - \sum_{\alpha} N_{\alpha} G_{\alpha}^{\circ}(\Phi) \\ &= RT \sum_{\alpha} N_{\alpha} \ln N_{\alpha} + \frac{1}{2} \sum_{\alpha} \sum_{\beta \neq \alpha} \frac{N_{\alpha} N_{\beta}}{(N_{\alpha} + N_{\beta})} [N_{\alpha} \Phi(\alpha, \beta) + N_{\beta} \Phi(\beta, \alpha)] \end{aligned} \quad (6)$$

where α is a running index ($\alpha = i, j, k$) and N_{α} refers to the atom fraction of the α th constituent ($\sum_{\alpha} N_{\alpha} = 1$). The quantities, N_{α} , are easily related to the binary atom fractions, x_{α} . The coefficients, $\Phi(\alpha, \beta)$ and $\Phi(\beta, \alpha)$, are those determined in the subsidiary binary, α - β [Eq. (2)]. Consequently, the calculations of the ternary thermodynamic properties can be carried out once the binary coefficients are determined. Using classical relations,

one can derive from Eq. (3), other thermodynamic functions such as $\overline{\Delta G}_\alpha(\phi)$, the partial Gibbs free energy of each element present in the solution, $\Delta S_{i,j,k}(\phi)$, the entropy of mixing and $\Delta H_{i,j,k}(\phi)$, the enthalpy of mixing:

$$\overline{\Delta G}_\alpha(\phi) = \frac{\partial}{\partial n_\alpha} [\Delta G_{i,j,k}(\phi)]_{T,P,n_\beta \neq n_\alpha} \quad (7)$$

$$\Delta S_{i,j,k}(\phi) = - \frac{\partial [\Delta G_{i,j,k}(\phi)]}{\partial T} \quad (8)$$

and

$$\Delta H_{i,j,k}(\phi) = \Delta G_{i,j,k}(\phi) + T \Delta S_{i,j,k}(\phi) \quad (9)$$

where n_α is the number of moles of the α th constituent. Finally, the fact that the Kohler equation is symmetrical with respect to each of the components is an advantage over other equations such as the Toop equation.⁹

2. Compound Phase Interactions

a. Binary Mixtures

For the sake of simplicity, all compounds will be considered as having a fixed stoichiometry, i.e., as line compounds. The Gibbs free energy of the compound, P, defined by a fixed stoichiometric composition, x_i^* and x_j^* , is expressed by:

$$G(P) = x_i^* G_i^\circ(\theta) + x_j^* G_j^\circ(\theta) + x_i^* x_j^* [L(x_i^*, x_j^*) - C] \quad (10)$$

where θ is designated as the base phase of the compound, P; $L(x_i^*, x_j^*)$ represents the interactions coefficient in the liquid mixture evaluated at the composition of the compound [Eq. (5)]; and C is defined as the compound parameter.

The choice of the base phase is arbitrary. However, for most of the cases, θ would be identical to the most stable form of either i

or j, at the temperature and pressure of interest. The Gibbs free energy of formation of the compound, P, can be derived from Eq. (10):

$$\begin{aligned}\Delta G_f(P) &= G(P) - x_1^* G_1^\circ(\theta) - x_j^* G_j^\circ(\theta) \\ &= x_1^* x_j^* [L(x_1^*, x_j^*) - C]\end{aligned}\quad (12)$$

The compound parameter, C, can be computed (i) from data on the thermodynamic functions of formation of the compound, if available; (ii) from the measured phase diagram utilizing mainly the melting point of the compound and some other characteristic liquidus temperatures; (iii) more often, by coupling thermodynamic information with phase diagram data. The compound parameter can be expressed in the following form:

$$C = c_1 + c_2 T \quad (13)$$

If the compound is unstable, C is usually set equal to zero.

b. Ternary Mixtures

In the ternary system, the present status of the calculations allows for the variation in compound stoichiometry.¹⁰ One can consider a compound, P, defined by a base phase, θ , and having a general composition, N_1 , N_j and N_k . The compound is assumed to run between the composition $[(x_1^*)', (x_j^*)']$ in the subsidiary binary, i-j, and the composition (x_j^*, x_k^*) in the adjacent binary, j-k. The general compositions, N_α , can be related to the x_α^* by:

$$\begin{aligned}N_1 &= (x_1^*)' - N_j(1+p) \\ N_j &= 1 - N_1 - N_k \\ N_k &= (x_j^*)' + N_j p\end{aligned}\quad (14)$$

where

$$p = [x_j^* - (x_j^*)'] / x_k^* \quad (15)$$

Then, the Gibbs free energy of the compound can be written as:

$$G(P) = \sum_{\alpha} N_{\alpha} G_{\alpha}^{\circ}(\theta) + RT[N_1 \ln N_1 + N_j \ln N_j - (1-N_k) \ln(1-N_k)] \quad (16)$$

$$+ [1 - (N_j/N_k)] \Delta G_f(A) + [N_j/(1-N_k)] \Delta G_f(B)$$

The compound, A, is usually the stable compound positioned on the i-j binary; the Gibbs free energy of formation, $\Delta G_f(A)$, is given by:

$$\Delta G_f(A) = (x_i^*)' (x_j^*)' \left[L[(x_i^*)', (x_j^*)'] - C' \right] \quad (17)$$

where L and C' are calculated from data on the binary, i-j. The compound, B, positioned on the j-k binary is the "counterphase" of A; the Gibbs free energy of formation of B, $\Delta G_f(B)$, is expressed by:

$$\Delta G_f(B) = x_j^* x_k^* [L(x_j^*, x_k^*) - C] \quad (18)$$

where L and C are also derived from data on the j-k binary. It should be noted that B can be, and often is, unstable* or even hypothetical; as mentioned earlier, in these cases, C is usually set equal to zero or to an arbitrary value less positive than the value corresponding to A. The compound parameter of B can be considered as an adjustable parameter; for example, if data on the stability of the ternary compound, P, are available, then one can more accurately determine the value of the compound parameter of the counterphase. In this context, the calculations could be improved and set to match the selected data and therefore predict with more reliability the existence of phases and their boundaries in regions inaccessible to measurements.

*By definition, when the Gibbs free energy of formation of a compound is positive, the compound is then metastable or unstable.

The Gibbs free energy of formation of P can be written as:

$$\Delta G_f(P) = G(P) - \sum_{\alpha} N_{\alpha} G_{\alpha}^{\circ}(\theta) \quad (19)$$

where $G(P)$ is given by Eq. (16). Therefore, the thermodynamic properties of ternary compounds, and consequently the interactions between compounds in the ternary system and the solution phases, are well defined.

II. Results and Discussion

The numerical program used to carry out the present computations has been purchased from L. Kaufman and Nesor (ManLabs, NPL Materials Data Bank). The algorithm has been described elsewhere.^{7,10} We will only mention that the interactions in the subsidiary binaries and in the ternary mixture have been calculated on a pair-wise basis.

1. The Al-Li System

As mentioned earlier, the Al-Li alloys appear to be useful as negative electrodes in a high-temperature battery. A rather divergent set of data on the phase diagram of Al-Li exist in the literature.¹¹⁻¹⁴ The results of the most recent investigation by DTA (differential thermal analyses) techniques complemented by careful metallographic and x-ray analyses are represented in Fig. 1a.¹⁵ Some of the significant differences between the phase diagram of Myles and Settle¹⁵ and that selected by Hansen et al.¹⁶ are:

(i) The shape of the boundary of the solid solutions in the Al-rich side is completely different (one is concave, while the other is convex).

(ii) The melting point of the compound β -LiAl (non-stoichiometric LiAl) is 966 K¹⁵ as opposed to 991 K.¹⁶ In addition, the limits of the solubility of the α -Al (FCC-Al) in the β -LiAl disagree considerably with earlier data.

(iii) The data of Myles and Settle confirm the existence of the compounds Al_2Li_3 and Al_4Li_9 observed first by Tebbe et al.¹⁴ and Hansen and Smith,¹³ respectively. The stability of the peritectically melting compound, AlLi_2 , remains questionable.

In our calculations of the phase diagram of Al-Li, we have tried to couple the thermodynamic information when available¹⁷⁻²⁰ and the phase diagram of Myles and Settle. The lattice stabilities of the constituents are given in Table I; some [such as $G_{\text{Al}}^\circ(\text{L}) - G_{\text{Al}}^\circ(\text{FCC})$] are selected from standard thermochemical tables,²¹ and others [such as $G_{\text{Al}}^\circ(\text{L}) - G_{\text{Al}}^\circ(\text{HCP})$] are estimated by Kaufman.²² The interaction coefficients of the solution phases are calculated from recent emf (electromotive force) measurements^{17,18} using Eqs. (2)-(4). The calculated values are given in Table II.

The three compounds, AlLi , Al_2Li_3 and Al_4Li_9 , are treated as line compounds. The compound parameter of AlLi was calculated from both emf data¹⁹ obtained between $T = 282\text{--}389^\circ\text{C}$ and the measured melting point ($T = 966\text{ K}$).

The Gibbs free energy of formation of Al_2Li_3 was calculated at the metastable melting point* from Eqs. (10)-(13). Some values of the liquidus temperatures were also used to calculate the variations of the compound parameter with temperature (Table III).

To our knowledge, there is no thermodynamic information available for Al_4Li_9 . Therefore, the liquidus temperatures were used to calculate the compound parameter, C (Table III).

In order to compute the phase diagram, the following interactions were considered: L vs. FCC, L referring to liquid; L vs. LiAl ; FCC vs. LiAl ; L vs. Al_2Li_3 ; and L vs. Al_4Li_9 . The resultant phase diagram is given in

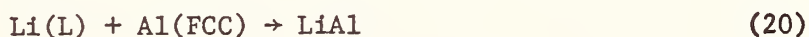
*The metastable melting point is determined by extrapolating the liquidus to the stoichiometric composition.

Fig. 1b. The calculated and experimental phase diagrams are in excellent agreement except in the Al-rich side; the shape of the computed solid solution boundary is closer to that selected by Hansen¹⁶ which is consistent with expectations for such solid solutions. The calculations also gave a better defined limit for the solubility of LiAl in Al(FCC). This limit has not been determined experimentally (note the dashed lines in Fig. 1a).

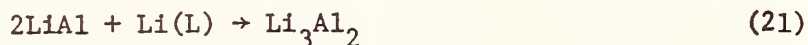
The computations are not only useful in constructing the phase diagrams but also in checking the self-consistency of the published thermodynamic data with the liquidus. For example, the computed Gibbs free energies of formation of the compounds (Table III) are in reasonable agreement with available measurements. For LiAl, our values compare well with those of Yao et al.¹⁹ (Table IV). However, at higher temperatures, the difference between our calculations and the values obtained by extrapolating the least-square fitted equation of Yao et al.¹⁹ increases somewhat: at $T = 773$ K, $\Delta G_f(\text{obs.}) = -3.24 \text{ kcal (g-atom)}^{-1}$ and $\Delta G_f(\text{calc.}) = -2.93 \text{ kcal (g-atom)}^{-1}$.

Recently, Selman et al.²⁰ estimated the Gibbs free energy of formation of Li_3Al_2 from pure liquid Li and pure solid Al(FCC), using emf data in the lithium-rich lithium-aluminum alloys. At 700 K, their value is $-14.1 \text{ kcal (g-atom)}^{-1}$, while we obtain $-15.5 \text{ kcal (g-atom)}^{-1}$. If one takes into account the different approximations in either calculation, one realizes that the differences between the two values are not significant.

On the one hand, Selman et al.²⁰ derived the free energy of formation of Li_3Al_2 from the reactions:



and



It implies that the solubility of Li in Al(FCC) was neglected and that data from the lithium-poor end member of the range of solid solutions were utilized.²⁰ In addition, the free energy of reaction (20) was derived from the extrapolation of the data of Yao et al.; the extrapolated values for $\Delta G_f^\circ(\text{LiAl})$ differ somewhat from our calculations. On the other hand, we have considered LiAl to be stoichiometric. We have also based our calculations on the experimental phase diagrams.

Finally, for Al_4Li_9 , we have derived values of the enthalpies of formation and entropies of formation (Table III). As mentioned earlier, the lack of thermodynamic information does not allow direct comparison between experiments and calculation. However, we believe that the values given in Table III could be considered as a reasonable approximation since the computed and the measured Li-rich portions of the liquidus are in good consonance.

2. The Al-Mg System

The phase diagram selected by Hultgren et al.²³ is given in Fig. 2a. The following compounds have been reported: $\beta\text{-Al}_3\text{Mg}_2$, $\gamma\text{-Al}_{12}\text{Mg}_{17}$, $\epsilon\text{-Al}_{30}\text{Mg}_{23}$, and γ' of unknown structure. While thermodynamic properties on liquid alloys (e.g., enthalpy, entropy, etc.) are available in selected tables,²³ there is not thermodynamic information on solid alloys. This lack of data led us to compute a slightly simplified version of the phase diagram. Only two compounds, Al_3Mg_2 and $\text{Al}_9\text{Mg}_{11}$, with a fixed stoichiometry have been considered. Therefore, the following interactions are calculated: L vs. FCC, L vs. HCP, L vs. Al_3Mg_2 , L vs. $\text{Al}_9\text{Mg}_{11}$, FCC vs. Al_3Mg_2 , and HCP vs. $\text{Al}_9\text{Mg}_{11}$. The values for the lattice stabilities of the components are given in Table I; the interactions in the solution phase (Table II) are approximated by a symmetrical function [$\phi(\text{Al}, \text{Mg}) = \phi(\text{Mg}, \text{Al})$ with $\phi = \text{L, FCC and HCP}$]. The

compound parameters for the two compounds are calculated using the phase field of the compounds and assuming an equal melting point, $T = 735 \text{ K}$.

The computed phase diagram is given in Fig. 2b. Except for the fact that the solubility of the compounds in Al(FCC) and in Mg(HCP) is neglected, there is excellent agreement between the two representations. The coordinates of the sets of points separating two different phases are very close (compare on the one hand $X_{\text{Mg}}(\text{obs.}) = 0.19$ and $X_{\text{Mg}}(\text{obs.}) = 0.379$ to $X_{\text{Mg}}(\text{calc.}) = 0.190$ and $X_{\text{Mg}}(\text{calc.}) = 0.350$ and on the other hand $X_{\text{Mg}}(\text{obs.}) = 0.699$ and $X_{\text{Mg}}(\text{obs.}) = 0.884$ to $X_{\text{Mg}}(\text{calc.}) = 0.700$ and $X_{\text{Mg}}(\text{calc.}) = 0.880$). The calculated enthalpy and entropy of formation for the compounds $\text{Al}_{0.45}\text{Mg}_{0.55}$ and $\text{Al}_{0.6}\text{Mg}_{0.4}$ are given in Table III.

3. The Li-Mg System

Hansen and Anderko¹⁶ report two completely different sets of liquidus and solidus curves for the lithium-rich side of the phase diagram of Li-Mg. There is no explanation for the inconsistency between the two sets of data since the experimental methods followed in the two investigations are identical. However, in the Mg-rich side, there is substantial agreement between all published results. In this specific case where a choice of liquidus and solidus curves would seem rather arbitrary, the computations of the phase diagram using a thermodynamically self-consistent method would provide a valuable tool for performing this selection.

There is also a rather significant discrepancy in the thermodynamic data for the liquid alloys.^{24,25} Recently, one of us has measured the activity of molten lithium-magnesium alloys using an emf technique.²⁵ The results differ considerably from those of Mashovets and Puchkov²⁴ derived from the Mg vapor pressure measurements. Mashovets et al. have calculated, using the Gibbs-Duhem equation, the activity of Li from that of Mg. There is no indication of the reproducibility of their data.

In these calculations, we have selected the emf data²⁵ to compute the liquid interaction coefficients, we have obtained $L(\text{Li}, \text{Mg}) = L(\text{Mg}, \text{Li}) = -11200 + 10 T \text{ (cal mol}^{-1}\text{)}$. The solid (FCC, HCP and BCC) interaction coefficients were evaluated using, on the one hand, $L(\text{Mg}, \text{Li})$ and $L(\text{Li}, \text{Mg})$ and on the other hand, liquidus temperatures on the Mg-rich side for which the published experimental results are in consonance. The values of $\phi(\text{Mg}, \text{Li})$ and $\phi(\text{Li}, \text{Mg})$ are given in Table II. The compound LiMg_2 was not included in our calculations since it has not been corroborated by more recent work. The computations of the phase diagram were performed by calculating the curves representing the following interactions*, L vs. HCP, L vs. BCC and HCP vs. BCC.

The resultant phase diagram, given in Fig. 3a, agrees best with the data of Grube et al.²⁶ (Fig. 3b), which are the higher set of liquidus and solidus curves from the two alternative sets of phase diagrams given by Hansen. This selection performed on thermodynamic self-consistency basis is different from the rather arbitrary choice of Hultgren et al.²³ It is desirable that such basis for selection would be adopted when several different data are published.

4. The Al-Li-Mg System

Alloys of Al-Li-Mg have been of interest from a practical point of view. They were primary candidates in a search for ductile, malleable structural materials.⁶ However, to our knowledge, there is rather incomplete and inconsistent information in the literature on the phase diagram.

Shamrai, in a series of papers, Ref. 3 being the last, reported the phase diagrams of Al-Li-Mg as well as isothermal sections at 20°C and 400°C. The ternary compound MgLiAl_2 was identified.

*Lithium is known to have two forms: The α -Li with the HCP structure isotopic with Mg and the β -Li with the BCC structure isotypic with W.²¹ In our calculations, Li is considered to be BCC since the transformation from the α -phase to the β -phase occurs at 80 K.

Frost et al.⁴ studied the phase relationships at 700°F ($\approx 371^\circ\text{C}$) for several compositions of the alloys.

Jones et al.⁵ reported the 500°F and 700°F isothermal sections of Al-Li-Mg alloys. The ternary compound MgLi_2Al was identified.

Finally, Rowland et al.⁵ investigated some isothermal sections of the magnesium-rich corner of the Al-Li-Mg system. Their metallographic and x-ray results did not confirm the existence of the compound MgLi_2Al at equilibrium.

When comparisons are possible, the different investigations show disagreement. The latest data are in contradiction with those of Shamrai; not only the compositions are irreproducible, but also there is a significant difference in the phases. It seems impossible to reconcile the data of Shamrai with the others even by considering the minor differences in temperature (400°C vs. 375°C or 371°C). The four latest investigations show an overall consistency with slight differences in the compositions of the boundaries of different phases. However, the x-ray diffractions data of Rowland et al.⁶ do not corroborate the existence of the ternary compound MgLi_2Al observed by Jones et al.⁵ and credited to the Dow Chemical Company. To quote them, "From this it must be assumed that an equilibrium compound MgLi_2Al does not exist in the temperature range 100° to 400°C " (Ref. 6, p. 357). We can conclude that if the ternary compound MgLi_2Al does exist, it should be metastable.

Finally, one has to be aware that even in the most recent investigation,⁶ the liquidus of the subsidiary binary Li-Al was not well defined. For example, Rowland et al.⁶ referred to Li_2Al as a stable compound; as mentioned earlier, it has been proven that Li_2Al is indeed Li_9Al_4 . Also, the existence of Li_3Al_2 was not yet known. As a consequence of the

uncertainties and without further experimental evidence, we did not include any ternary compound in our calculations.

The isothermal sections of the Al-Li-Mg system calculated are given in Fig. 4 for $T = 673$ K, Fig. 5 for $T = 728$ K, Fig. 6 for $T = 773$ K and Fig. 7 for $T = 648$ K. They were computer generated by considering all the possible interactions on a pair-wise basis:

At the Al-rich corner: FCC vs. LiAl, FCC vs. L, FCC vs. Al_3Mg_2 ,
L vs. Al_3Mg_2 , L vs. LiAl

At the Li-rich corner: L vs. Li_3Al_2 and L vs. BCC

At the Mg-rich corner: HCP vs. L, HCP vs. BCC, HCP vs. $\text{Al}_9\text{Mg}_{11}$
and L vs. $\text{Al}_9\text{Mg}_{11}$

The interaction coefficients $\phi(i,j)$ as well as the compound parameters, C , calculated in the subsidiary binaries are used in Eqs. (6)-(19).

Only the stable part of the curves representing each couple of interactions are drawn in the final plots given in Figs. 4-7. In the computation of the compound interactions, the counterphase (refer to Section II) always consisted of a hypothetical compound located on the adjacent binary and by definition less stable than the compound studied. In this particular case, we did not use any information from the experimental phase diagram in the calculations (i.e., solubility of LiAl in Mg, etc.). Therefore, we always set the compound parameter of the "counter-phase" equal to zero. It is important to realize the significance of this approximation on the shape of the boundaries between two different regions and even on the stability of some phases. For example, in Fig. 4, a hypothetical compound, H, on the Li-Mg binary was assumed to be the counterphase of Li_3Al_2 . If the compound parameter of H was different from zero, it is probable that the phase field of the two-phase region⁷ of $(\text{Li}_3\text{Al}_2 + \text{L})$ would be larger.

This illustrates the importance of the existence of reliable experimental data at "key" compositions of the Al-Li-Mg alloys.

At $T = 723$ K (Fig. 5), the liquid phase becomes more significant and the phase fields of the Al-Mg compounds less important. At $T = 773$ K (Fig. 6), only the LiAl and Li_3Al_2 binary phases are stable. As expected, the liquid phase covers a large area. The isothermal section at $T = 648$ K (375°C) was calculated in order to allow a better comparison with the data of Rowland et al.⁶ collected for the Mg-rich corner; indeed, a direct comparison cannot really be done since Rowland et al.⁶ were not aware of the existence of Li_3Al_2 . However, there is reasonable agreement between our computed isotherm and the experimental data, if one takes into consideration the differences in the binary Li-Al. What is the most striking similarity between Fig. 7 and the x-ray data of Rowland et al.⁶ is the non-existence of the liquid phase. Note that a 25 K difference led to the disappearance of the liquid in the Mg-rich side of the system.

Finally, it should be emphasized that these calculations must not be considered as final. It would be desirable to have some experimental information as feedback. Modifications can be easily performed to (i) include ternary compounds (stable or metastable); (ii) change the stability of the compounds generated from the binary compounds; and (iii) include any reliable data on the solubility of a component, C, in a binary solution, A-B. These changes can be easily performed within the framework of the present computer-program. However, there are different limitations inherent in the techniques and models used which one has to be aware.

It is not always possible to represent the thermodynamic properties of the binary solutions by equations such as Eqs. (2)-(4). It has been shown in detail by Darken²⁷ that simple polynomials could not always be

used for the excess Gibbs free energy of mixing of some binary systems such as Mg-Bi. Particularly in the case of Li-Pb,²⁸ we have shown that the curve representing the variations of $\overline{\Delta G}_{Li}^{xs}$ versus the atom fraction of Pb, X_{Pb} , exhibits an "S" shape and has an inflection point. In these cases, it would be preferable to use other numerical methods to solve the equations (i.e., one could use a spline function to interpolate the intermediate values).

The thermodynamic representation of ternary solutions can also be improved. The Kohler equations are not as precise as one would desire and particularly when the interactions in the subsidiary binaries are significant. A correctional term to these equations should be considered. In a study of ternary ionic systems, Saboungi and Blander²⁹ developed equations to represent the thermodynamic properties. Up to the third order expansion, they obtain:

$$\Delta G_m^E = \sum_{i < j} \sum a_{ij} N_i N_j + \sum_{i \neq j} \sum b_{ij} N_i^2 N_j + A N_1 N_2 N_3 \quad (22)$$

where A is related to the binary interaction coefficients by:

$$A = -(b_{12}^{1/3} + b_{13}^{1/3})(b_{21}^{1/3} + b_{23}^{1/3})(b_{31}^{1/3} + b_{32}^{1/3}) \quad (23)$$

A similar term might be introduced in the ternary alloy equations. Different theoretical, rather than empirical, equations should be tried.

CONCLUSION

The method of Kaufman and coworkers is used to provide an estimate of isothermal sections of the Al-Li-Mg system. One starts by calculating the lattice stability of the constituents, the binary interaction coefficients and the binary compound parameters. In the computations, thermodynamic data, when available, were coupled with measured phase diagrams

to provide thermodynamically self-consistent liquidus and solidus curves for the binary systems. Standard enthalpies of formation and entropies of formation were calculated for the reported compounds. The binary system Li-Mg illustrates the use of such calculations in selecting the most reliable representation of the phase diagram.

The calculated binary data were used to compute the phase diagram of Li-Al-Mg, assuming that no ternary compounds exist.

Despite some limitations due mainly to the formalism used (i.e., simple polynomials to fit binary data, the use of the Kohler equations for the thermodynamics of the ternary system), this numerical tool remains useful in providing a reasonable prediction of thermodynamically self-consistent ternary phase diagrams. One of the most attractive features is the fact that the accuracy of the calculations can be improved greatly with a very small amount of experimental information.

ACKNOWLEDGMENTS

We are indebted to both Larry Kaufman and Harvey Nesor for their often-needed help in "debugging" some problems encountered when running the program. Special thanks are due to Milton Blander for his continuous encouragement and advice. We also thank our colleagues Donald Vissers and Michael Roche for keeping us informed of arising technical problems. Finally, we are grateful to Janet Steinquist for typing this manuscript and to the unknown FTS operator who made this long-distance computation possible.

REFERENCES

*This work was performed under the auspices of the U. S. Energy Research and Development Administration,

1. P. A. Nelson et. al., USAEC Report ANL-8058, Argonne National Laboratory, Argonne, Illinois (1974).
2. P. A. Nelson et al., USAEC Report ANL-75-1, Argonne National Laboratory, Argonne, Illinois (1975).
3. F. I. Shamrai, Izvest. Akad. Nauk. S.S.S.R. Otdel. Khim. Nauk., 290-310 (1948).
4. P. D. Frost, J. G. Kura and L. W. Eastwood, Trans. AIME 188, 1277 (1950); Journal of Metals (Oct. 1950).
5. A. Jones, J. H. Lennon, R. R. Nash, W. H. Chang and E. G. Mac Peek, Technical Report 52-169 (1952), U. S. Air Force, Air Research and Development Command, Wright Paterson Air Force Base.
6. J. A. Rowland, Jr., C. E. Armantrout and D. F. Walsh, Trans. AIME, 355 (1955).
7. a) ManLabs - NPL Materials Data Bank
b) L. Kaufman and H. Nesor, "Treatise on Solid State Chemistry," N. B. Habbay, Ed., Plenum Press, New York 5 179-232, (1975).
8. F. Kohler, Monatsch f. Chemie 19, 738 (1960).
9. G. N. Toop, Trans. Met. Soc. AIME 233, 850 (1965).
10. L. Kaufman and H. Nesor, Z. Metallk. 64, 249 (1973).
11. G. Grube, L. Mohr and L. Breuning, Z. Elektroch. 41, 880 (1935).
12. F. I. Shamrai and P. Ya. Saldau, Izvest. Akad. Nauk. S.S.S.R., Otdel. Khim. Nauk., 631 (1937).
13. D. A. Hansen and J. F. Smith, Acta Cryst. 24, 913 (1968).

14. K. F. Tebbe, H. G. von Schnering, B. Ruter and G. Rabeneck, Z. Naturforsch. 28b, 600 (1973).
15. K. M. Myles, F. C. Mrazek, J. A. Smaga and J. L. Settle, in "Proceedings of the Symposium and Workshop on Advanced Battery Research and Design," March, 1976, U.S. ERDA Report, ANL-76-8, p. B-50.
16. M. Hansen and K. Anderko, Constitution of Binary Alloys, McGraw-Hill Book Co. Inc., New York, 1958.
17. S. P. Yatsenko and E. A. Saltykova, Russ. J. Chem. Phys. 48, 1402 (1974).
18. M. L. Saboungi and M. Blander, J. Electrochem. Soc. (in press).
19. N. P. Yao, L. A. Heredy and R. C. Saunders, J. Electrochem. Soc. 118, 1039 (1971).
20. J. R. Selman, D. K. DeNuccio, C. J. Sy and R. K. Steunenbergh (in press).
21. R. Hultgren, P. D. Desai, D. T. Hawkins, M. Gleiser, K. K. Kelley and D. D. Wagman, "Selected Values of the Thermodynamic Properties of the Elements," American Society for Metals, Metals Park, Ohio, 1973.
22. L. Kaufman, personal communication.
23. R. Hultgren, P. D. Desai, D. T. Hawkins, M. Gleiser and K. K. Kelley, "Selected Values of Thermodynamic Properties of Binary Alloys," American Society for Metals, Metals Park, Ohio, 1973.
24. V. P. Mashovets and L. V. Puchkov, Zh. Prikl. Khim. 38(8), 1875 (1965).
25. M. L. Saboungi and M. Blander, J. Electrochem. Soc. 122, 1631 (1975).
26. G. Grube, H. V. Zeppelin and H. Bumm, Z. Elektrochem. 40, 160 1934
27. L. S. Darken, Trans. Metall. Soc. AIME (Am. Inst. Min. Metall. Pet. Eng.) 239, 80 (1967).
28. M. L. Saboungi, J. J. Marr and M. Blander (to be published).
29. M. L. Saboungi and M. Blander, J. Chem. Phys. 63(1), 212 (1975).

Table I

Lattice Stability Values for Aluminum,
Lithium and Magnesium

Element	Lattice Stabilities (cal mol ⁻¹)
Al	$G^{\circ}(\text{L}) - G^{\circ}(\text{FCC}) = 2560 - 2.75 \text{ T}$
	$G^{\circ}(\text{L}) - G^{\circ}(\text{BCC}) = 150 - 1.60 \text{ T}$
	$G^{\circ}(\text{L}) - G^{\circ}(\text{HCP}) = 1250 - 2.32 \text{ T}$
Li	$G^{\circ}(\text{L}) - G^{\circ}(\text{FCC}) = 427 - 1.71 \text{ T}$
	$G^{\circ}(\text{L}) - G^{\circ}(\text{BCC}) = 717 - 1.58 \text{ T}$
	$G^{\circ}(\text{L}) - G^{\circ}(\text{HCP}) = 727 - 1.71 \text{ T}$
Mg	$G^{\circ}(\text{L}) - G^{\circ}(\text{FCC}) = 1675 - 2.75 \text{ T}$
	$G^{\circ}(\text{L}) - G^{\circ}(\text{BCC}) = 1040 - 1.60 \text{ T}$
	$G^{\circ}(\text{L}) - G^{\circ}(\text{HCP}) = 2140 - 2.32 \text{ T}$

Table II

Calculated Interaction Parameters* for the Solution
Phases of the Al-Li, Al-Mg and Li-Mg Systems

$\Phi(i,j)$ (cal mol ⁻¹)	Phase Φ			
	L	FCC	BCC	HCP
$\Phi(\text{Al,Li})$	-9600 + 8.0 T	-3000	9999	-3000
$\Phi(\text{Li,Al})$	-20,000 + 16.0 T	-22,000 + 16.0 T	9999	-22,000 + 16.0 T
$\Phi(\text{Al,Mg})$	-2400 + 0.8 T	-300	0	0
$\Phi(\text{Mg,Al})$	-2400 + 0.8 T	-300	0	0
$\Phi(\text{Li,Mg})$	-11,200 + 10.0 T	-5100 + 3.0 T	-9500 + 7.0 T	-5100 + 3.0 T
$\Phi(\text{Mg,Li})$	-11,200 + 10.0 T	-9000 + 7.0 T	-13,900 + 10.0 T	-9000 + 7.0 T

$$*\Delta G_{i,j}^E(\Phi) = x_i x_j [x_i \Phi(i,j) + x_j \Phi(j,i)]$$

Table III

Calculated Parameters,* Enthalpies of Formation,** and Entropies of Formation** of the Compounds of the Li-Al and Al-Mg Systems

Compound, P	Compound Parameter, C	$\Delta H_f(P)$	$\Delta S_f(P)$
$\text{Al}_{0.308}\text{Li}_{0.692}$	13,648 - 10.0 T	-7573	7.047
$\text{Al}_{0.40}\text{Li}_{0.60}$	15,688 - 11.0 T	-8847	7.838
$\text{Al}_{0.5}\text{Li}_{0.5}$	7839 + 0.19 T	-7153	5.182
$\text{Al}_{0.45}\text{Mg}_{0.55}$	3180	-3620	2.948
$\text{Al}_{0.60}\text{Mg}_{0.40}$	3180 + 0.21 T	-3545	2.892

*The compound parameters, C, are calculated using for the five compounds FCC as the base phase [cal (g-atom)⁻¹].

**The enthalpies of formation [in cal (g-atom)⁻¹] and entropies of formation [in cal(g-atom)⁻¹ K⁻¹] are defined as follows:

$$\Delta H_f(P) = H(P) - x_i^* H_i^\circ(L) - x_j^* H_j^\circ(L)$$

and

$$\Delta S_f(P) = S(P) - x_i^* S_i^\circ(L) - x_j^* S_j^\circ(L)$$

Table IV

Observed¹⁹ and Computed Gibbs Free
Energy of Formation of $\text{Li}_{0.5}\text{Al}_{0.5}$ *

T°K	$-\Delta G_f(\text{obs.})$ [kcal(g-atom) ⁻¹]	$-\Delta G_f(\text{calc.})$ [kcal(g-atom) ⁻¹]
573	3.74	3.69
623	3.62	3.50
653	3.54	3.39

$$\Delta G_f = G(\text{Li}_{0.5}\text{Al}) - 0.5 G_{\text{Al}}^{\circ}(\text{L}) - 0.5 G_{\text{Al}}^{\circ}(\text{FCC})$$

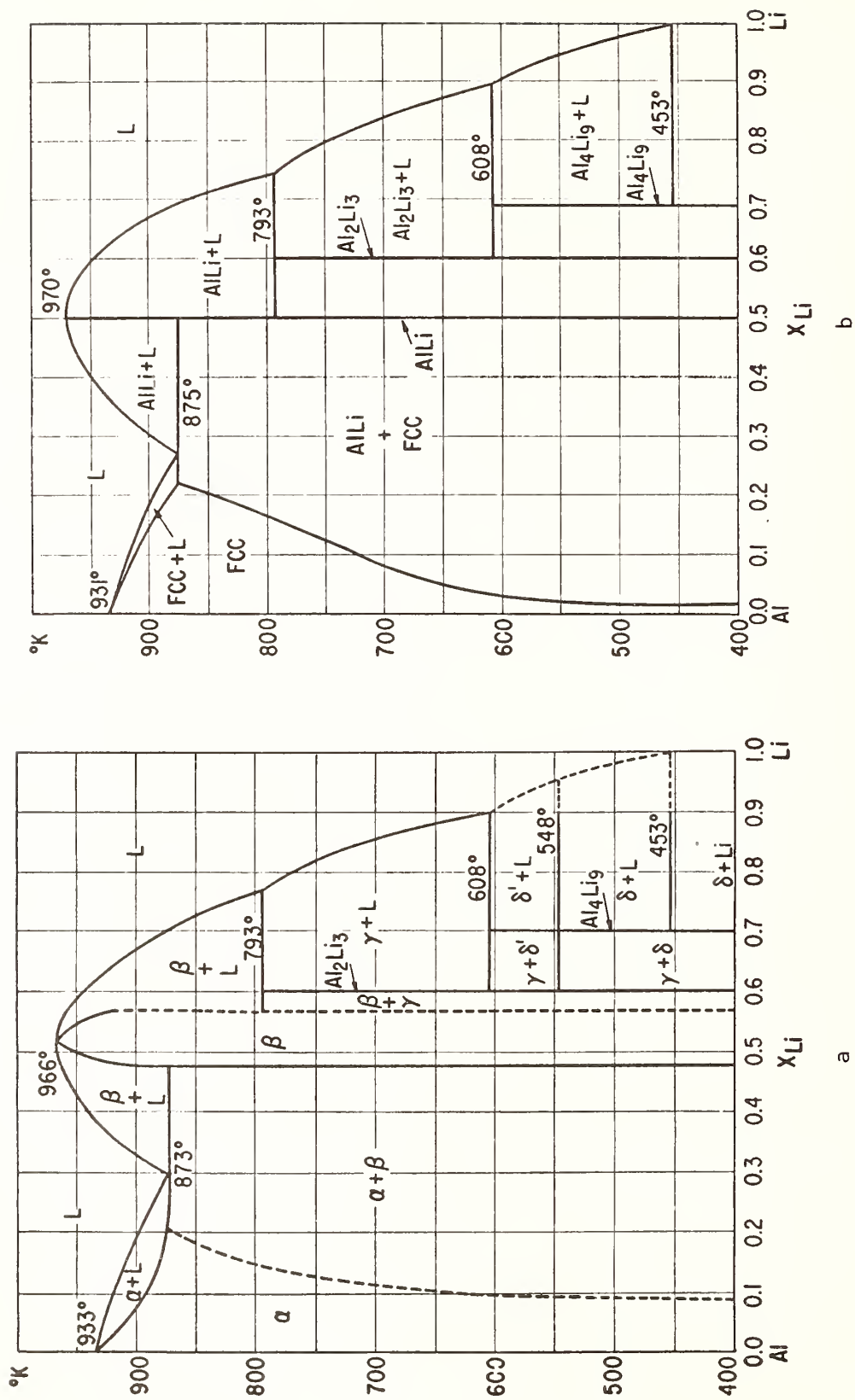


Fig. 1 a. The measured phase diagram of the Al-Li system (Ref. 15).
b. The calculated phase diagram.

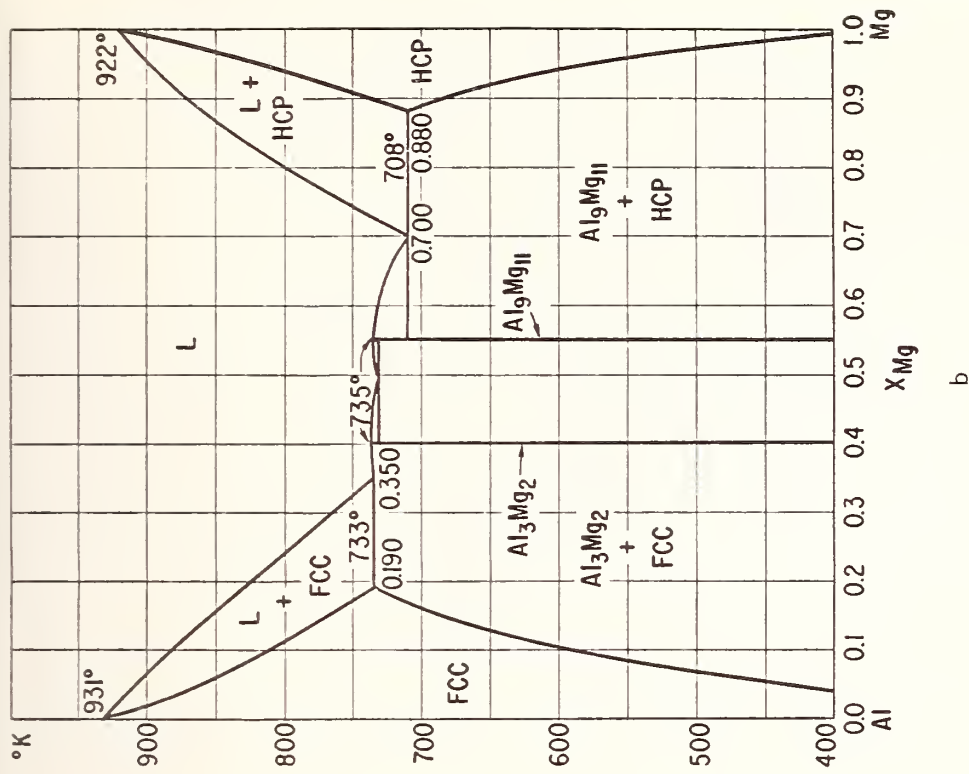
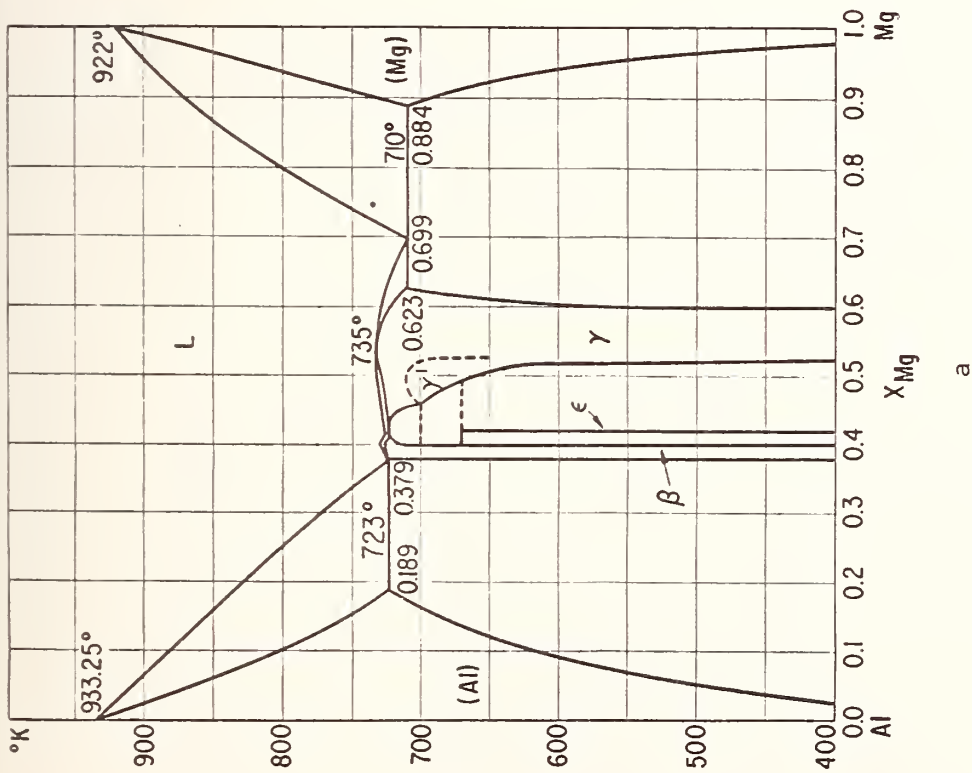


Fig. 2 a. The measured phase diagram of the Al-Mg system (Refs. 16 and 23).

b. The calculated phase diagram.

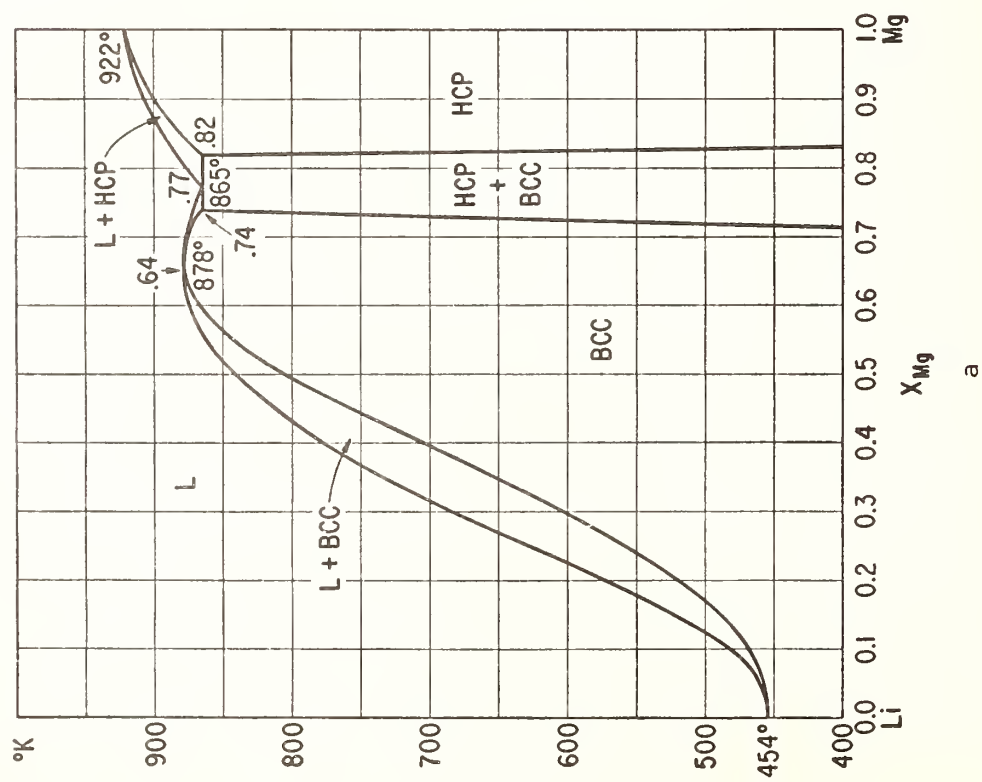
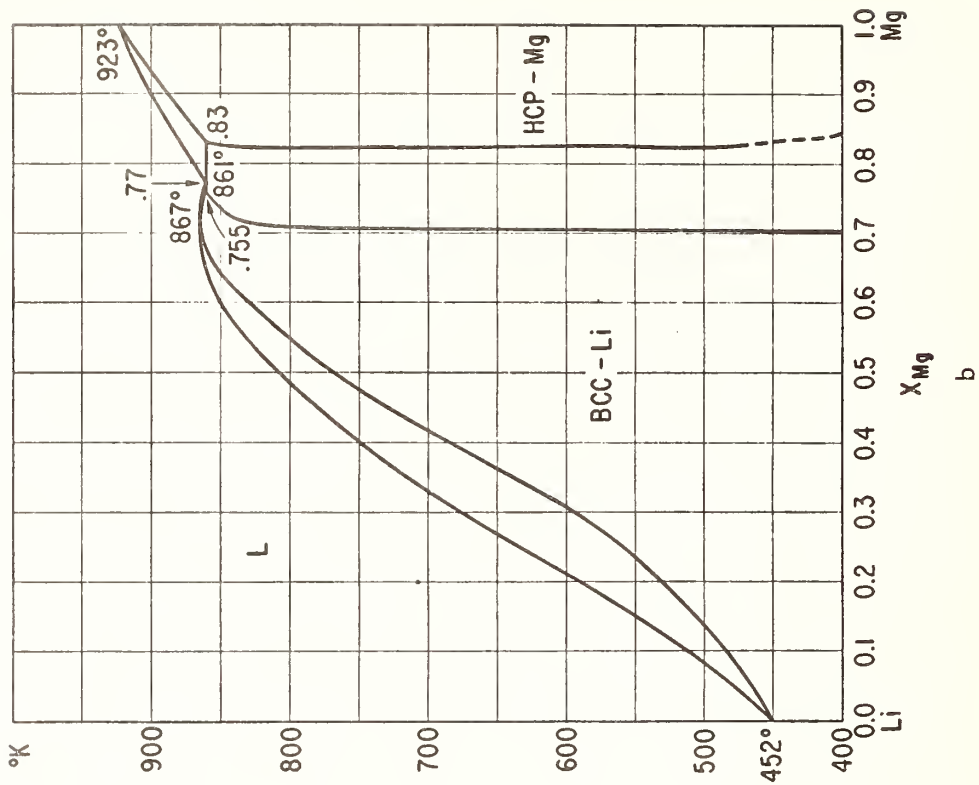


Fig. 3 a. The calculated phase diagram of the Li-Mg system.
b. The measured phase diagram (Refs. 16 and 26).

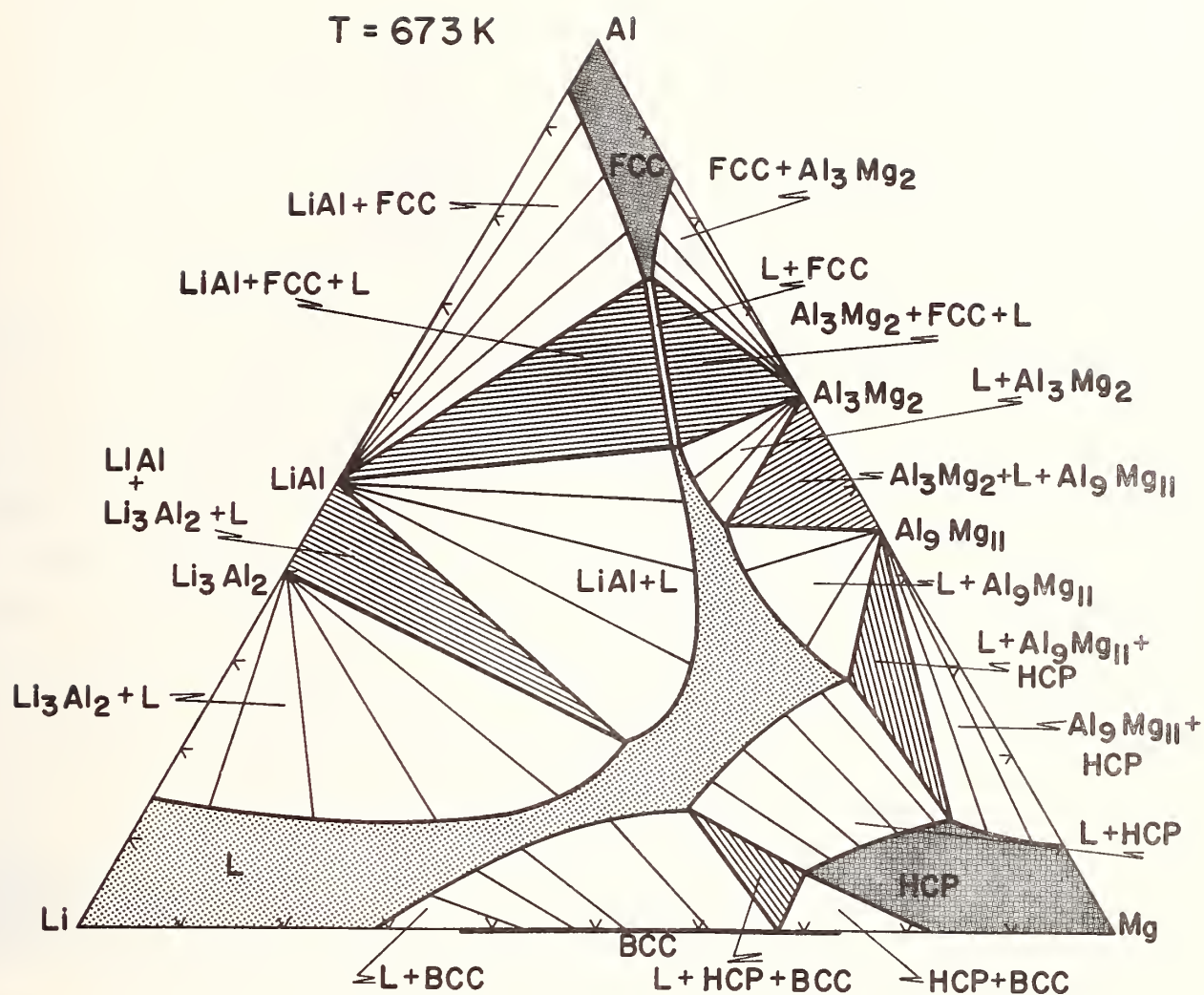


Fig. 4 Computed 673K isotherm of the Al-Li-Mg system.

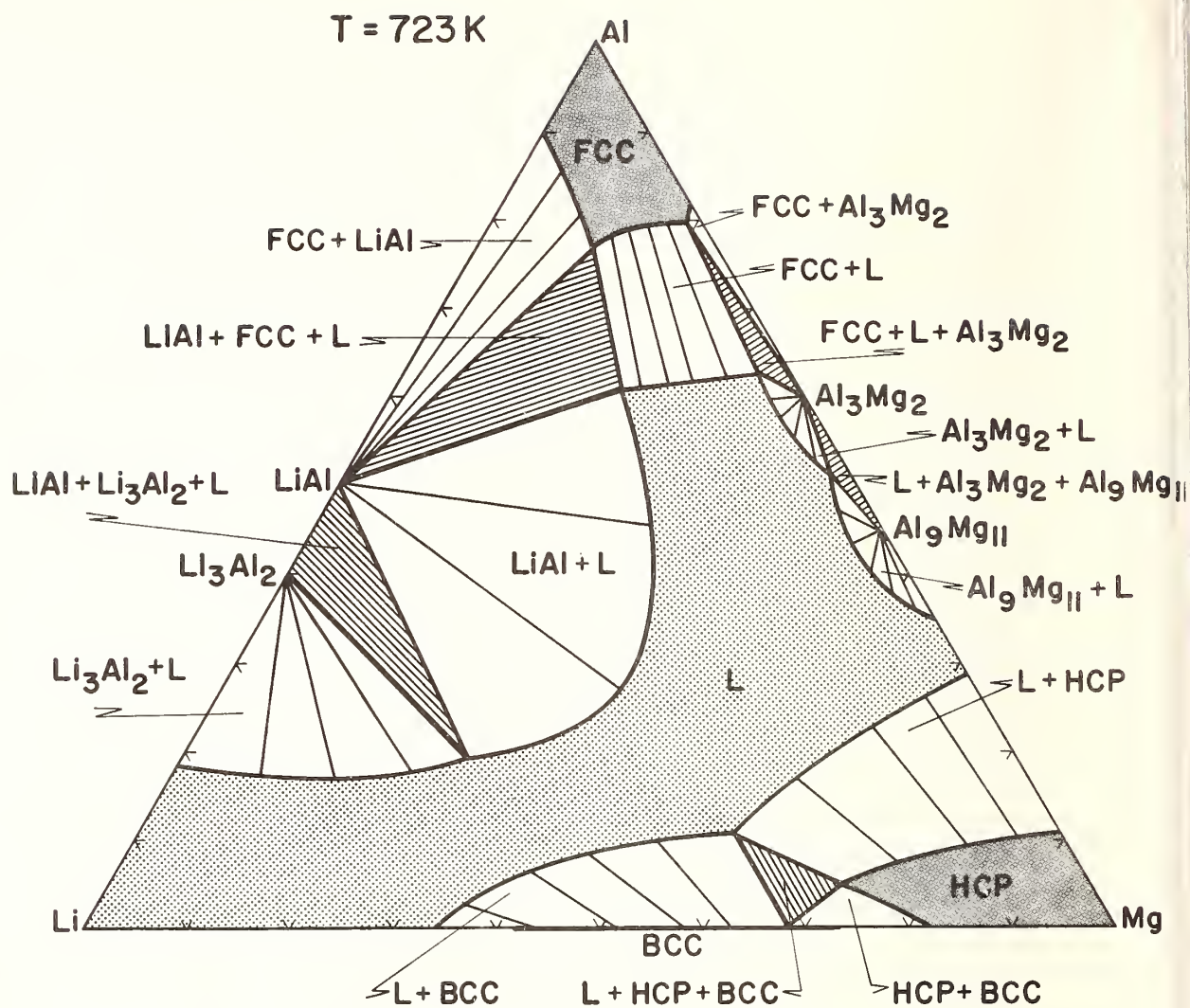


Fig. 5 Computed 723K isotherm of the Al-Li-Mg system.

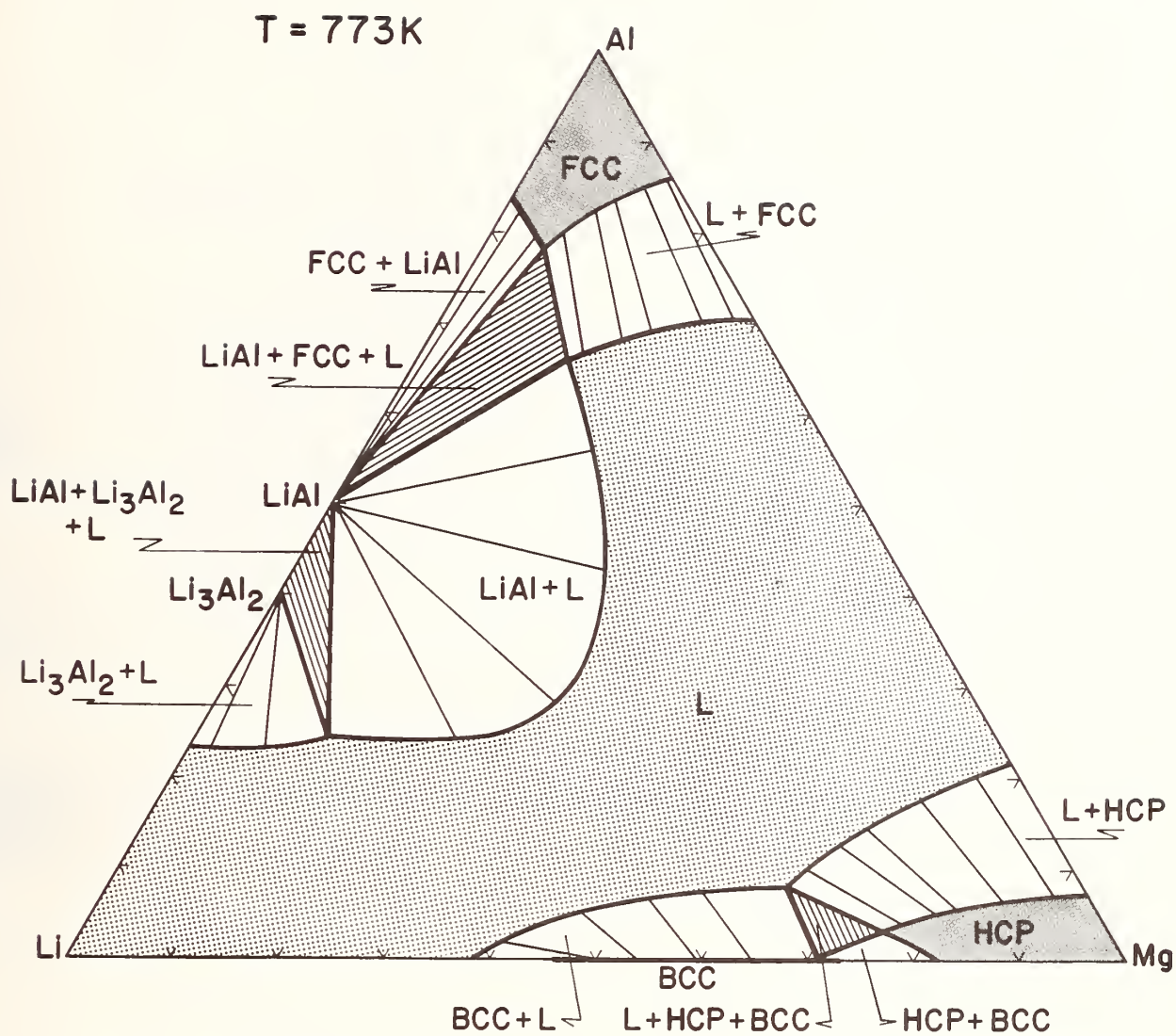


Fig. 6 Computed 773K isotherm of the Al-Li-Mg system.

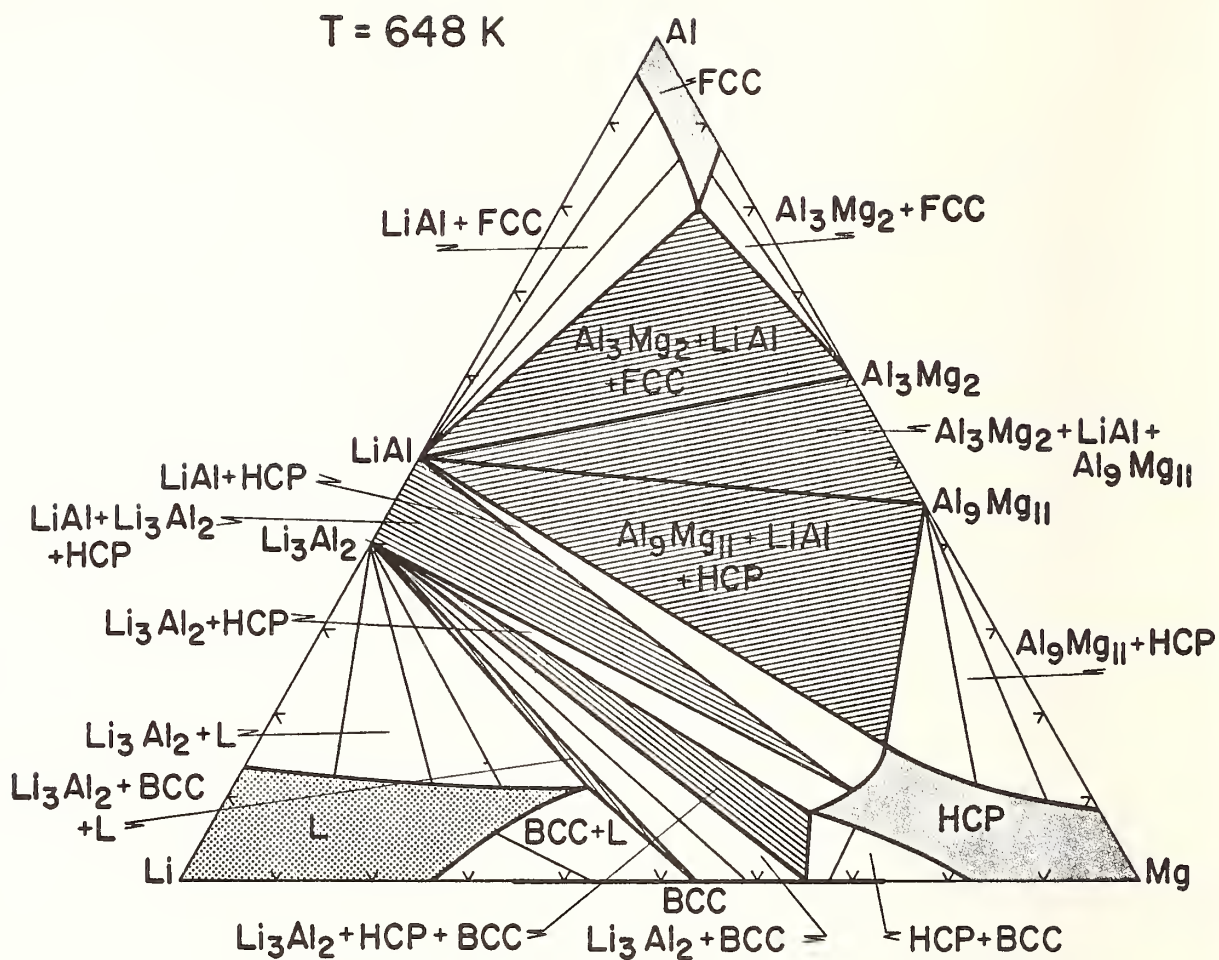


Fig. 7 Computed 648K isotherm of the Al-Li-Mg system.



Е.М.Савицкий, В.Б.Грибуля, Н.Н.Киселёва

Кибернетическое прогнозирование образования химических
соединений в неисследованных системах

Благодаря успехам физики твердого тела, сейчас известно, что все свойства металлов и неметаллов, кроме ядерных, при данном уровне дефектов определяются распределением электронов в поле положительных ионов. Однако расчет существования и устойчивости металлических и других неорганических фаз из "первых принципов" остается пока неразрешенной проблемой. С другой стороны, в химии и металлургии накоплено колоссальное количество экспериментальной информации о зависимости появления и существования фаз от различных факторов (свойств и размеров атомов, состава, температуры, давления, воздействия физико-химических сред, внешних физических полей, кинетики и т.д.). Эти факторы переменны и индивидуальны для конкретных фаз. Традиционные теоретические методы — квантовая механика, термодинамика — в большинстве случаев не дают возможностей для комплексного анализа этих данных с целью поиска новых материалов. Более того, эти методы сами опираются на эмпирические модели взаимодействия частиц, которые, как правило, включают понятия валентности, экранизации заряда ядра, размера атомов, потенциалов взаимодействия.

Принимая во внимание отсутствие эффективных методов использования накопленной информации для прогноза и расчета веществ и материалов, представляющих практический интерес, мы решили использовать новый подход к решению этих проблем. Подход состоит в применении некоторых идей кибернетики из области создания обучающихся автоматических систем к прогнозу физико-химических объектов. Такими объектами, в частности, являются химические элементы, их соединения и смеси, свойства которых определяют структуру фазовых диаграмм. Так как в настоящее время химические элементы изучены наиболее пол-

но по сравнению с более сложными веществами, то мы считаем целесообразным прежде всего использовать широко известные данные о свойствах элементов для прогноза поведения элементов в системах.

Нами была поставлена задача обучить машину различать сочетания химических элементов, обладающих и не обладающих заданным свойством, т.е. классифицировать объекты по свойствам. При этом исходной посылкой служило представление о взаимоотношении элементов в физико-химических системах как о сложной кибернетической системе с взаимобусловленными связями, где данные об элементах неизвестным нам образом обуславливают закономерности наблюдаемых эффектов в системах. После обучения на имевшихся экспериментальных примерах компьютер классифицирует все неисследованные сочетания элементов на заданные классы. Это и составляет задачу кибернетического прогнозирования.

В настоящей работе использованы кибернетические прогнозирующие системы разных типов. В основу первой из них первоначально была положена идеология обучения ЭВМ распознаванию образов / I,3,II/. Вторая система базировалась на методах обучения ЭВМ процессу индуктивного формирования понятий /9,IO/.

Первые исследования в данной области были начаты нами в 1966 году /I/. В настоящее время появился целый ряд химических и металлургических работ, авторы которых обращаются к идее использования распознавания образов /I2-I7/. Область применения этих кибернетических методов широка: от анализа масс-, ИК-, ЯМР-спектров органических веществ /I3,I4,I6/ до поиска новых сплавов с заранее заданными свойствами /I2/. При этом применяются различные методы распознавания образов, включая распознавание с обучением /I2-I4,I7/ и автоматическую классификацию /I4-I6/. Не столь важно, какой алгоритм распознавания образов используется для прогноза, если принимается во внимание спе-

цифика объектов, т.е. объективные и эвристические ограничения, накладываемые на выбор и классификацию объектов обучения для прогноза. Последнее является задачей собственно физико-химии или другой специальной области, но не математики как таковой. Выбор того или иного программного варианта часто определяется возможностями имеющейся вычислительной техники и математического обеспечения. Ввиду отсутствия общей теории распознавания образов, поиск соответствующего метода для решения конкретных задач является проблемой в значительной степени экспериментальной, нежели теоретической. При этом, конечно, нельзя забывать о математических ограничениях того или иного алгоритма.

Стремление получить прогноз из "первых принципов" подсказывает использование в качестве исходных данных фундаментальных характеристик атомов химических элементов – атомного номера, распределения электронов по энергетическим состояниям в атоме и других. Не в зависимости от задачи исследования могут быть использованы различные характеристики химических элементов или известных фаз, представления зонной теории и других физических теорий строения вещества.

Для иллюстрации приводим фрагменты прогноза существования двойных фаз Лавеса /4,5/, 6-фаз /6/, фаз типа A-15 /7/ (рис.1-3). На рисунках вертикальная ось соответствует компонентам А, а горизонтальная – компонентам В в соединениях A_mB_n , где $m \geq n$. Знак "+" указывает на прогноз существования фазы данного типа. Знак "⊕" соответствует известным химическим соединениям, которые могли быть использованы для обучения ЭВМ. В приводимых примерах прогноз получен по обучению на экспериментальных примерах существования и отсутствия фаз в системах, в которых химические элементы описаны исключительно данными о распределении электронов в изолированных атомах химических элементов. Оказалось возможным построить логическим путём

аналоги "существенных" признаков для прогнозируемых фаз только из этих данных.

Учитывая перспективность кибернетического прогнозирования, начаты исследования по прогнозу тройных химических соединений и созданию более мощной кибернетической системы, основанной на методе обучения универсальных вычислительных машин формированию понятий /9,10/. Такого рода методы пригодны для выделения сложных закономерностей в больших массивах информации /18/.

Метод формирования понятий был применен для прогнозирования тройных химических соединений состава $A_xB_yC_z$, где А и В – любые элементы периодической системы, а С – кислород или сера. В первую очередь прогнозировались наиболее представительные /по количеству экспериментальных примеров/ классы соединений, имеющие к тому же практический интерес / ABO_4 , AB_2O_4 , ABO_3 /9/, $A_2B_2O_7$, AB_2S_4 /, а также наиболее распространённые типы кристаллических структур /перовскиты, шпинели и пироклоры/. Достоверность прогноза не ниже 78 %.

В работах по прогнозу тройных соединений мы не ограничивались использованием в качестве системы признаков для описания соединений только совокупностью параметров электронного строения изолированных атомов. Помимо распределения электронов, для описания соединений были использованы ещё две системы признаков. Первая из них включала в себя параметры химических элементов А и В: тип незавершённой электронной оболочки, теплоёмкость элемента, радиус иона элемента в соединении, первые четыре потенциала ионизации, формальную степень окисления элемента в соединении заданного состава. В основу второй системы признаков были положены свойства простых окислов элементов А и В: энтальпия их образования, изобарная теплоёмкость, эффективный радиус катиона в окисле, а также соответствующая ему степень окисления элемента.

Все три системы признаков, используемые для описания соединений, тесно коррелируют. Поэтому прогнозы, полученные в результате обучения ЭВМ с использованием каждого из трёх признаков описаний, должны, в общем, совпадать. Сравнение прогнозов по разным системам признаков ведёт к значительному повышению достоверности результатов. При этом несовпадающие прогнозы исключаются из рассмотрения.

На рис.4 приведена часть прогнозов возможности образования соединений состава $A_2^{\text{III}}B_2^{\text{IV}}O_7$ (римскими цифрами помечены степени окисления элементов). Знаком "+" отмечены случаи существования соединений, "-" - отсутствия таковых в системе A-B-O; кружком обведены объекты, использованные для обучения ЭВМ.

На рис.5 дан прогноз соединений со структурой типа пироклора. В этом случае знак "+" свидетельствует о том, что соответствующее соединение $A_2^{\text{III}}B_2^{\text{IV}}O_7$ имеет пироклорную структуру, а "-" удостоверяет противоположное. Следует обратить особое внимание на большое количество прогнозируемых соединений со структурой пироклора, которые образуют трехвалентные редкоземельные металлы. Вполне возможно, что некоторые из этих соединений будут интересны для исследователей, ведущих поиск новых сегнетоэлектриков.

Следует отметить, что использованные нами кибернетические прогнозирующие системы носят адаптивный характер. Появление совершенно новых экспериментальных данных, неохваченных нашими прогнозами или противоречащих им, способствует дообучиванию системы, уточнению классифицирующих закономерностей и прогнозов. Такая гибкость предложенного подхода является следствием использования быстродействующих ЭВМ, способных для построения классификационной схемы перебрать огромное количество имеющихся вариантов и выбрать из них наилучший с точки зрения разделимости классов.

Полученные прогнозы значительно уменьшают время поиска материалов с заданными свойствами. Они расширяют наши возможности теоретического расчёта диаграмм состояния и новых фаз и показывают относительность существующих представлений о диаграммах состояния как инструменте познания физико-химических систем. Они требуют уточнения и формализации понятий химического соединения, условий его образования, стехиометричности, равновесного состояния, кинетических данных и более широкой формулировки термодинамического правила фаз с учётом воздействий различных физических полей, вакуума, дисперсности и т.д.

Литература

1. Е.М.Савицкий, Ю.В.Девингталь, В.Б.Грибуля, ДАН СССР, 1968, 178, №1, с.79-81.
2. E.M.Savitskii and V.B.Gribulya, J.Phys. Chem. Solids, 1972, v.33, 1853-1860.
3. Е.М.Савицкий, В.Б.Грибуля, Изв. АН СССР.Неорганические материалы, 1971, 7, №7, с.1097-1104.
4. Е.М.Савицкий, В.Б.Грибуля, ДАН СССР, 1972, 206, №4, с.848-851.
5. Е.М.Савицкий, В.Б.Грибуля. Предсказание фаз Лавеса при помощи ЭВМ. №4658-72 Деп., М., ВИНТИ, 1972.
6. Е.М.Савицкий, В.Б.Грибуля, ДАН СССР, 220, №5, 1975, с.1066-1069.
7. Е.М.Савицкий, В.Б.Грибуля, ДАН СССР, 1975, 223, №6, 1383-1386.
8. Е.М.Савицкий, В.Б.Грибуля, в сб. "Структура и свойства жаропрочных металлических материалов", М., "Наука", 1973, с. 3-10.
9. Н.Н.Киселёва, Б.И.Покровский, Н.Д.Вашенко, в сб. "Планирование и автоматизация эксперимента в научных исследованиях", М., "Советское радио", 1974, с.308-315.
10. В.П.Гладун, Кибернетика, 1972, №5, с.109-117; №6, с.28-36.
11. Ю.В.Девингталь, Изв. АН СССР. Техн. кибернетика, 1971, №3, 139-147.
12. Б.Б.Гуляев, Л.Ф.Павленко, Автоматика и телемеханика, 1973, №1, с.131-147.
13. T.R.Brunner, C.L.Wilkins, R.C.Williams, P.J.McCombie, Anal. Chem., 1975, v.47, N.4, pp. 662-665.
14. P.C.Jurs, T.L.Isenhour, "Chemical applications of pattern recognition", N.Y., John Wiley and Sons, 1975.
15. J.R.Koskinen, B.R.Kowalski, J. Chem. Inform. and Comput. Sci.,

- 1975, v.15, №.2, pp.119-123.
- 16.B.R.Kowalski, C.F.Bender, J. Amer. Chem. Soc., 1972, v.94, №.126
pp.5632-5639.
- 17.M.A.Pichler, S.P.Perone, Anal. Chem., 1974, v.46, №.12. pp.1790-
1798.
- 18.E.B.Hunt, J.K.Marin, P.J.Stone, "Experiments in Induction"
New York and London, "Academic press", 1966.

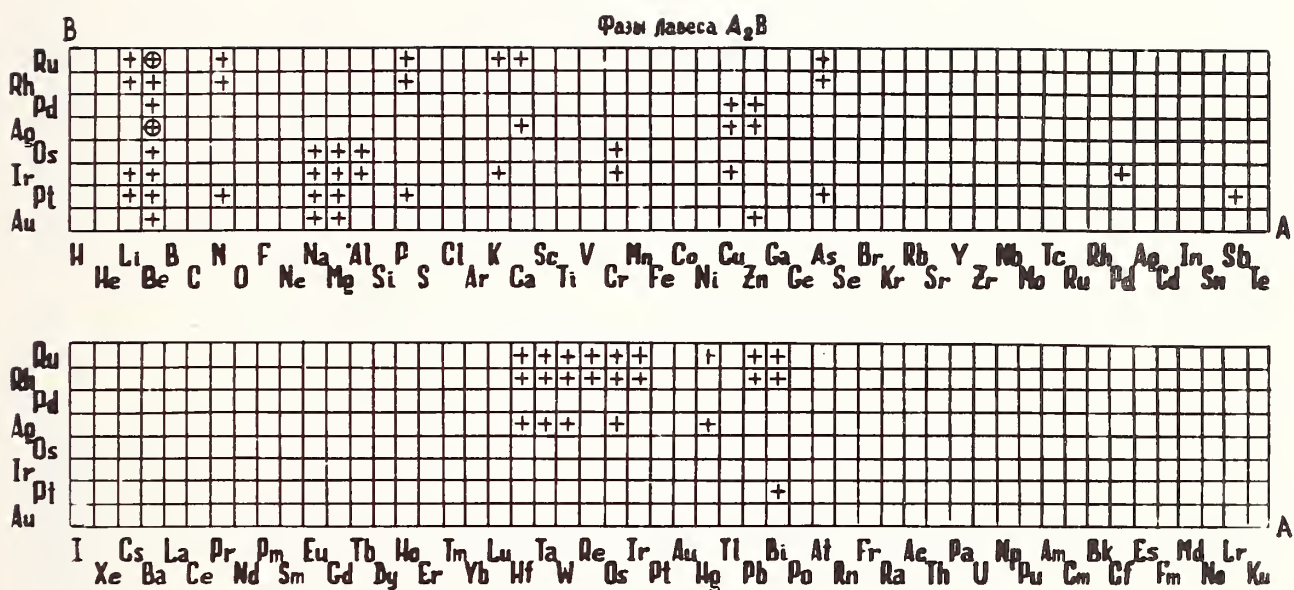


Рис. 1 Прогноз фаз Лавеса с благородными металлами.

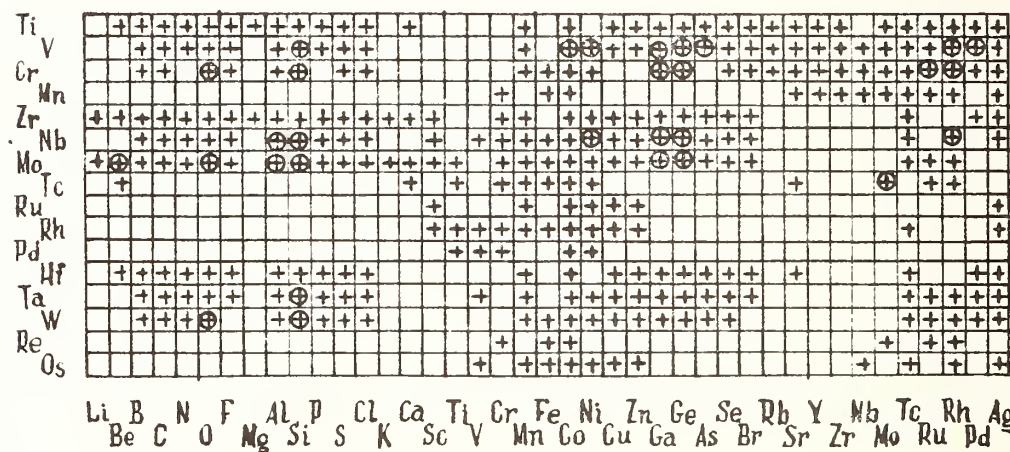
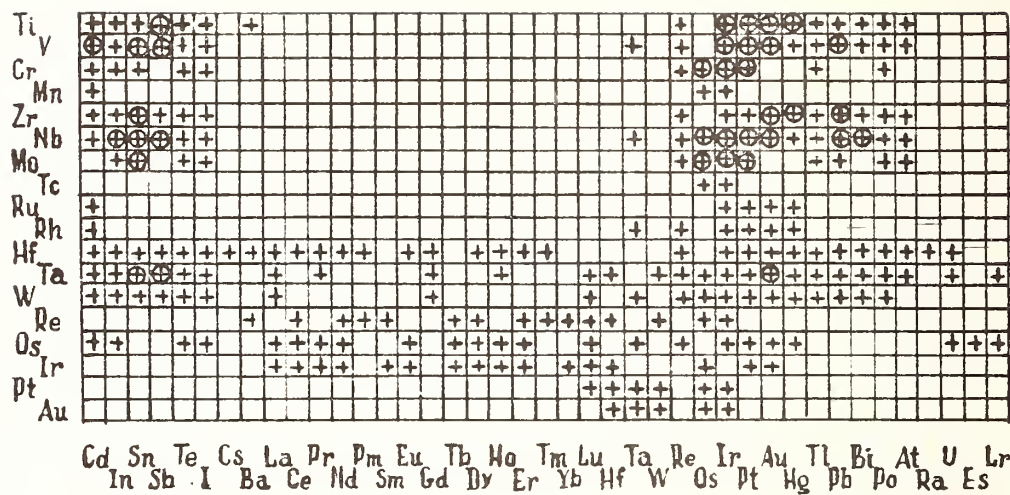


Рис. 2 Прогноз двойных фаз типа А-І5.



An English translation prepared by G. Marinenko, Analytical Chem. Div., NBS

Cybernetic Prediction of the Formation of Chemical Compounds
in Uninvestigated Systems

E. M. Savitskii, V. P. Gribulya and N. N. Kiselyeva

Baikov Institute of Metallurgy
USSR Academy of Sciences
Institute of Scientific Information
Moscow, USSR

As a result of the advances in solid state physics, it is now known that all properties of metals and nonmetals, with the exception of nuclear properties, under given conditions of defect level, are determined by the distribution of electrons in a field of positive ions. However, the calculation of the existence and the stability of metallic as well as of other inorganic phases on the basis of prima-facie principles still remains an unresolved problem. On the other hand, in chemistry and metal science, an enormous amount of experimental information on the dependence of the occurrence and of the existence of phases on different factors (the properties and atomic size dimensions, composition, temperature, pressure, interaction of physical-chemical media, the external physical fields, kinetics, etc.) has been collected. These factors are variable as well as unique for specific phases. The traditional theoretical methods - quantum mechanics, thermodynamics - in a majority of cases do not provide the possibility for complex analyses of these data in search of new materials. Moreover, these methods in themselves are dependent on the empirical models of the interaction of particles, which, as a rule, include the concepts of valency, nuclear charge shielding, atomic dimensions and interaction potentials.

Taking into account the absence of the effective methods for utilizing the accumulated information for the purposes of prediction and calculations of substances and materials, of practical interest, we have decided to utilize a new approach to the solution of these problems. The approach consists of utilization of certain ideas from cybernetics, from the field known as the generation of learning type of computer systems to the prediction of physical-chemical characteristics of various objects. Such objects in particular, are chemical elements and their compounds and mixtures, the properties of which determine the structure of phase diagrams. Since chemical elements have, at present, been studied in greater detail in comparison with more complex substances, we have decided that it is worthwhile first of all to utilize widely known data on the properties of elements for the prediction of the behavior of elements in various systems.

The problem which we have tackled was to teach the computer to differentiate among the combinations of various chemical elements, those which possess and those which do not possess a prescribed property i.e., objects

according to their properties. In this task the starting point was the concept of interrelationship of elements the physical-chemical systems as being a complex cybernetic system with preconditioned bonds, were the data on elements in a manner unknown to us form the basis for the effects which we observed in these systems. After the study of the available experimental examples, the computer classifies all uninvestigated combinations of elements into prescribed classes. This constitutes the problem of cybernetic prediction.

In this work cybernetic prediction was utilized for various types of systems. The basis for the first problem was to lay down the ideology for teaching the computer to recognize patterns [1,3,11]. The second system was based on the method of teaching the computer of inductive concept formation processes [9,10].

In this area, first investigations began in 1966 [1]. At present a number of chemical and metal science works have appeared, the authors of which turn to the idea of utilizing pattern recognition [12-17]. The area of obligation of their cybernetic methods is very broad; from analyses of mass spectra, IR spectra, NMR spectra of organic substances [13,14,16] to the search for new alloys with specific predesignated properties [12]. In this approach various pattern recognition methods are used, including recognition with learning [12-14,17] and automated classification [14-16]. It is not all that important what type, for the recognition of patterns is utilized for prognosis, if specific objects are taken into account, i.e. the objective and heuristic limitations which are placed on the choice and classifications of trained objects for prediction purposes. This latter is a problem of physical chemistry proper, or some other specialized discipline, and not that of mathematics per se. The choice of one or another program variation is frequently determined by the capability of a given computing technology and computation facility. In view of the absence of the general theory of pattern recognition, the search of an appropriate method for solving specific problems is a problem which is to a large extent experimental and not so much a theoretical one. Here one must not forget the mathematical limitations of the different algorithms.

The attempts to obtain prediction from "prima facie principles" suggest the use of fundamental characteristics of the atoms of chemical elements as the starting data-atomic number, distribution of electrons in the atom and others. However, depending on the problem facing the investigation different characteristics of chemical elements or the known phases can be utilized, as well as the concepts of the zone theory and other physical theories of the structure of matter.

For illustration let us cite fragments of the prediction of the existence of the binary Laves phase [4,5], beta-phase [6], A-15 type phase [7] (Figures 1-3). In the figures the vertical axes correspond to components A, while the horizontal axes correspond to component B in $A_n B_n$ type compounds, where n is equal or greater than 1. The positive sign indicates the prediction of the existence of a phase of a given type.

The sign "+" corresponds to known chemical compounds, which could have been used for teaching the computer. In cited examples, the prediction was obtained on teaching the machine using experimental examples in which phases in the various systems either existed or were absent, and in which chemical elements were described exclusively by the data on distribution of electrons in the isolated atoms of the corresponding chemical elements. It was thus found possible to construct in a logical way the analogs of "significant" indices for predicting the phases on the bases of these data alone.

In view of the promise of cybernetic prediction, investigations were started on prediction of ternary chemical compounds and creation of larger capacity cybernetic systems, based on the method of teaching universal computers the concept of formation [9-10]. Such methods are useful for isolation of complex concepts from a larger mass of information [18].

The method of formation concepts was used for predicting ternary chemical compounds of the following composition: $A_xB_yC_z$, where A and B are any elements of the periodic system, while C is either oxygen or sulfur. In the first place predictions were made on the most representative classes of compounds [from the standpoint of experimental examples], which are also of some practical interest [ABO_4 , AB_2O_4 , ABO_3 [9]], [A_2 , B_2 , O_7 , AB_2S_4], as well as the most wide-spread types of crystal structures [perovskite, spinels and pyrochlores]. The reliability of such prognoses is not lower than 78%.

In the work on ternary compounds we did not limit ourselves to utilization of only combinations of the parameters of electron structures of isolated atoms for the primary indices of the system and a description of the compounds. In addition to electron distribution, for the description of compounds two other indices were utilized. The first index included the parameters of chemical elements A and B; the type of unfilled electronic shell, the heat capacity of the element, the ionic radius of the element in a compound, the first four ionization potentials, and the formal oxidation state of the element in the compound of a given composition. The bases of the second system of indices included properties of simple oxides of the elements A and B; the enthalpy of formation, heat capacity at constant pressure, the effective radius of cation in the oxides, and also the corresponding degree of oxidation of the element.

All three systems of indices which were used for the description of compounds have high degree of correlation. Therefore, the prognosis obtained as a result of teaching the computer to use each of the three descriptive indices must, in general, coincide. The comparison of the predictions from different systems of indices leads to a significant increase in the reliability of the results. In using this approach, the predictions which do not coincide are excluded from consideration.

Figure 4 shows part of the prediction for the possibility of the formation of the compounds of the $A_2^{III}B_2^{IV}O_7$ composition (Roman numerals indicate the oxidation state of the element). The "+" sign denotes those cases when the compounds exists, "-" denotes the absence of such compounds in the A - B - O system; the circles indicate those compounds which were used for teaching the computer.

Figure 5 shows prediction of the existence of the compounds with pyrochlore structure. In this case "+" sign indicates that the existing compound $A_2^{III}B_2^{IV}O_7$ has a pyrochlore structure, while "-" indicates to the contrary. It is worthwhile to turn our attention to the large number of compounds which are being predicted with pyrochlore structure, which are formed by the trivalent rare-earth metals. It is quite possible some of these compounds will be of interest to the researchers who are seeking new piezoelectric materials.

It should be noted that the cybernetic predictory systems which were utilized are flexible in nature. The appearance of completely new experimental data which were not previously included into our predictory systems or which contradict the existing systems, aid in further educating the system, and to refine further the characteristics and prediction classifications. Such flexibility of the proposed approach resulted from the use of high speed electronic digital computers, capable of examining a tremendous number of possibilities for the construction of the classification scheme and then select from the analyzed variations the best suitable ones from the standpoint of separation of classes.

The predictions which were obtained by us decreased significantly the search time required for materials with the assemblage of desirable properties. They expand our capability of theoretically calculating phase diagrams and prediction of new phases as well as show the pertinence of the existing concepts regarding phase diagrams as an instrument for learning physical chemical systems. They require refinement and formulation of the concepts of chemical compounds, the conditions under which they are formed, stoichiometry, equilibrium state, kinetic data, as well as broader formulation of the thermodynamic phase rule which would take into account the interaction in various phase fields, vacuum, degree of dispersity, etc.

Bibliography

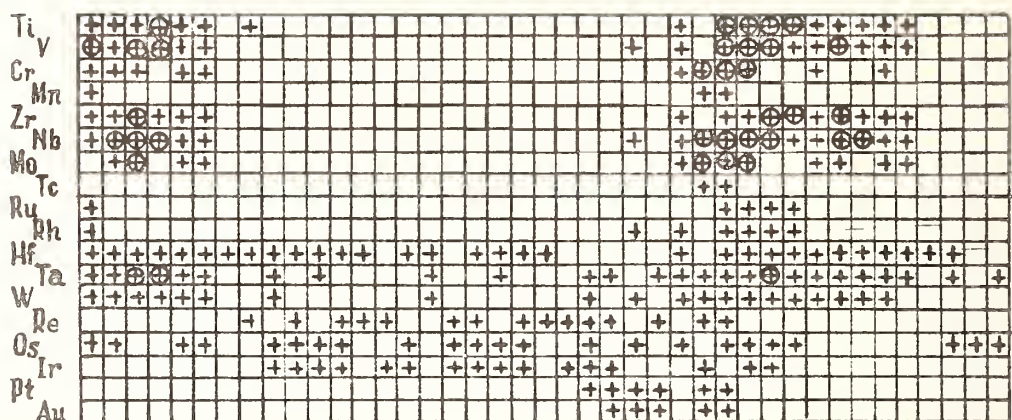
1. E. M. Savitskii, Yu. V. Devingtal', and V. P. Gribulya, Doklady Akad. Nauk. SSSR (Reports of the Academy of Sciences of the USSR), 1968, Vol. 178, No. 1, pp. 79-81.
2. E. M. Savitskii and V. B. Gribulya, J. Phys. Chem. Solids, 1972, Vol. 33, pp. 1853-1860.
3. E. M. Savitskii and V. P. Gribulya, Izv. Akad. Nauk. SSSR. Neorganicheskiye Materialy (The news of the Academy of Sciences of the USSR. Inorganic Materials), 1971, 7, No. 7, pp. 1097-1104.
4. E. M. Savitskii and V. P. Gribulya, Doklady Akad. Nauk. SSSR (Reports of the Academy of Sciences of the USSR), 1972, Vol. 206, No. 4, pp. 848-851.
5. E. M. Savitskii and V. P. Gribulya, Predskazaniye Faz Lavesa Pri Pomoshchi Evm. (Prediction of laves phases by means of the electronic digital computer), No. 4658-72, DEP, VINITI, Moscow, 1972.
6. E. M. Savitskii, Yu. V. Devingtal', and V. P. Gribulya, Doklady Akad. Nauk. SSSR (Reports of the Academy of Sciences of the USSR), 1975, Vol. 220, No. 5, pp. 1066-1069.
7. E. M. Savitskii, Yu. V. Devingtal', and V. P. Gribulya, Doklady Akad. Nauk. SSSR (Reports of the Academy of Sciences of the USSR), 1975, Vol. 223, No. 6, pp. 1383-1386.
8. E. M. Savitskii and V. P. Gribulya in the collection "Stiukdurae Svoystva, Zharoprochnyykh, Metallicheskih Materialov" (Structure and properties of refractory metallic materials) NAUKA Publishing House, Moscow, 1973, pp. 3-10.
9. N. N. Kiselyeva, B. I. Pokrovsakiy, N. V. Vashhenko, in a collection "Planiro-Vaniye i avtomatizatsiya eksperimenta v nauchnykh issledovaniyakh" (planning and automation of the experiment in scientific investigations) "SOVETSKOYE RADIO" Publishing House, Moscow, 1974, pp. 308-315.
10. V. P. Gladun, Kibernetika (Cybernetics), 1972, No. 5, pp. 109-117 and 28-36.
11. Yu. V. Devingtal', Izv. Akad. Nauk. SSSR. Tekh. Kibernetika (News of the Academy of Sciences of the USSR Technical Cybernetics), 1971, No. 3, pp. 139-147.
12. B. P. Gulyayev, and L. F. Pavanko, Avtomatika i telemek (automation and telemechanics), 1973, No. 1, pp. 131-147.

13. T. R. Brunner, C. L. Wilkinw, R. C. Williams, P. J. McCombie, *Anal. Chem.* 1975, v. 47, No. 4, pp. 662-665.
14. P. C. Jurs, T. L. Isenhour, "Chemical applications of pattern recognition", John Wiley and Sons, New York, 1975.
15. J. R. Koskinen, B. R. Kowalski, *J. Chem. Inform. and Comput. Sci.*, 1975, v. 15, No. 2, pp. 119-123.
16. B. R. Kowalski, C. F. Bender, *J. Amer. Chem. Soc.*, 1972, v. 94, No. 126 pp. 5632-5639.
17. M. A. Pichler, S. P. Perone, *Anal. Chem.*, 1974, v. 46, No. 12, pp. 1790-1798.
18. E. B. Hunt, J. K. Marin, P. J. Stone, "Experiments in Induction," Academic Press, New York and London, 1966.

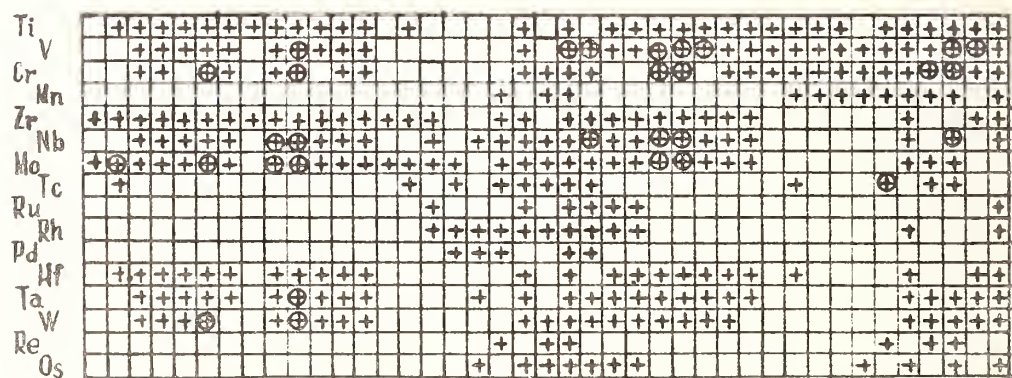
[illegible]

H Li B N F Na Al P Cl K Sc V Mn Co Cu Ga As Br Rb Y Nb Tc Rh Ag In Sb
He Be C O Ne Mg Si S Ar Ca Ti Cr Fe Ni Zn Ge Se Kr Sr Zr Mo Ru Pd Cd Sn Te

1157



Cd Sn Te Cs La Pr Pm Eu Tb Ho Tm Lu Ta Re Ir Au Tl Bi At U Lr
In Sb I Ba Ce Nd Sm Gd Dy Er Yb Hf W Os Pt Hg Pb Po Ra Es



Li B N F Al P Cl Ca Ti Cr Fe Ni Zn Ge Se Rb Y Nb Tc Rh Ag
Be C O Mg Si S K Sc V Mn Co Cu Ga As Br Sr Zr Mo Ru Pd

Figure 2. Prediction of binary phases of the A-15 type.

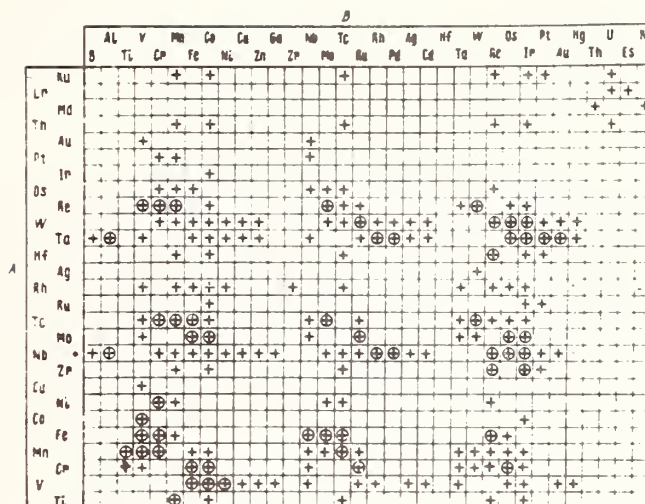


Figure 3. Prediction of the binary σ -phases.

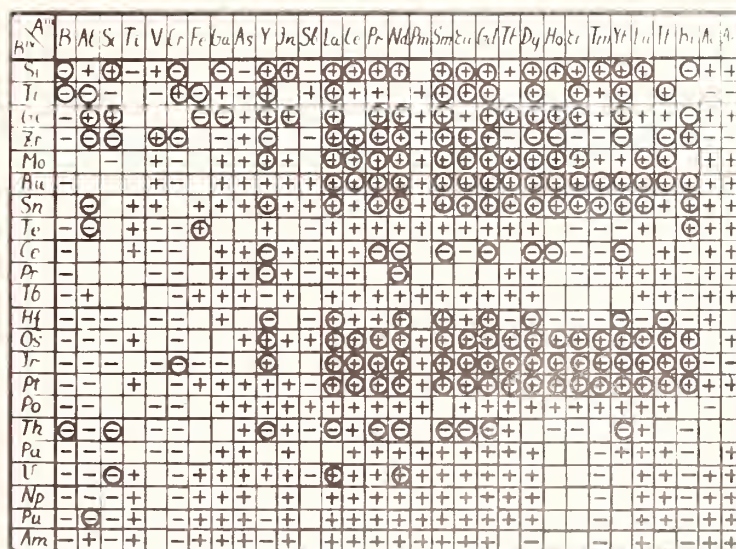


Figure 4. Prediction of chemical compounds of the $A_2^{III}B^{IV}O_7$ composition.

$A_{B''}^{IV}$	B	Al	Si	Ti	V	Cr	Fe	Ga	As	Y	In	Sc	Lu	U	Pr	Nd	Pm	Sm	Eu	Gd	Tb	Dy	Ho	Er	Tm	Yb	Lu	Tl	Hg	Au	Ag
Si	-	⊖							⊖	⊖	+	+	+	+	+	+	+	+	+	+	+	+	+	+	+	+	+	+	+	+	+
Ti					+	+	+	+	+	+	+	+	+	+	+	+	+	+	+	+	+	+	+	+	+	+	+	+	+	+	+
Ge	⊖	⊖							-	+	⊖	+	+	+	+	+	+	+	+	+	+	+	+	+	+	+	+	+	+	+	+
Zr				+				+					⊕	⊕	⊕	⊕	⊕	⊕	⊕	⊕	⊕	⊕	⊕	⊕	⊕	⊕	⊕	⊕	⊕	⊕	
Mo								+	⊖	⊖	⊖	⊖	⊖	⊖	⊖	⊖	⊖	⊖	⊖	⊖	⊖	⊖	⊖	⊖	⊖	⊖	⊖	⊖	⊖	⊖	⊖
Ru				+				+	+	+	+	+	+	+	+	+	+	+	+	+	+	+	+	+	+	+	+	+	+	+	+
Sn			+					+	+	+	+	+	+	+	+	+	+	+	+	+	+	+	+	+	+	+	+	+	+	+	+
Te				+					+	+	+	+	+	+	+	+	+	+	+	+	+	+	+	+	+	+	+	+	+	+	+
Ce				+				+	+			+	+	+	+	+	+	+	+	+	+	+	+	+	+	+	+	+	+	+	+
Pr																															
Tb								+	+				+	+	+	+	+	+	+	+	+	+	+	+	+	+	+	+	+	+	+
Hf								+																							
Os			+					+	+	+	+	+	+	+	+	+	+	+	+	+	+	+	+	+	+	+	+	+	+	+	+
Ir									⊕	⊕	⊕	⊕	⊕	⊕	⊕	⊕	⊕	⊕	⊕	⊕	⊕	⊕	⊕	⊕	⊕	⊕	⊕	⊕	⊕	⊕	
Pt			+					+	+	+	+	+	+	+	+	+	+	+	+	+	+	+	+	+	+	+	+	+	+	+	+
Po								+	+	+	+	+	+	+	+	+	+	+	+	+	+	+	+	+	+	+	+	+	+	+	+
Th																															
Pa																															
U			+					+	+	+	-	⊕	+	+	⊕	+	+	+	+	+	+	+	+	+	+	+	+	+	+	+	+
Np			+					+	+	+		+	+	+	+	+	+	+	+	+	+	+	+	+	+	+	+	+	+	+	+
Pu			+					+	+	+		+	+	+	+	+	+	+	+	+	+	+	+	+	+	+	+	+	+	+	+
Am	+	+						+	+	+	+	+	+	+	+	+	+	+	+	+	+	+	+	+	+	+	+	+	+	+	+

Figure 5. Prediction of the structure of pyrochlore type in compounds of the $A_2^{III}B^{IV}O_7$ composition.



THE DETERMINATION AND REPRESENTATION OF METASTABLE PHASE DIAGRAM FEATURES AND OTHER THERMAL CHARACTERISTICS OF METASTABLE ALLOYS, ESPECIALLY AMORPHOUS METALS

Bill C. Giessen

Institute of Chemical Analysis, Applications and Forensic Science
and Department of Chemistry, Northeastern University, Boston, Massachusetts 02115

INTRODUCTION

Recent advances in materials synthetic technology¹⁻⁴ have led to the preparation of a considerable number of metastable alloy phases; it was found that metastable phases can be prepared in virtually every alloy system if sufficiently effective nonequilibrium solidification or condensation methods are applied. These results have made it desirable to represent the new phases graphically in modified phase diagrams.

We first list the materials forming the subject of this review. One can differentiate four principal types of non-equilibrium phases^{1,2,4} (the term "phase" is used here in the Gibbsian sense to describe a homogeneous constitutional entity⁵ and does not necessarily indicate a local free energy minimum, or relate to the ability of the entity to participate in constrained equilibrium reactions, etc.). These materials are:

- A. Metastable elemental and near-elemental phases;
- B. Metastable extensions of terminal or intermediate solid solutions;
- C. Metastable intermediate phases;
- D. Amorphous alloys (metallic glasses).

Typical metastable phases representing these four types are listed in Table I, using information compiled primarily in Refs. 2, 4, 6-11. We limit our discussion to phases which require very rapid quenching methods or atomic deposition methods for their preparation and retention to room temperature. This excludes common metastable phases such as martensite and cementite.

Table I: Types of Metastable Alloy Phases

Type	Examples
1. Metastable Elemental Modifications	Ga
2. Extended Terminal or Intermediate Solid Solution	
a) Substitutional	Al(Ni), ϵ -Pu(Ti)
b) Interstitial or disubstitutional	Pb(Au), Gd(Cu)
c) Based on metastable elemental modification	γ -Sn(Pb), β' -Ga(In)
3. Metastable Intermediate Phases	
a) Disordered phases	
α) Hume-Rothery phases	ζ -(Au-Sb), γ -(Au-Sn)
β) Element-like B and T metal phases	Zn-Ga, In-Bi, ϵ (Nb-Ni)
b) Ordered phases	NiPb, Cu ₂ Al ₃ , Al ₃ Ge ₂
4. Amorphous Metals	
a) Transition metal - metalloid	Fe-B, Pd-Si
b) Transition metal - transition metal	Zr-Cu, Nb-Ni
c) Miscellaneous systems	
α) A metal - B metal	Mg-Zn
β) Actinide - T metal	U-Cr

Following present custom⁴ we do not differentiate between amorphous solids prepared from the melt (i.e. glasses in the original sense of the word) and those prepared by atomic deposition methods (e.g. from a vapor) and designate both materials as glasses; see Ref. 8 for a discussion of this point. The types of metastable phases listed above have been the subject of many recent extensive reviews, e.g. Refs. 1, 2, 4. Alloy constitutional aspects have been emphasized in Ref. 1; phase diagram aspects have been presented especially in Ref. 7. In Ref. 12, the constitutional requirements of metastable crystalline phase formation have been discussed in detail and the kinetic aspects have been treated in terms of solidification theory; the formation of amorphous metals is reviewed thoroughly in Ref. 13.

Further, because most of the metastable alloys studied to date either contain two components or components that can be divided into two groups

of closely related elements⁴ (such as amorphous metal-metalloid systems T-X where T = Fe, Co, Ni and X = B, C, P), we emphasize binary systems here; we also do not discuss pressure effects; last, because the phases of interest to us are principally prepared from the melt, we focus here on those regions of the phase diagrams which pertain to condensed phases.

Three principal types of data are of importance in the phase diagram representation of metastable phases and will be discussed:

1. Free energy diagrams;
2. Temperature-composition phase diagrams and related diagrams;
3. Diagrams presenting kinetic and other physical/chemical parameters.

We discuss, in order, types of phase diagram representations as listed here, pertinent experimental methods, phase diagram aspects of the formation of metastable phases, and, last, data needed in future research on amorphous metals.

PHASE DIAGRAM AND RELATED DIAGRAM REPRESENTATIONS

1. Free Energy - Composition Diagrams

As free energy diagrams are fundamental to phase diagram representations they are treated first. We begin this discussion by presenting an estimate of the maximum free energy excess ΔG^{exc} of a metastable phase over the equilibrium phases that can be achieved by different preparation methods. The estimate is based on a Carnot cycle thought experiment and has been given by Baker and Cahn.¹² It is readily seen that $\Delta G_{\text{max}}^{\text{exc}} \leq \frac{\Delta T}{T} \Delta H$ where ΔT is the undercooling and ΔH is the heat added in the first stage of the process. For solidification of a liquid into a crystalline phase, $\Delta H/T = 2$ e.u., $\Delta T/T < 0.3$, and $\Delta G_{\text{max}}^{\text{exc}} \sim 0.06$ eV (for a metal melting at 1000 K). For condensation of a vapor, $\Delta T/T$ may be unity, $\Delta H/T \sim 20$ e.u. and $\Delta G_{\text{max}}^{\text{exc}} \sim 2$ eV (for a metal evaporated at 2000 K). While this argument correctly yields the higher capability for metastable phase formation observed for atomic deposition processes, it appears to overestimate this potential considerably. First, this argument is valid only for a reversible process and irreversibility will reduce the $\Delta G_{\text{max}}^{\text{exc}}$; this will be the case for vapor quenching processes, which are conducted far from equilibrium conditions. Second, it can be expected that any high-energy metastable phase with free energy higher than the corresponding liquid or glass would not form under any conditions, but would relax spontaneously to form a melt or glass, releasing its free energy excess over the latter.

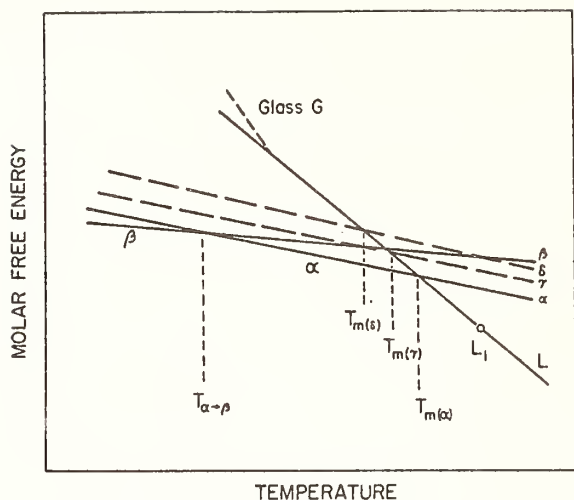
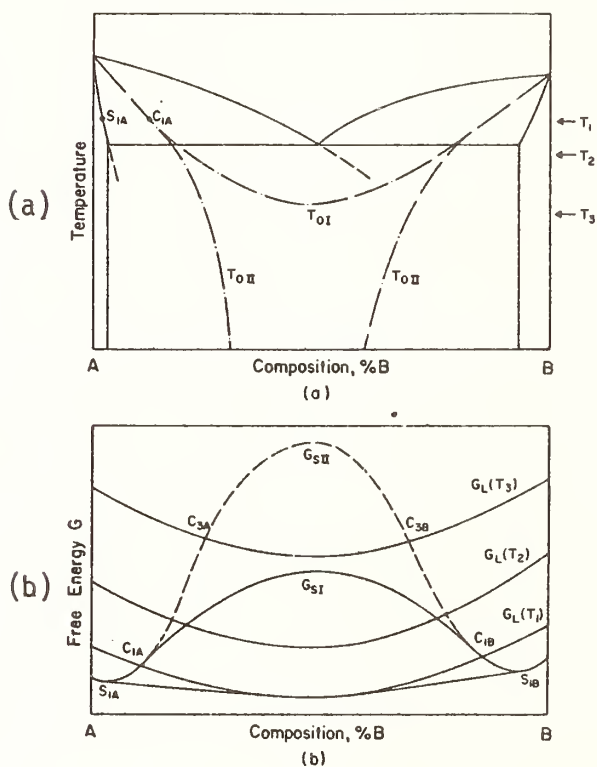


Figure 1. Schematic representation of the free energies of phases present in a hypothetical one-component system as a function of temperature at constant pressure. (From Ref. 1.)

Figure 2. Hypothetical eutectic binary system: (a) phase diagram indicating role of the parameter T_0 ; (b) free energy diagram for three temperatures $T_{1,2,3}$ and two solid solutions with different positive deviation from Raoult's law. (From Ref. 1.)



a. G-T diagrams: Metastable phase and glass formation can be presented particularly readily for one-component systems where free energy(G)-temperature(T) diagrams such as that given in Fig. 1 can be drawn.⁴ This figure shows that metastable γ and δ may form in local equilibrium if the system is constrained against the formation of the lowest-free-energy phase α and, subsequently, the phase β . The formation of the glass at G is also shown; this will occur if the supercooled liquid is no longer able to relax

internally as the temperature is reduced and passes through a glass transition.

b. G-x diagrams: A hypothetical, simple eutectic binary phase diagram A-B, where A and B are isostructural, is shown in Fig. 2a. The G-x diagram (x = composition) for this system is as shown schematically in Fig. 2b. These diagrams are discussed extensively in Refs: 1 and 4. The shape of G_s , the free energy curve of the solid, is the principal factor in determining which metastable phases are possible: for a G_s curve such as G_{sI} there exists a

range of temperatures for which G_S lies below G_L , the free energy of the liquid, over the whole composition range, while for G_{SII} no such temperature range exists down to the absolute zero of temperature. This situation is reflected in the T - x diagram by the important T_0 temperatures discussed below (see Fig. 2a). For metastable intermediate phases, G - x diagrams can give comprehensive graphic representations of all phases thermodynamically possible in any given system. An example of such a plot is given in Fig. 3c, which is closely patterned after (though not representative of) the In-Bi system in which many metastable phases have been prepared.¹⁴ This figure, discussed in detail in Ref. 1, shows a large number of competing phases with similar, low excesses of the free energy over those of the equilibrium phases and their combinations.

It may be considered that the G - T diagram of every unary system contains all possible elemental structures at their appropriate free energies if it is extended to sufficiently high values of G ; likewise, the free energy diagrams of binary systems contain all binary phases possible at the appropriate composition, both with correct stoichiometries or off-stoichiometrically, and with all values of atomic volume, axial ratio, internal parameters etc., of these phases. However, only a limited number of these phases will have free energies lying below the Carnot process excess free energy discussed previously and can possibly be retained by appropriate experimental techniques.

As an example, the G - x diagram of the Au-Sb system which is discussed below in more detail, is given in Fig. 4d;^{1,4} it shows two observed metastable phases ζ ¹⁵ and π ,¹⁶ for which thermodynamic properties have been determined.¹⁷ We also present a partial G - x diagram for the Zn-rich portion of the Ag-Zn system,¹⁸ Fig. 5a, which includes data for the metastable

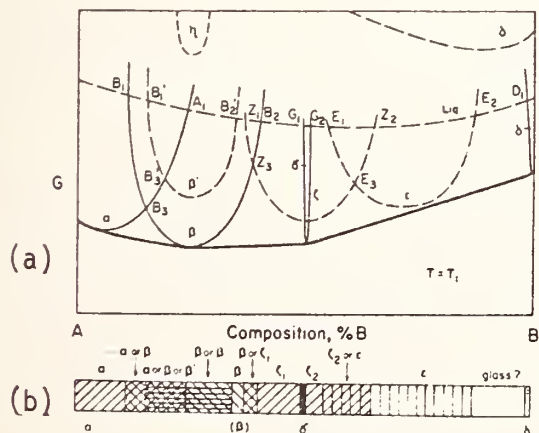


Figure 3. Hypothetical binary system with intermediate phases: (a) free-energy diagram; (b) phases which may be present after nonequilibrium solidification following supercooling of the melt to $T=T_1$. (From Ref. 1.)

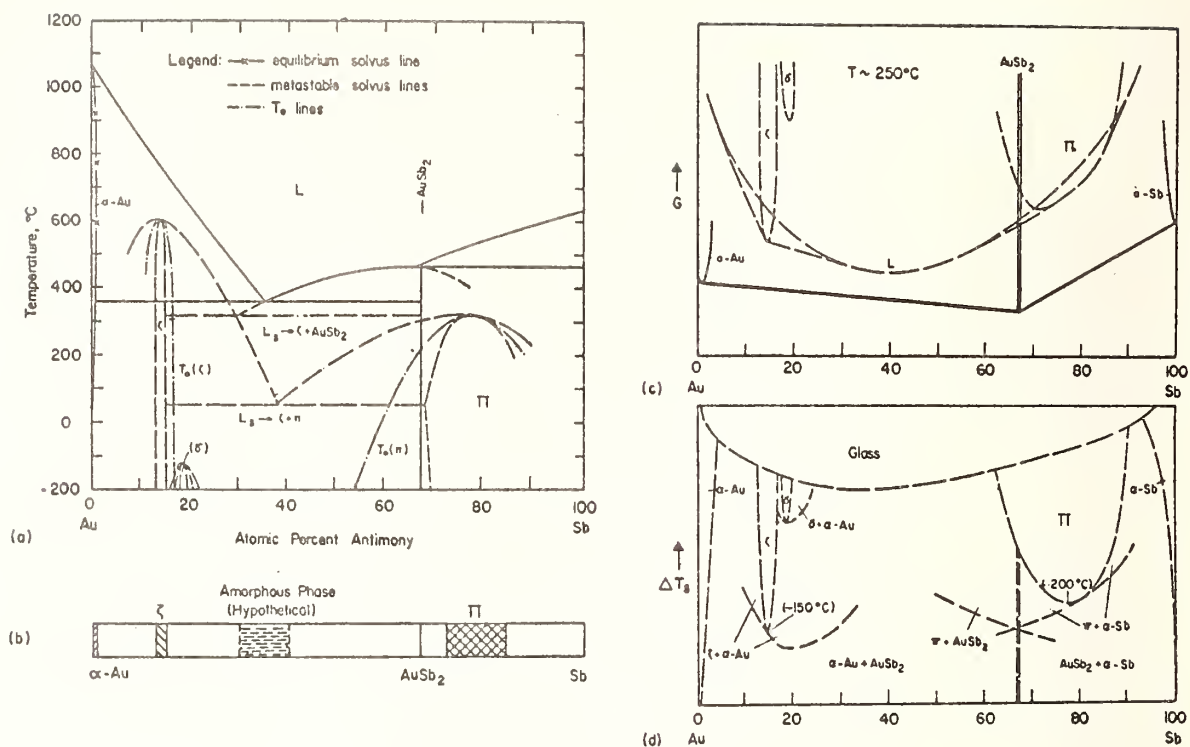


Figure 4. The system Au-Sb: (a) stable and metastable phase diagram; —x—, equilibrium solvus lines; — — —, metastable solvus lines; - · - · -, T_0 lines; (b) quenched-phase plot; (c) hypothetical free energy diagram at $T \sim 250^\circ\text{C}$; (d) ΔT_s - x diagram showing the role of supercooling in metastable phase formation. (From Refs. 1, 4.)

extensions of two hexagonal phases, terminal η -Zn(Ag) and intermediate ϵ . The atomic volumes and axial ratios of η and ϵ approach each other in the metastable range but do not become equal, leading to the proposed G- x diagram.¹⁹

2. Temperature-Composition Diagrams

The T- x diagrams are the diagrams of greatest general importance concerning metastable phase retention.

a. Phase-vs-composition diagrams: In systems where metastable phases have been prepared by cooling to a certain temperature but where there is no further information on their thermal properties, the most direct representation of metastable phases is in a "quenched phase plot", drawn as shown in Fig. 4b under the phase diagram, Fig. 4a.

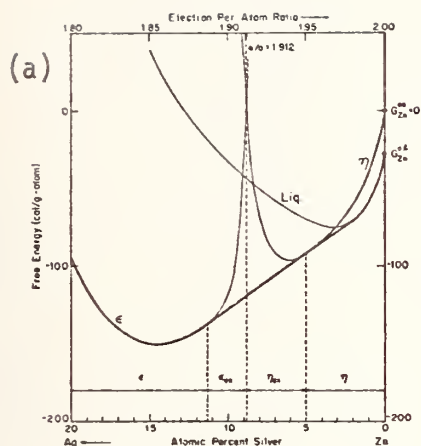
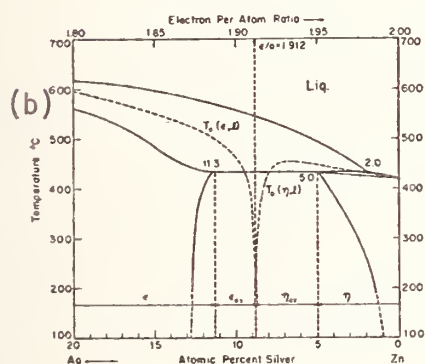


Figure 5.

(a) Free energy configuration for the solid ϵ and η phases and the liquid phase at the peritectic temperature (430°C) for zinc-silver. The free energy of each phase in its stability range has been calculated from thermodynamic data. The arbitrary energy references are $G_{\text{Zn}}^{\text{OS}} = 0$, $G_{\text{Ag}}^{\text{OS}} = +8000$ cal/g-atom. (From Refs. 18, 19.)

(b) Possible trends of the T_0 temperatures in the zinc-silver system. (From Refs. 18, 19.)



b. T-x diagrams with metastable phases: If thermal data are known from direct measurements, as discussed below for Ga^{20} or Bi alloys²¹ or by calculation from measured thermodynamic quantities, as shown below for the melting points of Au-Sb alloys,¹⁷ metastable phases and equilibria can be directly represented in a phase diagram as shown for Au-Sb in Fig. 4a. This type of presentation, using dashed lines, has long been standard for equilibria involving metastable phases that can be readily obtained such as those occurring in the metastable $\text{Fe-Fe}_3\text{C}$ portion of the Fe-C system²² or the Cd_4Sb_3 phase and the associated equilibria in the Cd-Sb system.²²

Ideally, such a T-x diagram should be completed as discussed above by including all metastable phases that are thermodynamically able to form from the liquid in constrained equilibrium upon supercooling of the liquid to any temperature, i.e. by including all phases that have lower free energies than the liquid at any temperature ≥ 0 K. At present only the upper temperature region down to 200-300 K below the melting point is

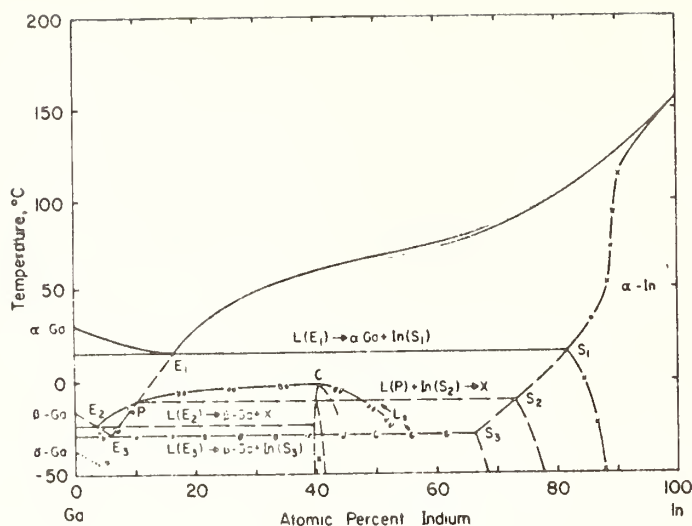


Figure 6. The system Ga-In; stable and metastable phase diagram (after Ref. 20) with additional, hypothetical reactions. —, equilibrium diagram α -Ga - In (measured); -x-, equilibrium diagram α -Ga - In (assumed); ---, nonequilibrium diagram β -Ga - In (X forms); -·-·-, nonequilibrium diagram β -Ga-In (X supercooled); - - - -, hypothetical congruent melting curve for X. (From Ref. 1.)

experimentally accessible to supercooling experiments because of the intervention of crystallization; moreover, upon supercooling of the liquid to lower temperatures, glass formation will intervene at the glass transition temperature and prevent the crystallization of metastable crystalline phases. However, at least in principle, the total temperature range is accessible by vapor quenching to 0 K. While at present it would be an impossible undertaking to attempt this kind of phase survey for more than a few selected systems, automated methods of examining thin films prepared at very low rates on substrates kept at very low temperatures may make vast portions of the metastable phase diagram accessible.

As examples of direct thermal determinations we present in Fig. 6 measurements on alloys in the metastable Ga-In system²⁰ which show the formation of metastable β -Ga²³ and its primary liquidus line as well as other equilibria involving a hypothetical metastable intermediate phase. Other examples are the metastable Ga-Al system, discussed in detail in Ref. 1, Fig. 6, and the metastable Sn-Pb system.^{24,25}

c. T_0 -x diagrams: In T-x diagrams, such as Fig. 2a, T_0 indicates the temperature for which the free energy curves of the liquid and the metastable solid intersect at a given composition x_0 in the corresponding G-x diagram; see Fig. 2b. Compositions with $x > x_0$ cannot be retained as metastable phases by cooling to $T > T_0$, because $G_{\text{solid}} > G_{\text{liquid}}$ for $x > x_0$ and $T > T_0$.

Alloys with $x = x_0$ can be retained from the melt only upon cooling to $T < T_0$; T_0 thus characterizes the minimum supercooling required for single metastable phase retention at composition x_0 .

T_0 curves such as those represented by T_{0I} in Fig. 2a indicate that, at least thermodynamically, a complete range of metastable solid solutions can be retained from the melt if equilibrium phase crystallization is prevented and glass formation does not intervene. By contrast, in the case of T_0 curves such as those represented by T_{0II} this is impossible even upon supercooling to $T = 0$ K. The Ag-Cu system²⁶ and probably also the Zn-Cd system²⁷ are of the former kind, although in the latter case only a small increase of the solid solubility of Cd in Zn has been achieved by splat cooling,²⁸ apparently due to the failure of reaching sufficiently large undercooling before crystallization occurred.

The T_0 - x curves of the Ag-Zn system^{18,19} which was introduced above are given together with the T - x phase diagram in Fig. 5b; it is seen that the rapid increases of G in the G - x curves (Fig. 5a) in the intermediate composition range and their intersection lead to a corresponding, deep valley and intersection of the T_0 curves in this region, indicating that supercooling temperatures of ~ 300 K are required to obtain a single phase alloy at every composition (and coexisting ϵ and η at the composition of the T_0 intersection).

d. T_C - x diagrams: Such diagrams show the composition dependence of the temperatures of phase transitions T_C involving some property of a metastable phase, such as a magnetic or superconducting transition; these plots are quite analogous to the corresponding ones for equilibrium phases. Examples are plots of the composition dependence of the superconducting transition temperature T_C of the metastable extension of the off-stoichiometric phase $Nb_3(Nb_xGe_{1-x})$ to Nb_3Ge ²⁹ and the plot of the saturation magnetization against composition for ferrimagnetic, amorphous Gd-Fe alloys³⁰ (see Ref. 4).

e. T_S - x diagrams: The minimum supercooling temperature ΔT_S required to prepare a given metastable phase at a given composition x can be read off from the stable-metastable T - x diagram (e.g., Fig. 4a) and can be plotted directly in a diagram bearing a certain resemblance to an inverted T - x diagram. An example is shown for the Au-Sb system in Fig. 4d;¹ the ΔT_S values for ζ and π are based on Fig. 4a while the other values have not been determined directly. A similar plot of the critical cooling rate \dot{T}_C required for the retention of a given metastable phase has also been introduced.³¹

3. Kinetic Parameters

Kinetic parameters are especially important in the characterization of amorphous metals,¹³ to which the discussion in this section will be limited. There are two principal pertinent quantities.

a. The glass transition temperature, T_g : T_g is the temperature at which properties such as the free energy (Fig. 1a), the atomic volume or some other property depart from a continuous extension of their values for the supercooled liquid due to the inability of the system to stay in internal equilibrium, as shown in Fig. 1a for the free energy. Other property changes taking place at T_g include a decrease of the specific heat by up to 100% and an increase of the viscosity by a factor of 10^5 ; for amorphous metals, T_g must be approached from below to prevent crystallization and the reverse of these changes is then observed.

T_g depends on the cooling rate of the liquid during supercooling and, if the measurement is made upon heating, the heating rate;³² thus it is not a quantity of state of the system. In many alloys, the glass transition cannot be observed upon heating because crystallization intervenes; in some systems, on the other hand, crystallization only occurred upon heating to 50 K above T_g .

b. The crystallization temperature, T_c : There may be a sequence of crystallization and recrystallization steps, characterized by T_{c1} , T_{c2} , etc.³³ Like T_g , these temperatures are heating rate dependent, increasing with increasing T ; the activation energy of crystallization can be deduced from the change of T_c with T .³⁴ Time-temperature-transformation (TTT) diagrams can be constructed for the equilibration process (see Ref. 8).

Another type of T-T-T diagram is of importance in the formation of amorphous metals; it contains information on the cooling conditions required for the retention of amorphous metals.³⁵ Representations of the composition dependence of T_g , T_c and the T-T-T diagrams would be useful; these data are presently available only in a few instances.

EXPERIMENTAL METHODS

1. Preparative methods

As the techniques employed to retain metastable phases (in the sense described above) have been discussed frequently in the literature,¹⁻⁴ we will limit ourselves here to a brief compilation of the principal methods,

given in Table II. As can be seen, preparative methods are generally classified into liquid (melt) quenching and atomic deposition methods, with the former subdivided into fast quenching (some of which are known as "splat cooling") and slow cooling methods, the latter divided into vapor or solution deposition techniques. There is special emphasis on the droplet supercooling method^{21,24} which is suitable for making thermal measurement during cooling, in contrast to the rapid quenching methods; it is primarily based on the prevention of heterogeneous nucleation during cooling and, possibly, a reduction of the equilibrating effect of homogeneous nucleation.

2. Investigative Methods ·

a. Free energy-composition diagrams: In principle, measurements of the free energy of formation can be made at temperatures sufficiently low to prevent decomposition or transformation of the metastable phases, e.g. by specific heat or EMF measurements. However, the latter measurements which require solid or liquid electrolytes are often difficult to perform at the required low temperatures. An alternate approach is to determine the enthalpy of formation by solution calorimetry and to make suitable assumptions on the entropy term.

b. Temperature-composition data:

i. Thermal analysis: Direct thermal analysis in the metastable range during cooling is readily possible for droplets during supercooling; it has also been attempted during the quenching (splat cooling) of alloy deposits;³⁶ see also Ref. 2. The thermal analysis of metastable phases by differential thermal analysis (DTA) or differential scanning calorimetry (DSC) during heating is also possible. There are some thermal measurements for metastable crystalline phases^{20,21} and a large number of such measurements on metallic glasses.^{37,38} For the former, the metastable melting temperatures are of prime interest; for the latter, the glass transition temperature, T_g , and the crystallization and recrystallization temperature(s), T_c , are objects of study. As mentioned, both T_g and T_c depend on the heating rates, as well as on the cooling rate during quenching; the effect of increasing heating rates is an increase (by different amounts) of T_g and T_c .

ii. Indirect methods: An indirect determination of the metastable melting points of crystalline nonequilibrium phases has been carried out for the two metastable Au-Sb phases shown in Fig. 7b;¹⁷ see also Fig. 4a. The

Table II. Methods for the Preparation of
Metastable Alloys, Especially Metallic Glasses

Method	Rate of Production	Estimated Cooling Rate, K/sec	Shape of Product
I. Melt Cooling			
A. Rapid Quenching			
1. Gun (splat) method	Very low	$10^6 - 10^9$	Irreg. foil fragments
2. Hammer-and-anvil method			
a) Arc furnace system	Very low	$10^6 - 10^7$	} Irreg. shaped flat foil
b) Induction system	Very low	$10^5 - 10^6$	
3. Melt spinning	Very high	10^6	Ribbon
4. Melt extraction	Very high	$10^4 - 10^5$	Profile wire
5. Dual roller method	low	10^6	Short ribbon
6. Plasma deposition	Medium	$10^4 - 10^6$	Porous sheet
7. Laser glazing	-	$10^5 - 10^6$ (est.)	Surface layer
B. Slow Quenching			
Droplet supercooling	Low - medium	$10^{-1} - 1$	Droplets
II. Atomic Deposition			
A. From Vapor Phase			
1. Vapor deposition	low	Very high*	Thin film
2. Sputtering	Medium	high*	Sheet
B. From Solution			
1. Electrodeposition	Medium	high*	Sheet
2. Electroless deposition	Medium	high*	Sheet

* Effective Cooling Rate

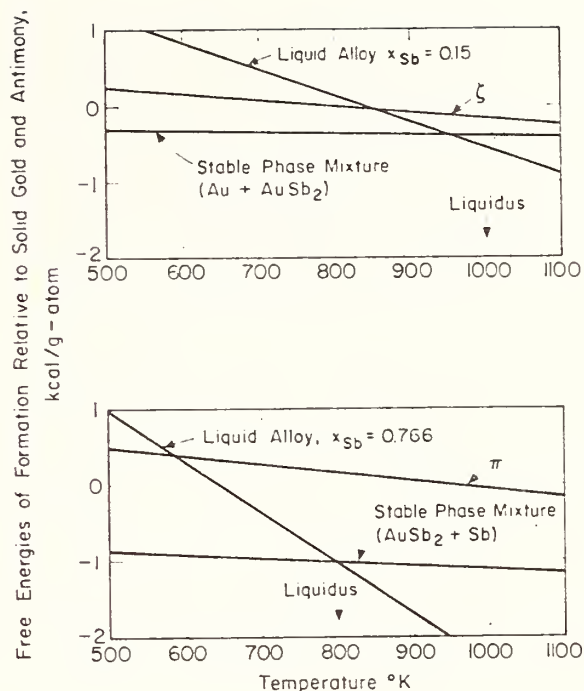
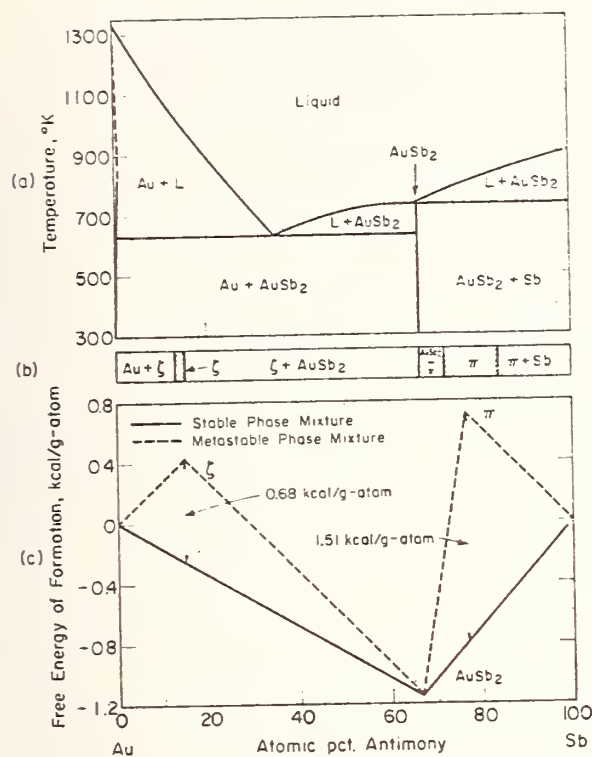


Figure 7. (a) Stable phases in the system gold-antimony. (b) Metastable and stable phases present at 298°K in the splat cooled gold-antimony alloys. (c) Free energies of formation at 298°K of mixtures of stable phases and mixtures of stable and metastable phases in the system gold-antimony. (From Ref. 17.)

Figure 8. Free energies of formation relative to solid gold and antimony of the ζ and π phases, the liquid gold-antimony alloys with $x_{Sb} = 0.15$ and $x_{Sb} = 0.766$ and the corresponding mixtures of stable phases. (From Ref. 17.)

heats of formation ΔH_F of ζ-(Au-Sb) and π-(Au-Sb) were measured by tin bath solution calorimetry. The free energies of formation were derived, making a proper assumption on the ΔS_F term, yielding the ΔG_F -x plot, Fig. 7c. This diagram shows that ζ and π are metastable not only with respect to the equilibrium phase mixtures but also with respect to the component mixture.

Further, free energy-temperature (G-T) diagrams can be constructed which yield the metastable melting points of ζ and π (Fig. 8a and b). These temperatures can subsequently be entered into the T-x phase diagram, as shown in Fig. 4a.

Insert shows calculated ratio of beryllium solubility in the hcp ternary solution divided by beryllium solubility in hcp binary solution

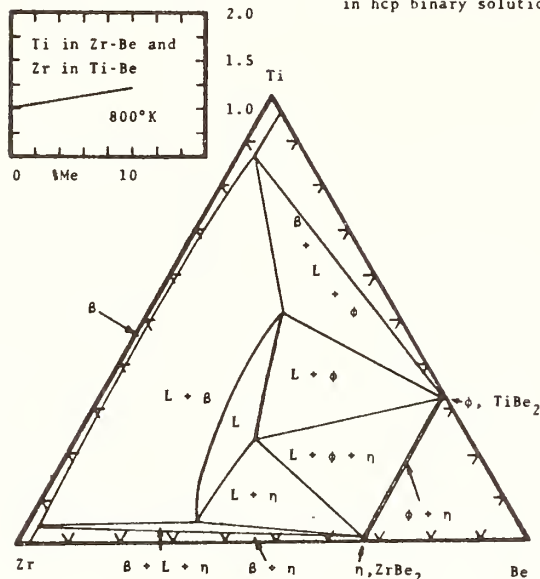


Figure 9. Calculated partial isothermal section in the Ti-Be-Zr system at 1180 K.⁴¹ (From Ref. 42.)

3. Computations

Definitive, first-principle calculations of the thermal data of metastable phases would represent an ideal method for the prediction of metastable phases;³⁹ unfortunately, at the present state of the art, the accuracy of such calculations is not yet sufficient. However, calculations such as those by Kaufman and others (see review, Ref. 40) can now be used to predict the supercooling required to obtain metastable elemental modifications and element-like intermediate phases in a number of cases. Further, the results of phase diagram calculations made to obtain eutectic compositions may be used to identify possible glass forming compositions in systems with more than two components using the low melting point criterion of ready glass formation discussed in more detail below. As an example, a calculated section of the Be-Ti-Zr system⁴¹ is shown in Fig. 9;^{41,42} a high glass forming ability was observed for a number of alloys in this system.⁴³

PHASE DIAGRAM ASPECTS OF THE FORMATION OF METASTABLE PHASES

1. Crystalline Phases

The metastable crystalline phases of interest here are of several kinds. For unary systems, there may be metastable modifications of the element or compound involved; for binary and higher order systems there may be metastable

modifications of one or more constituent element(s), with associated solid solution range(s), as well as melting curves and other multi-phase reactions involving these modifications. Further, there may be metastable intermediate phases, both disordered^{44,45} and ordered.¹¹ The alloy chemistry of these two types of phases in binary metallic systems has been reviewed extensively in the references given; these aspects are therefore not repeated here.

As shown above for the metastable Au-Sb phases ζ and π , metastable phases are readily represented in T-x diagrams. Besides the interest in metastable equilibria involving such phases, there would be a fundamental interest in "complete" phase diagrams containing all possible metastable phases that could be obtained in a given system by cooling the melt to 0 K, as discussed above. Such information could be used to establish connections between equilibrium diagrams by pointing out structural relationships and fields of isostructural phases or "metastability ranges", as discussed in Refs. 11 and 44. Also, it would provide a basis for the experimental verification of theoretical calculations of structural stability such as those of Heine and Weaire for B-metal phases.³⁹

The nucleation and growth rates of various metastable phases from supercooled liquids are generally not known. Ostwald's rule, according to which equilibrium is reached by small steps where possible, with the system passing through a series of metastable states, is sometimes quoted

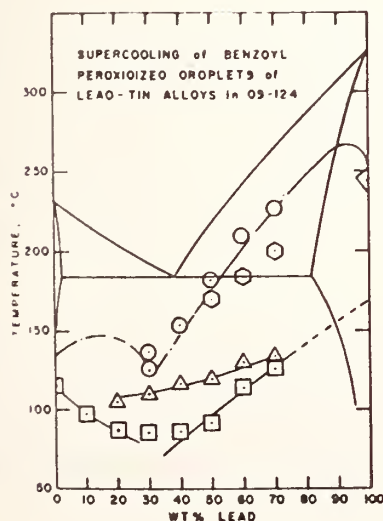


Figure 10. Phase diagram for Sn-Pb indicating undercoolings corresponding to various peroxidation reactions at the droplet surfaces. Squares represent maximum supercooling for benzoyl peroxidized emulsions. The maximum undercooling observed by Hollomon and Turnbull⁴⁶ is indicated by the - - - - curve. (From Ref. 24.)

as a general guide; however, as it is not known beforehand whether discrete intermediate steps (i.e. states of intermediate free energy) exist, this rule has little predictive value.

It would be of interest to relate the occurrence of metastable crystalline phases to features of the equilibrium T-x diagram. Thus, at least in some systems, metastable crystalline phases were found at compositions of relatively low melting point, e.g. in the Au-Si and Al-Ge systems.⁷

Further, we mention plots of other types of composition dependent thermal properties, such as plots of the maximum supercooling obtained, as shown in Fig. 10 for droplet-dispersed and supercooled Pb-Sn alloys.²⁴

2. Amorphous Phases

Phase diagram aspects and, particularly, T-x diagrams play an important role in the scientifically and technologically significant effort of categorizing and, hopefully, predicting the occurrence of the amorphous state in alloys prepared under nonequilibrium conditions, especially by rapid quenching from the melt. The latter may be possible because the phase diagram expresses, directly or indirectly, important aspects of the glass forming ability of a given alloy.^{4,8,13} Some of these aspects are summarized in Table III (following Ref. 8) and are briefly reviewed in the following; we limit our discussion mostly to systems in which glasses can be formed readily by melt quenching. The eight glass forming phase diagrams presented in Fig. 11¹³ may serve as illustrations of some of the principles involved.

a. Low liquidus temperatures: Probably the most obvious and best-known of the criteria for ready glass formation are connected with the liquidus temperatures. Soon after the accidental discovery that an amorphous Au-Si alloy can be prepared by rapid quenching⁴⁷ (splat cooling) the higher glass forming ability of low melting point compositions, frequently at and near eutectics, was recognized. This concept was formalized by Cohen and Turnbull,⁴⁸ who related glass forming ability to a low value of the reduced melting temperature

$$\tau_m = kT_m/\Delta H_v ,$$

where T_m , the melting (liquidus) temperature, reflects the thermal energy at the melting point and where ΔH_v , the vaporization enthalpy, is a measure of the activation energy required for diffusion processes involved in the nucleation and growth of the equilibrium phases whose formation

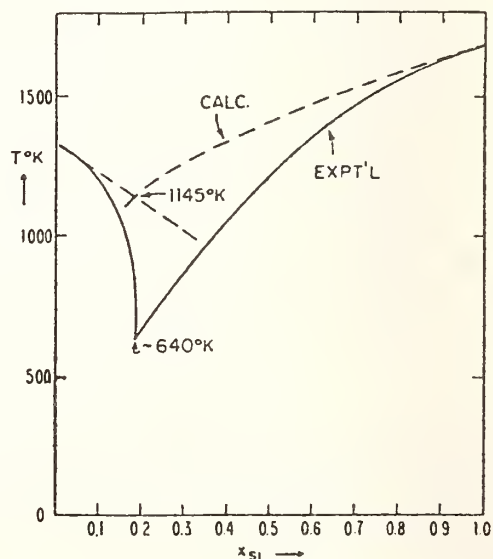
Table III. Criteria for Easy Glass Formation Expressed by the T-x Phase Diagram (After Ref. 8)

<u>Property</u>	<u>Examples</u>
1. Low liquidus temperatures	
a) Narrow region of low T_m (e.g. single deep eutectic)	Pd-Si, Mg-Zn
b) Low T_m over extended composition range	Nb-Ni, Zr-Cu
2. Atomic properties of constituents	
Size difference	Fe-B, Zr-Cu
3. Compositional properties	
a) Crystal chemistry of equilibrium phases	$\mu(\text{Nb-Ni})$, Mg_7Zn_3
b) "Confusion principle"	Fe-P-C, Fe-Ni-P-B

Note: Other important criteria not directly expressed by the phase diagram include:

atomic properties of the constituents such as valence difference;
compositional properties such as melt stoichiometry and alloy valence electron concentration.

Figure 12. Comparison of experimental phase equilibrium diagram ($p = 1$ atm) of Au-Si system with diagram calculated assuming that liquid solutions behave ideally. Experimental diagram from Refs. 22 and 49. (From Ref. 40.)



competes with glass formation taking place by continuous cooling of the liquid. τ_m thus is the ratio of the thermal energy available at the melting point to the energy of diffusion in the melt and measures its fluidity.

Composition ranges of relatively low liquidus temperatures thus become prime candidates in a search for readily glass forming alloys. The melting point depression may be expressed as

$$T_{mr} = (\bar{T}_m - T_m)/\bar{T}_m ,$$

the normalized reduction of the melting point T_m from the weighted average \bar{T}_m of the components.⁸ An alternate expression is based on the reduction of T_m from the hypothetical melting point as given by ideal solution theory;⁵¹ as an example, observed and calculated values are compared for the Au-Si system in Fig. 12.⁴⁰ It is found that the phase diagrams showing large T_{mr} values are primarily of two types:

- i. those having narrow regions of low melting points, e.g., a single deep eutectic; examples are transition metal-metalloid systems²² such as Pd-Si⁵² and non - transition metal systems such as Mg-Zn³³ (Fig. 11);
- ii. those having low melting points over extended composition ranges, such as Nb-Ni⁵³ and Zr-Cu;⁵⁴ systems of this type generally include one or more intermetallic phase(s) in the glass forming composition range.⁸

Large values of the reduced glass temperature

$$\tau_g = T_g/T_m ,$$

where T_g is the glass temperature, are also associated with high glass forming ability.¹³

- b. Atomic properties: Turning to atomic properties of the constituents that are of importance for glass formation and are expressed by features of the phase diagram, one finds the important criterion of atomic size. Generally, a component size ratio of ≥ 1.15 is required for glass formation; here, the size is not the atomic size of the elements but the "actual" size of the atoms as deduced from equilibrium phases in the system involved. These atomic sizes and their ratios are often reflected in the structure type and thermal stability of the observed equilibrium phases; thus glass forming systems with constituents having a size ratio differing from unity by an amount similar to that given above will often show Laves phases at the compositions appropriate for the formation of such phases (AB_2 , AB_3);⁴⁵ in general, these compositions are far removed from the glass forming ones.
- c. Compositional Properties: Properties of intermediate equilibrium phases may also be used to estimate glass forming ability in another way which is

classified in Table III under the heading of compositional properties. This approach is based on the fact that alloy phases found at or near glass forming compositions generally belong to certain, frequently complex crystal structure types and have similar atomic coordination characteristics. For metal-metalloid glasses, e.g., this observation was made by Polk⁵⁵ and was related to a model for the structure of such glasses. Another compositional criterion reflected by the phase diagram is the so-called "confusion principle" which expresses the experience¹⁰ that more complex alloy systems (i.e. systems containing more than two constituents) are often better glass formers than simpler ones; thus, alloys near the ternary eutectic Fe-Fe₃C-Fe₃P form glasses more readily than binary Fe-P or Fe-C alloys. Presumably, all of these factors affect glass forming ability by modifying the quenching T-T-T diagrams discussed above.

5. PHASE DIAGRAM RELATED DATA NEEDED IN FUTURE RESEARCH ON METASTABLE PHASES (ESPECIALLY AMORPHOUS METALS).

The present work on metastable phases, especially the intense current research on amorphous metals would be substantially aided if certain types of phase diagram related information were more readily available. Along with the common thermal data, we include in this discussion alloy chemical data such as the structural information commonly presented in phase diagram compilations and some other related properties. The following data are required:

1. Phase Diagram Information

a. Phase diagrams: There is a need for quantitatively correct phase diagrams, especially diagrams of binary systems with measured solidus and liquidus temperatures in those composition regions in which metastable phase formation is observed. These diagrams should also have well determined phase boundaries, especially for high temperature phases and other phases having limited stability ranges which are often absent in the qualitative phase diagrams on record.^{22,49,50} A present need exists particularly for diagrams of transition metals with the metalloids boron, phosphorus and silicon, phase diagrams of the alkaline earths, and a number of diagrams of transition metals and B metals. Liquidus temperatures and high temperature phases are especially important for amorphous metal research.

b. Surveys: There is a need for qualitative phase diagram surveys, especially for ternary systems containing one or two components that are of interest as base metals for metallic glasses. Such data may be useful in several respects. As mentioned above, it is often found that ternary alloys form glasses more readily than binary ones, as recently shown for Ti-Ni-Si alloys;⁵⁶ however, this helpful observation is often difficult to utilize without adequate ternary phase diagram data. Such data should include at least an isothermal section and the projection of the melting point troughs in the composition range of interest.

• Also, it is often of interest to assess the effect of ternary additions X to glass forming binary alloys (such as Pd-Si-X⁵⁷) [and of quaternary additions X to glass forming ternary alloys (such as Fe-C-P-X⁵⁸)] on the thermal stability (as measured by T_g and T_c) and mechanical properties (microhardness) of the base alloy glass. These measurements are generally more difficult to interpret if the effect of the ternary or quaternary addition on the equilibrium phase diagram is not known. Last, quaternary glass forming systems (i.e. systems with four major constituents) almost always have to be studied without guidance from equilibrium phase diagrams because of the absence of data for the systems of interest.

c. Metastable phases: Thermal data and phase equilibria involving metastable phases have been determined only in a few cases. As discussed above, some of these phases are of crystal chemical interest; others are important in connection with their glass forming ability or that of other alloys with the same components. More phase diagram studies of such systems are desirable.

2. Crystallographic Data

Besides the phase diagrams, crystal structure data on intermediate phases are needed. In particular, structure data are missing for many compounds occurring at or near glass forming compositions, where crystal structures would be of particular importance. Possibly, this is the case because compounds at such compositions tend to have complex structures (see previous section) and the structures have therefore not been worked out when the phase diagram was established. This is especially true for complex ternary phases,⁵⁹ of which very few are structurally well established.

3. Thermal Characteristics

For fundamental studies on metallic glasses, data on several thermal properties of equilibrium and metastable phases are required. A principal reason

for this is that glass forming systems are generally not among the alloy systems most commonly studied for which data are available in reviews such as Hultgren et al.⁶⁰ The following measurements would be useful:

a. Thermodynamic measurements: Data on $\Delta\bar{H}_F$ and $\Delta\bar{G}_F$ are needed for liquids and intermediate stable and metastable phases. This will involve solution calorimetry (generally, using a transition or noble metal bath) and EMF studies (using solid electrolyte cells). Differential scanning calorimetric (DSC) studies of the specific heats of metastable phases continue to be rewarding.

b. Kinetic parameters of metastable phases: Important data include the glass transition temperature $T_g(x, \dot{T})$ as a function of the heating rate (to obtain T_{g0} and $T_{g\infty}$),³² the crystallization temperature(s) $T_c(x, \dot{T})$, and the activation energies of crystallization as obtained by differential thermal analysis using different heating rates.³⁴

4. Other, Related Properties

For a theoretical correlation of the thermal parameters of metallic glasses, such as T_g , a quantity characteristic of the vibrational spectrum, such as the Debye temperature θ_D , is required for intermediate alloy phases. The change of θ_D on going from the crystalline to the amorphous state is also of fundamental interest; a substantial reduction of θ_D in alloy glasses had been predicted⁶¹ and observed.⁶² More data on other temperature-dependent properties such as the melt viscosity would also be useful.

ACKNOWLEDGEMENT

Research on metastable alloys at Northeastern University is partially sponsored by the Office of Naval Research; this support is gratefully acknowledged. I thank Dr. D.E. Polk for helpful discussions and Ms. T. Utterback for secretarial assistance.

DISCUSSION

T. Massalski - You showed that the bcc phase of Pu can be retained by rapidly quenching, but it would seem to me that by lattice quenching, you eliminate the entropy factor. Therefore, I am surprised that the entropy-stabilized bcc phase of Pu can actually be retained in this process.

W. Giessen - The competing lower temperature solid solutions rise very much in energy by adding a simple transition metal, like Ti, to Pu. You are suppressing the f-electron bonding in the 5f levels. The basic concept is that the f-electron bonding, which stabilizes the 3 low temperature forms of Pu, is suppressed as you add an early transition metal to it. You are, in fact, thermodynamically stabilizing the high temperature modifications to such a degree that you prevent nucleation of the low temperature forms. So your entropy term is certainly working against us, but our enthalpy term is very much in favor of us.

REFERENCES

1. B.C. Giessen and R.H. Willens in Phase Diagrams; Materials Science and Technology, Vol. III., A.M. Alper, Ed., Academic Press, N.Y., p. 103 (1970).
2. H. Jones, Rep. Prog. Phys. 36, 1425 (1973).
3. H. Jones, in Proc. Second Internat. Conf. on Rapidly Quenched Metals, Section I, N.J. Grant and B.C. Giessen, Eds., M.I.T. Press, Cambridge, Mass. p. 1 (1976).
4. A.K. Sinha, B.C. Giessen, and D.E. Polk, in Treatise on Solid State Chemistry, Vol. 3, N.B. Hannay, Ed., Plenum Press, N.Y., p. 1 (1976).
5. L.S. Darken and R.W. Gurry, Physical Chemistry of Metals, McGraw Hill, N.Y., p. 290 (1953).
6. H. Jones and C. Suryanarayana, J. Mater. Sci. 8, 705 (1973).
7. B.C. Giessen, in Developments in the Structural Chemistry of Alloy Phases, B.C. Giessen, Ed., Plenum Press, N.Y., p. 227 (1969).
8. D.E. Polk and B.C. Giessen, in Metallic Glasses, J.J. Gilman and J.H. Leamy, Eds., American Society for Metals, Metals Park, Ohio, p. 1 (1977).
9. S. Takayama, J. Mater. Sci. 11, 164 (1976).
10. P. Duwez, Annual Review of Materials Science, Vol. 6, p. 83 (1976).
11. B.C. Giessen, in Proc. Second Internat. Conf. on Rapidly Quenched Metals, Section I, N.J. Grant and B.C. Giessen, Eds., M.I.T. Press, Cambridge, Mass., p. 119 (1976).
12. J.C. Baker and J.W. Cahn, in Solidification, American Society of Metals, Metals Park, Ohio, p. 23, (1971).
13. F. Spaepen and D. Turnbull, in Proc. Second Internat. Conf. on Rapidly Quenched Metals, Section I, N.J. Grant and B.C. Giessen, Eds., M.I.T. Press, Cambridge, Mass., p. 205 (1976).

14. B.C. Giessen, M. Morris, and N.J. Grant, *Trans. Met. Soc. AIME* 239, 883 (1967).
15. P. Predecki, B.C. Giessen, and N.J. Grant, *Trans. Met. Soc. AIME* 233, 1438 (1965).
16. B.C. Giessen, U. Wolff, and N.J. Grant, *Trans. Met. Soc. AIME* 242, 597 (1968).
17. A.K. Jena, B.C. Giessen, M.B. Bever, and N.J. Grant, *Acta Met.* 16, 1047 (1968).
18. T.B. Massalski and T. Bienvenu, in Proc. Second Internat. Conf. on Rapidly Quenched Metals, Section I, N.J. Grant and B.C. Giessen, Eds., M.I.T. Press, Cambridge, Mass. p. 95 (1976).
19. T.B. Massalski, L.E. Vassamillet and T. Bienvenu, *Acta Met.* 21, 649 (1973).
20. E. Delcroix, A. Defrain, and I. Epelboin, *J. Phys. Radium* 24, 17 (1963).
21. J.H. Perepezko, D.H. Rasmussen, I.E. Anderson, and C.R. Loper, Jr., *Proc. Sheffield Internat. Conf. on Solidification and Casting* (July 1977), in print.
22. M. Hansen, Constitution of Binary Alloys, McGraw-Hill, N.Y., 1958.
23. L. Bosio, A. Defrain and I. Epelboin, *J. Physique* 27, 61 (1966).
24. D.H. Rasmussen, J.H. Perepezko and C.R. Loper, Jr., in Proc. Second Internat. Conf. on Rapidly Quenched Metals, Section I, N.J. Grant and B.C. Giessen, Eds., M.I.T. Press, Cambridge, Mass. p. 57 (1976).
25. B.C. Giessen and J. Barrick, to be published.
26. P. Duwez, R.H. Willens, and W. Klement, *J. Appl. Phys.* 31, 1136 (1960).
27. L. Kaufman, Private Communication.
28. J.C. Baker and J.W. Cahn, *Acta Met.* 17, 575 (1969).
29. C.C. Tsuei in Proc. Second Internat. Conf. on Rapidly Quenched Metals, Section I, N.J. Grant and B.C. Giessen, Eds. M.I.T. Press, Cambridge, Mass. p. 441 (1976).
30. J. Orehotzky and K. Schröder, *J. Appl. Phys.* 43, 2413 (1972).
31. T.R. Anantharaman, H.L. Luo, and W. Klement, Jr., *Trans. Met. Soc. AIME* 233, 2014 (1965).
32. M. Lasocka, in Proc. Second Internat. Conf. on Rapidly Quenched Metals, Section II, N.J. Grant and B.C. Giessen, Eds., *Mater. Sci. Eng.*, 23 173 (1976).
33. A. Calka, M. Madhava, D.E. Polk, B.C. Giessen, H. Matyja and J. Vander Sande, *Scripta Met.* 11, 65 (1977).
34. H.O.K. Kirchner, in Proc. Second Internat. Conf. on Rapidly Quenched Metals, Section II, N.J. Grant and B.C. Giessen, Eds., *Mater. Sci. Eng.* 23, 95 (1976).

35. D.R. Uhlmann, J. Noncryst. Sol. 7, 337 (1972).
36. P. Predecki, A. W. Mullendore and N.J. Grant, Trans. Met. Soc. AIME 233, 1581 (1965).
37. N.J. Grant and B.C. Giessen, Eds., Proc. Second Internat. Conf. on Rapidly Quenched Metals, Section I, M.I.T. Press, Cambridge, Mass. (1976).
38. N.J. Grant and B.C. Giessen, Eds., Proc. Second Internat. Conf. on Rapidly Quenched Metals, Section II, Mater. Sci. Eng. 23/2-3, (1976).
39. V. Heine and D. Weaire, in Solid State Physics, Vol. 24, H. Ehrenreich, F. Seitz, and D. Turnbull, Eds., Academic Press, N.Y., p. 249 (1970).
40. L. Kaufman, Calphad 1, 13 (1977).
41. L. Kaufman and H. Nesor, in Titanium Science and Technology, Vol. 2, R.I. Jaffee and H. Burte, Eds., Plenum Press, N.Y., p. 773 (1973).
42. L. Kaufman and H. Nesor, in Proc. Second Internat. Conf. on Rapidly Quenched Metals, Section II, Mat. Sci. Eng. 23, 119 (1976).
43. L.E. Tanner, R. Ray and C.F. Cline, U.S. Patent No. 3,989,517.
44. B.C. Giessen, in Adv. in X-Ray Analysis, Vol. 12, C.S. Barrett, G.R. Mallett, and J.B. Newkirk, Eds., Plenum Press, N.Y., p. 23 (1969).
45. W.B. Pearson, The Crystal Chemistry and Physics of Metals and Alloys, Wiley-Interscience, N.Y. (1972).
46. J.H. Hollomon and D. Turnbull, Trans. AIME 191, 803 (1951).
47. W. Klement, Jr., R.H. Willens, and P. Duwez, Nature 187, 809 (1960).
48. M.H. Cohen and D. Turnbull, J. Chem. Phys. 31, 1164 (1959).
49. R.P. Elliott, Constitution of Binary Alloys, First Supplement, McGraw-Hill, N.Y. (1965).
50. W.G. Moffatt, Binary Phase Diagrams Handbook, General Electric Co., Schenectady, N.Y. (1976).
51. M. Marcus and D. Turnbull, in Proc. Second Internat. Conf. on Rapidly Quenched Metals, Section II, Mat. Sci. Eng. 23, 211 (1976).
52. P. Duwez, R.H. Willens, and R.C. Crewdson, J. Appl. Phys. 36, 2267 (1965).
53. B.C. Giessen, M. Madhava, D.E. Polk, and J. Vander Sande, in Proc. Second Internat. Conf. on Rapidly Quenched Metals, Section II, N.J. Grant and B.C. Giessen, Eds., Mater. Sci. Eng. 23, 145 (1976).
54. R. Ray, B.C. Giessen, and N.J. Grant, Scripta Met. 2, 357 (1968).
55. D.E. Polk, Acta Met. 20, 485 (1972).
56. D.E. Polk, A. Calka and B.C. Giessen, Acta Met., to be published.
57. H.S. Chen and D. Turnbull, Acta Met. 17, 1021 (1969).
58. M. Naka, S. Tomizawa, T. Masumoto and T. Watanabe, in Proc. Second Internat. Conf. on Rapidly Quenched Metals, Section I, N.J. Grant and B.C. Giessen, Eds., M.I.T. Press, Cambridge, Mass., p. 273 (1976).
59. C.B. Shoemaker and D.P. Shoemaker, in Developments in the Structural Chemistry of Alloy Phases, B.C. Giessen, Ed., Plenum Press, N.Y., p. 107 (1969).
60. R. Hultgren, P.D. Desai, D.T. Hawkins, M. Gleiser, and K.K. Kelley, Selected Values of Thermodynamic Properties, American Society for Metals, Metals Park, Ohio (1973).
61. D. Weaire, M.F. Ashby, J. Logan, and M.J. Weins, Acta Met. 19, 779 (1971).
62. S.R. Nagel, J. Vassiliou, P.M. Horn and B.C. Giessen, Phys. Rev., to be published.



THE CALCULATION OF MULTICOMPONENT ALLOY PHASE DIAGRAMS
AT THE NATIONAL PHYSICAL LABORATORY

T G Chart

National Physical Laboratory,
Teddington, Middlesex, UK

ABSTRACT

Members of the Division of Chemical Standards, National Physical Laboratory, are currently engaged in the calculation of ternary and quaternary phase diagrams, of relevance to superalloys and other high-temperature materials, from the thermodynamic data for the binary systems concerned. Computer methods involving the minimization of Gibbs energy are utilized. The systems calculable at present involve the transition metals, carbon and aluminium. In order to extend this range a programme of critical assessment of thermodynamic data for binary systems, mainly involving transition metal-silicon and transition metal-boron systems, is being undertaken. Examples of recently calculated phase equilibria in the systems Al-Cr-Zr and Al-Cr-Nb are given.

INTRODUCTION

When accurate thermodynamic data are available for the various phases in a system the phase diagram can be calculated reliably. The modern digital computer allows such calculations to be made rapidly, and for multicomponent systems, very cost-effectively. This approach is an important complementary method to that of experimental determination, and in some cases, eg where equilibration is subject to diffusional delays, can be more reliable. In addition, metastable equilibria can be calculated.

For many years those involved in metallurgical thermodynamics at the National Physical Laboratory have been providing data and developing methods for the calculation of reliable phase diagrams for metallurgical systems of technological importance. This work was initiated by Kubaschewski^{*}, who demonstrated the advantages of calculation procedures when applied to certain binary systems, eg Bi-Zn, Hf-Zr and U-Fe;⁽¹⁾ Ga-Zn, Mg-Cd and Cr-Mo;⁽²⁾ Fe-Cr;⁽³⁾ Co-Cu;⁽⁴⁾ and Cu-Ni.⁽⁵⁾ Later, Counsell and Spencer^{*} made significant advances in the calculation of ternary and quaternary systems using a digital computer:⁽⁶⁾ ternary systems calculated by these investigators include Au-Pt-Pd,⁽⁷⁾ Fe-Cu-Ni and Fe-Cr-Ni,⁽⁸⁾ Fe-Cr-V,⁽⁹⁾ and Fe-Co-Cr.⁽¹⁰⁾

Currently, technologically important ternary and quaternary phase diagrams, mainly of relevance to superalloys and other high-temperature materials, are being calculated. A computerized data base is being established to maximize this effort, and collaboration and interchange

^{*} Now at the Rheinisch-Westfälische Technische Hochschule Aachen, Federal Republic of Germany.

of information with other groups in the field is being achieved via the CALPHAD (CALculation of PHase Diagrams) Project.

OUTLINE OF METHODS EMPLOYED

The principles of the calculation of phase diagrams from thermodynamic data are well established and have been described in a number of monographs, eg by Kaufman and Bernstein,⁽¹¹⁾ and by Prince.⁽¹²⁾ For multicomponent systems the Gibbs energies of formation of the various phases present are represented mathematically as functions of composition and temperature, and phase boundaries computed using minimization of Gibbs energy techniques.⁽⁶⁾ Because it would generally be too expensive to measure the thermodynamic properties of multicomponent phases these data are estimated from the thermodynamic properties of the binary systems involved, using empirical equations. The suitability of the equations used, when applied to different types of ternary system, has been scrutinized by various CALPHAD members.⁽¹³⁻¹⁵⁾ When multicomponent thermodynamic data or phase equilibria are available they are taken into account to produce the best possible overall representation.

For ternary systems three primary computer programs have been developed to calculate (a) the stable equilibria between various solution phases, eg fig 1(i), (b) the stable equilibria between stoichiometric compounds and various solutions, eg fig 1(ii), and (c) the stable equilibria between two compounds, which are either completely or partly miscible in each other, and various solutions, eg fig 1(iii). When two compounds which exist over a range of compositions are known to be mutually miscible they are represented as a solution, eg fig 1(iv). Any number of phases can be handled simultaneously. The boundaries of three-phase regions are established by the intersection of two two-phase regions, or alternatively, where this is impossible, eg when two compounds are in

equilibrium with a pseudo-binary solution between two other compounds (fig 1(v)), by minimizing the Gibbs energy of formation of a composition within the tie-triangle (point X) for different compositions along the pseudo-binary line (point Y). These programs enable a wide range of types of ternary phase diagram to be calculated. The computer programs which enable the stable equilibria between various solution phases, and between compounds and solutions to be calculated, have been modified to deal with quaternary systems.

EXAMPLES OF CALCULATED TERNARY PHASE DIAGRAMS

Recently calculated phase diagrams include the ternary isothermal sections at 1773, 1673, 1573 and 1523 K for the system Al-Cr-Zr shown in figs 2 to 5. Full details of the calculations and data used will be published shortly. No ternary compounds have been reported to exist in this system^(16,17) and the Laves phases ZrAl_2 (hexagonal, C14⁽¹⁷⁾) and Cr_2Zr (cubic, C15, at the temperatures for which calculations were made⁽¹⁸⁾) have been assumed to be insoluble in each other. The calculated diagrams are in good agreement with the experimental equilibria determined for these temperatures⁽¹⁹⁾ as indicated by fig 6, which shows the calculated and experimentally obtained equilibria⁽¹⁹⁾ for the pseudo-binary section indicated in fig 2, between pure zirconium and the composition represented by point Y. When making such comparisons it should be noted that some of the disagreement may be due to errors in the experimental diagrams, which in the present case indicate the melting point of zirconium to be about 2075 K,⁽¹⁹⁾ which is 50 K lower than the accepted value.⁽²⁰⁾

Fig 7 shows a calculated isothermal section at 1773 K for the system Al-Cr-Nb. The thermodynamic data employed for the three binary systems involved were those assessed by Kaufman and Nesor,^(21,22) who have also

calculated equilibria in this system.⁽²²⁾ The intermetallic compounds stable at this temperature have been considered stoichiometric and not to form ternary solutions, although there is evidence^(23,24) to suggest that the Laves compound Cr_2Nb (cubic, C15) does extend into the ternary phase field, towards NbAl_3 (tetragonal, DO_{22}). Nevertheless, the calculation provides a rapid and economic method of determining the composition and temperature ranges in which desired behaviour, such as eutectic solidification, occurs.

CURRENT STATUS AND DIRECTION OF FUTURE WORK

At present over 100 ternary alloy systems, mainly involving transition metal elements, carbon and aluminium, can be reliably calculated from thermodynamic data. A high proportion of the required binary data have been assessed by Kaufman.* The NPL data base is being enlarged so that phase equilibria can be calculated for high-temperature alloy systems involving most combinations of the elements B, C, Al, Si, Ti, Cr, Fe, Co, Ni, Zr, Nb, Mo, Hf, Ta and W. Extant thermodynamic data for binary alloys are being critically assessed to produce sets of values which are consistent with the reliable parts of the binary phase diagrams, (and this programme of work is therefore dependent on the availability of such information). Initially it is planned to deal with transition metal-silicon systems, for which reliable thermodynamic data are available,^(25,26) and then to extend the assessments to transition metal-boron systems. It is intended to disseminate these data assessments as widely as possible.

ACKNOWLEDGEMENT

The author gratefully acknowledges the advice received from Dr A J Head.

* ManLabs Inc, Massachusetts, USA

REFERENCES

- 1 Kubaschewski, O, in "Thermodynamics of Nuclear Materials", 1962, IAEA, Vienna, p 219.
- 2 Kubaschewski, O, Chart, T G, J Inst Met, 1965, 93, 329.
- 3 Müller, F, Kubaschewski, O, High Temp High Pressures, 1969, 1, 543.
- 4 Dench, W A, Kubaschewski, O, ibid, 1969, 1, 357.
- 5 Elford, L, Müller, F, Kubaschewski, O, Ber Bunsenges Phys Chem, 1969, 73, 601.
- 6 Counsell, J F, Lees, E B, Spencer, P J, Met Sci J, 1971, 5, 210.
- 7 Kubaschewski, O, Counsell, J F, Monatsh Chem, 1971, 102, 1724.
- 8 Counsell, J F, Lees, E B, Spencer, P J, in "Metallurgical Chemistry", ed Kubaschewski, O, 1972, HMSO, London, p 451.
- 9 Spencer, P J, Counsell, J F, Z Metallkd, 1973, 64, 662.
- 10 Chart, T G, Counsell, J F, Jones, G P, Slough, W, Spencer, P J, Int Metall Rev, 1975, 20, 57.
- 11 Kaufman, L, Bernstein, H, "Computer Calculation of Phase Diagrams", 1970, Academic Press, New York and London.
- 12 Prince, A, "Alloy Phase Equilibria", 1966, Elsevier, Amsterdam &c.
- 13 Ansara, I, in "Metallurgical Chemistry", ed Kubaschewski, O, 1972, HMSO, London, p 403.
- 14 Spencer, P J, Hayes, F H, Kubaschewski, O, Rev Chim Miner, 1972, 9, 13.
- 15 Spencer, P J, Hayes, F H, Elford, L, in "Chemical Metallurgy of Iron and Steel", 1973, Iron and Steel Institute, London, p 322.

- 16 Mondolfo, L F, "Aluminium Alloys: Structure and Properties", 1976, Butterworths, London &c.
- 17 Pearson, W B, "A Handbook of Lattice Spacings and Structures of Metals and Alloys", Vol 2, 1967, Pergamon, Oxford &c.
- 18 Eremenko, V N, Prima, S B, Tret'yachenko, L A, Poroshk Metall, 1973, (1), 54.
- 19 Gruzdeva, N M, Tregubov, I A, in "Diagrammy Sostoyaniya Metallicheskih Sistem", No 14, ed Ageev, N V, 1970, Viniti, Moscow, p 138.
- 20 Hultgren, R, Desai, P D, Hawkins, D T, Gleiser, M, Kelley, K K, Wagman, D D, "Selected Values of the Thermodynamic Properties of the Elements", 1973, ASM, Metals Park (Ohio).
- 21 Kaufman, L, Nesor, H, in "Proceedings of Conference on In-Situ Composites", Vol 3, 1973, National Academy of Sciences - National Academy of Engineering (Publication NMAB-308), Washington DC, p 21.
- 22 Kaufman, L, Nesor, H, Ann Rev Mater Sci, 1973, 3, 1.
- 23 Svechnikov, V N, Shurin, A K, Dmitriev, G P, in "Diagrammy Sostoyaniya Metallicheskih Sistem", No 10, ed Ageev, N V, 1967, Viniti, Moscow, p 125.
- 24 Hunt, C R, Raman, A, Z Metallkd, 1968, 59, 701.
- 25 Chart, T G, High Temp High Pressures, 1970, 2, 461.
- 26 Chart, T G, ibid, 1973, 5, 241.

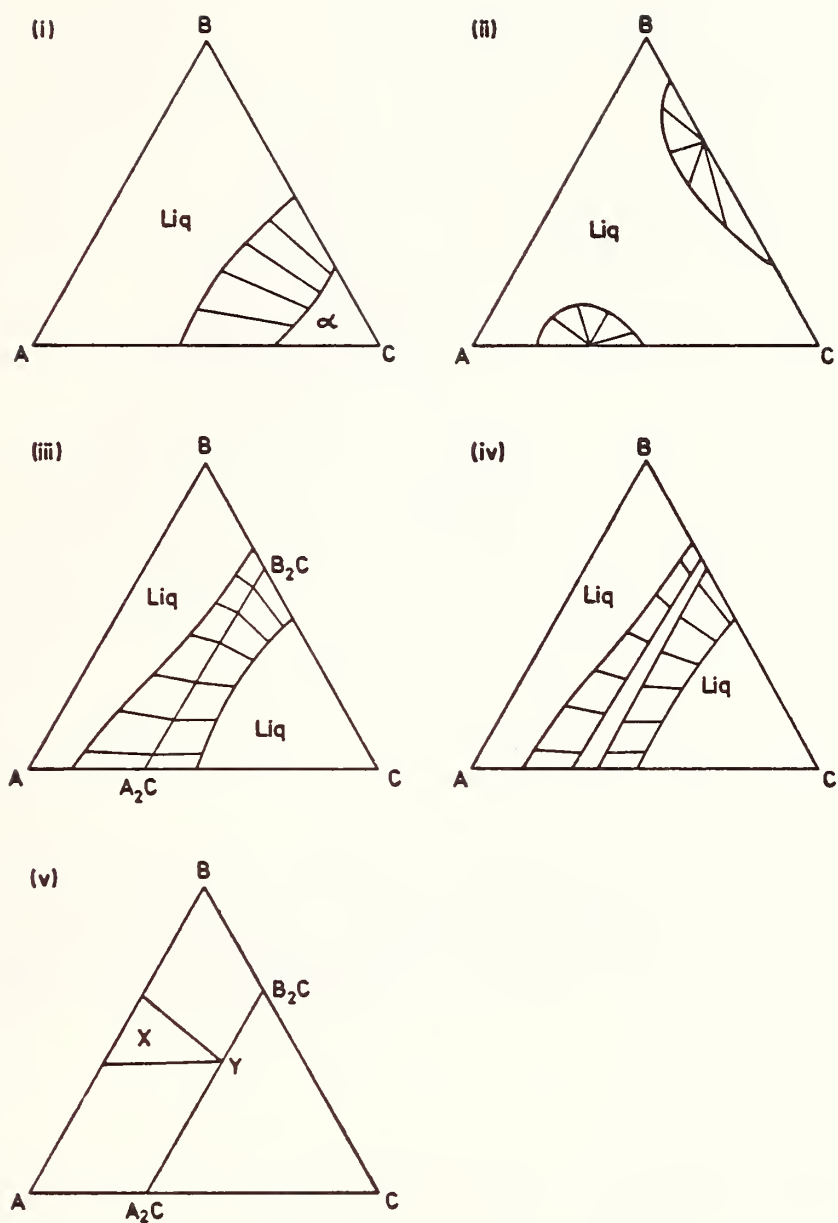


Figure 1 Schematic representation of basic types of ternary phase equilibria calculable from thermodynamic data.

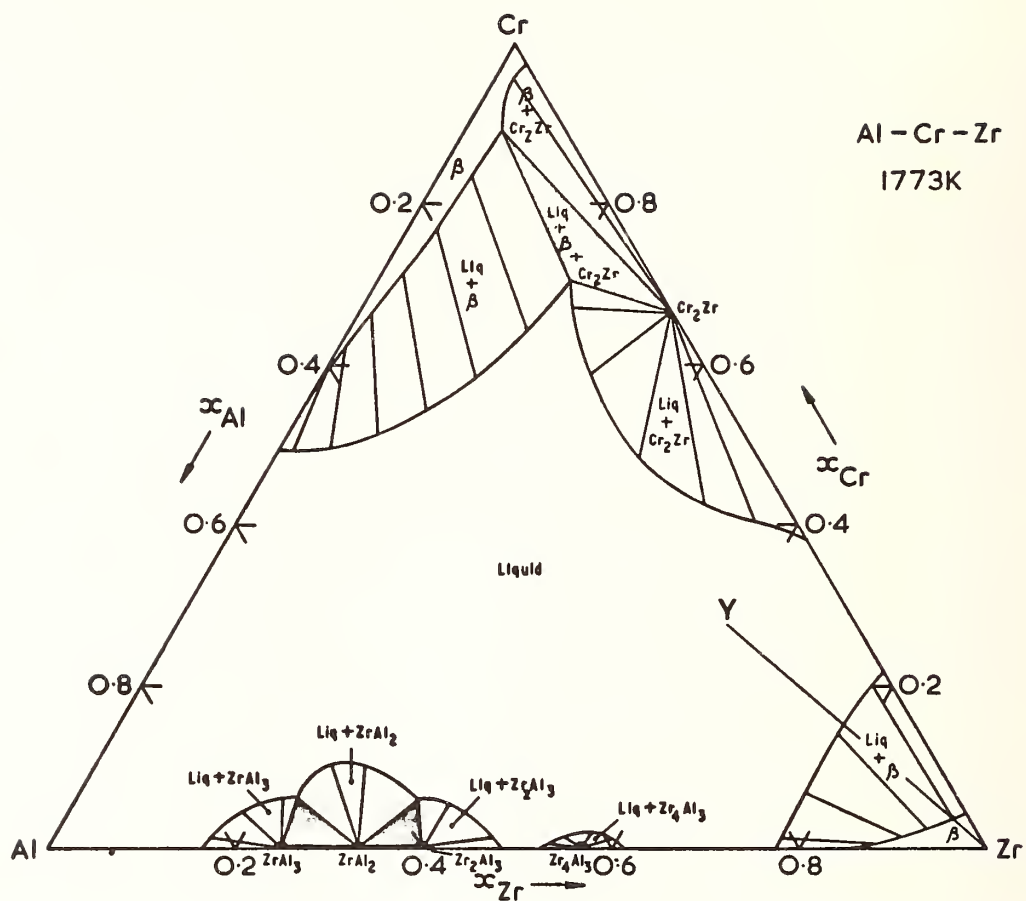


Figure 2 Calculated phase equilibria in the Al-Cr-Zr system at
1773 K.

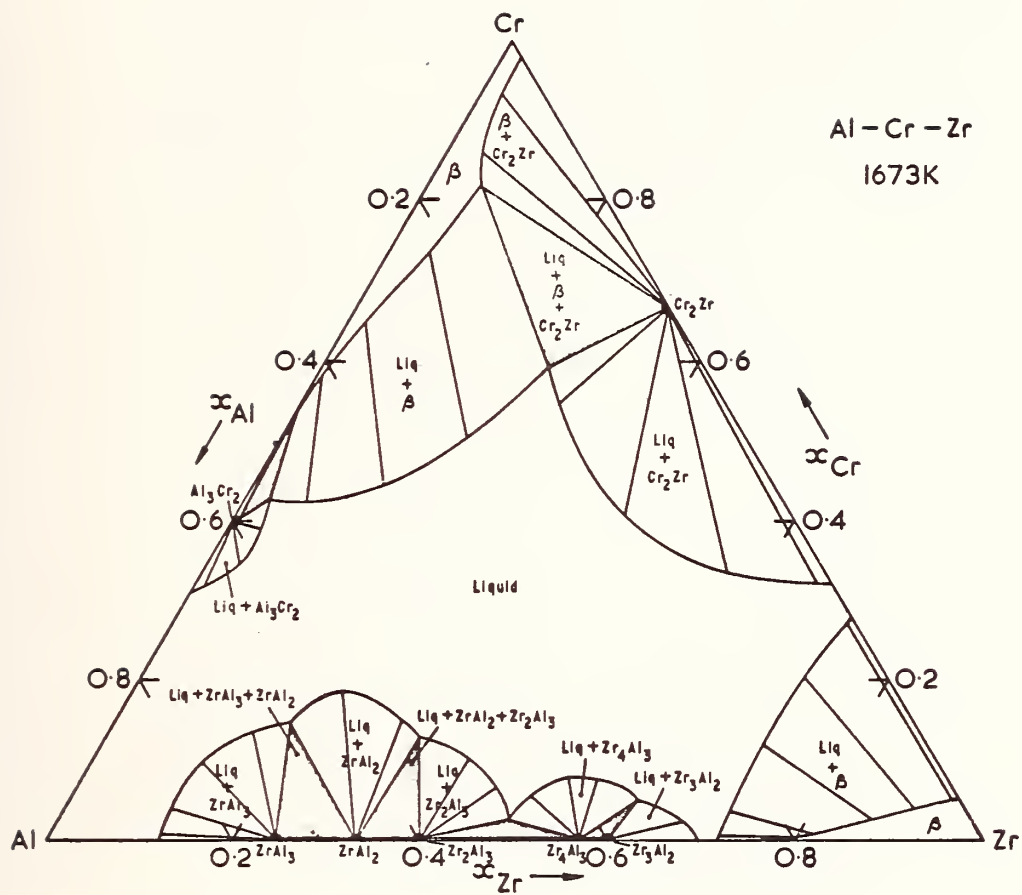


Figure 3 Calculated phase equilibria in the Al-Cr-Zr system at
1673 K.

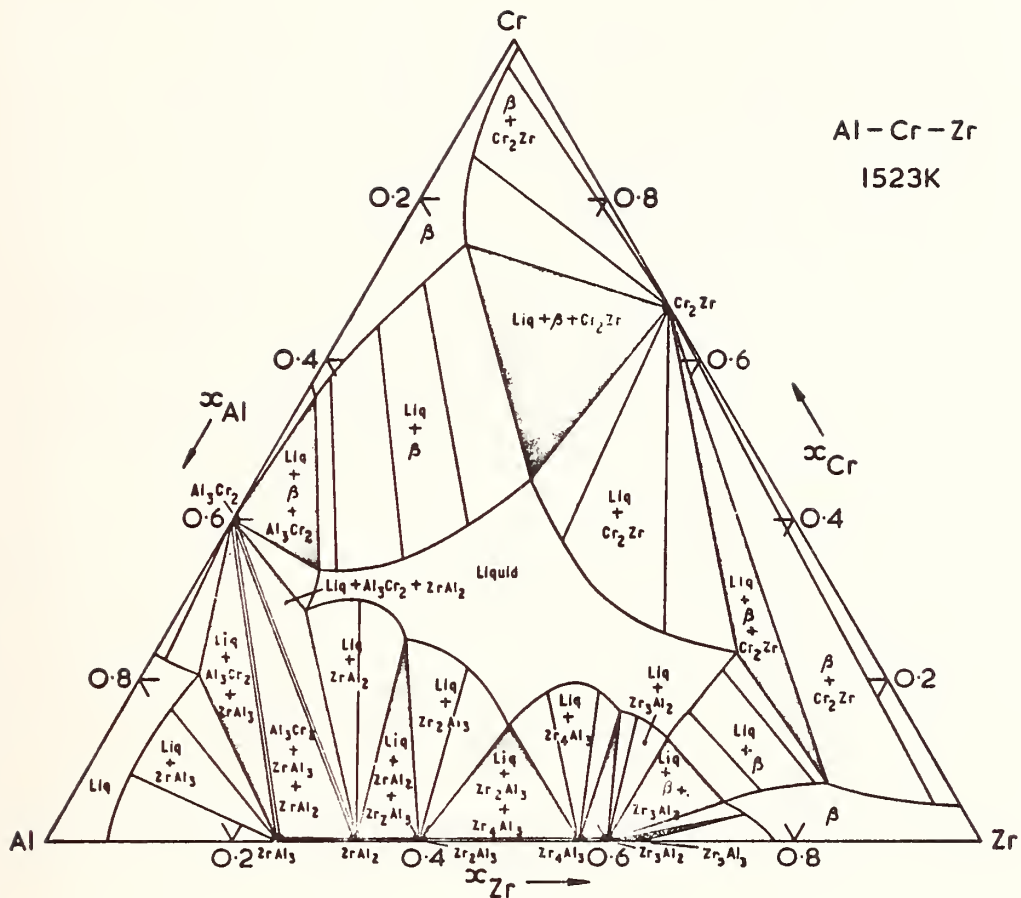


Figure 5 Calculated phase equilibria in the Al-Cr-Zr system at
1523 K.

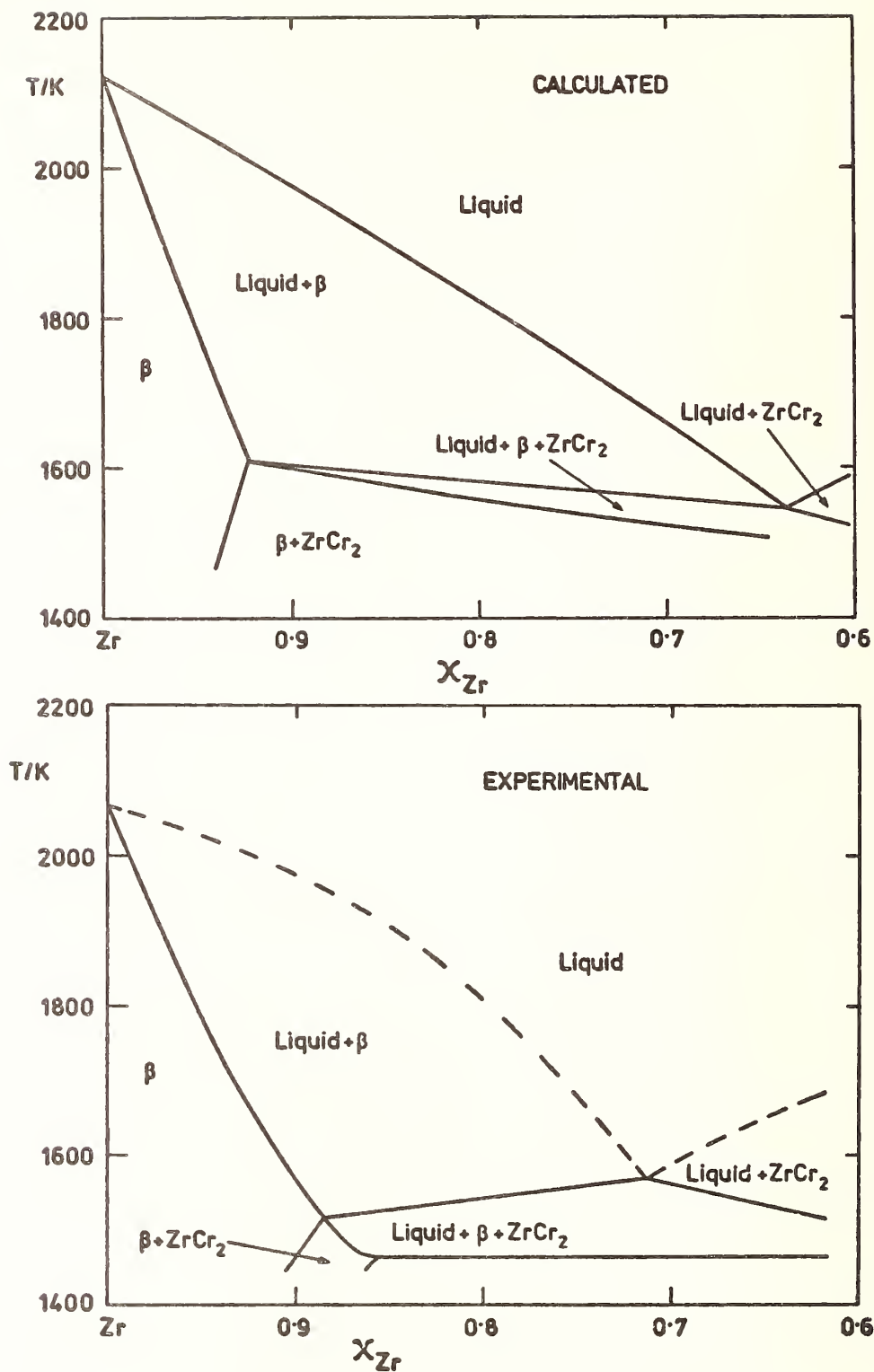


Figure 6 Calculated and experimental phase equilibria in the Al-Cr-Zr system for the pseudo-binary section indicated in figure 2 (see text).

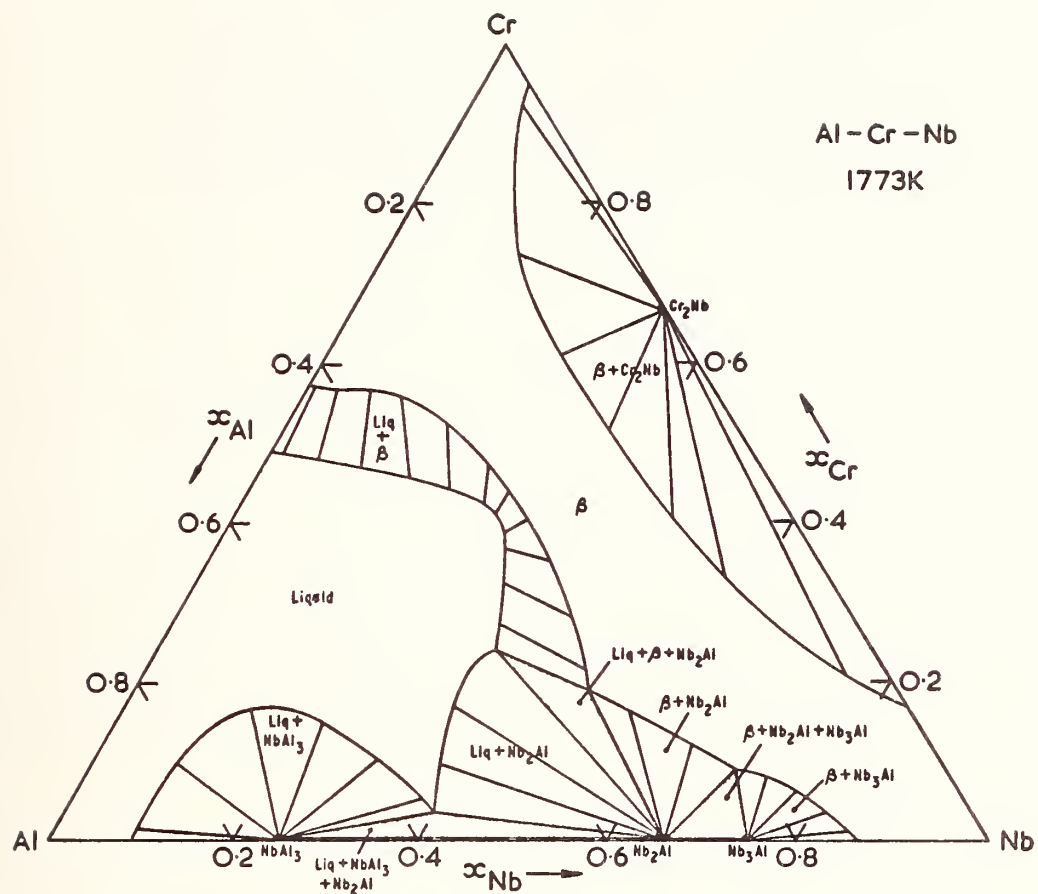


Figure 7 Calculated phase equilibria in the Al-Cr-Nb system at 1773 K.

SYNTHESIS OF BINARY METALLIC SYSTEMS

- I. ISMORPHOUS SYSTEMS
- II. SIMPLE EUTECTIC SYSTEMS

S.S. BALAKRISHNA AND A.K. MALLIK.[†]
Department of Metallurgical Engineering,
Indian Institute of Technology, Bombay,
INDIA

Introduction:

One of the most important sources of information regarding a materials system is its phase diagram. In fact, before any research or development work is done on a materials problem, it is important to study the phase diagram to know about the nature of the material. Information concerning phase compositions and phase stability are a function of temperature, composition and pressure, and can be obtained from the phase diagrams.

Theoretical synthesis of phase diagrams is a valuable aid in estimating thermodynamic properties in the absence of experimental data and for critical comparison. Using convenient mathematical expressions or statistical thermodynamic models for the free-energy functions involved, one can extend the calculations of the phase diagram to regions where no, or questionable, experimental data are available. This procedure thus forms the basis for extrapolation in phase diagrams.

In order to calculate the phase equilibria in an alloy system, one must express the free energy function of individual phases as a function of composition. Once the free energy functions

[†] Department of Metallurgical Engineering, Indian Institute of Technology, Bombay, INDIA.

of the phases in a system are known, it is in principle possible to calculate the equilibrium state for a certain alloy composition by directly minimising the total free energy. In the present investigation the binary isomorphous and simple eutectic phase diagrams are synthesized using models of statistical thermodynamics (i.e. regular and quasi-chemical) and ideal solution models using and neglecting the C_p data. To solve the system of equations to yield the phase boundaries, the method based on the Newton-Raphson iteration technique⁽¹⁾ offered by Kaufman and Bernstein⁽²⁾ is utilized.

Thermodynamic Definition of Binary Equilibrium:

Consider an alloy system A-B in which x represents the atom fraction of component B. Suppose that there are two phases liquid (L) and solid solution (α) which exist in the system. The free energy of the liquid phase (L) in the A-B system is defined by

$$F^L = (1-x) F_A^L + x F_B^L + RT [x \ln x + (1-x) \ln(1-x)] + F_E^L$$

cals/g.atom ... (1)

where F_A^L and F_B^L are the free energies of pure liquid A and pure liquid B, and F_E^L is the excess free energy of mixing which is zero when $x=0$ and 1.

The free energy of the solid solution phase (α) in the A-B system is defined in a similar manner to that of liquid phase.

$$F^\alpha = (1-x) F_A^\alpha + x F_B^\alpha + RT [x \ln x + (1-x) \ln(1-x)] + F_E^\alpha$$

cals/g.atom .. (2)

where F_A^α and F_B^α are the free energies of solid forms of pure A and B and F_E^α is the excess free energy of mixing in the solid state.

The partial molar free energies of A and B in an alloy containing x atom fraction of B are \bar{F}_A and \bar{F}_B respectively. These quantities are defined as follows:

$$\bar{F}_A = F - x \frac{\partial F}{\partial x} \quad \text{.. (3)}$$

$$\bar{F}_B = F + (1-x) \frac{\partial F}{\partial x} \quad \text{.. (4)}$$

If, at a temperature T, there exists a two phase (L+α) field bounded by compositions XL and Xα, then equilibrium requirements dictates that for the particular values of T, XL and Xα

$$\bar{F}_A^L \Big|_{XL} = \bar{F}_A^\alpha \Big|_{X\alpha} \quad \text{.. (5)}$$

$$\bar{F}_B^L \Big|_{XL} = \bar{F}_B^\alpha \Big|_{X\alpha} \quad \text{.. (6)}$$

equations (5) and (6) represent the equality of chemical potentials of the components in the two phases. They are the equivalent of the

rule of common tangents. Equations (1-4) yield:

$$\bar{F}_A^L = F_A^L + RT \ln (1-x) + [F_E^L - x \frac{\partial F_E^L}{\partial x}] \quad \dots (7)$$

$$\bar{F}_A^\alpha = F_A^\alpha + RT \ln (1-x) + [F_E^\alpha - x \frac{\partial F_E^\alpha}{\partial x}] \quad \dots (8)$$

$$\bar{F}_B^L = F_B^L + RT \ln x + [F_E^L + (1-x) \frac{\partial F_E^L}{\partial x}] \quad \dots (9)$$

$$\bar{F}_B^\alpha = F_B^\alpha + RT \ln x + [F_E^\alpha + (1-x) \frac{\partial F_E^\alpha}{\partial x}] \quad \dots (10)$$

Applying equations (5-6) to equations (7-10) yield:

$$\begin{aligned} \Delta F_A^{\alpha \rightarrow L} + RT \ln ((1-XL)/(1-X\alpha)) &= [F_E^\alpha - x \frac{\partial F_E^\alpha}{\partial x}]_{X\alpha} \\ &\quad - [F_E^L - x \frac{\partial F_E^L}{\partial x}]_{XL} \quad \dots (11) \end{aligned}$$

$$\begin{aligned} \Delta F_B^{\alpha \rightarrow L} + RT \ln (XL/X\alpha) &= [F_E^\alpha + (1-x) \frac{\partial F_E^\alpha}{\partial x}]_{X\alpha} \\ &\quad - [F_E^L + (1-x) \frac{\partial F_E^L}{\partial x}]_{XL} \quad \dots (12) \end{aligned}$$

as the condition for equilibrium. Equations (11) and (12) show directly how the difference in free energies between the two phases of components A and B contribute to final values of XL and X α at a temperature T and thereby lead to the establishment of

the equilibrium diagram.

I. Application to Isomorphous Systems:

a) Ideal Solution.

When $F_E = 0$, the solution is ideal. Equations (11) and (12) reduce to the form

$$\Delta F_A^{\alpha \rightarrow L} + RT \ln \left(\frac{(1-XL)}{(1-X\alpha)} \right) = 0 \quad \dots (13)$$

$$\Delta F_B^{\alpha \rightarrow L} + RT \ln (XL/X\alpha) = 0 \quad \dots (14)$$

Equations (13) and (14) are solved simultaneously for XL and $X\alpha$ at different temperatures using and neglecting C_p data. Using the C_p data, $\Delta F_i^{\alpha \rightarrow L}$ (for $i = A$ or B) is expressed as

$$\begin{aligned} (1/RT) \Delta F_i^{\alpha \rightarrow L} &= (1/R) \Delta H_i^{\alpha \rightarrow L} \left[\frac{1}{T} - \frac{1}{T_i} \right] \\ &+ \frac{\Delta a_i^{\alpha \rightarrow L}}{R} \left[1 - \frac{T_i}{T} + \ln \frac{T_i}{T} \right] - \frac{\Delta b_i^{\alpha \rightarrow L}}{2RT} [T - T_i]^2 \\ &- \frac{\Delta c_i^{\alpha \rightarrow L}}{2R} \left[\frac{1}{T} - \frac{1}{T_i} \right]^2 \quad \dots (15) \end{aligned}$$

Neglecting C_p data, $\Delta F_i^{\alpha \rightarrow L}$ is expressed as

$$(1/RT) \Delta F_i^{\alpha \rightarrow L} = (1/R) \Delta H_i^{\alpha \rightarrow L} \left[\frac{1}{T} - \frac{1}{T_i} \right] \quad \dots (16)$$

b) Regular Solution:

In the regular solution model⁽³⁾, F_E^L and F_E^α are given by

$$F_E^L = L \times (1-x) \quad \text{cal/g. atom} \quad \dots (17)$$

$$F_E^\alpha = B \times (1-x) \quad \text{cal/g. atom.} \quad \dots (18)$$

where L and B are the interaction parameters of liquid and solid phases respectively.

Introducing these equations (17) and (18) to equations (11) and (12) result

$$\Delta F_A^{\alpha \rightarrow L} + RT \ln \left(\frac{(1-XL)}{(1-X\alpha)} \right) = X\alpha^2 B - XL^2 L \quad \dots (19)$$

$$\Delta F_B^{\alpha \rightarrow L} + RT \ln (XL/X\alpha) = (1-X\alpha)^2 B - (1-XL)^2 L \quad \dots (20)$$

Equations (19) and (20) are solved simultaneously for XL and X α at different temperatures.

c) Quasi-chemical:

In the quasi-chemical model, the excess free energy of mixing is derived by Guggenheim and others⁽⁴⁾, (16) as

$$F_E = x(1-x) \frac{[1-x(1-x)]}{ZRT} \quad \dots (21)$$

neglecting the higher order terms than the second of (ω/ZRT), where ω is the interaction parameter and Z is the coordination number.

The excess free energy terms for liquid and solid phase are written as

$$F_E^L = x(1-x) L [1-x(1-x) L/ZRT] \quad \dots(22)$$

$$F_E^\alpha = x(1-x) B [1-x(1-x) B/ZRT] \quad \dots(23)$$

With the introduction of equations (22) and (23) to equations (11) and (12) yield

$$\Delta F_A^{\alpha \rightarrow L} + RT \ln \left(\frac{1-X_L}{1-X_\alpha} \right) = B X_\alpha^2 \left[1 - \frac{B}{ZRT} (1-X_\alpha)(3X_\alpha-1) \right] \\ - L X_L^2 \left[1 - \frac{L}{ZRT} (1-X_L)(3X_L-1) \right] \quad \dots(24)$$

$$\Delta F_B^{\alpha \rightarrow L} + RT \ln (X_L/X_\alpha) = B(1-X_\alpha)^2 \left[1 - \frac{B}{ZRT} X_\alpha(2-3X_\alpha) \right] \\ - L(1-X_L)^2 \left[1 - \frac{L}{ZRT} X_L(2-3X_L) \right] \quad \dots (25)$$

Equations (24) and (25) are solved simultaneously for X_L and X_α at different temperatures.

II. Application to Simple Eutectic Systems:

a) Ideal Solution:

For the case of simple eutectic system (i.e. no mutual

solid solubilities in each), $X_\alpha = 0$ and $X_L = X_{AL}$ in equation (13) and $X_\alpha = 1$ and $X_L = X_{BL}$ in equation (14) and $r = s$, a pure solid. These two requirements reduce the equations (13) and (14) to

$$\Delta F_A^{S \rightarrow L} + RT \ln (1 - X_{AL}) = 0 \quad \dots (26)$$

$$\Delta F_B^{S \rightarrow L} + RT \ln X_{BL} = 0 \quad \dots (27)$$

The equations (26) and (27) are solved for X_{AL} and X_{BL} at different temperatures using and neglecting C_p data. The expressions (15) and (16) are valid to apply in equations (26) and (27) using and neglecting C_p data.

b) Regular Solution:

In this case $X_\alpha = 0$ and $X_L = X_{AL}$ in equation (19) and $X_\alpha = 1$ and $X_L = X_{BL}$ in equation (20). These two requirements reduce the equations (19) and (20) to

$$\Delta F_A^{S \rightarrow L} + RT \ln (1 - X_{AL}) = -L(X_{AL})^2 \quad \dots (28)$$

$$\Delta F_B^{S \rightarrow L} + RT \ln (X_{BL}) = -L(1 - X_{BL})^2 \quad \dots (29)$$

The equations (28) and (29) are solved for X_{AL} and X_{BL} at different temperatures.

c) Quasi-chemical:

In this case $X_\alpha = 0$ and $X_L = X_{AL}$ in equation (24) and $X_\alpha = 1$ and $X_L = X_{BL}$ in equation (25). These two requirements reduce the equation (24) and (25) to

$$\Delta F_A^{S \rightarrow L} + RT \ln (1 - X_{AL}) = -L X_{AL}^2 \left[1 - \frac{L}{ZRT} (1 - X_{AL}) (3X_{AL} - 1) \right] \dots (30)$$

$$\Delta F_B^{S \rightarrow L} + RT \ln X_{BL} = -L (1 - X_{BL})^2 \left[1 - \frac{L}{ZRT} X_{BL} (2 - 3X_{BL}) \right] \dots (31)$$

The equations (30) and (31) are solved for X_{AL} and X_{BL} at different temperatures.

Numerical Techniques for Solving the System of Equations:

Rudman's trial and error method⁽⁵⁾ has been used to solve the system of equations (19) and (20), (24) and (25), (28) and (29) and (30) and (31) by assigning arbitrary values to the couple of unknown X_L and X_α or X_{AL} and X_{BL} , so that the whole range of possible compositions is covered, and then selecting the couple of values that best fits the equations. This procedure is time consuming and so the Kaufman and Bernstein method⁽²⁾ based on Newton-Raphson iteration technique⁽¹⁾ has been used. This method

consists in selecting a couple of approximate equilibrium compositions XL and $X\alpha$ and then calculating a more precise solution XL' and $X\alpha'$ using successive approximations computed by the following formulae:

$$\begin{aligned}
 XL_{n+1} &= XL_n - \frac{1}{J(XL_n, X\alpha_n)} \begin{vmatrix} F(XL_n, X\alpha_n) & F'_{X\alpha}(XL_n, X\alpha_n) \\ G(XL_n, X\alpha_n) & G'_{X\alpha}(XL_n, X\alpha_n) \end{vmatrix} \\
 &= XL_n - \frac{\Delta_{XL}(n)}{J(XL_n, X\alpha_n)} \quad \dots (32)
 \end{aligned}$$

$$\begin{aligned}
 X\alpha_{n+1} &= X\alpha_n - \frac{1}{J(XL_n, X\alpha_n)} \begin{vmatrix} F'_{XL}(XL_n, X\alpha_n) & F(XL_n, X\alpha_n) \\ G'_{XL}(XL_n, X\alpha_n) & G(XL_n, X\alpha_n) \end{vmatrix} \\
 &= X\alpha_n - \frac{\Delta_{X\alpha}(n)}{J(XL_n, X\alpha_n)} \quad \dots (33)
 \end{aligned}$$

where $F(XL, X\alpha) = 0$, $G(XL, X\alpha) = 0$,

$$\begin{aligned}
 \Delta_{XL}(n) &= \begin{vmatrix} F(XL_n, X\alpha_n) & F'_{X\alpha}(XL_n, X\alpha_n) \\ G(XL_n, X\alpha_n) & G'_{X\alpha}(XL_n, X\alpha_n) \end{vmatrix} , \\
 \Delta_{X\alpha}(n) &= \begin{vmatrix} F'_{XL}(XL_n, X\alpha_n) & F(XL_n, X\alpha_n) \\ G'_{XL}(XL_n, X\alpha_n) & G(XL_n, X\alpha_n) \end{vmatrix} ,
 \end{aligned}$$

and the Jacobian

$$J(XL, X\alpha) = \begin{vmatrix} F'_{XL}(XL, X\alpha) & F'_{X\alpha}(XL, X\alpha) \\ G'_{XL}(XL, X\alpha) & G'_{X\alpha}(XL, X\alpha) \end{vmatrix} \neq 0$$

This method is effective only when the initial selection of a couple of approximation is sufficiently close to the solution of a system.

Estimation of Interaction Parameters:

The 'electronic component' e_o and the internal pressure term e_p of L described by Kaufman and Bernstein⁽²⁾ are

$$e_o = 2[\phi_L \left(\frac{A+B}{2} \right) - \frac{1}{2} \phi_L(A) - \frac{1}{2} \phi_L(B)] \text{ cal/g.atom} \quad \dots (34)$$

$$e_p = 0.3 (V_A + V_B) \left[\left(-\frac{H_A}{V_A} \right)^{\frac{1}{2}} - \left(-\frac{H_B}{V_B} \right)^{\frac{1}{2}} \right] \text{ cal/g.atom} \quad \dots (35)$$

$$\text{and } L = e_o + e_p \quad \dots (36)$$

The strain energy term e_1 , the other terms e_2 , e_3 and e_4 given by Kaufman and Bernstein⁽²⁾ are

$$e_1 = -0.5 (H_A + H_B) (V_A - V_B)^2 (V_A + V_B)^{-2} \text{ cal/g.atom.} \quad \dots (37)$$

$$e_2 = 2[\phi_2 \left(\frac{A+B}{2} \right) - \frac{1}{2} \phi_2(A) - \frac{1}{2} \phi_2(B)] \quad \dots(38)$$

$$e_3 = 2[\phi_3 \left(\frac{A+B}{2} \right) - \frac{1}{2} \phi_3(A) - \frac{1}{2} \phi_3(B)] \quad \dots(39)$$

$$e_4 = 2[\phi_4 \left(\frac{A+B}{2} \right) - \frac{1}{2} \phi_4(A) - \frac{1}{2} \phi_4(B)] \quad \dots(40)$$

$$B = L + e_1 + e_2 \quad \dots(41)$$

These terms are calculated for the estimation of the interaction parameters of L and B and utilized in the computations of phase equilibria using regular solution and quasi-chemical models.

Results and Discussion:

The regular solution and quasi-chemical solution phase diagrams of the isomorphous and simple eutectic binary systems are computed using the thermodynamic data of heats of fusion, heat capacities, melting temperatures and the interaction parameters using heats of vaporization, molar volumes. The systems considered are Ag-Pd, Cu-Ti, Mo-W, Mo-V, V-W, and Cu-W for isomorphous type and Ag-Si, Sn-Al, Au-Si, Be-Si, and Bi-Cd for simple eutectic type.

The T_0 -x computation is the first step in computing the phase diagram, since it discloses the temperature and composition range where the various phases are stable. In the case of isomorphous systems of Cb-Ti, Mo-W, Mo-V, V-W and Cb-W it is found using T_0 -x computation that the phases to be considered are only liquid and bcc phases and in case of isomorphous Ag-Pd system, the phases to be considered are liquid and fcc phases. Consequently, the next step in the synthesis is to calculate the two-phase boundaries associated with each T_0 -x curve by utilising equations (19) and (20) using regular solution model and equations (24) and (25) using quasi-chemical solution model for isomorphous systems considered. The computations are made using the Newton-Raphson iteration technique described earlier.

In case of simple eutectic systems since liquid phase is in equilibrium with pure components only, the Newton-Raphson iteration technique is relatively simple since it involves the solution of a single variable.

The ideal isomorphous phase diagrams in which the interaction parameters are zero are calculated using equations (13) and (14). With the consideration of C_p data of the pure components, these diagrams are calculated utilizing equations (15) in equations (13) and (14).

The ideal simple eutectic phase diagrams with zero interaction parameters are calculated using equations (26) and (27). With the

consideration of C_p data of the pure components, these diagrams are calculated using equation (15) in equations (26) and (27).

The numerical values of e_o, e_p, e_1, e_2, e_3 and e_4 obtained for the isomorphous systems considered are summarized in table 1, and the resultant interaction parameters are presented in table 2.

Table:1. Interaction Parameters (Cal/g. atom)

System	e_o	e_p	e_1	e_2	e_3	e_4
Ag-Pd	-139,000	2302	438.4	-4110	1990	1415
Cb-Ti	0	3334	28.3	0	0	0
Mo-W	0	1381	7.2	0	0	0
Mo-V	0	585	256	0	0	0
V-W	0	3681	391.3	0	0	0
Cb-W	0	2276	783	0	0	0

Table 2: Resultant Interaction Parameters (Cals/g. atom)

System	$L = e_o + e_p$	$B = L + e_1 + e_2$	$E = B + e_3$	$A = E + e_4$
Ag-Pd ^φ	-136698	-140370	-138380	-136964
Cb-Ti	3334	3362	3362	3362
Mo-W	1381	1388	1388	1388
Mo-V	585	841	841	841
V-W	3681	4072	4072	4072
Cb-W	2276	3064	3064	3064

^φ In case of Ag-Pd system, A is used instead of B, since it forms fcc solid phase.

The interaction parameters computed for the simple eutectic systems are presented in table 3.

Table 3: Interaction Parameters for Simple Eutectic Systems (Cal/g.atom)

System	e_o	e_p	L
Ag-Si	0	+ 190	+ 190
Be-Si	-3689	+ 7254	+ 3565
Bi-Cd	-922.4	+ 80.7	- 842
Au-Si	- 5763	+ 214.2	- 5549
Sn-Al	- 2075.4	+ 3595	+ 1520

The diagrams calculated using ideal, regular and quasi-chemical models are compared in figs. (1) (i.e. a,b,c,d,e,f) and (2) (i.e. g,h,i,j,k) for isomorphous type and simple eutectic type respectively, with the experimental phase diagrams taken from ASM Hand Book⁽⁶⁾ and Hansen and Anderko⁽⁷⁾.

In the case of phase diagrams of Mo-W, Mo-V, Cb-W and Ti-Cb the experimental solidus lines are in agreement with that computed by the regular solution model and better agreement with that computed by quasi-chemical model. In the V-W diagram, the synthesized solidus lines of regular solution and quasi-chemical models, are away from the idealised solidus lines but lie in between the ideal solidus line and experimental solidus line. In case of Ag-Pd system the agreement is very poor. In all the isomorphous systems,

the synthesized liquidus lines show poor agreement with the experimental liquidus lines.

The ideal model calculations with C_p or without C_p consideration have shown negligible effect on the Ag-Pd, Ti-Cb, and Mo-V systems whereas in other isomorphous systems considered deviation is observed.

In all the simple eutectic systems considered, both the regular solution and quasi-chemical models improved the phase diagrams from ideal to experimental. Though the synthesized models do not agree well with the experimental diagrams, the shape of the synthesized diagrams, agree well with the experimental ones. The ideal model with out without C_p data remain same in all the systems considered.

Summary:

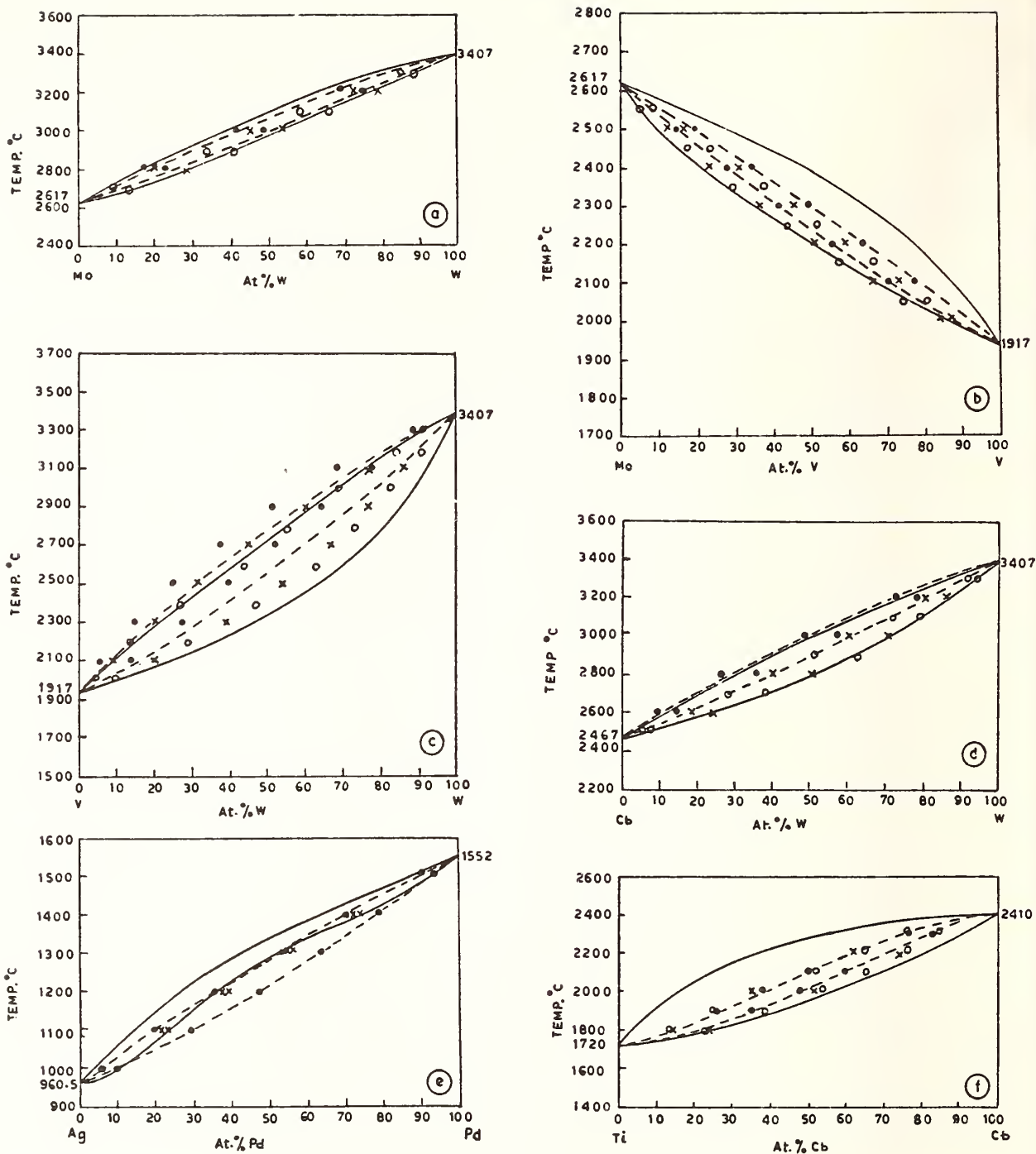
1. The isomorphous binary metallic systems of Ag-Pd, Cb-Ti, Mo-W, Mo-V, V-W and Cb-W have been synthesized. The synthesized solidus lines of Mo-W, Mo-V, Cb-W, and Cb-Ti diagrams are in agreement with the experimental solidus lines. The agreement is poor in Ag-Pd systems. The synthesized solidus line of V-W diagram tends to the experimental solidus line from that of ideal solidus line. In general the synthesized liquidus lines show poor agreement with the experimental liquidus lines.

2. The simple eutectic systems of Ag-Si, Be-Si, Bi-Cd, Au-Si and Sn-Al have been synthesized. The shape of the synthesized diagrams agree well with the experimental ones. The synthesized diagrams tend to approach the experimental diagram from that of ideal diagrams, with the refinement of the statistical thermodynamic models.

References:

1. Kopchenova.N.V and Maron. I.A, 'Computational Mathematics', MIR Publishers, Moscow, 1972.
2. Kaufman.L and Bernstein.H, 'Computer Calculation of Phase diagrams'. Academic Press, New York, 1970.
3. Wagner C, 'Thermodynamics of Alloys', Addison Wesley,Mass, 1952.
4. Rudman, Averbach, Oriani, Acta Met 1954, P 576, Vol.2.
5. Rudman.P.S, 'Advances in Materials Research', Vol.IV, pp.147-293, Interscience Publishers, New York,1969.
6. ASM Metals Hand Book, 'Metallography, Structures and Phase Diagrams', Vol.8., 1973.
7. Hansen.M. and Anderko.K.'Constitution of Binary Alloys', McGraw Hill Book Co., New York,1958.
8. Hultgren.R, Orr.L.R, and Kelley K.K, 'Selected Values of Thermodynamic Properties of Metals and Alloys', John Wiley and Sons,Inc, New York, 1963.
9. Lupis.C.H.P. and Elliott J.F. Acta Met., 1966, Vol.14, PP 529-38: 1967, Vol.15, PP 265-76.
10. Lupis C.H.P. Acta Met, 1968, Vol.16, PP 1365-75
11. Hiskes.R and Tillier W.A. Mater.Sci.Eng. 1967-68, Vol.2, PP 320-30; 1969, Vol.4, PP 163-84.

12. Kaufman L., Acta Met, 1959, Vol.7, PP 575-587.
13. Henri Gaye and Lupis C.H.P., Met. Trans, 1975, Vol.6A, PP 1049-1056.
14. Rao.S.V and Misra S, Trans.IIM, Vol.27, No.5, 1974, PP 311-316.
15. Swalin R.A. 'Thermodynamics of Solids', John Wiley and Sons Inc., New York (1962).
16. Shunk F.A. 'Constitution of Binary Alloys' McPraw-Hill Book Co., New York, (1969).



the notations are as follows:

- Experimental
- Ideal neglecting C_p
- Ideal with C_p
- xxxxxx Regular
- ooooo Quasi - chemical

Fig. 1. Isomorphous phase diagrams.

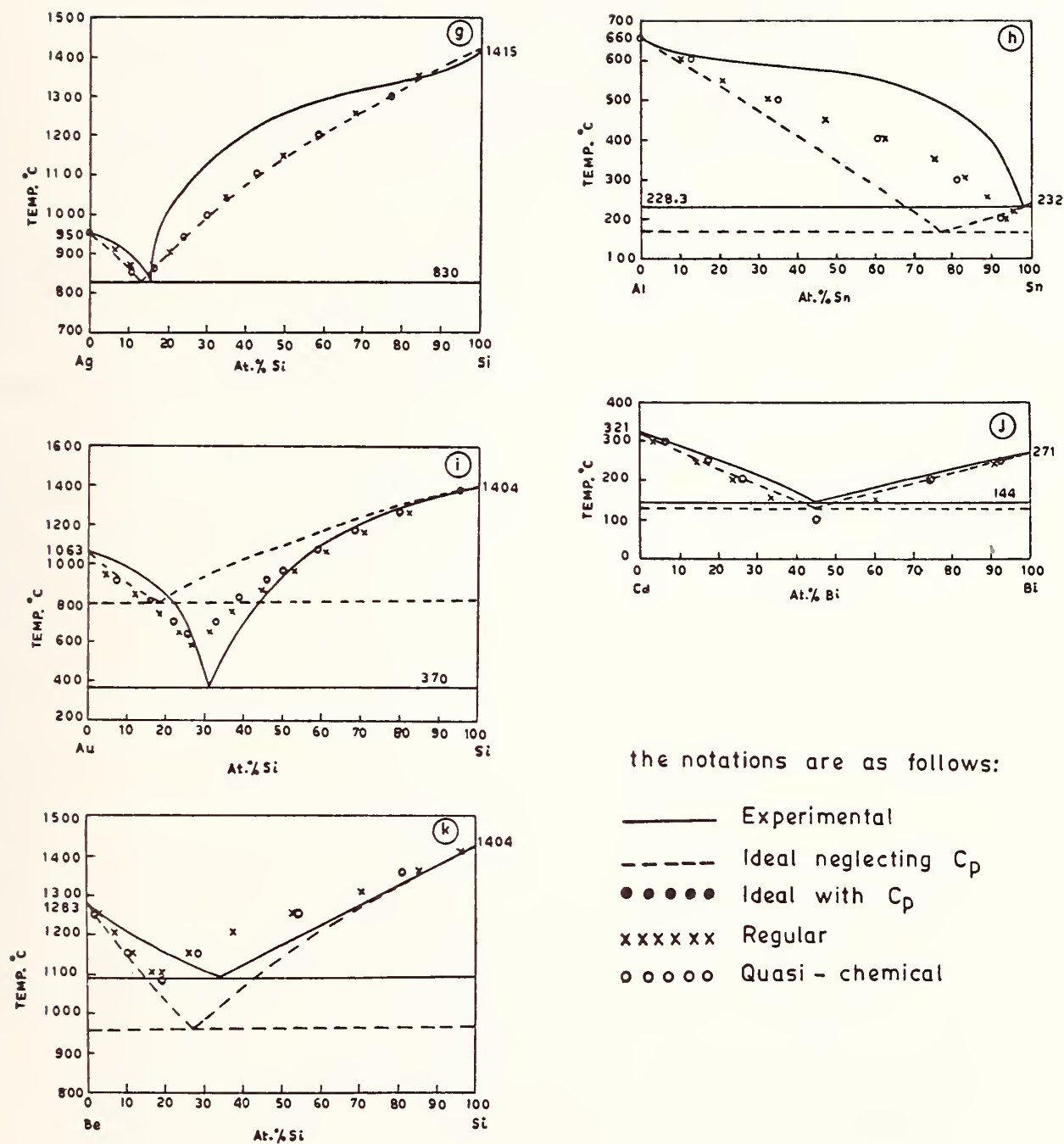


Fig.2. Simple Eutectic phase diagrams.



Quantitative Fits to Phase Lines and High Temperature Thermodynamic Data for Systems Forming Semiconductor Compounds

Robert F. Brebrick
Metallurgy and Materials Science Program
Marquette University, Milwaukee, WI 53233

Introduction

We are primarily interested in binary systems involving compound or elemental semiconductors. Theoretical construction of the phase diagrams involves knowing the appropriate thermodynamic models for the various phases occurring and the values of the parameters in these models that differentiate among specific systems. Although it is commonly believed that the appropriate model is established for a compound semiconductor with not too wide a deviation from stoichiometry, or for an elemental semiconductor containing a small amount of a second component, the same cannot be generally claimed for the liquid phases. Moreover, it has not yet been established that the model parameters, although some progress has been made for crystalline semiconductor phases,^{1,2} can be reliably calculated. Therefore the task is to fit available experimental phase diagram lines, as well as any other available high temperature thermodynamic data, in an effort to identify appropriate phase models for chemically similar systems and to establish values for the model parameters. We discuss efforts in this direction below for an A-B system forming a congruently-melting, narrow homogeneity range compound, $A_m B_n(c)$.

Thermodynamic Equation for the Liquidus Line

The appropriate liquidus equation has recently been derived³ and only the main points are indicated here. An equation is desired that is general in so far as the liquid phase is concerned and which takes account of the

temperature dependence of the enthalpy of formation, ΔH_f , and entropy of formation, ΔS_f , per formula weight of $A_m B_n(c)$ from the pure, liquid elements. As already implied, a basic, plausible, approximation is that at any temperature, T , the integral molar properties are essentially the same at both composition limits of the compound. An important feature of the derivation is that enroute to obtaining the desired liquidus equation, two auxiliary equations are used which link the properties of solid and liquid phases at the congruent melting point, T_{mn} , and the nominal compound composition $x = x^* = n/(m+n)$.

The starting point is in two equilibrium equalities, one between the chemical potentials of A in the coexisting liquid and solid phases, the other between those for component B. Multiplying the former by m , the latter by n , adding, and rearranging gives

$$\begin{aligned}
 m(h_A - Ts_A^e) + n(h_B - Ts_B^e) + RT \ln(1-x)^m x^n \\
 = m\mu_A(c) + n\mu_B(c) - m\mu_A^O(l) - n\mu_B^O(l)
 \end{aligned}
 \quad (1)$$

where if $i = A, B$ then h_i is the relative partial molar enthalpy of i in the liquid, s_i^e is the relative partial molar, excess entropy, and x is the atom fraction of B. The quantity $\mu_i^O(l)$ is the chemical potential of pure liquid i . For a narrow homogeneity range compound we assume, with justification from both theory and experiment,⁴ that the right hand member of Eq. (1) differs insignificantly from the Gibbs free enthalpy of formation of $A_m B_n(c)$ from the pure liquid elements. This quantity as well as the other integral properties of the compounds are in effect then functions of T alone. Writing

$$\Delta G_f = \Delta H_f - T\Delta S_f \quad (2)$$

and replacing the r.h.m. of Eq. (1) by that of Eq. (2) gives a liquidus equation called⁴ the $\Delta H_f - \Delta S_f$ liquidus equation, since these quantities enter as experimentally determined parameters. Since congruent melting implies a zero change in the Gibbs free enthalpy, two auxiliary relations can be written as

$$\Delta H_f(T_{mn}) = mh_A^* + nh_B^* - H_{mn} \quad (3)$$

$$\Delta S_f(T_{mn}) = ms_A^{*,e} + ns_B^{*,e} - H_{mn}/T_{mn} - R \ln[(1-x^*)^m (x^*)^n] \quad (4)$$

where the asterisk superscript indicates the partial molar quantities for the liquid are evaluated at $x = x^* = n/(m+n)$ and $T = T_{mn}$. In any specific case Eqs. (3) and (4) are two equations between the liquid phase model parameters. Using Eqs. (2), (3) and (4) in (1) and rearranging gives

$$T = \frac{H_{mn} + m(h_A - h_A^*) + n(h_B - h_B^*) - \Delta H_f + \Delta H_f(T_{mn}) + T\{\Delta S_f - \Delta S_f(T_{mn})\}}{H_{mn}/T_{mn} + m(s_A^e - s_A^{*,e}) + n(s_B^e - s_B^{*,e}) + R \ln \left[\left(\frac{1-x^*}{1-x} \right)^m \left(\frac{x^*}{x} \right)^n \right]} \quad (5)$$

This is the desired "heat-of-fusion" liquidus equation in which the temperature dependence of the enthalpy of compound formation, $\Delta H_f - \Delta H_f(T_{mn})$, and that of the corresponding entropy, $\Delta S_f - \Delta S_f(T_{mn})$, can be written more explicitly as a function of T in a specific case.⁵ In general we do not have an explicit equation for T and must resort to iterative methods for solution. In Eq. (5) the behavior of the relative heat capacity of both the compound and the liquid phase are general. The former is to be fixed by experiment, the latter is fixed upon adoption of a liquid phase model.

In certain cases Eq. (5) can be put into an approximate form, whose validity must be checked in each case, but which has the advantage of being an explicit equation for the liquidus temperature T and so more rapidly solved using a computer.³ Suppose the Gibbs free enthalpy of compound

formation turns out to depend very nearly linearly upon T . Then one can write

$$\Delta G_f(c) = \Delta \bar{H}_f - T \Delta \bar{S}_f + \delta(T) \quad (6)$$

where the enthalpy and entropy are average, constant quantities and $\delta(T)$ is small in a sense made clear below. One can also write

$$\Delta \bar{H}_f = \Delta H_f(T_{mn}) + \Delta \quad (7)$$

$$\Delta \bar{S}_f = \Delta S_f(T_{mn}) + \Delta/T_{mn} + \delta(T_{mn})/T_{mn} \quad (8)$$

Once the quantity Δ is defined by Eq. (7), then Eq. (8) must follow in order that the correct value of $\Delta G_f(c)$ at T_{mn} be given by Eq. (6). The auxiliary relations, Eqs. (3) and (4) can now be written in terms of the average enthalpy and entropy of formation to give

$$\Delta \bar{H}_f = m h_A^* + n h_B^* - (H_{mn} - \Delta) \quad (3b)$$

$$\Delta \bar{S}_f = m s_A^{*,e} + n s_B^{*,e} - (H_{mn} - \Delta - \delta(T_{mn}))/T_{mn} - R \ln[(1-x^*)^m (x^*)^n] \quad (4b)$$

Eliminating $\Delta \bar{H}_f$ and $\Delta \bar{S}_f$ in Eq. (6) using these equations and then substituting the resulting r.h.m. of Eq. (6) for that of Eq. (1) and rearranging gives

$$T = \frac{H_{mn} - \Delta - \delta(T) + m(h_A - h_A^*) + n(h_B - h_B^*)}{\frac{H_{mn} - \Delta - \delta(T_{mn})}{T_{mn}} + m(s_A^e - s_A^{*,e}) + n(s_B^e - s_B^{*,e}) + R \ln \left[\left(\frac{1-x^*}{1-x} \right)^m \left(\frac{x^*}{x} \right)^n \right]} \quad (9)$$

This liquidus equation is still as exact as that given by Eq. (5). It is always possible to choose $\Delta \bar{H}_f$ and $\Delta \bar{S}_f$ so that the correction term in Eq. (6) is zero at the melting point, i.e. $\delta(T_{mn}) = 0$. However we now neglect the quantity $\delta(T)$ in the numerator of Eq. (9). The assumption is not that $\delta(T) = 0$ everywhere, only that the values of T calculated from Eq. (9) with

$\delta(T) = 0$ and with $\delta(T)$ present differ insignificantly for the purpose at hand. This of course can be checked in a specific case by calculating the denominator of Eq. (9), the error in T incurred by neglecting $\delta(T)$ being the ratio of $\delta(T)$ to this denominator. The approximate equation obtained by setting $\delta(T) = 0$ in the numerator of Eq. (9) is an explicit equation for T whenever the enthalpy and excess entropy of mixing for the liquid phase are independent of T .

One question still remains in the application of these equations when the liquidus line for the compound extends to temperatures below the melting point of either of its elements. The thermodynamic properties of the metastable, supercooled elements are required to obtain ΔH_f and ΔS_f . For definiteness we define the properties of the supercooled melts by taking a zero difference in the constant temperature heat capacity of stable solid element and supercooled melt. This choice can effect the behavior of a particular choice for a liquid phase model, in fact it becomes part of the model, but it does not effect the properties of any stable phase.

An earlier derivation⁶ of the liquidus equation of a congruently-melting, narrow homogeneity range compound, $A_m B_n$, was given by Vieland for the special case, $m=n=1$. The derivation did not explicitly emphasize the auxiliary relations given here by Eqs. (3) and (4) and relied upon the difference in the constant pressure heat capacity of the compound and that of the supercooled liquid of the same composition. Vieland's liquidus equation has been commonly used in the literature with this ΔC_p set equal to zero. This amounts to a neglect of the temperature dependence of ΔH_f and ΔS_f when the liquid phase model is characterized by a temperature independent enthalpy and excess entropy of mixing (h_i , s_i^e in Eq. (5) independent of T). The liquidus equation is then similar to the approximate

form of Eq. (9), i.e. Eq. (9) with $\delta(T)=0$, differing in absence of the terms Δ and $\delta(T_{mn})$. However the validity of the approximate form of Eq. (9) does not rely upon setting the above ΔC_p equal to zero.

Jordan and Weiner⁷ has also derived a liquidus equation for a congruently-melting, narrow homogeneity range compound, AB(s). Their equation (15) can be shown to be equivalent to Eq. (5) with $m=n=1$, but, in our opinion, is in a relatively awkward form. Again the importance of what we call the auxiliary relations is not emphasized in obtaining the heat-of-fusion liquidus equation. Separate derivations are given for the heat-of-fusion and heat-of-formation liquidus equations whereas a straight forward analysis suffices to obtain both in a single, connected chain of argument.

Liquid Phase Model

Thus far our efforts are most complete for III-V binary systems. It appears that an adequate liquid phase model is one in which the heat and excess entropy of mixing are written in terms of four composition and temperature parameters, W , a , V , and c as

$$\Delta H_M^L = Wx(1-x)\{1+a(x-1/2)\} \quad (10)$$

$$\Delta S_M^{e,L} = Vx(1-x)\{1+c(x-1/2)\} \quad (11)$$

The partial molar quantities necessary to describe the liquidus line can be obtained using thermodynamic definitions. It is seen that the enthalpy and excess entropy of mixing are temperature independent and that the Kopp-Neumann rule for ΔC_p is implicitly assumed for the liquid solution. A number of commonly used models such as the ideal, strictly regular, athermal, and quasi-regular are obtained by setting various parameters in Eq. (10) and (11) equal to zero and so are special cases of this model.

Moreover the model defined by Eqs. (10) and (11) is mathematically equivalent to one used by Kaufmann and Nesor⁸ to reproduce the phase diagrams and available thermochemical data in metallic systems. (They also find it necessary to use a more complicated model in certain cases in which ΔH_M^L and $\Delta S_M^{e,L}$ are temperature dependent.) Lupis^{9,10} has discussed a model in which ΔH_M^L and $\Delta S_M^{L,e}$ are also independent of T and are given as infinite series in x , the series being truncated where necessary to reproduce the experimental data. The connection between the model used here and other simpler ones, which are derivable from a Braggs-William approximation for nearest neighbor bonding and therefore considered to have a theoretical basis, has already been discussed by Hardy.¹¹ It should be noted that the choice of factors $a(x-1/2)$ and $c(x-1/2)$ in Eqs. (10) and (11) is one of convenience in that application of the auxiliary relations, Eqs. (3) and (4) then impose restrictions upon W and V alone, a and c not entering. On the other hand, replacement of these factors by any others linear in x yield mathematically equivalent expressions.

Application

The above liquid model has been applied elsewhere¹² in detail to the In-Sb, Ga-Sb, In-As, and Ga-As systems and the experimental data used are tabulated or cited there. Some of these data are shown in Table I. The analysis is described below as a series of steps. For all four compounds a linear temperature dependence with $\delta(T_{mn}) = 0$ and $\delta(T)$ less than 40 cal/mole describes $\Delta G_f(c)$ (see Eq. (6)). Generally the liquidus temperatures calculated using the approximate liquidus equation, Eq. (9) with $\delta(T) = 0$, gives T accurate to 1°C or better, which is sufficient for our purposes. For each system W and V were fixed by Eqs. (3) and (4) and for each given liquidus composition, x_j , a calculated liquidus temperature,

$T_{j,cal}$, was obtained for some fixed values of a and c . These then were varied in an iterative search technique,¹³ until a minimum was found for $\sigma(T)$ where

$$\sigma^2(T) = \sum_{i=1}^N (T_{j,cal} - T_{j,obs})^2 / N \quad (12)$$

For the liquid model to be considered adequate it is necessary that $\sigma(T)$ be less than a critical value chosen as characterizing the experimental accuracy of the liquidus points. As a corollary, all fits with $\sigma(T)$ less than the critical value are considered equally acceptable at this stage. The corresponding values of a and c lie within a narrow, elongated ellipse in the a - c plane. The major axis of the ellipse is so much longer than the minor axis that one can consider the acceptable values of a and c to be along a "best-fit" line. A similar behavior has been found in the analysis of solidus and liquidus lines in pseudobinary sections between two III-V compounds¹⁴ and in the extraction of second law enthalpies and entropies from Gibbs free enthalpy-temperature measurements.¹⁵ Such behavior can be expected to occur generally in the quantitative fitting of phase diagrams.

Eutectic temperatures are potentially more accurately determined than liquidus temperatures in general and, except for GaAs, were so considered. Moreover an adequate fit to the liquidus points does not necessarily guarantee a eutectic temperature agreeing with the experimental value to within the latter's error. In the second step, only summarized here, the thermodynamic equations between the liquidus of the compound and that of one of the pure elements at their eutectic point were formulated. Specification of a eutectic temperature generates a eutectic composition and another line in the a - c plane, or allowing for the experimental error in

the eutectic temperature, a narrow band in the a-c plane. The intersection of this with the best-fit line, fixed by a fit to the liquidus points, serves to fix the liquid model parameters, \underline{a} and \underline{c} to within a negligible uncertainty. In this second step, the eutectic with the Group V element was used, but not that with the Group III element. The latter eutectic is very nearly degenerate with the pure element and variations in the eutectic temperature that are well within experimental error, cause such large shifts in the constraint line between a and c that it is not useful in fixing a and c.

At the end of the second step all the liquid parameters are fixed. The third step consisted of comparing the experimental points on the liquidus of the pure Group V element with that calculated and making a similar quantitative comparison for other high temperature properties. These included the chemical potential of In in In-Sb melt at 627°C, the enthalpy of mixing at $x=1/2$ for InSb and GaSb melts, and the partial pressures of As_2 over In-saturated InAs(c) and Ga-saturated GaAs(c). In all cases the predicted properties were in quantitative agreement with those measured. A summary is given in Table II.

The final step consisted in allowing for experimental errors in $\Delta H_f(T_{mn})$ and $\Delta S_f(T_{mn})$ which serve to fix the liquid parameters W and V through the auxiliary relations. It was found that the quality of the fits could be maintained over our estimate of the error range for the selected values of $\Delta H_f(T_{mn})$ and $\Delta S_f(T_{mn})$.

In summary it is found that the liquidus lines, Group V eutectic temperatures and compositions, and other high temperature data can all be simultaneously fit in a quantitatively satisfactory way with liquid phase

parameters that are consistent with the measured enthalpy and entropy of compound formation and the temperature dependence of these quantities.

In addition it was also shown that these simultaneous fits cannot be achieved with the special case of the liquid model in which $a=c=0$ (quasi-regular model). This is illustrated in part for InSb by the plots in the W-V plane shown in Fig. 1. At the best fit point to the InSb liquidus, shown as a square, the value of σ is 7.6°C. However at the point fixed by the auxiliary relations, shown by the cross near $W = -3.7$ kcal, the value of σ is 18.8°C and too large to be considered satisfactory. The latter point can be made to correspond to a value of 10°C for σ only by assuming it should be shifted to within the 10°C contour for σ due to errors in our selected values for $\Delta H_f(T_{mn}) + H_{mn}$ and for $\Delta S_f(T_{mn}) + H_{mn}/T_{mn}$. These would have to be simultaneous, negative errors of about -2 kcal/mole and -3 e.u./mole which, in view of the overall picture, seem unlikely. Furthermore, as shown in Fig. 1 only an InSb-Sb eutectic temperature of 470°C (lowest dashed line) will allow a value of σ less than 10°C. This is significantly different than the experimental value of $494 \pm 0.5^\circ\text{C}$.

The agreement between theory and experiment for the four III-V systems considered is so good and so extensive, that we are prompted to suggest that the liquid phase model given by Eqs. (10) and (11) is adequate for all the III-V melts. The agreement also suggests that some of the experimental data for the compounds considered that do not agree with the calculated values be redetermined, e.g. the GaAs-As eutectic temperature. On the other hand, it should be pointed out that the liquid model used here does not give a satisfactory fit to the liquidus lines in more ionic systems such as Pb-Te and Cd-Te when the values of W and V are fixed by the auxiliary relations.¹⁶

Solidus Lines of a Compound Semiconductor

We now turn to perhaps the most important aspect of the phase diagram for a solid-state chemist, the solidus lines of a semiconductor compound. As an illustration of a somewhat unusual analysis PbTe(c) is considered. The solidus lines have been determined experimentally in terms of electronic carrier concentration for PbTe.¹⁷ The partial pressure of Te₂ has also been measured along the Te-rich leg of the three-phase curve for PbTe and along a short portion of the Pb-rich leg.¹⁸ Thus the solidus lines can be analyzed without reference to the PbTe liquidus lines. The crystalline PbTe is considered to be a non-degenerate semiconductor. It can exist over a range of composition while maintaining the rock-salt structure by the inclusion of the appropriate kind and concentration of atomic point defects. Those associated with an excess of Pb are assumed to be donors that are always z-fold ionized, e.g. Pb interstitials or Te-vacancies. Those associated with an excess of Te are assumed to be acceptors that are also always z-fold ionized. Both kinds of atomic defects are assumed to be randomly distributed upon the appropriate sites of the PbTe lattice and to increase the excess Gibbs free enthalpy of the crystal by an amount per defect that is constant for each type. The resulting equations can be put into a compact form¹⁹ involving the relevant variables as

$$\mu_{\text{Te}} = \mu_{\text{Te}}(\text{int}) + z RT \sinh^{-1} \left(\frac{p-n}{2n_i} \right) + RT \sinh^{-1} \left(\frac{p-n}{2zk_s^{1/2}} \right) \quad (13)$$

where μ_{Te} is the chemical potential of Te in the pure crystal of fixed composition and hence fixed excess of valence band holes over conduction band electrons, $p-n$; $\mu_{\text{Te}}(\text{int})$ is the chemical potential of Te in the pure, intrinsic crystal for which $p-n=0$; n_i is the concentration of electrons in the intrinsic crystals, and k_s is the equilibrium constant equal to the

product of the concentration of z-ionized native donors and that of z-ionized native acceptors. The intrinsic material parameters are therefore $\mu_{\text{Te}}(\text{int})$, n_i , and k_s . Assuming an ideal vapor we have

$$\mu_{\text{Te}} - \mu_{\text{Te}}(\text{int}) = 1/2 RT \ln [p_{\text{Te}_2}/p_{\text{Te}_2}(\text{int})] \quad (14)$$

so that $p_{\text{Te}_2}(\text{int})$ replaces $\mu_{\text{Te}}(\text{int})$. If each of the three intrinsic parameters depend exponentially upon T as expected then there are six adjustable parameters. The particular difficulty here lies in the fact that the experimental data considered here require that all six parameters be considered simultaneously. The analysis commonly used in the literature would handle isothermal values of p-n vs p_{Te_2} . Nevertheless it has proved possible to obtain very good fits to the experimental data for PbTe using Eq. (13) with μ_{Te} replaced by p_{Te_2} through Eq. (14). The results are summarized in Table III for two different assumed states of ionization. Recent ion implantation studies²⁰ give z=2 for Pb-vacancy acceptors and also for Te-vacancy donors. What is not completely indicated in Table III, nor completely developed here, is that the parameters quoted are not unique. Rather there exists a range for each parameter, that for each parameter being correlated, over which almost equally good fits are obtained. It remains to investigate this problem and to apply a similar analysis to SnTe, PbSe, and PbS. Hopefully this can be done and some systematics identified in the values of the intrinsic materials parameters. Then one may be in a position to construct the solidus lines for the solid solutions formed among these compound semiconductors.

This work has been supported by NSF Grant DMR75-09332.

References

1. J. A. VanVechten, J. Electrochem. Soc., 122, 419 (1975).
2. G. B. Stringfellow, J. Phys. Chem. Solids, 33, 665 (1972).
3. R. F. Brebrick, Met. Trans., 7A, 1609 (1976).
4. R. F. Brebrick, Met. Trans., 2, 1657 (1971).
5. In ref. 3 these quantities were given a specific form.
6. L. J. Vieland, Acta Met., 11, 137 (1963).
7. A. S. Jordan and M. E. Weiner, J. Phys. Chem. Solids, 36, 1335 (1975).
8. L. Kaufman and H. Nesor in "Treatise on Solid State Chemistry", Vol. 5, Ed. N. B. Hannay, Plenum Press, N.Y. (1975).
9. C. H. P. Lupis and J. K. Elliott, Acta Met., 14, 529 (1966).
10. H. Gaye and C. H. P. Lupis, Met. Trans., 6A, 1049 (1975).
11. H. K. Hardy, Acta Met., 1, 202 (1953).
12. R. F. Brebrick, Met. Trans. A (in press) Quantitative Fits to the Liquidus Line and High Temperature Thermodynamic Data for InSb, GaSb, InAs, and GaAs.
13. J. A. Nelder and R. Mead, Computer J., 7, 308 (1965).
14. R. F. Brebrick and R. J. Panlener, J. Electrochem. Soc., 121, 932 (1974).
15. R. F. Brebrick, High Temp. Sci., 8, 11 (1976).
16. D. N. Abu-Judom, unpublished, Master's Thesis in Materials Science, Marquette University, Milwaukee, WI (1975).
17. R. F. Brebrick and E. Gubner, J. Chem. Phys., 36, 1283 (1962).
18. R. F. Brebrick and A. J. Strauss, J. Chem. Phys., 40, 3230 (1964).
19. R. F. Brebrick in "Progress in Solid State Chemistry", Vol. 3, p. 244, Ed. H. Reiss, Pergamon Press, Oxford and New York, (1966).
R. F. Brebrick, J. Solid State Chem., 1, 88 (1969).
20. H. Heinrich, A. Lopez-Otero, L. Palmetshofer and L. D. Haas, Inst. Phys. Conf. Ser. No. 23, Ch. 3, p. 264 (1975).

Table 1. Thermodynamic Properties of the Compounds AB(c).
Enthalpies in kcal/mole, entropies in e.u./mole, T in °C.

	T_{mn}	H_{mn}	$-\Delta H_f^O(298)$	$-\Delta S_f^O(298)$	$-\Delta H_f(T_{mn})$	$-\Delta S_f(T_{mn})$	$-\Delta \bar{H}_f$	$-\Delta \bar{S}_f$	T_{eu}	Eutectic with V x_V
InSb	525	11.41	7.40	3.82	13.27	11.53	13.020	11.22	494 \pm .5	0.69
GaSb	709.2	15.80	9.88	2.56	16.30	13.10	16.231	13.03	589 \pm .5	0.88
InAs	942	18.40	14.8	4.25	21.30	11.668	21.458	11.79	731 \pm	0.87
GaAs	1240	25.18	20.67	2.86	27.753	13.05	27.886	13.14	810?	--

Table 11. Summary of Fits to Thermodynamic Data
 $\sigma(T,V)$ is the measure of fit to the Group V element liquidus line.
 $x_V(\text{eu})$ is the calculated atom fraction of the Group V element at the eutectic temperature, T_{eu} .
 $\sigma(p)$ is the root mean square of the fractional difference between calculated and observed values of the partial pressure of As_2 .

	W cal	a	V e.u.	c	$\sigma(T)$ °C	$\sigma(T,V)$	T_{eu} °C	$x_V(\text{eu})$	$\Delta H_M^L(1/2)$ cal/gm-atom	$\sigma(\mu(\ln))$ cal/gm-atom
InSb	-3720	1.559	0.02377	-395.83	7.2	6.0	494	.689	-930(900°K)	94
GaSb	-1000	12.350	0.4602	-31.35	5.8	1.0	589	.887	-250(1023°K)	--
									$\sigma(p)$	
InAs	-5780	1.98	1.440	-7.80	12.9	15.0	731	.859	0.12	
GaAs	-5186	1.830	1.6735	-4.052	5.7	--	788	.947	0.15	

Table III. Comparison of Experimental and Calculated Values of $p-n$ for PbTe(c) given T and p_{Te_2} . If $\delta = p-n$,

$$\sigma^2 = \sum_{i=1}^{36} [\ln(\delta_{i,\text{cal}}/\delta_{i,\text{exp}})]^2/36$$

z	W	A	V	B	C	D	σ
2.0	-2939	21.63	-14,790	8.668	-4179	22.32	.164
1.0	-1344	20.116	-11,920	6.148	-5389	23.23	.168

$$\log_{10} n_i = W/T + A : n_i, \text{ cm}^{-3}$$

$$\log_{10} p_{\text{Te}_2}(\text{int}) = V/T + B : p_{\text{Te}_2}, \text{ atm}$$

$$\log_{10} (2zk_s^{1/2}) = C/T + D ; k_s^{1/2}, \text{ cm}^{-3}$$

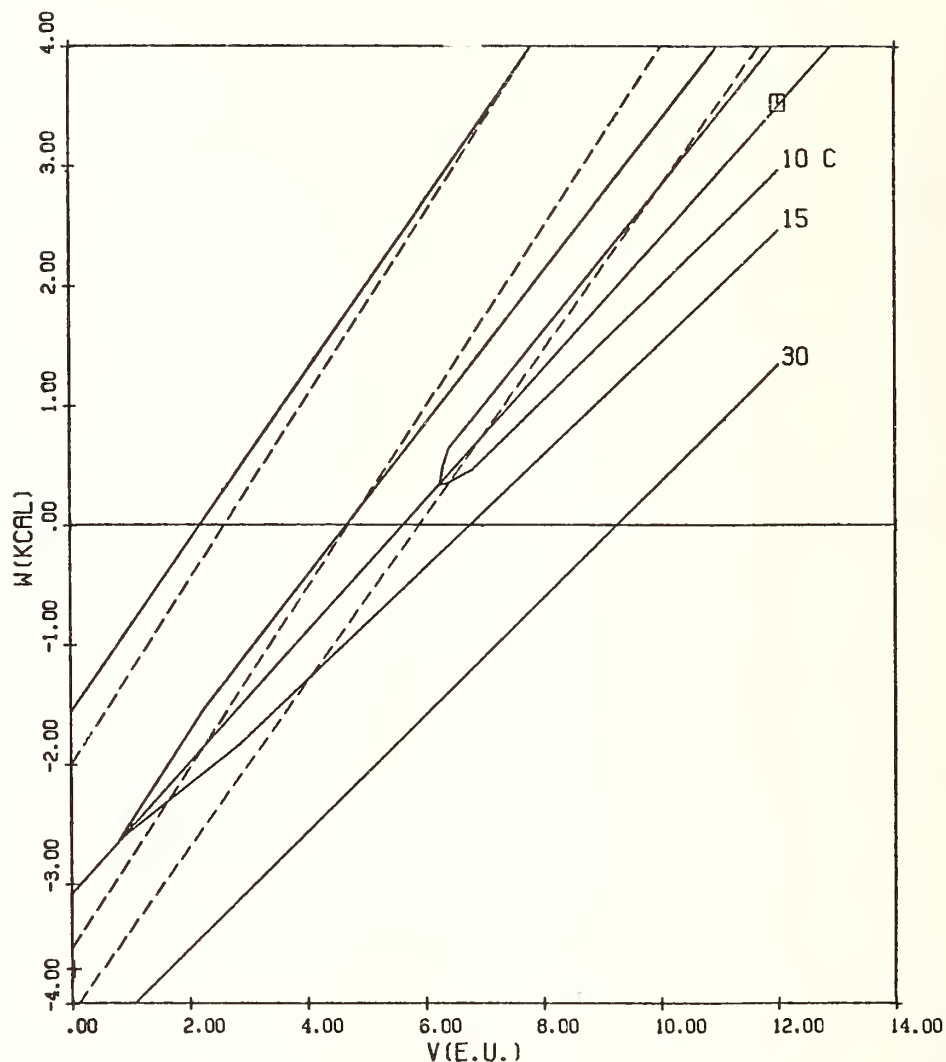


Figure 1 Fit to the InSb liquidus line using the quasiregular model i.e. $a=c=0$. The best-fit point is the square at the upper right. The lower halves of contours of constant σ are shown as solid curves. The solid straight line bisecting these contours and going through the best-fit point is the so-called best-fit line. The three dashed lines define those values of W and V consistent with an InSb-Sb eutectic temperature of 494°C (upper), 480°C (middle), and 470°C (bottom).



National Bureau of Standards SP-496, Applications of Phase Diagrams in Metallurgy and Ceramics
Proceedings of Workshop held at NBS, Gaithersburg, Md., January 10-12, 1977

NASA TECHNICAL TRANSLATION

NASA TT F-17296

PHASE DIAGRAMS OF METALLIC SYSTEMS (ALPHABETICAL CUMULATIVE
ALLOY SYSTEM INDEX AND TABLE OF CONTENTS)

BY N. V. AGEEV, EDITOR

MOSCOW, "VINITI" PRESS, 1959 - 1976

NATIONAL AERONAUTICS AND SPACE ADMINISTRATION

WASHINGTON, D.C. 20546

1. Report No. NASA TT F-17296		2. Government Accession No.		3. Recipient's Catalog No.	
4. Title and Subtitle PHASE DIAGRAMS OF METALLIC SYSTEMS (Alphabetical Cumulative Alloy System Index and Table of Contents)				5. Report Date December 1976	
				6. Performing Organization Code	
7. Author(s) N. V. Ageev, Editor				8. Performing Organization Report No.	
9. Performing Organization Name and Address NASA Lewis Research Center Cleveland, Ohio 44135				10. Work Unit No.	
				11. Contract or Grant No.	
				13. Type of Report and Period Covered Translation	
12. Sponsoring Agency Name and Address National Aeronautics and Space Administration Washington, D. C. 20546				14. Sponsoring Agency Code	
15. Supplementary Notes Translation of "Diagrammy Sostoyaniya Metallicheskih Sistem." Volumes I - XIX, Moscow, "VINITI" Press, 1959 - 1976, Selected pages. Translated and compiled by Coulson M. Schenermann, Lewis Research Center, Cleveland, Ohio 44135					
16. Abstract The compilation of phase diagram information edited by N. V. Ageev and published in Russian is the most comprehensive publication available on phase diagram information for binary, ternary, and higher order alloy systems. The Tables of Contents in volumes 1 through 17 of the compilation do not list the contents by alphabetic chemical symbols, but in Russian. Volumes 18 and 19 have their Tables of Contents listed by alphabetic chemical symbol. It is a laborious task to use this compilation because no cumulative alloy system index is available. This translation provides individual volume listing of contents by page number with alphabetic chemical symbols and it provides a cumulative alloy system index, listing alloy systems alphabetically by chemical symbol. This publication should facilitate the use of this valuable information source.					
17. Key Words (Suggested by Author(s)) Phase diagrams Alloy systems Binary alloy systems Ternary alloy systems order alloy systems				18. Distribution Statement Unclassified - unlimited Subject category 26	
19. Security Classif. (of this report) Unclassified		20. Security Classif. (of this page) Unclassified		21. No. of Pages 106	
				22. Price*	

For sale by the National Technical Information Service, Springfield, Virginia 22161

PREFACE

Phase diagram information is an important factor in the design and development of alloys. Phase diagram information is reasonably accessible for binary systems. Information for higher order systems, however, is not as readily accessible. The most comprehensive source of phase diagram information for binary and higher order systems is the annual compilations edited by N. V. Ageev and produced by the USSR Academy of Sciences.

Several difficulties face the potential user of the Ageev compilations. Typical lag times between cited literature publication dates and supplement publication is about three years. The compilations are somewhat difficult and cumbersome to use by those who cannot read the Russian language because the Tables of Contents through volume 17 are in Russian and because they do not have a cumulative index. Availability of the Ageev compilations is limited within the United States. Volumes 1 through 17 are currently available on microfilm through the Library of Congress. Other partial sets are located at private research laboratories.

This translation addresses the problems of those who cannot read Russian and those who want a cumulative index to aid them in their searches in these Ageev compilations. It is composed of two sections. The first section gives the Tables of Contents for volumes 1 through 19 (1959 - 1976) with the phase diagrams identified by chemical symbol. These volumes are listed in the Bibliography.

The second section of this translation is a cumulative index of phase diagrams included in the Ageev compilations, volumes 1 through 19 (1959 through 1976). The phase diagrams are listed in alphabetical order by chemical symbol. Throughout Section 2, the following convention is used. The volume is given by Roman numerals. Pages are designated by Arabic numerals. For example, the notation 'VII-205' refers to volume 7, page 205. Where data for one system extends to following pages, only the first page is given.

It is hoped that this publication will facilitate use of the Ageev compilations and the enormous amount of phase diagram information which they contain.

Coulson M. Scheuermann
Lewis Research Center

CUMULATIVE ALLOY SYSTEM INDEX

VOLUMES 1 - 19

CUMULATIVE ALLOY SYSTEM INDEX

<u>System</u>	<u>Location</u>
Ag-Al-Cd	VI-97
Ag-Al-Cu	VII-151, XIX-92
Ag-Al-Cu-Pd	XVIII-244
Ag-Al-Fe	XIX-93
Ag-Al-Mg	V-113, XV-117, XVII-208, XVIII-94
Ag-Al-Mn	III-84, VI-104, VIII-140
Ag-Al-Pd	XV-135
Ag-Al-Sn	IV-110
Ag-Al-Ti	III-86
Ag-Al-Zn	IV-111
Ag-As	V-74
Ag-As-S	XVI-279
Ag-As-Se	XVIII-95
Ag-Au-Co	IV-140
Ag-Au-Cu-Zn	XV-252
Ag-Au-Ge	X-152
Ag-Au-Pt	IV-141
Ag-Au-Si	VIII-183
Ag-Be	XIV-15
Ag-Bi	VIII-26
Ag-Bi-Pb-Te	IX-259
Ag-Bi-Sb-Se-Te	IV-182
Ag-Bi-Te	IX-179
Ag-C	XV-85
Ag-Ca	XVI-65
Ag-Cd	VI-52
Ag-Cd-Cu	I-117, II-73
Ag-Cd-Cu-Sn	VI-172
Ag-Cd-Cu-Zn	I-133, II-99, XIV-266
Ag-Cd-Sb	XIX-93
Ag-Cd-Sn	V-145
Ag-Cd-Zn	VII-205, VIII-191
Ag-Co-Ge	XVIII-97
Ag-Co-Si	XIV-205
Ag-Cr-Pd	VI-162

<u>System</u>	<u>Location</u>
Ag-Cu	XV-60
Ag-Cu-Pd	I-124
Ag-Cu-Se	XVII-345
Ag-Cu-Sn	V-155
Ag-Cu-Ti	XV-207, XVI-259
Ag-Cu-Zn	VIII-205
Ag-D-Pd	XVIII-99
Ag-Dy	XVI-36
Ag-Er	XVI-107
Ag-Eu	XI-62
Ag-Fe	IV-48
Ag-Fe-Ge	XVIII-98
Ag-Fe-Pd	VI-134, VIII-180
Ag-Fe-S	XVI-229
Ag-Fe-Si	II-68
Ag-Ga	V-34
Ag-Ga-In	VIII-171
Ag-Ga-Mg	XVII-265
Ag-Ga-Te	XII-190
Ag-Gd	XVI-28, XVIII-5
Ag-Ge	XII-64
Ag-Ge-Mn	XVIII-98
Ag-Ge-Ni	XVIII-99
Ag-H	XVII-52
Ag-H-Pd	XIX-94
Ag-Hg	IV-86
Ag-Ho	IX-47, XII-67
Ag-In	XVI-53
Ag-In-Mg	XVII-297
Ag-In-Sb	XVII-301
Ag-In-Se	XIII-214
Ag-In-Te	XIII-216
Ag-Ir-Pd	VIII-189
Ag-La	XIII-95
Ag-Lu	XVI-73
Ag-Na	VII-87, XIV-85
Ag-Ni-Si	XIV-214
Ag-O	I-43, XIV-69
Ag-P	V-97

<u>System</u>	<u>Location</u>
Ag-Pb-Sb-Te	IX-269
Ag-Pb-Se	XIII-254
Ag-Pb-Te	XIII-255
Ag-Pd-Rh	VII-234
Ag-Pd-Si	III-114
Ag-Pd-Te	XIV-245
Ag-Pt	III-67
Ag-Pu	XIII-117
Ag-Rh	V-94
Ag-Ru	V-95
Ag-S	IV-88, XIII-130, XVII-162
Ag-S-Sb	V-159, XVI-292
Ag-Sb-Se	XVII-384
Ag-Sb-Sn	IV-168
Ag-Sb-Te	VII-236, IX-252
Ag-Sc	XVI-103
Ag-Se	XVII-161
Ag-Si	XII-97
Ag-Sm	XI-127, XVI-101
Ag-Sr	XVI-104
Ag-Tb	XVI-105
Ag-Te	XVII-165
Ag-Ti	V-96, VI-87, XV-84
Ag-Tm	XVI-106
Ag-Y	XVI-62
Ag-Yb	XVI-58
Ag-Zr	XV-86
Al-As	I-11
Al-As-Ga	XVII-188
Al-As-Ga-Sn	XIX-242
Al-Au	XIII-11
Al-B	VII-5, XIII-6
Al-B-Ce	XVII-183
Al-B-Co	VIII-127, XIX-95
Al-B-Cr	XIX-96
Al-B-Cr-Fe-Si-Ti	IX-271, XIII-271
Al-B-Fe	XII-132
Al-B-La	XVII-182
Al-B-Mn	XIX-97

<u>System</u>	<u>Location</u>
Al-B-Ni	VIII-128, XIX-98
Al-B-Re	XVIII-100
Al-B-Ti	XVIII-101
Al-B-Y	XVII-181
Al-Ba	XVIII-6
Al-Be	XII-5, XVIII-6
Al-Be-Ce	XII-131
Al-Be-Cu	III-80, IV-95
Al-Be-Mg	XII-130
Al-Be-Si	XVIII-102
Al-Be-Ti	XVI-118, XVII-175
Al-Be-Zr	VI-93
Al-Bi	XII-6, XV-7
Al-Bi-Sb	IX-140
Al-C-Co	VI-98
Al-C-Cr-Mo-Nb-Ni-Ti-W	IV-183
Al-C-Fe	V-109, XIV-112, XV-106
Al-C-Fe-Si	XV-239
Al-C-Mo	IX-159
Al-C-Ni-Ti	IV-178
Al-C-W	IX-141
Al-C-Y	XI-146
Al-Ca-Fe	XV-103, XVI-123
Al-Ca-Mg	III-81, V-111
Al-Ca-Mg-Mn	VI-166
Al-Ca-Mn	XV-110
Al-Cd	II-5, XI-7, XIII-13
Al-Cd-Cu	VIII-134, XI-147, XII-140
Al-Cd-Cu-Mn	XI-259, XII-251
Al-Cd-Mn	IX-145, X-115
Al-Cd-Sb	V-110
Al-Cd-Sb-Zn	III-121
Al-Cd-Sn	X-116, XIII-147
Al-Ce	III-12, VII-16, XII-13, XIII-23, XV-15
Al-Ce-Cu	VII-152
Al-Ce-Fe	XV-108
Al-Ce-Ge	XVI-122
Al-Ce-Mg	XIII-150

<u>System</u>	<u>Location</u>
Al-Ce-Mn	IX-153
Al-Ce-Sb	XII-148
Al-Ce-Si	IX-148
Al-Ce-Th	VII-155
Al-Co	XVII-23
Al-Co-Cr	IV-103, VI-99
Al-Co-Cu	XII-142, XVII-205
Al-Co-Cu-Fe-Nb-Ni	XII-265
Al-Co-Cu-Fe-Ni-Si	XII-264
Al-Co-Cu-Fe-Ni-Si-Zr	XII-267
Al-Co-Cu-Fe-Ni-Ta	XII-266
Al-Co-Cu-Fe-Ni-V	XII-263
Al-Co-Fe	IV-100, XII-138, XV-104
Al-Co-Hf	XVII-189
Al-Co-Mn	XVIII-104
Al-Co-Nb	XIV-117
Al-Co-Ni	XII-141
Al-Co-Ta	XIV-118
Al-Co-Ti	XII-143, XIII-148, XV-112
Al-Co-U	X-117, XIV-119
Al-Co-Y	XVII-198
Al-Cr	VI-12, IX-17, XVI-9
Al-Cr-Cu	IV-108, V-115, XIII-152, XVIII-109
Al-Cr-Cu-Zr	XIII-264
Al-Cr-Fe	XV-107, XVI-129
Al-Cr-Fe-Ni	XVIII-245
Al-Cr-Fe-Ni-Ti	III-124
Al-Cr-Fe-Ni-Ti-W	I-135
Al-Cr-Fe-Si-Ti	VI-173, IX-270
Al-Cr-Mg	XIX-99
Al-Cr-Mg-Mn	XIX-243
Al-Cr-Mn	XI-158, XVIII-110
Al-Cr-Mo-Nb-Ni-Ti-W	VII-258, X-219
Al-Cr-Mo-Ni-Ti	XVI-304
Al-Cr-Nb	X-125, XIV-132
Al-Cr-Ni	I-92, IV-109, VII-153
Al-Cr-Ni-Ti	X-213
Al-Cr-Ni-Ti-W	II-101, III-123
Al-Cr-Ni-W	VII-248, VIII-221, X-211
Al-Cr-Si	VII-147, XI-155

<u>System</u>	<u>Location</u>
Al-Cr-Ti	IV-112, IX-162
Al-Cr-Zr	XIII-156, XIV-138, XVI-148, XVIII-113
Al-Cu	I-10, IV-7, VII-9, IX-9, XVIII-7
Al-Cu-Fe	I-81, XVII-196
Al-Cu-Fe-Mn	X-212
Al-Cu-Fe-Ni	III-120
Al-Cu-Fe-Si	VI-165
Al-Cu-In	I-82, II-56
Al-Cu-La	XV-115
Al-Cu-Li	II-58, VI-102, VII-148, IX-151, XI-157
Al-Cu-Li-Mg	XV-241
Al-Cu-Li-Mn	XIV-258
Al-Cu-Mg	I-86, III-83
Al-Cu-Mg-Mn	IX-256
Al-Cu-Mg-Ni	IV-176
Al-Cu-Mg-Si	I-130, VII-249
Al-Cu-Mg-Zn	I-132, V-162, VI-167, VII-250
Al-Cu-Mn	I-88, X-120, XII-144
Al-Cu-Mn-Ni	IV-177
Al-Cu-Mn-Si	I-131
Al-Cu-Nb	XIV-125
Al-Cu-Pd	X-122, XVIII-114
Al-Cu-Si	XIV-120
Al-Cu-Sn	XIV-126
Al-Cu-Ti	IV-106, VI-105, VIII-141, IX-154, XI-160, XVII-209, XIX-99
Al-Cu-V	VII-138, XI-140
Al-Cu-Y	XIV-115, XVII-202, XVIII-115
Al-Cu-Zn	III-85, VI-106, XVIII-116
Al-Cu-Zr	X-123, XIII-153, XVI-137
Al-Dy	XIII-8
Al-Dy-Fe	XIX-100
Al-Dy-U	XIII-144
Al-Er	XI-16, XIII-24
Al-Er-Fe	XVIII-117
Al-Er-Y	XIV-116

<u>System</u>	<u>Location</u>
Al-Fe	IV-4, VI-8, VII-7, XIII-9, XVI-7, XVII-20
Al-Fe-Gd	XIX-105
Al-Fe-Ge	XVIII-118
Al-Fe-Hf	XV-101
Al-Fe-La	XIV-110
Al-Fe-Mg-Si	IV-175
Al-Fe-Mn	VI-95
Al-Fe-Mn-U	XII-252, XIV-255
Al-Fe-Mo	XVI-124
Al-Fe-Mo-Ti-Zr	XVII-413
Al-Fe-Nb	XII-139
Al-Fe-Nd	XVI-126
Al-Fe-Ni	II-55
Al-Fe-Ni-Ti	XIV-256
Al-Fe-Sc	XVI-127
Al-Fe-Si	I-80, VI-94, VII-142, XIII-145, XIV-109
Al-Fe-Si-U	XIX-245
Al-Fe-Ta	XIV-111
Al-Fe-Ti	IV-101, IX-142, XV-105, XVI-128, XVII-197, XIX-101
Al-Fe-U	VI-96, VIII-133, IX-143, X-114, XIII-146
Al-Fe-Y	XVII-194
Al-Fe-Zn	XVI-130, XIX-103
Al-Fe-Zr	XIV-113, XV-109
Al-Ga	III-7, IV-3, XIV-7
Al-Ga-In-Sb	I-129, XII-250
Al-Ga-Mg	VII-141, VIII-130, X-113
Al-Ga-Nb	XIX-104
Al-Ga-P	XIX-105
Al-Ga-Sb	I-79, IV-97, V-108
Al-Gd	XI-5, XIII-7
Al-Ge	XVII-19
Al-Ge-La	XVI-121
Al-Ge-Mg	IV-99, XV-102
Al-Ge-Nb	XVII-191
Al-Ge-Nb-Sn	XI-258

<u>System</u>	<u>Location</u>
Al-Ge-P	VIII-132, XI-145
Al-Ge-Sb	VIII-131, XI-144
Al-Ge-Sn	XIX-106
Al-Ge-Y	XVII-190
Al-H	XVII-18
Al-H-Ni	XV-99
Al-Hf	VI-7, VIII-6, XII-7, XVI-6
Al-Hf-Ni	XV-100
Al-Ho	XII-8
Al-In	II-4, XI-6
Al-In-Sb	I-83
Al-La	III-9, XI-8, XIII-15, XV-11
Al-La-V	XV-93
Al-Li	II-6, IV-5, VIII-7, IX-6
Al-Li-Mg	I-84, II-57, XIX-108
Al-Li-Mg-Mn	XVII-393
Al-Li-Mg-Sn	XIX-246
Al-Li-Mg-Zn	XVII-395
Al-Li-Mn	IX-150, XIII-149
Al-Mg	III-10, IX-7
Al-Mg-Mn	III-82, XIX-110
Al-Mg-Mn-Sn	XVI-295
Al-Mg-Nd	XIV-123, XV-116
Al-Mg-Si-Sn	XIV-257
Al-Mg-Sn	IV-104, V-112, XIV-124, XIX-111
Al-Mg-Ti	XIX-111
Al-Mg-Zn	I-87, V-114, VI-103, VII-149, VIII-139
Al-Mg-Zr	XV-118
Al-Mn	IV-6, VI-9, IX-8, XVII-26
Al-Mn-Ni	I-90
Al-Mn-Si	X-118, XI-151
Al-Mn-Ti	I-91, IV-105, IX-152
Al-Mn-U	X-121, XIII-151
Al-Mn-V	XV-94
Al-Mn-Y	XVII-200
Al-Mo	V-8, VI-11, X-7, XVII-28, XVIII-8
Al-Mo-Nb	XIV-128
Al-Mo-Nb-Ni	XV-243
Al-Mo-Nb-Sn	IX-257
Al-Mo-Ni	VI-109, XV-120, XVII-213

<u>System</u>	<u>Location</u>
Al-Mo-Si	VI-100, VII-143
Al-Mo-Ti	VIII-142, IX-155, XV-123, XVI-138, XVIII-119
Al-Mo-Ti-V	X-209
Al-Mo-Ti-Zr	XIV-259
Al-Mo-U	X-124, XV-125, XVII-215
Al-Mo-V	V-107, XII-133
Al-Mo-Zr	XIV-127, XVI-139
Al-Nb	V-9, VII-10, X-8, XII-11, XIV-9
Al-Nb-Ni	VIII-143, XI-161, XII-145, XV-127, XVI-140, XVII-220
Al-Nb-Rh	XVI-142
Al-Nb-Si	VII-144, XIX-112
Al-Nb-Ta	XVI-143
Al-Nb-Ti	V-116, VIII-145, IX-160, XV-130, XVI-144
Al-Nb-V	VII-139, XII-134
Al-Nb-Zr	XIV-133, XVI-146
Al-Nd	XI-9, XIII-16, XV-12
Al-Ni	XVIII-9
Al-Ni-Sc	XIV-129
Al-Ni-Si	VI-101, XVI-136
Al-Ni-Ta	XIV-130
Al-Ni-Ti	VIII-144, XI-162, XIII-154, XIX-113
Al-Ni-U	XIV-131
Al-Ni-V	XI-142, XVII-184
Al-Ni-W	IV-96
Al-Ni-Y	XIV-114
Al-Ni-Zr	XII-147, XV-129
Al-O-Ti	XI-149, XV-111
Al-P	XVII-29
Al-P-Si	VIII-138, XI-154, XVII-207
Al-Pb	XIII-21
Al-Pb-Sn	II-59
Al-Pd	IX-10, X-9
Al-Pr	XII-12, XIII-18, XV-13
Al-Pt	X-10
Al-Pu	VIII-8, X-11, XIII-17
Al-Re	VII-12, IX-11, XVIII-10
Al-Ru	IX-12

<u>System</u>	<u>Location</u>
Al-S-Sb	XI-163
Al-Sb-Si	VIII-136, XI-152
Al-Sb-Y	XVII-204
Al-Sc	XI-11, XIX-3
Al-Si	I-9, III-8, XIII-14, XIV-8, XV-10, XVII-24
Al-Si-Sn	VIII-135
Al-Si-Ta	VII-145
Al-Si-Ti	IX-146, XI-153, XIV-121
Al-Si-U	VII-146, VIII-137, IX-147, X-119
Al-Si-V	VII-137
Al-Si-W	VII-140
Al-Si-Y	XVII-199
Al-Si-Zr	XI-156, XIV-122
Al-Sm	XI-10, XIII-19
Al-Sm-U	XIII-155
Al-Sn	II-7
Al-Sn-Ti	VI-111, VII-154, VIII-146, XV-134
Al-Sn-Ti-Zr	XI-260, XVI-296
Al-Sn-Zn	XIV-134
Al-Sn-Zr	XIV-135
Al-Ta	II-9, V-11, XIX-3
Al-Ta-Ti	IX-161, XII-149
Al-Ta-V	XII-135
Al-Th	V-13, VII-14
Al-Ti	I-12, II-10, III-11, V-12, VII-13, IX-13, XI-12, XII-9, XIII-22
Al-Ti-V	I-78, IX-139, XI-143, XII-136, XIV-107, XV-96, XVI-120, XVII-186
Al-Ti-W	XIX-113
Al-Ti-Zr	X-126, XI-164, XIV-136, XV-136, XVI-147
Al-Tl	IX-15, XV-14
Al-U	VII-15, IX-16, X-12
Al-U-Zr	VII-156, X-129, XIV-137
Al-V	I-7, III-6, V-6, XIX-4
Al-V-Zr	XII-137

SystemLocation

Al-W	VI-6
Al-Y	V-7, VII-8, XIII-12, XV-9
Al-Yb	XV-8, XVII-22, XVIII-10
Al-Zn	II-12, VII-17, VIII-11
Al-Zr	V-14, VIII-9, XI-15, XIV-10, XVI-10, XVIII-13
Am-Pu	XII-14
As-Bi	XI-33
As-Bi-Se	VIII-160
As-Bi-Sn	XVIII-120
As-C-Fe	III-105
As-C-Fe-Mn	VI-170
As-Cd	XVI-64, XVIII-13
As-Cd-Ge-In	IX-262
As-Cd-Ge-Sn	XII-258
As-Cd-I-In	XI-263
As-Cd-In	XI-219
As-Cd-Se-Zn	XVII-405
As-Cd-Te	XVIII-122
As-Cd-Zn	X-172
As-Cu	III-53, XI-105, XVIII-14
As-Cu-Fe	XI-209
As-Cu-Ni	XI-238
As-Cu-Pb	XIII-231
As-Cu-Sn	XII-230
As-Eu	XVII-83
As-Fe	III-31, IV-44
As-Fe-Ni	XIII-202
As-Ga	I-25, XV-27
As-Ga-Ge	IX-187, XII-187
As-Ga-Ge-Sn	XIX-247
As-Ga-In	I-101, XII-188, XV-173
As-Ga-P	XVII-267
As-Ga-Sb	I-104, XVII-266
As-Ga-Se-Zn	V-163
As-Ga-Sn	XI-198, XII-189, XIII-187, XVIII-123, XIX-116
As-Ga-Te	XIII-188, XVIII-124
As-Ga-Zn	IV-128, XVIII-125

<u>System</u>	<u>Location</u>
As-Ge-In	IX-193
As-Ge-In-Zn	IX-263
As-Ge-P	XVIII-126
As-Hg	IX-117
As-In-P	IV-144, XVI-237
As-In-Pb	XIII-211
As-In-Pd	XVI-236
As-In-Sb	I-113, II-72
As-In-Se	IV-142, V-141, X-166
As-In-Sn	XIII-210
As-In-Sn-Zn	IX-267
As-In-Te	IV-143, XII-209, XIII-212
As-In-Zn	XIII-213
As-Ni-Sn	XI-246
As-Pb	XIX-5
As-Pb-Sn	XIX-116
As-Pd	IX-95
As-Pd-Te	XVII-364
As-Se	VIII-97
As-Sn-Te	XVI-276, XVII-361
As-Sn-Zn	IX-238
As-Te	XIV-82
As-Te-Zn	XVII-365
As-Th	XIV-84
Au-Be	VIII-10
Au-Bi	VIII-21
Au-Bi-Te	X-140
Au-Bi-Zn	XII-175
Au-C	XV-40
Au-Cd	IV-52, VIII-57
Au-Cd-In	IV-139
Au-Cd-Sb	XIX-120
Au-Co	II-29
Au-Co-Cu	XIII-206
Au-Co-Fe	XVI-212
Au-Co-Pd	II-71
Au-Cr	VI-49
Au-Cs	VII-63

SystemLocation

Au-Cu	I-37, III-36, IV-53, V-44, VIII-58
Au-Cu-Fe	XIII-196
Au-Cu-Pb	I-111
Au-Cu-Pd	I-110
Au-Cu-Zn	XI-218
Au-Dy	XI-58, XIX-6
Au-Er	XI-73
Au-Fe	IX-49
Au-Fe-Ni	VII-192
Au-Ga	XII-52
Au-Ga-Ge	XVII-263
Au-Gd	XI-39
Au-Ge	XII-61
Au-Ge-Sb	X-153, XIV-175, XVII-275
Au-H-Ni	XV-167
Au-Hf	VIII-43
Au-Hg	IV-55, XIII-77
Au-Ho	IX-45, XI-57
Au-In	IV-51, X-50, XVII-91
Au-In-Sb	XIII-205
Au-K	VII-57
Au-Li	VII-58
Au-Lu	XI-68
Au-Mg	XI-69
Au-Mn	X-51
Au-Na	VII-59
Au-Nb	XIX-7
Au-Ni	IV-54, XIV-56, XVII-93
Au-Ni-Pd	VIII-184
Au-Ni-Pt	XIX-121
Au-P	V-48
Au-Pb	I-38, IV-56, V-47, XVII-95
Au-Pb-Sn	XII-208, XIII-207, XIV-194
Au-Pb-Te	XV-194
Au-Pd-Pt	I-112
Au-Pd-Rh	VI-138
Au-Pd-Ru	VIII-185
Au-Pd-W	XV-170

<u>System</u>	<u>Location</u>
Au-Pr	XVII-94
Au-Pt	VI-48
Au-Pt-Rh	X-165
Au-Pu	XIII-75
Au-Rb	VII-60
Au-Rh	V-45, X-52
Au-Ru	V-46
Au-S	VII-62
Au-Sb	XVIII-14
Au-Sb-Si	XVII-294
Au-Sc	XI-70
Au-Se	VII-61, XVII-96
Au-Sm	XIX-8
Au-Sn	XIV-57
Au-Tb	XI-71
Au-Ti	II-30, VIII-59
Au-Tu	XI-72
Au-V	I-14, VI-21, VIII-14
Au-Yb	XI-67, XVI-50
Au-Zn	XVIII-15
Au-Zr	VIII-61
B-Be	VII-18, XIX-9
B-C	IV-10, VII-21
B-C-Cr-Fe	XII-254
B-C-Cr-Fe-Ni	XII-262
B-C-Fe	IX-166, XIII-162
B-C-Hf	VII-159
B-C-Mo	IX-168
B-C-Nb	IX-170, XI-174
B-C-Si	VI-114
B-C-Ta	IX-171, XI-175
B-C-Th	VII-162
B-C-Ti	VII-161
B-C-U	VII-164
B-C-V	IX-163, XI-167
B-C-W	IX-165, XIV-145
B-C-Zr	VII-165

<u>System</u>	<u>Location</u>
B-Ce	XI-26
B-Ce-Cr	XIX-123
B-Ce-Fe	XVIII-127
B-Ce-Ni	XVII-236
B-Ce-Si	XVII-232
B-Ce-Th	XI-176, XIII-168
B-Ce-U	XI-177, XIII-169
B-Co	VI-17, IX-20, XII-22
B-Co-Cr	XII-160, XIV-150
B-Co-Ga	XIX-124
B-Co-Hf	XV-145, XVIII-128
B-Co-In	XVII-228
B-Co-Mn	XII-157
B-Co-Mo	XII-158
B-Co-Nb	XII-161, XIV-149
B-Co-Ni	V-119
B-Co-Re	XIX-124
B-Co-Sb	XI-169
B-Co-Si	V-118, XIX-126
B-Co-Sn	VIII-147
B-Co-Ta	X-132
B-Co-Ti	XIII-163, XVII-230
B-Co-V	XI-166, XIX-127
B-Co-W	XIII-158
B-Co-Zn	IX-167
B-Co-Zr	XI-170, XV-147
B-Cr	IV-11, X-16, XV-17
B-Cr-Fe	XII-156, XVI-155, XIX-127
B-Cr-La	XIX-128
B-Cr-Mn	XV-151
B-Cr-Mo	XV-153
B-Cr-Nb	XV-156
B-Cr-Ni	VI-118, VIII-149, XVIII-128
B-Cr-Re	XV-157, XVI-162
B-Cr-Si	IV-116
B-Cr-Ta	XVIII-129

<u>System</u>	<u>Location</u>
B-Cr-Ti	VI-119
B-Cr-V	XV-140
B-Cr-W	XIV-146
B-Cr-Y	XVI-156
B-Cr-Zr	XIII-170
B-Cu	XI-21, XVI-14, XVII-37
B-Cu-Ni	XI-171
B-Eu	XVII-36
B-Fe	XV-16, XVI-13
B-Fe-Ga	XIX-129
B-Fe-Mn	XII-153
B-Fe-Mo	XII-154
B-Fe-Nb	XIV-148
B-Fe-Ni	XII-155, XV-146, XVIII-130
B-Fe-Si	V-117, XVI-154
B-Fe-Ta	XVII-227
B-Fe-Ti	XIII-161
B-Fe-V	XIX-129
B-Fe-Zr	XI-168
B-Ga-Ni	XV-144, XIX-130
B-Ge	XVI-12
B-Ge-Ni	X-130
B-Hf	XVII-35
B-Hf-N	VII-131
B-Hf-Nb	XVIII-131
B-Hf-Ni	XII-152, XVIII-132
B-Hf-Re	XVI-153
B-Hf-Ta	XVII-226
B-Hf-U	XIII-160
B-Hf-W	XVI-150
B-In-Ni	X-131
B-La	VII-19
B-La-Mo	XVIII-132
B-La-Ni	XIX-131
B-La-Si	XVII-231
B-La-W	XVIII-133
B-Mg-Ni	X-133
B-Mn	XI-20
B-Mn-Mo	XVII-233
B-Mn-Nb	XVIII-134

<u>System</u>	<u>Location</u>
B-Mn-Ni	XV-148
B-Mn-Re	XV-149, XVI-158
B-Mn-Si	V-120, XVI-157
B-Mn-Ti	XV-150
B-Mn-V	XVII-222
B-Mn-W	XVII-223
B-Mo	X-15, XIII-29, XVII-38, XVIII-16
B-Mo-Nb	XVII-234
B-Mo-Ni	VII-160, X-134, XII-162, XV-152
B-Mo-Re	XVI-159
B-Mo-Si	III-88
B-Mo-Ta	XIV-151
B-Mo-Ti	VI-117, XVIII-134
B-Mo-W	XIV-142, XV-141, XVIII-136
B-Mo-Y	XIX-132
B-Mo-Zr	IV-117, XIII-164, XVIII-137, XIX-132
B-N-Ti	I-77, VII-132
B-N-V	XIV-105
B-N-Zr	VII-133
B-Nb	V-20, XVII-40
B-Nb-Ni	X-135
B-Nb-Re	XVI-161
B-Nb-Si	III-89
B-Nb-Ti	I-95, IX-169, XVII-237
B-Nb-W	XII-151
B-Nb-Zr	XVII-240
B-Ni	III-16, VI-18, XI-22, XII-23, XIII-30, XVII-39
B-Ni-P	XIII-165
B-Ni-Re	XVIII-139
B-Ni-Sb	X-136
B-Ni-Si	XVIII-139, XIX-134
B-Ni-Sm	XVI-160
B-Ni-Sn	VIII-148
B-Ni-Ta	X-137, XVII-235
B-Ni-Ti	XI-172, XV-155
B-Ni-V	XIII-157, XIX-135
B-Ni-W	XV-143, XVIII-140
B-Ni-Zn	VIII-150
B-Ni-Zr	XI-173, XIII-166

<u>System</u>	<u>Location</u>
B-Pd	VI-19
B-Pt	XI-24
B-Re	XIV-19
B-Re-Si	XVIII-141
B-Re-Ta	XVII-243
B-Re-Ti	XVII-244
B-Re-V	XV-138, XVI-149
B-Re-W	XIV-144, XVI-151
B-Re-Zr	XIV-152, XVI-163
B-Ru	IX-22
B-Si	V-18, VIII-13, IX-21, XIV-18
B-Si-Ta	III-90
B-Si-V	IV-114
B-Si-W	III-87, IV-115
B-Si-Y	XVII-229
B-Si-Zr	VI-116
B-Ta	V-21, VII-20, XVII-41
B-Ta-Ti	XIV-153
B-Ta-W	XVII-224
B-Ta-Zr	XIII-167
B-Th	XI-25
B-Th-U	VII-163
B-Ti-V	XV-139
B-Ti-W	IX-164, XVI-152, XVII-225
B-U	V-22
B-U-Zr	VIII-151
B-V	V-17
B-W	III-15, XIII-28
B-W-Y	XIX-136
B-W-Zr	XIII-159, XIV-147
B-Zr	III-17, IV-12, XVI-15
Ba-Bi	XII-15
Ba-Cd	XVIII-17
Ba-Cu	V-15, XVII-30
Ba-Ga	XII-16
Ba-Ge	XII-17

<u>System</u>	<u>Location</u>
Ba-In	XII-18
Ba-Li	IV-8
Ba-Mg	III-13
Ba-Mn	X-14, XI-18
Ba-Mn-Si	XI-165
Ba-Na	III-14, VI-13
Ba-Ni	XI-19
Ba-Pd	XVI-11, XVII-31
Ba-Pr	XVII-34
Ba-Pt	XVII-32
Ba-Si	X-13, XI-17
Ba-Sr	II-13
Be-Bi	IV-9, XII-19
Be-C-Si	XII-150
Be-C-U	I-94, XV-137
Be-Ca	XIII-25, XIV-12
Be-Ce	XII-21
Be-Cr	II-14, XIV-16
Be-Cu	VIII-11, XIV-13
Be-Cu-Mn	VI-113
Be-Cu-Ni	IV-113
Be-Cu-Ni-Ti	XV-244
Be-Fe	VI-14, XIV-11
Be-Fe-P	I-93
Be-Fe-Si	VI-112
Be-Fe-Zr	XIV-139
Be-Li	V-16, XIII-26
Be-Na	XIII-27
Be-Nb	IX-18, XIV-14
Be-Nb-Zr	XIV-140
Be-Ni	VI-15
Be-Pu	I-13
Be-Ru	IX-19
Be-Si-U	XVIII-142
Be-Sn-Zr	XIV-141
Be-Th-U	VII-158
Be-Ti	VIII-12
Be-Ti-V	VII-157
Be-W	XII-20
Be-Zr	VI-16, XIV-17

<u>System</u>	<u>Location</u>
Bi-Ca	IX-28, XII-33
Bi-Ca-Pb	III-96
Bi-Cd	XVIII-17
Bi-Cd-Hg	XVI-174
Bi-Cd-In	VII-175
Bi-Cd-Sn	V-124, VII-177
Bi-Cd-Te	XVI-175
Bi-Co	XII-34
Bi-Cs	IV-21
Bi-Cu	VII-28, VIII-22
Bi-Cu-Mg	III-97
Bi-Cu-S	II-61
Bi-Cu-Te	XVII-252
Bi-Cu-U	VIII-159
Bi-Cu-Zn	XII-178
Bi-Dy	XIII-38
Bi-Eu	XVIII-19
Bi-Eu-Th	XVIII-143
Bi-Fe-S	VI-123
Bi-Ga	VI-26
Bi-Gd	XIII-37
Bi-Ge-Te	XI-187
Bi-Hf	XII-31
Bi-Hg	XI-34
Bi-Hg-Pb	XV-163
Bi-Hg-Sn	XV-161, XVI-176
Bi-Hg-Tl	XVI-179
Bi-I-Te	XVII-251
Bi-In	XIX-10
Bi-In-Sb	VII-176
Bi-In-Sb-Te	XIX-248
Bi-In-Sn	XVIII-143
Bi-In-Te	IX-176, XII-176, XIV-168
Bi-Ir	XI-32
Bi-La-Th	XVIII-146
Bi-Lu	XII-36

<u>System</u>	<u>Location</u>
Bi-Mg	XII-37
Bi-Mg-Pb	VI-124, VIII-158
Bi-Mg-Sn	VIII-157
Bi-Mn	II-16, XII-38
Bi-Mn-Sb	IX-177, XIX-136
Bi-Mo	IV-16
Bi-Na	XVI-21
Bi-Na-Sn	XIX-137
Bi-Nb	XII-39
Bi-Nd	XVI-22, XVII-44
Bi-Ni-Rh	XV-160
Bi-O-Te	XIX-138
Bi-Pb	III-21, IV-19, XIII-39
Bi-Pb-Se	VII-178
Bi-Pb-Sn	IV-121
Bi-Pb-Te	V-125, IX-178, XIII-179, XV-164, XVI-180
Bi-Pd	V-25
Bi-Pd-Te	XVII-254
Bi-Pt	VIII-24, XII-40
Bi-Pr	XVII-45
Bi-Rb	III-20, IV-17
Bi-Rh	VIII-25, IX-29
Bi-S	VI-28
Bi-S-Se	V-126, XIII-180
Bi-S-Te	V-127, XVI-181
Bi-Sb	XIV-24
Bi-Sb-Se-Te	IX-260, XI-261
Bi-Sb-Te	XI-188, XIV-169
Bi-Se	I-20, V-26, VI-27
Bi-Se-Sn	XIII-177
Bi-Se-Te	VI-125
Bi-Si	XII-35
Bi-Sn	VIII-23, X-22, XVI-23
Bi-Sn-Te	XIII-178
Bi-Sr	II-17, XII-41
Bi-Te	III-22, IV-20, V-27, XIV-26
Bi-Te-Tl	IX-180
Bi-Th-U	VII-179

<u>System</u>	<u>Location</u>
Bi-Ti	VI-29, XII-42
Bi-Tl	XVI-24
Bi-U	V-28, VII-29, VIII-27
Bi-U-Zr	VII-180
Bi-V	XII-24
Bi-Yb	XII-32
Bi-Zn	I-21
Bi-Zr	IX-30
C-Ce	X-111
C-Ce-Mo	X-190
C-Ce-Th	X-204, XIII-260
C-Ce-U	X-207, XIII-261, XVIII-146
C-Ce-Zr	X-208
C-Co	XIV-72, XVII-113
C-Co-Cr	XV-200, XVII-318, XVIII-147
C-Co-Cr-W	XIV-263, XV-248
C-Co-Fe	XV-185, XVIII-148
C-Co-Mo	XV-199, XIX-139
C-Co-Nb	XI-228, XVIII-148
C-Co-Sn	VI-144
C-Co-Ti	II-80, V-151, VII-208
C-Co-U	IX-218
C-Co-W	VII-185, XVI-187
C-Co-Zn	VII-209
C-Co-Zr	XI-229, XIX-140
C-Cr	III-76, XIII-137
C-Cr-Fe	IV-137, VIII-181, XVI-232, XVIII-149, XIX-141
C-Cr-Fe-Mn-N	XIV-268
C-Cr-Fe-Mo	VIII-224, XIII-266, XVII-401
C-Cr-Fe-N	XII-249, XIII-262, XV-233, XVIII-245
C-Cr-Fe-Ni	VIII-225, XIV-265, XVIII-253
C-Cr-Fe-U	X-218, XIII-268
C-Cr-Fe-V	VIII-222, XIII-265, XIV-260
C-Cr-Fe-W	VIII-223, XVI-299, XVII-396
C-Cr-Hf	XII-195
C-Cr-Mo	XI-243, XVIII-152
C-Cr-Mo-Zr	XVII-412

<u>System</u>	<u>Location</u>
C-Cr-N	XIII-143
C-Cr-Nb	XIV-240, XVIII-153
C-Cr-Ni	I-125
C-Cr-Ni-Ti	XI-265
C-Cr-Re	XII-242
C-Cr-Ta	XIV-252
C-Cr-Ti	I-128, VIII-219, XII-248, XIX-143
C-Cr-U	VII-245, IX-255, X-206
C-Cr-V	XII-173, XIV-167
C-Cr-W	X-150, XIII-186
C-Cr-Zr	XI-257, XIX-144
C-Cu	XV-62
C-Cu-Fe	XI-210, XVIII-153
C-Cu-Ni	VIII-204
C-Cu-U	IX-230
C-Cu-V	VII-171
C-Fe	I-33, V-41, VI-43, VII-55, X-46, XI-66, XII-76, XIV-55, XVI-45, XVII-89, XVIII-19, XIX-10
C-Fe-H	XIX-144
C-Fe-Hf	VIII-173
C-Fe-Mn	X-158, XVII-287, XVIII-155, XIX-145
C-Fe-Mn-Si	III-122, IV-179
C-Fe-Mo	XIV-187, XV-190, XVI-221, XVIII-155
C-Fe-N	VIII-126, XI-138, XIII-140
C-Fe-Nb	XI-212, XVIII-158
C-Fe-Ni	X-161, XV-191, XVI-225, XVIII-159
C-Fe-Ni-Pb	VI-171
C-Fe-Ni-U	XIII-267
C-Fe-Ni-W	X-215
C-Fe-O	VIII-175
C-Fe-P	XVIII-159
C-Fe-Pu	X-162
C-Fe-S	VII-201, XIV-192, XIX-148
C-Fe-Si	V-138, XII-204, XIII-199, XIV-181, XVI-217, XVII-280, XVIII-160
C-Fe-Sn	VII-200
C-Fe-Ti	II-70, III-107, XV-193
C-Fe-U	VII-202, IX-209, X-164

<u>System</u>	<u>Location</u>
C-Fe-V	IX-174, XII-165, XIV-156, XV-158, XVIII-160
C-Fe-W	XIV-170, XVI-182
C-Fe-Zn	VI-137
C-Ge	V-37, XIII-58
C-H-V	XIX-148
C-Hf	VIII-46, XI-52, XVIII-21
C-Hf-Mo	XII-193, XIII-191, XV-175, XVII-272, XVIII-162, XIX-149
C-Hf-Nb	X-151, XI-202, XIII-192, XVII-273
C-Hf-Nb-Zr	IX-261, XII-257
C-Hf-Re	XII-194, XVIII-165
C-Hf-Ta	IX-191, XIII-194
C-Hf-Ti	V-132, XIII-195
C-Hf-U	VII-189, IX-192
C-In-Ni	VI-139
C-Ir	XV-47
C-La	VI-57
C-La-U	XVIII-165
C-Li	III-48
C-Mn	XIX-14
C-Mn-Mo	XVII-334
C-Mn-Si	IV-153
C-Mn-W	XVII-255
C-Mo	XI-106, XII-103, XIII-101, XV-65, XVI-82
C-Mo-N	XVI-117
C-Mo-Nb	VII-213, XIII-234, XVII-356, XIX-150
C-Mo-Nb-Zr	XVII-409
C-Mo-Ni	XV-212, XVII-354, XVIII-166, XIX-150
C-Mo-Ni-Zr	XIX-249
C-Mo-Pu	XIII-236
C-Mo-Re	X-185, XIX-152
C-Mo-Ta	XIV-229, XIX-153
C-Mo-Th	IX-235
C-Mo-Ti	II-89, XI-241, XIII-237, XIV-231, XV-216, XVI-266, XVII-357, XIX-153
C-Mo-Ti-Zr	XVII-410, XIX-251

<u>System</u>	<u>Location</u>
C-Mo-U	IX-236, X-188, XII-232, XIII-240, XIV-234, XVII-358, XIX-154
C-Mo-W	II-62, XVII-258, XIX-157
C-Mo-Zr	IX-237, XI-244, XIII-241, XV-219, XVI-273, XVII-360
C-N-Nb	V-105, VI-92
C-N-O-U	XVII-392
C-N-Ta	V-106
C-N-V	X-112
C-Nb	V-79, VII-102, XIV-91, XVII-140, XVIII-22
C-Nb-Ni	XVIII-167, XIX-158
C-Nb-Re	XIII-246, XIV-239, XVI-285, XVIII-168
C-Nb-Ti	I-126, X-193, XI-247, XVIII-168
C-Nb-U	IV-165, VII-229, X-197, XII-238, XVII-372
C-Nb-W	X-145, XI-193, XIII-184, XVII-260, XVIII-170, XIX-158
C-Nb-W-Zr	XIX-252
C-Nb-Zr	X-198, XI-249, XII-239, XIII-248, XVIII-170
C-Nd-U	XVIII-171
C-Ni	IX-99, X-87, XI-112, XII-109, XIV-89, XVII-137, XIX-14
C-Ni-Pb	VI-159
C-Ni-Ti	II-91, VI-160, VII-225, VIII-213
C-Ni-U	VII-226, IX-239, X-192, XIII-245
C-Ni-W	VII-187
C-Ni-Zn	VII-227
C-Ni-Zr	XIX-159
C-O-Pu	XI-225, XIV-200
C-O-Ta	XIV-201
C-O-Te-U	XVII-406
C-O-Ti	II-76
C-O-U	XII-219, XVI-253
C-O-V	IV-118
C-Pu	VII-114, IX-109
C-Pu-Si	XIII-227
C-Pu-Th	XIII-252
C-Pu-Ti-U	XIII-270

<u>System</u>	<u>Location</u>
C-Pu-U	IX-251, X-199
C-Pu-U-W	XIX-252
C-Pu-W	XVIII-172, XIX-159
C-Re	V-91, IX-112, XI-124, XII-119
C-Re-Ta	XIII-253, XIV-247, XV-224, XVII-382
C-Re-Ti	XIV-248
C-Re-U	X-200
C-Re-W	IX-186, X-147, XIX-161
C-Re-Zr	XV-225, XIX-160
C-Rh	XV-83, XIX-15
C-Ru	XIX-16
C-Ru-U	XVI-289, XVIII-173
C-Si	V-61
C-Si-U	XIII-229, XIV-216
C-Ta	IX-129, XI-132
C-Ta-Ti	V-160
C-Ta-Ti-W	XIX-253
C-Ta-U	IV-170, VII-238
C-Ta-V	XVI-171
C-Ta-W	VIII-170, XIX-162
C-Ta-Zr	X-202, XII-246
C-Te-U	XVII-391
C-Th	IV-91, XIII-135
C-Th-U	IV-171, VII-240
C-Th-U-Zr	IV-181, VII-257
C-Th-Zr	VII-243, VIII-220, IX-254
C-Ti	II-52, V-102, VII-122
C-Ti-V	X-139, XI-184, XII-169
C-Ti-W	XIX-162
C-Ti-Zr	XIII-258
C-U	VII-129, X-109, XI-134, XII-128, XV-90
C-U-V	XVI-172
C-U-W	X-149, XII-186, XVI-197, XVII-262, XVIII-173, XIX-167
C-U-Y	X-171
C-U-Zr	IV-174, VII-246, XIV-254, XVII-390
C-V	III-19, VIII-19, XI-30, XII-29, XIV-23, XIX-16
C-V-W	VIII-152

<u>System</u>	<u>Location</u>
C-W	IX-33, X-25, XI-37, XII-49, XIX-17
C-W-Zr	XI-194, XVIII-174
C-Y	X-59, XIV-66, XIX-18
C-Zr	XI-135, XII-129
Ca-Cd	XVIII-23
Ca-Ce-Cl	I-118
Ca-Cu	XVII-107
Ca-Eu	XV-35
Ca-Fe-P	II-63
Ca-Fe-Si	VIII-174, XIV-176, XV-179
Ca-Ga	XII-54
Ca-Ge	XI-55, XVII-75
Ca-Hg	XIX-19
Ca-La	IV-61
Ca-Li	III-40
Ca-Mg	I-41, IX-86
Ca-Mg-Mn	V-149
Ca-Mg-Si	XV-195
Ca-Mn	IX-71
Ca-Mn-Si	IX-214, XI-224
Ca-Na	II-34
Ca-Na-Pb	IX-216
Ca-Ni	XI-83
Ca-Pb	V-54
Ca-S-U	XVII-309
Ca-Si	XVIII-24
Ca-Sr	IV-62
Ca-Ti	VI-53
Ca-Zn	IX-73
Cd-Cr-Se	XIX-168
Cd-Cu	VIII-74
Cd-Cu-Mg	I-116, XVI-248
Cd-Cu-Mg-Zn	II-98
Cd-Cu-Sb	XVI-243, XIX-169
Cd-Cu-Sn	V-144
Cd-Cu-Zn	II-75, VIII-190, XIII-219
Cd-Eu	XI-61

<u>System</u>	<u>Location</u>
Cd-Ga	IV-32
Cd-Ga-Pb	VII-188
Cd-Ga-Sb	XI-197
Cd-Ga-Se	XVI-202
Cd-Gd	XVII-63
Cd-Ge-Sb	XV-178, XVI-207
Cd-Hg	XV-49
Cd-Hg-Pb	XVIII-175
Cd-Hg-Sn	XVIII-178
Cd-Hg-Te	XIII-221
Cd-In	V-49, XVII-98
Cd-In-Sb	XVII-296
Cd-In-Sb-Sn	XII-260
Cd-In-Sb-Te	IX-266
Cd-In-Te	IX-211
Cd-La	XIX-20
Cd-Mg	XIII-83, XVII-105, XIX-21
Cd-Mn-S	XIV-199
Cd-Ni	IX-69, XV-48
Cd-Pb	XVIII-27
Cd-Pb-Sb	XVI-245
Cd-Pb-Se	XI-223
Cd-Pb-Sn-Zn	XIII-269
Cd-Pb-Te	X-174
Cd-Pb-Zn	XIII-222
Cd-Pu	XI-79
Cd-S	IX-70
Cd-Sb	VII-71, XIII-84
Cd-Sb-Sn	XII-216, XIX-170
Cd-Sb-Te	XVI-246
Cd-Sb-Zn	V-148, VIII-192, IX-213, X-175
Cd-Se	XII-87
Cd-Sn	V-52, X-61, XIV-67
Cd-Sn-Te	X-173
Cd-Sn-Tl	V-146
Cd-Sn-Zn	IV-146, V-147, XVI-244
Cd-Sr	XI-81
Cd-Te	VIII-75
Cd-Te-Zn	XVI-247

<u>System</u>	<u>Location</u>
Cd-Ti	XVIII-27
Cd-Tl	X-62
Cd-Yb	XVII-100
Cd-Zn	XI-82
Ce-Co	V-58, XII-94, XVII-115
Ce-Co-Fe	V-137
Ce-Co-H	XVIII-182
Ce-Co-La	XIX-170
Ce-Co-Pu	V-150, XII-222
Ce-Co-Si	XVI-255, XVII-314
Ce-Cr	V-104, XV-92, XVI-110
Ce-Cr-O	XVI-254
Ce-Cu	X-77
Ce-Cu-Mn	XIX-171
Ce-Cu-Mn-Zr	XIX-254
Ce-Cu-Pu	XI-239
Ce-Cu-Zr	XVII-350
Ce-Fe	I-36, V-43
Ce-Fe-N	XIX-172
Ce-Fe-Ni-Si	X-217
Ce-Fe-Pu	XIII-204
Ce-Fe-Si	XVI-218, XVII-285
Ce-Ga-V	XVI-164
Ce-Gd	IX-34, X-29
Ce-Ge	XVII-80, XIX-22
Ce-Ge-Se	XVIII-182
Ce-Ge-Si	XII-196
Ce-H	XIX-23
Ce-Hf	XVII-71
Ce-Hg	XII-51
Ce-Ir	XIX-23
Ce-K	XVII-106
Ce-La	IV-66
Ce-La-Mg	XVIII-183
Ce-Mg	VIII-86, XI-102, XVII-123
Ce-Mg-Mn	III-115
Ce-Mg-Zn	XVII-332
Ce-Mn	III-52
Ce-N	XVI-5, XVII-17
Ce-N-V	XIX-173

<u>System</u>	<u>Location</u>
Ce-Na	XIV-86
Ce-Nb	V-80
Ce-Ni	X-88
Ce-Ni-Pu	XIII-243
Ce-Ni-Si	XV-205, XVII-322, XIX-173
Ce-Pd	XIII-112
Ce-Ru	VIII-118
Ce-S-Ti	XVII-388
Ce-Sc	X-106
Ce-Si	XII-98
Ce-Si-Th	XII-226, XIII-228
Ce-Sm	XIV-102
Ce-Te	XIII-132
Ce-Th	III-73, VII-125
Ce-Th-Zr	X-205
Ce-Ti	III-71
Ce-V	VIII-20, XIII-36
Ce-Zn	XI-137
Co-Cr	VI-56, VII-76, XVIII-28
Co-Cr-Fe	V-136, VI-127, IX-197, XIX-174
Co-Cr-Fe-Mo-Ni	XV-258
Co-Cr-Fe-Ni-W	XV-257
Co-Cr-Mo	I-119
Co-Cr-Mo-Ni	XV-253
Co-Cr-Ni	XIX-175
Co-Cr-Ni-W	XV-247
Co-Cr-Si	XI-226
Co-Cr-Ti	IV-148, VI-145, VIII-198
Co-Cr-W	XVIII-185
Co-Cr-Zr	XVIII-186
Co-Cu	II-36, IV-63, XII-91, XVIII-29
Co-Cu-Mn	IV-147
Co-Cu-Pd	II-77
Co-Cu-Si	XIV-202
Co-Dy	XVII-82
Co-Er	XII-95, XVII-116

<u>System</u>	<u>Location</u>
Co-Fe	III-30, XIV-48, XVI-40
Co-Fe-Ge	XIX-176
Co-Fe-Mn	VIII-176
Co-Fe-Mn-U	IX-264
Co-Fe-Mo	XVIII-187
Co-Fe-Ni	XV-183
Co-Fe-O	II-64
Co-Fe-Pd	IV-130, V-135, VII-194
Co-Fe-S	IV-131
Co-Fe-Si	XI-206
Co-Fe-Sn	XIV-183
Co-Fe-U	IX-196, X-157, XI-207
Co-Fe-V	I-96
Co-Fe-Zn	II-67
Co-Gd	VIII-36, XV-23, XVII-65, XIX-24
Co-Ge-Mo	X-154
Co-Ge-Ni	XIX-176
Co-Ge-Si	XVII-276
Co-H	XVII-47
Co-H-La	XVIII-188
Co-Hf	XIV-35, XV-28
Co-Hf-Zr	XVIII-188
Co-Hg	IX-78
Co-Ho	XVII-81
Co-In	XVI-51
Co-La	XIII-90
Co-Mg	XI-86
Co-Mn	VIII-77, XVII-109
Co-Mn-Mo	VI-143
Co-Mn-Pd	X-177
Co-Mn-Si	VIII-197, X-176
Co-Mn-Sn	XIV-207
Co-Mn-Ti	XV-198
Co-Mn-U	IX-217, X-178, XI-227
Co-Mn-Zr	XVIII-189
Co-Mo	IX-77
Co-Mo-Si	XII-220
Co-Mo-Zr	XVII-315

<u>System</u>	<u>Location</u>
Co-Nb	X-67, XII-92, XIII-91, XVI-68, XVIII-30
Co-Nb-Si	XIV-204, XVIII-190
Co-Nb-Sn	XVII-316
Co-Nb-Zr	XIV-208, XVIII-190
Co-Ni-Pd	II-78
Co-Ni-Pd-V	XIV-261
Co-Ni-S	XIX-177
Co-Ni-Sb	III-111, XIX-178
Co-Ni-Si	XIV-203, XIX-178
Co-Ni-Sn	I-120, XIX-179
Co-Ni-U	I-121
Co-Ni-V	III-92
Co-Ni-Zn	II-79
Co-O-W	XI-190
Co-Pb	I-46
Co-Pb-Te	XIV-209
Co-Pd-V	XIV-158
Co-Pu	V-56
Co-S	VII-75, XI-87
Co-Sb	XIX-25
Co-Sb-Si	XIV-206
Co-Se	XVII-111
Co-Si	XIII-89
Co-Si-Ti	XII-221
Co-Si-V	XII-166
Co-Sm	XIV-70, XV-52, XIX-26
Co-Sn	XVII-110
Co-Ta	XIII-92, XVIII-31
Co-Te	V-57, XVIII-32
Co-Th	XII-93
Co-Ti	I-47, VI-54, XIV-71, XVII-112
Co-Ti-Zr	XVII-317
Co-V	I-16
Co-V-Zr	XVIII-191
Co-W	XIII-44
Co-Y	XI-77, XVII-103
Co-Zn	I-48
Co-Zr	XI-88, XVI-69, XVIII-33

<u>System</u>	<u>Location</u>
Cr-Cu	III-54
Cr-Cu-Fe-Mn-Ni	II-102
Cr-Cu-Fe-Ni	II-97
Cr-Cu-Mn-Ni	II-100
Cr-Cu-Nb	XVIII-192
Cr-Cu-Ni	III-117, XIII-233
Cr-Cu-Pd	VI-152
Cr-Cu-Ti	XVI-263
Cr-Cu-Zr	II-87, III-118, XVIII-193
Cr-Fe	VI-45, VIII-55, X-48, XV-39, XVI-48, XVIII-34, XIX-27
Cr-Fe-Mn	IV-135, XIV-186, XIX-179
Cr-Fe-Mn-N-Ni	XIX-265
Cr-Fe-Mn-Nb-Ni-Si-V	VIII-227
Cr-Fe-Mn-Ni	II-96, V-164
Cr-Fe-Mo	III-103, VIII-178, X-160
Cr-Fe-Mo-Ni	XV-251
Cr-Fe-Mo-V	XVIII-254
Cr-Fe-N	IV-94, IX-137, XI-139, XIII-141
Cr-Fe-Nb-Ni	XVIII-248
Cr-Fe-Ni	III-100, VI-133, VII-199, IX-204, XII-207, XVII-290, XVIII-193, XIX-180
Cr-Fe-Ni-Si	XVIII-259
Cr-Fe-Ni-Ti	V-165, XII-259, XVIII-260
Cr-Fe-Ni-W	XV-246
Cr-Fe-O	I-106, XIV-177, XVI-216
Cr-Fe-O-S	XI-262
Cr-Fe-P	XI-216
Cr-Fe-S	IX-206
Cr-Fe-Si	VII-197, VIII-177, XII-206
Cr-Fe-Ti	VI-136, X-163, XI-215
Cr-Fe-V	III-91, XVI-167, XIX-181
Cr-Fe-W	X-142
Cr-Fe-Zr	VIII-182, IX-210, XVI-234, XVIII-195
Cr-Ga	XI-50, XVIII-38
Cr-Gd	X-28
Cr-Ge	XII-66, XIII-59, XIV-44, XVIII-37
Cr-Hf	XI-53, XIV-39, XIX-28
Cr-Hg	IX-122
Cr-Ho	XVIII-38

<u>System</u>	<u>Location</u>
Cr-Ir	XIX-29
Cr-La	VI-58, XIX-30
Cr-Mn	XII-100
Cr-Mn-N	XIV-106
Cr-Mn-Ni	VIII-203
Cr-Mn-Si	XVII-320
Cr-Mn-Zr	XIX-182
Cr-Mo	IX-94, X-83, XII-104, XVII-134
Cr-Mo-Nb	VI-154, VII-217, VIII-208, X-183, XI-240, XV-214
Cr-Mo-Nb-W	XII-256
Cr-Mo-Ni	VIII-207, XIX-182
Cr-Mo-Si	X-182, XII-224
Cr-Mo-Ti	VI-155, VIII-209, XII-231
Cr-Mo-Ti-V	XIV-262
Cr-Mo-U	IV-159, VII-220
Cr-Mo-W	IV-123, V-129, VII-186, VIII-168
Cr-Mo-Zr	XVI-275, XVII-359, XIX-183
Cr-N	III-5, XVII-15, XVIII-38
Cr-N-Pu	XVIII-196
Cr-N-U	XVII-174
Cr-Nb	II-44, IV-80, VII-106, VIII-103, X-94
Cr-Nb-Ni	VI-157, VII-223, VIII-211, XII-234
Cr-Nb-Si	VII-210
Cr-Nb-Ta-Ti	XII-261
Cr-Nb-Ta-Ti-Zr	XV-259, XVII-414
Cr-Nb-Ti	VIII-214, IX-243, X-194, XI-248
Cr-Nb-Ti-Zr	XV-254
Cr-Nb-U	IX-247
Cr-Nb-V	IV-119, V-123
Cr-Nb-Zr	XI-250, XIV-241, XV-222
Cr-Nd	XV-67, XVI-86
Cr-Ni	I-65, III-61, VI-72, VII-93, VIII-99, XVI-89, XVIII-39
Cr-Ni-S	XIX-184
Cr-Ni-Si	VI-147, IX-222
Cr-Ni-Ti	II-92
Cr-Ni-W	III-99

<u>Page</u>	<u>System</u>
3	N-Nb
4	N-Ta
5	Al-B
7	Al-Fe
8	Al-Y
9	Al-Cu
10	Al-Nb
12	Al-Re
13	Al-Ti
14	Al-Th
15	Al-U
16	Al-Ce
17	Al-Zn
18	B-Be
19	B-La
20	B-Ta
21	B-C
22	V-W
23	Hf-V
24	V-Y
25	Sn-V
26	Re-V
27	Th-V
28	Bi-Cu
29	Bi-U
30	Os-W
31	Pd-W
32	Cr-W
33	Fe-Gd
34	Gd-Mg
35	Gd-Zr
36	Ga-K
37	Ga-Na
38	Ga-Hg
40	Ga-Te
41	Fe-Hf
42	Hf-Mo
43	Hf-Ni
44	Fe-Ge
45	Ge-Mn
46	Fe-Y
47	Fe-O
48	Fe-Si
50	Fe-Mo

<u>Page</u>	<u>System</u>
51	Fe-Ni
52	Fe-Nb
53	Fe-S
54	Fe-Te
55	C-Fe
56	Fe-Zn
57	Au-K
58	Au-Li
59	Au-Na
60	Au-Rb
61	Au-Se
62	Au-S
63	Au-Cs
64	Hg-In
65	Mg-Y
66	Cu-Y
67	Nd-Y
68	Ni-Y
69	Ti-Y
70	Cr-Y
71	Cd-Sb
72	O-Pu
73	O-Zr
75	Co-S
76	Co-Cr
78	Mn-Si
80	Nb-Si
81	Si-Th
82	Mn-Re
83	Cu-Nb
84	Cu-Pu
85	Mo-U
87	Ag-Na
88	Np-Pu
90	Ni-Ru
91	Ni-Se
92	Ni-S
93	Cr-Ni
95	Ni-Zr
96	Nb-Pd
97	Nb-Pt
98	Nb-Re
101	Nb-Ti
102	C-Nb

<u>Page</u>	<u>System</u>
104	Nb-U
106	Cr-Nb
108	Nb-Zr
109	Hg-Sn
110	S-Sn
111	Sn-Tl
112	Pb-Te
113	Pu-Ru
114	C-Pu
115	Re-Th
116	Cr-Ru
117	Sc-Ti
118	Tl-Zn
119	Ta-Th
120	Cr-Ta
122	C-Ti
123	Ti-U
124	Ti-Zr
125	Ce-Th
126	Th-Zr
129	C-U
130	U-Zr
131	B-Hf-N
132	B-N-Ti
133	B-N-Zr
134	Fe-N-Si
135	Fe-Mn-N
136	Fe-N-Zn
137	Al-Si-V
138	Al-Cu-V
139	Al-Nb-V
140	Al-Si-W
141	Al-Ga-Mg
142	Al-Fe-Si
143	Al-Mo-Si
144	Al-Nb-Si
145	Al-Si-Ta
146	Al-Si-U
147	Al-Cr-Si
148	Al-Cu-Li
149	Al-Mg-Zn
151	Ag-Al-Cu
152	Al-Ce-Cu
153	Al-Cr-Ni

<u>System</u>	<u>Location</u>
Cr-O	III-41
Cr-Os	III-66
Cr-Pd	XIII-111
Cr-Pr	XV-79, XVI-97
Cr-Pt	XIX-31
Cr-Pu	I-71
Cr-Re	V-92
Cr-Rh	XIX-32
Cr-Ru	VII-116, X-105
Cr-Sc	XVIII-40
Cr-Si	III-44, IX-82, X-73, XIV-75
Cr-Si-Ti	XVII-325
Cr-Si-W	VIII-166
Cr-Si-Y	XVII-305
Cr-Sm	XIX-33
Cr-Sn	X-98, XV-74
Cr-Sn-Zr	IV-169, IX-249
Cr-Ta	V-101, VII-120, XIX-33
Cr-Ta-Ti	XII-245, XV-227, XVI-293
Cr-Ta-Zr	XII-247, XIII-257, XV-229
Cr-Tb	XVII-166
Cr-Ti	III-70, IV-90, VIII-121, IX-130, XVII-167
Cr-Ti-V	VIII-155, XI-186, XII-172, XIII-175
Cr-Ti-W	IV-125
Cr-Ti-Zr	XI-256, XIII-259, XV-230
Cr-U	I-75, IX-132
Cr-V	V-24, VI-25
Cr-V-Zr	XVI-173, XVIII-196, XIX-186
Cr-W	VII-32
Cr-W-Zr	XIX-187
Cr-Y	VII-70, XIX-34
Cr-Yb	XIX-35
Cr-Zr	IX-134, XIV-104, XVII-171, XIX-36
Cs-Ga	XIX-36
Cs-Mg	XIII-98
Cs-Na	XVII-135

<u>System</u>	<u>Location</u>
Cu-Er	XVI-81
Cu-Fe	IV-43, VI-40, XII-69, XIII-69, XVIII-41
Cu-Fe-Mn-Ni	II-95
Cu-Fe-Ni	XVII-289
Cu-Fe-P	XIII-201
Cu-Fe-P-Zn	XIV-264
Cu-Fe-Pd	IX-201
Cu-Fe-Ti	XVI-219
Cu-Ga	XI-44
Cu-Ga-Ge	I-100
Cu-Ga-Ge-Se	XVI-302
Cu-Ga-Te	XIX-187
Cu-Ge	III-29, XII-63
Cu-Ge-Ni	V-134
Cu-Ge-Sb	VII-191
Cu-Ge-Sn	XII-199
Cu-Ge-Te	XIX-188
Cu-H	XVII-48
Cu-Hf	XII-59
Cu-Hg	IX-89, XVII-131
Cu-Ho	IX-46
Cu-In	XVIII-41
Cu-In-Sb	XVII-298
Cu-In-Se	XIII-208
Cu-In-Sn	XVIII-197
Cu-In-Te	XIII-209
Cu-Ir	XV-46
Cu-Li	IV-67
Cu-Mg	III-50
Cu-Mg-Ni	II-82, XVIII-204
Cu-Mg-Sb	V-154
Cu-Mg-Sn	II-83, IX-226
Cu-Mg-Ti	XII-227
Cu-Mg-Zn	I-122, II-84, VI-150
Cu-Mn	VIII-87, XVII-124
Cu-Mn-Ni	IV-154
Cu-Mn-Si	IV-149, VIII-200
Cu-Mn-Sn	XIX-189
Cu-Mn-Zr	XVIII-206

<u>System</u>	<u>Location</u>
Cu-Mo-Nb	XVI-258
Cu-Mo-Ni	XIX-189
Cu-Mo-Zr	XIV-219, XVII-335
Cu-Nb	VII-83, XV-59, XVI-79
Cu-Nb-Ta	XIV-223
Cu-Nb-W	XV-172, XVI-191
Cu-Nb-Zr	XIV-224, XVIII-207
Cu-Ni	IV-71, XVII-126, XVIII-42
Cu-Ni-P	XVII-344
Cu-Ni-Pb	III-116
Cu-Ni-Pd	XI-236, XVII-340
Cu-Ni-S	VI-151
Cu-Ni-Si	III-112, IV-150, XVII-324, XVIII-207, XIX-191
Cu-Ni-Sn	XVII-337
Cu-Ni-Ta	XI-237
Cu-Ni-Ti	XIII-232, XIV-220, XVII-342
Cu-Ni-W	XVI-190
Cu-Ni-Zr	XIV-221
Cu-O	XII-88, XIV-68
Cu-O-Pt	XV-196
Cu-O-Sn	XII-217
Cu-P	XVIII-43
Cu-Pb	I-57, II-40, XVIII-44
Cu-Pb-Te	II-86
Cu-Pu	VII-84, XIII-100
Cu-Rh	XVII-130
Cu-S	VI-64
Cu-Sb	IV-72
Cu-Se-Sn	XIX-192
Cu-Si-Ti	XV-202
Cu-Si-Zn	III-113, V-152, IX-220, X-180
Cu-Si-Zr	XI-233
Cu-Sn	XVI-80, XVII-129
Cu-Sn-Zr	XIV-225
Cu-Sr	XVII-132
Cu-Te	II-41, XIX-37
Cu-Te-Tl	XVII-349
Cu-Th	XVII-133

<u>System</u>	<u>Location</u>
Cu-Ti	IV-73, VI-65, VIII-91, IX-90, XII-101
Cu-Ti-Zn	VIII-206
Cu-Ti-Zr	VII-212
Cu-Tl	I-59, XV-61
Cu-V	VIII-17, X-20, XIII-35
Cu-Y	VII-66
Cu-Yb	XVI-57, XVII-102
Cu-Zn	III-55, VIII-92, XV-63
Cu-Zr	VIII-93, X-78, XVIII-44
D-Lu	XVIII-60
D-Nb	XVIII-60
D-Ni	XVIII-61
D-Pd	XVIII-62
D-Ta	XVIII-63
D-V	XVIII-63, XIX-38
D-Zr	IX-48
Dy-Er	XIX-38
Dy-Hg	XII-51
Dy-Ho	XVI-34, XIX-39
Dy-Ho-Y	XVI-211
Dy-Mg	XI-59
Dy-Mn	XIII-64
Dy-Nd	XVIII-45
Dy-Pb	XIV-45
Dy-Pd	XIX-40
Dy-Sb	XIII-65
Dy-Th	XV-34
Dy-Y	XIII-63
Er-Fe	XVII-90
Er-Gd	X-30
Er-Hf	XVII-73
Er-Hg	XII-51
Er-Ho	XIX-41
Er-Mn	XIII-99
Er-Nd	XVIII-46
Er-Pd	XIX-42
Er-Pt	XVII-154
Er-Rh	XIX-43

<u>System</u>	<u>Location</u>
Er-Sc	X-107
Er-Tb	XIX-44
Er-Th	XV-89
Er-Y	X-60, XIX-45
Eu-In	XI-60
Eu-Mg	XV-36
Eu-Pb	XIII-66
Eu-Te	XVI-37
Fe-Ga	XI-41, XIII-48
Fe-Ga-N	VIII-124
Fe-Gd	VII-33
Fe-Ge	VII-44, X-41, XI-54, XVIII-47
Fe-Ge-Ni	XIX-196
Fe-Ge-S	XV-177
Fe-H	XVII-46
Fe-Hf	VII-41, XII-57, XIV-34, XIX-45
Fe-Hf-Zr	XVIII-209
Fe-Ho	XVI-35
Fe-In	XIII-67, XV-37, XVI-38
Fe-Ir	IX-50, X-42
Fe-Ir-Rh	XIII-197
Fe-La-N	XIX-196
Fe-La-Si	XVIII-209
Fe-Lu	XVIII-48
Fe-Mg	XII-68
Fe-Mg-Ni-O	XVI-303
Fe-Mn	VIII-52, X-44
Fe-Mn-N	VII-135
Fe-Mn-Ni-Zn	VII-254
Fe-Mn-O	XV-181, XVI-213
Fe-Mn-O-S	XVIII-260
Fe-Mn-S	IX-199, XVII-286
Fe-Mn-Si	IV-132
Fe-Mn-Si-V	XII-255
Fe-Mn-Sn	XIV-184
Fe-Mn-Ti	IV-133, XV-189
Fe-Mn-U	IX-200, X-159, XIV-185, XIX-197
Fe-Mn-Zr	XVIII-210

<u>System</u>	<u>Location</u>
Fe-Mo	VII-50, XII-70, XIII-70, XVI-42, XIX-46
Fe-Mo-P	XI-211
Fe-Mo-S	IX-203
Fe-Mo-Si	VII-196, XII-202
Fe-Mo-W	XIX-199
Fe-Mo-Zr	XIV-188
Fe-N	I-5, II-3, XIV-5, XVIII-49, XIX-47
Fe-N-Nb	VIII-125, XIX-200
Fe-N-Si	II-54, III-79, VII-134, XVI-111
Fe-N-U	IX-136
Fe-N-V	XIX-200
Fe-N-Zn	VII-136
Fe-Nb	III-33, VI-41, VII-52, XII-71, XIII-71, XVI-43
Fe-Nb-P	VIII-179, XI-213
Fe-Nb-S	IX-205
Fe-Nb-Si	VI-129, XVIII-211
Fe-Nb-Zr	XIV-190
Fe-Nd	XI-64
Fe-Ni	II-26, III-32, VII-51, XI-65
Fe-Ni-O	I-105, XVI-215, XVII-278
Fe-Ni-P	XVI-226
Fe-Ni-P-S	IX-265
Fe-Ni-Pb	VI-132
Fe-Ni-Pd	VI-131
Fe-Ni-Re	XVI-224
Fe-Ni-S	I-107, III-106, VII-198
Fe-Ni-Sb	XIX-201
Fe-Ni-Si	VI-128, XI-208, XIV-178
Fe-Ni-Sn	XIX-202
Fe-Ni-Ti	XIII-203
Fe-Ni-U	I-108
Fe-Ni-W	III-98, XV-169
Fe-Ni-Zn	IV-136
Fe-Ni-Zr	XIV-189, XIX-202
Fe-O	IV-42, VI-38, VII-47, XIV-46, XVI-39
Fe-O-S	XI-205
Fe-O-Ti	II-65
Fe-O-V	IX-172
Fe-O-Zr	VII-193
Fe-Os	IX-52

<u>System</u>	<u>Location</u>
Fe-P	IV-50, IX-58
Fe-P-S	XIV-193
Fe-P-Si	V-139
Fe-P-Sn	I-109
Fe-P-Ti	V-140, XI-214
Fe-P-V	I-97, XI-180
Fe-P-W	I-99
Fe-P-Zr	IV-138, XI-217
Fe-Pb-Te	XV-192
Fe-Pd	IV-45, V-38, IX-53
Fe-Pt	V-39
Fe-Pu	I-31, III-34
Fe-Rh	IV-46, XIII-73, XVII-85
Fe-Ru	IV-47, VI-42
Fe-S	VII-53, XIV-54, XVII-87, XVIII-50
Fe-S-Sb	VI-135
Fe-S-Si	XIII-198, XIV-180
Fe-S-Ti	IX-208
Fe-S-V	IX-173
Fe-S-W	VII-184
Fe-S-Zr	IX-207
Fe-Sb	XIX-48
Fe-Sb-Si	III-102
Fe-Sc	VIII-53, XV-38
Fe-Se	XIV-53
Fe-Si	II-24, VI-39, VII-48, VIII-50, IX-51, X-43, XI-63, XIII-68, XIV-49, XVI-41
Fe-Si-Sn	VI-130
Fe-Si-Ti	II-69, XII-203
Fe-Si-U	XIX-204
Fe-Si-V	XI-179, XII-164
Fe-Si-W	X-141
Fe-Si-Zn	XIV-182, XV-186
Fe-Sm	XVII-86
Fe-Sn	X-45, XIII-72, XIV-52, XVII-84, XVIII-51
Fe-Sn-Zr	XIV-191

<u>System</u>	<u>Location</u>
Fe-Ta	V-40, XII-73, XIII-74, XVI-44
Fe-Tc	IX-54
Fe-Te	I-32, VII-54
Fe-Th	XII-75
Fe-Ti	II-27, III-35, VIII-54, IX-55, XII-74
Fe-Ti-V	V-121, VI-120, VII-167
Fe-Ti-Zr	XVII-293
Fe-Tm	XVIII-52
Fe-U	IV-49, IX-57, XII-79
Fe-V	XI-28, XVI-16, XIX-49
Fe-V-Zr	XVIII-211
Fe-W	XII-48, XIII-43, XVI-26, XIX-49
Fe-Y	VII-46
Fe-Zn	VII-56, X-49, XVIII-53, XIX-51
Fe-Zr	VI-46, VIII-56, IX-59, XII-80, XVI-49, XIX-52
Ps-Pu-U	XI-251, XII-241
Ga-Ge	I-24, III-25, IV-31, XVII-59
Ga-Ge-Nb	XVIII-212
Ga-Ge-Ni	XIX-204
Ga-Ge-P	IX-188
Ga-Ge-Si-V	XVIII-261
Ga-Ge-Sn	XIX-205
Ga-Ge-Ti	XI-195
Ga-Ge-Zr	XI-196
Ga-Hf	VIII-39
Ga-Hg	VI-35, VII-38
Ga-In	IX-35, XII-53, XV-26, XVIII-54, XIX-53
Ga-In-P	XVI-201, XVII-264, XVIII-213
Ga-In-S	XV-174
Ga-In-Sb	I-102, IV-126, V-130, VIII-172, XVIII-214
Ga-In-Se	XVI-200
Ga-In-Sn	XVI-199
Ga-In-Te	IV-127, V-131

<u>System</u>	<u>Location</u>
Ga-K	VII-36, XIX-54
Ga-La-V	XIV-155
Ga-Li	XIX-54
Ga-Mn	XI-43
Ga-Mo	XIX-55
Ga-Na	II-21, VI-34, VII-37
Ga-Nb	X-31, XI-45, XIV-31, XVIII-54
Ga-Ni	III-26
Ga-O-V	XII-163
Ga-P	X-34
Ga-P-Zn	XII-192
Ga-Pb	IV-34, V-33
Ga-Pd-Zn	XIX-206
Ga-Pt	XIV-33
Ga-Pr-V	XVII-247
Ga-Pu	X-33, XI-47, XIII-49, XVII-61
Ga-Rb	XIX-56
Ga-S	XIII-52
Ga-S-Te	XI-199
Ga-Sb	I-26, IV-35
Ga-Sb-Te	XII-191
Ga-Se	XI-48, XII-55
Ga-Si	IV-33, XVII-60
Ga-Sn	VIII-40, IX-36, X-32, XIV-32
Ga-Sn-Te	XIII-189
Ga-Sr	XII-56
Ga-Ta	XI-49
Ga-Te	VII-40, IX-37
Ga-Ti	III-27, IV-36, VIII-41
Ga-Ti-Zn	XI-200
Ga-Tl	I-28, V-35
Ga-V	X-18, XI-27, XII-26, XIII-32, XIV-20
Ga-V-Y	XVII-245
Ga-Zn	IV-37, IX-38, XI-51
Ga-Zn-Zr	XI-201
Ga-Zr	IV-38, VIII-42, XVI-29
Gd-Hg	XII-51
Gd-La	VIII-37
Gd-Mg	VII-34, XI-40
Gd-Mn	XIII-45

<u>System</u>	<u>Location</u>
Gd-Mo	XII-50
Gd-Pb	XV-24
Gd-Pd	XIX-57
Gd-Pu	XIII-46
Gd-Sb	XIII-47
Gd-Sc	X-26
Gd-Sm	XIV-30
Gd-Tb	X-27
Gd-Th	XV-25
Gd-Ti	VIII-38
Gd-Y	VIII-35
Gd-Zr	VII-35
Ge-In	XVII-74
Ge-In-P	IX-194
Ge-In-Sb	V-133
Ge-In-Te	XI-203, XIX-207
Ge-La	XVII-76, XIX-57
Ge-Li	III-28, XII-62
Ge-Mg	XIV-41
Ge-Mg-Pb	XII-198
Ge-Mg-Sn	XII-197
Ge-Mn	VII-45, XV-32, XVI-30
Ge-Mn-Te	VII-190
Ge-Mo	IX-41
Ge-Mo-W	IX-183
Ge-Nb	XIII-57
Ge-Nb-Ti	XIX-209
Ge-Ni	XVII-77
Ge-O	I-29
Ge-P	VIII-49
Ge-Pb-Se	XII-200
Ge-Pb-Te	X-156, XVIII-215
Ge-Pd-Te	XVII-277
Ge-Pr	XIX-60
Ge-Pt	XII-65
Ge-Rh	II-22
Ge-Ru	VIII-47

<u>System</u>	<u>Location</u>
Ge-S	IX-42
Ge-Sb	XVII-79
Ge-Sb-Si	XVIII-215
Ge-Sb-Sn	XVI-208, XIX-210
Ge-Sb-Te	XI-204, XVI-209
Ge-Se	VIII-48, XIV-42
Ge-Se-Te	XII-201
Ge-Si-Te	X-155
Ge-Si-Th	IX-195
Ge-Si-V	XI-178
Ge-Si-W	VII-183
Ge-Sn-Te	IV-129
Ge-Sr	XVI-33
Ge-Te	VI-36, XI-56, XV-33
Ge-Th	IX-43
Ge-Ti	I-30, IV-4.1
Ge-Tl	IV-40
Ge-U	VI-37
Ge-V	IV-13
Ge-W	XVII-57
Ge-Y	XVIII-55
Ge-Zr	II-23
H-Hf	VI-30, VIII-28
H-Hf-Zr	XI-189
H-Ir	XIX-61
H-La-Ni	XVIII-216
H-Mo	XVIII-56
H-Mo-Ni	XV-168
H-N-V	XIX-212
H-Nb	IV-22, VI-31, XI-35, XII-43, XV-19, XVIII-57
H-Nb-Ti	VIII-162
H-Nb-Zr	XII-180, XVIII-217
H-Nd	XVII-49
H-Ni	XVII-50, XIX-62
H-Ni-W	XV-166
H-Ni-Zr	IV-122

<u>System</u>	<u>Location</u>
H-O-Ti	VIII-161, XII-179, XIX-212
H-O-V	XIX-213
H-O-Zr	I-98, VII-181, IX-182
H-Pd	XVII-51
H-Rh	XIX-63
H-Ru	XIX-63
H-Sc	XI-36
H-Ta	II-18, VIII-29, XV-20
H-Th	XVII-54
H-Ti	II-19, IV-23, XII-44, XVII-53
H-Ti-Zr	VIII-163
H-U	IV-24, XIII-41, XIV-27
H-U-Zr	V-128, VII-182
H-V	X-17, XII-25, XIX-64
H-Y-Zr	XVIII-219
H-Zr	I-22, II-20, III-23, IV-25, V-29, VI-32, VIII-30, XII-46, XIII-42, XIV-28, XV-21, XVII-55, XVIII-59
Hf-Mn	XIV-36, XV-29
Hf-Mo	VII-42, XIII-53, XVIII-64, XIX-65
Hf-Mo-Nb	XVI-205
Hf-Mo-Re	IX-189, XVI-206
Hf-Mo-Si	XVII-270
Hf-Mo-W	XIII-181
Hf-N-Nb	XIII-139
Hf-N-V	XIX-214
Hf-Nb	X-36, XV-30, XVII-67, XIX-66
Hf-Nb-O	XIII-190, XVI-204, XVII-268
Hf-Nb-Ru	XIX-215
Hf-Nb-Sn	IX-190
Hf-Nb-Ti	XIX-215
Hf-Nb-Ti-Zr	XV-249, XVII-398
Hf-Nb-Zr	XIII-193
Hf-Ni	VII-43, XIII-54, XIV-37, XIX-67
Hf-Ni-O	XVI-203
Hf-O	IX-39, XII-58

SystemLocation

Hf-Pd	XVIII-65
Hf-Pr	XVII-69
Hf-Pu	XIII-55, XIV-38
Hf-Re	VIII-45, IX-40, XV-31
Hf-Re-W	XII-181
Hf-Ru-Ti	XVIII-219
Hf-Ru-V	XIX-217
Hf-Sc	XIII-56
Hf-Si	XVII-66
Hf-Sn	XVII-68
Hf-Ta	X-39
Hf-Th	IV-39
Hf-Ti	V-36
Hf-Ta-V	XVI-165
Hf-U	XVII-70
Hf-V	VII-23, XIV-21, XIX-67
Hf-W	VI-33, VIII-33, XVIII-66
Hf-Y	VIII-44
Hf-Zr	XII-60, XVII-72
Hg-In	VII-64, VIII-62, IX-61, XVI-52
Hg-La	XII-51
Hg-Mn	IX-87
Hg-Mn-Te	IX-229
Hg-Ni	IX-97
Hg-Pb	XIII-128
Hg-Pb-Se	XIV-249
Hg-Pb-Sn	XVII-375
Hg-Pb-Te	XIV-250
Hg-Pb-Tl	XVI-288, XIX-217
Hg-Pd	XI-120
Hg-Pr	XII-51, XVII-157
Hg-Pt	XIX-68
Hg-Pu	V-88
Hg-Rh	XIII-126
Hg-Sb	VIII-117, IX-118
Hg-Se-Te	VI-163
Hg-Se-Tl	XVII-383
Hg-Sm	XII-51
Hg-Sn	VII-109, IX-103, X-95, XIII-109, XV-72

<u>System</u>	<u>Location</u>
Hg-Tb	XIV-100
Hg-Te	XVI-100
Hg-Th	IX-120
Hg-Ti	IX-119, XIX-69
Hg-Tl	XIX-69
Hg-U	IX-121
Hg-Y	XII-51
Hg-Yb	XIV-61
Ho-Mn	XIII-61
Ho-Pd	XIX-70
Ho-Tb	XIX-71
Ho-Th	XIII-62
Ho-Y	XIII-60
I-In	II-31
I-Pb-Se	XII-215
I-Pb-Te	XIII-218, XVI-239
I-Sb-Se	XVIII-221
I-Tl	XVII-104
In-Li	XV-41
In-Mg	XIV-58, XV-42
In-Na	XV-43
In-Ni	XV-44, XIX-72
In-P	III-38, IV-59, XVI-54
In-Pb	IV-57, XV-45
In-Pb-Sb	VIII-187, IX-212
In-Pb-Sb-Sn	XVII-404
In-Pb-Se	XI-220
In-Pb-Sn	I-114
In-Pb-Te	X-168
In-Pb-Tl	IV-145
In-Pd	V-50
In-Pd-Sn	XVIII-221
In-Pr-Se-Te	XI-264
In-Pt	XIX-73
In-Pu	XI-74, XIII-78
In-S	XVIII-66
In-S-Se	XIX-219
In-S-Te	XVII-299

<u>System</u>	<u>Location</u>
In-Sb	IX-65
In-Sb-Se	XII-211, XIII-215, XVI-238
In-Sb-Se-Te	XVIII-262
In-Sb-Sn	I-115, V-142, VIII-186, XII-210, XIV-195
In-Sb-Te	VI-140, X-169, XII-212, XIII-217, XIV-196, XVII-302
In-Sb-Zn	X-170
In-Se	IX-62
In-Se-Sn	XIX-220
In-Se-Te	XI-221
In-Sn	II-32, III-37, X-53
In-Sn-Te	X-167, XVIII-223
In-Sr	XII-81
In-Ta	IX-67
In-Te	X-54
In-Te-Zn	XI-222, XVII-303
In-Th	V-51
In-Ti	IV-58, VIII-65, XVIII-67
In-Tl	IX-66, XII-82
In-V	XVI-17
In-Yb	XVII-97
In-Zr	IV-60
Ir-Mn	I-39
Ir-Mo	XII-83
Ir-Nb	X-55
Ir-Ni-Ta	XIX-221
Ir-O-Zr	VII-204
Ir-Os	X-56
Ir-Pd	III-39, VIII-66
Ir-Pr	XVII-99
Ir-Pt	II-33
Ir-Re	VIII-67
Ir-Re-W	XVI-183
Ir-Ru	X-57, XIX-74
Ir-Th	X-58
Ir-Ti	XI-75, XVI-55
Ir-U	XIV-59
Ir-V	XIII-33
Ir-W	IX-31

<u>System</u>	<u>Location</u>
K-Mg	XIII-85
K-Na	I-40
K-Pb	V-53
K-Yb	XIV-60
La-Mg	XI-95, XVIII-68
La-Nb	V-63
La-Ni	XVIII-68
La-Ni-Re	XVI-256, XVIII-224
La-Pu	XIII-94
La-Re	XIV-76
La-Rh	XV-54
La-Sc	XVI-72
La-Th	XIV-77
La-Ti	III-45
La-V	VI-22, XIII-34
La-Y	VIII-68
Li-Mg-Sn	XV-206, XVII-326, XVIII-224
Li-Mg-Zn	II-81, IV-151, VI-148
Li-Mg-Zr	IX-225
Li-Mn	X-74, XI-96
Li-Mn-Si	XI-230
Li-N	V-5
Li-Na	III-47
Li-Ni	V-64, XI-97
Li-Si	I-50, III-46, V-59, VIII-78, X-68, XI-89
Li-Sr	VIII-83
Li-Ti	IX-83
Li-U	V-65
Li-Zr	V-66
Lu-Mg	XI-98
Lu-Th	XV-55
Mg-Mn	III-49
Mg-Mn-Nd	VIII-202
Mg-Mn-Nd-Ni	XIV-267
Mg-Mn-Ni	XIV-217
Mg-Mn-Th	V-153, VI-149
Mg-Mn-Y	XIV-197, XVI-240
Mg-Mn-Zr	XIII-230

<u>System</u>	<u>Location</u>
Mg-Na	XIII-96
Mg-Nb	IX-85
Mg-Nd	IV-68, VIII-84, IX-84, XI-99
Mg-Nd-Ni	XII-228
Mg-Nd-Pr	XVIII-226
Mg-Nd-Y	XVII-306
Mg-Nd-Y-Zn	XVIII-263, XIX-255
Mg-Nd-Zn	XVII-328
Mg-Pb	XI-101, XVI-74, XVII-122
Mg-Pb-Si	XI-231, XIV-210
Mg-Pd	VIII-85
Mg-Pr	XI-100, XVII-121
Mg-Rb	XIII-97
Mg-Sb-Si	IX-219, XIV-211
Mg-Sb-Sn	IX-228
Mg-Sc	XVIII-69
Mg-Si	XIV-73
Mg-Si-Sn	XII-223
Mg-Sn	XV-56, XIX-74
Mg-Th	IV-69, VI-59
Mg-Th-Zr	IV-152
Mg-Ti	I-52, V-67, XIV-78
Mg-U	II-38
Mg-V	IX-24
Mg-Y	VI-50, VII-65, XI-78, XIV-63
Mg-Y-Zn	XIV-198
Mg-Yb	XI-76
Mg-Zn	III-51
Mg-Zr	X-75
Mn-N	VIII-5, XIII-5
Mn-Nb	VI-60
Mn-Nd	XVI-75
Mn-Ni	XV-57
Mn-Ni-Pd	IV-155
Mn-Ni-Si	VIII-201, X-179
Mn-Ni-Sn	XI-235
Mn-Ni-U	I-123
Mn-Ni-V	XIII-173

<u>System</u>	<u>Location</u>
Mg-Na	XIII-96
Mg-Nb	IX-85
Mg-Nd	IV-68, VIII-84, IX-84, XI-99
Mg-Nd-Ni	XII-228
Mg-Nd-Pr	XVIII-226
Mg-Nd-Y	XVII-306
Mg-Nd-Y-Zn	XVIII-263, XIX-255
Mg-Nd-Zn	XVII-328
Mg-Pb	XI-101, XVI-74, XVII-122
Mg-Pb-Si	XI-231, XIV-210
Mg-Pd	VIII-85
Mg-Pr	XI-100, XVII-121
Mg-Rb	XIII-97
Mg-Sb-Si	IX-219, XIV-211
Mg-Sb-Sn	IX-228
Mg-Sc	XVIII-69
Mg-Si	XIV-73
Mg-Si-Sn	XII-223
Mg-Sn	XV-56, XIX-74
Mg-Th	IV-69, VI-59
Mg-Th-Zr	IV-152
Mg-Ti	I-52, V-67, XIV-78
Mg-U	II-38
Mg-V	IX-24
Mg-Y	VI-50, VII-65, XI-78, XIV-63
Mg-Y-Zn	XIV-198
Mg-Yb	XI-76
Mg-Zn	III-51
Mg-Zr	X-75
Mn-N	VIII-5, XIII-5
Mn-Nb	VI-60
Mn-Nd	XVI-75
Mn-Ni	XV-57
Mn-Ni-Pd	IV-155
Mn-Ni-Si	VIII-201, X-179
Mn-Ni-Sn	XI-235
Mn-Ni-U	I-123
Mn-Ni-V	XIII-173

<u>System</u>	<u>Location</u>
Mo-Nb-U	IV-157, VII-214, IX-231, XIX-222
Mo-Nb-U-Zr	IV-180, VII-255, IX-268, XVII-407
Mo-Nb-V	VI-121
Mo-Nb-W	VIII-167
Mo-Nb-W-Zr	X-216
Mo-Nb-Zr	IX-233, X-184, XIV-227
Mo-Ni	X-79, XIX-76
Mo-Ni-Re	XVIII-227
Mo-Ni-Si	VI-146, XIII-225, XIV-212, XV-203
Mo-Ni-Ta	XV-211
Mo-Ni-Ti	VI-153, XVIII-228
Mo-Ni-W	XIX-222
Mo-Ni-Zr	XIV-226, XV-213, XIX-223
Mo-O	XI-84
Mo-Os	VIII-95
Mo-Os-W	XI-191
Mo-Pd	V-68, X-80
Mo-Pt	IV-75, V-69, XIV-81, XIX-76
Mo-Pt-Re	XVI-264
Mo-Re	III-57, IV-76, V-70, XV-64
Mo-Re-W	VI-126, XIV-172
Mo-Re-Zr	XVI-265
Mo-Rh	V-73, VI-66
Mo-Ru	VI-67
Mo-Si	XIV-74, XVII-117
Mo-Si-Ti	XVIII-229
Mo-Si-V	VIII-153
Mo-Si-W	VIII-164
Mo-Sn-Zr	IV-158, V-156
Mo-Ta-Ti-V	XIX-259
Mo-Ta-V	XI-182
Mo-Ta-W	XVII-257
Mo-Ta-Zr	XIV-230
Mo-Tc	IX-91
Mo-Th	VIII-96
Mo-Th-Zr	X-187
Mo-Ti	IX-92
Mo-Ti-V	II-60, VI-122, VII-172
Mo-Ti-W	XII-182
Mo-Ti-Zr	VIII-210, XIII-238, XIV-232

<u>System</u>	<u>Location</u>
Mo-U	III-58, IV-77, VI-68, VII-85, IX-93, X-82, XVI-83, XVIII-71
Mo-U-V	VIII-154
Mo-U-Zr	IV-160, VI-156, VII-221
Mo-V	IV-14
Mo-V-Zr	XIV-160, XIX-224
Mo-W-Zr	X-144, XI-192, XII-183
Mo-Zr	XIII-103, XVI-84, XVIII-71
N-Nb	VI-5, VII-3, IX-5, X-5
N-Nb-O	VI-91
N-Nb-W	XIII-138
N-Ni-U	IX-138
N-O-Th	XVIII-232
N-O-U	XVI-112
N-Pr-V	XIX-227
N-Pu-U	XIX-228
N-Re	XVII-14, XVIII-72
N-Sc-V	XIX-229
N-Ta	VII-4, XIX-77
N-Ti-V	XIX-229
N-U	XIV-6
N-V	XV-5, XVII-5
N-V-Y	XIX-230
N-V-Zr	XIX-231
N-W	XV-6, XVII-8
N-Y	XIX-78
Na-O	XVII-108
Na-O-V	XVII-249
Na-Pb	I-60
Na-Pb-Te	XVII-366
Na-Sr	III-59
Na-Zn	XIV-87
Nb-Ni	X-84, XII-107, XVIII-73
Nb-Ni-Si	XIV-213, XV-204
Nb-Ni-Sn	XVII-368
Nb-Ni-Ta	II-90
Nb-Ni-Ta-Ti	VII-256
Nb-Ni-Ti	IV-161, XII-233
Nb-Ni-W	XVI-192, XVIII-234
Nb-Ni-Zr	XIV-235, XVI-283

<u>System</u>	<u>Location</u>
Nb-O	VIII-76, IX-74, X-63, XII-89, XIII-86, , XVIII-73
Nb-O-Re	VIII-194
Nb-O-Ru	VIII-195
Nb-O-S	XIX-232
Nb-O-Sn-Zr	XIX-261
Nb-O-Ti	VIII-196, XIX-232
Nb-O-W	XIII-182
Nb-O-Zr	XII-218, XVI-250, XVII-310
Nb-Pd	VII-96
Nb-Pt	VII-97
Nb-Re	V-77, VII-98, XV-69
Nb-Re-Ta	XIX-233
Nb-Re-W	XIV-173
Nb-Rh	X-92
Nb-Ru	IX-102, X-93, XI-116
Nb-Ru-Ta	XII-235
Nb-Ru-Ti	XIX-235
Nb-Ru-Zr	XVII-369, XVIII-234, XIX-235
Nb-Sb	XII-110
Nb-Se	XI-117
Nb-Si	I-51, II-37, IV-64, VII-80, XIII-93, XIX-79
Nb-Si-Sn	IX-223
Nb-Si-V	IX-175, X-138
Nb-Si-W	VIII-165, IX-184, X-143
Nb-Sn	V-76, VIII-101, IX-101, X-89, XI-113, XIII-106, XVI-90, XIX-79
Nb-Sn-Ti	IX-240
Nb-Sn-Zr	IV-163, IX-241, XVIII-236
Nb-Ta	IV-78
Nb-Ta-Ti	XV-221
Nb-Ta-Ti-W	XIX-263
Nb-Ta-V	XI-183, XII-168, XIV-163
Nb-Ta-W	XVII-259
Nb-Ta-Zr	IV-164
Nb-Te	VI-75, XI-118, XVIII-74
Nb-Th	I-66, II-43
Nb-Th-Zr	IX-246, X-196

<u>System</u>	<u>Location</u>
Nb-Ti	VII-101, VIII-102, XII-111, XV-70
Nb-Ti-U	IX-242, XIX-237
Nb-Ti-V	III-94, V-122, VII-173
Nb-Ti-V-W	XIX-263
Nb-Ti-W	XII-184, XVI-194
Nb-Ti-W-Zr	XVI-301
Nb-Ti-Zr	VII-228, VIII-217, XII-236, XIII-247, XIV-237, XVI-286, XVII-370
Nb-U	III-63, IV-79, VII-104, XVI-91, XVII-141
Nb-U-Zr	IV-166, VII-230, XVII-373
Nb-V	I-18
Nb-V-Zr	XIII-174, XIV-164, XV-159, XVI-168
Nb-W	IV-28, XVIII-75
Nb-W-Zr	VIII-169, IX-185, XVI-195
Nb-Y	VIII-70
Nb-Zn	XI-119
Nb-Zr	I-67, III-64, VII-108, VIII-104, XV-71, XVII-142, XVIII-75, XIX-80
Nd-Pr	XII-105
Nd-Pt	IX-96, XVII-136
Nd-Pu	XIII-104, XV-66
Nd-Rh	XVI-85
Nd-Sb	XVIII-76
Nd-Te	XI-108, XII-106
Nd-Th	XIII-105, XIV-88
Nd-Ti	VI-69
Nd-Y	VII-67
Ni-O	I-42
Ni-O-Ta	XVI-249
Ni-O-W	XVI-186
Ni-Pb	I-63, VI-70, XV-68
Ni-Pd-V	XIV-161
Ni-Pu	I-62
Ni-Re	XVI-87
Ni-Re-Sc	XVI-284, XVIII-236
Ni-Re-Y	XVI-242, XVIII-237
Ni-Rh	XI-110
Ni-Ru	VII-90, X-86

<u>System</u>	<u>Location</u>
Ni-S	II-42, VII-92
Ni-Sb-Sn	X-191
Ni-Se	VII-91
Ni-Si	VIII-80, XI-91
Ni-Si-Ti	XII-225, XVII-321
Ni-Si-V	XII-167
Ni-Si-W	XIV-171
Ni-Si-Y	XVII-304
Ni-Si-Zn	XIV-215
Ni-Si-Zr	XIII-226
Ni-Sn	I-61, X-85
Ni-Sr	XI-111
Ni-Ta	VIII-98
Ni-Ta-Ti	IV-162
Ni-Te	VI-71, XVI-88
Ni-Th	XVIII-77
Ni-Ti	I-64, III-60, IX-98
Ni-U	IX-100, XVII-139
Ni-V	XVI-19
Ni-V-Zr	XIV-162
Ni-W	XVI-27, XVIII-78
Ni-W-Zr	XVI-193
Ni-Y	VI-51, VII-68
Ni-Yb	XIX-81
Ni-Zr	III-62, VI-74, VII-95, XVIII-79
Np-Pu	VII-88
Np-U	V-75
O-Pt-Zr	VII-206
O-Pu	VII-72
O-Rh-Zr	VII-207
O-Sc	XV-50
O-Si-V	XIV-157
O-Sn-Ti	XVI-251, XVIII-238
O-Ta	I-44, V-55, X-64, XII-90, XVI-66, XVIII-80
O-Te	X-65
O-Te-U	XVII-312
O-Th	XV-51

<u>System</u>	<u>Location</u>
O-Ti	I-45, II-35, IX-75, X-66
O-Ti-V	VII-169
O-Ti-W	XIII-183
O-Ti-Zr	XIII-224, XVII-313
O-U	IX-76, XI-85, XIII-87, XVI-67
O-U-Zr	III-110
O-V	I-15, III-18, XVI-18, XVII-42, XVIII-81
O-W	VIII-34
O-Y	XIX-82
O-Zr	VII-73, XIII-88
Os-Pd	IX-104
Os-Pr	XVII-148
Os-Pu	I-69
Os-Re	VIII-110
Os-Re-Ru	IX-250
Os-Ru	VIII-111, XIX-82
Os-Ti	XVII-149, XVIII-82
Os-U	IX-105
Os-V	XII-28
Os-W	VII-30
P-Pd	XII-116
P-S	IV-87
P-Si	V-62, VIII-82
P-Th	XIII-136
P-Ti	XI-133
Pb-Pd	XIX-83
Pb-Pd-Te	XVII-380
Pb-Pr	XVII-158
Pb-Pu	I-70, XV-77
Pb-Rh	XVIII-83
Pb-S-Sb	VI-164
Pb-S-Te	XII-243
Pb-Sb-Se	VII-235
Pb-Sb-Sn	IX-248
Pb-Sb-Te	XI-253, XIII-256, XVI-291
Pb-Sb-Zn	V-157

<u>System</u>	<u>Location</u>
Pb-Se	II-48, XII-121
Pb-Se-Sn-Te	XIX-264
Pb-Se-Te	II-94, XI-252, XVI-290
Pb-Si	XVII-119
Pb-Sn	IV-82, VIII-106, XVI-93
Pb-Sn-Te	IV-167, XIII-249
Pb-Sn-Zn	XIII-250
Pb-Te	II-49, VII-112, XI-128
Pb-Te-Tl	XV-226
Pb-Te-U	XVIII-239
Pb-Ti	I-72
Pb-Tl	XVI-102
Pb-Y	XIII-80
Pb-Yb	XIII-79
Pb-Zr	IX-126
Pd-Pt-Ru	II-93
Pd-Pu	XIII-110
Pd-Re	VIII-112
Pd-Re-W	X-146
Pd-Rh	V-85
Pd-Ru	II-46, V-86, VI-79, XIX-84
Pd-Sb	XVII-151
Pd-Sb-Te	XVII-381
Pd-Sc	XVII-150
Pd-Si	III-42, XVII-119
Pd-Sm	XIX-84
Pd-Sn	V-81
Pd-Ta	X-99
Pd-Tc	IX-106
Pd-Th	X-100
Pd-Ti	IV-84, VI-80, XI-121, XIV-94, XVIII-84, XIX-85
Pd-U	II-47, X-101, XIV-95
Pd-V	IV-15
Pd-W	VII-31, X-23
Pd-Y	XIX-86
Pd-Zr	V-87, VIII-113, XVII-152

<u>System</u>	<u>Location</u>
Pr-Pt	XVII-153
Pr-Pu	XIII-114, XV-75
Pr-Re	XVII-156
Pr-Se	XII-117
Pr-Te	XVI-95
Pr-Th	XIII-125, XIV-96
Pr-Tl	XVII-159
Pr-Zn	XVI-98
Pt-Pu	XIII-113
Pt-Ru	XVIII-85, XIX-87
Pt-Si	X-71, XV-53
Pt-Ta	XI-122
Pt-Tc	IX-108
Pt-Te	IX-107
Pt-Th	X-102
Pt-U	VI-81
Pt-Zr	XIX-88
Pu-Rh	XIII-115
Pu-Ru	VII-113, XIII-116
Pu-Si	XI-92, XIII-118
Pu-Sm	XV-76
Pu-Th	III-68, XI-123, XIII-121
Pu-Ti	XIII-119, XVII-155
Pu-U	V-89
Pu-U-Zr	XIV-246
Pu-V	I-17
Pu-Y	XIII-81
Pu-Zn	XIII-122
Pu-Zr	VI-82, X-103, XIII-123, XV-78
Re-Rh	VIII-114
Re-Ru	VIII-115
Re-Sc	XII-118
Re-Si-W	XV-171
Re-Sn	XVI-92, XVII-143
Re-Ta	VI-83, XV-80
Re-Ta-W	XIII-185, XIV-174, XIX-237
Re-Tb	XIV-97
Re-Tc	IX-111
Re-Th	VII-115, XIV-98
Re-Ti	V-90, XV-81

<u>System</u>	<u>Location</u>
Re-U	IX-113
Re-V	VI-23, VII-26, XV-18
Re-W	V-31, XV-22
Re-W-Zr	XVI-196
Re-Zr	V-93, XV-82
Rh-Ru	XIX-88
Rh-Sb	IV-85, IX-114
Rh-Se	XIII-127
Rh-Ta	X-104
Rh-Tc	IX-115
Rh-Th	IX-116
Rh-Ti	XI-125, XII-120, XVIII-86, XIX-89
Rh-U	XIV-99
Ru-Sc	XVII-160
Ru-Si	XI-93
Ru-Ta	XI-126
Ru-Th	IX-124
Ru-Ti	IX-123, XVIII-86
Ru-U	XIV-101
Ru-V	IX-25
Ru-V-Zr	XIX-238
Ru-W	X-24
Ru-Y	XVIII-87
Ru-Zr	IX-125
S-Sb	VI-86
S-Sn	IV-83, VII-110, XII-113
S-Sr-U	XVII-387
S-Te-U	XIX-239
S-Ti	XIII-131
S-U	XVII-164
Sb-Se-Sn	XIV-242
Sb-Se-Te	XI-255
Sb-Se-Tl	I-127, XIX-240
Sb-Si	XVII-120
Sb-Sn	VI-76, XII-114, XVII-144
Sb-Sn-Te	XII-240, XIII-251
Sb-Sn-Te-Tl	VIII-226
Sb-Te	V-98, IX-127, XIV-103
Sb-Te-Tl	XII-244, XIV-251
Sb-Te-Zn	XVII-389

<u>System</u>	<u>Location</u>
Sb-Tl	XVI-108
Sb-U	VI-88
Sb-Y	XVI-63
Sb-Zn	IV-89
Sc-Ti	VII-117, VIII-119
Sc-V	XVII-43
Sc-Y	XII-84
Sc-Zr	XII-123
Se-Sn	XII-112, XIV-92
Se-Sn-Te	XIV-243
Se-Ta	II-50, XI-129
Se-Te	VI-85, XII-122
Se-Te-Tl	V-158
Se-U	XVII-163
Si-Sn	V-60
Si-Sr	X-72, XI-94
Si-Ta-V	III-93
Si-Th	VII-81, IX-80
Si-Th-U	IX-224
Si-Ti	VIII-81, IX-79, XVI-71
Si-Ti-V	VII-170, XI-181
Si-Ti-W	XVI-188
Si-Tl	IV-65
Si-U	III-43, IX-81
Si-U-Zr	VII-211
Si-V	II-15, IX-23
Si-V-W	XIII-171
Si-W	III-24, XIX-90
Si-Zn	XVIII-88
Sm-Zn	XIII-129
Sn-Te	X-96
Sn-Te-U	XVIII-240
Sn-Th	X-97
Sn-Ti	I-68, II-45, III-65, VI-77, VIII-108
Sn-Ti-V	III-95
Sn-Ti-Zr	VI-161, VII-232, VIII-218, XIV-244, XVI-287

<u>System</u>	<u>Location</u>
Sn-Tl	V-82, VII-111, VIII-107, XII-115, XIV-93, XVI-94, XVII-146
Sn-Tl-V	XIX-241
Sn-V	VII-25, XIX-91
Sn-Y	IX-68, XIV-64
Sn-Zn	V-84
Ta-Te	V-100, XI-131
Ta-Th	VII-119, XVIII-88
Ta-Ti	IX-128, XV-88
Ta-Ti-V	VII-174, XVI-169
Ta-Ti-W	XVIII-240
Ta-Ti-Zr	X-201
Ta-V	V-23, VI-24, VIII-18, X-21, XI-29
Ta-V-W	XIV-154
Ta-V-Zr	XIV-166
Ta-W	XVIII-89
Ta-W-Zr	X-148
Ta-Y	VIII-71
Ta-Zr	III-69, VIII-120, XII-124, XVIII-90
Tb-Th	XIII-134
Tb-Y	XIII-82
Tc-V	XIV-22
Tc-W	IX-32
Tc-Zn	X-108
Te-Tl	VI-89
Te-Yb	XVI-61
Th-Ti	II-51
Th-Ti-Zr	IX-253, X-203
Th-U	IV-92, XVIII-90
Th-U-W	XVIII-242
Th-U-Zr	IV-172, VII-244, XVIII-243
Th-V	VII-27, IX-27
Th-W	XVIII-91
Th-Zn	III-75
Th-Zr	IV-93, V-103, VII-126, XVIII-92

<u>System</u>	<u>Location</u>
Ti-U	I-74, VII-123
Ti-U-Zr	III-119, V-161, VII-239, XIV-253, XIX-242
Ti-V	IX-26
Ti-V-W	VII-166
Ti-V-Zr	IV-120, VIII-156
Ti-W	IV-30, XIV-29, XVII-58, XVIII-92
Ti-W-Zr	XII-185
Ti-Y	VII-69, VIII-72, XIV-65
Ti-Zn	VIII-123, XII-125
Ti-Zr	VII-124, XII-126, XVII-168
Tl-Zn	I-73, VII-118, XI-130
U-W	I-23
U-Zn	III-77
U-Zr	I-76, II-53, III-78, VII-130, IX-133, XVI-109, XVII-169
V-W	VI-20, VII-22
V-Y	VII-24, VIII-15
V-Zn	XII-30
V-Zr	I-19, XVIII-93
W-Zr	XVIII-93
Y-Zn	XII-85
Y-Zr	VIII-73
Yb-Zn	XII-86, XIV-62
Zn-Zr	VI-90

BIBLIOGRAPHY

The following is a list of the volumes of "Diagrammy Sostoyaniya Metallicheskih Sistem," edited by N. V. Ageev and published by VINITI in Moscow, USSR, which were used in making this compilation.

<u>Volume</u>	<u>Publ. Date</u>
I	1959
II	1959
III	1960
IV	1961
V	1962
VI	1962
VII	1963
VIII	1964
IX	1966
X	1966
XI	1968
XII	1968
XIII	1970
XIV	1970
XV	1971
XVI	1972
XVII	1973
XVIII	1975
XIX	1976



Standards for Publication of Phase Equilibrium Studies

Eric R. Kreidler

General Electric Company, Lighting Research and Technical
Services Operation, Nela Park, Cleveland, Ohio

INTRODUCTION

A paper on phase equilibria typically receives a review before publication and may not be critically evaluated again until it is included in a compilation. Since most phase diagrams will eventually be published in handbooks or compilations such as Phase Diagrams for Ceramists, it is important that the initial review process be critical and constructive. Critical evaluations after publication are of limited value because there is usually no opportunity for a response from the original authors. It is suggested that a set of published standards for phase equilibrium papers would assure more uniform treatment of data and would help both journal reviewers and compilers to properly assess the value of individual papers. A brief survey of the literature quickly reveals the wide variation in quality. Papers range from speculations based on a few haphazard experiments to thorough studies based on hundreds of experiments and using complementary experimental techniques. The purpose of standards should not be to preclude publication of incomplete or exploratory work, but to assure that such works are based upon sound data. Standards should be used to prevent publication of erroneous diagrams, and if properly written and disseminated can help improve the general quality of phase equilibrium studies.

The establishment of standards raises some difficult questions. Among them being: how demanding should standards be?; how rigorously should standards be applied?; and what aspects of phase equilibrium work should be subject to standardization? If a set of standards is to gain

wide acceptance, it must represent a concensus of informed opinion and satisfy the main needs of all concerned disciplines. For these reasons, the establishment of standards should be the responsibility of the scientific community. A committee of phase equilibrium experts representing the disciplines metallurgy, ceramics, mineralogy, geochemistry, semi-conductor technology, etc. could accomplish the task.

The purpose of this work is not to formulate standards but to point out some of the problem areas and suggest ways to handle them. Most of the comments and opinions result from the author's experiences while handling the review process for thirty phase equilibrium papers over the last three years. The most significant impression gained from that activity is that a majority of phase equilibrium studies are poorly conceived and conducted. Furthermore, there seems to be a widespread lack of understanding of basic phase rule principles among scientists engaged in phase equilibrium studies. It is important to explore ways of upgrading the field; hence the motivation for this discourse.

The majority of problems fit into one or more of the following broad categories, ranked in order of importance.

- A. Failure to test for equilibrium.
- B. Use of inappropriate experimental methods.
- C. Accuracy and precision of experimental results.
- D. Failure to provide adequate documentation of experimental data.
- E. Diagrams which violate the phase rule.
- F. Terminology and phase diagram format.
- G. Poor exposition.

Each of these areas are discussed in greater detail in the following sections.

A. Tests of equilibrium

Although the phase rule applies only to systems at equilibrium, tests of equilibrium are a widely ignored aspect of experimental phase diagram determinations. This single factor probably leads to more errors than any other. It is estimated that if sensible tests of equilibrium were a prerequisite to publication, fewer than one in five diagrams would be published. Admittedly, tests of equilibrium are sometimes difficult, but several methods are available and should be put to more extensive use.

Theoretically a system is at equilibrium when the components have interacted in such a way as to obtain the minimum free energy possible with those components for a given composition, temperature, and pressure. Furthermore at equilibrium, there cannot be any gradients in chemical potential, temperature, or pressure. Although these are the best criteria for equilibrium, they are seldom used because adequate thermodynamic data are lacking and because it is tedious to prove that individual phases have reached homogeneous equilibrium (i.e. they are free of composition gradients).

The experimental test most often employed is to perform periodic phase analyses on samples held at specified conditions. If the phase assemblage remains constant with time, equilibrium is then assumed. The test is frequently abused because the time intervals studied are too short. This test is usually open to question because it is impossible to determine a priori what the time scale should be.

A better test is to approach equilibrium from two (or more) directions. This technique is much more flexible and generally yields more information than the "constancy with time" criterion. For rapid reversible reactions,

such a test can take the form of DTA scans in both the upward and downward directions at several heating and cooling rates. If sharp heat effects are observed in both directions, one can evaluate, from the thermal hysteresis, how readily the system approaches equilibrium. For sluggish systems, it is often possible to obtain more than one set of phases for a given composition. These can be studied in paired experiments to determine if a common set of assemblages is reached from the two different initial sets. If so, equilibrium can be reasonably assumed. If both initial sets of phases remain unchanged or fail to converge, the investigator immediately knows that equilibrium has not been attained.

At equilibrium, the number of observed phases must be in accord with the predictions of the phase rule. If there is a discrepancy, either the system is not at equilibrium, or the components were incorrectly chosen. This simple criterion is often overlooked, and incorrect diagrams for condensed binary systems have been occasionally presented, showing extensive areas of three and even four phase coexistence. Fortunately, most errors of this sort are eliminated during the review process.

A first rate study should contain convincing tests of equilibrium. The "time invariance" criterion should give way to the "two directions" criterion whenever possible. In all cases the number of observed phases must be in accord with the predictions of the phase rule.

B. Inappropriate Experimental Techniques

In order to select appropriate experimental techniques, something must be known of the system kinetics. The rate at which reactions proceed should dictate the methods used. Generally little is known about the kinetics of phase reactions in new systems, and such knowledge

must be generated by various tests of equilibrium. The two extremes are most easily studied. Rapid reversible reactions are amenable to dynamic methods such as DTA or hot stage microscopy. Very sluggish reactions are best evaluated by static methods such as quenching. Serious experimental problems can lie between the two extremes and may require the use of in situ high temperature methods. Generally these should be static measurements.

In general no one method is suitable for an entire system, and a judicious mixture of static and dynamic methods will yield the greatest amount of information. A classic example is the system SiO_2 where both rapid reversible (α - β quartz transition) and sluggish (cristobalite - liquid) reactions are encountered.

Many other errors in experimental technique can be found in the literature. One of the more common is to fail to control or specify the oxygen fugacity in systems containing multivalent oxides. These errors lead to inaccurate results as indicated in the next section.

C. Accuracy and Precision of Experimental Results

A phase diagram is only as good as the accuracy with which temperature, pressure, and composition are measured and controlled. Temperature measurements, although the easiest to make, are frequently of questionable accuracy. One of the more common errors is the use of dynamic methods to measure sluggish transitions. It is not uncommon to find polymorphic transitions which are off by 20°C or more due to superheating and supercooling effects. The precision in temperatures should be realistically stated, taking into account such factors as stability of furnaces, possible temperature gradients, and pyrometer calibration. If a furnace used for equilibration studies is stable to

only $\pm 5^{\circ}\text{C}$ it is not valid to claim precision of $\pm 1^{\circ}\text{C}$ which may be the accuracy of a thermocouple calibration. It appears that the precision of temperature measurements made by optical pyrometry is often grossly overstated.

Pressure measurements have many difficulties which need not be discussed here. As with temperature measurements, estimates of the accuracy and precision of such measurements is mandatory.

Compositional inaccuracy can arise from a number of causes: reactions with containers, reactions with atmospheric components, incongruent vaporization, etc. For this reason, it is essential that investigators state as accurately and completely as possible the nature of containers or other materials in contact with samples as well as the atmospheres used. Where applicable, possible changes in oxidation state should be evaluated and commented upon. Any assumptions regarding the final composition of samples derived by pyrolysis of more complex materials should be checked by chemical analysis. It is not always valid to assume that all CO_2 , H_2O , etc. has been removed by heating to high temperatures. Aside from the problem of gross composition, one is faced with a myriad of problems relating to the composition of liquid and solid solutions.

X-ray lattice parameter shifts are commonly used to estimate compositions of solid solutions. Often as not, the method is misused because the calibration curve is obtained from mixtures of phases rather than single phase samples. For the method to be valid, the actual compositions of the solid solutions used in constructing the calibration curve must be accurately known. If a mixture of phases is involved, this is not possible unless the phases can be separated and chemically

analyzed. Liquid compositions are infrequently determined by chemical analysis, but if more effective methods of separating high temperature melts from their conjugate solids could be devised, the problem of accurate liquidus determinations could be greatly simplified.

D. Failure to Provide Adequate Documentation of Experimental Data

Since many journals no longer publish extensive tabular data, it is becoming more and more common for authors not to provide such information. Other, less desirable, methods of documenting phase equilibrium data are being used. One method is to place symbols directly on the phase diagram in an effort to indicate what experiments were done. Although somewhat useful, such symbols do not convey as much information as a well constructed table. The lack of well organized tables often leads to lengthy verbal descriptions of the data. Such discussions tend to read poorly, becoming so bogged down in details that the main points are missed. In some cases the experimental data are simply not documented, and only the phase diagram itself is given.

Tables of well documented phase equilibrium data should be provided along with any diagram submitted for publication! Such tables are placed in data depositories and are available to interested readers. From the viewpoint of the reviewer (or other critical reader), it is inherently unfair to expect that the conclusions of a study (i.e. a phase diagram) be accepted, when the data upon which they are based is unavailable for inspection.

A well constructed table should contain at least the following information:

1. Sample composition

2. Initial phases present
3. Equilibration conditions -- temperature, time at temperature, pressure, atmosphere, etc.
4. Phases present after equilibration
5. Methods of phase analyses -- x-ray diffraction, microscopy, others.

Any conditions or methods common to the entire study should be stated in a footnote and not be endlessly repeated in the table. A sample table incorporating these ideas is shown in Table I. The information density in such a table can be very high, and one might consider replacing the "Experimental" section of a study with such an annotated table. With such a presentation it is an easy matter to document the history of any given sample along with the phase assemblage finally obtained. Table I shows that by indentation of temperatures alone, the sequence of heat treatments given any sample is easily documented. Thus Sample #2 was heated at 900°C for 48 hours in an open platinum crucible, cooled, a portion was packed into a platinum tube which was then sealed, held at 1200°C for 15 hours, and finally quenched into water.

With this kind of detailed information the reviewer is able to fairly judge the plausibility of the author's conclusions. Without it he cannot exercise much independent judgement, and the value of the review declines accordingly.

E. Diagrams Which Violate the Phase Rule

The geometry of phase diagrams must be consistent with the phase rule. There is a tendency among less expert workers to "pepper" a system with experimental points and then map out areas of like phase assemblages without much regard for the requirements of the phase rule. The resulting

diagrams can be very strange and their various parts sometimes cannot be connected together to make a correct, whole diagram. Non-equilibrium phase assemblages are frequently the underlying cause of such implausible diagrams.

Impossible geometries are sometimes found in published diagrams. They can be grouped into "absolutely impossible" and "impossible but approachable in the limit" categories. A few examples of each type which have been found in the recent literature are illustrated in Figures 1 - 4. A greater variety and higher frequency of errors can be found in ternary and quaternary systems. Some of the impossible configurations probably result from poor draftsmanship, but whatever their cause, they should be eliminated before a diagram is published. A brief set of rules for the geometric construction of unary, binary, ternary and quaternary systems and their various sections might be useful. A short compendium of impossible configurations might also help.

F. Formats and Terminology

The formatting of phase diagrams need some attention. Although some conventions do exist, and are in wide use, a formalized statement of these conventions would be of great value both to authors and reviewers. A principal concern is that speculative phase relationships be clearly indicated on the diagrams. This is commonly done by using dashed curves for speculative portions of the diagram. However, this convention is not universally followed. Extraneous material such as the height of DTA peaks should not be superimposed on phase diagrams. Isofracts, lattice parameters or other data useful in constructing the phase diagram may be displayed on separate "property" diagrams but should not be plotted on the phase diagram itself.

A uniform terminology across all disciplines, using phase diagrams, should be possible and is desirable. Our present terminology is incomplete in some respects and confusing in others. Even in simple binary systems, a few rather common features either have no names or are referred to by cumbersome phrases such as "lower temperature limit of stability" (Fig. 5e). A few of these unnamed features are shown in Figures 5a - 5f.

Invention of jargon to supplant more suitable terminology, already in existence, must be strenuously discouraged. The use of generic terms such as "invariant point" should be discouraged whenever the use of a more specific term such as "eutectic point" or "peritectic point" is possible.

An example of faulty terminology is illustrated by Figure 6. This diagram was repeatedly referred to as a "planar square iso-electronic phase diagram". Granted the diagram is planar and square, but it certainly is not iso-electronic. (The number of electrons per formula unit are given in parentheses.) The diagram is iso-equivalent which is what the author meant. A lot of trouble could have been saved if the diagram had been referred to by its proper term "reciprocal salt system". Surprisingly, this obviously faulty term almost made it into the literature.

G. Poor Exposition

The exposition of phase equilibrium studies is probably no better or worse than is to be found in other fields of science. A long discourse could be written about what constitutes good and bad scientific writing, but it is not appropriate here. From the reviewer's point of view, there are several particularly annoying faults which should be avoided:

1. Do not expect reviewers to be ghost authors. The English

in some manuscripts is appalling. The responsibility of writing well belongs to the author not his reviewers or editors. The reviewer's main responsibility is to judge the scientific aspects of the work, his responsibility for exposition should be secondary and mostly of a cosmetic nature.

2. Do not engage in extensive discussions which are unsupported by well documented experimental evidence. Speculations should be clearly stated, labeled as such, and occupy the minimum possible space. A corollary is -- Do not build an extensive case on data which are really of questionable value.
3. Keep the use of jargon to a minimum. The aim of writing is to communicate, and jargon or excessive use of specialized terminology can only restrict the size of the potential audience.
4. Do not indulge in criticism of prior work unless your own work is clearly more definitive.
5. Do yourself justice. Do not negate a good piece of work with sloppy writing.

CONCLUSION

Much can and should be done to improve the quality of published work on phase equilibria. It is suggested that an interdisciplinary committee of experts could formulate a set of standards or guidelines for the publication of phase equilibrium studies. Although incomplete and certainly debatable in some particulars, it is hoped that the remarks herein might serve as a starting point for such an effort.

A set of well written standards could make the review process more constructive and less subject to the vagaries of individual tastes and expectations. If potential authors could know what standards their work would be evaluated against, they could do a better job of planning and executing their work. The end result should be a general improvement in the quality of phase equilibrium studies.

Table I

Suggested Format for Reporting Phase Equilibrium Data

Composition	T (°C)	Time (hr.)	Phases Present	Comments
ABC	900	48	AB + C	a, x
	1200	15	AB + LIQ.	b, x, m
	1500	5	LIQUID	b, x, m
	1400	20	LIQUID	a, m
	900	48	AB + C	b, x, m
	1000	48	AB + C	b, x, m
	1100	48	AB + C	b, x, m
A ₂ BC	900	48	A ₂ B + C	a, x
	1000	1	A ₂ B + LIQ.	b, x, m

a. Open Pt crucibles, cooled by plunging into air, ~10 gram samples.

b. Sealed Pt capsule, quenched into water, ~10 mg. samples.

x = x-ray diffraction, m = microscopy in polarized light.

The atmosphere in contact with all samples was air.

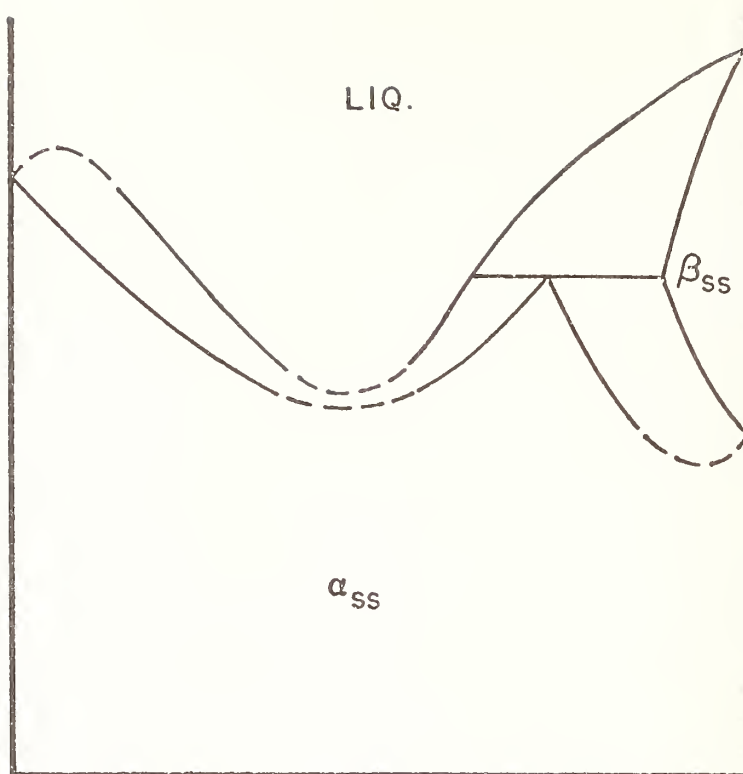


FIGURE 1

Some impossible configurations (dashed curves). Liquidus and solidus curves must be tangent in such a system.

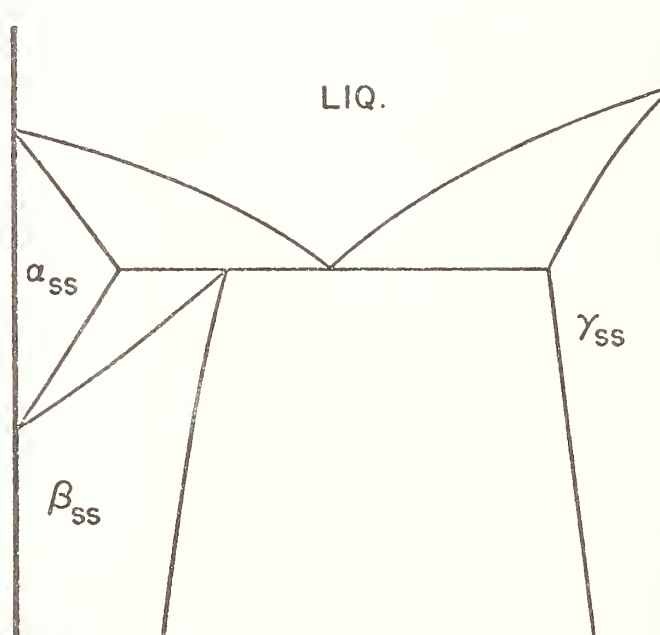


FIGURE 2

However narrow, there must be an $\alpha_{ss} + \gamma_{ss}$ region.

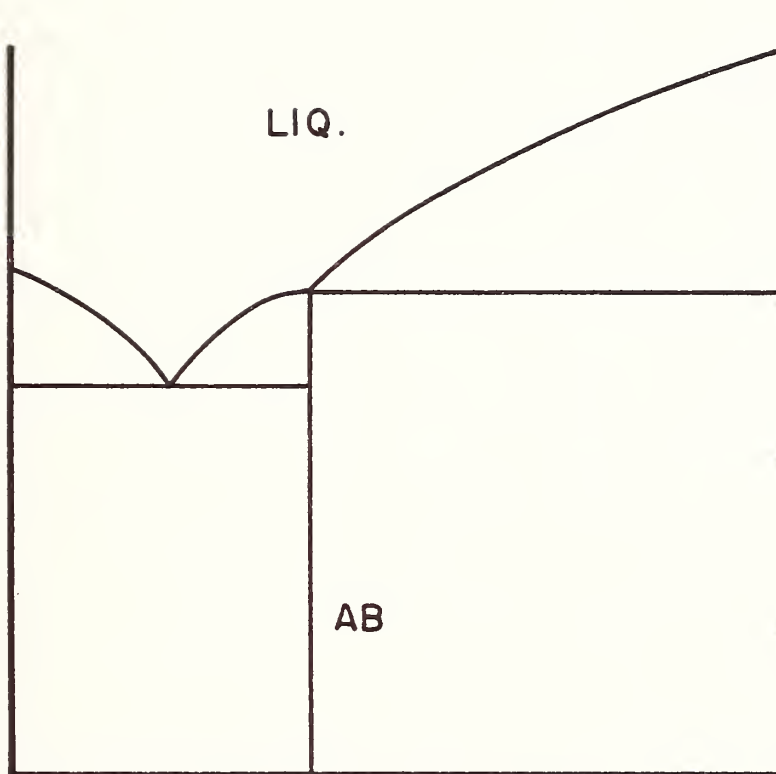


FIGURE 3

Approachable as a limit, but generally the compound AB must melt either congruently or incongruently.

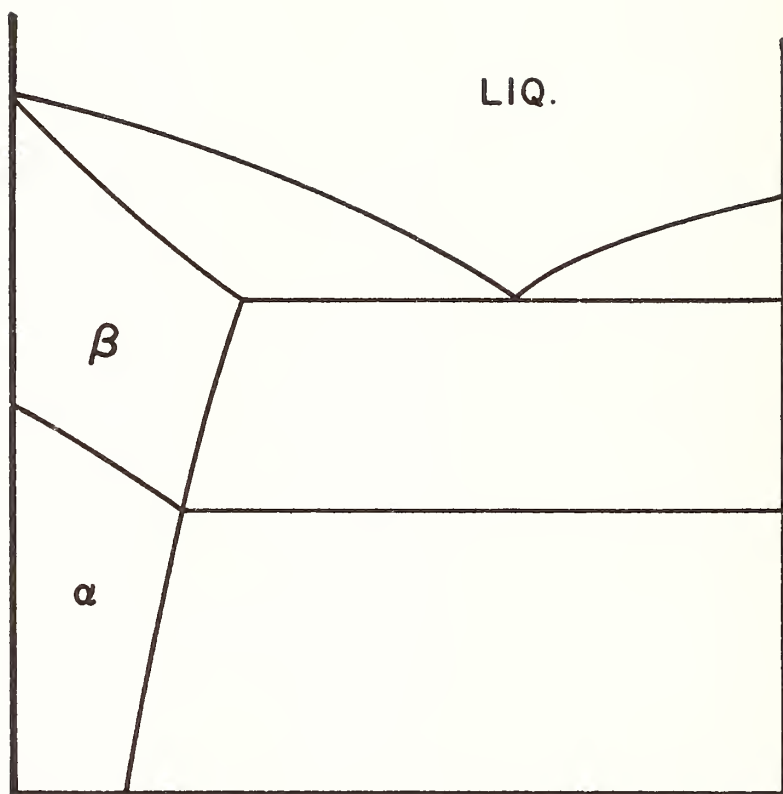


FIGURE 4

If α and β are distinct phases, they must be separated by an $\alpha + \beta$ region.

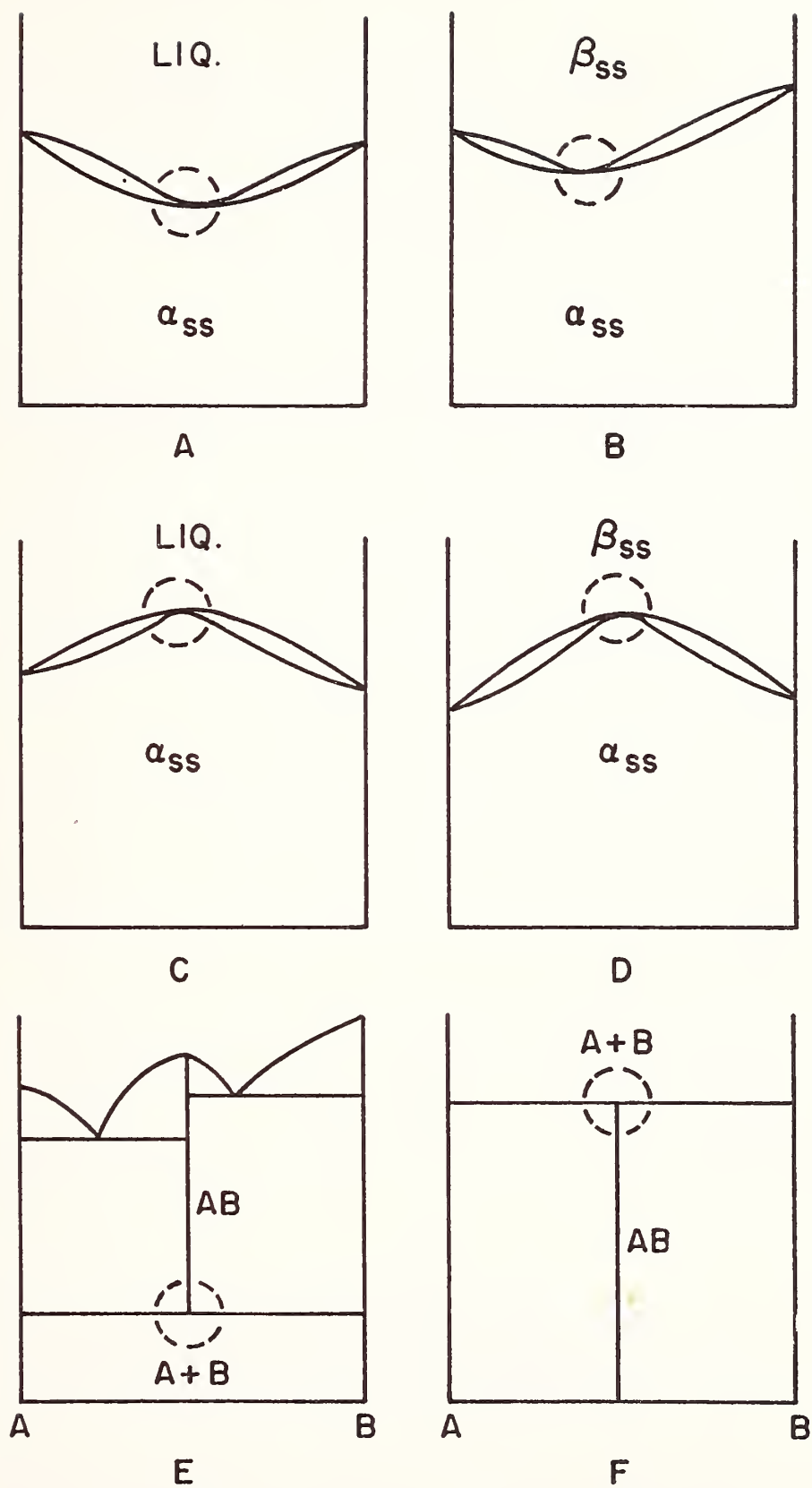


FIGURE 5

Some unnamed features in binary condensed systems (circled).

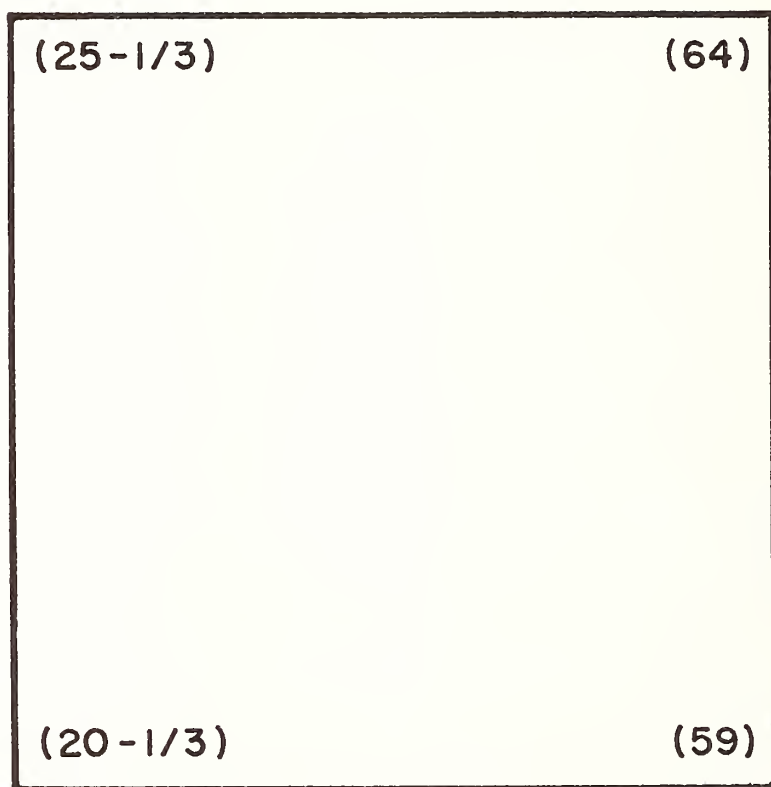
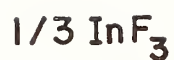


FIGURE 6

An example of poor terminology. "Planar square iso-electronic phase diagram" or "Reciprocal salt diagram"? (Number of electrons per formula unit given in parentheses.)



FORMATTING AND DISTRIBUTING EVALUATED REFERENCE DATA:
THE OFFICE OF STANDARD REFERENCE DATA
AT THE NATIONAL BUREAU OF STANDARDS

S. P. Fivozinsky and G. B. Sherwood
Office of Standard Reference Data
National Bureau of Standards
Washington, D.C. 20234

The Office of Standard Reference Data at the National Bureau of Standards manages a complex of data evaluation centers located in university, industrial, and other Government laboratories as well as within NBS. The centers are engaged in the compilation and critical evaluation of numerical data on physical and chemical properties retrieved from the world scientific literature. This system of centers, the National Standard Reference Data System (NSRDS), is a means of coordinating on a national scale the production and dissemination of critically evaluated reference data in the physical sciences. The primary focus of the NSRDS is on well-defined physical and chemical properties of well-characterized materials or systems.

The Office of Standard Reference Data, as coordinator of the system:

- establishes needed data centers in technical areas which fall within the scope of the program
- maintains close contact with other data compilation activities both in the U.S. and abroad to encourage exchange of data and avoid needless duplication of effort
- identifies, by contacts with users, areas where needs for evaluated reference data are increasing or decreasing, and formatting procedures which will make the outputs of the system as useful as possible
- distributes evaluated reference data through a variety of output channels

The output channels include:

- Journal of Physical and Chemical Reference Data
a quarterly journal containing data compilations and critical data reviews, published for the National Bureau of Standards by the American Institute of Physics and the American Chemical Society.
- NSRDS-NBS Series
a publication series distributed by the Superintendent of Documents, U.S. Government Printing Office

- appropriate publications of technical societies and commercial publishers. Handbook publications are an important element of this category
- magnetic tape data files - sold through the National Technical Information Service

The outputs of several NSRDS centers are directly or indirectly related to phase diagram applications in metallurgy and ceramics; examples include alloy data, data on diffusion in metallic systems, properties of substances at high pressures; properties of superconducting materials, and thermodynamic data of minerals. Some recent publications on these subjects are:

1. Butrymowicz, Daniel B., Manning, John R., Read, Michael E., "Diffusion in Copper and Copper Alloys, Part IV. Diffusion in Systems Involving Elements of Group VIII," J. Phys. Chem. Ref. Data, 5(1) 103-200 (1976).
2. Chang, Y. Austin, "Phase Diagrams and Thermodynamic Properties of Ternary Copper-Silver Systems," J. Phys. Chem. Ref. Data (in process).
3. Donnay, J.D.H. and Ondik, Helen M., Crystal Data Determinative Tables, Third Edition, Vol. 1, Organic Compounds, Vol. 2, Inorganic Compounds, Swarthmore, PA, Joint Committee on Powder Diffraction Standards, Vol. 1 (1972), Vol. 2 (1973).
4. Hultgren, R. and Desai, P. D., Selected Thermodynamic Values and Phase Diagrams for Copper and Some of Its Binary Alloys, New York, International Copper Research Association, Inc. (1973).
5. Roberts, B. W., "Survey of Superconductive Materials and Critical Evaluation of Selected Properties," J. Phys. Chem. Ref. Data, 5(3) 281-821 (1976).
6. Stull, D. R. and Prophet, H., JANAF Thermochemical Tables, Second Edition, NSRDS-NBS 37, U.S. GPO (1971).

Reprint No. 50, "JANAF Thermochemical Tables, 1974 Supplement," J. Phys. Chem. Ref. Data, 3(2) 311-480 (1974).

Reprint No. 60, "JANAF Thermochemical Tables, 1975 Supplement," J. Phys. Chem. Ref. Data, 4(1) 1-175 (1975).

In general, current NSRDS projects fall into the following categories:

Energy and Environmental Data - This program includes projects dealing with data that have an important application in some aspect of energy R&D or environmental quality improvement. Projects in chemical kinetics, nuclear properties, spectroscopic data, and interaction of radiation with matter are currently incorporated in this program. The output of these projects is particularly important in R&D on new energy sources, environmental monitoring techniques, and prediction of the effects of pollutants introduced into air, water, or land.

Industrial Process Data - Projects dealing with thermodynamic, transport, colloid and surface, and physical properties of industrially important substances are included in this program. Such data have particular application to design of new processes in the chemical and metallurgical industries, optimization of currently used processes, and general productivity enhancement.

Materials Utilization Data - This program covers properties required for material selection and R&D on new materials. The structural, optical, electric, magnetic and mechanical properties of solid materials are included.

Physical Science Data - Projects which involve basic data of very broad applicability, or which are associated with an important frontier field of science, are included in this program. Examples are fundamental physical constants, data on fundamental particles, and data relevant to radioastronomy.

The data centers currently included in the National Standard Reference Data System are given below. Inquiries on data may be directed to all these centers.

Energy and Environmental Data

Atomic Energy Levels Data Center

Dr. W. C. Martin
Optical Physics Division
National Bureau of Standards
Washington, D.C. 20234
Telephone: (301) 921-2011

Data Center for Atomic Transition Probabilities and Atomic Line Shapes and Shifts

Dr. W. L. Wiese
Optical Physics Division
National Bureau of Standards
Washington, D.C. 20234
Telephone: (301) 921-2071

Direct inquiries to: Ms. Georgia Martin, (301) 921-3374

Atomic Collision Cross Section Information Center

Dr. E. C. Beaty
Joint Institute for Laboratory Astrophysics
University of Colorado
Boulder, Colorado 80309
Telephone: (303) 499-3672

Data Center for Atomic and Molecular Ionization Processes

Dr. H. M. Rosenstock
Physical Chemistry Division
National Bureau of Standards
Washington, D.C. 20234
Telephone: (301) 921-2792

Chemical Kinetics Information Center

Dr. R. F. Hampson, Jr.
Physical Chemistry Division
National Bureau of Standards
Washington, D.C. 20234
Telephone: (301) 921-2174

Radiation Chemistry Data Center

Dr. Alberta B. Ross
University of Notre Dame
Radiation Laboratory
Notre Dame, Indiana 46556
Telephone: (219) 283-6527

Molten Salts Data Center

Dr. G. J. Janz
Rensselaer Polytechnic Institute
Department of Chemistry
Troy, New York 12181
Telephone: (518) 270-6356

X-ray and Ionizing Radiation Data Center

Mr. J. H. Hubbell
Center for Radiation Research
National Bureau of Standards
Washington, D.C. 20234
Telephone: (301) 921-2685

Photonuclear Data Center

Dr. E. G. Fuller
Nuclear Sciences Division
National Bureau of Standards
Washington, D.C. 20234
Telephone: (301) 921-2625

Table of Isotopes Center

Dr. M. Lederer
Lawrence Radiation Laboratory
University of California
Berkeley, California 94720
Telephone: (415) 843-2740 x5995

Industrial Process Data

Chemical Thermodynamics Data Center

Mr. D. D. Wagman
Physical Chemistry Division
National Bureau of Standards
Washington, D.C. 20234
Telephone: (301) 921-2773

Aqueous Electrolyte Data Center

Dr. B. R. Stanles
Physical Chemistry Division
National Bureau of Standards
Washington, D.C. 20234
Telephone: (301) 921-3632

Thermodynamics Research Center

Dr. B. J. Zwolinski
Texas A & M University
Department of Chemistry
College Station, Texas 77843
Telephone: (713) 846-8765

Cryogenic Data Center

Mr. N. A. Olien
Cryogenics Division
National Bureau of Standards
Boulder, Colorado 80302
Telephone: (303) 499-1000 x3257

Center for Information & Numerical Analysis and Synthesis

Dr. Y. Touloukian
Purdue University
CINDAS
2595 Yeager Road
W. Lafayette, Indiana 47906
Telephone: (317) 463-1581

Direct inquiries to: Mr. W. H. Shafer

High Pressure Data Center

Dr. H. T. Hall
574 Clark Library
Brigham Young University
Provo, Utah 84601
Telephone: (801) 374-1211 x3477

Direct inquiries to: Dr. Leo Merrill

Alloy Data Center

Dr. L. H. Bennett
Metallurgy Division
National Bureau of Standards
Washington, D.C. 20234
Telephone: (301) 921-2917

Materials Utilization Data

Crystal Data Center

Dr. H. M. Ondik
Inorganic Materials Division
National Bureau of Standards
Washington, D.C. 20234
Telephone: (301) 921-2900

Diffusion in Metals Data Center

Dr. J. R. Manning
Metallurgy Division
National Bureau of Standards
Washington, D.C. 20234
Telephone: (301) 921-3351

Superconductive Materials Data Center

Dr. B. W. Roberts
General Electric Company
Research & Development Center
P.O. Box 8
Schenectady, New York 12301
Telephone: (518) 377-2271

Physical Science Data

Fundamental Particle Data Center

Dr. A. H. Rosenfeld
Lawrence Radiation Laboratory
University of California
Berkeley, California 94720
Telephone: (415) 843-2740 x6301

Microwave Spectral Data Center

Dr. F. J. Lovas
Optical Physics Division
National Bureau of Standards
Washington, D.C. 20234
Telephone: (301) 921-2021

PANEL II

PRIMARY METAL PRODUCTION

(User Needs for Phase Diagram Information)

Moderator: Prof. John F. Elliott, Dept. of Materials
Science and Engineering, M.I.T.
Cambridge, MA

Panel Members:

Dr. Peter Crimes, Ledgemont Laboratory,
Kennecott Copper Corp., Lexington, MA

Dr. Harold R. Larson, American Smelting and
Refining Company, Plainfield, NJ

Dr. Robert D. Pehlke, Metallurgy Division,
University of Michigan, Ann Arbor, MI



PANEL DISCUSSION: PRIMARY METAL PRODUCTION

John F. Elliott
Dept. of Materials Science
and Engineering, M.I.T.
Cambridge, MA

To start the ball rolling, I would like to make a few comments on how phase equilibria and phase diagrams fit in extractive metallurgy. The pyrometallurgy of copper is the area from which the example is drawn. Figure 1¹ is a stability diagram for the copper-iron-silica-oxygen system at 1200°C in which the sides are the copper-iron-oxygen, iron-silica-oxygen and copper-silica-oxygen systems. Log P_{O_2} is the vertical axis. This is a type of phase diagram that is coming into more general use today. The iron-silicate phase on the right is reasonably well understood. There is also the liquid copper-silicate slag at the upper left which is stable at relatively high oxygen pressures. A point of interest technically for newer methods for smelting sulfide copper ores is how the two liquid slag fields may join as the temperature is raised. We think that the joining occurs at approximately 1250°C. The fields of stability of these slags are important to our understanding of what controls the loss of copper to the smelting slags, particularly for newer processes. Dr. Crimes will probably have more to say on the matter in a few minutes.

The copper-oxygen-silica ternary system is a portion of the quaternary system just mentioned. We have devoted considerable attention to this system in the recent past. Reference 2 covers the results of a portion of our work.

It is interesting to note that the liquid field in the Cu-Fe-O-S-SiO₂ system at 1400°C extends continuously from pure liquid copper through the oxysulfid phase (matte) to the silicate phase.

One of the diagrams of importance in nonferrous extractive metallurgy is the iron-copper-sulfur system (Fig. 2). We know quite a bit about this system from the work of Krivsky and Schumann³. Technically we are interested in the regions of stability of the liquid sulfide field (matte) near saturation with iron and with copper. There is also great technical interest in this phase with additions of oxygen, of lead, of nickel, etc., but our information on the phase relationships in the pertinent quaternary systems are relatively meager.

The principal point to be made is that these systems are of great technical importance, but our knowledge of them is rather incomplete, principally because of experimental compilations.

References

1. J. F. Elliott; Met. Trans., 1976, vol. 7B, p. 17.
2. A. Luraschi and J. F. Elliott; Proceedings, International Symposium on Copper Extraction and Refining, J. C. Yannopoulos and J. Agarwal, ed., TMS-AIME, 1976, p. 90.
3. W. A. Krivsky and R. Schuhmann; Trans., TMS-AIME, 1957, vol. 209, p. 981.

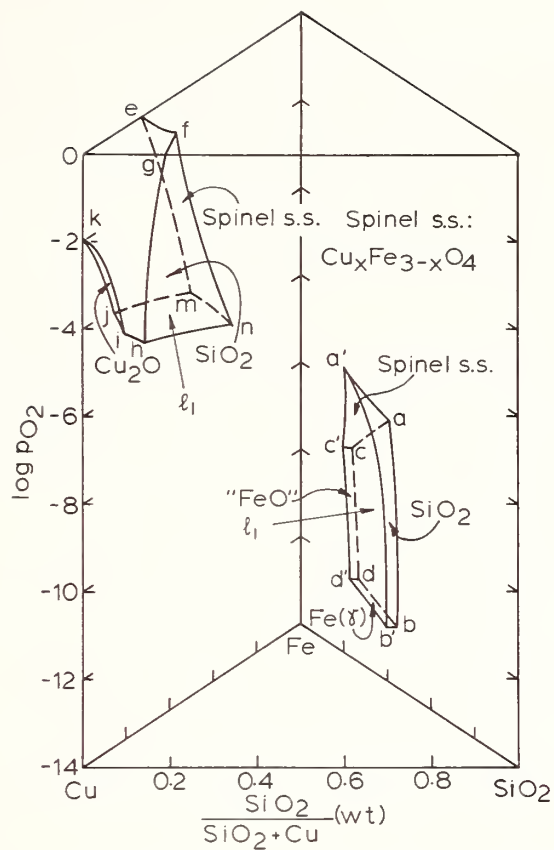


Fig. 1 Stability Diagram of the Cu-Fe-O-SiO₂ System at 1200°C¹.

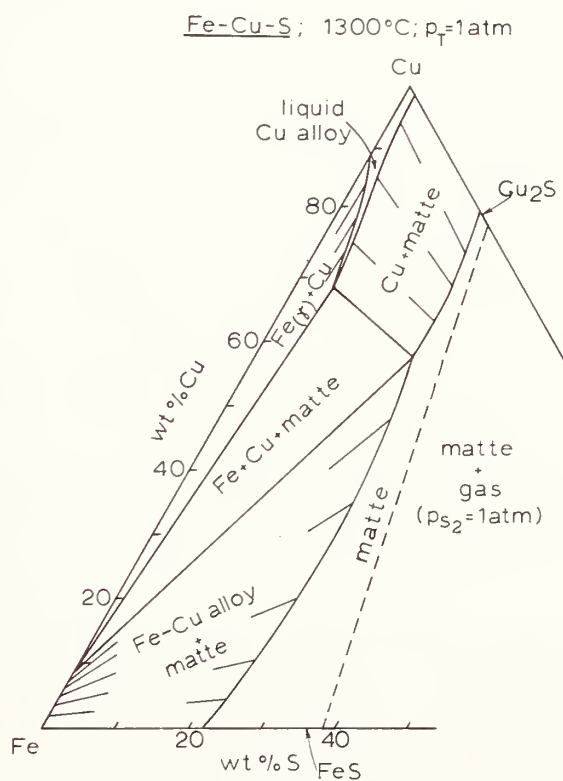


Fig. 2 The Cu-Fe-S System at 1300°C³.



Needs for Phase Diagram Information in Non-Ferrous Industry

P. R. Ammann⁽¹⁾

Kennecott Copper Corporation
Ledgemont Laboratory
Lexington, Massachusetts

Introduction

Professor Elliott, members of the panel, and ladies and gentlemen. I am pleased to have an opportunity to convey to you some of our thoughts on the future of the non-ferrous industry and the need for and use of fundamental data.

A large fraction of primary copper, nickel, cobalt, zinc, etc. is produced by the conversion of intermediate concentrates into metal through pyrometallurgical processes. In these processes, the sulfides are heated and reacted with air to produce sulfur-dioxide-bearing offgases and molten metal or metal intermediates and molten slag wastes. For many years, copper, nickel, cobalt (as well as lead and zinc) have been produced in smelters. In the modern plants, as well as in their age-old predecessors, the key to the pyrometallurgical process is the highly favorable separation of the desirable metal from the undesirable molten wastes (e.g., iron).

Now the non-ferrous metal industry, particularly in the United States, is in a state of change. Both economic and environmental pressures have reduced the profitability of the copper and nickel businesses, as well as those of other non-ferrous industries. These pressures pose both a threat to the health of these businesses and a challenge to these industries to continue to provide the world needs for these metals. The future health of primary metals production lies in a technological base for improving present operations and for innovation in the areas of metal production such that a new generation of processes will develop. Such an evolution could be akin to the transition from the vacuum tube computers of twenty-years ago to solid-state systems we know today.

In the next few minutes I would like to make some remarks on the use of phase diagram information from the point of view of Industrial Research and Development. The metals industry may respond to economic and environmental pressures in several ways.

⁽¹⁾ Paper given by Dr. P. B. Crimes, Ledgemont Laboratory

SLIDE 1

One response is to improve the performance and operability of existing plants. In such systems, the process metallurgy is known. But, improvements in the systems, such as:

- (1) closer process control,
- (2) higher metal throughput,
- (3) minimization of gaseous and other waste products, and
- (4) improved quality of the product,

may require a better definition of the process thermodynamics.

SLIDE 2

The second alternative is to replace conventional process plants by new processes which will lower operating costs. Examples of this approach are:

- (1) the development of the Outokompu Flash Furnace, the Noranda Direct Converting and Mitsubishi Continuous Smelting Processes to replace the reverberatory furnace-converter system for making copper; and
- (2) the development of an alternative process to the Hall Cell for making aluminum.

The substitute processes derive their advantage largely for advances in engineering design. However, more sophisticated processes reach their maximum potential from a complete definition of the thermodynamics in each step.

SLIDE 3

A third direction for R & D is to combine with existing or future processes the capability for the recovery of byproduct metals. Cobalt, and often copper, are byproducts of treating nickel sulfide concentrates. Gold and silver are profitable byproducts of producing copper from copper sulfide concentrates. But there are other metals, such as molybdenum and iron, which could be profitably produced from the non-ferrous smelters as well.

SLIDE 4

Fourth, plants which smelt metal sulfide concentrates generate wastes, such as slags and dusts from offgas streams. These materials contain metal values, which because of present technology limitations, are discarded without being recovered.

SLIDE 5 Finally, metals may derive from new raw materials. For example, many companies now look at deep sea nodules as a source for nickel, copper, cobalt, and perhaps even manganese. Although much published information on processing sea nodules describes hydrometallurgical processes, at least one process has been described by Inco in which the dried material is smelted to separate the small mass of metals from the bulk of the nodule material.

Let us now look at the role of the phase diagram in a couple of copper and nickel smelting processes.

(1) Copper Smelting.

SLIDE 6 Copper sulfide concentrates consist of chalcopyrite, CuFeS_2 and pyrite, FeS_2 . These sulfides are oxidized and heated to 1250°C where a molten iron-copper sulfide matte is produced. Sulfur dioxide gas is generated and iron oxide is fluxed with silica to make a molten slag which is a waste product. These reactions are described simply in the next slide. The molten copper-iron sulfide matte is denser than, and completely immiscible with, the iron silicate which thus permits separation of copper from most of the iron. Depending upon composition, mattes are molten above 1000 to 1100°C . Slags, on the other hand, are more complex, containing in addition to FeO and SiO_2 , Fe_2O_3 , CaO , Al_2O_3 , Na_2O and MgO . Fayalite ($2\text{FeO}\cdot\text{SiO}_2$), the principle slag former has a stated melting point of 1205°C , but higher slag temperatures are used in furnaces.

SLIDE 7 The smelting process is described by the two-phase diagrams in the next slide. A typical copper concentrate contains about 30 per cent copper, 30 per cent sulfur and 40 per cent iron, as shown at the center of the phase diagram on the right. When the sulfide is heated to say 1000°C and oxidized, the sulfide phase becomes enriched in copper, as shown by the red line on the diagram. As the iron is oxidized to FeO , silica is added to produce a low melting, low density slag phase which is immiscible with the sulfide phase. A range of acceptable slag compositions is shown in the $\text{FeO}-\text{Fe}_2\text{O}_3-\text{SiO}_2$ diagram to the left of the slide. When the iron is completely oxidized, the sulfide or matte phase will consist essentially of Cu_2S , plus small amounts of valuable metals such as gold, silver and

trace amounts of impurities such as bismuth, and arsenic. In the final step of the process, the Cu_2S is oxidized with air to blister copper and SO_2 .

The overall process may be carried out in one step (and one vessel), or it may be carried out in several steps.

SLIDE 8 An example of improving existing operations is related to the smelting of the copper sulfide concentrates in reverberatory furnaces. These furnaces are long - over 100 feet - and have a relatively wide but shallow bath of about 5 feet, as shown in this side and top view. In routine operation, sections of the bath solidify, reducing the effective volume of the furnace bath and consequently, the performance of the equipment. In a study described by Kim et al, at the 1976 Annual AIME Meeting, a determination was made of the cause of the formation of these solid materials. Samples were taken throughout the furnace to establish composition profiles and they showed extensive buildups in the furnace. SLIDE 9 The solids were found to be composed of FeO , SiO_2 , Al_2O_3 , and Cr_2O_3 . An $\text{FeO} \cdot (\text{Al Cr})_2\text{O}_3$ (aluminum chromite) phase crystallized in the slag bath as shown here. SLIDE 10 The study showed that by better control over

- (1) the amount of chrome-alumina in the furnace,
- (2) the bath temperature, and
- (3) the depth of the slag,

the rate of bottom buildup could be reduced and, therefore, the productivity and performance of the furnace enhanced.

For this slag system, only part of the phase equilibria is known but with this limited information, some improvements could still be made in future operations. However, if the complete system equilibrium were known, it might be possible to make even further improvements in productivity.

SLIDE 11 As an example of new process technology, the reverberatory furnace just described is being replaced by new copper smelting processes, for example, the Noranda Process. Copper sulfide concentrates are oxidized in one step to crude copper, as shown in the diagram. Such a one-step conversion produces a highly oxidized slag which contains 5 to 10 per

SLIDE 12

cent copper - a significant fraction of the feed copper. To recover this copper, the slag is slow-cooled from 1200°C to 550°C under controlled conditions, in which oxidized copper in the slag is transformed to particles of copper sulfide. These phases are shown in the next slide. The copper values are recovered selectively by milling and flotation; and the copper sulfide is resmelted. This process is an improvement over the conventional reverberatory furnace-converter process. It achieves high copper recovery (better than 95 per cent overall) and acceptable capital and operating costs. In addition, plants can be designed to capture most of the sulfur dioxide and dust emissions, thus meeting today's environmental standards.

But what about opportunities for byproduct metal recoveries? In the flowsheet shown, copper, gold and silver are recovered from the cooled slag, but the iron and the nickel or molybdenum, which occur in some slags in appreciable concentrations, are not recovered. Furthermore, significant amounts of dusts are carried with the furnace gases and are cooled and recovered. Although the dusts contain copper, they are enriched in other elements such as zinc, lead, and antimony.

SLIDE 13

The Noranda process can be modified to employ an electric furnace for recovery of copper from slags. The costs are competitive with the slag milling flowsheet shown in the previous slide, but it allows two other options:

- (1) recovery of iron, molybdenum, nickel, cobalt (if any), zinc and lead from the slag by reduction in a second furnace,
- (2) dusts containing metal impurities can be processed in the electric furnace. If we are clever enough, a process could be developed for the total recovery of not only copper, gold and silver; but also separation and recovery of other metals such as bismuth, lead, and zinc.

We are exploring a number of process flowsheets, for separating and recovering some of the byproduct and metal impurities, but we find that

the required phase diagrams are not available for defining appropriate process conditions to make the necessary metal separations.

(2) Nickel Smelting.

A large amount of the world's nickel is recovered from sulfide minerals. Copper sulfides usually occur in the same ores, so that when metal sulfides, including iron sulfide, are concentrated from the ore, the copper/nickel ratio may vary from 1/2 or 1/3, to as low as 1/12 (Cobalt is another co-product which occurs in these sulfides, but in smaller concentrations.) The smelting processes involve melting the concentrate at about 1250°C, and then oxidizing the iron and sulfur, (making slag and SO₂ gas), and leaving a nickel-copper sulfide matte which contains less than 2 per cent iron. This first step, making a nickel copper sulfide matte, may be carried out by any of several smelting processes. However, the second step, of separating the nickel-copper values, is the most important.

In one early pyrometallurgical process - the now extinct Orford Process - sodium sulfide was added to the liquid nickel-copper sulfide matte. The copper sulfide would selectively dissolve in the sodium sulfide and the lighter copper-sodium and heavier nickel phases would separate upon cooling.

SLIDE 14

This process was replaced by Inco, at Copper Cliff, Canada, in 1948, with a slow-cooling process in which Cu₂S and Ni₃S₂ are selectively formed. Matte from the converter is poured into large pits where it cools slowly over about 3 days. When the temperature reaches about 1700°F, Cu₂S crystallizes first, and when the temperature reaches about 1300°F, a copper/nickel alloy precipitates. Finally at 1070°F, Ni₃S₂ crystals form. The advantage of this process is that the solubility of nickel in the Cu₂S is low (less than 0.5 per cent) and copper in the nickel sulfide is also relatively low. Although Ni₃S₂ contains 6 per cent copper at 1067°F, in slow cooling to 700°F, copper is rejected resulting in a phase containing less than 0.5 per cent copper. This

SLIDE 15

micrograph shows the resulting phases. At the Inco Copper Cliff plant, the cooled matte is crushed, milled to a fine size and the phases separated by flotation.

This process is probably a classic example of the use of phase equilibria for the primary production of non-ferrous metals. Through the knowledge of the phase behavior of the copper-nickel-sulfur system, Inco can achieve both high recovery and high separation of the copper and nickel values.

I would now like to mention briefly some future needs for Phase Diagram information. The extensive information published on binary and ternary systems is used in developing new processes for primary metal production, and also for processes to recover byproduct metals and for processing wastes, such as flue dusts. To predict specific needs for phase diagram information in the future is to crystal ball the directions industry will take in the future to produce the primary metals. And this, of course, is a chancy business.

SLIDE 16

Let me suggest generally that the quaternary systems need more definition. In particular, we have been looking at a process to extract molybdenum from copper smelting slags. It involves the reduction of molybdenum from slags into a sulfide phase. There is only limited information on the metallic-sulfide phase, Mo-Fe-Cu-S, as shown in the slide. Our researchers have attempted to obtain some data on this system. Of interest also is the slag phase, consisting principally of Mo-Fe-SiO₂-oxygen. (As I noted earlier, such slags usually contain other important components such as MgO, Al₂O₃, CaO, which have an impact on equilibria and melting points.) After the molybdenum and copper have been extracted from the slag into the metal sulfide, it is necessary to separate and recover the molybdenum and copper values. Although this step can be achieved by conventional hydrometallurgical processes, we have been intrigued by Inco's slow-cooling process, just described as a possible alternative route.

The recovery of byproduct nickel and cobalt from certain smelter slags is analogous to the molybdenum system, and should be important in

the future. In addition, the smelting of nickel sulfide concentrates will probably undergo some important changes in the near future in order to meet environmental requirements and to accommodate new ores. Therefore, I see a need for further information on this system.

Another system of interest includes bismuth and lead in copper smelting. The need is two-fold: (1) to control the level of these impurities in the copper product, and (2) to devise processes for separating and recovering these metals. At present, there is a lack of pertinent information on the phase relationships in these complex systems. I might just add another area of importance - the presence of trace elements in copper products. Small amounts of impurities such as As, Bi, Te, S, Sb, Pb, etc., can affect the properties of copper product markedly and additional information on these systems is also needed.

Summary

To summarize; in the future, pyrometallurgical processes for producing copper and nickel will become more efficient and sophisticated. A sound thermodynamic base is essential for smelting processes to meet our future needs in these areas. In these past few minutes I have tried to show how phase diagrams are used and to suggest some future directions for equilibria studies in commercially important systems.

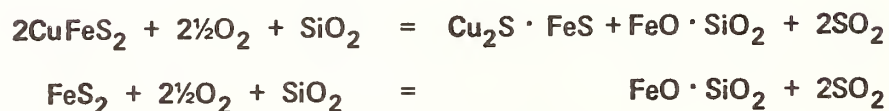
OPPORTUNITIES FOR R & D IN
NON-FERROUS METAL PRODUCTION

1. IMPROVE PERFORMANCE AND OPERABILITY OF EXISTING PROCESSES
2. DEVELOP NEW PROCESSES WITH LOWER COSTS
3. INCREASE RECOVERY OF BY-PRODUCT METALS
4. PROCESS WASTE STREAMS FOR SAFE DISCARD OR FOR METAL PRODUCTION
5. TREAT NEW RAW MATERIALS

SLIDES 1 to 5

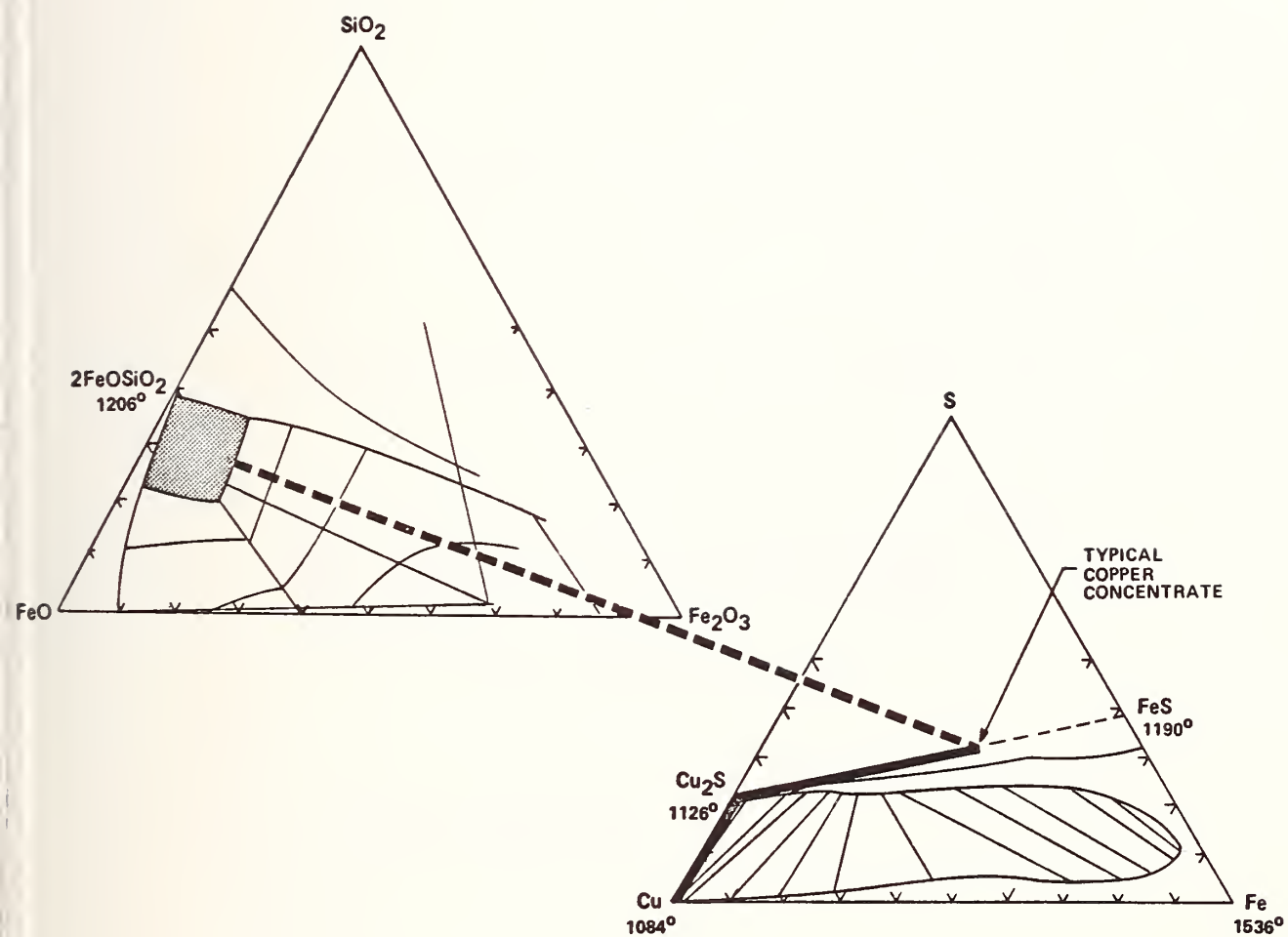
Description of Opportunities for R&D in
Non-Ferrous Metal Industry

PRINCIPLE COPPER SMELTING REACTIONS



Slide 6

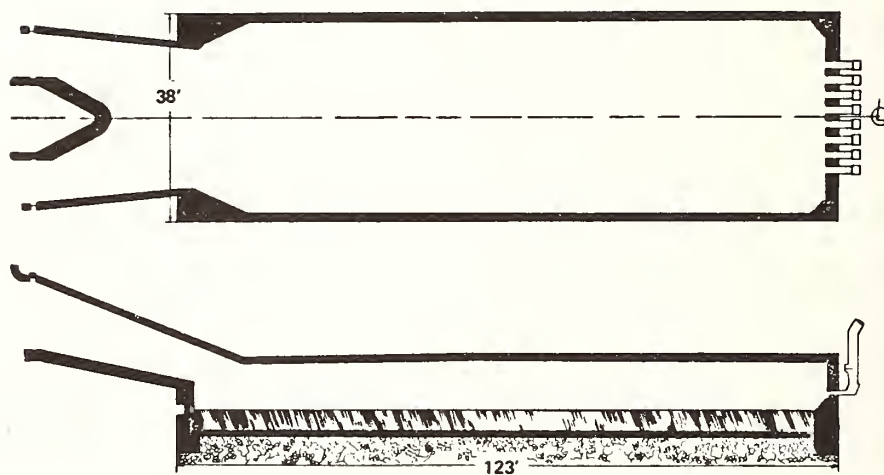
Principle Oxidation Reactions for
Smelting Copper Concentrates



Slide 7

PRA1677

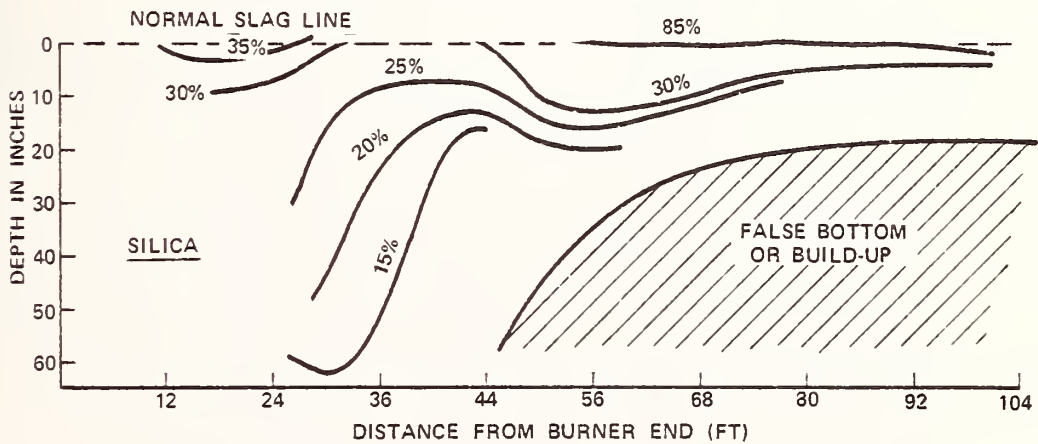
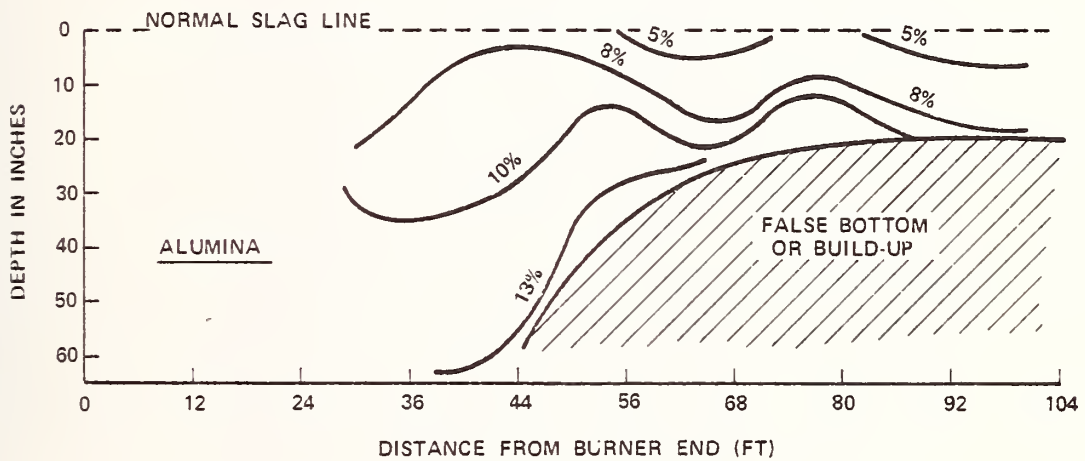
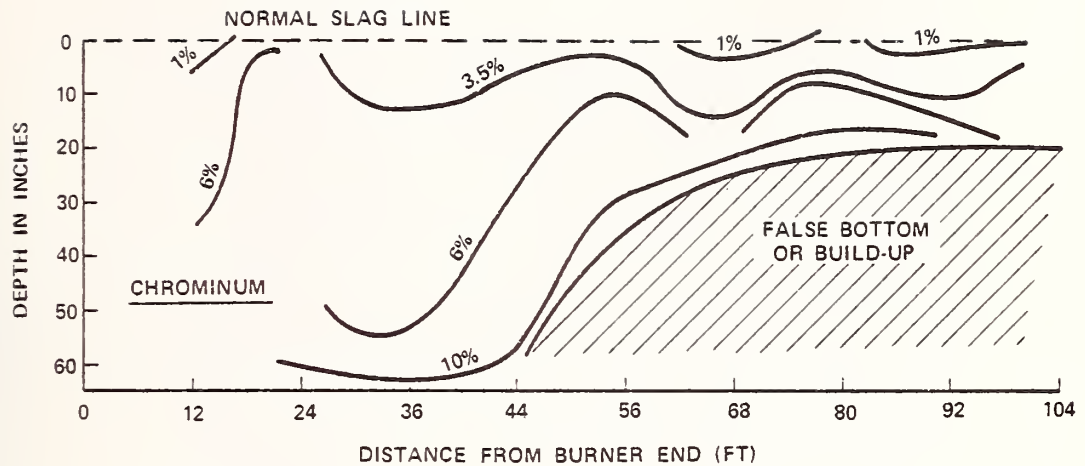
Key Phase Diagrams for Smelting Copper Concentrates
Showing Formation of Matte/Copper and Slag Phases



PLAN — REVERBERATORY FURNACE

Slide 8

Plan and Side Views for Typical Reverberatory
Furnace Used For Smelting Copper Concentrates



CONCENTRATION PROFILE OF SLAG

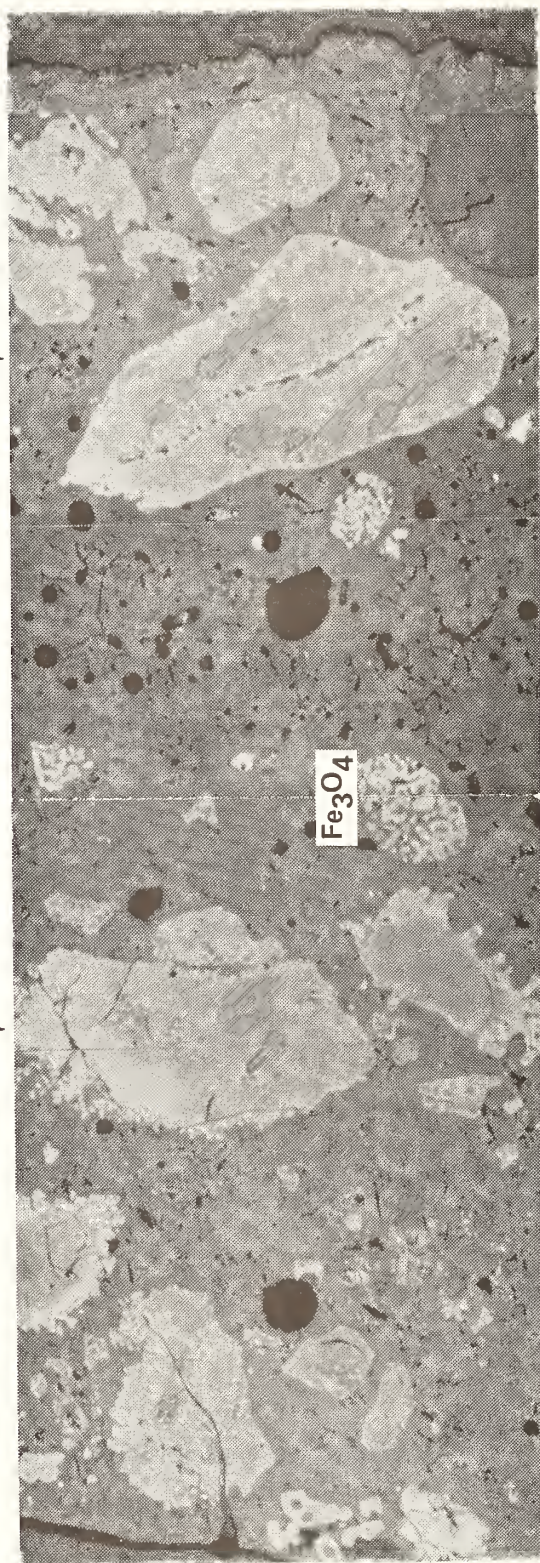
Slide 9

Concentration Profiles for Chromium, Alumina
and Silica in Reverberatory Furnace

MICROGRAPH OF BOTTOM LAYER OF SLAG

$\text{FeO} \cdot (\text{Al Cr})_2 \text{O}_3$

Normal Slag Matrix



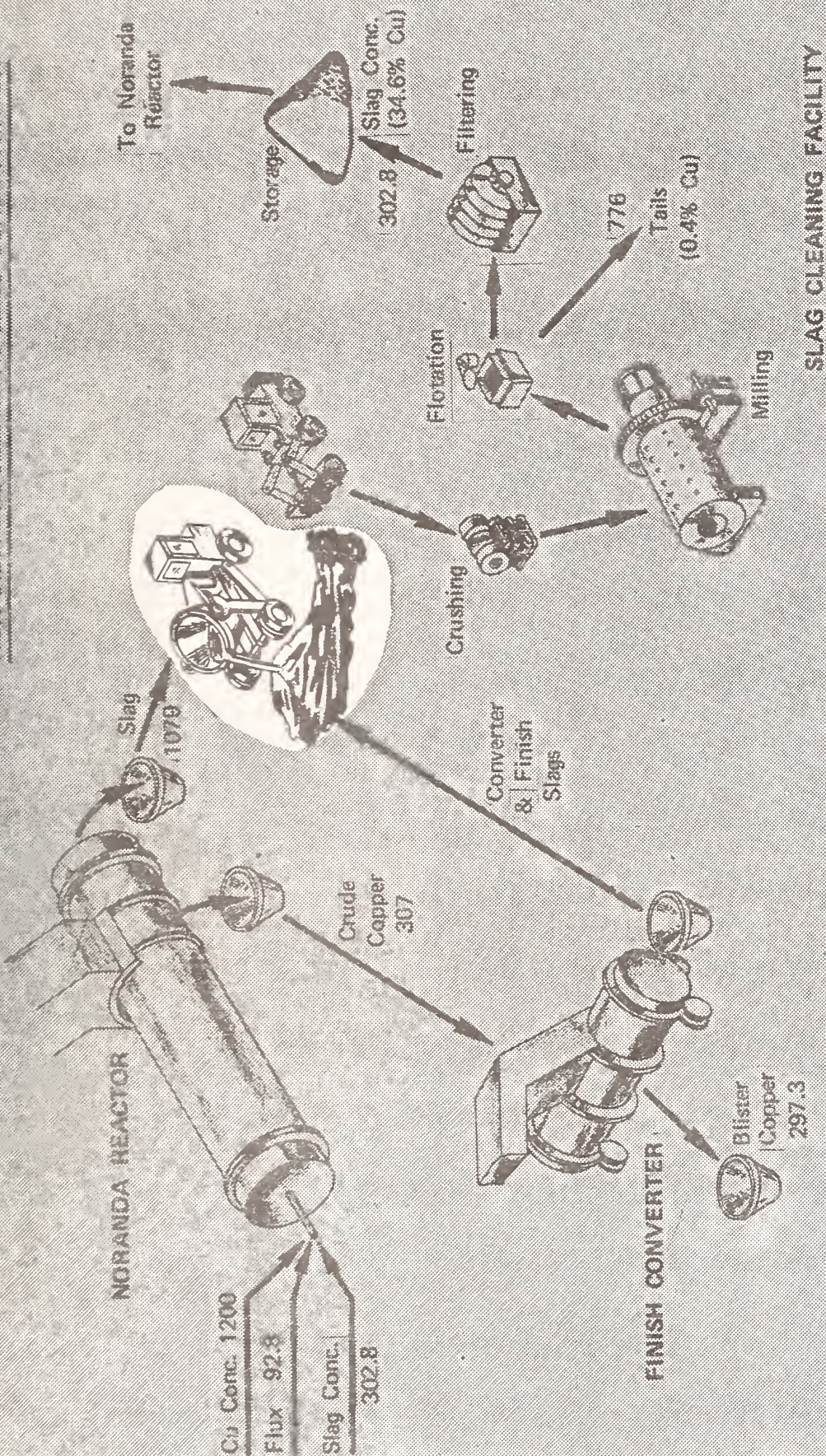
Fe_3O_4

1 MM

Slide 10

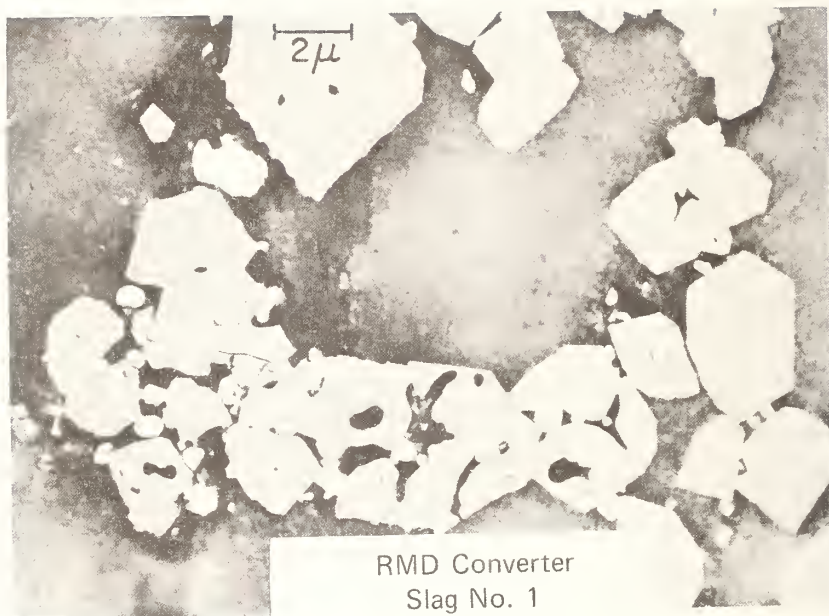
Photomicrograph Showing Major Phases in
Reverberatory Furnace Bottom
(Ref. Kim, J.J. et al, Int. Symposium on Copper
Extraction & Refining, AIME, Feb. 22-26, 1976,
pp 139-153)

NORANDA PROCESS WITH SLAG CONCENTRATOR



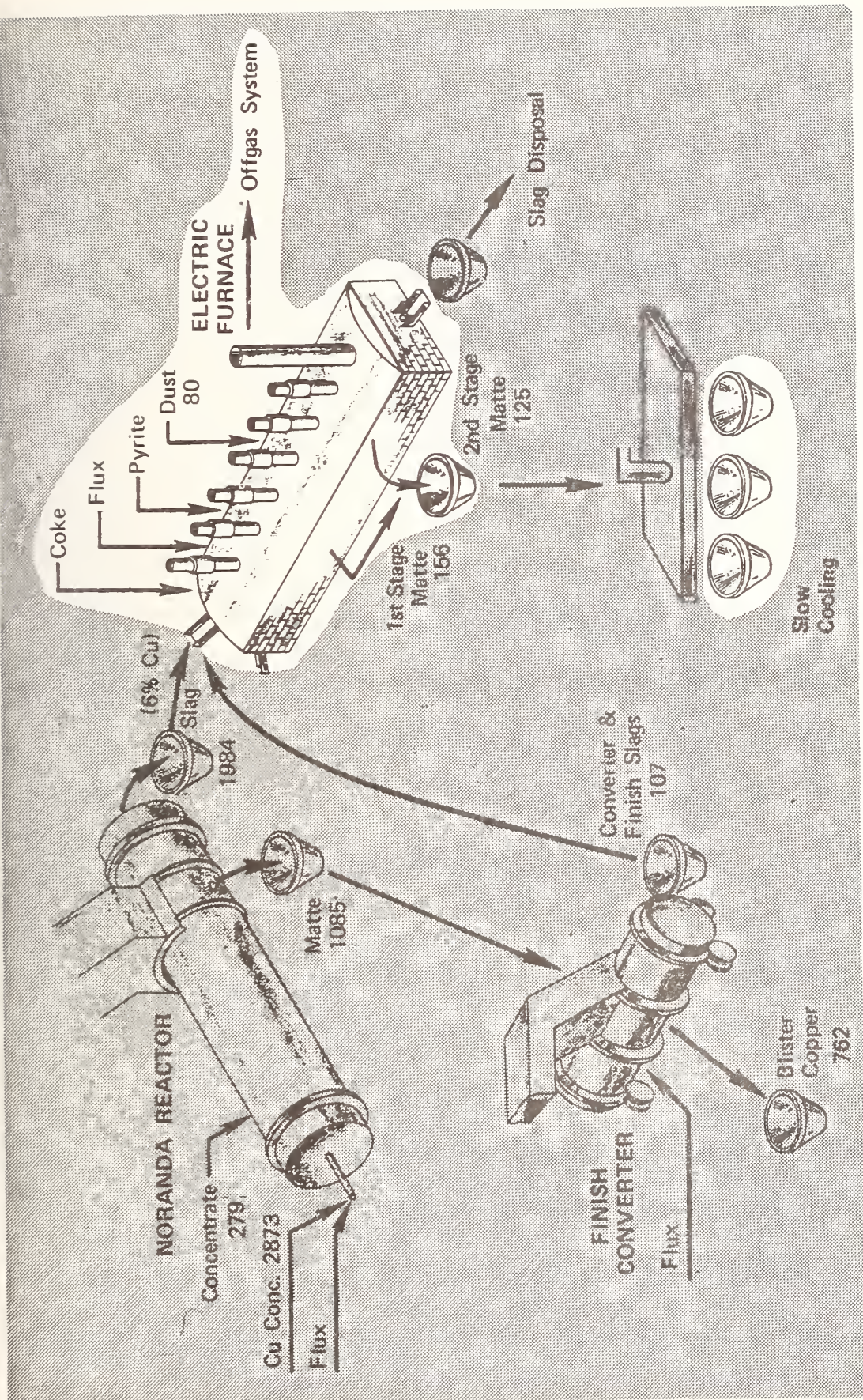
Slide 11

Schematic Diagram of Noranda Process Showing Cooling of Slag as Important Process Step



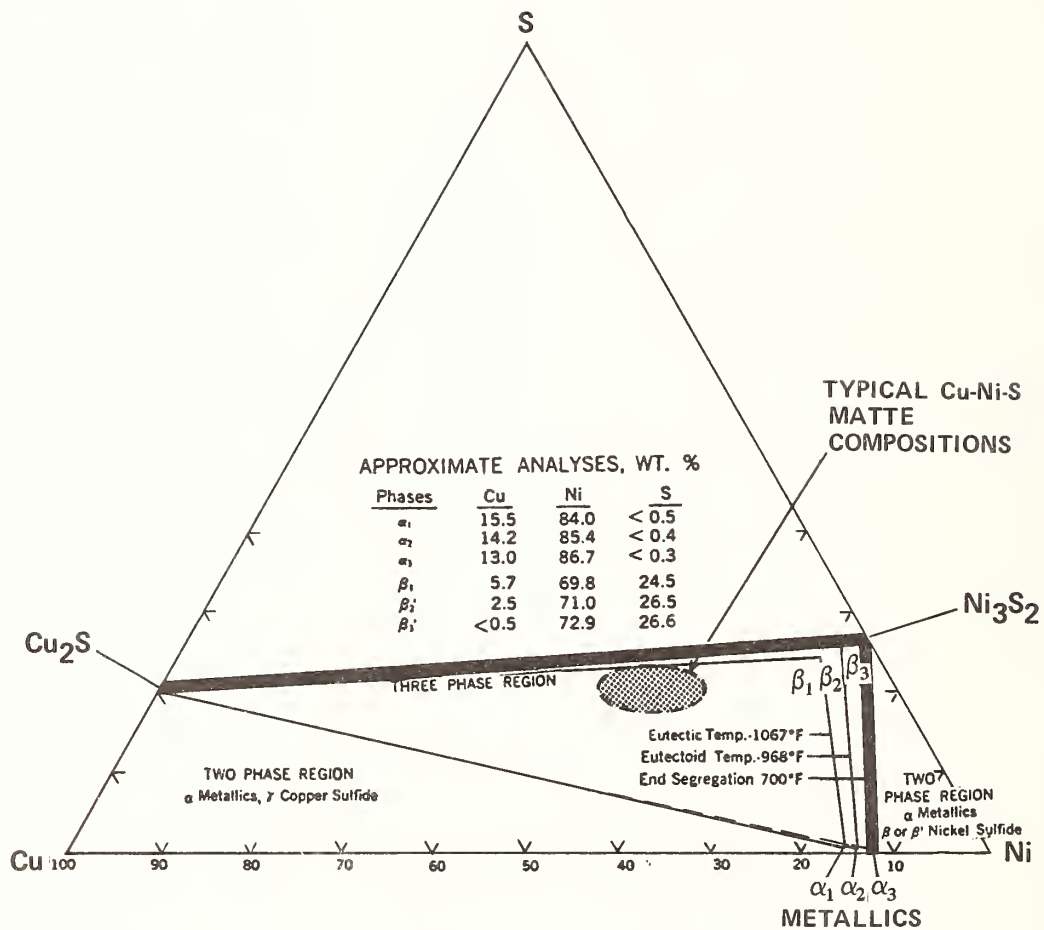
Slide 12

Photomicrograph Showing Copper and Magnetite
Phases in Cooled Converter Slag



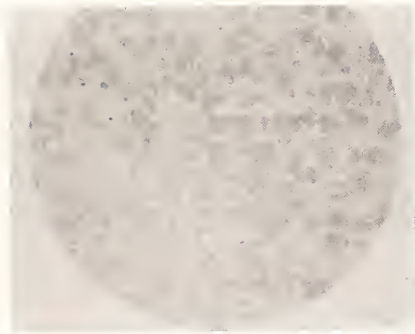
Slide 13

Schematic Diagram Showing Electric
Furnace Slag Cleaning for Noranda Process



Slide 14

Diagram Showing the Phase Separation for Copper–Nickel Sulfide Matte as a Function of Temperature and Composition (Ref. Boldt, J.R. & Queneau, P., "The Winning of Nickel," D. Van Nostrand Company, Inc., Princeton, N.J., p. 278)



QUENCHED MATTE



SLOW COOLED MATTE

Ref: The Winning of Nickel

Slide 15

Photomicrograph Showing Effect of Cooling Rate on Grain Size for Copper and Nickel Sulfides (Ref. Boldt, J.R. & Queneau, P., "The Winning of Nickel," D. Van Nostrand Company, Inc., Princeton, N.J., p. 276)

SYSTEMS OF POSSIBLE
FUTURE INTEREST

- { Mo - Fe - Cu - S
Mo - Fe - SiO₂ - O
- Bi - Pb - Cu - Fe - S - (O)
- Cu - Fe - SiO₂ - O - (S)
- Ni(Co) - Fe - SiO₂ - O - (S)

Slide 16

Metallurgical Systems of Future Interest

DISCUSSION

J. F. Elliott - Thank you, Peter, for your interesting remarks. I might add that phase diagrams often are equivalent to road maps for the process metallurgist. He uses them to find his way through the equivalent of unfamiliar terrain.

Bruce Connor - I wish to thank Dr. Crimes for his excellent review of important aspects of copper and nickel smelting. I would like to add that we have a lot of other phase equilibria that need to be understood in the handling of recycling of secondary copper and nickel alloys. Because precious metals, such as iridium, platinum, pladium, gold and silver are obtained when processing copper and nickel ores, we also have need for more information on the binary, ternary and quaternary phase diagrams of these metals.

J. F. Elliott - It might be noted that nonferrous metals producers usually have to contend with virtually all of the metals and many of the nonmetals in the periodic table. Accordingly, they face great complexity in their systems.

P. Crimes - It may be of interest to the audience to know that we have made considerable progress in understanding kinetic and mass-transfer aspects of our systems, and now we are greatly in need of more and better information on equilibrium relationships.



Primary Metals Production

Dr. H. R. Larson
ASARCO Incorporated
Central Research Department

Asarco is a large, diverse, primary non-ferrous company involved among other things in the smelting of Cu, Pb, Zn and precious metals. We are largely a custom smelter treating a wide variety of materials. This fact has an important effect on our outlook and on some of the remarks I will make today. Our metallurgy is extremely complex. We have many materials flowing between plants i.e., from Cu smelter to Pb smelter, etc. In addition to the primary metals we recover a large array of by-product elements which are very important to us. Several of our plants have what must be considered high impurity loads. This adds to the complexity.

What is our interest in Phase Diagrams?

We are of course interested in anything that improves our understanding of the processes used in our plants. I think however that there are a few areas of practical considerations where phase diagrams can be especially important. (Slide 1) First, factors controlling or affecting metal losses to slag are highly important. Our operating revenues are derived from a smelting charge. Obviously, metal losses reduce profitability. Secondly, we are interested in multi-component multiphase equilibria. The distribution of elements between phases during smelting and pyrometallurgical refining operations is of importance. In particular, the distribution of impurity, by-product elements between phases is of interest. Third, a good deal of our work at the Research Department involves the theoretical evaluation of process alternatives. This can range anywhere from minor changes in an existing process to consideration of a new continuous smelting process. In any of these considerations phase diagrams can be of particular use when they are available. As an example, I could point to the published work of Queneau and Schuhmann on the application of the Q-S process to lead smelting.

Let me start off by making the point that our use of phase diagrams is limited. This is primarily because they are not readily available for the systems of most interest to us. We do use the standard compilations of diagrams, such as: 1. Hansen and 2. Elliott and Shunk's supplements, 3. "Phase Diagrams for Ceramicists" by Muan and Osborn, and I tend to also use 4. W. Guertler et.al. "Compendium of Constitutional Ternary Diagrams of Metallic Systems" as translated from German and published by the U. S. Department of Commerce. In general, the real world systems of interest are more complex than those for which diagrams are available. We use the compilations of diagrams to gain insight into our real systems. Often we are interested in multicomponent systems not adequately described in the literature.

Let me digress for a minute and say something about the phases that are of most interest to us. (Slide 2)

Metal

Here we are in the best shape. Good information is available on all binary systems and many ternary systems. Impurity elements of interest are often in relatively dilute solutions. In the case of lead refining, concentrations may be appreciable and available data serves us well. There is a lack of information on impurity interactions. Activity data would be of great use were it available particularly at varying sulfur and oxygen potentials. The formalization of interaction coefficients available for elements dissolved in iron which has been used for many years should be extended to Cu solutions and Pb solutions. In some cases, such as Pb, the activity of alloying elements would be of interest in the liquid state over a fairly large temperature range.

Alloy development work, i.e., brasses, bronzes and solders is hampered by the lack of phase diagrams or their equivalent for multicomponent systems. Here I am talking of conditions where the substitution of a relatively small amount of a substance can have rather profound effects on alloy properties.

Slag

Of all the phases I have listed slags are perhaps the most interesting, most important, most investigated and least well understood. Metal losses to slag are a major concern. The copper content of reverb slag put to waste at a single smelter can easily exceed \$1,000,000/yr. The Cu content of throw away slags is nearly as high as the ore that is mined from the earth.

Our slags are essentially CaO-FeO-SiO_2 , a system well defined in the literature. However, our slag will contain several percent Al_2O_3 and usually more than 1% MgO . The slag may or may not be saturated with magnetite. ZnO is usually present and, in the case of lead slags, can run to levels of 10-15%. Frequently the slags are equilibrated with a sulfur bearing matte and the slag will contain some sulfur. These complex real slags are not adequately described by phase diagrams. A recent monogram by Prof. Diaz sponsored by INCRA "The Thermodynamic Properties of Copper-Slag Systems" has gathered a great deal of information on copper smelting slags. Similar data is not available for lead smelting slags.

Metal losses in slag occur both as solution and as particulate entrainment. The interrelation of composition and slag viscosity and surface tension are of importance.

The operation of conventional lead blast furnaces requires special properties in sinter. Up until the time of fusion the sinter must maintain enough strength to support a column of burden on top of it. A sharp melting point is important. Once smelted it must form a free flowing low viscosity slag. The presence of a mush or partially molten mass can be disastrous. Selection and control of slag composition is important in this regard. Additional phase diagrams could be of help.

Matte

Matte is a phase consisting of several sulfides in solution. In its simplest form we think of matte as a mixture of Cu_2S and FeS . Again this binary is well defined as is the Cu-Fe-S ternary. Real mattes, especially at a custom smelter, will contain PbS , As_2S_3 , Sb_2S_3 , NiS and in the case of dross reverb matte Na_2S_x .

Added confusion comes from the ability of matte to dissolve magnetite. Activities of impurities in matte are not well known. Interaction data is almost totally non-existent.

Speiss

Speiss is a very interesting phase that is often overlooked. Speiss can be thought of as a solution of metal arsenides. It consists primarily of Cu, Pb, As and Sb. Antimony can substitute fairly freely with As. Several intermetallic compounds are present. I have never seen a Cu-Pb-As-Sb phase diagram. Little data is available on the ternary systems. It would be especially interesting. Speiss can also contain appreciable quantities of Fe, Ni, Sn, In, Ag, S and Bi. Phase diagrams for complex, multicomponent, arsenide systems are non-existent.

Perhaps the most complex thermochemistry occurring anywhere takes place in the dross reverberatory furnace of a lead smelter. Three phases, bullion, speiss and matte interact with each other with a considerable temperature gradient existing across the three phase bath. The distribution of at least 7 elements between these phases is of importance. These include Pb, Cu, As, S, Sb, Na and Ag.

DISCUSSION

J. F. Elliott - Thank you very much, Dr. Larson. There certainly are a number of interesting phase relationships in the field in which you work.

Reed Howald - Are there good data on the binary systems in the copper-lead-arsenic-antimony system?

Dr. Larson - The binaries are reasonably well known; the ternaries are not. We know essentially nothing about the quaternary system.

PRACTICAL CONSIDERATIONS

1. METAL LOSSES TO SLAG

2. DISTRIBUTION OF ELEMENTS BETWEEN PHASES

**3. THEORETICAL BASIS FOR THE EVALUATION OF ALTERNATE
TECHNOLOGIES**

PHASES

1. METAL

Blister Cu, Anode Cu, Lead Bullion

2. SLAG

Reverb Slag, Converter Slag, Blast Furnace Slag

3. MATTE

Reverb Matte, Converter Matte, Dross Reverb Matte

4. SPEISS

Dross Reverb Speiss



Use of Phase Diagrams in Iron and Steelmaking

Robert D. Pehlke

Department of Materials and Metallurgical Engineering
The University of Michigan, Ann Arbor, MI 48109

INTRODUCTION

Phase diagrams are particularly important in iron and steelmaking. In fact, the processing and products of the iron and steel industry can be described essentially in terms of the iron-carbon phase diagram. Furthermore, the phase relationships, particularly in oxide systems, reflect the refining steps during smelting and converting of iron in the ironmaking and steelmaking processes, respectively.

The iron and steel industry is presented with several processing problems that can be solved in part on the basis of phase diagrams. Consequently, there is a pressing demand for the study of certain phase relationships in iron and steelmaking systems. The following paragraphs summarize current processing and the requirements for solution of several problems, as well as the development of new processing based on these thermochemical relationships.

IRON AND STEELMAKING VIA PHASE RELATIONSHIPS

The phase diagram central to iron and steel production is that for the iron-carbon system, as illustrated in Figure 1. This phase diagram reflects the structural relationships which define the wide variety of cast irons and steels, as reflected in their heat treatment, in terms of the temperature-composition diagram for the iron-carbon system.

Recognizing that phase equilibrium relationships are of direct importance in iron and steelmaking, several challenges in processing as well as the potential for new processes, should be considered in terms of phase relationships. Some examples are presented in the following paragraphs.

EXAMPLES OF PHASE EQUILIBRIA REQUIRED FOR IMPROVED IRON AND STEELMAKING

The iron and steel industry faces a wide variety of challenges in terms of raw materials, energy and the environment. New and improved processes are necessary to meet these needs. In many cases, phase equilibria are required for the development of new technologies. The following examples are representative of instances where phase equilibria must be defined to accomplish these processing advances.

The iron blast furnace must utilize new charge materials, some of which contain higher concentrations of the alkali oxides, K_2O and Na_2O which have recently become a major concern to the ironmaking industry. High slag basicities and high hearth temperatures can result in concentration of these materials, even at relatively low concentrations in the burden, to cause operating problems such as high blast pressures, burden hangup and coke deterioration, and also to reduce lining life by inducing physical abrasion and chemical attack of refractories.

At the present time several blast furnaces in the industry are being monitored with respect to alkali input. However, an opportunity exists for control of these alkali metals in terms of the particular slag and fluxing

agents employed, as well as by controlling gas phase reactions in terms of oxygen potentials, CN reactions, and other aspects of the gas phase composition and temperature profiles in the furnace. It is widely recognized that recirculation with possible concentration of elements exists for alkali metals and also for silicon, in terms of SiO formation. Further studies of these phase equilibria are required.

The iron and steel industry has periodically undergone reviews of substitutes for fluorspar as a flux, particularly in steelmaking. At the present time the supply of fluorspar and its relative cost, as well as an increase in usage with the adoption of the oxygen steelmaking process, require that substitutes be developed. First of all, the fluxing role of fluorspar, particularly in reducing the liquidus temperatures for phases in equilibrium with dicalcium silicate, has not been fully defined, nor has the chemical role of fluorspar in the steelmaking process. In considering a potential shortage of fluorspar, the steel industry has undertaken a wide variety of full scale plant tests on many substitutes. These include the boron-bearing materials colmonite, razorite and borax. Manganese-bearing materials such as manganese ore, cametco briquettes and urucum ore have been studied. Materials relatively high in calcium oxide and containing some iron oxide including red lime, BOP dust mixed with lime, and alaflex have been tested. Aluminum oxide-bearing materials have been employed in plant trials on aluminum dross, bauxite, and topaz as fluxing agents. In addition, the titanium-bearing materials, ilmenite and soreflux, have also been considered.

A dozen or more specific processing steps for heat treatment, stress relieving, preheating for welding, carburizing, nitriding, solution treating, preparation for forging, and other hot working operations, as well as the development of desired structures, can be described in terms of this basic phase diagram, as shown in Figure 2. Furthermore, the influence on this phase diagram on various elements which commonly appear in steels has been developed for most alloying additions.

The refining of iron and steel is dependent upon the use of a suitable slag system. Normally, basic processing is used in which a slag with relatively high concentrations of calcium oxide (and magnesium oxide) is used to refine the iron-base liquid. Phase relationships in the $\text{CaO-SiO}_2\text{-FeO}$ system represent a base system for steelmaking; calcium oxide is added as lime flux, silica is a reaction product in the steelmaking process, and iron oxide is developed by oxidation of the iron bath during the conversion of steel. This phase diagram is presented in Figure 3. Of particular interest are the liquidus phase equilibria for dicalcium silicate ($2\text{CaO}\cdot\text{SiO}_2$), a high melting reaction product which must be fluxed in the steelmaking process.

In the iron blast furnace process, the $\text{CaO-SiO}_2\text{-Al}_2\text{O}_3$ (or $\text{AlO}_{1.5}$), system is particularly important. An activity plot for SiO_2 in this system is presented in Figure 4 to emphasize the importance of the interrelationship between activities of components in systems and their phase equilibria. It should be noted that this diagram was developed by John Chipman utilizing both phase equilibria and thermochemical data to calculate the activity of silica in this system, an important chemical parameter in the blast furnace process.

The fact that plant tests have been conducted indicates the seriousness of the problem, as well as the commitment of the industry to adoption of new fluxing materials. In all cases, phase relationship information is lacking and sorely needed.

Tramp elements represent a serious threat to the economical production of many high quality steel products. Arsenic and antimony which are present in some iron ores, and copper, nickel and tin which result from the use of relatively low quality scrap present challenges to current processes. These elements have a deleterious influence on product properties and service performance, and are not removed in the standard practices for iron or steelmaking. A knowledge of phase equilibria is required to develop control of tramp elements. This question can be presented in a different manner. The result is to be a processing step in which these tramp elements are selectively removed from the iron-base product. The processing systems to be used, which typically are specified, in this case remain to be defined.

Finally, an understanding of phase equilibrium relationships is needed for control of sulfur and phosphorus, the bane of a steelmaker's existence. A number of studies have been made of sulfur distribution between metal and slag under a wide variety of conditions. Unfortunately, in many instances the oxygen potential was undefined and the studies are of questionable value in terms of development of new processing systems to improve sulfur removal. A substantial amount of capital investment and operating costs are now being directed toward sulfur control. These industrial processing steps could be

enhanced by a better understanding of the role of oxygen potential as well as the phase distribution relationships for sulfur between slag, metal, and gas under a wide variety of composition and temperature conditions. Phase equilibria in liquid and solid iron are required for sulfides and oxy-sulfides of various alloying elements and refining additives.

Phosphorus has not presented a major problem for western hemisphere steelmaking in that for the most part we have been blessed by relatively low phosphorus burden materials. However, as new iron-steelmaking processing systems are being adopted worldwide, e.g. the direct reduction-electric furnace melting system, the role of phosphorus has taken on a new aspect. First of all, phosphate phase equilibria in normal iron and steelmaking slags have not been thoroughly defined. Furthermore, pre-reduced iron ores containing phosphates can be greatly improved if the phosphorus remains as phosphate and is not reduced during direct reduction processing. An improvement in quality and development of control measures to optimize direct reduction processing of iron ore for use in subsequent steelmaking operations requires additional information on the phase equilibria which prevail during phosphate reduction.

The few examples presented here are only illustrative of the wide variety of challenges and potential improvement in iron and steelmaking processing which can be accomplished through a knowledge of phase equilibria. The further spinoff of such knowledge in areas of nonferrous processing as well as other high temperature processing such as coal conversion and other energy generating systems should also be recognized. One example is the thermochemistry of iron oxides. This system is central to slag formation

in iron and steelmaking, but also is important in magnetic separation of iron concentrates in mineral processing systems, the undesirable formation of high melting magnetite-rich phases in copper concentrate smelting, and the processing of iron-bearing materials in the production of various electronic components. The control of iron oxide chemistries in a wide variety of high temperature chemical reactions is dependent upon a knowledge of the thermochemistry and phase relationships in the iron-oxygen system.

SUMMARY

Phase relationships play a very significant and prominent role in production of iron and steel. These phase relationships are reflected in the variety of products and structures which can be produced, and are particularly important in the processing steps that are utilized to achieve them. The refining of iron and steel as reflected by slag-metal equilibria and the corresponding phase relationships are most important to development of present and future industrial processes.

A wide variety of specific systems relating to present and future iron and steelmaking processes are in need of further investigation and clarification. The interrelationship between thermochemical data and phase diagrams should be recognized and applied to interpret and evaluate phase equilibria, and should be utilized in their deployment as the foundations of process development.

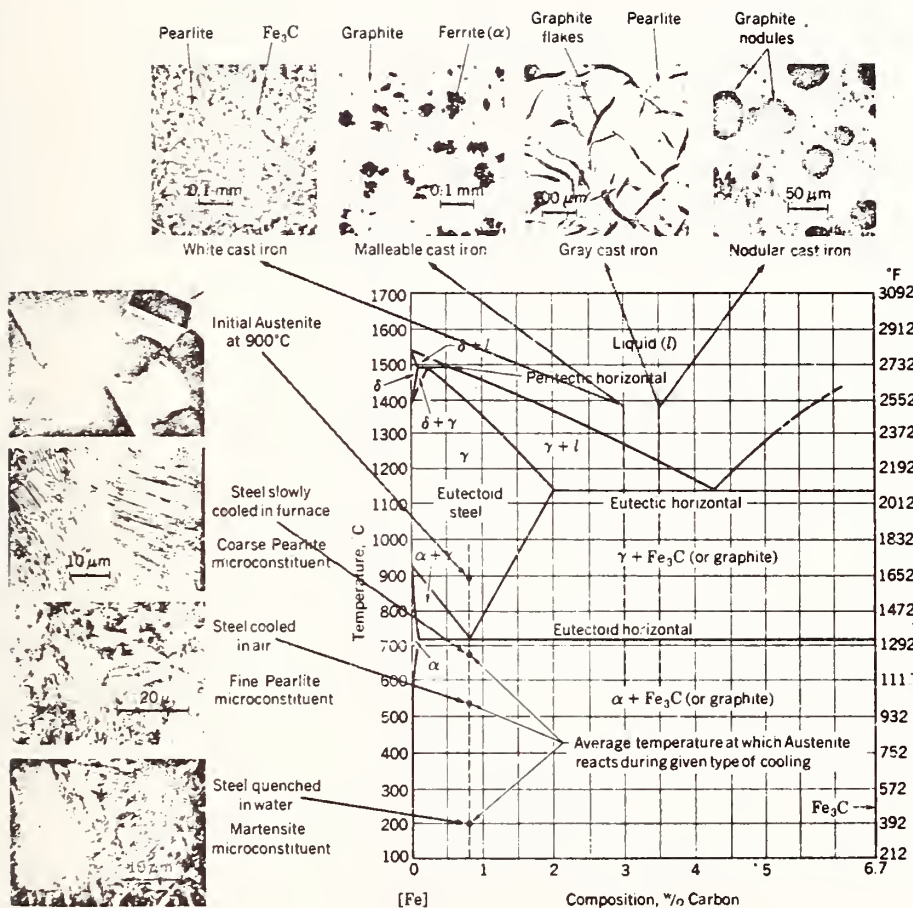
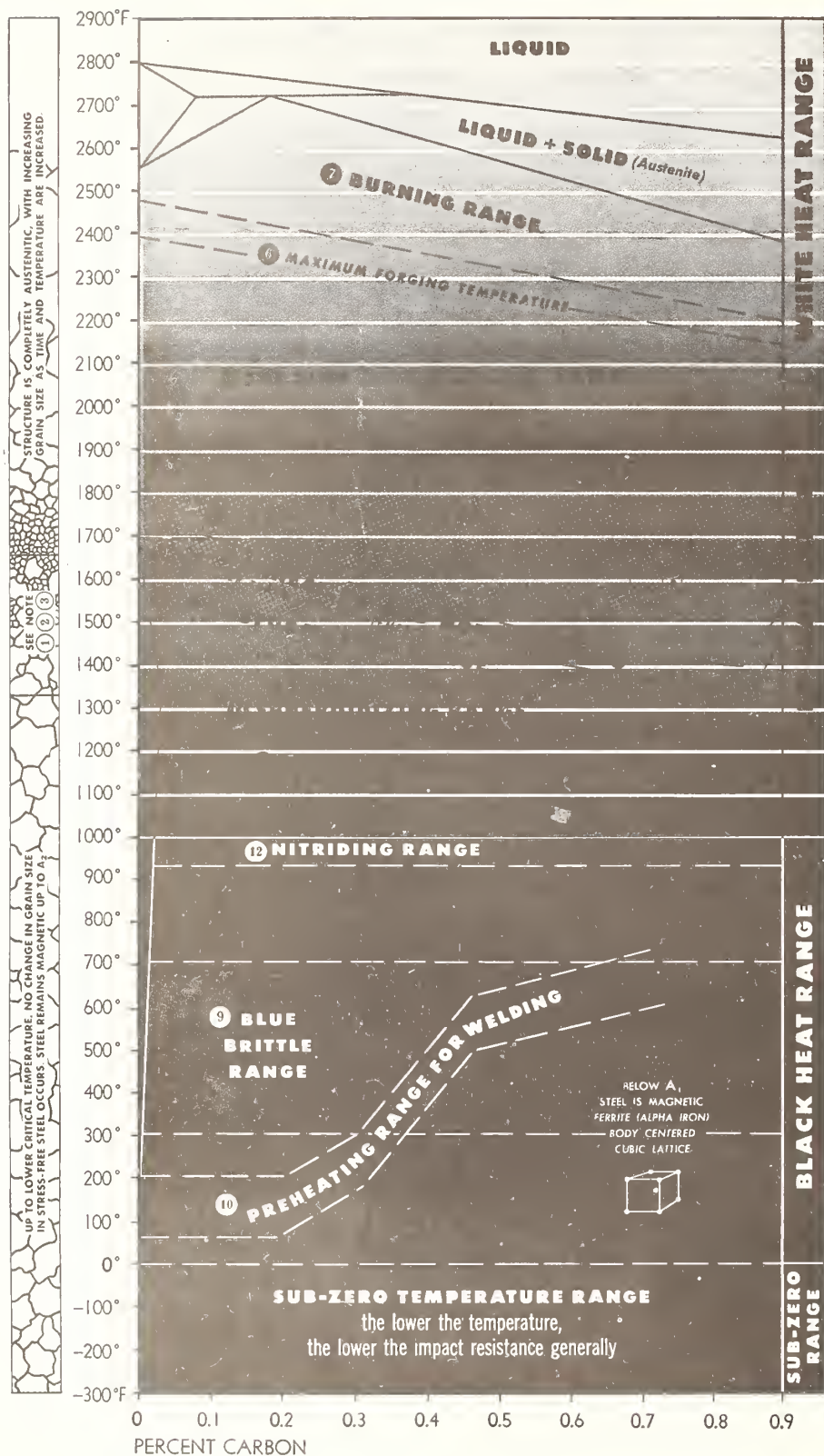


Figure 1. The iron-carbon phase diagram and photomicrographs illustrating the nonequilibrium behavior of a eutectoid steel (0.8 % C) and of typical cast irons. (Photomicrographs from Research Laboratory, U.S. Steel Corporation, Malleable Research and Development Foundation, and International Nickel Company.) From: Essentials of Materials Science, A.G. Guy, McGraw-Hill, 1976, p. 93.

Basic Guide to Ferrous Metallurgy



- 1 **TRANSFORMATION RANGE.** In this range steels undergo internal atomic changes which radically affect the properties of the material.
- 2 **LOWER TRANSFORMATION TEMPERATURE (A₁).** Termed A₁ on heating, A₁ on cooling. Below A₁ structure ordinarily consists of FERRITE and PEARLITE (see below). On heating through A₁ these constituents begin to dissolve in each other to form AUSTENITE (see below) which is non-magnetic. This dissolving action continues on heating through the TRANSFORMATION RANGE until the solid solution is complete at the upper transformation temperature.
- 3 **UPPER TRANSFORMATION TEMPERATURE (A₃).** Termed A₃ on heating, A₃ on cooling. Above this temperature the structure consists wholly of AUSTENITE which coarsens with increasing time and temperature. Upper transformation temperature is lowered as carbon increases to 0.85% (eutectoid point).
- 4 **FERRITE** is practically pure iron (in plain carbon steels) existing below the lower transformation temperature. It is magnetic and has very slight solid solubility for carbon.
- 5 **PEARLITE** is a mechanical mixture of FERRITE and CEMENTITE.
- 6 **CEMENTITE** or IRON CARBIDE is a compound of iron and carbon, Fe₃C.
- 7 **AUSTENITE** is the non-magnetic form of iron and has the power to dissolve carbon and alloying elements.
- 8 **ANNEALING**, frequently referred to as FULL ANNEALING, consists of heating steels to slightly above A₃, holding for AUSTENITE to form, then *slowly* cooling in order to produce small grain size, softness, good ductility and other desirable properties. On cooling slowly the AUSTENITE transforms to FERRITE and PEARLITE.
- 9 **NORMALIZING** consists of heating steels to slightly above A₃, holding for AUSTENITE to form, then followed by cooling (in still air). On cooling, AUSTENITE transforms giving somewhat higher strength and hardness and slightly less ductility than in annealing.
- 10 **FORGING RANGE** extends to several hundred degrees above the UPPER TRANSFORMATION TEMPERATURE.
- 11 **BURNING RANGE** is above the FORGING RANGE. Burned steel is ruined and *cannot be cured* except by remelting.
- 12 **STRESS RELIEVING** consists of heating to a point below the LOWER TRANSFORMATION TEMPERATURE, A₁, holding for a sufficiently long period to relieve locked-up stresses, then slowly cooling. This process is sometimes called PROCESS ANNEALING.
- 13 **BLUE BRITTLE RANGE** occurs approximately from 300° to 700° F. Peening or working of steels should not be done between these temperatures, since they are more brittle in this range than above or below it.
- 14 **PREHEATING FOR WELDING** is carried out to prevent crack formation. See TEMPIL® PREHEATING CHART for recommended temperature for various steels and non-ferrous metals.
- 15 **CARBURIZING** consists of dissolving carbon into surface of steel by heating to above transformation range in presence of carburizing compounds.
- 16 **NITRIDING** consists of heating certain *special steels* to about 1000° F for long periods in the presence of ammonia gas. Nitrogen is absorbed into the surface to produce extremely hard "skins".
- 17 **SPHEROIDIZING** consists of heating to just below the lower transformation temperature, A₁, for a sufficient length of time to put the CEMENTITE constituent of PEARLITE into globular form. This produces softness and in many cases good machinability.
- 18 **MARTENSITE** is the hardest of the transformation products of AUSTENITE and is formed only on cooling below a certain temperature known as the M_s temperature (about 400° to 600° F for carbon steels). Cooling to this temperature must be sufficiently rapid to prevent AUSTENITE from transforming to softer constituents at higher temperatures.
- 19 **EUTECTOID STEEL** contains approximately 0.85% carbon.
- 20 **FLAKING** occurs in many alloy steels and is a defect characterized by localized micro-cracking and "flake-like" fracturing. It is usually attributed to hydrogen bursts. Cure consists of cycle cooling to at least 600° F before air-cooling.
- 21 **OPEN OR RIMMING STEEL** has not been completely deoxidized and the ingot solidifies with a sound surface ("rim") and a core portion containing blowholes which are welded in subsequent hot rolling.
- 22 **KILLED STEEL** has been deoxidized at least sufficiently to solidify without appreciable gas evolution.
- 23 **SEMI-KILLED STEEL** has been partially deoxidized to reduce solidification shrinkage in the ingot.
- 24 **A SIMPLE RULE.** Brinell Hardness divided by two, times 1000, equals approximate Tensile Strength in pounds per square inch. (200 Brinell \times 2 \times 1000 = approx. 100,000 Tensile Strength, p.s.i.)

Figure 2. Iron-Carbon phase diagram showing processing temperatures for steels. (Permission is granted by Tempil Corporation to use its Basic Guide to Ferrous Metallurgy in these proceedings).

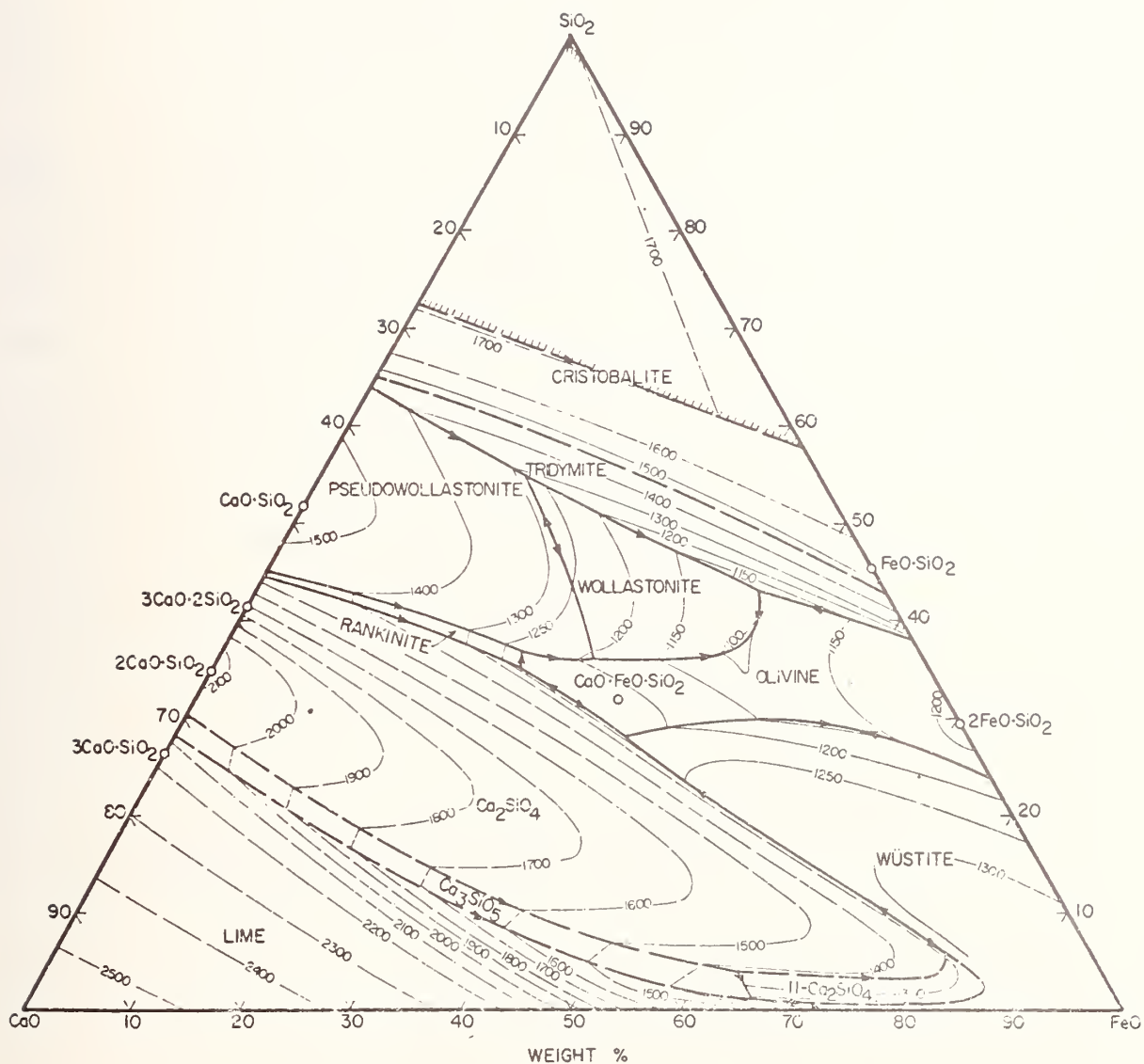


Figure 3. Phase relations in the system CaO-iron oxide-SiO₂ in contact with metallic iron, based mainly on data of Bowen, Schairer, and Posnjak⁽²⁷⁴⁾ and of Allen and Snow.⁽²⁷⁵⁾ The system is not ternary. From: Phase Equilibria Among Oxides in Steelmaking, A. Muan and E.F. Osborn, Addison-Wesley, 1965, p. 113.

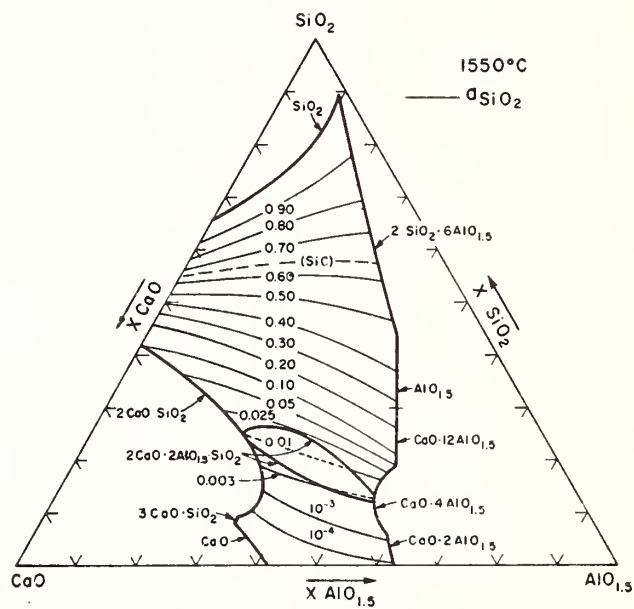


Figure 4. Activity of SiO_2 in SiO_2 - CaO - Al_2O_3 slags at 1550°C . From: J. Chipman, Trans. Met. Soc.-AIME, Vol. 233, 1965, p. 419.

DISCUSSION

J. F. Elliott - Thank you, Professor Pehlke, for a very succinct statement concerning some very interesting problems where phase equilibria are important. Would you comment on the possible importance of phase diagrams in problems of solidification of steels?

R. Pehlke - One area where phase relationships are of great importance in determining the properties of steel products is that governing the formation of oxysulfides during solidification. Specifically, the Mn-Fe-O-S system. Another is equilibria between gases and the liquid and solid metal phases during solidification of steels.

Gil Speich - What is the state of our understanding of the phase relationships related to the use of calcium as an agent for deoxidizing and desulfurizing steels?

R. Pehlke - That is a good question because just now I am looking at desulfurization of liquid iron-base alloys. The desulfurization with calcium forms calcium sulfide and other products. The equilibrium constant for the reaction to form calcium sulfide is reasonably well known. Also calcium is very effective as a desulfurizer. An interesting aspect in the use of calcium is that it is a vapor at steelmaking temperatures, but a liquid at temperatures employed in ironmaking and iron foundry operations. This, of course, influences the choice of agents and addition methods when using calcium as a deoxidizer or desulfurizer.

J. F. Elliott - Currently there is a strong interest in the use of rare earths for control of sulfides in steels.

R. Pehlke - Yes, and there is very little information on the phase relationships involved. Work on the use of rare earths for this purpose is in progress at McMaster University in Canada.

D. DeFontaine (excerpted) - I would like to raise a point regarding the size of the task ahead of us if we are to meet the needs of the industrial world. If we take 80 elements as being important, there are 3,000 possible binary systems. In the last 50 years, it appears on the average that we have completed work on one binary a week. There are approximately 50,000 ternaries. Assuming conservatively that at the same tempo of work it takes five times as long to complete a study on a ternary system as it does on a binary, it would be possible to complete 10 a year. This takes us forward 5,000 years. If we go to quaternary systems and assume that by that time our techniques have advanced sufficiently so that we can then do a complete quaternary system in about the same time it now takes us to do a ternary system, it would appear that an additional 100,000 years would be required. This overly simplified statement brings out the enormity of the task before us. It seems to me that we must ask ourselves what are the realistic goals and where do we stop. We must be honest with the industrialists and say that we never really are going to be able to develop all of the information that is needed in the next hundred thousand years.

J. F. Elliott - I feel that the question is highly pertinent. One of the answers is that we must be highly selective as to the systems on which we work because of limitations of funding and of the available manpower. It seems to me that the latter is the more important constraint. We must also be aware that there are limits

to the patience of those who ultimately must pay the bills - the public. We must provide the industrial researcher with background information to assist him to get started in his work even though he may have to develop detailed information on the system that is of immediate interest to him.

Question - Are there common interests in phase relationships across the industrial world where what is known in one area can be used to assist workers in another?

J. F. Elliott - One example that comes readily to mind is the liquid oxide systems CuO-FeO-SiO_2 and $\text{CaO-SiO}_2\text{-Al}_2\text{O}_3$ which are the bases for many slags that are used in the ferrous and nonferrous systems. Another example is the iron-oxygen system which is very broadly applicable. The answer would be yes.

F. L. Carter - In response to Professor DeFontaine's problem, it appears to me that we should fix our attention on some of the systems of major importance and then use various types of simple and sophisticated chemical and computer models to help us determine the behavior of minor constituents when added to these systems.

P. Crimes - We know quite a bit about a number of basic systems which we have discussed. However, it seems improbable that in the near future we can develop models of sufficient precision to predict in an acceptable way the behavior of all of the components

that might be found in the basic systems that are of interest to process metallurgy. As in the past, we may be forced to continue to rely on empiricism for our predictions.

F. L. Carter - Professor Brewer is not here so I must respond on his behalf. It is absolutely necessary that we develop predictive models because of the scale of our problem, as has been pointed out earlier.

I would like to bring to the panel the questions before the workshop: that is, the questions of the relative importance of depth of coverage versus range of materials covered, and the importance of factors such as high precision, presence of metastable phases, magnetic transitions. Can the panel respond?

R. Pehlke - On the issue of magnetic properties. Magnetic processing is of great importance in the treatment of iron-bearing minerals. With regard to the other questions, it depends on the specific system. One does not really know how much detail one needs on a specific system until one encounters an obstacle. It is only then that one needs detailed information. One has to decide case by case and I find it difficult to generalize on these matters.

H. Larson - I would say that we do not have general information on a number of systems as yet. The calcium-iron-silica system at various potentials of sulfur and oxygen is not well known, even though we know the system quite well at low oxygen pressures.

Other examples are the iron-copper-sulfur system to which arsenic or lead has been added. One can also point out that very little is known about the distribution of elements such as arsenic, antimony and tellurium between the matte and slag phases.

J. F. Elliott - It is unusual to find four liquid phases in a system. In the hearth of a blast furnace there may be bullion, matte speiss and slag - a very complex system which is poorly understood.

P. Crimes - The equilibria involving the distribution of minor elements between phases is indeed of great interest in process metallurgy. Elements such as arsenic, antimony, tellurium, selenium and bismuth, as well as most of the previous metals, are important.

B. Connor - There are four general levels of information that I think are needed in a compilation on phase equilibria. The first is a picture of the phase diagram. The second is an evaluated diagram with annotated references and with the name of the evaluator given to permit one to judge the evaluation itself. The third is a reference which notes from whom and where one can obtain computer-based treatments of the system. The fourth level is fitting in with the diagram quantitative information on the thermodynamic behavior of components of phases and the thermodynamics of reactions involving components in the system.

J. F. Elliott - You place a very tall order with the compiler.
However, this has been the goal of several compilations in the field.

B. Rosof - The needs of minor industries in the area of phase diagrams are often not met. The companies in these industries (my company being one) are important to the general economy and often have a high technical base.

J. F. Elliott - I would like to thank our panel members and the audience for a fruitful session. The session is adjourned.

PANEL III

MATERIALS PROCESSING (fabricating, machining, heat treating, etc.)

(User Needs for Phase Diagram Information)

Moderator: W. Rostoker, Dept. of Materials Engineering,
University of Illinois, Chicago, IL

Panel Members:

E. R. Kreidler, Lamp Business Div., General
Electric Co., Cleveland, OH

R. McNally, Ceramics Research, Corning Glass
Works, Corning, NY

L. Mondolfo, Consultant, Clinton, NY

S. Prochazka, Ceramics Branch, Physical Chemistry
Laboratory, General Electric Co.

G. R. Speich, Research Laboratories, United
States Steel, Monroeville, PA



User Needs for Phase Diagrams for Materials Processing: Glasses

R. C. Doman
R. N. McNally

Corning Glass Works
Corning, NY 14830

Introduction:

Phase diagrams are essential for the understanding of materials. These data are employed on a routine basis for developing new products. In many of our developments the phase diagrams were either not available or incomplete resulting in substantial phase equilibria studies to understand the manufacturing and end use. It is imperative that basic phase equilibria data be done in the temperature range 1500°C to 3500°C and in varying atmospheres where materials with unique properties exist. Outlined below are only a few of the important parameters, applications and examples of our requirements for phase equilibria data.

- I. Applications for High Temperature Materials ($>1000^{\circ}\text{C}$)
 - A. Glasses
 - B. Glass-Ceramics
 - C. Ceramics
- II. Important Phase Equilibria Systems
 - A. Oxides
 - B. Intermetallics
 - C. Metals
 - D. Composites

- III. Processes Related to Phase Equilibria
 - A. Melting
 - B. Forming
 - C. Sintering
- IV. Commercial Applications Where Phase Equilibria is Important
 - A. Refractories for steel and glass industry
 - B. Technical ceramics - zirconia; nitrogen containing materials
 - C. Honeycomb ceramics - auto exhaust; engine components
 - D. Glass systems
 - E. Glass-ceramics
- V. Type Data Needed
 - A. Melting points, liquidus curves
 - B. Eutectics, peritectics, compound formation, solid solutions, sub-solidus, kinetics of solution - exsolution
 - C. Environment - oxidizing, reducing, neutral, vacuum
 - D. Vapor pressure data
- VI. Some Key Data Needed for Determining Phase Equilibria Diagrams at High Temperatures
 - A. Chemical analysis
 - B. Microstructural analysis
 - C. Physical properties
 - D. Instrumental analysis
- VII. Some Problems
 - A. Greatest need is at higher temperatures - 1500 to 4000°C where experimental problems increase by 4th power

- B. Time = money
- C. Basic supporting data isn't known

VIII. Examples

Example I: Fusion-Cast MgO-Chromite Product in order to understand this system it was necessary to:

- A. Break up nine components system to binarys, ternarys, quaternarys etc. systems.
- B. Had to determine melting points of end members.
- C. Work out all binary systems - $\text{MgO-Al}_2\text{O}_3$, $\text{MgO-Cr}_2\text{O}_3$ - MgO-CaO etc. - liquidus, solidus, sub-solidus, solid solutions, etc.
- D. Ditto ternarys etc.
- E. Ditto in various atmosphere conditions
- F. Determine - surface tension at liquidus, vapor pressure, vapor species.
- G. Determine phase equilibria data between metallurgical stage and refractory materials
- H. Without this work there would not be commercial progress because of the strong relationship of phase equilibria to properties

Example II: up to 3500°C

- A. Group IVB, VB, VIB, carbides, borides, silicides, nitrides, oxycarbides, oxynitrides, oxyborides; the need for phase equilibria data even more imperative for the current need for these type materials

Example III: ZrO_2 Solid Solutions - Effect of phase distributions on resulting properties of ZrO_2

A. Example - ZrO_2 electrolytes

B. Example - Relationship to strength

Example IV: Li_2O Stabilization of $\text{MgO-R}_2\text{O}_3$ Solid
Solutions

A. Without original work on $\text{MgO-R}_2\text{O}_3$ phase equilibria,
this work would not have been done



EQUILIBRIUM DIAGRAMS IN NON-FERROUS ALLOYS

L. F. Mondolfo

Dept. of Chemical Engineering and Materials Science
Syracuse University
Syracuse, New York 13210

SUMMARY

In non-ferrous alloys, the equilibrium diagram explains why in the continuous casting of brasses, the 60/40 brass cannot be cast with the same technique as used for the 70/30 and 80/20 brasses and suggests the technique changes necessary. The location of the cracking in the welding of AlMgZn alloys is explained by the equilibrium diagram, and the effect of Cu additions. In Mg base alloys the equilibrium diagram indicates that better castability can be obtained by Si additions; in the zone refining of Al the diagrams indicate the movement of impurities and, in a general way, the amount of refining obtainable. Equilibrium diagrams explain the neutralization of Pb in zinc die casting alloys, the choice of heat treatment temperature for dural as function of Si content, Mn additions to improve the corrosion resistance of AlMg alloys, additions of Co or Mn to AlSi alloys to improve the ductility.

The two major difficulties with equilibrium diagrams, namely reliability and availability are discussed, together with the problems arising, especially in Al alloys, because of the complexity of the alloys and the necessity to account for every element present. Also mentioned are some reasons for the decrease of research on equilibrium diagrams and some of the difficulties in equilibrium diagram work.

The equilibrium diagram is for the material engineer what a map is for a surveyor. Not only the map tells the actual relief, but oftentimes when the relief is masked by overgrowth, the knowledge of the location of the ground, even if not visible, permits the surveyor to predict how much to cut to reach bare ground. Similarly for the material engineer non-equilibrium conditions may mask the true equilibrium, but to know where and how far the material has to go to reach equilibrium is often more valuable. Although materials can be handled without equilibrium diagrams, the use of the diagram makes life much easier. In the 100 or so years that equilibrium diagrams have been in use, material science has made more progress than the thousands of years that preceeded it! Every material engineer can tell about the many cases in which the equilibrium diagram has been of great help if not essential, the few examples reported here will show some of the cases in the author's experience.

In the continuous casting of large slabs of brass for subsequent rolling to coils, the casting conditions that produce good slabs are very similar for the 80/20 and the 70/30 brasses: same mold, same settings for the cooling water, same speed of descent. The only difference is that the 80/20 brass requires a pouring temperature some 50°C higher than the 70/30. However when one tries to cast the 60/40 brass with the same conditions as the 70/30, the results are appalling; after a few inches of ingot have been cast, molten metal starts to pour into the pit. The metal shell that forms inside the mold is not solid enough to support the hydrostatic pressure and molten metal breaks through. The obvious answer is to increase the cooling in the mold to build up a stronger shell. This

produces the desired result: no more spill-out. However the problem only changes, casting can proceed to completion, but when one goes to remove the ingot from the pit, one is faced with two half ingots, most times completely split. In Fig. 1 is shown the pertinent part of the diagram Cu-Zn, as given by Hansen and Anderko⁽¹⁾. The three vertical lines mark the 80/20, 70/30 and 60/40 alloys. As can be seen, the difference of composition between the first solid and last liquid to freeze is relatively small and approximately the same for the 80/20 (A) and the 70/30 (B) brasses, but the range of freezing temperature is some 50°C higher for the 80/20. The 60/40 on the other hand freezes over approximately the same range of temperature of the 70/30, but the difference in composition between the first solid and the last liquid (C) is much larger. In addition both the 80/20 and the 70/30 in the solid state are composed mostly if not all of alpha phase, whereas the 60/40 is mostly beta phase. Freezing during continuous casting is definitely in non-equilibrium conditions; solidification may start with a solid with the composition shown by the equilibrium diagram, but at the point at which in equilibrium conditions it should end, there is still an appreciable amount of liquid, of a composition more or less corresponding to that shown by the diagram. Thus solidification continues and ends at a temperature lower than required by the equilibrium diagram. The lowering of the solidification end is proportional to the difference in composition between solid and liquid. This explains why in the 60/40 brass the shell formed in the mold is not as strong as in the other brasses, the actual range of solidification is larger and more mushy metal is present.

When increased cooling in the mold is used to thicken the shell, internal tensions, due to the quenching of the shell, build up. The shell, mostly of beta phase, is less plastic than if it were composed of the more ductile alpha phase and because of the internal tensions, cracks. Once this information is available, the cure is obvious. The splitting requires a reduction of the internal tensions which means a lesser quenching, the spill-out requires more build up of the shell. Reduction of the cooling in the mold and below reduces the internal tensions and eliminates the splitting, a slower descent speed that allows more time in the mold permits the thickening of the shell necessary to avoid spill-out. Of course all of this could have been done without equilibrium diagram by varying the casting conditions one at the time and then two at the time and so on, until the proper set-up was found. This was actually done at the beginning, but an enormous amount of work was expended and once the proper conditions were found, nobody knew what to do when minor accidental variations of practice crept in and suddenly all the production was scrap!

Fig. 2 shows the equilibrium diagram of the AlMgZn alloys⁽²⁾, with the crosshatched square marking the range of commercial compositions. As can be seen by comparing the liquidus and the solid state distribution of the phases, the alloys when in equilibrium are well within the range of solid solutions and so far away from the eutectic line, that even the non-equilibrium conditions that may result from commercial welding practice, do not produce sufficient coring to cause the appearance of eutectics. Thus the alloys freeze as solid solutions and toward the end of freezing there is little liquid to feed the shrinkage. Microporosity develops in

the weld, that weakens the weld zone and concentrates in it cracking due to internal tensions. When Cu is added to the alloys, the equilibrium diagram, if available, would show the presence of an eutectic near the alloy composition range. This eutectic toward the end of freezing of the weld acts to feed the shrinkage, thus reducing substantially the micro-porosity and its weakening effect. No more cracking of the weld zone results. However in the zone surrounding the fused metal eutectic melting takes place, that weakens the material and cracking due to internal tensions concentrates there. Of course the advantage of the equilibrium diagram in this case is limited, it explains what is happening, but not how to remedy it. However, once it is known what the problem is, it is usually reasonably easy to find an answer.

A similar case in which the equilibrium diagram does not give the right answer is that of the Mg base alloys that contain Al and Zn in amounts well below their maximum solubility. They freeze as solid solutions and, also because of the high shrinkage coefficient of Mg, they show extensive microshrinkage in all but the simplest castings. In the MgSi diagram (Fig. 3) at the Mg end there is an eutectic at 1.4% Si⁽¹⁾. This suggests that if some Si is added to the MgAlZn alloys, the problem of lack of eutectic should be solved. Experiments show that this is the case, as little as 0.4 - 0.5% Si produces all the eutectic that is necessary, and sound castings are produced. What the equilibrium diagram does not tell is that the Si addition so embrittles the castings, that they may shatter if dropped on a hard floor!

In the zone refining of aluminum a look at the binary equilibrium

diagrams will predict that Cu, Mg, Zn, Si whose eutectic composition is quite different from the solid solubility limit, can be moved to the end fairly rapidly and easily, whereas Mn, which has an eutectic point very close to the solid solution limit, will move only extremely slowly, Cr, Ti, V, Zr which undergo peritectic reactions with Al, will move backwards to the starting end. Experimental results shown in Table I confirm the predictions. It is to be noticed that in this case use of the binary diagrams

TABLE I
ANALYSES OF Al (PRODUCED BY DEPOSITION FROM ORGANIC SALTS)
BEFORE AND AFTER ZONE REFINING⁽³⁾

Element	Before	After	Change	k Factor *
Cu	0.3	0.006	- 150	0.17
Cr	0.004	0.01	+ 2.5	2.0
Mg	1.0	0.01	- 100	0.5
Mn	0.031	0.030	- 0.3	0.94
Si	1.0	0.05	- 20	0.13
Ti	0.05	0.5	+ 10	11.0
V	0.01	0.03	+ 3	4.0
Zn	0.06	<0.001	- 100(?)	0.88
Zr	0.04	0.05	+ 0.25	2.5

for multi-component alloys will predict the right direction, but not even an order of magnitude change. For example Si, with the lowest k factor,

*k = ratio of amount of addition soluble in the solid to amount soluble in the liquid at freezing temperature,

should be the easiest to be removed, followed in the order by Cu and Mg, and far away by Zn and Mn. For the peritectic elements, Ti should be the most concentrated and then in order V, Zr, Cr. Instead the most easily removed is Cu, followed by Zn, Mg and with Si far behind. The only element that follows predictions of the binary diagram is Mn. In the peritectics, Ti concentrates in the right amount but the changes for the other elements are in the proper direction, but not in the proper order or of the right magnitude.

Zinc-base die casting alloys contain some 4 - 5% Al which give to the alloy its excellent castability and strength. Accordingly Zn die castings are extensively used because they are cheap, easily polished and plated to excellent appearance, and stronger than plastics. Most Zn, unless specially refined, contains a few thousandths of a percent of Pb. Neither Zn nor Al form compounds with Pb, thus the Pb is present in the alloys as elemental Pb. Solubility of Pb in Zn decreases with decreasing temperature. The age hardening phenomena that result from it have little effect on the mechanical properties, but make the alloys susceptible to intergranular corrosion, to the point that early failure may result even in mildly corrosive conditions. Since removal of the last amount of Pb is expensive, neutralization of the Pb is necessary. As shown by the MgPb diagram, (Fig. 4) a compound Mg_2Pb is formed⁽¹⁾, which is very stable and does not dissolve to any great extent in Zn. This reduces the precipitation of Pb and eliminates the intergranular corrosion susceptibility. The amount of Mg necessary for the neutralization is only a few thousandths of a percent and even if for safety sake few

hundreds are added, the cost is infinitesimal, especially if one compares it to the cost of refining Zn to remove the last trace of Pb.

Many commercial Al alloys are subjected to heat treatment, which permits a 3 - 4 fold increase of strength over the annealed properties. Heat treatment relies upon producing a supersaturated solid solution and then controlling its movement toward equilibrium to produce the structure with the desired properties. The best means of supersaturating a solution is to heat the alloy at the highest temperature possible to dissolve the largest amount of solute possible. Since solid solubility increases exponentially, even a few degrees make a substantial difference in the amount dissolved. On the other hand exceeding the lower melting point of the alloy, even by few degrees and for few seconds, deteriorates the alloy beyond repair. In most heat treatments of Al alloys the margin of safety is small: heat treatment temperatures only 5 to 10°C below the melting point of the lowest eutectic are common. Obviously knowledge of the eutectics present in the alloy is necessary.

A typical case are the duralums. These are alloys that contain Cu and Mg and sometimes added Si. In addition they contain Mn and the normal impurities of Al: Fe and Si. Neither Mn nor Fe have an appreciable effect on low melting eutectics; the structure of the alloys is basically controlled by the Mg/Si ratio; depending on it several different eutectics can be present in the alloys. Fig. 5 shows the quaternary diagram AlCuMgSi⁽²⁾. As can be seen, 3 eutectics are formed in that part of the diagram that covers the duralums. In Table II are listed three typical dural compositions, their Mg/Si ratios, the eutectics in them and the

TABLE II
NOMINAL COMPOSITION OF COMMERCIAL DURALS, THEIR Mg/Si RATIO
EUTECTICS PRESENT IN THEM WITH THEIR MELTING POINT AND
HEAT TREATMENT TEMPERATURE RECOMMENDED

Alloy	Cu	Mg	Si	Ratio Mg/Si	Eutectic	Melting Point	Heat Treatment Temperature °C
2014	4.4	0.5	0.8	<1	Al + CuAl ₂ + Cu ₂ Mg ₈ Si ₆ Al ₅ + Si(?)	507	500 ± 5
2017	4.0	0.5	0.25	≈1.7	Al + Mg ₂ Si + CuAl ₂	515	505 ± 5
2024	4.4	1.5	0.25	>>1.7	Al + CuAl ₂ + Mg ₂ Si + CuMgAl ₂	500	490 ± 5

prescribed heat treatment temperature. It is to be noticed that in the first alloy listed the Si content is insufficient for the Si phase to appear, thus there is no quaternary eutectic in it. The lowest melting point of the alloy is somewhere on the line between the points Q (512°C) and R (507°C). With the equilibrium diagram and the analysis of the alloy, heat treatment temperature can be set with assurance that maximum benefit will be obtained, without danger of deterioration.

AlMg alloys have excellent resistance to corrosion, if properly compounded and treated. The usual Al impurities Fe and Si, form in them the two compounds FeAl₃ and Mg₂Si. Mg₂Si has an electrolytic potential anodic to the matrix⁽⁴⁾ and in corrosive conditions Mg₂Si is rapidly dissolved to protect the matrix, leaving a pit more or less the size of the Mg₂Si particle. Since Si is kept low and Mg₂Si particles are easily dispersed, and thus small, their solution produces only a slight roughening of the surface. FeAl₃ on the other hand, is strongly positive to the matrix⁽⁴⁾

thus the matrix around the FeAl_3 particle corrodes to protect it, until the particle comes loose. When this happens a pit several times larger than the particle has formed. If one looks at the AlFeMn diagram (Fig. 6) (one should really look at the AlFeMgMnSi diagram or at least to the AlFeMgMn diagram, but neither of the two diagrams is sufficiently known for the purpose) one sees that when Mn is present, the Fe tends to replace Mn in the MnAl_6 compound, giving rise to a $(\text{FeMn})\text{Al}_6$ compound, that has a structure and properties very close of those of the MnAl_6 . Of interest in this case: the MnAl_6 has an electrolytic potential very close to that of $\text{Al}^{(4)}$, and so does the $(\text{FeMn})\text{Al}_6$. As a result addition of Mn to AlMg alloys in amounts equal to the Fe content replaces the FeAl_3 compound, strongly positive in respect to the matrix, with a $(\text{FeMn})\text{Al}_6$ one with practically the same potential as the matrix, and which therefore will not give rise to pronounced pitting corrosion.

Al alloys with more than 12% Si have excellent wear resistance, low thermal expansion coefficients, good castability and, if they contain sufficient high melting point metals, reasonably good strength at elevated temperatures. Thus they are extensively used in the automotive industry for pistons and cylinder blocks. In the Al foundry iron pickup is always a serious problem; sources for iron are innumerable. Even if one does not use cast iron pots for holding the melts, iron can come from stirring tools, mold washes, galvanized iron roofs, steel chips from the saws that cut the ingots and risers, etc., etc. In addition the automotive industry is extremely cost conscious and secondary metal, which usually contains more Fe than primary, is the rule for their castings.

The high Si alloys are particularly sensitive to Fe contamination, if the Fe content is above 0.7 - 0.8% Fe correction is necessary or else the castings may be as brittle as glass. A look at the AlFeSi diagram explains the Fe limit: with Fe above 0.7% the FeSiAl_5 phase is primary. This phase is extremely brittle and tends to form large platelets (Figure 7). The problem is to prevent the formation of these primary crystals. The best way would be to reduce the Fe content, but this is economically impossible, sweetening an alloy with 0.9% Fe down to an acceptable 0.6% Fe requires the addition of almost the same amount of low Fe metal!

Several elements combine with Fe to form compounds less embrittling than FeSiAl_5 : the most common are: Cr, Mn, Ni and Co. The equilibrium diagrams (Fig. 8) can help in the choice of the best corrector. In the AlCrFeSi diagram (Fig. 8a) the compound in equilibrium with Al is most probably $(\text{CrFe})_4\text{Si}_4\text{Al}_{13}$ which contains large amounts of Si and Cr, but little Fe. A large amount of it forms, which reduces the fluidity of the alloy, with only a limited improvement on ductility. In the AlFeMnSi system (Fig. 8b) the compound formed is $(\text{FeMn})_3\text{Si}_2\text{Al}_{15}$ which contains less Si and in which Fe can greatly exceed the Mn, thus a small addition of Mn can absorb a large amount of Fe. Ni and Co do not form compounds with Si thus the Fe is absorbed by them through the formation of FeNiAl_9 (Fig. 8c) or by displacing up to 50% of the Co in Co_2Al_9 to form a $(\text{CoFe})_2\text{Al}_9$ compound (Fig. 8d). The FeNiAl_9 compound unfortunately crystallizes as long needles which, although better than FeSiAl_5 still embrittle the alloys. Thus neither Cr nor Ni are suitable for the purpose and the choice is

between Mn and Co. Co is better because for any given amount of Fe to be neutralized less compound is formed. For example in the alloy marked x in Figs. 8b and d, using the lever rule, the ratio of Si to $(\text{CoFe})_2\text{Al}_9$ can be calculated at approximately 0.12; in the AlFeMnSi diagram, for the same alloy, the ratio is approximately 0.18. Thus in the latter alloy there is some 50% more Fe bearing compound. However the price of Co is much higher than that of Mn, thus economically Mn is more attractive, whereas functionally Co is better. At this point equilibrium diagrams give place to economics: if quality is the major factor, Co wins, if cost, Mn is preferred.

In most examples shown it is obvious that the equilibrium diagram alone is not sufficient and that additional information is needed to solve the problems. However the role of the diagram is basic: it is the framework to which additional information is attached to give a complete, coherent picture.

There are two problems in the use of equilibrium diagrams: availability and complexity. Not only many diagrams are only partially known or even completely unknown, but even those supposedly well established may not be as reliable as one would expect from work widely accepted. Fig. 9 shows several AlZn equilibrium diagrams. As shown by the references⁽⁵⁻¹³⁾, the names of many well known metallurgists are attached to them. Obviously only one of them can be correct and there is a good probability that the last one is not it. There are good reasons to expect that the actual diagram is the one shown by Hanson and Gayler, published in 1922, and later discarded.

The other serious problem is that the more knowledge of metals increases, the more one becomes aware of the disproportionate role that some small impurity may play on structure and properties. Thus to account, even approximately, for the structure of commercial alloys one has to consider multicomponent systems. In steel and most Cu or Ni alloys many alloying elements are in solution and only small modifications to the binary or ternary systems can account, at least approximately, for these additions. An easily legible diagram can serve for most purposes. In Al alloys the contrary is true. Even commercially pure Al, which contains Fe and Si as normal impurities is a multiphase alloy: in addition to the Al phase, FeAl_3 , Fe_2SiAl_8 , FeSiAl_5 and Si may be present (Fig. 10). Thus even before the start of alloying, one is dealing with a ternary diagram. Very few commercial alloys contain only one addition and many of them contain three or four. For example durals are AlCuFeMgMnSi alloys (6 elements), the 7000 group alloys AlCuFeMgSiZn alloys (also 6 elements) but usually with additions of at least one of Cr, Mn, Zr, Ag and often Ti, B.

Ternary diagrams are easily plotted: liquidus and one or two sections can give a reasonably complete and accurate picture. Quaternary diagrams can be plotted by the method of Phragmen⁽¹⁴⁾ in which the pyramid vertex that represents the base element is used as projection point for the diagram (Fig. 11). The picture that one obtains is not as accurate, but one can gather a reasonable idea of invariant reactions, phases present and their approximate distribution. For a quinary system this is impossible: sections have to be used and following a phase or a reaction

through them becomes a major project. Until computers can be trained to read equilibrium diagrams there is little that can be done on this problem.

In the early years of this century every fourth paper published was an investigation of an equilibrium diagram, today one has to wade through an enormous amount of literature to find equilibrium diagram work. Granted that the most important parts of binary diagrams are already established reasonably accurately, but how many useful ternary or quaternary diagrams are known with certainty, if at all?

This dearth of equilibrium diagram work is particularly noticeable in American publications; Russian, Japanese, German magazines still report a fair amount of equilibrium diagram work. One of the reasons for this is that in American Universities equilibrium diagram work is considered routine and unfit for PhD. theses. It is true that a good part of the work is routine and repetitive, but so is most good research. Granted that one can take a bunch of alloys, prepared by a technician and give them to another technician to determine their X-ray diffraction pattern, and from this work publish an equilibrium diagram, but how much reliance can one put on this kind of research? With the large number of variables in any research one experiment, no matter how brilliantly conceived or executed, is not sufficient to prove anything. One of the most important principles of research is that unless an experimental result can be confirmed by another method, preferably also by another investigator, it should be considered only tentative.

In equilibrium diagram work, where non-equilibrium conditions are

the rule, rather than the exception, one should use as many methods of investigation as possible. On the other hand a judicious selection of methods is necessary. There is no method invented for investigating metals that cannot be used for the determination of equilibrium diagrams. Already the selection of the methods to be used is a series of decisions that require both knowledge and judgement: it is useless to make the most accurate lattice parameter measurements to determine a solid solubility that is below 0.1%! Any one who has investigated equilibrium diagrams knows how much ingenuity and hard work are necessary to assemble all the experimental data and to coordinate them to make them fit a smooth and plausible picture that obeys all the thermodynamic laws.

Among the non-ferrous metals, Al and Mg, which were born in an era when metallurgy was becoming a science, are in a favorite position: many more complex equilibrium diagrams are available for Al and Mg alloys than for the older metals. However even in the Al and Mg industries there is need for more diagram work. The Concorde plane uses large amount of Hyduminiums, which are AlCuFeMgNiSi alloys, yet the AlCuFeNi diagram, that is vital for the understanding of these alloys is very poorly investigated and far from established. Those people that have the money to fly the Concorde should be asked "How does it feel to fly a plane whose equilibrium diagram is not known?".

REFERENCES

1. M. Hansen and K. Anderko, "Constitution of Binary Alloys," McGraw-Hill New York, 1958.
2. L. F. Mondolfo, "Aluminum Alloys, Structure and Properties," Butterworths, 1976.
3. G. Revel, Mem. Artillerie Franc., 1969, 43, 343.
4. E. Franke, Werkstoffe u. Korrr., 1953, 4, 4.
5. E. S. Shepard, J. Phys. Chem., 1905, 9, 504.
6. W. Rosenhaim, S. L. Archbutt, Phil. Tr. Roy. Soc., 1912, 212, 315.
7. O. Bauer, O. Vogel, Inter. Z. Metallographie, 1916, 8, 101.
8. D. Hanson, M. L. V. Gayler, J. Inst. Metals, 1922, 27, 267.
9. T. Tanabe, J. Inst. Metals, 1924, 32, 415.
10. T. Tshiwara, J. Inst. Metals, 1925, 33, 73.
11. E. Schmid, G. Wassermann, Z. Metallkunde, 1934, 26, 145.
12. W. L. Fink, L. A. Willey, AIME Tr., 1936, 122, 244.
13. A. A. Presnyakov, Y. A. Gorban, V. V. Chernyakova, Zh. Fiz. Khim, 1961, 35, 1289.
14. G. Phragmen, J. Inst. Metals, 1950, 77, 489.

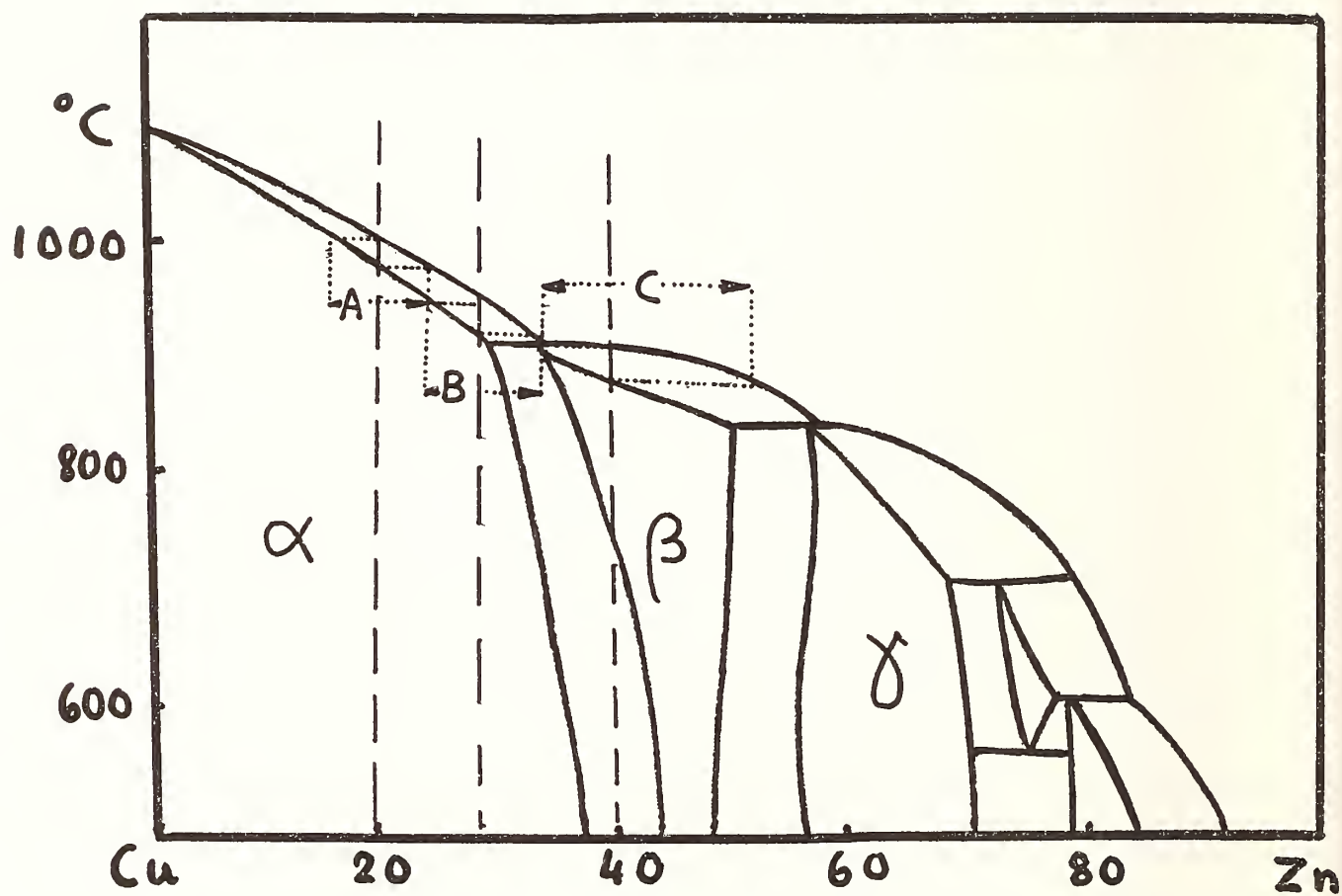


FIG. 1 CuZn DIAGRAM, SHOWING THE 80/20, 70/30, 60/40 BRASSES AND THE SIZE OF THE DIFFERENCE OF COMPOSITION BETWEEN THE FIRST SOLID AND THE LAST LIQUID TO FREEZE IN EQUILIBRIUM CONDITIONS.

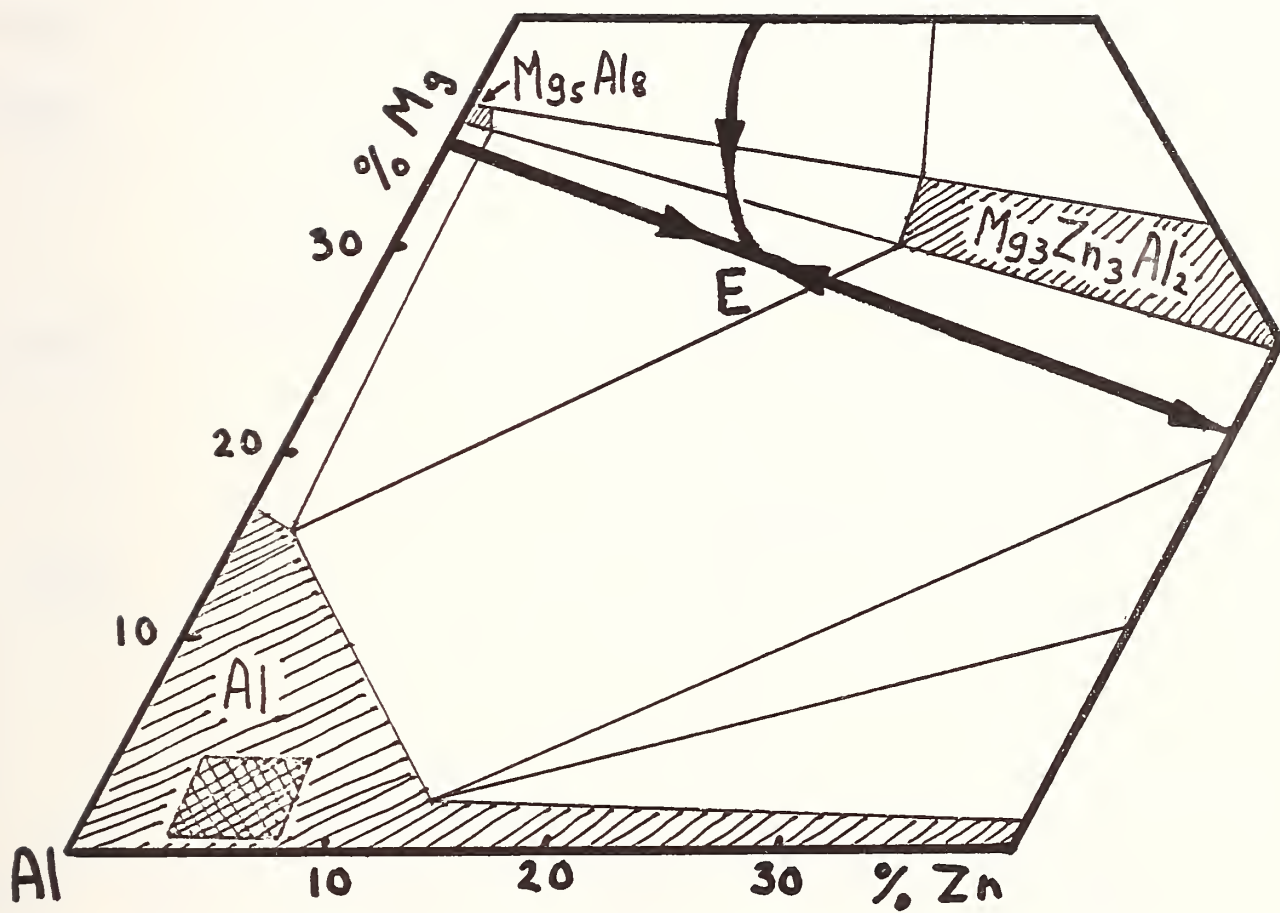


FIG. 2 AlMgZn DIAGRAM, Al CORNER, LIQUIDUS LINES (HEAVY), EUTECTIC E AND PHASE DISTRIBUTION IN THE SOLID STATE (LIGHT LINES). THE CROSSHATCHED AREA REPRESENTS THE RANGE OF COMPOSITION OF COMMERCIAL ALLOYS. NOTICE ITS DISTANCE FROM THE EUTECTIC LINES.

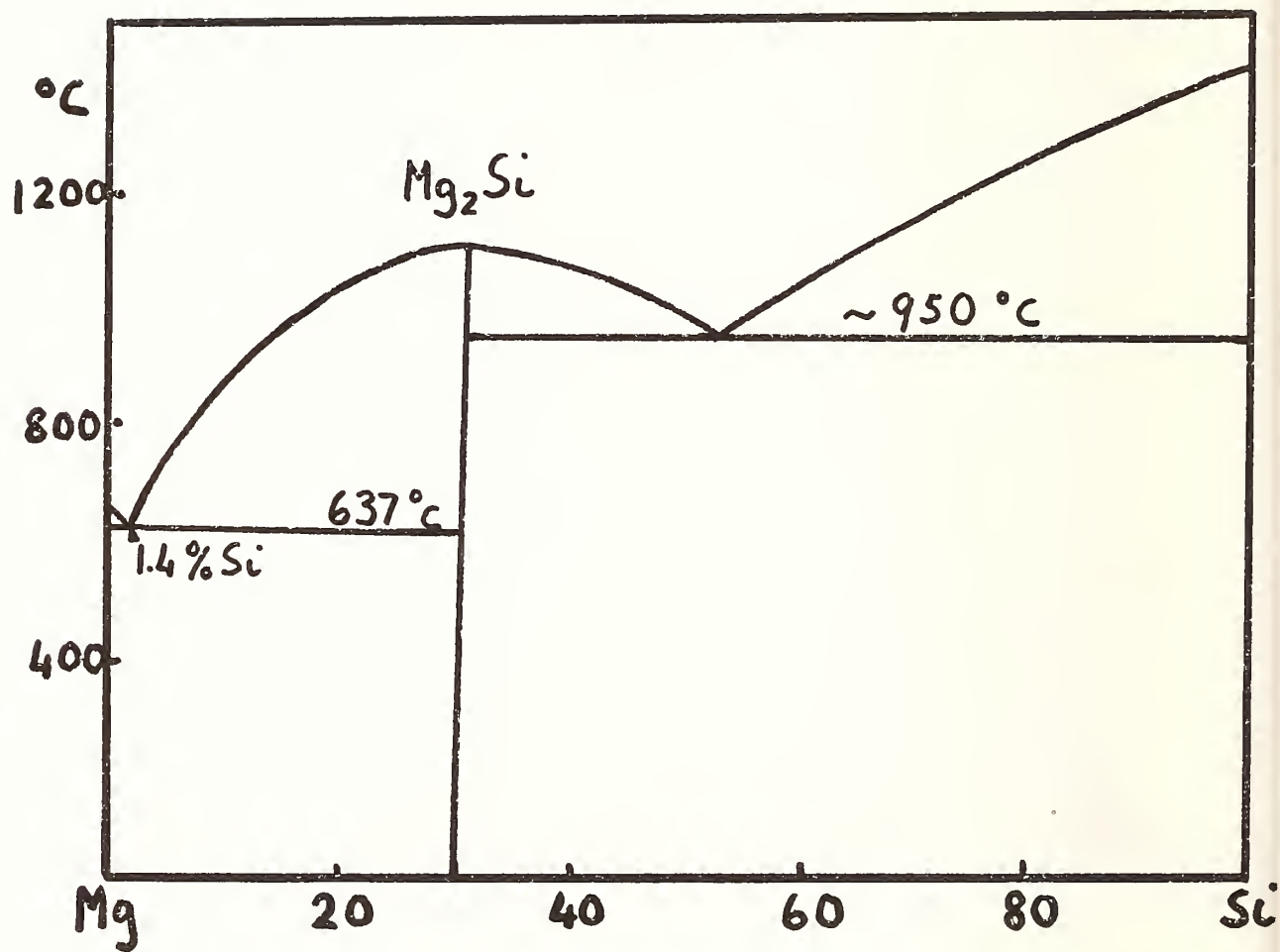


FIG. 3 MgSi EQUILIBRIUM DIAGRAM SHOWING THE PRESENCE OF AN EUTECTIC AT 1.4% Si.

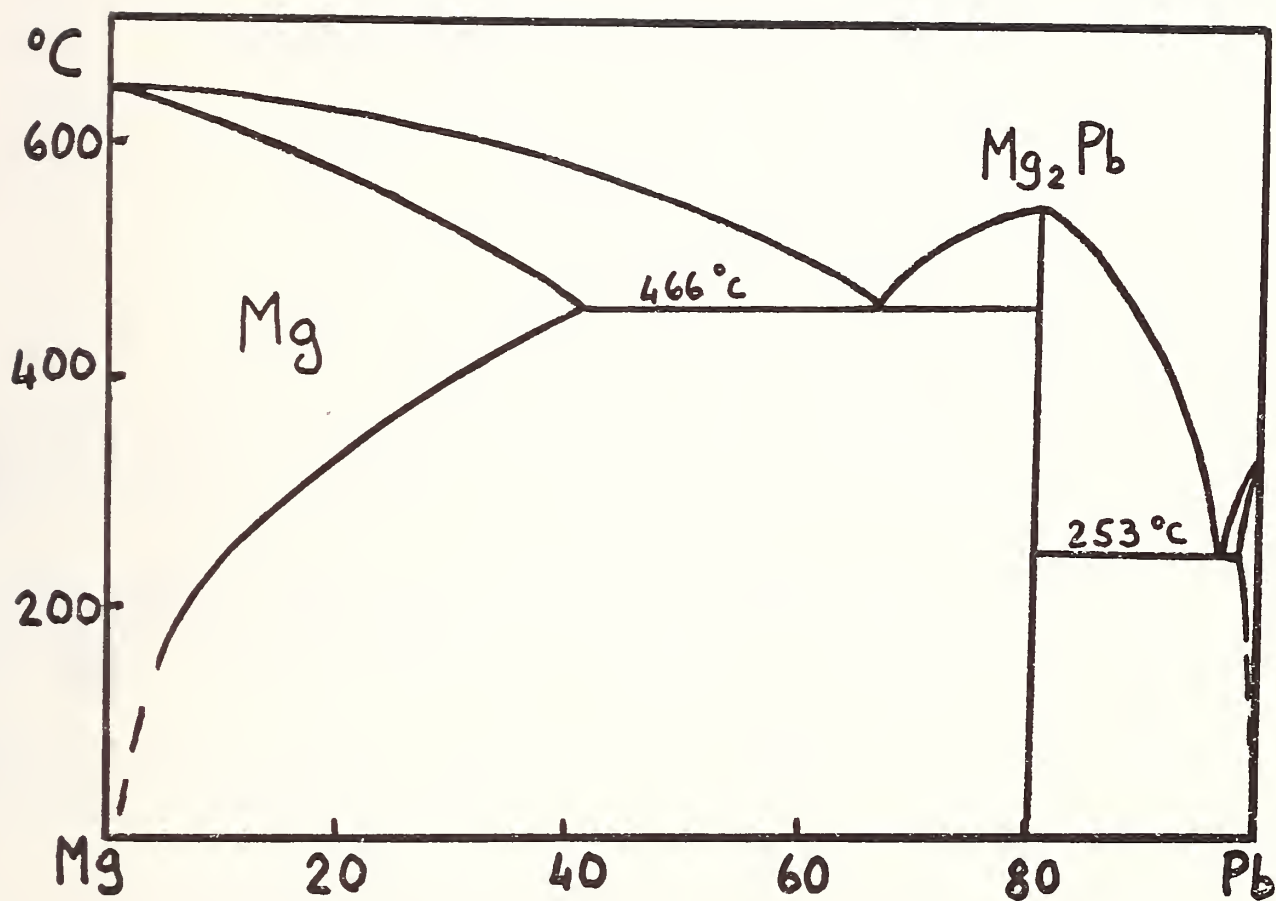


FIG. 4 MgPb DIAGRAM SHOWING THE PRESENCE OF A Mg_2Pb COMPOUND, WITH HIGH Pb CONTENT.

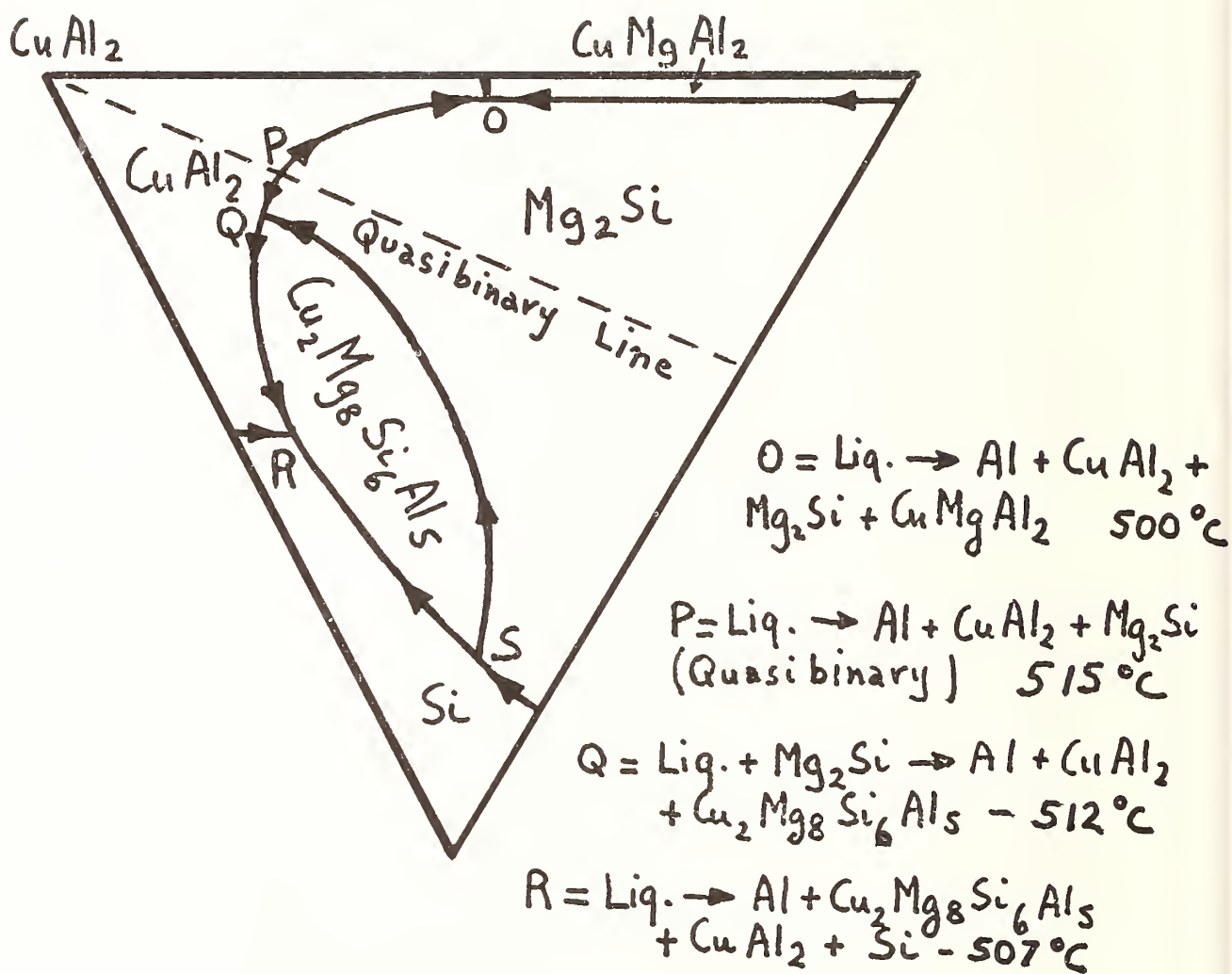


FIG. 5 CORNER OF THE PROJECTION OF THE AlCuMgSi LIQUIDUS, SHOWING THE LOCATION OF THE QUATERNARY EUTECTICS, THE PHASES PRESENT IN THEM AND THEIR MELTING POINT.

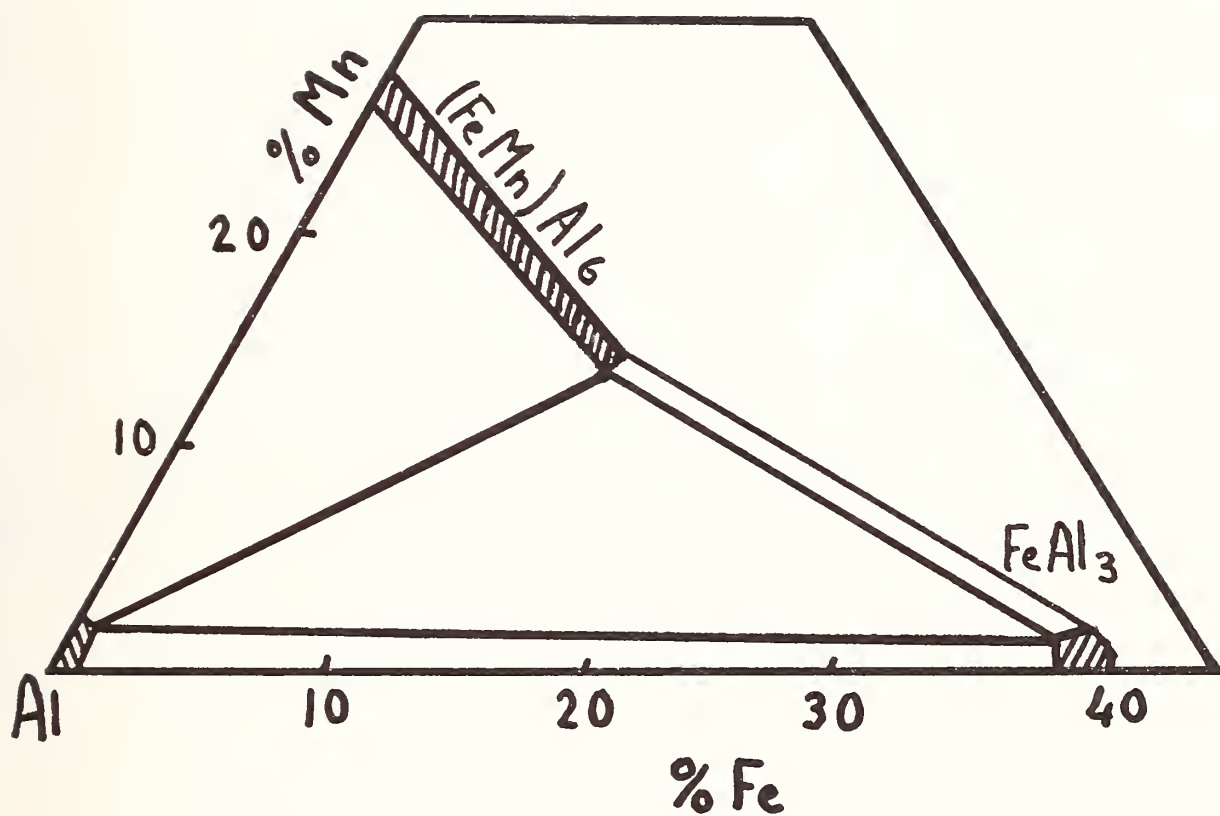


FIG. 6 Al CORNER OF THE AlFeMn DIAGRAM SHOWING THE RANGE OF COMPOSITION OF THE $(\text{FeMn})\text{Al}_6$ PHASE.



FIG. 7 Al ALLOY WITH 10% Si, 0.9% Fe, SAND CAST. LARGE PRIMARY NEEDLES
OF FeSiAl_5 (LIGHT) IN A BACKGROUND OF EUTECTIC AlSi . X 250 NOT
ETCHED.

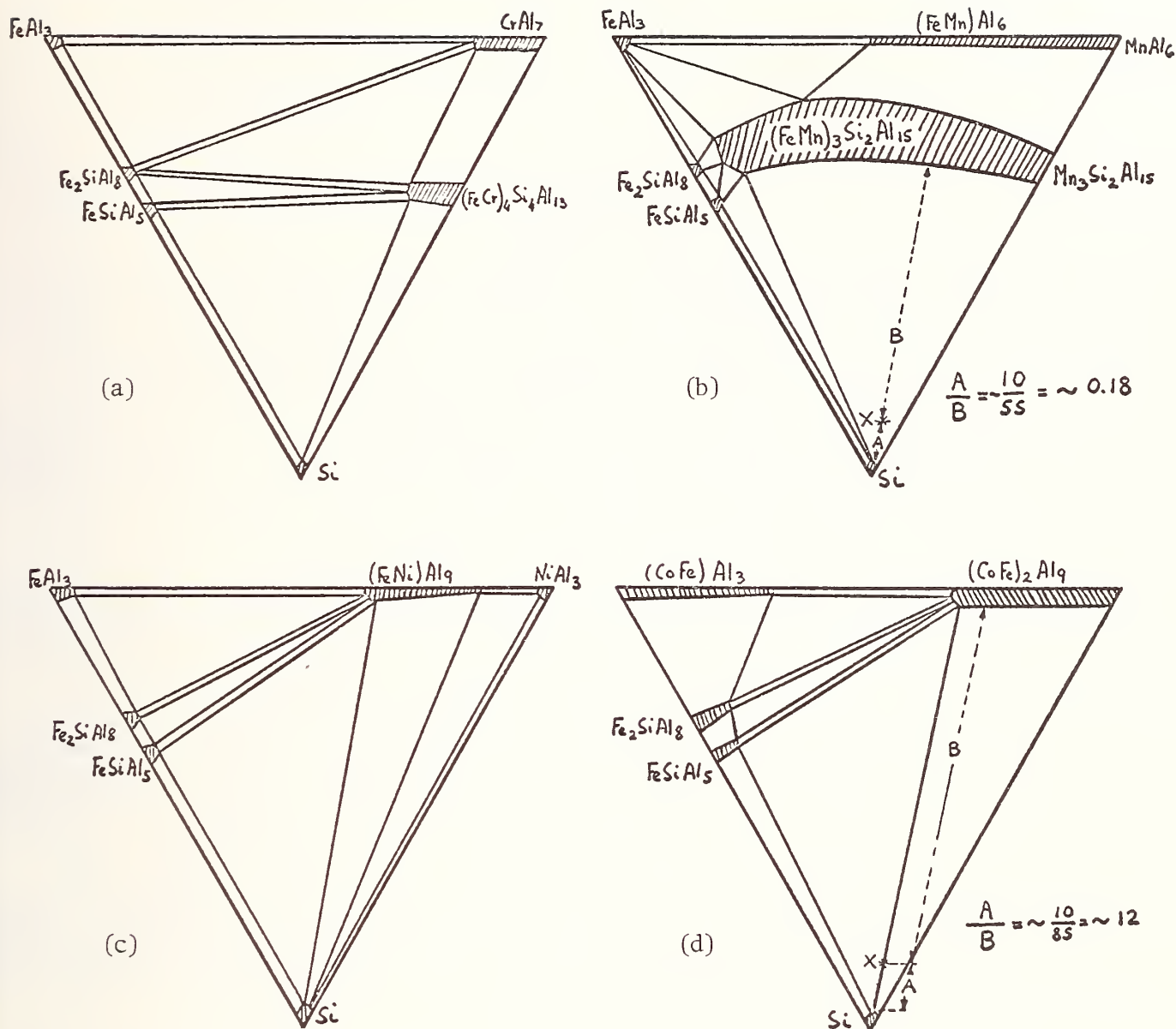


FIG. 8 PROJECTION OF THE PHASE DISTRIBUTION IN THE SOLID IN THE DIAGRAMS a) AlCrFeSi, b) AlFeMnSi, c) AlFeNiSi, d) AlCoFeSi. NOTICE SMALL AMOUNT OF Fe in $(\text{FeCr})_4\text{Si}_4\text{Al}_{13}$ AND THE LARGE AMOUNT OF Si, AS EVIDENCED BY THE LIMITED PROTRUSION IN THE QUATERNARY FIELD AND PROXIMITY TO THE Si CORNER. ALSO NOTICE HOW IN THE ALLOY X THE RATIO OF COMPOUND TO Si IS 0.18 IN THE AlFeMnSi DIAGRAM, BUT ONLY 0.12 IN THE AlCoFeSi SYSTEM.

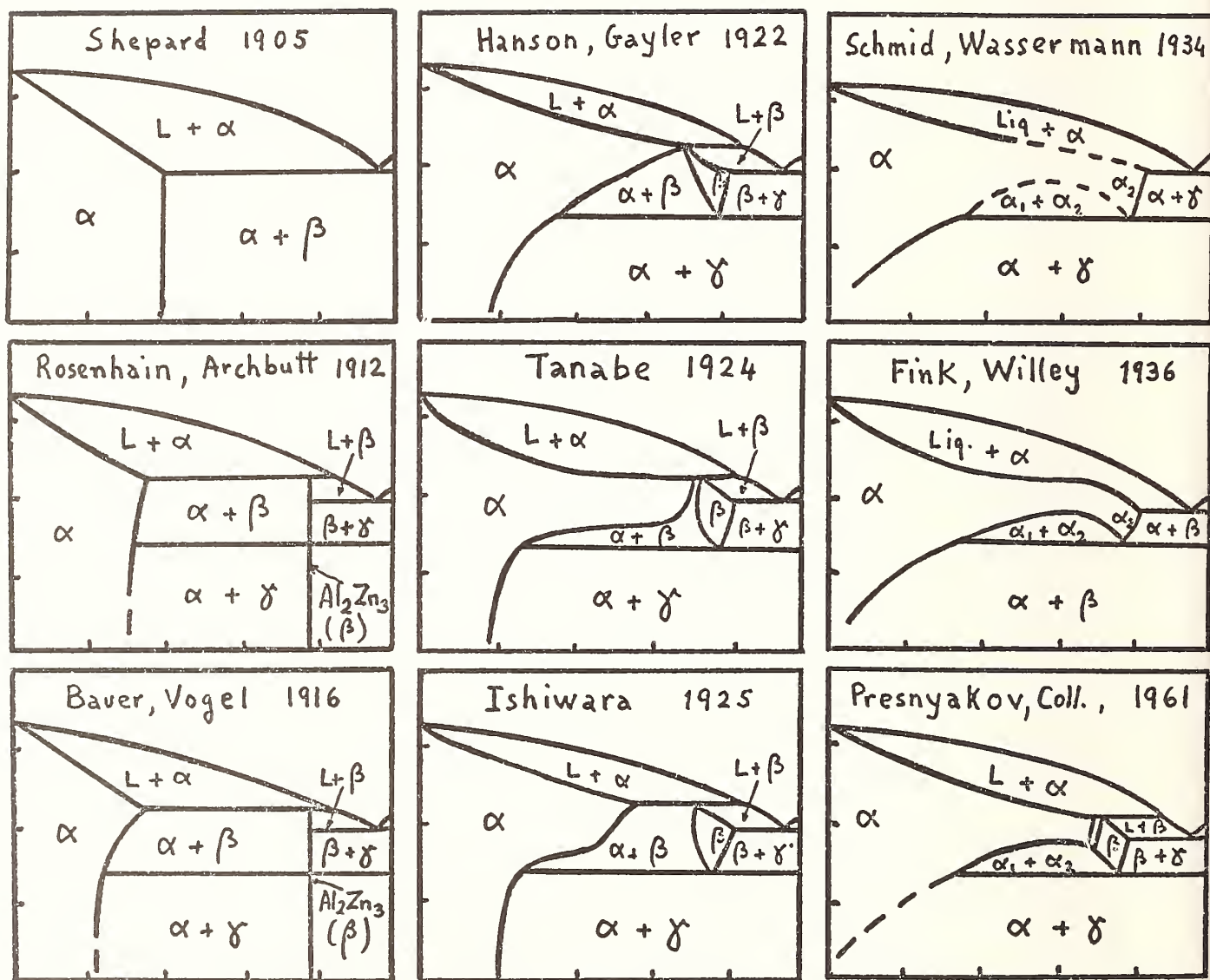


FIG. 9 SOME OF THE AlZn EQUILIBRIUM DIAGRAMS PUBLISHED WITH NAMES OF THE INVESTIGATORS AND DATE (SEE ALSO REFERENCES).

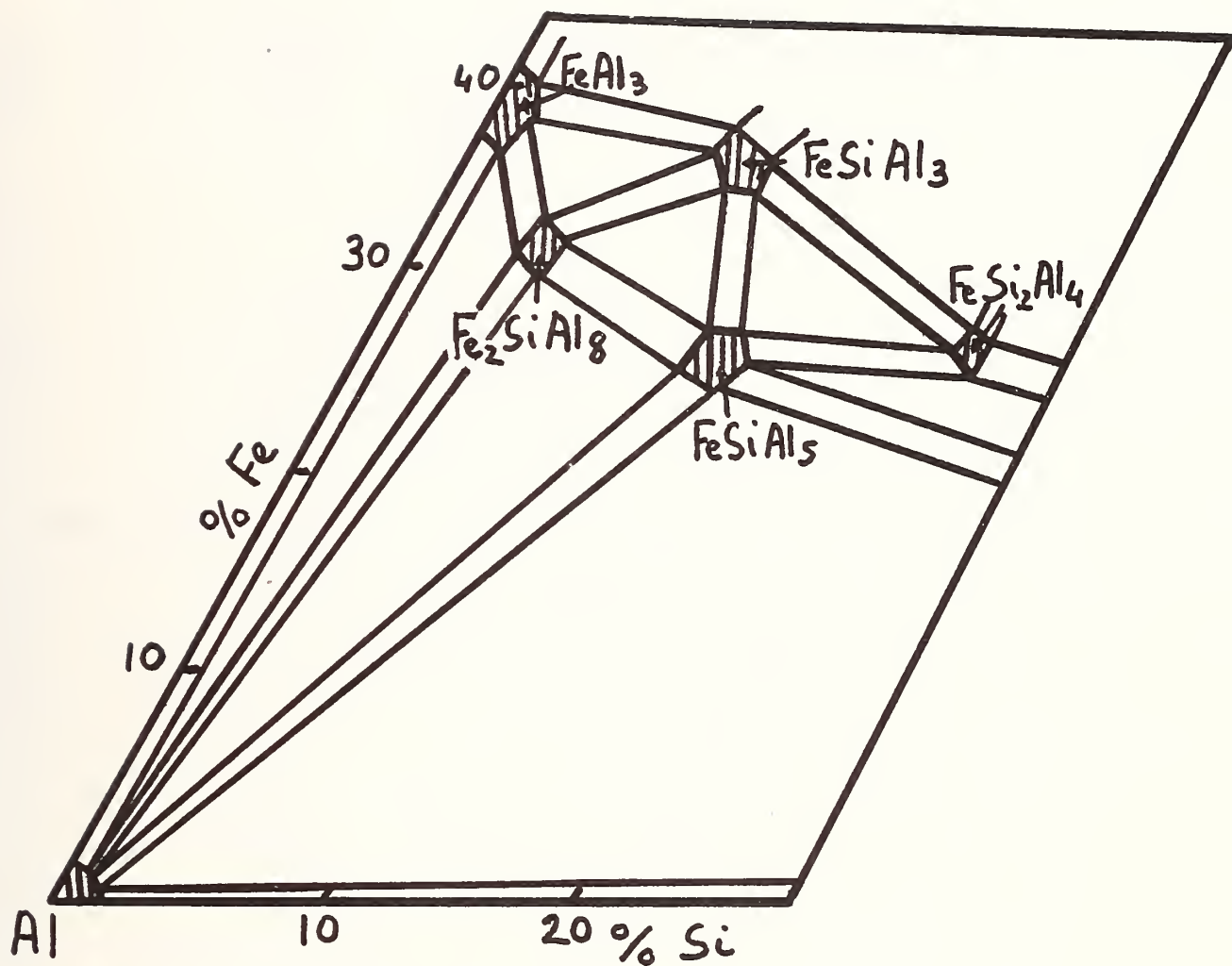


FIG. 10 THE AlFeSi EQUILIBRIUM DIAGRAM, THAT REPRESENTS THE STRUCTURE OF COMMERCIAL PURE Al.

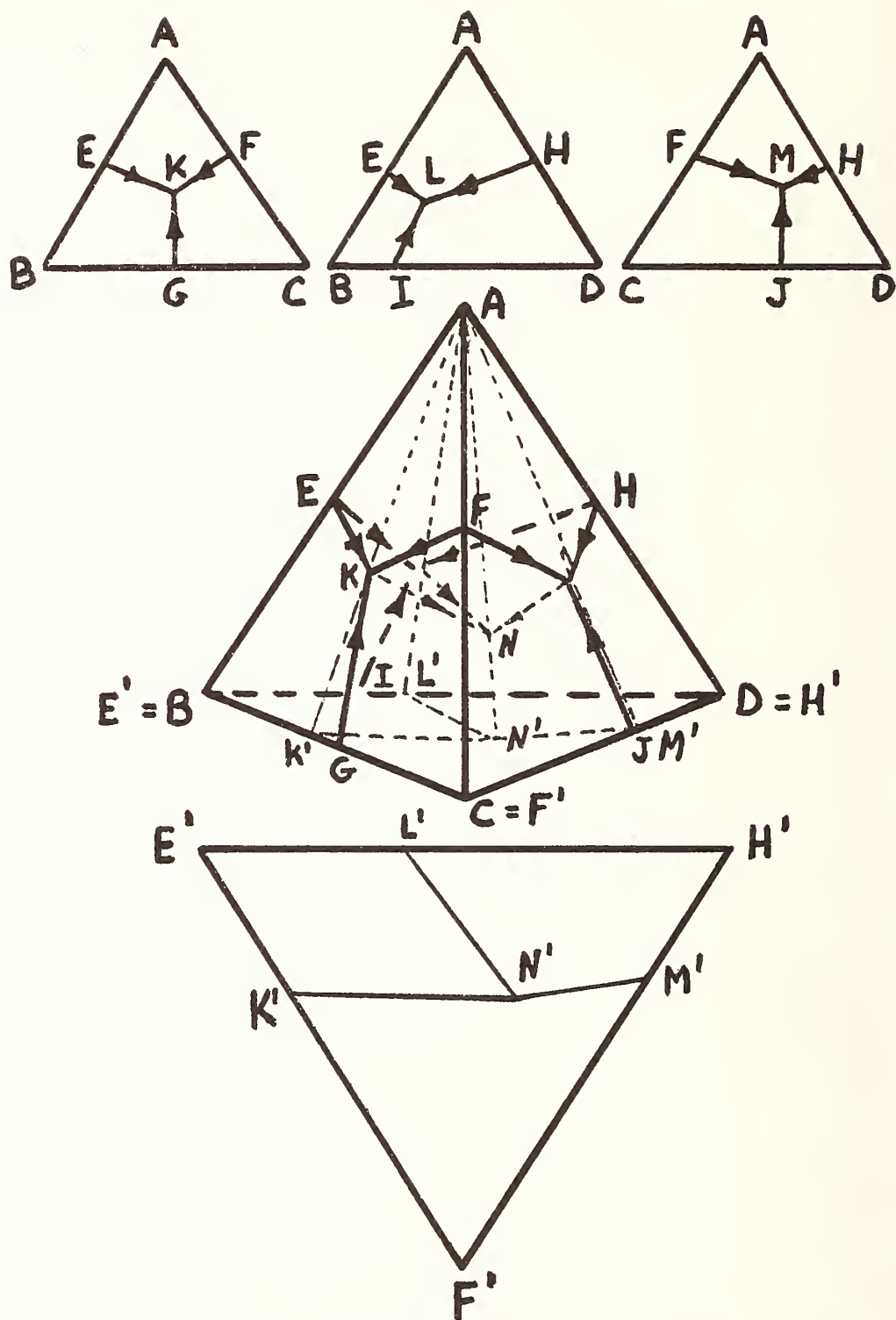


FIG. 11 PHRAGMEN'S METHOD OF PROJECTING QUATERNARY DIAGRAM ON A PLANE. AT THE TOP THE LIQUIDUS OF THREE HYPOTHETICAL DIAGRAMS ABC , ACD , ABD . IN THE CENTER THE QUATERNARY PYRAMID AND (DASHED) THE EUTECTIC LINES IN THE QUATERNARY DIAGRAM. DOTTED LINES SHOW HOW THE PERTINENT POINTS ARE PROJECTED ON THE BASIS OF THE PYRAMID, AND BELOW IS SHOWN THE PROJECTION THAT RESULTS.



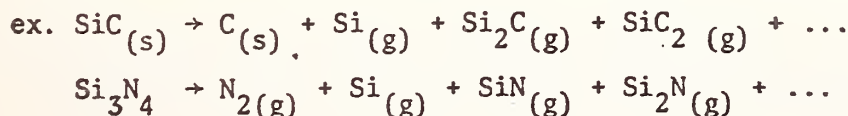
Phase Equilibria in the Development
of High Temperature Structural
Ceramics

Savante Prochazka
General Electric Research and Development
P.O. Box 8
Schenectady, New York 12345

Oxidation resistance, low thermal expansion and low creep rates are first-approach criteria for the development of high-temperature engineering ceramics (temperatures 1300°C and above). Prime candidates are covalently bonded compounds, SiC, Si₃N₄, Si-Al-O-N solid solutions and perhaps AlN, some transition metal borides and materials based on combinations of these compounds. Single phase ceramics are believed to offer the highest temperature capability, but the presence of some other specific phases is usually required for fabrication purposes and for microstructural control and control of related properties. All consolidation processes developed for these materials involve chemical reactions, additions and thermal treatments. Information on phase equilibria is essential for understanding fabrication processes, which are usually established empirically, and the behavior of the materials at high temperature and their interactions with the environments.

The types of chemical processes and equilibria which need to be understood in this field of ceramics may be grouped into the following categories.

A. Pure compound in equilibrium with its decomposition products:



B. Stability of polymorphs and the effect of some species on phase transitions between polymorphs:

ex. β - SiC \rightarrow α - SiC

effect of N_2 , O_2 , metals (Si) etc.

α - Si_3N_4 \rightarrow β Si_3N_4

effect of O_2 , metals (Si) etc.

C. Limits of nonstoichiometry in pure compounds.

D. Solubility limits in pure compounds of species used to promote sintering.

ex. B, Be, Al, La, in SiC

E. Phase relations, composition ranges and esp. solidus and liquidus temperatures in systems of interest:

ex. Si - Al - N - O

Si - Mg - N - O

Si - C - B

Si - Al - C - N

F. Phase relations in oxidation products:

ex. $Si_3N_4 + MgO \rightarrow SiO_2 + Mg_2SiO_4 \rightarrow 2 MgSiO_3$

G. Interaction of the parent material and its oxidation products in the environment of combustion products containing

CO , SO_2 , Na_2O , V_2O_5 etc.

H. Interaction of nickel and cobalt based refractory alloys with the base material.

Much of the information does not exist; its generation will be slow and will require unconventional techniques.



Phase Diagram Information for Processing of Superconductors *

David Dew-Hughes
Metallurgy and Materials Science Division
Department of Applied Science
Brookhaven National Laboratory
Upton, New York 11973

High critical temperature (>20 K) superconductors, and conductors developed therefrom, are essential if superconductivity is to make a serious impact upon electrical engineering practice. The highest critical temperatures are found in compounds with the A15 crystal structure based upon vanadium or niobium. V_3Ga and Nb_3Sn are already established as commercially available conductors, with T_c 's of 15 K and 18 K, respectively. The potentially superior compounds Nb_3Al (19 K), Nb_3Ga (20.3 K) and Nb_3Ge (22.5 K) have yet to be developed as conductors.

The superconducting properties of A15 compounds are maximized in well-ordered, stoichiometric samples (see, for example, reference ⁽¹⁾ for a review of the properties of A15 superconductors). In the Nb-Al, Nb-Ga and Nb-Ge systems the equilibrium A15 phase field does not include the stoichiometric composition. The problem is that of phase competition referred to by Professor Massalski in the first session of this meeting. The presence of a stable σ or σ -related compound pushes the range of homogeneity of the A15 compound to the niobium-rich side of the 3:1 composition, as shown in figure 1. The extreme example is Nb_3Ge , which can have a T_c as high as 23 K. When prepared by

*Research carried out under the auspices of the United States Energy Research and Development Administration under Contract No. EY-76-C-02-0016.

bulk melting techniques, the composition of the Al5 phase corresponds to Nb_4Ge with T_c of only 6 K. The phase diagram can be beaten by non-equilibrium techniques such as sputtering, chemical vapor deposition, and high vacuum evaporation, all of which can yield thin film material with T_c 22-23 K. It is possible that the addition of a third element will alter the relative stability of the Al5 and σ phases, allowing the Al5 phase to form at stoichiometry. A precise understanding of phase stability might enable the nature of this third element to be predicted. In the Nb-Al-Ge ternary system, an Al5 compound, $\text{Nb}_3(\text{Al}_{.8}\text{Ge}_{.2})$ forms close to stoichiometry. This is believed to be due to a miscibility gap between Nb_2Al and Nb_5Ge_3 just allowing the Al5 phase field to advance to the stoichiometric composition, figure 2. A similar situation exists in the Nb-Al-Si system. The existence of the miscibility gap has been related to the presence of a eutectic in the Al-Ge and Al-Si systems⁽¹⁾. There is also a eutectic in the Al-Ga system, and a miscibility gap between Nb_2Al and Nb_5Ga_3 ⁽²⁾. It is important to know if this is a general rule, and if so, are there other ternary systems based on niobium which allow of the formation of a high T_c stoichiometric Al5 phase.

Conductor wire based on Nb_3Sn is fabricated by the 'bronze' process⁽³⁾. In this process, filaments of niobium are drawn down in a bronze (Cu-Sn) matrix and subsequently reacted to form a layer of Nb_3Sn . The process is also applicable to V_3Ga , but not to Nb_3Al , Nb_3Ga and Nb_3Ge . Again, the more stable σ and $\bar{\sigma}$ -related phases intervene. The system is now a ternary between niobium, copper and a third element. Diffusion between two phases in a ternary system follows the two-phase tie-lines⁽⁴⁾. If there is no tie-line route leading directly from the copper

solid solution to the Al₅ phase, then it is unlikely that the phase will form. In the case of Nb-Cu-Sn, there are direct tie-lines from the copper-tin solid solution (bronze) to the Al₅ phase, Nb₃Sn, figure 3, and the process is successful for Nb₃Sn. In the Nb-Cu-Ge ternary the tie-lines from the copper-germanium solid solution lead only to either of the phases Nb₅Ge₃ or Nb₃Ge₂, at low and high germanium concentrations, respectively⁽⁵⁾ (see Fig. 4). These phases are more stable than Nb₃Ge, and therefore do not allow the latter to form⁽⁶⁾. A Nb-Al-Cu ternary μ -phase intervenes between the Cu-Al solid solution and Nb₃Al in the Nb-Al-Cu ternary⁽⁷⁾. In the V-Cu-Si system the tielines lead to V₃Si at low, $\sim 1\%$ Si concentrations in the copper but to V₅Si₃ as the silicon content is increased⁽⁸⁾.

A knowledge of the various ternary diagrams is necessary in order to predict diffusion routes. It would also be advantageous to know whether the addition of a fourth element is likely to alter phase stability and tie-lines such that the desired Al₅ phases become accessible by a direct diffusion path.

References

1. D. Dew-Hughes, Cryogenics 15, 435 (1975).
2. M. Drys, J. Less Common Metals 44, 229 (1976).
3. M. Suenaga, W. B. Sampson and C. J. Klamut, IEEE Transactions on Magnetics MAG-11, 231 (1975).
4. J. B. Clark and F. N. Rhines, Trans. A.S.M. 51, 199 (1959).
5. R. H. Hopkins, G. W. Roland and M. R. Daniel, Metallurgical Transactions 8A, 91 (1977).
6. T. S. Luhman, O. Horigami and D. Dew-Hughes, Applied Polymer Symposium No. 29, 61 (1976).
7. C. R. Hunt, Jr. and A. Raman, Zeit. Metallkunde 59, 701 (1968).
8. J. D. Livingston, to be published.

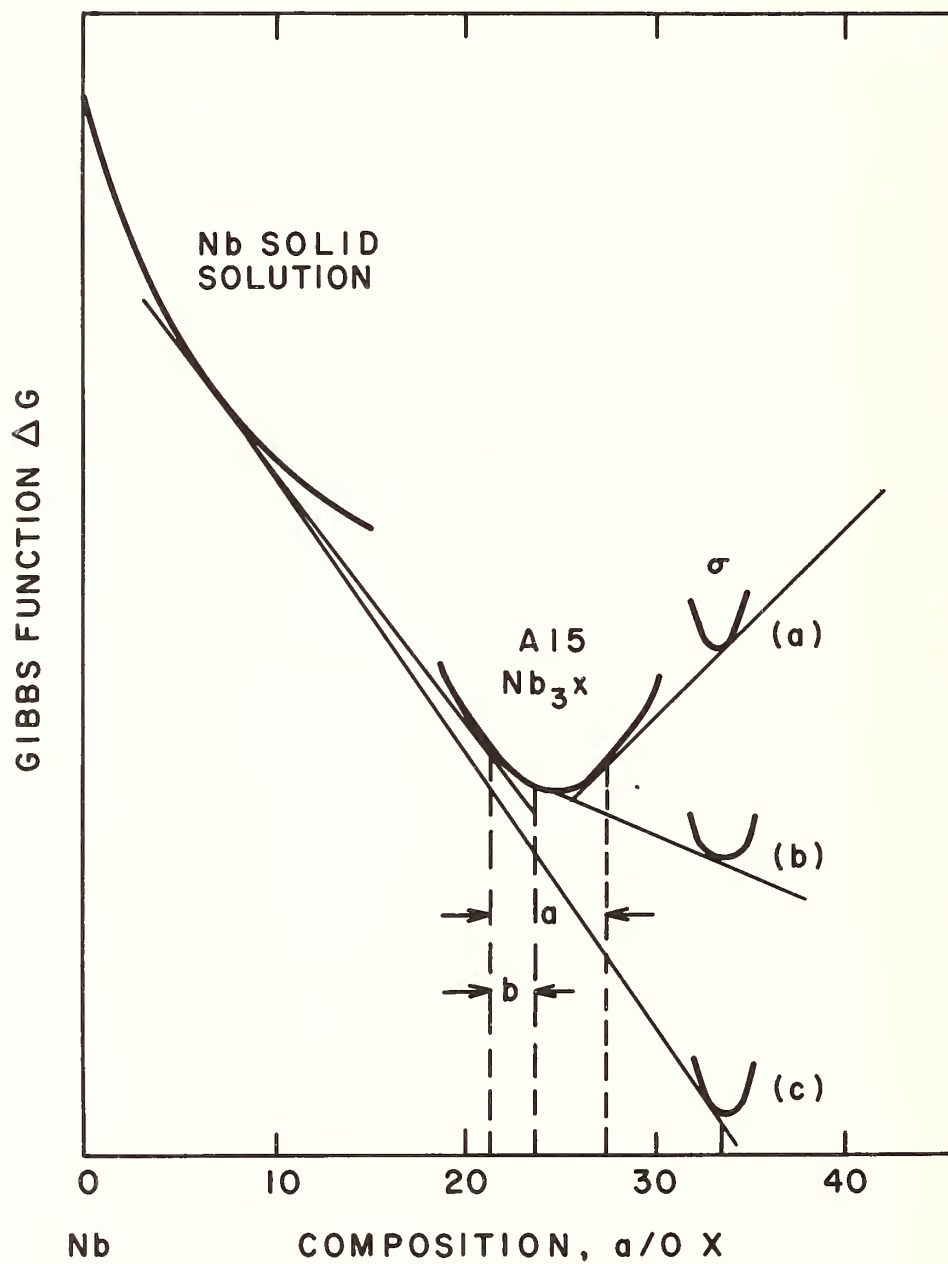


FIGURE 1. Hypothetical Nb-X binary system, showing how the range of homogeneity of the Nb₃X Al₅ phase is reduced by increasing stability (lower ΔG) of the competing σ phase.

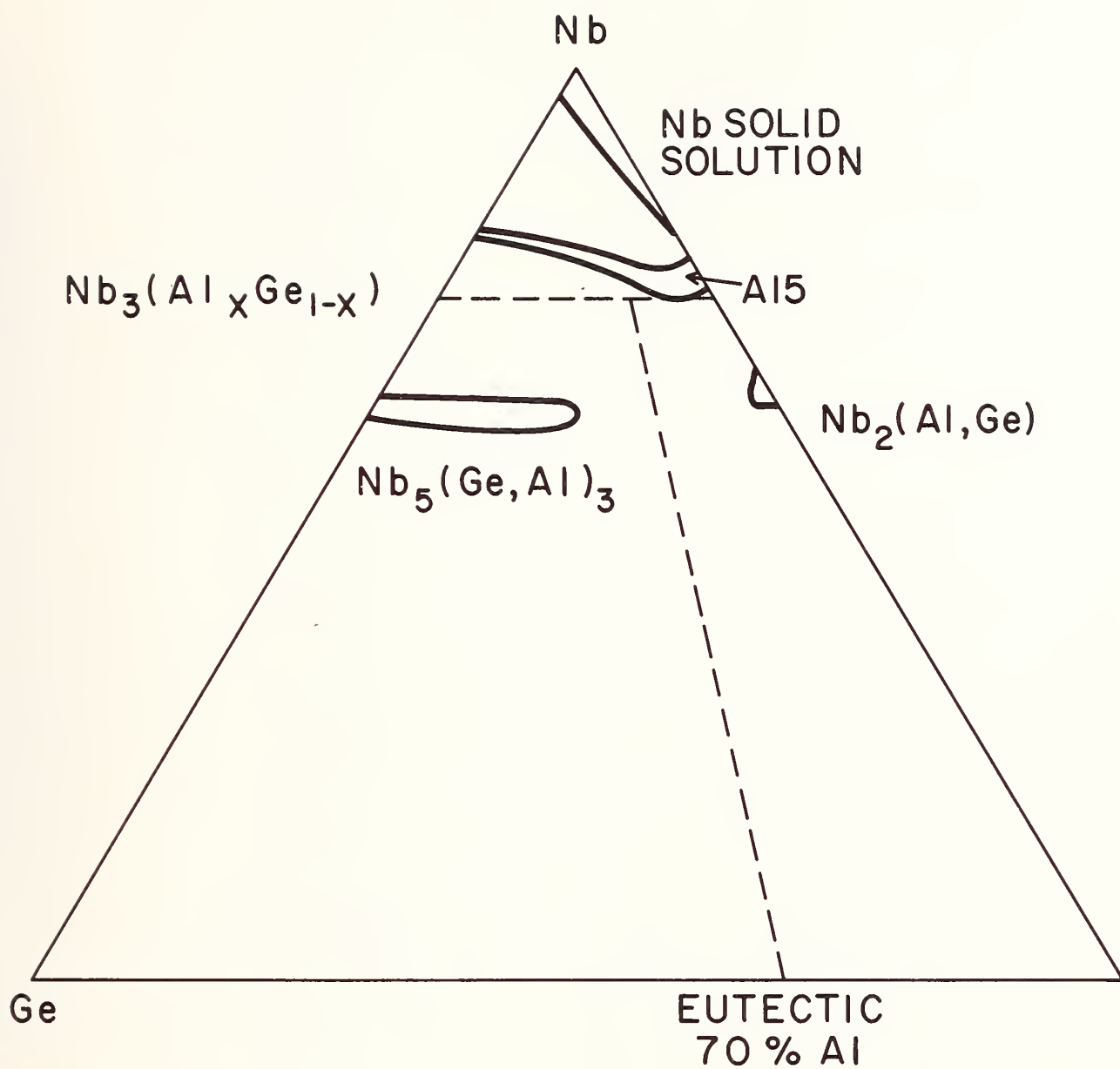


FIGURE 2. A section of the Nb-Al-Ge ternary phase diagram at 1840°C (after reference (1)).

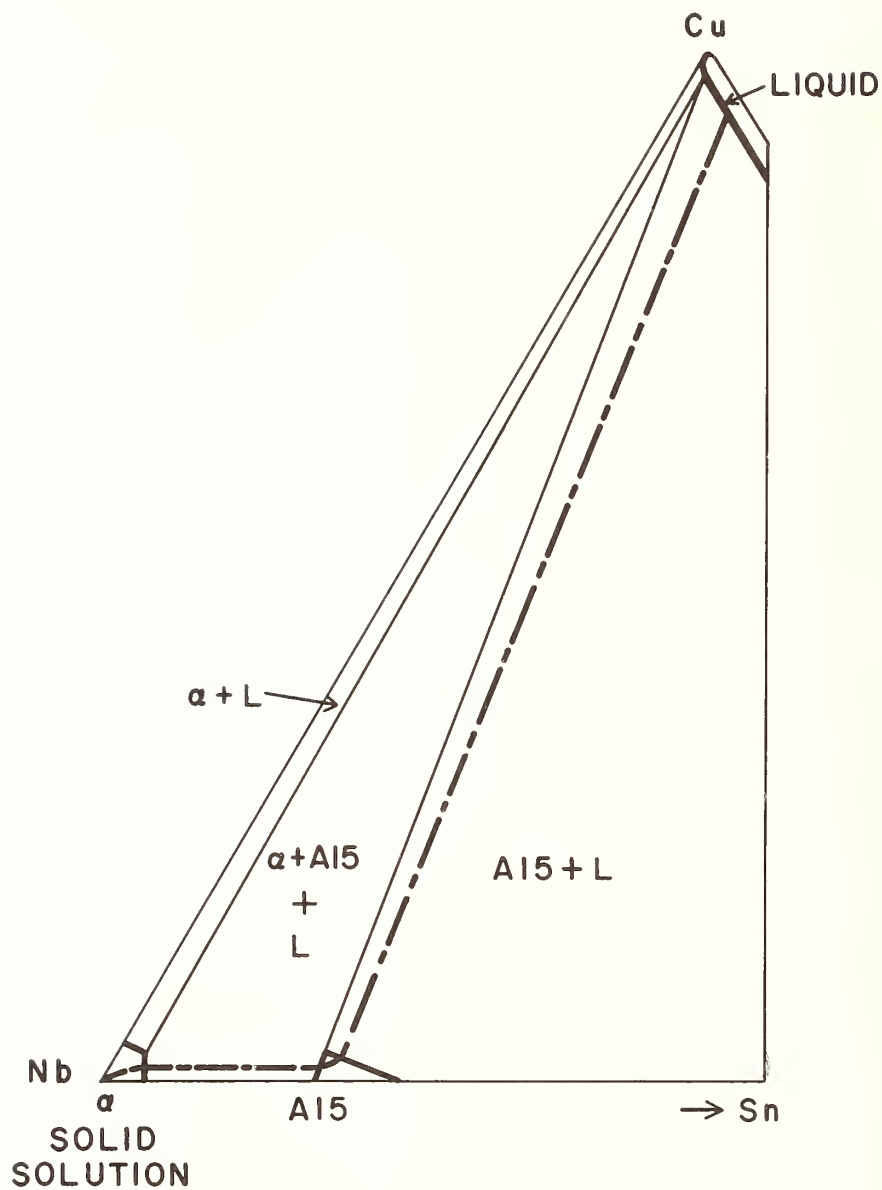


FIGURE 3. A section of the Nb-Sn-Cu ternary phase diagram at 1100°C, showing the diffusion path between Nb and Cu-Sn solid solution, via Nb_3Sn (after reference (5)).

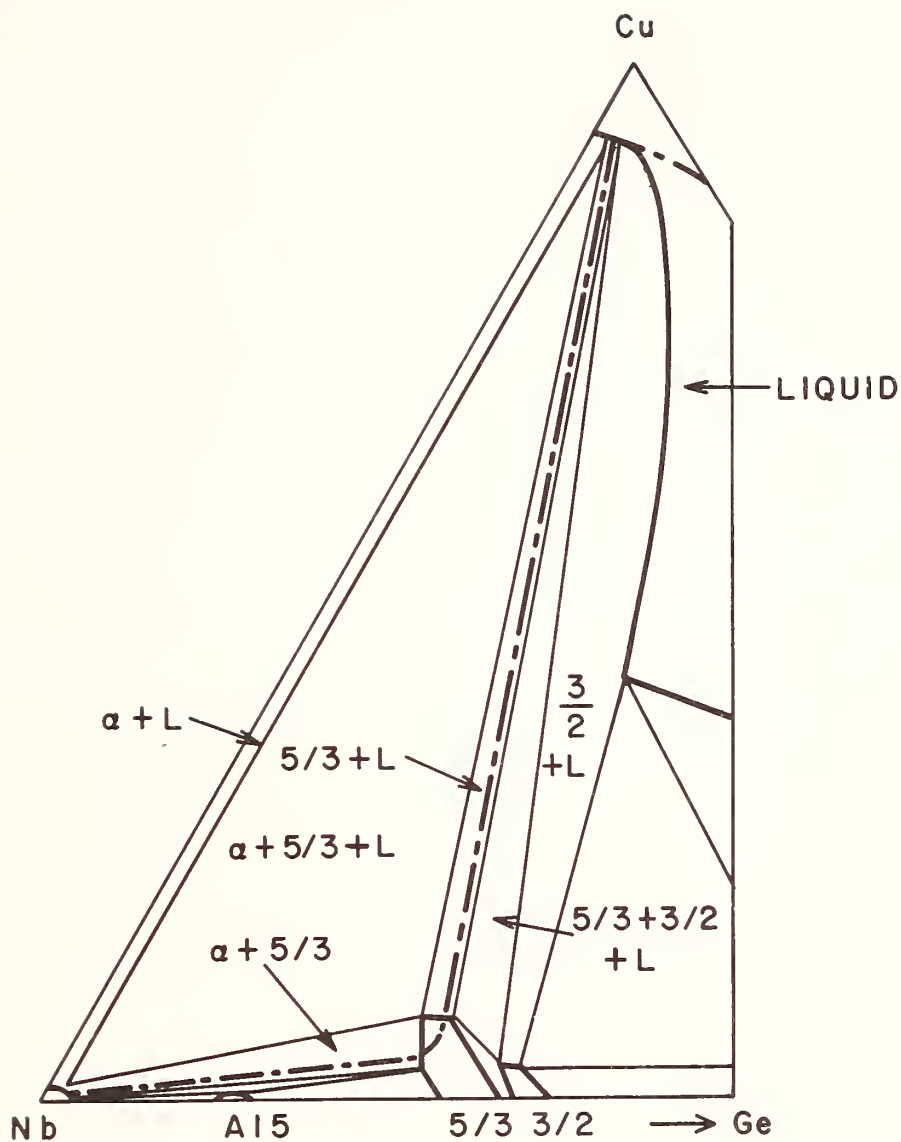


FIGURE 4. A section of the Nb-Ge-Cu ternary phase diagram at 1100°C, showing the diffusion path between Nb and Cu-Ge solid solution. The Nb_3Ge phase is cut off by the intervention of the $5/3$ phase (after reference (5)).

PANEL IV

Product Applications

(User Needs for Phase Diagram Information)

Moderator: F. L. VerSnyder, Materials Engineering
and Research, Pratt and Whitney Aircraft,
U.T.C., E. Hartford, CT

Panel Members:

C. Greskovich, Research and Development Center,
General Electric Co., Schenectady, NY

R. I. Jaffee, Fossil Fuel & Advanced Systems
Div., Electric Power Research Institute,
Palo Alto, CA

B. H. Kear, Materials Engineering and Research
Laboratory, Pratt and Whitney Aircraft, U.T.C.,
Middletown, CT

A. I. Mlavsky, Sr. Vice President of Technology,
Tyco Laboratories, Inc., Waltham, MA

P. Slick, Bell Telephone Laboratories,
Allentown, PA



PANEL DISCUSSION: PRODUCT APPLICATIONS

Opening Remarks by the Moderator

F. L. VerSnyder

Materials and Engineering Research*

Pratt and Whitney Aircraft, U.T.C.

E. Hartford, CT 06108

After introducing the panel members, Chairman VerSnyder gave a brief example of phase diagram applications to a bonding method called Transient Liquid Phase Bonding which is used in the production of gas turbine engines. This method produces high quality bonds with properties that are equivalent to the materials being joined, with the simplicity in production that is characteristic of a simple brazing operation, thus avoiding exceedingly costly processes.

A summary of VerSnyder description of the Transient Liquid Phase Bond (TLP Bond), follows in these paragraphs.

In TLP bonding a thin (.001 - .004") interlayer alloy of specific composition is placed between the mating surfaces of the parts to be joined. The parts are held together under slight compressive pressure (only a few psi is necessary) and heated to the bonding temperature (typically 2000 - 2200°F) in protective atmosphere (vacuum or inert gas). At the bonding temperature, the interlayer initially melts filling the gaps between the mating surfaces with a thin liquid layer. While the parts are held at the bonding temperature, interdiffusion between the interlayer and the parent material raises the melting point of the joint and causes it to solidify isothermally, thus forming a bond. At the completion of isothermal solidification, the joint microstructure generally resembles that of the base metal except for some residual compositional and structural heterogeneity. At this stage the bond has excellent properties although not fully equivalent to the parent metal. To obtain bonds with strengths similar to that of the parent metal, the bond thermal cycle can be continued to further homogenize the joint composition and structure until it is essentially equivalent to the base metal.

Unlike most other practical metallurgical processes, the TLP bonding process occurs under equilibrium conditions. For this reason, the pertinent phase relationships existing during a TLP bond cycle can be viewed with respect to a classic equilibrium phase diagram. The TLP interlayer alloys are designed so they are similar in composition to the alloys being joined, with the principle exceptions that 1) some parent metal elements are either excluded or limited in amount to avoid unwanted phase formation and 2) a melting point depressant is added (currently, boron is utilized as our primary melting point depressant).

*presently Manager, Materials Technology, United Technologies Research Center,
East Hartford, CT 06108

This view of TLP bonding as an equilibrium process aids further in understanding the influence of many of the bond process variables, the principal variables being base alloy and interlayer composition, bond temperature and bond time. Depending on the base alloy being bonded (or dissimilar metal combination, which is also possible), the interlayer is "tailored" to provide as homogeneous a joint in as short a time as possible. This is done by matching the solute/hardener content of the interlayer as close as possible to the base alloy. For example, titanium is normally excluded since it promotes the formation of undesirable stable precipitates in the joint. Also, the melting point depressant, boron, is added at levels just sufficient to cause enough melting for good bonding. In most cases, less than 100% melting is required (interlayer composition is in the $\alpha + L$ region at the bond temperature). While these interlayers are brittle in bulk form, P&WA has developed and patented a method for making them as ductile foil.

The TLP bonding process is now utilized for the production bonding of low pressure turbine vane clusters for the JT9D engine. By clustering vanes in this manner, significant engine performance improvements are realized primarily as a result of reduced turbine air leakage between vanes. Simple ceramic fixtures are used to hold the vanes in the proper position and also to provide the dead weight loading used during the bond cycle. Both new and previously used vanes (for retrofit into existing engines) have been clustered. Since 1972 over 116,000 clusters have been bonded at a yield well in excess of 99%. These figures demonstrate the production applicability and reliability of this joining process.

VerSnyder concluded:

"I do not think we would ever expect anyone to try to work out all of the details of the foil composition, because, like the superalloy itself, it contains at least five or six components, perhaps not ten, but, at least five or six. General phase information on these superalloy systems is very helpful and with an adequate supply of information we then can carry forward and complete the in-depth process of getting information that finally leads to the application."



"IMPORTANCE OF PHASE DIAGRAMS IN THE ELECTRIC POWER INDUSTRY"

R. I. Jaffee

Electric Power Research Institute
Palo Alto, California 94304

To talk on behalf of phase diagrams is like talking on behalf of truth and love, because everybody is in favor of them. In the electrical power industry, equipment must last for lifetimes of 20-40 years at elevated temperatures in many cases. Under these conditions, equilibrium has a very good chance of being attained. In fact, many problems occur because materials are placed in service that are not in equilibrium, and become equilibrated in service, with an accompanying detrimental change in properties.

It is true that many commercial alloys are complex with many alloying components, generally greater than four. Thus, phase diagram information, which is generally limited to ternary equilibrium at best, is not strictly applicable. However, it is my observation that most alloys are dominated by two or three elements, and that a great deal of useful information can be obtained from binary and ternary phase diagrams. In cases where more accurate information is needed, quaternary and even quintanary sections, where the base composition is kept fixed, and alloy elements are varied over limited alloying ranges, can be developed. It is surprising, therefore, that the conference is so negative about the difficulty of the problem of dealing with multi-component equilibrium. Generally, one is concerned with a fairly specific composition, whose deviation from equilibrium is of primary concern. This problem certainly can be handled.

A major problem is metastable equilibrium, which is usually encountered in industry. A typical example is carbide equilibrium in steel. The formation of carbides takes place by kinetic and not equilibrium forces, such that the easiest carbide to form generally forms first. It then may transform to other carbides during elevated temperature service. Ultimately, the carbide itself may be metastable, and one ends up as graphite. No one would develop a practical steel on the basis of the iron-graphite diagram. In real life, one must deal with metastable equilibrium systems.

As an example, take pressure vessel steels for coal conversion. The pressure vessel is generally maintained at 400-500°C maximum. In the case of coal liquefaction, it contains 40-50% hydrogen and hydrogen sulfide at pressures up to several hundred atmospheres. A type of phase diagram is used to design such pressure vessels. It is called a Nelson diagram in which the safe operating temperatures and hydrogen pressures are plotted for various pressure vessel steels. A typical Nelson curve is shown in Figure 1. These curves are based on operating experience, in that at some time decarburization or actual failure of pressure vessels made of the particular steel occurred under T-P conditions above the line, and satisfactory operation has been obtained below the line.

The pressure vessels may fail by hydrogen attack at elevated temperatures or hydrogen embrittlement at low temperatures. In the hydrogen attack case, hydrogen diffuses into the steel and reacts with carbides, forming

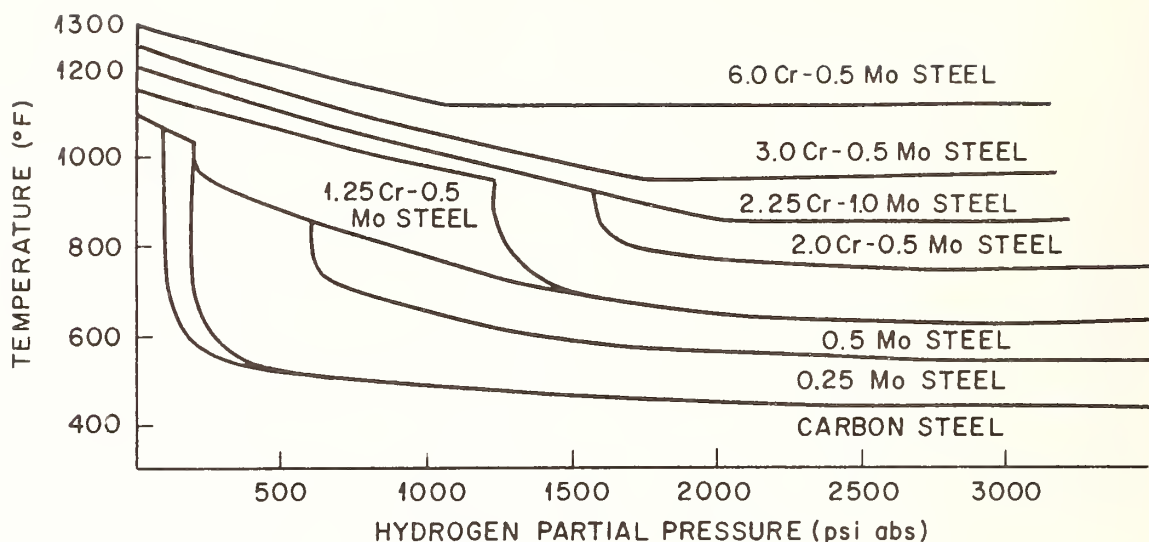


Fig. 1. Operating limits for steels in hydrogen service - the Nelson curves.

internal methane at high pressure, which is trapped at the point of formation, and facilitates crack propagation. In the case of hydrogen embrittlement, the solubility of hydrogen decreases with temperature. A high internal hydrogen pressure may develop if the vessel is cooled too rapidly for the hydrogen to diffuse out of the steel. These are all situations that can be described by phase diagrams involving hydrogen and methane in equilibrium with steel. The carbide in the steel may itself be in a stage of metastable equilibrium. Much higher methane pressures are developed with iron carbide than with alloy carbides. Thus, for safe operation of pressure vessels, it is important to employ heat treatment schedules which develop the equilibrium carbides.

Another example of interest to the electric power industry has to do with the segregation of non-metallic elements such as phosphorus, antimony,

tin and silicon to the grain boundaries of steel during elevated temperature operation. Grain boundary segregation reduces low temperature ductility and is called temper embrittlement. The problem was not properly understood for many years until improved methods to study grain boundaries were developed. The principal technique was Auger electron spectroscopy, which permits the extent of grain boundary segregation to be measured. In this regard, it is clear that phase equilibrium at grain boundaries is considerably different from equilibrium within the grain itself. It might be worthwhile to develop phase diagrams in which equilibrium at grain boundaries and surfaces are described.

Another industrial problem of interest to both steam and gas turbines is the phase stability of the alloys, which are exposed to elevated temperatures over long periods of service. It is desirable to be able to predict the approach to equilibrium. Considerable use has been made of the electron vacancy concept known as "Phacomp".* This is essentially an adaptation of the rigid band model of electron structure of transition metals. If the maximum number of stable d electrons is taken as 10, the electron vacancy is the average group number subtracted from 10 after allowing for the stable compounds such as carbides that precipitate from solid solution before the alloy is placed in service. The electron vacancy number of alloys is then correlated with the occurrence of embrittling phases such as Laves or sigma phases, which are found to occur in specific ranges. The alloy designer tries to keep his alloy composition away from these ranges. Another phase stability method being developed

*Editor's note: The paper by R. L. Dreshfield (Panel I) in these proceedings gives a more detailed description of the Phacomp concept.

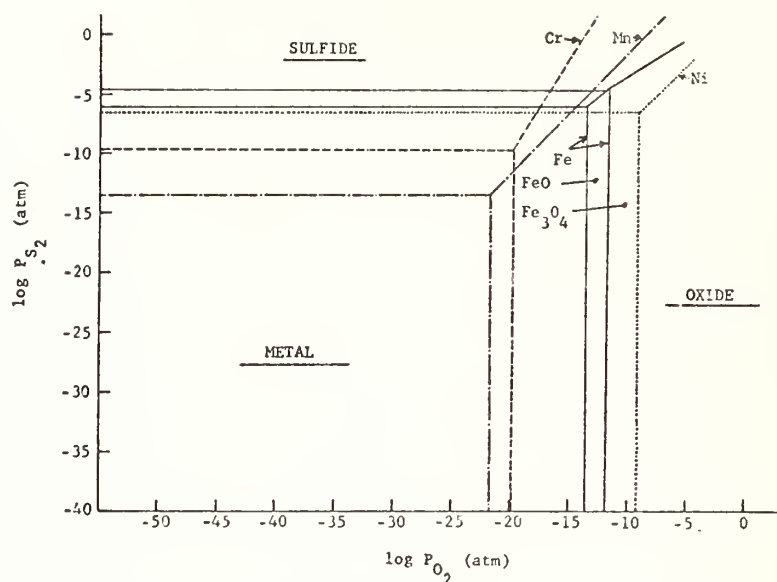


Fig. 2. Comparison of Metal-S-O Diagrams at 1366°K (2000°F) for Cr, Mn, Fe and Ni.

by Machlin at Columbia uses a pair potential method, where the energy in the complex alloy is summed up and minimized. The pair potential method has an advantage over Phacomp in that it does not require the constant electron vacancy value for each group of the Periodic table.

Another type of phase diagram of interest in the power industry has to do with equilibrium between non-metallic phases and alloys. These are important in hot corrosion of turbines and boilers. An area of current interest is the solubility of impurities in steam. In the low pressure steam turbine, highest concentration of impurities precipitate first, and can cause pitting and stress corrosion. For example, high caustic concentration droplets may form on the blades, discs and shafts of the LP turbine, which creates a stress corrosion and corrosion fatigue hazard.

The last example is the use of so-called phase stability diagrams in hot corrosion. These are Pourbaix-Ellingham diagrams which are constructed from the standard free energy formation of the oxides, sulfides or carbides converted to an equivalent dissociation pressure from the relationship,

$$\Delta G^0 = RT \ln K. \text{ For the reaction } M + \frac{1}{2}O_2 = MO, K = \frac{a_{MO}}{a_M \times P_{O_2}^{1/2}}$$

Taking activities of the solids at unity, $\Delta G^0 = RT \ln P_{O_2}^{-1/2}$

This permits the oxygen partial pressure to be calculated as a function of temperature. Figure 2 shows Metal-S-O diagrams for Cr, Mn, Fe, and Ni. The stable phases that form as a function of P_{O_2} , P_{S_2} , and a_C of a multi-component gas or condensed salts in contact with metallic alloys can be predicted from these diagrams. They are also helpful in guiding conditions of operations to avoid excessive corrosion that might occur if the reaction products are molten.



Summary of Presentation on User Needs of Phase Diagrams: The Solar Energy Field

A. I. Mlavsky
Sr. Vice President of Technology
Tyco Laboratories, Inc.
Waltham, MA

Several requirements in the solar energy field were outlined that could be met with better phase diagram information.

Heat Storage

The ability to store heat at various pre-selected temperatures in compact systems would be of great value in a variety of solar energy systems. Salt mixtures with eutectic temperatures of 160°F for space heating and hot water, 220°F for absorption air conditioners, and 500 - 800°F for steam turbine or Rankin cycle engines would be of great value.

Solar Cells

Low cost silicon solar cells for terrestrial use require non-noble metal contacts to silicon surfaces, these contacts meeting certain stringent criteria. They must be ohmic, and of low resistance; they must be applied to the silicon by low cost techniques such as plating (electro or electroless) or screen printing; they must be adaptable to either copper or aluminum wires as power leads. Although there clearly have been developed many excellent ohmic contacts to silicon, the criteria of low cost both in the metals chosen and their means of application are quite specific to the solar cell requirements. Detailed phase information will be necessary to permit the development of such contacts. Although simple binaries between metal and silicon are well defined, there is seldom any detailed information in the 99 - 99.9% silicon-rich range. The interface region at a contact is indeed in this range.

The problem becomes even more acute in making contact to compound semiconductors where at least three component systems must be considered.

Any information which could be generated by practitioners of classical phase equilibria techniques would find a very ready audience among developers of low cost solar cells.



Summary of Presentation given for Panel IV by

P. Slick

Bell Telephone Laboratories

Allentown, PA 18103

on

The Use of Phase Equilibria in the Manufacture of Spinel Ferrites

(summary prepared by the editor of these proceedings)

The importance of use of the condensed and phase equilibria for the manufacture of low-loss manganese-zinc-ferrites was discussed by Slick. Multicomponent equilibrium diagrams were said not to be available for the complex processes of deriving manganese-zinc-ferrite spinels, but existing information on condensed phase equilibria for simpler, related systems was said to be used to infer this information for the actual processes. To better understand the mechanisms involved, additional data on phase equilibria were said to be important.

The material manganese-zinc-ferrite, discussed by Slick, is employed in magnetic components of inductors used in filter circuits for telecommunication networks and these materials were said to require close control manufacturing conditions, since the important properties are very dependent on chemistry, microstructure, and defect state (i.e. cation vacancies, nonmagnetic inclusions of second phase and porosity, and compositional inhomogeneity).

Slick noted that one of the most important requirements for low loss ferrite materials is to have a high resistivity phase at grain boundaries. The formation of a high resistivity phase at grain boundaries is needed to reduce eddy current losses, and is exemplified by a condensed phase equilibrium. Minute quantities of calcia and silica, added to the spinel ferrites were said to produce this high resistivity boundary. The exact composition and phase, or phases are not known in the grain boundary, but analysis confirms the segregation of calcia and silica in the grain boundary.

Slick indicated that it is felt that the segregation of calcia and silica, at grain boundaries in manganese-zinc-ferrites may be manifested by a low temperature eutectic of some composition, even though no local phase has been found for the amounts of calcium silicate added in these materials. He noted that it would be of specific interest in this application to develop a phase equilibrium diagram of minute amounts of phases with a specific manganese-zinc-ferrite or any particular ferrite composition, calcia and silica, to better understand the mechanism for producing the segregation of calcium silicate in the grain boundary and especially its influence on high quality manganese-zinc-ferrite properties.



THE APPLICATION OF THE PHASE DIAGRAM TO THERMAL ENERGY STORAGE TECHNOLOGY

Jerry E. Beam
Air Force Aero Propulsion Laboratory
Wright-Patterson Air Force Base, OH 45433

and

Joseph E. Davison, Ph.D.
University of Dayton Research Institute
Dayton, OH 45469

1.0 INTRODUCTION

In our program, we are evaluating the potential of phase change thermal energy storage devices to provide heat energy to operate a Vuillieumier cooler for space satellite applications. We have selected the liquid-solid transformation as the energy storage mechanism. Our next step has been to identify liquid-solid transformations which have the largest storage capacity in the temperature range for our application. In this presentation, we have identified those pure components which are of primary interest and the type of data available in the phase diagram which can be utilized to assess the relative merits of different materials.

2.0 SELECTION OF MATERIALS

The tabulated values for the enthalpy of fusion and the melting temperature of the pure components provide a quantitative basis for the selection of phase change thermal energy storage materials. Values for selected elements, inorganic oxides, and inorganic fluorides are presented in Table 1. Extensive compilations of these values for different classes of pure components have been prepared and are available (1-11). The selection of a pure component as the energy storage media limits the application temperature to the melting temperature of the component. This limitation can be circumvented to some extent by selecting intermediate compositions between or among pure components. These intermediate compositions can be readily identified from the appropriate phase diagram. As an example, the melting points of the fluorides of lithium and magnesium are respectively 848°C and 1242°C.

TABLE 1
SELECTED VALUES FOR THE ENTHALPY OF FUSION AND
THE MELTING TEMPERATURE

	Enthalpy of Fusion	Melting Temperature	
	K Joules/gram	Deg. C	Ref.
a. Elements			
Carbon	(8.71)	(4327)	5
Boron	(2.05)	2027	5
Silicon	1.80	1412	5
Beryllium	1.36	1287	5
Phosphorus (red)	0.61	597	1
Germanium	0.51	937	5
Lithium	0.43	181	5
Vanadium	(0.41)	1902	5
Aluminum	0.40	660	5
b. Oxides			
ThO ₂	4.61	2952	3
BeO	2.53	2547	1
Li ₂ O	(1.96)	1570	1
MgO	(1.92)	2825	1
Al ₂ O ₃	1.16	2042	1
c. Fluorides			
LiF	1.04	848	1
MgF ₂	0.93	1242	1
NaF	0.79	996	1
CaF ₂	0.61	1127	1
FeF ₂	(0.55)	(1100)	1
ScF ₃	0.49	1227	3
TiF ₃	0.48	1227	3
KF	0.47	858	1

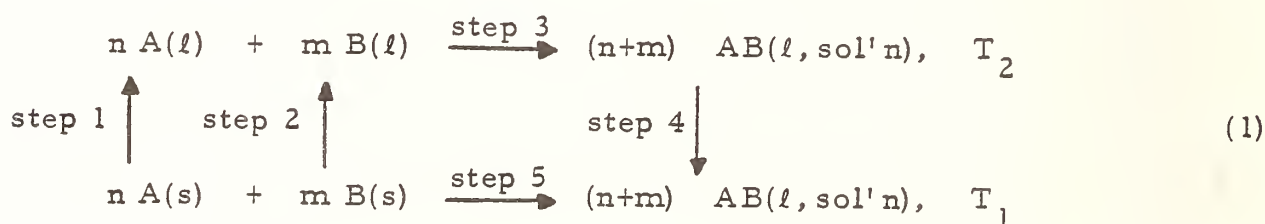
The phase relations in the binary system of these two components has been studied (11,12) and an eutectic transformation has been identified at 724°C and at 33 mole percent MgF₂. Additional invariant points of ternary eutectic compositions at lower temperatures may be obtained by adding NaF or KF. Thus, the temperature of the liquid-solid transformation can be tailored to the particular application. The types of liquid-solid transformations which

we have identified for our applications are the eutectic transformation and the congruent melting of an intermediate compound. The selection of these transformations is based on their reproducibility during cycling between the liquid and solid states. Although the peritectic reaction is reversible in a thermodynamic sense, the time required to attain an equilibrium state on cooling through the peritectic horizontal was judged to be unsatisfactory for short duty cycles.

2.1 THE ENTHALPY OF THE LIQUID-SOLID TRANSFORMATION

The amount of heat energy which can be stored or released in the isothermal and reversible transformation between a pure solid and liquid phase at constant pressure is obtained directly from the value for the enthalpy of fusion of the substance. However, when two solid phases of different compositions react to form a single liquid phase, then the value for the enthalpy of mixing must be taken into account to determine the amount of heat energy involved in the liquid-solid transformation.

The effect of the enthalpy of mixing on the energy storage capacity of a liquid-solid transformation can be assessed by consideration of the following thermodynamic cycle. The isothermal and reversible reaction between two solid phases may be considered as the sum of the following processes:



Step 1: Heat " n " moles of component A from temperature T_1 to T_2 . The enthalpy change of this step is given by,

$$\Delta H_1 = n \int_{T_1}^{T_A} C_{P,A} dT + n \Delta H_{M,A} + n \int_{T_A}^{T_2} C_{P,A} dT, \tag{2}$$

where T_A represents the melting point of pure A.

Step 2: Heat "m" moles of component B from temperature T_1 to T_2 . The enthalpy change for this step is given by,

$$\Delta H_2 = m \int_{T_1}^{T_B} C_{P,B} dT + m \Delta H_{M,B} + m \int_{T_B}^{T_2} C_{P,B} dT, \quad (3)$$

where T_B represents the melting point of pure B.

Step 3: React the two separate liquid components to form the AB liquid solution at a temperature of T_2 . The enthalpy change for this step is given by,

$$\Delta H_3 = (n+m) \Delta H(\text{mix}). \quad (4)$$

Step 4: Cool the AB liquid solution from temperature T_2 to T_1 . The enthalpy change for this step is given by,

$$\Delta H_4 = (n+m) \int_{T_2}^{T_1} C_{P,AB} dT. \quad (5)$$

Step 5: The value for the enthalpy of the liquid-solid transformation between the two solid phases, A and B, and the liquid solution, AB, at the temperature, T_1 , can be expressed as the sum of the enthalpies of the first four steps, and is as follows,

$$\begin{aligned} \Delta H_5 = & n \Delta H_{M,A} + m \Delta H_{M,B} + (n+m) \Delta H(\text{mix.}) + \\ & n \int_{T_1}^{T_A} C_{P,A} dT + n \int_{T_A}^{T_2} C_{P,A} dT + m \int_{T_1}^{T_B} C_{P,B} dT + \\ & m \int_{T_B}^{T_2} C_{P,B} dT + (n+m) \int_{T_2}^{T_1} C_{P,AB} dT. \end{aligned} \quad (6)$$

In the absence of data for the heat capacities of the liquid phase, the Neumann-Kopf Rule states that the heat capacity of a substance may be taken as the sum of the heat capacities of the elemental constituents. The application of this rule in the present analysis gives a zero value to the sum of heat capacity terms. As a result, the heat energy which can be stored in the isothermal liquid-solid transformation is given by,

$$\Delta H_5 \approx n \Delta H_{M,A} + m \Delta H_{M,B} + (n+m) \Delta H(\text{mix}). \quad (7)$$

The first two terms on the right-hand side of this expression are properties of the individual components. The last term on the right is the contribution due to the enthalpy of mixing. The effect of the enthalpy of mixing on the heat of the liquid-solid transformation can be either positive or negative depending on whether the reaction is endothermic or exothermic. If the reaction is endothermic, then the enthalpy of mixing is positive and additional heat energy can be stored in the transformation. If the reaction is exothermic, then the converse is true and less heat energy can be stored in the transformation than would be predicted from the properties of the individual components.

Unfortunately, the data for the enthalpy of mixing are available for relatively few systems. In order to obtain values for the enthalpy of mixing we have combined experimental data which is presented in the phase diagrams with analytical thermodynamic models to obtain the required data.

2.2 THE ENTHALPY OF MIXING

Analytical expressions for the liquidus and solidus phase boundaries can be obtained by combining basic thermodynamic principles with a thermodynamic model of the alloying behavior of the system. When the regular solution model is utilized to represent the alloying characteristics of the system, the following expressions have been obtained for the liquidus and solidus boundaries (13).

$$\Delta H_{fA}(T/T_A - 1) - RT \ln (X_A^\alpha / X_A^L) = W_1^\alpha (X_B^\alpha)^2 - W_1^L (X_B^L)^2, \quad (8)$$

and

$$\Delta H_{fB}(T/T_B - 1) - RT \ln (X_B^\alpha / X_B^L) = W_1^\alpha (X_A^\alpha)^2 - W_1^L (X_A^L)^2. \quad (9)$$

The values of the parameters, W^α and W_1^L , were calculated from Equations (8) and (9) with the known values for the enthalpies of fusion, ΔH_{fA} and ΔH_{fB} , the melting points, T_A and T_B , of the pure constituents, and the composition of the liquidus boundary, X_A^L and X_B^L , and the solidus boundaries, X_A^α and X_B^α , at the temperature, T . The enthalpy of mixing of the liquid solution is related to the parameter, W_1^L , by the expression,

$$\Delta H (\text{mix}) = X_A^L X_B^L W_1^L. \quad (10)$$

An underlying assumption in this approach is that the crystal structures of the two solid phases, A and B, are the same. If the crystal structures are different, then the enthalpy of the solid state transformation between the two structures must be known to obtain an exact solution. In the absence of any data, a zero value was assigned to the enthalpy of the solid state transformation. The data taken from selected phase diagrams and the results of the computations for the parameters W_L and W_S are presented in Table 2. The values of the composition of the solidus boundary were available on only a few of the systems studied. In the absence of any experimental data, a value of 0.999999 was assigned to the solidus composition. The calculated values for the enthalpy of mixing at a mole fraction of 0.5 are compared to experimental values which have been measured on these systems in Table 3. The negative values for the enthalpy of mixing have the effect of decreasing the energy storage capacity of the binary systems in accord with the relation 7. However, the magnitude of the decrease for the system, LiF - KF, represents less than 15 percent of the value for the enthalpy of fusion of the LiF.

3.0 SPECIFIC USER NEEDS

The phase diagrams which are of special interest to a phase change thermal storage technology base for space satellite applications are those which have the largest value for the enthalpy of the liquid-solid transformation

TABLE 2

EXPERIMENTAL DATA FOR THE TEMPERATURE AND COMPOSITION
OF THE LIQUIDUS AND SOLIDUS PHASE BOUNDARIES

System		Temp.	Mole Fraction		W _L	W _S
A	B	Deg. C	Liquidus	Solidus	K	Joules per Mole
a. Chlorides:						
AgCl	KCl	306	0.695	*	-10.2	---
AlCl ₃	KCl	250	0.495	*	-40.5	---
AlCl ₃	NaCl	152	0.490	*	-60.4	---
CaCl ₂	FeCl ₂	592	0.445	*	4.0	---
CaCl ₂	MgCl ₂	621	0.428	0.877	5.3	20.1
CaCl ₂	NaCl	500	0.52	*	-11.4	---
FeCl ₂	NaCl	370	0.43	*	-19.4	-4.8
FeCl ₃	NaCl	158	0.54	*	-39.5	---
KCl	LiCl	358	0.586	*	-16.8	---
LiCl	RbCl	312	0.5525	*	-19.2	---
b. Fluorides:						
KF	LiF	492	0.5	*	-17.2	---
KF	MgF ₂	778	0.85	*	-47.6	---
KF	NaF ₂	710	0.6	0.88	-0.01	22.4
LiF	MgF ₂	724	0.68	0.94	-1.3	37.5
LiF	NaF ₂	649	0.61	*	-6.4	---
LiF	RbF	450	0.47	*	-18.0	---
MgF ₂	NaF	987	0.64	*	-39.5	---
MgF ₂	RbF	883	0.625	*	-65.9	---
NaF ₂	RbF	664	0.33	*	-0.1	---
c. Oxides:						
B ₂ O ₃	Li ₂ O	715	0.55	*	-27.2	---
Bi ₂ O ₃	Li ₂ O	730	0.92	*	-272.	---
Li ₂ O ₃	MoO ₃	570	0.75	*	-25.3	---
Li ₂ O	V ₂ O ₅	621	0.835	*	-10.4	---
Li ₂ O	WO ₃	800	0.63	*	-41.1	---

* In the absence of any experimental information, the mole fraction of the solidus boundary is assumed to be 1.000.

TABLE 3
CALCULATED AND EXPERIMENTAL VALUES
FOR THE ENTHALPY OF MIXING

System		$\Delta H_{\text{mix}}, N = 0.5$ K Joules per Mole	
		Calc.	Exp.
AgCl	KCl	-2.5	-0.84 ¹ , -2.31 ²
KCl	LiCl	-4.2	-4.39 ² , -3.98 ³
LiCl	RbCl	-4.8	-5.02 ²
LiF	KF	-4.3	-4.47 ³
$\text{Li}_2\text{O} \cdot 2\text{B}_2\text{O}_3^*$		-6.0 [*]	-3.3 ^{4*}

1. K. Stern, J. Phys. Chem. 60, 679, (1956).
 2. L.S. Hersch, O.J. Kleppa, J. Phys. Chem. 42, 3752, (1956).
 3. E. Aukrost, B. Bjorge, H. Flood, T. Forlan, Amer. N.Y. Acad. Sci. 79, 830, (1960).
 4. JANAF Thermochemical Tables, Dow Chemical Company, Midland, Mich. (1962).
- * The calculated and experimental values are for the composition of $\text{Li}_2\text{O} \cdot 2\text{B}_2\text{O}_3$.

on a per-unit mass basis. The value for this transformation depends for the most part on the values of the enthalpy of fusion of the pure components and the enthalpy of mixing of the pure components in the liquid phase. The pure components can be selected on the basis of the tabulated values for their enthalpies of fusion. In Table 1 we presented these values for metal oxides and metal fluorides which have the largest values in their respected groups on a per gram basis. Next, we reviewed the number of phase diagrams compiled by the American Ceramic Society (14) which contain one of these pure components. In Table 4 are tabulated the pure component and the total number of phase diagrams presented which contain that component, and many of the systems which have been compiled have been only partially investigated. More comprehensive coverage of systems which contain these components would be of significant value in the selection process.

TABLE 4

THE NUMBER OF PHASE DIAGRAMS COMPILED WHICH CONTAIN A
PURE COMPONENT WITH A LARGE VALUE FOR THE ENTHALPY
OF FUSION ON A PER-UNIT WEIGHT BASIS

System	Total No. of Systems	No. of Binary Systems	No. of Ternary Systems
LiF	128	42	50
MgF ₂	27	12	14
NaF	195	46	91
CoF ₂	3	3	0
FeF ₂	2	2	0
ScF ₃	8	6	2
TiF ₃	---	--	--
KF	134	37	52
ThO ₂	25	13	11
BeO	36	17	18
Li ₂ O	94	16	52
MgO	158	35	70
Al ₂ O ₃	207	53	70

The data of primary interest within a particular system are the composition, temperature, and type of liquid-solid transformation.

An assessment of the reliability and the accuracy of thermodynamic models to calculate the enthalpy of mixing from data presented in the phase diagram would likewise be of significant value. If this method can produce reliable thermodynamic data, then a significant increase in our data base for values for the enthalpy of mixing can be made available from the phase diagrams which have been compiled.

4.0 SUMMARY

The applications of the phase diagram to phase change energy storage technology has been presented. Our particular needs are for materials which have large values for the enthalpy of the liquid-solid transformations. Two properties which determine this enthalpy value are the enthalpies of fusion of the pure components and the enthalpy of mixing of the pure components. Values for the enthalpy of mixing can be determined from the data presented in the phase diagram when coupled with a thermodynamic model of the alloying behavior. We hope that our comments will have been of value to assist investigators in assessing the importance of phase diagrams in providing for a technology base for thermal energy storage.

REFERENCES

1. JANAF Thermochemical Tables, 2nd Edition, Dow Chemical Company, Midland, Michigan.
2. Kabaschewski and Evans, Metallurgical Thermochemistry, 3rd Edition, Pergamon Press, New York, 1958.
3. Wicks and Block, Thermodynamic Properties of 65 Elements, Bureau of Mines Bulletin, 605, 1963.
4. Handbook of Materials Science, Volume 1, General Properties, CRC Press, Cleveland, Ohio, 1974.
5. Hultgren et al., Supplement to Selected Values of Thermodynamic Properties of Metals and Alloys, ASM, Metals Park, Ohio, 1974.
6. Thermal and Other Properties of Refractories, LA-5937-MS Informal Report dated March 1975 by Dwayne T. Vier of the Los Alamos Scientific Laboratory, Los Alamos, New Mexico.
7. Janz, George J., Molten Salts Handbook, Academic Press, New York, 1967.
8. Phase Change Materials Handbook, NASA Contractor Report Number NASA CR-61363, dated September 1971 by Hale, Hoover, and O'Neill of Lockheed Missiles and Space Company, Huntsville, Alabama.
9. Determination and Analysis of the Potentialities of Thermal Energy Storage Materials, ASD Technical Report 61-187 dated June 1961 by Wilson, Beahm, and Cooper of the Callery Chemical Company, Callery, Pennsylvania.
10. Survey and Selection of Inorganic Salts for Application to Thermal Energy Storage, ERDA-59 dated June 1975 by Alina Borucka, Borucka Research Company, Livingston, New Jersey.
11. Evaluation of Eutectic Fluoride Thermal Energy Storage Unit Compatibility, AFAPL-TR-79-92-Part 1 by Joseph E. Davison, dated October 1975, University of Dayton, Dayton, Ohio.
12. Voskresenskaya, N.K., Handbook of Solid-Liquid Equilibria in Systems of Anhydrous Inorganic Salts, Volume 1. Available from the U.S. Department of Commerce Clearinghouse for Federal Scientific and Technical Information, Springfield, Virginia.

REFERENCES (concluded)

13. Davison and Rice, Application of Computer Generated Phase Diagrams to Composite Synthesis, NMAB 308-III, dated January 1973. Proceedings of the Conference on In-Situ Composites, September 5-8, 1972, Reported by the National Materials Advisory Board, Washington, D.C.
14. Levin, Robbins, and McMurdie, Phase Diagrams for Ceramists, 1964 (also see the 1969 and 1975 Supplements), The American Ceramic Society, Columbus, Ohio.



THE NEEDS FOR PHASE EQUILIBRIA DATA IN THE DEVELOPMENT OF MAGNETOHYDRODYNAMICS*

R. A. Howald and I. Eliezer
Chemistry Department
Montana State University
Bozeman, MT 59715

ABSTRACT

The study of magnetohydrodynamic power production with the use of coal, necessitates a major effort to elucidate the phase equilibria and thermodynamic properties of a variety of inorganic substances: Liquid or gaseous slag constituents, sulfur compounds and other inorganic materials dissolve protective oxide layers on alloys and have deteriorating effects on ceramic materials used in MHD channels and other components of the MHD power plant. The electrical conductivity in the MHD power generators and the emission of pollutants are also affected by the slag constituents, seed and sulfur compounds, and other inorganic materials. The study of the high temperature equilibria of the materials involved in MHD power generation includes broad ranges of temperature, pressure and oxidation potential, i.e. 1000-2500 K, 1-20 bars, excess oxygen, excess carbon, various moisture contents, etc.

The addition of potassium seed compounds (K_2SO_4 , K_2CO_3 , etc.) is essential to achieve sufficiently high electrical conductivity in open cycle MHD, and so the interactions between potassium oxide and various refractory oxides are particularly important. Coal slag has actually been used in operating MHD channels as a continually replaced protective coating over the electrodes. Thus the vapor pressures of potassium oxide over typical slag compositions have to be known. For economic reasons

it will be necessary to recover and recycle most of the seed compound, presumably as K_2SO_4 . In this connection additional phase equilibria data on solubilities of various oxides in liquid potassium sulfate are needed. Cesium compounds should also be studied since they are used in closed cycle MHD systems.

Large high temperature heat exchangers constitute one of the major capital expenses for MHD. Thus phase relations involved in the preparation and useful lifetime of high temperature ceramics should be investigated in detail.

To summarize, information on the solid, liquid and gas phase relations in a variety of MHD systems is vital both to establish the extent of interaction and to locate temperature and pressure regimes in which deleterious reactions will and will not occur.

Much of the above information is useful for gas turbine engine development as well as for MHD.

Introduction

Of the several alternative energy sources to the conventional power plant, the MHD system seems to have the best efficiency potential which derives mainly from the very high temperature generation of the MHD generator.¹⁻³ The thermodynamic characteristics of the materials involved at these temperatures are thus of crucial importance to the proper design and operation of an MHD power plant.⁴ However, in most cases such information is scant or totally lacking. Therefore a major research program on the thermodynamic properties and phase equilibria of the substances involved is essential if magnetohydrodynamic power production is to become competitive.

Open Cycle MHD Power Generation From Coal

In open cycle MHD power generation the operating substance is a high-temperature plasma made up of hot combustion products and preheated air. In order to obtain the required electrical conductivity, it is necessary to add ionizable substances such as potassium carbonate or sulfate. It is generally accepted that in an economically feasible MHD power generating system the MHD generator is to be coupled to a steam bottoming plant. A schematic representation of an MHD/steam combined cycle plant is given in Figure 1.

Oxidation and Corrosion

Open cycle MHD systems have been operated for periods of up to a hundred hours burning clean fuels. However, MHD can provide a significant contribution to world energy needs only if it can utilize a fuel available in larger, cheaper quantities such as coal. All coals contain substantial quantities of ash and slag constituents causing corrosion of ceramic and metal parts, as is the case for other high temperature systems such as gas turbines.

Metallic and ceramic materials that are exposed to high temperatures are usually protected from oxidation and corrosion by an adhering layer of oxide such as Al_2O_3 or Cr_2O_3 . The combustion gases contain vapor species and particulates which condense to liquid sulfates, carbonates, oxides, etc. These liquids are corrosive under both oxidizing and reducing conditions, and may dissolve the protective oxide layers on alloys and ceramics causing serious deterioration of the ceramic or metal parts of the system. Since the physico-chemical interactions in

question will obviously impose severe limitations on the design and operation of the system they must be elucidated. This necessitates thermodynamic information on the vapor pressures of the various species in question, their free energies, their solubilities, the activities of the volatile species when dissolved in typical coal slag liquid oxides, the heat of mixing of the oxides, and the temperature dependence of all these quantities.

The slag may also have beneficial effects on the MHD components, acting as a continually renewable protective coating of the electrode and insulator surfaces and preventing arcing. These effects will again depend on the composition and properties of the slag.

Electrical Conductivity

In the MHD process, the combustion gases are expanded from combustor pressure (1-20 bars) and temperature (1-3 kK) through a duct with a transverse magnetic field (3-7 Tesla) for production of electric power. The gas velocity is of the order of Mach 1. The electrical conductivity of the gas is dependent on the free electron density and the electron mobility. In principle, the conductivity is also dependent on the ions but these are too heavy to contribute appreciably to the conductivity.

The electron density will be reduced by the presence of gaseous species with high electron affinities. The resultant ions can also have adverse effects on the conductivity because they reduce the electron mobility due to their large scattering cross-section. It is therefore important to know the negative ions which are likely to be formed, their electron affinities and their concentrations.

At the temperatures attainable by the combustion of coal with preheated air, it is essential to have a material with a low ionization potential (seed) present to achieve sufficient electrical conductivity. The ionization potential of sodium atoms is slightly too high, but one can use the heavier alkali metals. At the high temperatures involved, substantial alkali metal atom concentrations are obtained from practically any compound. However, it is best to avoid halides because of the electron affinities of halogen atoms. For closed cycle MHD, one can probably recover enough of the seed to consider using expensive material such as cesium metal. With open cycle systems, less seed can be recovered and cost considerations together with the ionization potential and electron affinity considerations mentioned above limit one almost completely to K_2CO_3 and K_2SO_4 as seed compounds. Thus the most important data for the calculation of electron concentrations and conductivities are the equilibria involving potassium atoms and all major potassium containing gaseous species. Much of this information is currently available;⁵⁻⁸ however, there is still room for improvement in the thermodynamic data for such important species as $K_2SO_4(g)$, $KOH(g)$, $K_2O_2(g)$, and $KO_2(g)$. In addition, data are needed on the interaction of potassium and potassium oxide with various materials which may be present on or in the channel walls.

In MHD coal combustion the main species involved in the formation of negative ions will be carbon, sulfur, nitrogen and metal oxides. Precise thermodynamic data will be necessary for these negative ions as well as the related gases and liquids, since neutral species with high electron momentum transfer collision cross sections, such as SiO , are also important.

Pollution and Seed Recovery

In MHD, as in other power plants, a basic requirement is that pollution levels be kept below EPA requirements. The main species in question are sulfur dioxide and nitrogen oxides.

Another requirement, if MHD is to be economically feasible, is that most of the seed material must be recovered and recycled.

Fortunately, these two requirements interact favorably because the reaction with seed will control sulfur dioxide emission, i.e., the precipitation of potassium sulfate can reduce sulfur in the effluent to very low levels. However, achievement of such a combination of seed recovery and SO_2 emission reduction requires thermodynamic data on the K-S-H-O system at the relevant temperatures and pressures.

Proper separation of the seed from the slag will require phase equilibria data on seed-slag oxide systems including K_2SO_4 - K_2O - Al_2O_3 - SiO_2 - FeO - Fe_2O_3 - MgO - CaO . Vaporization data on these seed-slag oxides systems are essential. Gaseous species like K_2SiO_3 and KAlO_2 may be stable and data for gaseous aluminum species such as AlO_2 and HAlO_2 are poor.

Inorganic oxide systems like the above are very far from ideal. At present, only a few of the binary and ternary subsystems have been analyzed thermodynamically. However, this is sufficient to show that general power series such as the Redlich-Kister⁹ and Bale-Pelton¹⁰ equations can represent the data for binary systems, and that it is possible in principle to extend the treatment to multi-component oxide solutions. Working with high temperature oxide systems is very frustrating because while there is a lot of experimental data bearing on the

thermodynamics of these systems, in most cases it has not been collected and evaluated, and there is no standard form for expressing activities and heats of mixing for the few systems which have been analyzed in detail.

At the present time we have available computers and programs which make possible a fully consistent thermodynamic treatment of four or five component oxide systems. In many cases additional activity data from vapor pressures, high temperature e.m.f., solubility, redox equilibria, etc., is required. Many of these systems are slow to reach equilibrium on a macroscopic scale. However, the recent work of Aksay and Pask¹¹ illustrates how improved solubility data can be obtained with modern techniques such as electron microprobe analysis of diffusion couples. The major additional requirement in most of the systems is good enthalpy data so that activity data can be accurately extended to additional temperatures.

Improved enthalpy data can be obtained either by high temperature calorimetry or by room temperature calorimetry coupled with accurate heat capacity measurements or drop calorimetry for the same compositions. In many cases all that would be required is careful DTA measurement of heats of melting for pure compounds and eutectic compositions. Collection of this data is not particularly glamorous work because there will be few surprises. However, it is essential to supplement the more interesting activity measurements, and those involved in funding research should recognize the importance of obtaining and interpreting enthalpy data on high temperature solutions.

Thus the design of the entire seed regenerator section of the MHD system is subject to the availability of thermodynamic and, in particular, phase equilibria data. For closed cycle MHD systems similar data will be required for cesium compounds.

As to nitrogen oxides, these may be controlled by fuel rich combustion, adding additional oxygen downstream from the MHD channel, but a better way would be their recovery and conversion into fertilizer. This again requires data on the equilibria involved.

Another potential pollution problem in MHD power generation concerns the distribution of toxic trace elements in particulate emissions. In conventional power plants the very small fly ash particles, ($<1\mu$) have been found to be enriched in arsenic, antimony, cadmium, lead, selenium, and thallium.^{12,13} This effect and also the concentration of various elements at the surface of fly ash particles¹⁴ is related to partial vaporization of the oxides during combustion. The effects of higher temperature combustion in the MHD process upon these phenomena have not yet been investigated either experimentally or theoretically. However, it is clear that additional data on the high temperature vaporization equilibria of complex oxide systems will be required for a full understanding of the distribution of toxic trace elements in particulate emissions of any coal combustion system.

Refractory Materials

High temperature refractory materials are of major importance in MHD power generation both in the large heat exchangers which constitute a major item of the MHD system and for other purposes, e.g., as conducting

ceramics for electrode materials. Many of them are new materials such as LaCrO_3 , SiN_4 , ZrB_2 , etc. Thermodynamic data and phase relations involved in the preparation and useful lifetime of high temperature ceramics and their reactions and products with slag and combustion gases should be known in detail.

Conclusion

Thermodynamic and phase equilibria data needed for the development of MHD include seed and slag interaction with metal alloys and ceramics, slag protection of electrodes, control of polluting effluents, seed recovery and gaseous ions and neutral species influencing electrical conductivity.

The main species involved are gaseous and liquid coal slag components (mostly oxides such as SiO_2 , Al_2O_3 , FeO , Fe_2O_3 , CaO , MgO), seed compounds (such as K_2SO_4 , K_2CO_3 , Cs_2SO_4 , Rb_2CO_3) and related sulfur compounds (such as K_2S , SO_2 , $\text{K}_2\text{S}_2\text{O}_3$), slag-seed interaction compounds (such as K_2SiO_3 , $\text{K}_2\text{Al}_{22}\text{O}_{34}$, $\text{K}_2\text{Al}_2\text{Si}_2\text{O}_6$, FeSiO_3), refractory materials (such as Al_2O_3 , SiO_2 , ZrO_2 , LaCrO_3 , BN) and combustion gases and ions (such as K^+ , e^- , OH^- , SO_4^- , AlO_2^- , CO_3^- , NO_2^-).

Thermodynamic and phase equilibria data such as the above are needed not only for MHD power generation but also for gas turbine engine development and for other high-temperature coal conversion processes.

ACKNOWLEDGEMENT

We should like to acknowledge helpful comments by W. Beezhold.

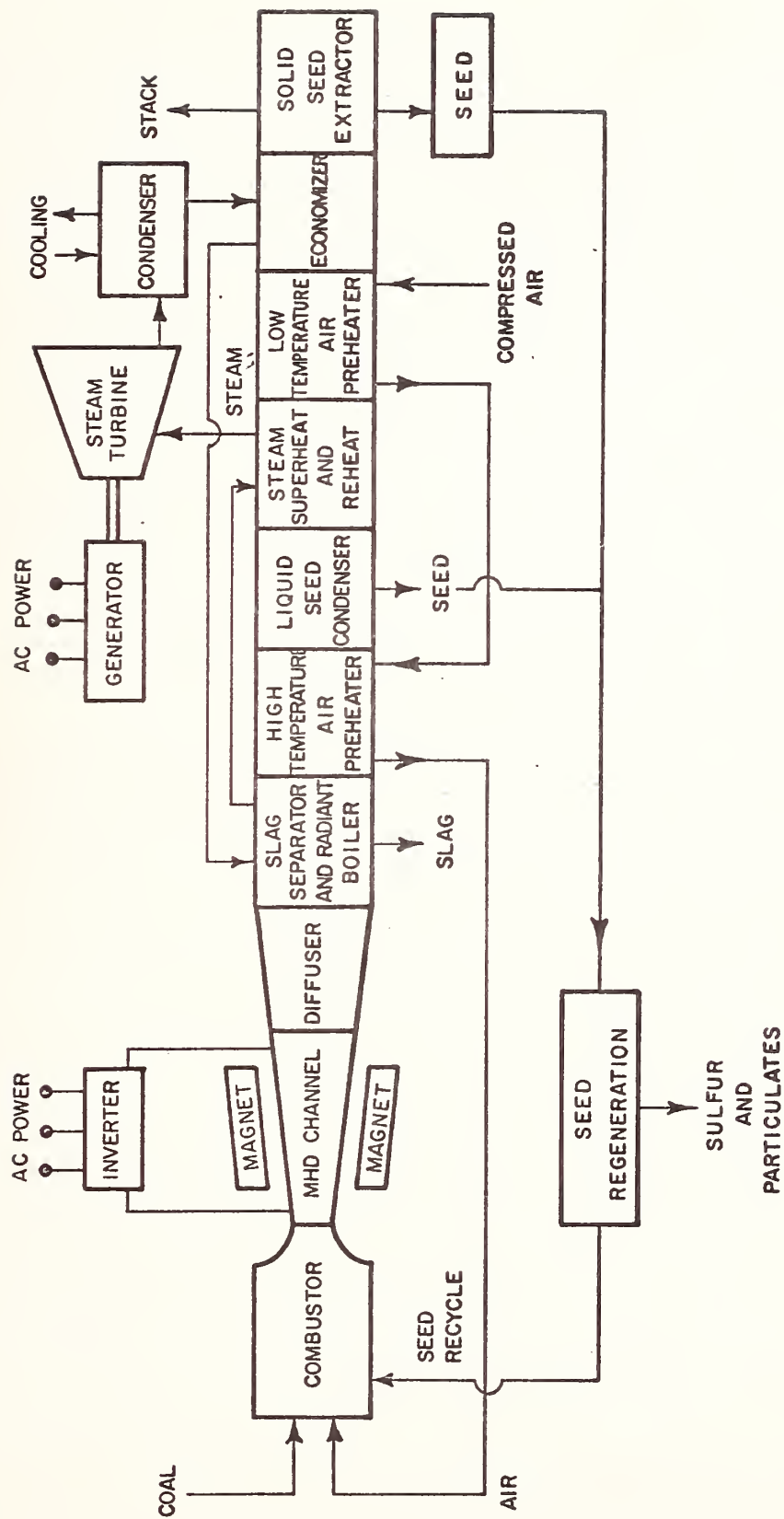


FIGURE 1. A schematic representation of an MHD/steam combined cycle plant.

References

*This work was supported by ERDA under Contract No. E(49-18)-1811.

1. W. D. Jackson, "MHD Electrical Power Generation: Prospects and Issues," AIAA 9th Fluid and Plasma Dyn. Conf., San Diego, California, July 14-16 (1976).
2. ECAS [Energy Conversion Alternatives Study], Westinghouse Electric Corporation Research Laboratories, NASA, CR-134941 (1976).
3. R. J. Rosa, "Magnetohydrodynamic Energy Conversion," McGraw-Hill, New York (1968).
4. J. B. Heywood and G. J. Womack, "Open Cycle MHD Power Generation," Pergamon Press, Oxford (1969).
5. I. Eliezer and R. A. Howald, J. Chem. Phys. 65, 3053 (1976).
6. JANAF Thermochemical Tables, Nat. Stand. Ref. Data Ser., Nat. Bur. Stand. 37 (1971).
7. JANAF Supplements, J. Phys. Chem. Ref. Data 3, 311 (1974); 4, 1 (1975).
8. E. R. Plante, C. D. Olson and T. Negas, 6th International Conference on MHD Electrical Power Generation, Volume II, p. 211, Washington, D.C., June 9-13 (1975).
9. O. Redlich, A. T. Kister and C. E. Turnquist, Chem. Eng. Progr. Symp. Ser. 48 (1952).
10. C. W. Bale and A. D. Pelton, Metal. Trans. 5, 2323 (1974); 6A (1963, 1975).
11. I. A. Aksay and J. A. Pask, J. Amer. Ceram. Soc. 58, 507 (1975).
12. D. F. S. Natusch, J. R. Wallace and C. A. Evans, Jr., Science 183, 202 (1973).
13. J. W. Kaakinen, R. M. Jorden, M. H. Lawasani and R. E. West, Environ. Sci. Technol., 9, 826 (1975).
14. R. W. Linton, D. F. S. Natusch, C. A. Evans, Jr. and P. Williams, Science 191, 852 (1976).

DISCUSSION

L. Kaufman - I would like to make a general comment. I believe that it was pointed out yesterday that you must couple in this environment the thermochemistry and phase diagrams to provide guidance for all these areas. I would like to list several. In the case of Bill Speich's talk, we have much data stored in the [Man Labs - NPL] data-base on solubility products for alloying elements of steels. Those are data that are there now. We have similar data on the range of stability of austenitic martensite. Those data are stored there now. We can carry out calculations of tie lines, in copper-niobium or copper-aluminum-X, that's information that's available now. Procedures are being developed to deal with oxides, carbides and borides. That data-base is more fragmentary but the techniques are available now. We don't yet know in general how to do an 8-component system. But 10 years ago we could barely do a binary system and in the last 10 years those of us who operate in this field have advanced from doing binaries routinely, to ternaries routinely and some to quaternaries routinely. So my two points are: a) the correlation and compilation of phase diagrams must be coupled with thermochemistry if we're going to make rational progress, and b) those of you who are interested in phase diagram information, don't stop there. Ask "is there thermochemistry available?" Because often times, information may really be what you want to know.

B. Rosof - I also have a general comment. We have talked about elegant uses of phase diagrams or how important it would be to have a phase diagram solve an elegant problem. All of us here, I'm sure, use phase diagrams in elegant ways. But most [outside] people, we use phase diagrams, don't. I'll tell you a little short research problem I had that will illustrate this point and is most typical of phase diagram users. I was melting, let's call it, a 10 component alloy in an arc furnace with the usual problems of chrome and carbon equilibrium, of silicon control and aluminum control, etc. And somewhere in this big complex problem I had to add some tantalum. Now you just don't throw tantalum into a furnace. It will sink to the bottom and its melting point is too high, so it doesn't alloy properly. You want to add this as a Ta-X alloy so it will melt in quickly. You go and grab Hansen off the shelf. You look up... let's see... Ta-Al, Ta-Fe, Ta-Ni, and go through all the components of your system with tantalum.. You find one that would make a suitable alloy with a suitably low melting point and in basically less than half an hour you have a solution to your problem. Ah!... the Ta-Fe system looks much better than the Ta-Co system. So you tell the technician, "take the tantalum, put some iron with it, put it in a vacuum - induction furnace", and now you have your ferro-alloy which is useful, and a solution to the research problem. The point here is that so many of our research problems in the use of phase diagrams are little tiny problems relative to the full complex problems encountered in research. We have to make sure that our phase diagrams are useful in this sense as well as in the elegant senses that everybody else here talked about.

C. Williams - I'd just like to make some sort of an "amen" to what the gentleman just said in terms of specific information that you can get from a phase diagram. In my particular application [at Union Carbide], I deal with ceramics and metals, also in combinations of these two, not necessarily only in the binaries, but usually in the ternary type situation. I think that maybe it would be somewhat helpful if ceramists and metallurgists would get together in sense of compiling some data that would be a little more useful in terms of what's happening at that particular interface and what kind of phases are forming at that particular interfacing. I also would like to ask more or less a question that was not answered, relating to this question of metals-and-ceramics. If anyone of you in the audience or on the panel would have any information or could direct me to some source of information concerning this metals-and-ceramics problem, it would be very much appreciated.

Also, I would like to thank the Bureau for the occasion and thank the committee and the various people that contributed to this session.



SUMMARY REMARKS

by

John F. Elliott
Dept. of Materials Science
and Engineering, M.I.T.
Cambridge, MA

Summarization of a workshop of the type held at the National Bureau of Standards this week should include these things. First, one should capture the general feeling that the participants have had towards the formal and informal parts of the workshop. Second, there should be some remarks covering what might be termed the "sense of the meeting" regarding the major issues that have been expressed explicitly and implicitly. Third, some conclusions should be drawn from the results of all facets of the workshop. The summary should not be all inclusive, nor should it necessarily reflect but one final opinion on each of the primary points being considered.

GENERAL REMARKS

From the nature of the formal and informal discussions during the three days of the workshop, it seems clear that the plan to bring people together from diverse areas to discuss a common general interest in phase diagrams was very successful. On the other hand, some came only to sessions of the workshop which were of particular interest to them, and they did not attend all sessions. Fortunately there were many who stayed for the full three

days, and they provided continuity in the discussion which is so essential to a successful workshop.

The informal discussions in the halls, at meals, and at poster sessions indicated that the participants found the sessions stimulating and enjoyable. The times set aside for discussion during the sessions necessarily were limited, particularly during the early part of the workshop, and the informal discussions served to compensate. The organization of the workshop did bring together people from very diverse fields who have a common interest in phase diagrams. All attending the workshop profited from sharing very different points of view with others whom they ordinarily would not meet in their usual professional activities. Such interactions help to develop a better perspective for all involved as to the development and use of thermodynamic data and phase diagrams. It also brings home the international character of the work in progress in the field.

The poster sessions were highly successful in bringing together people with different perceptions of the development and use of phase diagrams. Both the posters and posters provided the participants with stimulating and productive exposures regarding many topics. Of particular interest was the use of computers, computational methods and graphical methods for treating data.

The participation in the workshop has shown again that the interest in phase diagrams is international. This is advantageous

because, as will be noted later, pertinent data are generated in many countries, the results of any work is shared across the world, and the task of assembling, compiling and collating data on phase diagrams is enormous. It can be assumed that the task must be shared by groups and laboratories across the world.

DISCUSSION OF AREAS OF COVERAGE

It is helpful in a summary to look at the general issues covered in the workshop from a different point of view than that presented in the formal organization. Thus it may be useful to start with a discussion of where and how data on phase relationships and phase diagrams are utilized, and then move back through the sessions in reverse order.

User Needs

The speakers in the three areas of primary production of metals, materials processing and product application pointed out that the need for information on phase relationships and phase diagrams for each particular application being discussed was extensive and detailed. Often the success of a processing sequence or the property of a material depends on the fine detail of a small area of a phase diagram. The cases cited were numerous and need not be reexamined here. A few examples can be listed to illustrate the range: (a) more complete information is needed on

fields of stability in terms of temperature, pressures of oxygen and sulfur, and composition of the matte and slag phases in copper-iron-sulfur-oxygen-silica systems and how the presence of minor elements such as nickel, lead, etc., influences these fields of stability; (b) a better understanding of the condition of equilibrium between the crystalline phase and the parent liquid phase is required for the conditons existing when semiconductor materials are grown from the melt; and (c) information of a detailed nature is needed for each of the many phase relationships that are pertinent to the processing of metals, alloys and various ceramic materials. It was interesting for people to see the sophisticated ways in which information on phase diagrams is employed by many users. It was also apparent that a user quickly ran out of information when progressing from binary to ternary and then quaternary systems.

Another point of interest was that users seek information on phase relationships in many different forms. The traditional T-X or P-T-X types of diagrams are useful, but other types such as the various types of stability diagrams are desired. It was clear that much more powerful means are needed to handle information about ternary, quaternary and higher order systems because the usual two dimensional charts and plots in most cases are inadequate to meet the user's requirements. This points up the general need for information on phase relationships to be put in forms that are readily adapted to computer use. Perhaps in the longer term it will be possible to prescribe ways of presenting information by investigators to facilitate the use by the computer in various ways and

thus make data of more direct use by many users.

In certain respects, the academic world has some special requirements for information on phase diagrams. There is the need in many research areas for information on phase relationships which is similar in many respects to that which has been expressed for the industrial area. In addition, however, there is the need for this information in forms that facilitate the teaching and learning about phase stability, phase diagrams of all sorts and the uses of these diagrams. Several interesting instructional movies to meet this need were presented during the workshop. However, it would appear that much more must be done, especially with multicomponent systems. It would seem that greater use of computer methods will be helpful in meeting this need.

Methods of Phase Diagram Calculations

The poster and discussion sections on this subject were very helpful in acquainting the participants of the workshop with current activities in a wide range of efforts. As the program schedule shows, the work includes: the treatment of methods for correlating experimental data, use of mathematical methods for expressing thermodynamic functions, development of methods for computing information on activities and other thermodynamic functions from data on phase diagrams, and the reverse in using thermodynamic data for calculating phase relationships. In a number of cases,

the work was directed quite effectively towards meeting some of the user needs as outlined earlier. The methods discussed often involved the use of the computer. These sessions indicated that a diversity of approaches was being employed. It is anticipated that the information displayed and the discussions during the meeting will lead to the development of greater harmony and unity in the use of computer methods. Calphad will undoubtedly help in this.

Review of Phase Diagram Representations

The papers and discussion in this session, the results of Dr. Carter's questionnaire and the various statements from the users' panels present us with the principal dilemma of the compiler of data of any kind. This dilemma arises because, on the one hand, the compiler may not have the time and resources to treat in great detail the information that may be available on a given system. This was noted in the session Present Status of Phase Diagrams. On the other hand, it was clear in the later sessions of the workshop that many users look for a high degree of sophistication and detail in the compiled information, often in a small and obscure portion of a system. In contrast, many who responded to the questionnaire indicated a need for only a moderate degree of sophistication in phase diagrams and phase relationships.

A possible means of resolving this dilemma is to focus the programs of compilation and collation on areas of need. Then one places principal emphasis on the materials, system, and phases of primary interest in an area and either borrows from other compilations or gives less time and effort to that which is of secondary or collateral interest. As an example, in compiling data pertinent to the pyrometallurgical processing of iron and steel¹, emphasis was placed on iron and its alloys and oxide systems typical of slags utilized in the blast furnace and steelmaking furnaces. Systems involving copper, zinc, etc., and liquid alkali-silicate systems were given less detailed coverage. If compilation work were focussed in this manner, it probably would be possible to provide for the needs of people in the current principal areas of application. The areas of lesser emphasis and possible newer areas of scientific and technical interest would be short-changed by this strategy.

The results of the questionnaire also indicate other general needs. As has already been noted, much more must be done with ternary and multicomponent systems. Treatment of metastable phases and of special crystal structures also was considered to be of medium importance. Coverage of these topics adds greatly to the work of the compiler for many systems. Surprisingly, surface phases were not considered to be of great interest. There may be three explanations for this: (a) the interest may in fact be low,

(b) people working in areas with surface phenomena did not respond to the questionnaire, or (c) those people do not perceive how knowledge of phase diagrams are of importance to their work. It seems probable that surface phases may receive much greater emphasis in the future. [Editor's note: Some very fine research on surface phases is being carried out by Prof. G. A. Somorjai et al. at U.C., Berkeley. Unfortunately, this group was unable to attend our workshop, thus causing this topic to seem less important than it is. Applications are, of course, in materials such as used, for example, in catalysis].

SUMMARY

Those of us working in various areas of science and technology see many places and problems where both in the short and long term there are serious and critical needs for continued effort to assimilate, collate and compile information on phase diagrams and phase equilibria. It is apparent that there is much pertinent information now in the literature, particularly with regard to alloy systems, that has not been sought out and compiled for general use. With the present levels of publication of scientific information in the world as compared to the present levels of effort at compilation, we are falling ever farther behind as the years pass in utilizing the information that becomes available. The demands for information on phase equilibria and phase diagrams continues to expand as new devices, materials and processes are developed. Inherent in this situation is the certainty that our technological advancement is slower and more expensive than might be the case. An engineer designing a system must make allowances in the materials chosen and the design of a system for deficiencies

and uncertainties in the behavior of materials and substances in the system. Accordingly, the failure to have up-to-date information on phase stability and equilibria may be costly in the design and operation of a system, and may lead to unexpected failure of that system. For example, those of us who work with energy conversion systems see many places where problems of the type described above ultimately could possibly limit severely the performance and economic viability of many systems being planned today.

The proposals for definitive and exhaustive compilations of phase diagrams and phase equilibria on a grand scale are appealing because it would be desirable to have all such information collected in a usable form in one place. This is a Herculean task, and it seems highly doubtful that it would be possible in the foreseeable future to find funding and talent necessary to carry it out. Thus we collectively are caught up in the dilemma that was mentioned earlier of breadth versus depth of coverage for a compilation. From the discussions of the past three days, it is apparent that a number of steps can be taken to increase the effectiveness of use of resources that are available. One of the most productive steps would be to obtain better coordination of the work of compilation of groups in various countries. Another step, which might be a series of steps, is to break down the work of compilation into smaller and more manageable pieces

rather than undertake a massive overall effort. The preparation of a complete bibliography of phase diagrams that is kept up-to-date could serve as a Baedeker for investigators who were looking for sources, particularly where specific and detailed information is being sought. The next level of sophistication would be to use very simple and compact methods to cover information on simple systems, particularly those that have been covered reasonably well in the literature previously. An example is the section in Landolt-Börnstein² where binary systems are collected by type; simple eutectics, peritectics, etc. There a system is covered in a single line on the page in which, for a eutectic, there is a two-numbered entry giving the eutectic composition and entries for the melting point of each component and numbers giving the principal references for the diagram. One could easily add columns giving the limits of solubility of component 1 in component 2, and vice versa, at the eutectic temperature, etc., and reference numbers to guide the reader to an acceptable diagram from a relatively easily available source. This number might in the future also indicate a computer file from which data and diagrams could be extracted. These two relatively simple and compact ways of storing information are inexpensive to prepare and distribute. They also permit the application of resources and expert talent to more complex, difficult and demanding analyses and systems.

The next level of complexity and coverage is to direct the attention of a compiler, or group of compilers, to an area of science and technology where information on phase diagrams and phase equilibria are of importance. An example of this is the volume Selected Thermodynamic Values and Phase Diagrams for Copper and Some of Its Binary Alloys by Hultgren and co-workers of the INCRA Monograph Series on the Metallurgy of Copper³. In such a compilation, the systems of principal interest to the field would be covered carefully and in as much detail as is permitted by the available data. Several types of diagrams might be employed to represent the compiled information. Systems that are peripheral to the main interests of the field would be covered in much less detail and might be taken directly from other sources. The compilers for such an effort should be conversant with the field of interest, or should be advised as to the level and coverage of systems by someone who was. It appears that this type of compilation has been reasonably successful in recent years. One of the problems to be faced is that fields tend to broaden, and the task of revising a work may be very large. Another problem is that there may not be sufficient support or interest in a field to develop information at a critical stage in the growth of the field.

The next step in level of coverage is to concentrate the work of compilers on classes of materials. Examples of this are the Phase Diagrams for Ceramists by Levin and co-workers⁴, which has

been carried out over the years by the National Bureau of Standards, and the Hansen, Anderko, Elliott and Shunk series on The Constitution of Binary Alloys⁵. The use of advisory groups to aid in coordinating the work and even in selecting areas to be covered as has been followed in the ceramics work is effective and useful. It is perhaps important to raise again the point that one should be wary of undertaking the effort of covering a class of materials in depth with inadequate resources. If the program is started with a high degree of sophistication, and then it is necessary later to draw back in part from such a commitment in quality, the reputation of the whole effort may suffer.

There is interest in seeking out methods and models by which it is possible from first principles to "predict" the phase diagrams of higher-order systems, and the behavior of many different solutes in multi-component solvents. Models by which this may be done still elude us, but people of talent and originality should be encouraged to pursue these efforts.

Computer modelling today is still very limited and tends to be quite empirical in character. It does, however, show promise in being able to provide a user with a limited class of answers on a somewhat limited number of systems. A great deal more needs to be done with this modelling effort to expand its capability and utility.

The Workshop has shown that the business of compilation of data on phase diagrams and phase equilibria is in a state of disarray. There are data in the literature that need attention and pertinent new information continues to appear day by day. Users have many needs that are not being met. The resources and manpower available for compilation of this type of data are neither adequate to keep up with the newly found information, nor to put the information in forms as needed by the users. An aftermath of the Workshop could be the crystallization of a small group of people who will be able to generate a program and attract resources that will begin to dispel this disarray.

REFERENCES

1. J. F. Elliott, M. Gleiser and V. Ramakrishna; Thermochemistry for Steelmaking, Vol. I and II, Addison-Wesley Press, No. Reading, Mass., 1960, 1963.
2. Landolt-Bornstein, Zahlenwerte und Funktionen, II Band, 3. Teil. Schmelzgleichgewichte und Grenzflächenerscheinungen; K. Schafer und Ellen Lax, ed., Springer-Verlag, Berlin, 1956.
3. R. Hultgren and P. D. Desai; Selected Thermodynamic Values and Phase Diagrams for Copper and Some of Its Binary Alloys, International Copper Research Association, Inc., New York City, 1971.
4. E. M. Levin, C. R. Robbins and H. F. McMurdie; Phase Diagrams for Ceramists and Supplements, The American Ceramic Society, Columbus, Ohio, 1964, 1969 and 1975.
5. M. Hansen and K. Anderko; Constitution of Binary Alloys, Mc-Graw Hill Book Co., Inc., New York, 1958. Also R. P. Elliott, First Supplement, 1965; and F. A. Shunk, Second Supplement, 1969.

DISCUSSION:

J. F. Elliott - Can we now have some general remarks about the Workshop?

R. Howald - The Workshop was valuable to me because it provided information on many activities where phase equilibria are important of which I was not aware.

J. F. Elliott - Dr. F. L. Carter raised the question earlier as to when and if there should be another workshop or conference of this type. Does anyone wish to comment?

B. Rosof - Until I have been able to digest what has been reported and discussed, I am not able to give an opinion.

(In a brief general discussion on the question, there was consensus that the meeting was successful, and that holding another of similar character at some undefined future time would be desirable. J. Westbrook suggested that CODATA's International Committee on Industrial Needs for basic scientific information might be helpful in planning future meetings of this kind.)

I. Ansara - The topic of the Workshop was of interest to many people in Europe. More would have attended had it been publicized more widely.

G. Armstrong - With the broad demands for use of information on phase equilibria, there appears to be little choice but to follow

Professor Brewer's statement that more systematic means are needed for interpreting the behavior of systems. Such means will help to maximize the use of data, and extend its use in predicting the behavior of related systems.

M. McNeil - It might be useful to use the vehicle of a brief annual review in one or two journals to keep people abreast of activities in the field of phase diagrams. One example of such a review is the annual article titled "What is Going on in Process Metallurgy" that appears in the Journal of Metals.

H. White, Jr. - There is a large variety of needs to be met in a work of compilation. As has been noted, this is what makes the effort both challenging and interesting. The needs are increasing rather than decreasing. This is usually not appreciated by people who are not familiar with the field. One often encounters a remark like "Are there not enough phase diagrams already?".

J. F. Elliott - Although many people ask for a great deal of information in a compilation of phase diagrams, there is a danger to the compiler who strives to meet this need. The amount of work in covering a large number of systems at this level is enormous, and there is

serious danger of not being able to maintain the level for all systems. It may be wiser not to attempt too much because a sin of commission seems to be worse than one of omission.

S. Snyder - It appears to me from my experience with phase diagrams that it is better to summarize data where possible in a compilation. Also the reporting of two reasonable, but conflicting diagrams may be the best way out when the compiler cannot choose between them.

J. Livingston - Many have commented on the large amount of effort that is required to treat ternary and high order systems. It appears that it would be wise for a compiler working on them to limit his coverage to the best developed and most important systems with the aim of completing the work in two to three years.

J. F. Elliott - It appears that we have had a highly successful Workshop. (Adjournment)



Evaluation of Conference

by

Reed A. Howald
Chemistry Department
Montana State University
Bozeman, MT

There are a lot of different viewpoints represented at this conference so it is not surprising that it is not easy or even possible to reach a consensus on what kind of evaluated compilation of phase diagram data is required. The range of conference papers makes it clear that there are rapid new phase diagram developments on a variety of fronts. This means that many of our individual prejudices are now seriously outdated, and perhaps the most significant achievement of the workshop is an increased openness of the participants to developments beyond their own areas: in pure theory or in power series representation of empirical data, in experimental techniques or in thermodynamic interpretation of data, in large computer data banks or in hand calculators. Probably we need time to digest these new perspectives before we make any definitive recommendations, but I would like to take the opportunity provided by the workshop proceedings for a few comments of my own on the future direction of phase diagram compilations.

I believe that within ten years we will be seeing the regular publication of updated thermodynamically evaluated computer drawn phase diagrams. Whenever new thermodynamic data for a phase become available from either a theoretical computation or new measurements, a revised phase diagram for the binary and ternary systems containing it could be calculated and made available. This job could be delegated to a large centralized facility, but I do not believe that this will be the direction taken by the United States. I see instead a large group of academic and industrial users with similar programs using compatible files of thermodynamic data and power series coefficients from which phase diagrams are computed.



Evaluation of Conference

by

J. E. Selle
Oak Ridge National Laboratory
P.O. Box X
Oak Ridge, Tennessee 37830

Throughout this conference several participants have made appeals, either directly or indirectly, for complete and unequivocal accuracy in phase diagram compilations. Referring to the 2nd Supplement to Hansen by Shunk, it has been inferred that unless a compilation is 100% accurate and complete it is not worth doing at all. I strongly disagree. Strict interpretation and adherence to this philosophy will only serve to intimidate the compilers with the end result that only a few diagrams will be completed each year. I understand the thermodynamicists and theoreticians need for such accuracy and can appreciate their needs, but they are in the distinct minority and if they need the accuracy they claim, they should do their own reviews. The overwhelming percentage of users of phase diagrams, the people in the shops and laboratories do not always need the accuracy or detail demanded. They need information on solid solution, eutectic temperatures (5-10°C in usually accurate enough), potential for compound formation, or potential for second phase formation after heat treatment. Insistence on complete accuracy and its attendant delays in transmitting this information to users will be a catastrophe. The time delay since the publication of Shunk is excessive and it is time to get on with an update and not force a slow down in order to satisfy a very small (through vocal) minority of phase diagram users.

I would hope that somewhere in the NBS budget there will be room for programs to determine phase diagrams for systems that have never been worked on. My own survey of Hansen Elliott and Shunk, the wall chart, "Summary of Binary Phase Diagrams", indicates that for about 15% of the possible binary systems for 55 of the more common metals, no information is available. This is another deficiency that should be addressed.

The NBS should be complimented on their initiative in organizing this conference and attempting to get on with the very crucial task of disseminating phase diagram information to potential users.



COMMENTS ON THE
PHASE DIAGRAM WORKSHOP

JAN. 10-12, 1977

by

Didier deFontaine, Professor of Engineering
School of Engineering and Applied Science
Materials Department
University of California, Los Angeles, CA

This was a timely meeting, indeed, on a very important topic. As a most interested participant, I would like to comment briefly on the meeting itself (1st, 2nd, and 3rd days) and then offer general impressions and even recommendations.

FIRST DAY

The first day's program was the one which I felt to be most relevant to the purpose of the workshop. The presentations on compilation, given in the morning, were most welcomed and the information presented will hopefully be accessible to a large audience; it is of the utmost importance.

The afternoon program was noteworthy as it proved, once again, the effectiveness of poster sessions, particularly in fields such as this one where a great deal of rather intricate graphical information has to be conveyed to the participants.

SECOND DAY

It was a particularly good idea to bring in a solid-state theorist to present the status of current work in the field. This, Dr. Watson did admirably, although, perhaps purposely, he did not attempt to predict when and if reliable computations of such things as alloying potentials would be forthcoming.

Currently, there is no cause for rejoicing: although in principle one knows quite well how to proceed; the business of getting reliable numbers is enormously difficult. Extremely lengthy computations are required to obtain just a single number, say a heat of mixing, and it is not surprising that present computations often result in numbers which are incorrect in both magnitude and sign! The problem of predicting crystal structures of compounds from first principles is many orders of magnitude more difficult yet: in principle, one should perform calculations on all possible structures, then decide on the correct one by minimizing the energy. This means that a small numerical error of perhaps less than one percent will lead to an incorrect structure.

Clearly, the theoretical determination of phase diagrams, even binaries, is presently out of the question. In fact, it appears that such calculations may never reach the truly predictive stage. To some participants of the workshop, this was very discouraging. But are we not asking for too much? After all, despite early optimism, dislocation theory still cannot help us predict work hardening properties of a given polycrystalline alloy, say, and probably never will. Yet dislocation theory is essential for an understanding of plasticity and mechanical behaviour, and has helped to completely reorient our thinking on such matters. Hence, theories (and theorists) should generally be required to give ideas, principles, guidelines. Accurate numbers can only be provided by Nature itself; actual experimental determination of phase diagrams must remain the only reliable way of proceeding.

This brings me to the topic of "computation and prediction of phase diagrams" the object of the morning panel, of which I was a member. First of all, the people working in this field who claim that they are predicting phase diagrams

are kidding themselves. There can be no "prediction", as such with the methods employed (nor, as stated above, with my other method known presently or projected). At best, sub-regular solution methods used currently can be regarded as convenient analytical representations of phase diagram data which can, under favorable circumstances, be extrapolated into unknown domains. The solution models on which these extrapolations are based have little theoretical validity and are, in fact, basically incorrect. This is not to minimize this line of approach; on the contrary, the techniques used by Kaufman, Ansara and others can be most useful from a practical standpoint, and constitute in fact the only currently practical methods available for extrapolation into the unknown for the purpose of making educated guesses. However, these methods should not be considered for attempting to extract basic physical parameters for a given system, as values of parameters obtained by such curve-fitting procedures do not have a clear physical meaning.

The Cluster Variation method proposed by Kikuchi and deFontaine is theoretically meaningful, but is presently limited to a small class of phase diagrams, the so-called "coherent" ones, as explained in our contributed papers. Again, this method can in no way be considered as "predictive", in the strict sense of the word.

What we can do now, but perhaps was not sufficiently discussed, is what I would call a perturbation approach to phase diagram calculations. For example, given an experimentally determined binary diagram, how will small additions of a ternary component modify the equilibria? Or, given a quaternary system containing a small percentage of element X, how will its replacement by Y affect the equilibrium? Answering these questions quantitatively is quite feasible provided that the "perturbation" on the given system to be in some way "small". Also,

this is not an idle academic pursuit, but has real practical applications.

Afternoon talks, were, for me, particularly enjoyable.

THIRD DAY

I found the presentation of industry's needs very disappointing: I could detect no trend, no policy, no clear general statement of requirements. Most panel members told a little anecdote about their favorite phase diagram, and generally made the profound statement that "much more work is needed". The questions of "how much work?" and "who is going to do it?" and "with what funds?" were hardly touched upon.

Of these questions, the one dealing with how much work can be done is the easiest to answer. I suggested that it would take about 8000 years to do all 32,160 possible ternary phase diagrams (based on a total of 80 components), and 100,000 years to do all 15,181,580 quaternaries. These are sobering numbers. Even if we could determine all ternaries, say, in a reasonable amount of time, storing that information (at an average of let us say five book pages per diagram) would require about 160,000 pages or roughly 200 volumes! Hence the first question to be answered is "what do we really want to do, what can we conceivably do?"

It appears that what can be done, and should be done, is a complete determination, evaluation, and compilation of binary phase diagrams. There are but 3,160 of these (again on the basis of 80 elements), so that this is a reachable goal. The problem is finite: once the goal has been reached, a mere six-volume set of binary diagrams, let us say, should satisfy all needs for generations to come.

GENERAL REMARKS

Thermodynamical measurements and phase diagram determinations are no longer regarded as glamorous fields. A few highly experienced and trustworthy old-timers

are still active, but little new blood is being transfused. Consequently, this type of work is often performed nowadays by ill-prepared teams whose primary interest is to obtain specific, immediate answers to specific questions. Phase diagrams result as bi-products, and the published data cannot always be taken very seriously. Frequently, published phase diagrams are even found to violate the phase rule.

Surely, this haphazard uncoordinated and random approach to data collection cannot endure. One group, one organism should take charge and exercise the most rigid scientific control over published data. One cannot insist too much on the need of absolutely top-flight people to preside over such a project: Thermodynamics is a very demanding field, where even long-time practitioners are often guilty of ignoring fundamental principles. There is perhaps no basic field in which so many bad mistakes are consistently made. A case in point: a certain number of educational films shown at the workshop were made (presumably at a considerable cost) by a group (I believe) at Penn State. Well, every single Gibbs free energy curve I saw depicted in these movies was drawn incorrectly: if the drawings are taken seriously, then the problem of purifying materials becomes trivial (and the semiconductor industry could save billions if they could only use the Penn State free energy curves) and phase diagrams which violate the phase rule could logically be constructed.

The question is then: "how do we bring very gifted young people into the field?" Unfortunately, I do not know the answer, but a generous injection of funds would help. Probably the type of support needed could be found in Europe where long-term funding policy of basic research is far more sensible than it is in this country right now.

SOME RECOMMENDATIONS

In summary, the workshop accomplished something important; it got people together from various disciplines, initiated dialogues, and made representatives from various fields aware of common needs (Thermodynamics is a great equalizer!) Unfortunately, the participants did not delineate objectives, define realistic goals, or propose methods of implementing these.

Perhaps a second get-together is now required to look into these matters in detail. This should be done quite soon, before too much grass is allowed to grow on the field. I would recommend participation by invitation only, and limited to about 50 persons at most. Participants should be discouraged from elaborating on their own pet projects, concentrating instead on general objectives and modes of implementation.

As mentioned above, the first question to be asked should be: "what can one actually accomplish in the relatively near future?" I would answer "the complete determination, evaluation, compilation, and publication of some 3000 "elemental" binaries (as opposed to "pseudo-binaries" such as NaCl-KCl for example)". In practice, this merely means doubling the size of the present Hansen-Elliott-Shunk series, surely an attainable goal.

Second question: "who shall do this?" It seems to me that since the disappearance of the Hultgren and K.K.Kelley groups, only the National Bureau of Standards can do the job. The NBS's task should not only be that of collecting data and publishing it, but also of evaluating and even generating it. I see no alternative to setting up a well-equipped central facility to crank out phase diagrams in a systematic and consistent manner, with well trained full-time technicians doing practically nothing but that, under the supervision of one top-flight thermodynamist, perhaps assisted by "rotating" post-docs. I repeat, the

task is a finite one; it can be done in reasonable time and gotten over with.

Next in order of complexity are the pseudo-binaries, usually regarded as the province of ceramist. Here, for the time being, I would only envision compilation and evaluation.

Ternaries pose an almost insurmountable problem (8000 years!). The best we can hope for at present is mere compilation and, in parallel, calculations à la Kaufman, with increased attention paid to the "perturbation techniques" alluded to above.

These are challenging tasks. Let us hope that means can be found to reach some limited goals. Needless to say, major technological problems confronting society today cannot be solved without adequate phase diagrams and thermodynamic data.



THE RELATION BETWEEN BOND LENGTH

AND

CRYSTAL STRUCTURES IN METALS

A. P. Miodownik
University of Surrey
Guildford, UK GU2 5XH

Introduction

The changes which occur in the distance of closest approach when an element is placed into a different lattice ^(1,2) are important in connection with the calculation of lattice strains ⁽³⁾, the estimation of critical size ratios ^(5,6), and the assessment of solid solubility limits ^(7,8). Such changes are usually associated with a corresponding change in bond strength and/or the type of bonding arrangement, and therefore also form a useful indicator for the estimation of hardness, melting point, heats of formation, and other properties of alloys and intermetallic compounds ^(5,6,8,10)

One of the earliest attempts to give general guidance on the magnitude of these changes is the set of predicted percentage changes known as the Goldschmidt conversion factors ⁽¹¹⁾. These have been extensively used in the tabulation of atomic diameters appropriate to 12-fold co-ordination, particularly for the conversion of the diameters of those elements which occur naturally in the BCC lattice with its 8-fold first co-ordination shell. The figure of 3% given by Goldschmidt for a change in Z from $12 \rightarrow 8$ was derived empirically from very limited evidence (iron and a copper-palladium alloy); this figure has nonetheless gained wide acceptance, and is in fact a very good approximation for the changes subsequently observed in similar transformations that have now been observed in some 14 other elements [1,12]. Although there is some controversy over the use of Goldschmidt correction factors in relation to solid solubility limits ⁽⁹⁾, their use is sufficiently wide-spread for several attempts too have been made to produce the same values theoretically. Thus Pauling ⁽¹³⁾ has applied the relationship:-

Note* Reader in Physical Metallurgy, Department of Metallurgy
and Materials Technology, The University of Surrey, Guildford.

$$d_n = d_1 - 0.60 \log_{10} n \dots\dots\dots(1)$$

which was derived from an empirical expression originally applied to organic compounds. Although this equation is not based on rigorous quantum mechanical foundations, it provides a convenient framework through which extensive crystallographic data can be readily interpreted in terms of simple bonding concepts. (d_n) represents the metallic diameter for bond number n , and (d_1) the single bond length, and metallic radii formulated on this basis have been used in a variety of ways to account for interatomic distances in alloys and compounds. In the original application of Pauling's equation only nearest neighbour interactions were considered significant, so that the value of $n_{FCC} = V_{FCC}/12$ and the corresponding value of $n_{BCC} = V_{BCC}/8$ (where V_{FCC} and V_{BCC} represent the total bond strength of any one atom in the two configurations). If it is further assumed that $V_{FCC} = V_{BCC}$, it follows immediately from equation (1) that:-

$$d_{BCC} - d_{FCC} = 0.60 \log(3/2) \dots\dots\dots(2)$$

$$\text{or } \Delta d_{\text{theor}} = 0.106 \text{ KK} \dots\dots\dots(3)$$

where d_{BCC} and d_{FCC} are the distances of closest approach in the respective lattices, and Δd the difference between these two values. This treatment predicts a value of Δd which is independant of the value of d , and considerably larger than the observed values for several common allotropic metals ($\Delta d_{\text{expt}} .072 - .092 \text{ KK}$).

In order to overcome this discrepancy, Thewlis⁽¹⁴⁾ recalculated (Δd) on the basis that the second nearest neighbours in the BCC lattice had a significant effect on bonding. If it is assumed that only a fraction f of the total bond strength V is associated with 8 nearest neighbours then a portion $(1 - f)$ of the bond strength is associated with the 6 atoms of the next co-ordination shell. The interatomic distance for atoms in the next co-ordination shell is $(2/\sqrt{3})d$; applying Pauling's equation to atoms at both

distances it follows that:-

$$d_{\text{BCC}} = d_1 - 0.60 \log f \ V/8 \dots\dots\dots(4)$$

$$\text{and } (2/\sqrt{3})d_{\text{BCC}} = d_1 - 0.60 \log (1 - f) \ V/6 \dots\dots\dots(5)$$

$$\text{whence } 0.60 \log 3f/4(1 - f) = 0.155d_{\text{BCC}} \dots\dots\dots(6)$$

From the introduction of the parameter (f), it follows that equation (2) must be replaced by equation (7) where:-

$$\Delta d = (d_{\text{BCC}} - d_{\text{FCC}}) = 0.60 \log 3f/2 \dots\dots\dots(7)$$

The value of f can be determined from equation (6), and it can be seen by inspection that Δd (BCC - FCC) for a given element will now be smaller than the value derived with equation (2), and that the value of Δd is no longer constant, but a function of d (equation 5). (Table I) shows the agreement between theory and experiment obtained by Thewlis for the elements Fe, Ti, Zr and Tl, and the marked improvement obtained by including second nearest neighbour interactions.

This improved fit between theory and experiment must nonetheless be considered partly a consequence of the restricted number of elements analysed by Thewlis. (Figure 1) shows that the value of Δd predicted by equation (7) underestimates the values obtained by experiment for a larger range of elements, particularly those with a large atomic radius. Since the basic Pauling equation does not appear to account for the observed changes in the newly discovered allotropic elements, metallurgical practice to obtain the appropriate atomic radius for a change in co-ordination number has generally reverted to the use of the empirical Goldschmidt factor, or an interpolated value taken directly from the experimental data summarised in Figure 1 (8). The criterion of a zero volume change for the BCC - FCC transformation leads to a predicted 2.6% change in diameter, and can be invoked on the grounds of current electron theory⁽¹⁵⁾, but clearly does not account for the large volume changes that occur in transformations involving lattices with other co-ordination numbers.

In the context of this situation the present paper

attempts to reconsider the basis of Pauling's equation and to apply a modified form of this equation to a more accurate prediction of changes in interatomic spacing resulting from FCC/CPH to BCC transformations.

A general relation between bond strength and interatomic distances

Gilman⁽¹⁶⁾ has shown that the shear modulus for elements of a given crystal structure is a simple function of the distance of closest approach, a family of straight lines of characteristic slope being obtained when these two variables are plotted on logarithmic axes. (Figures 2,3) show that a similar relationship occurs if the bulk modulus is substituted for the shear modulus, which is to be expected with the values of Poisson's ratio characteristic for most metals. All bulk moduli have been taken from the compilation of Küster and Franz⁽¹⁷⁾ with the exception of the data for the allotropes of tin⁽¹⁸⁾ This relationship can be expressed in the form:-

$$\log(K_a/K_b) = k_G \log (d_a/d_b) \dots\dots\dots(8)$$

where the constant (k_G) has the characteristic values shown in Table II.

At this point it is necessary to enquire whether any systematic error is introduced into the measured slopes through the use of room temperature values of the variables in question, rather than the values appropriate to a series of homologous temperatures. Examination of the expression derived by Mott and Jones⁽¹⁹⁾ for the variation of compressibility with temperature suggests that, to a first approximation, the slopes may well remain largely unaffected providing both variables are referred to the same temperature:-

$$\text{According to Mott } \frac{dX}{dT} = - \frac{\alpha X}{\gamma} V^2 d^2 (\log \gamma)/dV^2 \dots\dots\dots(9)$$

where X is the compressibility, V the atomic volume, α the coefficient of expansion, γ the characteristic vibration frequency of the lattice, and γ is Grünheisen's constant^(19,20). Since α and X are inversely proportional to each other, and Grünheisen's constant equals $-d(\log \gamma)/d(\log V)$, the rate of change of compressibility with temperature appears to be largely

a function of V^2 , or the sixth power of the interatomic distance. This is of the same order as the slopes of the bulk modulus versus interatomic distance plots.

Table II lists the slopes derived from Figure 2 and 3 for various crystal structures and bond types. In the light of the variations accepted in numerous other groupings of physical constants, such as Lindemann's constant and Leibfried numbers⁽²⁰⁾, it seems valid to use the relationship expressed by equation 8, and the average slopes given in Table I as a valid basis for further discussion of the changes in bond distance occurring during phase transformations. Also included for comparison in Table II are the equivalent slopes calculated for several materials on the basis of various simple bonding models (21 - 24).

The relationship between the Pauling's Equation and the Gilman formulation

Equation (8) clearly indicates that a reduction in interatomic distance will result from an increase in bond strength, where changes in the latter variable are produced by moving from one element to another. The Pauling equation expresses the same conclusion, but relates to changes in bond strength which result from varying the number of bonds between otherwise identical atoms. There is obviously a close connection between the two formulations as can be seen from (Figure 3), where the force constants (f) appropriate to various carbon bonds have been plotted on a logarithmic basis. A slope of approximately -3 is obtained, which forms the basis of Badger's Rule⁽²⁵⁾. It is significant that the dimensional relationship between force constants and modulus values is given by $K = f \cdot d^{-1}$, so that Badger's rule corresponds to a slope of ~ -4 for plots of modulus versus interatomic distance. Although many attempts have been made to combine interatomic distances, force constants and bond number^(26 - 28) there does not seem to exist a formal description of how the Pauling equation (1) can be related to logarithmic plots of the type used by Gilman.

Alternative form of the Pauling equation

The general form of Pauling's equation is expressed by:-

$$d_e - d_b = k_p \log (n_b/n_a) \quad \dots\dots\dots(9)$$

where the constant k_p is left unspecified instead of entering a specific value such as 0.70.

Dividing both sides by d_b

$$(d_a - d_b)/d_b = (k_p/d_b) \log (n_b/n_a) \quad \dots\dots\dots(9a)$$

Since $x \approx 2.3 \log (1 + x)$ when x is small, $(d_a - d_b)/d_b$ can be replaced by $2.3 \log \left[1 + (d_a - d_b)/d_b \right]$ and hence:-

$$2.3 \log (d_a/d_b) \approx (k_p/d_b) \log (n_b/n_a) \quad \dots\dots\dots(10)$$

Rearrangement yields:-

$$\log (n_b/n_a) \approx \left(\frac{-2.3d_b}{k_p} \right) \log (d_a/d_b) \quad \dots\dots\dots(11)$$

and comparison with equation (8) shows that the slope A in Gilman plots should be related to the constant k_p of Pauling's equation by the simple relationship:-

$$k_p \approx -2.3d_b/k_G \quad \dots\dots\dots(12)$$

if it is accepted that the bulk modulus is equivalent to the bond number as a criterion of bond strength. The validity of equation (12) can be tested by comparing the calculated values of (k_p) for carbon and a typical metal such as iron, with the empirical values used by Pauling (Equations 1 and 2); Table III shows that values of the correct magnitude are obtained.

The dependence of $\Delta d_{FCC \rightarrow BCC}$ on the distance of closest approach

Equation (12) suggests that the value of k_p in Pauling's equation will be directly proportional to the distance of closest approach for groups of elements whose bonding characteristics are similar (constant value of k_G). This has a number of interesting consequences.

Thus replacing $k_P = 0.60$ by $k_P = 2.3 d_{BCC}/k_G$ in equation (6):-

$$\log 3f/4(1-f) = \frac{-0.155 k_G}{2.3} \dots\dots\dots(13)$$

Hence the value of f is now a constant independent of the value of d_{BCC} and only a function of the value of (k_G) . A similar substitution in equation (7) yields the result that:-

$$\Delta d = d_{BCC} - d_{FCC} = \frac{-2.3 d_B}{k_G} \log(3f/2) \dots\dots\dots(14)$$

This leads to the conclusion that the value of Δd should be directly proportional to the distance of closest approach d . Figure 2 indicates that, for BCC/FCC/CPH transformations, A has a value lying between 8 and 9, and the derived values of Δd calculated on this basis are shown in Table IV. It can be seen that there is good agreement with the experimental values available in the literature^(8,12) and equations (13 and 14) in effect define the pragmatic dependence of Δd as used by Gschneidner⁽⁸⁾, and illustrated in Figure 1. Substituting a value of k_G equal to 8.7 (Table IV) into equation (13) yields $f = 0.84$, and substituting this value into equation (14) and rearranging gives:-

$$\begin{aligned} \Delta d_{BCC-FCC}/d &= \frac{-2.3}{8.7} \log \frac{3 \times 0.84}{2} \\ &= -2.6\% \dots\dots\dots(15) \end{aligned}$$

This confirms the initial empirical value of 3% suggested by Goldschmidt. It should however be noted that the small difference between 2.6% and 3% may become significant in high pressure experiments and cases where transformation stresses are important. The inherent geometrical volume change that will occur on changing from FCC to BCC configuration assuming no change in atomic diameter is easily deduced to be:-

$$\frac{V_{BCC} \cdot N_{FCC}}{V_{FCC} \cdot N_{BCC}} = 2 \left(\sqrt{\frac{2}{3}} \right)^3 = 1.0872 \dots\dots\dots(16)$$

Where V_{BCC} and V_{FCC} are the appropriate volumes of the unit cells, and N_{BCC} and N_{FCC} the corresponding numbers of atoms per unit cell.

The net volume change which occurs when a change in atomic diameter is included is given by:-

$$\Delta V_{\text{net}} = 1.0872 (d_{\text{BCC}}/d_{\text{FCC}})^3 \dots\dots\dots(17)$$

Since $(1.026)^3$ equals 1.0799 and $(1.03)^3$ equals 1.0927, the two criteria therefore predict net volume changes of opposite sign.

The effect of a change in co-ordination from 12 \rightarrow 6 nearest neighbours

The Goldschmidt correction factor for this change in co-ordination is quoted as a contraction of 4%, which is not very different from the 3% quoted for the change to 8 nearest neighbours. The original reference⁽¹¹⁾ shows that this value was derived from the behaviour of a single material (SbSn) which cannot be considered typical of this class of transformation. An examination of some cubic transition metal carbides with the B3 structure shows that the appropriate reduction for a change in co-ordination from 12 \rightarrow 6 may be nearer 7% (Table V). This is the value derived by calculating the effective carbon radius for sixfold co-ordination with equation (9) (using the appropriate value of k_p derived from equation 12), subtracting this result from the distance of closest approach in the carbides concerned, and comparing the effective metallic radius with the distance of closest approach in the pure metal (for co-ordination 12).

An independent estimate of the expected contraction for the metal atom can be made by using the same principle already outlined for the FCC-BCC transformation (equations 13 and 14), namely by first establishing the expected partition of the total bond strength between the six metal-carbon bonds and a further 12 second nearest metal-metal bonds. Since the metal-metal bond distance is 41% greater than the metal-carbon bond, it is found that 95% of bond strength is associated with these latter bonds; applying the appropriate analogues of equations (14 and 15):-

$$\begin{aligned} \Delta d_{\text{NaCl-FCC}}/d &= -(2.3/8.7) \log (2 \times 0.95) \\ &= -7.4\% \dots\dots\dots(18) \end{aligned}$$

This value is in good agreement with the mean value derived from the carbides listed in Table V ($6.9 \pm 1.5\%$) and it may therefore be worth considering that this is a more suitable value to use in metallic systems.

Since the sodium chloride lattice is also favoured by ionic bonding, it is interesting to note that Pauling⁽¹³⁾ calculates an expected expansion of 9.1% for a change in ligancy from 6 \rightarrow 12, with an average Born exponent of 9 which is equivalent to an 8.4% contraction based on 12 fold co-ordination).

A change in the proportion of ionic bonding is therefore not going to produce a great deal of difference in the interatomic distances observed in practise, and this situation favours a high degree of resonance consistent with the high melting point and hardness of these carbides. These considerations serve to complement the arguments used by Robins⁽¹⁰⁾ to account for the existence of these carbides, and remove some of the anomalies which result when a conventional Pauling analysis is made of the apparent bond numbers in these compounds⁽¹⁰⁾.

III The A4 \rightarrow A5 Transformation in Group IV Elements

Jamieson⁽²⁹⁾ has shown that the allotropic transformation which occurs in pure tin can occur under pressure in other materials possessing a diamond structure (Table VI). It is therefore of interest to see whether the observed changes in interatomic distance can be predicted by means of the . . present treatment. The A5 (white tin) structure is characterised by two distances of closest approach⁽¹⁾:-

$$4 \text{ atoms at } (a^2/4 + c^2/16)^{1/2} \dots\dots\dots(19)$$

$$\text{and } 2 \text{ atoms at } c \dots\dots\dots(20)$$

This can be rearranged to yield the difference between the two distances of closest approach Δd_{1-2} :

$$\Delta d_{1-2} = a \left[\frac{c}{a} - 0.518 \right] \dots\dots\dots(21)$$

The fraction of the total bond strength (f) associated with the four nearest neighbours may be calculated in an analogous way to the method used for BCC structures (equations 4 to 6), and this value then used to calculate the expected change in interatomic distance for the $A4 \rightarrow A5$ transformation. Since there is here some doubt as to whether the bonds should be considered metallic or covalent, both values of the constant B have been used in Table VII. Pauling originally treated the tin transformation as an example where there is a change in the effective valency of the element as well as a change in the number of ligands, attributing a metallic valency of 2.5 for white tin as compared to 4 in the case of the diamond structure of grey tin⁽¹³⁾. However a comparison of the experimental results in Table VI with the predicted values from Table VII indicates that the transformation may equally well be considered in terms of an unaltered valency of 4 together with predominantly covalent bonding in both allotropes. Covalent bonding in white tin structures has also been suggested by Yoshioka and Beck⁽³²⁾ on the basis of the alloying behaviour of group IV elements.

The effect of ionic bonding and the $B3 - B1$ Transformation

It may be noted from Table VII that an increasing value of Δd ($A4 \rightarrow 5$) in the case of III - V compounds correlates with an increase in polarisability of these compounds as determined by Folberth and Welker⁽³⁰⁾. It therefore seems likely that there is some proportion of ionic bonding involved in this transformation.

While the $A5$ structure may be considered as a deformed six-fold co-ordination (since the two sets of interatomic distances are reasonably similar) there is no doubt that it is a less suitable structure for ionic bonding than either the sodium chloride lattice or the diamond lattice. Consequently it may be expected that whereas in a transformation from $B3(ZnS) \rightarrow B1(NaCl)$ the proportion of ionic bonding is likely to increase, in the transformation $A4(or B3) \rightarrow A5$ the proportion of ionic bonding is likely to decrease. With increasing polarisability there then arises a situation where in the $A4(B3)$ structure there

will be an increasingly large contribution to resonance bonding whereas there will be a decreasing contribution to resonance in the corresponding A5 structure. This situation is consistent with the observed variation of Δd with polarisability.

According to Folberth and Welker⁽³⁰⁾ when the polarisability factor exceeds a critical value the ZnS lattice becomes unstable with respect to the NaCl (or CsCl) lattice, since ionic bonding now predominates over the covalent component. Folberth and Welker placed this critical point between InSb and InP, and it is significant that the results as Drickamer⁽³¹⁾ shows that InP and InAs (which have very similar values of polarisability) both transform to a B1 (NaCl) lattice in preference to the white tin modification. Table VIII shows that the changes in the distance of closest approach for this transformation also lie very close together (between +7.4% and +3.6%); Table X shows the corresponding calculated values based on both fully ionic and fully covalent models, it can be seen that, as might be expected, the experimental values fall in between these two extremes.

Changes in the interatomic distance arising from a change in co-ordination from 12 \rightarrow 4

(Table X) shows that the changes in atomic diameter for silicon, germanium and tin dissolved in FCC lattices center around 14% relative to the diameter in their normal lattice⁽¹⁾, which is good agreement with the value suggested by Goldschmidt (his correction factor of 12% is based on the FCC lattice as a reference point, and this is nearer 14% relative to CN = 4). With this large change in co-ordination, correspondingly larger differences might be expected for different bonding models, as shown in Table XI.³ The large differences in apparent atomic volume for these elements when present in various intermetallic compounds⁽³²⁾ can be readily rationalised in terms of varying proportions of covalent and metallic bonding, providing the purely geometric volume changes associated with the various structural changes are first eliminated (see Appendix A). According to the principles already used for the other

types of transformation, the calculated values are given by:-

$$\frac{\Delta_{\text{FCC} \rightarrow \text{DIAMOND}}}{d} = \frac{-2.3}{k_G} \log 3 \dots\dots\dots(22)$$

Where in this case it is clearly not to be expected that either $k_G = 8.7$ or $k_G = 4.5$ will lead to a universally applicable answer. It is interesting to note that the range of experimentally determined results does lie generally between the two values obtained by assuming totally covalent or totally metallic bonding in both co-ordinations. The suggested intermediate case in Table XI assumes that there is covalent bonding for the co-ordination change $4 \rightarrow 6$ and metallic bonding for the change $6 \rightarrow 12$. Both these changes have been discussed in other sections of this paper, and together total +16%.

It is interesting that if the experimentally determined values for these two sets of transformations are added, the average value and scatter is almost identical $+14 \pm 4\%$ with the results of Table X. Attributing a definite metallic diameter to the Group IV elements (Si, Ge, Sn) is thus difficult, but it seems clear that the appropriate value will be considerably larger than the estimate made by Rudman⁽¹²⁾ on the basis of the effective diameter in the A5 structure.

Conclusion

Table XII compares changes in the distance of closest approach, calculated for various transformations on the basis of the modified Pauling equation used in this paper, with the average experimental values obtainable from literature. It may be concluded that this treatment offers a satisfactory general method of rationalising the observed data, and also relates various other empirical methods currently in use. A summary of the effect of different types of bonds (Figure 4) shows that there is considerable similarity in the dimensional changes expected from the major kinds of bonding, and this no doubt contributes to the general uniformity of the observed overall trend. Although this allows more confidence in estimating dimensional changes where the nature of the bond is not known, it means that the reverse procedure of estimating the nature of the bond from observed changes in interatomic distances must be treated with caution.

Acknowledgements

A debt of gratitude is due to Professor F. C. Thompson, who encouraged the author to persist in tackling this topic, and also to the many students and colleagues whose questions have acted as a spur to finding the solution presented here.

Appendix A

The necessary information to evaluate the changes in volume which occur due to geometric factors only is assembled in (Table A1). The ratio of atomic volumes to be expected can then be expressed in terms of a purely geometric factor and a ratio of the effective atomic diameters in the two structures (Table A2).

If it is assumed that no changes occur in the size of the atoms concerned during transformation, the equivalent values of $\Delta V\%$ are very similar for the $A4 \rightarrow A5$ and $A4 \rightarrow B1$ transformation, but markedly different from the value of the $A4 \rightarrow A1$ transformation (Table A3). It can be seen that if allowances are made for the average change in (d) observed for these transformations an entirely different set of values is obtained. The formulae in the main body of the paper can be used to derive the likely changes in ΔV for different bond strengths.

It is clear that similar calculations should be made for each type of lattice change before any significant comparison can be made between the effective atomic volumes per atom.

TABLE A1

Crystal Lattice	Distance of Closest Approach (d)	Volume/Atom
Diamond A4	$(\sqrt{3}/4)a$	$a^3/8 = (8/3\sqrt{3})d_{A4}^3$
White Tin A5	$\frac{a}{4} \left[4 + (c/a)^2 \right]^{1/2}$	$a^2 c/4 = \frac{1}{4}(c/a)(d_{A5}/.518)^3$
NaCl B1	$(1/2)a$	$a^3/8 = d_{B1}^3$
FCC A1	$(1/\sqrt{2})a$	$a^3/4 = (\sqrt{2}/2)d_{A1}^3$

TABLE A2

Transformation	Ratio of Atomic Volumes
$A4 \rightarrow A5^*$	$.63 \times (d_{A5}/d_{A4})^3$
$A4 \rightarrow B1$	$.65 \times (d_{B1}/d_{A4})^3$
$A4 \rightarrow A1$	$.46 \times (d_{A1}/d_{A4})^3$

(*based on c/a ratio of 0.55; only marginal differences in c/a observed for this group of products)

TABLE A3

Transformation	$\Delta d\%$	Ratio d/d_{A4}	Equivalent $\Delta V\%$
$A4 \rightarrow A5$	0%	1.00	- 37%
$A4 \rightarrow B1$	0%	1.00	- 35%
$A4 \rightarrow A1$	0%	1.00	- 54%
$A4 \rightarrow A5$	+7%	1.07	- 23%
$A4 \rightarrow B1$	+8%	1.08	- 18%
$A4 \rightarrow A1$	+14%	1.14	- 32%

(a 1% increase in Δd is approximately equivalent to a change of +2% in ΔV)

REFERENCES

1. Pearson, W. B. A Handbook of Lattice Spacings, Pergamon 1958
2. Massalski, T. B. Met. Reviews 1958 3 (9) 45
3. Friedel, T. Advances in Physics 1954 3 504
4. Eshelby, J. D. Solid State Physics 1956 3 79
5. Leves, F. Theory of Alloy Phases 1956 ASM p. 124
6. Stringer, Ed. J. Rudman, P. and Jaffee, J., Phase Stability in Metals and Alloys, McGraw Hill 1967.
7. Waber, J. T. et al. Trans. Met. Soc. AIME 1963 227 717
8. Gschneidner K. et al. U.S. Dept. Commerce Publication LA 2345 1960
9. Hume Rothery, W. Acta Metallurgica 1966 14 17
10. Robins, D. A. Powder Metallurgy 1958 1/2 172
11. Goldschmidt, V. M. Z. Phys. Chem. 1928 133 397
12. Rudman, P. S. Trans. Met. Soc.(AIME) 1965 233 864
13. Pauling, L., The Nature of the Chemical Bond, O.U.P. 1960
14. Thewlis, J. J. Amer. Chem. Soc. 1953 75 (2) 2279
15. Mott, N. F. Proc. Phys. Soc. 1962 25 218-243
16. Gilman, J. J. Amer. Ceram. Soc. Symp. Nat. Bureau of Standards Publication No. 59 p.79 1963
17. Koster, W. and Franz, H. Metallurgical Reviews 1961 6 (21) 1
18. Musgrave, M. J. P. Proc. Roy. Soc. (A) 1963 272 503
19. Mott, N. F. and Jones, H., The Theory of the Properties of Metals and Alloys, O.U.P. 1936
20. Gschneidner, K. A. (Jr.) Solid State Physics 1964 16 275
21. Smith, C. S. ASM Symposium on Resonance and Relaxation in Metals 1959
22. Pice, O. K. Phase Transformations in Solids 1951 (John Wiley) (7) 212
23. Raynor, G. V. Inst. of Metals Monograph No. 4 1947 90
24. Gurney, V., Ions in Solution, Dover 1939
25. Badger, R. M. J. Chem. Phys. 1934 2 128 ibid 1935 3 710
26. Walsh, A. D. Trans. Farad. Soc. 1946 42 779 et.seq.
27. Gordy, W. J. Chem. Phys. 1947 15 305
28. Waser, J. and Pauling, L. J. Chem. Phys. 1950 18 (5) 747
29. Jamieson, J. C. Science 1963 March 1 845
30. Folberth, O. G. and Welker, H. J. Phys. Chem. Solids 1959 8 14-20

31. Minomura, S. and Drickamer, H. G. Phys. Chem. Solids 1962 Vol. 23
pp. 451-456
32. Yoshioka, T. and Beck, P. A. Trans. AIME Met. Soc. 1965 233 1788
33. Huggins, M. L. Phase Transformations in Solids 1951 (John Wiley)
(8) p. 238

TABLE I

Effect of second neighbour interaction on the prediction of changes in the distance of closest approach in FCC allotropic transformations

Element	d CN12 KX (at T_A)	Δd First neighbour interaction only Pauling (13)	Δd First and second neighbour interactions Thewlis (14)	Observed Δd (at T_A) (1,12)
Fe	2.57	4.1%	2.5%	2.5%
Ti	2.95	3.6%	2.4%	2.8%
Zr	3.13	3.3%	2.4%	2.9%
Tl	3.45	3.1%	2.4%	2.7%

TABLE II

Experimental and calculated values of $d(\log K)/d(\log d)$ for groups of elements with different crystal structures

	Structure	$d(\log K)/d(\log d)$	Reference
Experimental Values	FCC A1	$-(8 \rightarrow 9)$	Data from Pearson (1)
	BCC A2	$-(8 \rightarrow 9)$	
	CPH A3	$-(8 \rightarrow 9)$	
	Diamond A4	$-(4 \rightarrow 5)$	Gilmen (16) and Köster (17)
	NaCl B1	-4	
Calculated Values	Aluminium	-8	Smith (21)
	Sodium	$-(7 \rightarrow 8)$	Smith (21)
	Vander Waal	$-(6 \rightarrow 8)$	Rice (22)
	"Fermi" Metal	-5	Raynor (23)
	Ionic	-4	Gurney (24)

TABLE III

Comparison of calculated values of the Pauling
constant with standard values used in the literature

Element	Interatomic Distance(d)	Gilman constant(k_G)	Pauling constant(k_P)	Calculated Pauling constant (Equation 12)
C	1.54	4.7	0.70	0.75
Fe	2.47	8.7	0.60	0.65

TABLE IV_a

Comparison of experimental and calculated values
of Δd for transformations from BCC to close packed
structures

Element	d (CN12) KX (at T_A)	Δd OBSERVED (Refs 1,8,12)	Δd CALCULATED ($k_G = 8.7$)
Fe	2.57	.063	.069
Mn	2.73	.069	.074
Ti	2.94	.078	.080
Zr	3.23	.090	.088
Tl	3.45	.097	.094
Th	3.65	.101	.099
Ce	3.66	.100	.100
Na	3.76	.103	.102
Ca	3.97	.110	.109
Sr	4.33	.127	.120

TABLE IV b

Variation in the partition coefficient f_{BCC} with the Gilman constant G_K , and the resultant changes in Δd for BCC - CPH and FCC - FCC transformations

Gilman constant k_G	8.0	8.5	8.7	9.0	OBSERVED
Partition coefficient f_{BCC}	0.82	0.83	0.84	0.85	Δd ↓
Calculated $\Delta d_{\text{CPH}}^{\text{BCC}}$ Ti	.075	.077	.080	.083	.078
Calculated $\Delta d_{\text{FCC}}^{\text{BCC}}$ Ca	.102	.106	.109	.112	.110

TABLE V

Distances of closest approach in cubic transition metal carbides and their relation to the radius for twelvefold co-ordination

System	Metal Carbon distance (10)	Carbon Radius for Z=6 (13)	Effective Metal Radius	Pure Metal Radius for Z=12 (1)	$\Delta\%$
Ti-C	2.16	0.84	1.32	1.44	8.3%
Zr-C	2.34	0.84	1.50	1.60	6.3%
Hf-C	2.32	0.84	1.48	1.58	6.3%
V-C	2.08	0.84	1.24	1.34	7.5%
Nb-C	2.23	0.84	1.39	1.43	5.6%

TABLE VI

Experimental values for changes in interatomic distance for A4-A5 transformations

Element	Δd	$c/a(A5)$	Polarization Factor $J(30)$	Refs
Si	7.0%	0.554	-	(31,32)
Ge	6.3%	0.551	-	"
Sn	7.5%	0.546	-	"
AlSb	5.2%	0.538	35	(29)
GaSb	5.4%	0.549	55	"
InSb	8.9%	0.536	95	"

TABLE VII

Predictions of the change in interatomic distance for the A4 \rightarrow A5 transformation in Tin

Valency A4 A5		Partition Coefficient $f(A5) \downarrow$	Type of Bond	Gilman Constant k_G	Calculated Δd	References
4	4	.72	Ionic	4	8.0%	Present
		.72	Covalent	4.5	7.1%	Work
		.76	Metallic	8 \rightarrow 9	3 \rightarrow 4%	
4	2.5	(.79)*	A4 Covalent A5 Metallic	(10)*	6.6%	Pauling (5,13)

* Equivalent values derived from Pauling and Equation (12) based on the transformation in Tin.

\downarrow The partition coefficient will be a function of c/a ratio, but for the range of c/a observed in these transformations (Table VI) this is only a second order effect.

TABLE VIII

Experimental values of the change in the distance of closest approach for the $B3 \rightarrow B1$ transformation

Compound	d NaCl	$\Delta d(B3 \rightarrow B1)$	Ref
Ag I	3.04	+ 8.6%	(33)
In As	5.51	+ 7.9%	(31)
In P	5.71	+ 7.4%	(31)

TABLE IX

Predicted values for the change in the distance of closest approach for the $B3 \rightarrow B1$ transformation

Type of Bond	$\Delta d(B3 \rightarrow B1)$	Ref
100% Ionic (Born exponent = 9)	+ 5.1%	13
100% Covalent ($k_G = 4.5$)	+ 9.2%	-

TABLE Xa

Variation in apparent atomic diameter for Tin, Silicon and Germanium in various crystal structures (1)

		d_{Si}	d_{Ge}	d_{Sn}
Elemental Form	A4	2.34	2.44	2.80
White Tin Structure	A5	2.52	2.60	3.02
FCC Solid Solution	A1			
(a) Al base		2.73	2.96	-
(b) Cu base		2.59	2.78	3.26
(c) Ag base		-	2.90	3.18

TABLE Xb

Apparent changes in the distances of closest approach
in FCC structures relative to the diamond structure

Element	$\Delta d \text{ A4} \rightarrow \text{A1}$		
	in Al	in Cu	in Ag
Si	14%	10%	-
Ge	17%	12%	16%
Sn	-	14%	12%

TABLE XI

Predicted change in interatomic distances for
the $\text{A4} \rightarrow \text{A1}$ transformation

Assumed Bonding	Gilman Constant k_G	Predicted $\Delta d/d_{\text{A4}}$
Totally Metallic	8.7	+ 12.6%
Totally Covalent	4.5	+ 24.3%
Covalent ($Z = 4 \rightarrow 6$) + Metallic ($Z = 6 \rightarrow 12$)	4.5 } + 8.7 }	+ 16.5%
Totally Ionic (13)	-	+ 14.2%
Based on ($Z = 6 \rightarrow 4$) + ($Z = 6 \rightarrow 12$)		

TABLE XII

Comparison of experimentally observed Δd values
with the predictions of the modified Pauling equation

Transformation	Δd predicted	Δd observed
FCC - BCC (A1 - A2)	- 2.6%	- 2.8% ($\pm 0.3\%$)
FCC - NaCl (A1 - E1)	- 7.4%	- 6.8% ($\pm 1.5\%$)
Diamond - White Tin (A4 \rightarrow A5)	+ 7.1%	+ 6.6% ($\pm 1.4\%$)
Diamond - NaCl (A4 \rightarrow E1)	+ 9.2%	+ 8.0% ($\pm 0.6\%$)
Diamond - FCC (A4 \rightarrow A1)	+ 16.5%	+ 14% ($\pm 4\%$)

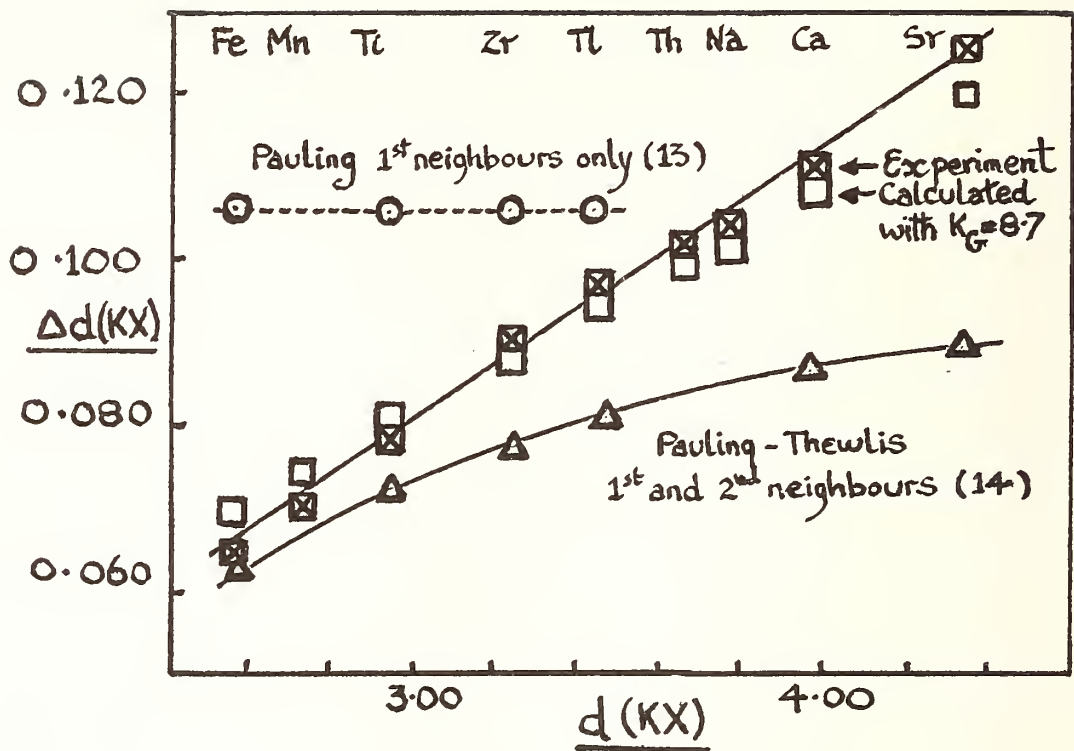


FIG.1.

The Variation of Δd with d for elements which exhibit BCC-FCC or BCC-CPH transformations

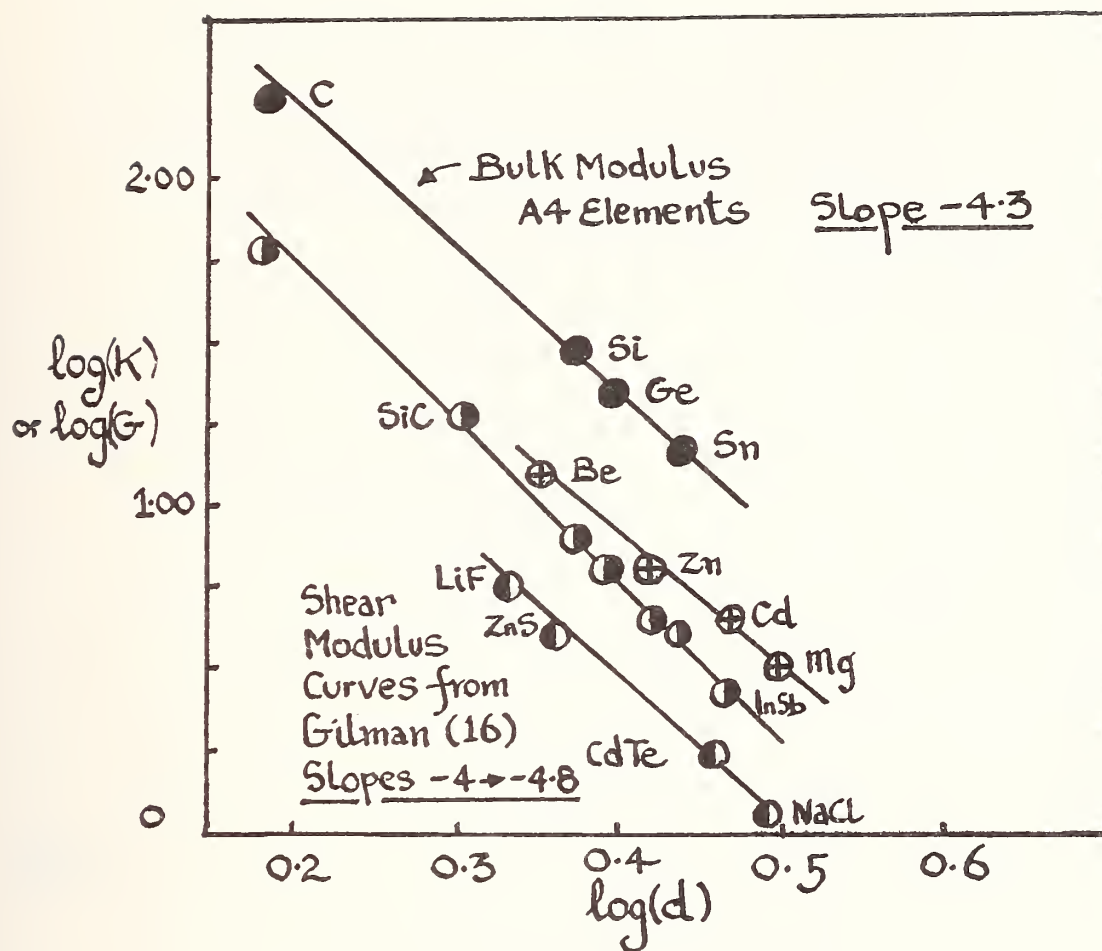


FIG. 2.

The relationship between the elastic modulus and the distance of closest approach for elements and compounds with predominantly covalent and ionic bonding.

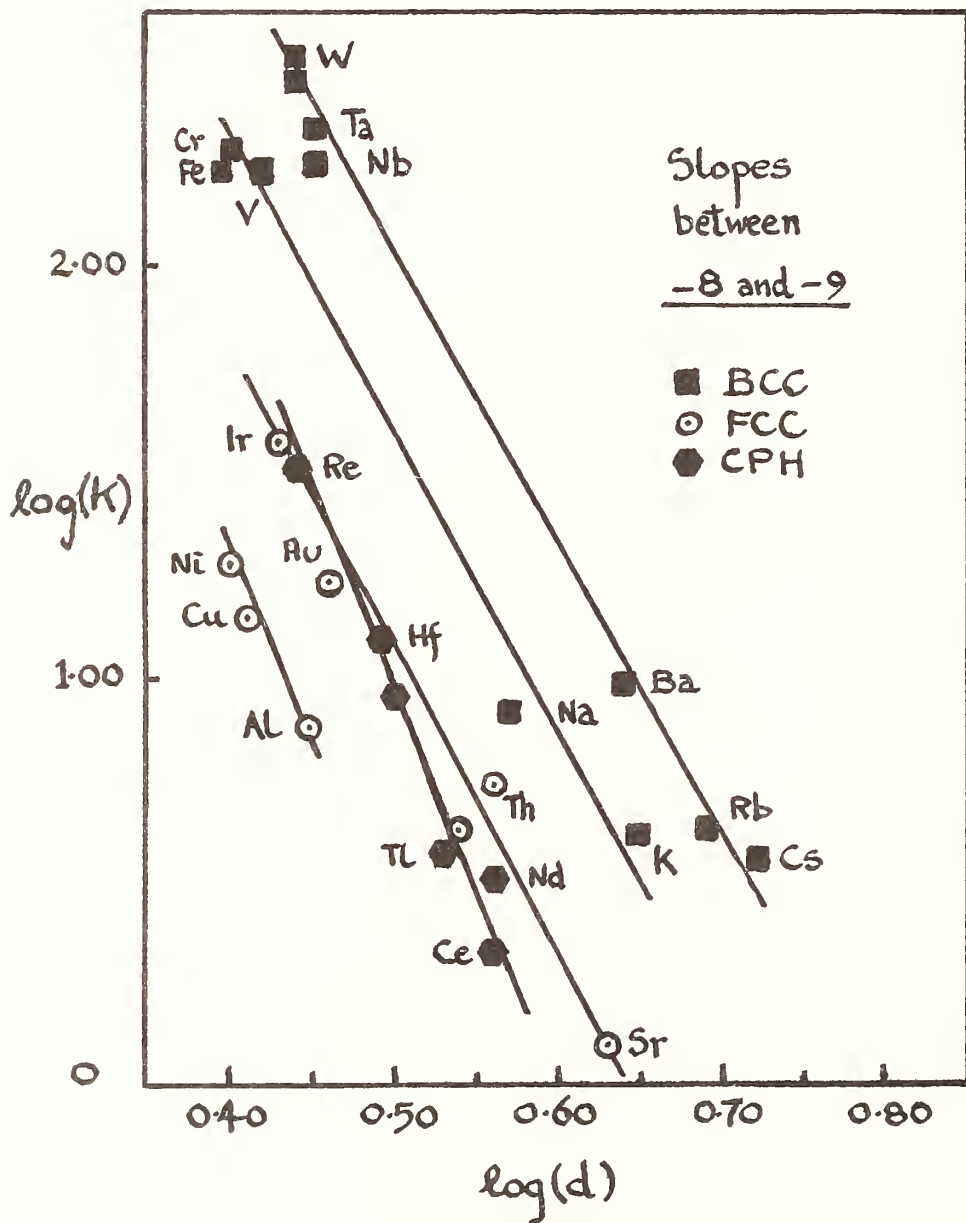
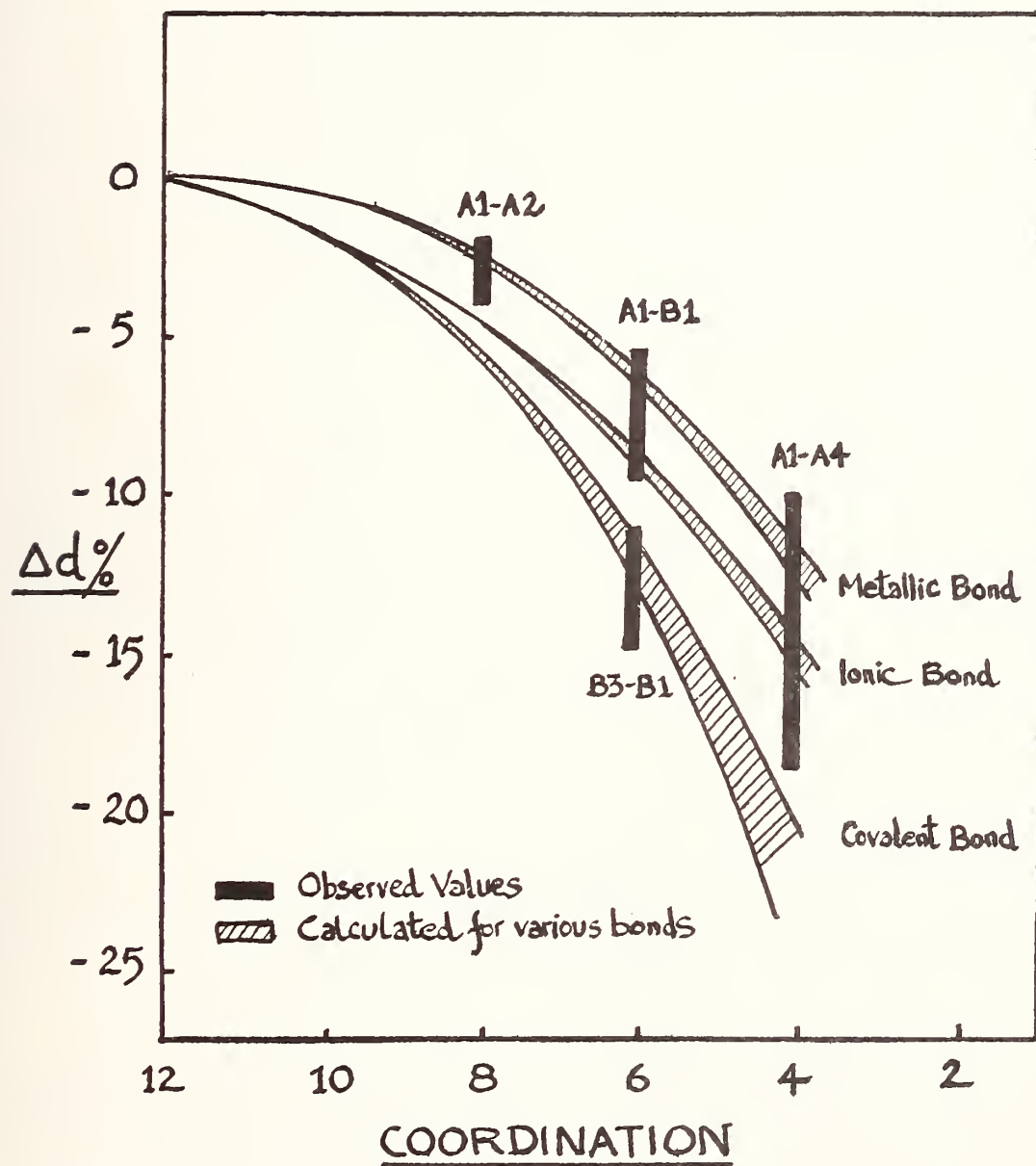


FIG.3. The Variation of Elastic Modulus with the distance of closest approach in metals with BCC, FCC, and CPH structures.

FIG 4. The variation of Δd with type
of bond for different changes
in coordination





On Computerized Construction of Multidimensional Phase Diagrams in a Factographic IRS

I. V. Tulupova and V. S. Stein

"Phase Diagrams" (PD) is a field of knowledge belonging to several sciences--chemistry, physical metallurgy, petrography, etc. Phase diagram data are widely used by scientists and engineers in various professional fields. Naturally, there are quite a number of studies summing up the published data on the PD of two-component systems, including the handbooks by M. Hansen and K. Anderko, R. P. Elliott, F. A. Schunk, and others. A sign of the great importance of PD for various fields of science and technology is the fact that VINITI puts out special collections of abstracts on "Phase Diagrams of Metallic Systems" and "Phase Diagrams of Nonmetallic Systems" on the basis of material covered in its abstract journals "Chemistry" and "Metallurgy."

Constructing a phase diagram from experimental data is a laborious, expensive, and sometimes even practically unfeasible job. This has given rise to several calculative methods of PD construction, some of them computer-based. Methods of computer-based PD construction are being developed by various authors in the USSR and in other countries (D. S. Kamenetskaya, I. L. Aptekar', O. S. Ivanov, A. L. Udovsky, L. Kaufman, G. H. P. Lupis, etc.). A number of studies deal with predictions of the PD pattern and its particular features, for instance, the chemical compounds (V. M. Vozdvizhensky, E. M. Savitsky, and V. B. Gribulya; G. Petzow; and others). Other studies are concerned with experiment planning, which is also very important (F. S. Novik, Yu. P. Adler, etc.). All those studies, however, deal either with particular boundaries or with PD of two-component systems and two-dimensional (isothermal) sections of three-component systems.

Yet PD of multicomponent systems which reflect the interaction of several components are of a particular practical importance. A case in point is PD of materials having special physical properties.

Normally, multicomponent PD are represented by individual sections both in primary publications and in secondary (reference) materials.

Conventional techniques of plotting the PD of a multicomponent system by experimental points (using descriptive geometry) are laborious, lack visuality, and cause difficulties when the PD are put to use in solving calculative problems. So it is clear that reconstruction by computer of PD of multicomponent systems is needed.

The objective of describing a complete PD by means of a computer with a view to its subsequent storage, retrospective searching, and

olution of computational and physical metallurgy problems was first stated by V. S. Stein.

His earlier publications (especially [1,2,3]) described the first attempts at devising machine methods for PD input into a computer (the input information language of PD) and for PD representation in the computer memory (internal information language, PD storage language), and attempts at devising, on this basis, a computer-based information retrieval system.

The concept was to enter PD into the computer in a topological and an analytic notation, describing, respectively, the qualitative and the quantitative aspect of PD structure.

A computer used for information recording, storage, and processing offers, in principle, a mighty capability for highly sophisticated PD calculations and for PD modeling. This is to be done on the basis of experimental data and all information published earlier and accumulated in the system's data base. Since this means bringing together experimental results obtained at different times by different research schools all over the world, one can only conceive such PD modeling within the framework of a computer-based information retrieval system handling a retrospective file of PD data. Such IR systems must be, by their nature, factographic only. Moreover, with the processing of primary information, especially of that extracted from primary texts and graphic material being a very complicated matter, a system of that kind will probably be efficient only if operated as a part of a general integrated IRS. The data items that must be known about each PD are: (1) materials used for PD construction, (2) method used for the study of the sample, (3) constitution of the diagram and the pattern of points and lines, (4) characteristics of system phases, and (5) bibliographic data about the source from which the information has been taken. Data to be extracted from text for items 1, 2, 4, and 5 are not reflected in the geometrical image of PD. Yet, even though the textual information about PD is less important than graphic information, it is very essential for a correct and thorough interpretation of graphic data. This means that the general aspects of automatic text processing should not be overlooked by a designer of an IRS for PD, even though, with the high informativity of geometric description of PD, this is a less urgent issue than in an IRS mainly concerned with verbal information.

This is a difficult problem, but even more difficult is that of the pre-computer description of PD geometry (i.e., creation of the input information language); this must be a description enabling all semantic information about PD stored in a text to be represented by geometrical means. Alongside problems of PD computer system design, this task involves both mathematical problems, e.g., describing the geometrical elements, and pattern recognition problems, particularly during information retrieval and computer input of PD.

A further great difficulty is the absence of automatic printers for efficacious input of PD.

The underlying principles of IRS for PD described in [1,2,3] has been mainly retained and elaborated in [4,5], where a version of topological notation has been developed for PD of condensed simple (nonreciprocal) constant-pressure three- and four-component systems (in principle applicable also to systems of more than four components); it was intended for modeling PD of multicomponent systems from binary PD, two-dimensional sections of PD of multicomponent systems, and projections of the individual surfaces and hypersurfaces of PD.

The information retrieval system under development is to become a part of the integrated IRS for chemistry, itself a component of the ASSISTENT System being designed at VINITI. Along with graphic information, the system will be able to handle natural language text.

In [4], an index of boundary was introduced, which served as an element of the topological notation and denoted the set of names of phase regions adjoining at that boundary. For example, the index of the boundary of the eutectic or peritectic point of PD of two-component systems (figs. 1 and 2) appears as $\mathcal{K}/\mathcal{K}\alpha/\mathcal{K}\beta/\mathcal{K}\alpha\beta$, where "/" separates the sets of symbols denoting the phases of each of the phase regions adjoining at the point.

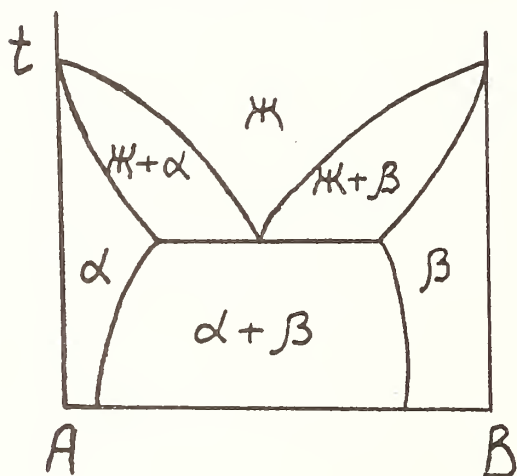


Figure 1

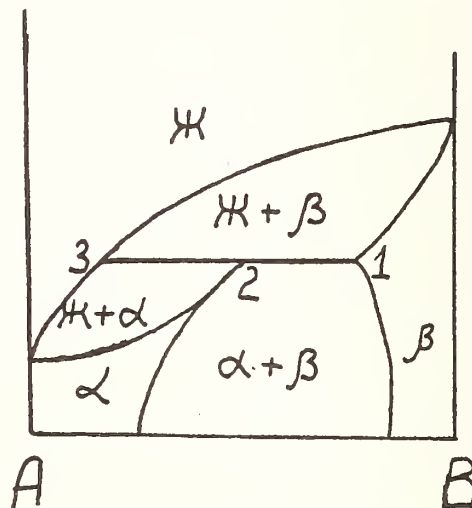


Figure 2

The boundary index gives an expression to one important rule of PD construction. It is the rule of phase grouping, formulated by L.S. Palatnik and A. I. Landau [6], which has several important corollaries. For convenient handling of boundary notations, the so-called index convolution has been introduced. Its left part (to be denoted x) fixes the symbols of the phases of the region which has the least number of phases; the right part (denoted y), does so with those of the region which has most phases. The right and left part of a convolution are separated by "//". The convolution of the above index appears as $\mathcal{K} // \mathcal{K}\alpha\beta$.

An index should in some fashion indicate all those phase equilibrium regions which, because of a low solubility of components, have merged in the PD with the axis, edge, or face of the coordinates network, degenerated to a point, a vertical straight segment, etc. (i.e., which have undergone a relative degeneration, to use the expression introduced in [6]).

Similarly, the topological notation should record all those phase regions which in the diagram have undergone the so-called absolute degeneration due to the presence of an intensive parameter (temperature). The absolute degeneration is expressed in the fact that a phase equilibrium region having $\bar{r} = \bar{n} + 1$ phases, where \bar{n} is the number of components, has one dimension less than the other regions do. In figures 1 and 2, only absolute degeneration has not been eliminated; in figure 3 the relative degeneration has not been eliminated either. Figure 4 shows an example of eutectic-type PD, with both absolute and relative degeneration having been eliminated. Proceeding from the general laws of PD construction, one can obtain a topological notation of a PD even lacking some of its constitutional data.

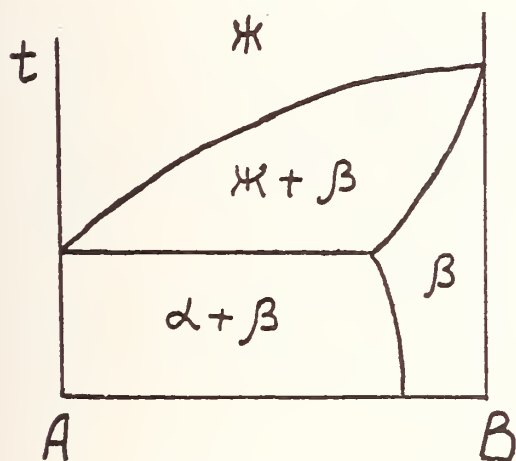


Figure 3

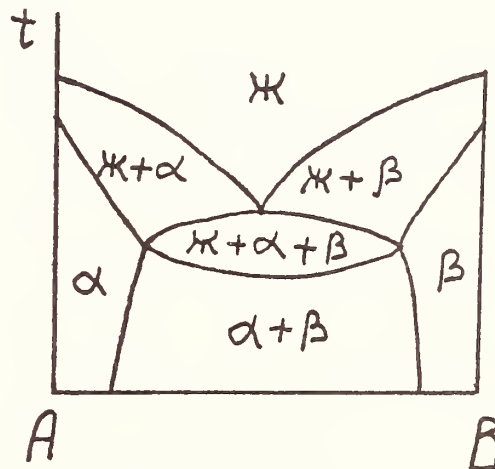


Figure 4

For example, figure 3 shows PD where the phase regions (α) and ($K + \alpha$) are absent and it is not known whether subsequent investigation will prove the PD to be eutectic (fig. 1) or peritectic (fig. 2). Nevertheless, it is possible in this case, like in many others, to get a full topological notation of PD. All subsequent refinements of the PD structure will only affect its analytical notation.

An analysis of the convolution of boundary indexes makes it possible to determine the dimensions of (1) the boundary R_b ($R_b = \bar{n} - \bar{y} + \bar{x}$), (2) the directrix of boundary R_{di} ($R_{di} = \bar{n} - \bar{y} + 1$), and (3) the generator simplex R_{ge} ($R_{ge} = \bar{x} - 1$). Since there is a one-one correspondence between boundaries and their index convolutions, it is possible to determine the index for any boundary, and, conversely, given the number of components of a PD, it is possible to determine the nature of each of its boundaries. Index

convolutions are liable to some operations (union, intersection, etc.) which allow the determination of: (1) all phase equilibrium regions adjoining through a boundary obtained by union or intersection of several boundaries, and (2) the dimensions and the type of the new boundary. For example, if boundaries A and B intersect along the boundary C, the index convolution of C is obtained thus: the left term of the C index convolution includes those and only those phases which are comprised at the same time in x_A and x_B , respectively, of the index convolutions of A and B, and the right term of the index convolution of C, (y_C) includes the sum of all phases contained in y_A and y_B of the index convolutions of the respective boundaries. If, for example, we consider the boundaries whose index convolutions are: $\mathcal{H}\alpha//\mathcal{H}\alpha\beta$ (A), and $\mathcal{H}\alpha\gamma//\mathcal{H}\alpha\gamma\delta\epsilon$ (B), these boundaries may intersect (i.e., give rise to a new boundary, C) whose index convolution will appear as $\mathcal{H}\alpha//\mathcal{H}\alpha\beta\gamma\delta\epsilon$. Introducing the sign \odot to denote intersection of boundaries we can represent the derivation of the index convolution of the new boundary as follows:

$$\mathcal{H}\alpha//\mathcal{H}\alpha\beta \odot \mathcal{H}\alpha\gamma//\mathcal{H}\alpha\gamma\delta\epsilon \rightarrow \mathcal{H}\alpha//\mathcal{H}\alpha\beta\gamma\delta\epsilon.$$

Since PD contains so-called critical elements (CE) (critical points, critical curves, etc.) and critical figures (CF)* (critical tie-lines, critical tie-triangles, etc.) to which the rule of phase grouping does not apply, a special rule [5] has been formulated enabling the approach described above to be applied for their notation, i.e., index convolutions to be applied for topological notation of CE and CF and the CF boundaries. An example of such a PD is given in figure 5, which shows a possible binary section of a ternary PD with the vanishing line of the binary eutectic.

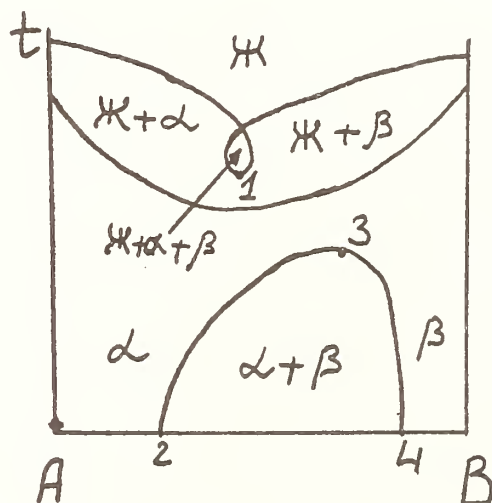


Figure 5

*Critical figure is a geometrical image of whose boundaries at least one is a critical element.

Table 1

		Curvilinear CF	Regular and flat CF and CF boundaries	
Index convolu- tion		$\mathcal{K}_1 = \mathcal{K}_2 \int \mathcal{K}_1 \mathcal{K}_2$		
Dimensions of PD	2	Critical point (extremal)		
	3	Critical curve		
	4	Critical surface		
Index convolu- tion		$\mathcal{K}_1 = \mathcal{K}_2 \int \mathcal{K}_1 \mathcal{K}_2 \alpha$	$(\mathcal{K}_1 = \mathcal{K}_2) \alpha \int \mathcal{K}_1 \mathcal{K}_2 \alpha$	
Dimensions of PD	2	-	-	-
	3	Terminal critical point (vertex of critical tie line)	Critical tie-line (extremal)	
	4	Terminal critical curve	Critical regular surface	
Index convolu- tion		$\mathcal{K}_1 = \mathcal{K}_2 \int \mathcal{K}_1 \mathcal{K}_2 \alpha \beta$	$(\mathcal{K}_1 = \mathcal{K}_2) \alpha \int \mathcal{K}_1 \mathcal{K}_2 \alpha \beta$	$(\mathcal{K}_1 = \mathcal{K}_2) \alpha \beta \int \mathcal{K}_1 \mathcal{K}_2 \alpha \beta$
Dimensions of PD	2	-	-	-
	3	-	-	-
	4	Angular critical point (vertex of critical tie-tri- angle)	Terminal criti- cal tie-line (side of criti- cal tie-triangle)	Critical tie- triangle (ex- tremal)

Table 2

		Curvilinear noncritical CF boundaries	Linear noncritical CF boundaries
Index convolution		$\alpha \parallel \mathcal{H}_1 \mathcal{H}_2 \alpha$	
Dimensions of PD	2	-	
	3	Noncritical terminal point	
	4	Noncritical curve (boundary of critical regular surface)	
Index convolution		$\alpha \parallel \mathcal{H}_1 \mathcal{H}_2 \alpha \beta$	$\alpha \beta \parallel \mathcal{H}_1 \mathcal{H}_2 \alpha \beta$
Dimensions of PD	2	-	-
	3	-	-
	4	Noncritical angular point (vertex of critical tie- triangle)	Terminal noncritical tie-line (side of critical tie-trian- gle)

Figure 6 shows a fragment of a hypothetical PD of a four-component system with miscibility gap in the quaternary system and in two ternary systems and without miscibility gap in binary systems. In the quaternary system, the miscibility gap region intersects with the surface of the binary eutectic along the closed curve 2- α '-8-b'-2. A fragment of this PD is presented in order to illustrate how the CF and its boundaries are recorded as index convolutions and complete indexes. Note also that 5- α -7, 5-b-7, and 4-6 are monovariant curves defining the equilibrium of two liquid (\mathcal{K}_1 and \mathcal{K}_2) and one solid (α) phases in one of the three-component systems, 3-4-5-2 is a critical regular surface of the four-component system, and 1-2-3 is a critical tie-triangle. For this PD, it is the temperature maximum of the four-phase region ($\mathcal{K}_1 + \mathcal{K}_2 + \alpha + \beta$). Point 2 is the critical angular point; points 1 and 3 are noncritical angular points.

For the geometrical elements 3-4-5-2, 3-2, 3-2-1, 2, and 3, the index convolutions are:

$$(\mathcal{K}_1 = \mathcal{K}_2)\alpha \mathcal{K}_1 \mathcal{K}_2 \alpha,$$

$$(\mathcal{K}_1 = \mathcal{K}_2)\alpha \mathcal{K}_1 \mathcal{K}_2 \alpha \beta,$$

$$(\mathcal{K}_1 = \mathcal{K}_2)\alpha \beta \mathcal{K}_1 \mathcal{K}_2 \alpha \beta,$$

$$\mathcal{K}_1 = \mathcal{K}_2 \mathcal{K}_1 \mathcal{K}_2 \alpha \beta,$$

and

$$\alpha \mathcal{K}_1 \mathcal{K}_2 \alpha \beta.$$

The complete indexes are, respectively:

$$(\mathcal{K}_1 = \mathcal{K}_2)\alpha / \mathcal{K}_1 \mathcal{K}_2 \alpha$$

(the index convolution coincides with the index),

$$(\mathcal{K}_1 = \mathcal{K}_2)\alpha / \mathcal{K}_1 \mathcal{K}_2 \alpha / (\mathcal{K}_1 = \mathcal{K}_2)\alpha \beta / \mathcal{K}_1 \mathcal{K}_2 \alpha \beta, (\mathcal{K}_1 = \mathcal{K}_2)\alpha \beta / \mathcal{K}_1 \mathcal{K}_2 \alpha \beta$$

(the index convolution coincides with the index),

$$\mathcal{K}_1 = \mathcal{K}_2 / \mathcal{K}_1 \mathcal{K}_2 / (\mathcal{K}_1 = \mathcal{K}_2)\alpha / (\mathcal{K}_1 = \mathcal{K}_2)\beta / \mathcal{K}_1 \mathcal{K}_2 \alpha / \mathcal{K}_1 \mathcal{K}_2 \beta / (\mathcal{K}_1 = \mathcal{K}_2)\alpha \beta / \mathcal{K}_1 \mathcal{K}_2 \alpha \beta,$$

$$\alpha / (\mathcal{K}_1 = \mathcal{K}_2)\alpha / \alpha \beta / (\mathcal{K}_1 = \mathcal{K}_2)\alpha \beta / \mathcal{K}_1 \mathcal{K}_2 \alpha \beta.$$

The specific feature of the PD fragment is the fact that it has such geometrical elements whose index convolutions would coincide if we do not introduce some additional symbolism (for example, this refers to the critical tie-lines in the three-component PD with a dome). Similar cases also occur in PD without a critical phase--a PD containing both

polymorphism and extremums and the like. On one side of the extremal (by temperature) critical figures (critical tie-triangle, critical regular surface) in figure 6, there lie phase regions separated by usual boundaries; the regions whose phases become identical on the other side of the critical figure merge pairwise, the respective boundaries disappear and in the notations of the phase regions comprised in the index, the sign "V" is introduced.

Let us enumerate the possible alternative positions of phase equilibrium regions relatively to the extremum critical figures.

1. All phase equilibrium regions are treated as ordinary in the following cases:
 - 1.1 At temperatures above CF, if CF is the minimum of the temperature (isothermal critical tie-figure) or temperatures (regular critical tie-figure with the parallelism plane perpendicular to the axis of temperatures).
 - 1.2 At temperatures below CF, if CF is the maximum of the temperature or temperatures.
2. Every two phase equilibrium regions each of which comprises the same phases and one differing phase, this differing phase becoming identical on the CE to which the CF directrix belongs, merge pairwise in the following cases:
 - 2.1 At temperatures below CF, if the latter is the minimum of the temperature or temperatures.
 - 2.2 At temperatures above CF, if CF is the maximum of the temperature or temperatures.

Index convolutions of CF boundaries can be obtained by the operation of intersection of CE, CF and their boundaries with the ordinary boundaries.

By introducing index convolutions of boundaries, it is possible to write down in the computer memory not only the complete PD, but also PD that have been built just partially.

Apart from points, curves, straight lines, curvilinear and regular surfaces, etc., CE and CF of PD are characterized by the presence of saddle points and extremums, which, in general, are not reflected in index convolutions. Therefore, in reconstructing the complete PD model, it is necessary somehow to include these features in the topological notation. The appearance of extremums and saddle points can be predicted proceeding from the qualitative and quantitative features of PD sections and from the thermodynamic rules. The quantitative description of PD is also affected by the factual insolubility of the components in one or several phases, the presence of polymorphous modifications of phases, etc.

When sections and projections of PD are constructed from the data of two or more experimentors, the experimental points are not normally reported, e.g., in some handbooks and similar publications. When, however, experimental points are not given even in publications by individual authors, i.e., when no thorough preliminary generalization of the results of various authors has been carried out and no estimates of the adequacy of the construction of the particular parts of the PD are given, the process of inputting the sections into the computer building a complete PD is greatly complicated and the reliability of information obtained from processing of input data is weakened.

In plotting PD of a multicomponent system from experimental data, one can resort to methods of descriptive geometry. The drawing of PD and the information about the multidimensional figure it represents express both the qualitative and the quantitative aspect of the PD structure. Applications of descriptive geometry in PD research are discussed by a number of Soviet scientists (V. N. Pervikova, M. G. Podylina, L. N. Lambin, A. G. Kraeva, Yu. A. Maleyev, F. S. Veselova, etc.).

V. N. Pervikova demonstrated (e.g., in [8]) that by attaching a coordinate system to a multidimensional figure to be represented by a drawing, one can dispense with defining the projection mechanisms and replace them with space transformations; a matrix interpretation of drawings makes it possible to pass over from the graphic plottings to the algebraic tools of the present-day geometry.

Some studies use the computer to solve certain special graphic problems in retaining the logic of the graphic method but replacing the geometric plotting with algebraic solutions typical of the analytical method (e.g., finding the common point of four hyperplanes of the four-dimensional space in [9]).

For qualitative description of PD of both binary systems and individual boundaries of the phase regions of the PD of multicomponent systems, the physico-chemical analysts nowadays make use of interpolation and approximation by polynomials of various orders. The polynomial method, however, has a limited application, as it only produces satisfactory results for piece-wise-smooth surfaces.

But, as mentioned, the structure of PD is largely determined by the special points.

In the system under development, the operations performed to reconstruct a complete PD from index convolutions, i.e., operations conducted on the elements of the topological notation, are inseparably linked with those conducted on those elements of the analytical notation which correspond to these index convolutions, e.g., on the equations describing the boundaries whose semantic is expressed by the topological notations.

From Soviet and other publications on the PD of metallic and non-metallic systems, certain rules based on thermodynamics have been selected. Those rules allow prediction of some features of PD structure and verification of the primary experimental data and their interpretations in the very process of PD plotting.

Descriptive-type rules have to be formalized before being entered into the computer. Formalization involves creating a system of concepts and terms and developing the appropriate predicate calculus on which to base a language for description of those rules.

The work on the system of concepts and terms has started by selecting the terms (some 350 altogether) to be in a certain manner correlated with the elements of the graphic image of PD. For the most part, these are names of the phase processes (such as "primary crystallization," "eutectic reaction") and the corresponding geometric elements (e.g., "regular surface"); terms serving to describe the network of coordinates (e.g., "concentration," "weight percentage"); and terms denoting physico-chemical properties ("solubility," "heterogeneity").

Various ways of description of concepts can be used. For example, Hillert's criterion, which determines the type of process (whether eutectic or peritectic), can be represented either mathematically or graphically. The determination of the quasi-binarity of a section can be interpreted as a pattern recognition problem. By feeding into the computer textual information alongside graphic information, it is possible to make corrections and refinements of the description of PD structure. Textual information will be of a particular value where there is no graphic image of PD but just a verbal description of its fragments. Textual information can also be used to add data to a PD which has been built and entered into the IRS earlier.

The IRS under development will make it possible to enter into the computer both graphic and textual information from published sources. Algorithms kept in the computer memory can, not only reconstruct the complete PD from its sections, but also cope with problems involving the plotting of isothermal and polythermal sections, calculation of the quantities of equilibrium phases depending on the mixture composition, etc.

As has been noted, the IRS for PD is to be incorporated in a larger system--the integrated IRS for chemistry, itself a part of the ASSISTENT System under development at VINITI. Along with the data bases of the IRS for PD, files of data will be prepared for other systems as well, including the subsystems for chemical compounds, properties, etc., all incorporated in the ASSISTENT. Data accumulated in these files will eventually allow predictions to be made about properties of chemical structures, the planning of experiments, and so on. It will be also possible to edit all sorts of printed information services on PD and to conduct SDI on permanent interest profiles as well as retrospective searches. All these capabilities will largely expand the scope of applications of ASSISTENT, and particularly of the IRS for PD.

Summary

1. The paper discusses a group of problems involved in the design of an automated information system for PD (in the framework of the integrated IRS for chemistry, a component of VINITI's ASSISTENT System).
2. PD will be constructed on the basis of formal descriptions of the boundaries of two-dimensional sections entered into the computer.
3. The complete record of a PD in the computer will consist of a topological part and an analytical part, expressing the qualitative and the quantitative aspects of PD structure, respectively.
4. The topological notation is based on the so-called boundary index and its convolution. Both index and index convolution serve to record ordinary boundaries as well as CE, CF, and CF boundaries.
5. Algorithms for computer modeling of PD make use of various substantial rules based on laws of thermodynamics. Along with graphic information about PD, some textual information will be used.
6. The IRS under development will allow the carrying out of a variety of operations in PD studies and computations and will provide information services to users in SDI and retrospective-search mode.

References

1. Stein, V. S., Solution of some information problems of the physico-chemical analysis using electronic computers. Thesis for the awardment of the degree of Candidate of Sciences (Technology), Moscow, 1965. (In Russian)
2. Stein, V. S., Design of an information retrieval system for physico-chemical analysis, in "Prikladnaya dokumentalistika," Moscow, Nauka Publishers, 1968. (In Russian).
3. Adler, Yu. P. and Stein, V. S., Composition-property diagrams representation of information for computers, Inform. Stor. and Retr. 4, 1969.
4. Tulupova, I. V. and Stein, V. S., Topology of equilibrium diagrams of multicomponent systems and formal methods of its description, in "Struktura faz, fazovye prevrascheniya i diagrammy sostoyaniya metallicheskih sistem," Moscow, Nauka Publishers, 1974. (In Russian).
5. Tulupova, I. V. and Stein, V. S., Topology of equilibrium diagrams of multicomponent systems with a critical phase and formal methods of its description, 2454-2474, VINITI, deposited on 9 September 1974. (In Russian).

6. Palatnik, L. S. and Landau, A. I., Phase equilibrium in multicomponent systems, Kharkov, Kharkov University Press, 1961. (In Russian)
7. Cayron, R., Étude théorique des diagrammes d'équilibre dans les systèmes quaternaires, 1, 2, Louvain, 1960.
8. Pervikova, V. N., Theoretical principles of the construction of drawings of multidimensional figures in a synthetic and vectorical presentation as applied to the study of multi-component systems. Thesis for the awardment of degree of Doctor of Sciences (Technology), Moscow, 1972. (In Russian)
9. Frolov, S. A., Automation of the process of graphic solution of problems. Thesis for the awardment of the degree of Doctor of Sciences (Technology), Moscow, 1964. (In Russian)

REGISTRATION LIST

Nazir Ahmad
University of Birmingham
Birmingham, England

Frank Ajersch
Ecole Polytechnique
C.P. 6079 Succ. "A"
Montreal, Quebec H2V-2W8

I. Aldinger
Max-Planck-Institut Für Metallforschung
Busnauerstr. 175
D-7000 Stuttgart, W. Germany

Ernest Ambler
Office of the Director
National Bureau of Standards
Washington, DC 20234

Paul R. Ammann
Kennecott Copper Corp.
Ledgemont Lab
128 Spring Street
Lexington, MA 02173

I. Ansara
Domaine Universitaire
B.P. 44-38401
St. Martin-d'Heres, France

George T. Armstrong
Physical Chemistry Division
National Bureau of Standards
Washington, DC 20234

N. Ault
Norton Co.
Worcester, MA 01606

Donald M. Bailey
Iowa State University
130 Metallurgy Bldg.
Ames, IA 50011

Hugh Baker
American Society for Metals
Metals Park, OH 44073

Chris Bale
Ecole Polytechnique
C.P. 6079
Montreal, Quebec H3C3A7

S. K. Banerji
Foote Mineral Company
Route 100
Exton, PA 19341

Ian R. Bartky
Institute for Materials Research
National Bureau of Standards
Washington, DC 20234

C. J. Bechtoldt
Metallurgy Division
National Bureau of Standards
Washington, DC 20234

Larry H. Bennett
Metallurgy Division
National Bureau of Standards
Washington, DC 20234

Milton Blander
Argonne Nat'l Lab
9700 S. Cass Ave.
Argonne, IL 60439

John H. Blanks
Pennsylvania State University
271 Mat. Res. Lab.
University Park, PA 16802

Edward L. Brady
Office of Information Programs
National Bureau of Standards
Washington, DC 20234

Robert F. Brebrick
Marquette University
1515 W. Wisconsin Ave.
Milwaukee, WI 53233

Leo Brewer
Lawrence Berkeley Laboratory
Univ. of California
Berkeley, CA 94720

Jesse J. Brown, Jr.
VPI & SU
302 Holden Hall
Blacksburg, VA 24061

Daniel Butrymowicz
Metallurgy Division
National Bureau of Standards
Washington, DC 20234

J. W. Cahn
Metallurgy Division
National Bureau of Standards
Washington, DC 20234

Thomas B. Cameron
University of Connecticut
U - 136
Storrs, CT 06268

Cynthia Carter
Metallurgy Division
National Bureau of Standards
Washington, DC 20234

Forrest L. Carter
Naval Research Laboratory
Code 6132
Washington, DC 20034

Y. Austin Chang
College of Engineering
University of Wisconsin-Milwaukee
Milwaukee, WI 53201

James R. Chelikowsky
Bell Labs
600 Mountain Ave.
Murry Hill, NJ 07974

U. V. Choudary
College of Engineering
University of Wisconsin-Milwaukee
Milwaukee, WI 53201

G. W. Cleek
Consultant
5512 N. 24th St.
Arlington, VA 22205

W. Dale Compton
Ford Motor Company
20000 Rotunda Drive
Dearborn, MI 48124

Bruce R. Conard
INCO, Ltd.
Sheridan Park
Mississauga, Ontario, Canada

Lawrence P. Cook
Inorganic Materials Division
National Bureau of Standards
Room B214, Materials Building
Washington, DC 20234

S. R. Coriell
Metallurgy Division
National Bureau of Standards
Washington, DC 20234

Joseph Cox
Watervliet Arsenal
Watervliet, NY 12189

John R. Cuthill
Metallurgy Division
National Bureau of Standards
Washington, DC 20234

Amit DasGupta
Oak Ridge National Lab
Oak Ridge, TN 37830

Didier de Fontaine
University of California
6532 Boelter Hall
Los Angeles, CA 90024

Peter R. Debruyne
Industrial Liaison
National Bureau of Standards
Washington, DC 20234

Joseph E. Davison
Univ. of Dayton
300 College Park
Dayton, OH 45469

R. C. Devries
General Electric
General Electric R & D Center K-1
Schenectady, NY 12345

R. L. Dreshfield
Materials Processing and Joining Section
NASA Lewis Research Center
Cleveland, OH 44135

J. Elliott
Department of Metallurgy & Metals
MIT
Cambridge, MA 02139

S. G. Epstein
Aluminum Association
New York, NY 10017

Maria-Luise Fiedler
North Carolina State University
Raleigh, NC 27607

H. Alan Fine
University of Arizona
Dept. of Met. Eng.
Tucson, AZ 85721

Gerhard R. Fischer
Corning Glass Works
SP, FR 1
Corning, NY 14830

Julius Fister
Metals Research Laboratories
Olin Corp.
91 Shelton Ave.
New Haven, CT 06504

Sherman P. Fivozinsky
Office of Standard Reference Data
National Bureau of Standards
Washington, DC 20234

René Flukiger
Dept. Phys. Mat. Cond.
32, Bd. d'Yvoy
Geneva, Switzerland

Paul Fopiano
Watertown Arsenal
Arsenal Street
Watertown, MA 02172

Patrick K. Gallagher
Bell Laboratories
Rm. 6D - 311
Murray Hill, NJ 07974

B. C. Giessen
Department of Chemistry &
Mechanical Engineering
Northwestern University
Boston, MA 02115

F. P. Glasser
University of Aberdeen
Old Aberdeen
Scotland, UK AB9 ZUE

Joseph I. Goldstein
Lehigh University
Bethlehem, PA 18015

J. Ronald Gonterman
Owens/Corning Fiberglas
Technical Center
Granville, OH 43023

Chuck Greskovich
General Electric Co.
K-1, 3C12, P.O. Box 8
Schenectady, NY 12301

K. A. Gschneidner, Jr.
Rare Earth Information Center
Iowa State University
Ames, IA 50010

John L. Haas, Jr.
U.S. Geological Survey
National Center, Stop 959
Reston, VA 22092

David Hansen
Ballistics Research Laboratory
Aberdeen, MD 21005

Ernst-Theo Henig
Max-Planck-Institut für Werkstoffwissensch
Buesnauerstr. 175
D-7000 Stuttgart-80, Germany

Keith A. Hill
Carpenter Technology Corporation
P.O. Box 662
Reading, PA 19603

J. Hilsenrath
National Bureau of Standards
Washington, DC 20234

Michael Hoch
University of Cincinnati
Location 12
Cincinnati, OH 45221

John D. Holder
Oak Ridge National Laboratory
Box X, 4500S S280
Oak Ridge, TN 37830

Emanuel Horowitz
Institute for Materials Research
National Bureau of Standards
Washington, DC 20234

R. A. Howald
Chemistry Dept.
Montana State University
Bozeman, MT 59715

Chen-Chao Hsu
Argonne National Laboratory
9700 S. Cass Ave.
Argonne, IL 60439

David Dew-Hughes
Brookhaven National Laboratory
Building 480
Upton, NY 11973

F. A. Hummel
Pennsylvania State University
Room 214 M.I. Bldg.
University Park, PA 16802

M. R. Jackson
General Electric Co.
CRD, K-1 223 Met
Schenectady, NY 12309

R. I. Jaffee
Electric Power Research Institute
Palo Alto, CA 94303

Ronald B. Johnson
Institute for Materials Research
National Bureau of Standards
Washington, DC 20234

Daniel J. Kahan
Metallurgy Division
National Bureau of Standards
Washington, DC 20234

Larry Kaufman
Manlabs Inc.
21 Erie St.
Cambridge, MA 02146

B. H. Kear
Pratt and Whitney
Materials Engineering &
Research Lab
E. Hartford, CT

S. E. Khalafalla
Dept. of the Interior
P.O. Box 1660
Twin Cities, MN 55111

R. Kikuchi
Hughes Research Laboratories
3011 Malibu Canyon Road
Malibu, CA 90265

R. Kirsch
Applied Mathematics Division
National Bureau of Standards
Washington, DC 20234

O. J. Kleppa
The James Franck Institute
University of Chicago
Chicago, IL 60637

Michael J. Koczak
Drexel University
Dept. of Materials Engineering
Philadelphia, PA 19104

Tamara Kolesnikova
Academy of Sciences of the USSR
Baltiyskaya ul., 14
Moscow, USSR

Ram Kossowsky
Westinghouse Research Laboratories
1310 Beulah Road
Pittsburgh, PA 15235

John Krc, Jr.
Parke, Davis & Company
Joseph Campau at the River
Detroit, MI 48232

Eric R. Kreidler
General Electric Co.
Nela Park
Cleveland, OH 44143

A. K. Kuriakose
Norton Research Corp. (Canada) Ltd.
8001 Daly St.
Niagara Falls, Ont., Canada

R. Laudise
Materials Research
Bell Telephone Labs
Murray Hill, NJ 07974

Y. E. Lee
Union Carbide Corp. Metals Div.
4625 Royal Ave.
Niagara Falls, NY 14302

David R. Lide, Jr.
Office of Standard Reference Data
National Bureau of Standards
Washington, DC 20234

James D. Livingston
General Electric Co.
Corp. Res. & Dev.
Schenectady, NY 12308

C. H. P. Lupis
Institute Für Eisenhüttenkunde
Aachen, Germany

Lottie T. McClendon
Institute for Materials Research
National Bureau of Standards
Washington, DC 20234

Scott McCormick
Illinois Institute of Technology
Dept. of Metallurgical and Matls, Eng.
Chicago, IL 60616

H. McKinstry
Materials Research Lab
Pennsylvania State University
University Park, PA 16802

R. McNally
Ceramic Research
Corning Glass Works
Corning, NY 14830

Michael McNeil
National Bureau of Standards
Room A129, Technology Building
Washington, DC 20234

H. F. McMurdie
Inorganic Materials Division
National Bureau of Standards
Washington, DC 20234

Richard Magin
Nat'l Institutes of Health
9000 Rockville Pike
Bethesda, MD 20795

A. I. Malausky
Tyco Laboratories
Waltham, PA

John R. Manning
Metallurgy Division
National Bureau of Standards
Washington, DC 20234

Vincent C. Marcotte
IBM
D/45K B/300 -95
Hopewell Jen, NY 12533

Dennis Marshall
Globe-Union, Inc.
5757 N. Greenbay Ave.
Milwaukee, WI 53201

Robert F. Martin
Institute for Materials Research
National Bureau of Standards
Washington, DC 20234

Thadeus B. Massalski
Carnegie-Mellon University
Schenley Park
Pittsburgh, PA 15213

Leo Merrill
High Pressure Data Center
5093 HBLL, Brigham Young University
Provo, UT 84602

Peter J. Meschter
Univ. of Tennessee
Dept. Chem. & Met. Eng.
Knoxville, TN 37919

Alan D. Mighell
Inorganic Materials Division
National Bureau of Standards
Washington, DC 20234

D. B. Minor
Inorganic Materials Division
National Bureau of Standards
Washington, DC 20234

A. P. Miodownik
University of Surrey
Guildford, UK GU2 5XH

W. G. Moffatt
General Electric Co.
1 River Road P.O. Box 8
Schenectady, NY 12301

B. J. Molino
Office of Standard Reference Data
National Bureau of Standards
Washington, DC 20234

L. F. Mondolfo
Syracuse University
Syracuse, NY 13210

John E. Morral
University of Connecticut
U-136
Storrs, CT 06268

Arnulf Muan
Penn State Univ.
118 M. S. Bldg.
University Park, PA 16802

A. Navrotsky
Chemistry Division
National Science Foundation
Washington, DC 20555

Taki Negas
Inorganic Materials Division
National Bureau of Standards
Washington, DC 20234

T. Nishizawa
Dept. of Metallurgy, Materials
Science & Metal Processing
Tohoku University
Japan

E. F. Osborn
Carnegie Institution of Washington
2801 Upton St., NW
Washington, DC 20008

Robert L. Parker
Metallurgy Division
National Bureau of Standards
Washington, DC 20234

P. Parish
U.S. Army Research Office
Box 12211
Research Triangle Park, NC 27709

Elio Passaglia
Institute for Materials Research
National Bureau of Standards
Washington, DC 20234

David D. Pearson
United Technologies Research Center
Silver Lane
East Hartford, CT 06108

W. B. Pearson
Faculty of Science
University of Waterloo
Waterloo, Canada

Arthur Pelton
Ecole Polytechnique
C.P. 6079
Montreal, Quebec H3C3A7

Guenter Petzow
Met-Planck-Inst. Metallforschung
Buesnauerstr 175
7000 Stuttgart 80, W. Germany

Sri Prakash
Union Carbide Corporation
P.O. Box 5928
Greenville, SC 29606

Svante Prochazka
GE CR & D
P.O. Box 8
Schenectady, NY 11301

Alan Prince
Hirst Research Centre
East Lane, Wembley
Middlesex HA9 7PP, England

Schrade F. Radtke
International Lead-Zinc Research Org.
292 Madison Ave.
New York, NY 10017

Dennis Readey
Division of Physical Research
ERDA
Washington, DC 20545

Curt W. Reimann
Institute for Materials Research
National Bureau of Standards
Washington, DC 20234

R. C. Reno
Dept. of Physics
University of Maryland
Baltimore, MD 21228

Robert J. Reynik
National Science Foundation
1800 G St., NW
Washington, DC 20550

Frederick N. Rhines
University of Florida
Dept. of Mat-Sci. & Eng.
Gainesville, FL 32611

A. D. Romig
Lehigh University
Whitaker Lab. # 5
Bethlehem, PA 18015

Barry H. Rosof
Technology Division, Cabot Corp.
1020 Park Avenue
Kokomo, IN 46901

W. Rostoker
University of Illinois
Chicago Circle, P.O. Box 4348
Chicago, IL 60680

Robert S. Roth
Inorganic Materials Division
Room B214, Materials Building
Washington, DC 20234

William Ruff
Metallurgy Division
National Bureau of Standards
Washington, DC 20234

M. L. Saboungi
Argonne National Lab
Chemical Engineering Div.
Argonne, IL 60439

Saed Safai
Materials Sci. Dept.
SUNY at Stony Brook
Stony Brook, L. I., NY 11794

E. Salkovitz
Office of Naval Research
Arlington, VA 22217

Gary Sandrock
International Nickel Co.
Sterling Forest
Suffern, NY 10901

L. M. Schetky
International Copper Research Assoc.
825 Third Ave.
New York, NY 10022

Coulson M. Scheuermann
NASA Lewis Research Center
21000 Brookpark Road
Cleveland, OH 44135

Fred C. Schwerer
U. S. Steel Research, MS #98
Monroeville, PA 15146

J. E. Selle
Metals and Ceramics Div.
Oak Ridge National Lab
Oak Ridge, TN 37830

M. Semchyshen
Research Laboratory
Climax Molybdenum Corp.
1600 Huron Pkwy.
Ann Arbor, MI 48105

Charles E. Semler
Ohio State Univ.
Refractories Research Center
2041 College Rd.
Columbus, OH 43210

Gertrude B. Sherwood
Office of Standard Reference Data
National Bureau of Standards
Washington, DC 20234

John Shyne
NSF
1800 G St., NW
Washington, DC 20550

W. C. Simmons
AFOSR
Bldg. 410
Bolling AFB, DC 20332

Satish P. Singhal
State University of New York
Materials Science Dept.
Stony Brook, NY 11794

P. Slick
Bell Telephone Laboratories
Murray Hill, NJ 07974

J. F. Smith
Iowa State University
Ames, IA 50010

J. E. Smugeresky
Sandia Labs
Div. 8312
Livermore, CA 94550

Shigeyuki Sômiya
Tokyo Institute of Technology
Ookayama, Meguro, Tokyo, 152
Tokoyo, Japan

Charles A. Sorrell
Dept. of Ceramic Engineering
Univ. of Missouri
Rolla, MI 65401

Karl E. Spear
Pennsylvania State University
Materials Research Laboratory
University Park, PA 16802

G. R. Speich
U. S. Steel, Research Labs
Monroeville, PA 15146

G. Springer
Falconbridge Nickel Mines Ltd.
8810 Yonge Street, P.O. Box 900
Thornhill, Ontario

Judith K. Stalick
Inorganic Materials Division
National Bureau of Standards
Washington, DC 20234

Kurt H. Stern
Naval Research Laboratory
Code 6130
Washington, DC 20375

C. P. Stroble
Allegheny Ludlum Steel Corp.
Research Center
Brackenridge, PA 15065

Lydon J. Swartzendruber
Metallurgy Division
National Bureau of Standards
Washington, DC 20234

J. Swisher
Energy Research & Development Admin.
Washington, DC 20545

R. E. Thoma
Union Carbide Corporation
P.O. Box X
Oak Ridge, TN 37830

Marshall K. Thomas, Jr.
Naval Air Devel. Center (30231)
Warminster, PA 18974

William Thompson
McGill University
Montreal, Quebec

C. Thurmond
Bell Telephone Labs
Murray Hill, NJ 07974

H. van Olphen
Numerical Data Advisory Board
National Research Council
2101 Constitution Avenue
Washington, DC 20418

E. C. van Reuth
DARPA
1400 Wilson Blvd.
Arlington, VA 22209

Chester J. Van Tyne
Lehigh University
Whitaker Laboratory #5
Bethlehem, PA 18015

Francis L. Ver Snyder
Pratt & Whitney Aircraft Group
400 Main Street
East Hartford, CT 06108

Walter E. Wahnsiedler
Alcoa Laboratories
Alcoa Technical Center
Alcoa Center, PA 15069

J. Waldman
Frankford Arsenal
Bridge & Tacony Streets
Philadelphia, PA 19137

Chang-F. Wan
Pennsylvania State University
271 Materials Res. Lab
University Park, PA 16802

Frederick E. Wang
NSWC
Silver Spring, MD 20910

Richard M. Waterstrat
Polymers Division
National Bureau of Standards
Washington, DC 20234

R. E. Watson
Brookhaven National Laboratory
Upton, NY 11973

Alan Webb
Naval Research Laboratory
Code 6434
Washington, DC 20375

George Wei
ORNL
P. O. Box X
Oak Ridge, TN 37830

J. H. Westbrook
General Electric Co. Bldg. 5-327
1 River Road
Schenectady, NY 12345

Howard J. White, Jr.
National Bureau of Standards
Office of Standard Reference Data
Washington, DC 20234

William B. White
The Pennsylvania State University
Materials Research Laboratory
University Park, PA 16802

Calvin S. Williams
Union Carbide Corporation
P.O. Box 5928
Greenville, SC 29606

Ray Woodruff
Roberts Hall
Montana State University
Bozeman, MT 59715

L. Richard Woodyatt
Bethlehem Steel Corp.
Homer Research Labs
Bethlehem, PA 18015

Han-Il Yoo
Inorganic Materials Division
Room B214, Materials Bldg.
Washington, DC 20234

William Vincent Youdelis
Dept. Engineering Materials
University of Windsor
Windsor, Ontario N9B 3P4

Author Index

- Ageev, N. V., 90
 Ageeva, D. L., 90
 Aldinger, F., 164
 Ammann, P., 1334
 Ansara, I., 121
- Badie, T. M., 550
 Bailey, D. M., 1027
 Balakrishna, S. S., 1200
 Bale, C. W., 1077
 Beam, J. E., 1428
 Bennett, L. H., 261, 450, 592
 Bilimoria, Y., 1047
 Blander, M., 1093
 Boreni, R., 259
 Boyle, M. L., 726
 Brebrick, R. F., 1220
 Brown, J. J., Jr., 272
- Cameron, T. B., 566
 Carter, F. L., 763
 Carter, G. C., 36, 261, 450
 Cassidy, R. T., 272
 Chang, L. L. Y., 165
 Chang, Y. A., 229, 774
 Chart, T. G., 1186
 Choudary, U. V., 229, 774
 Cleek, G. W., 1, 257
 Cook, L. P., 1, 257, 440
 Craig, D. F., 272
- Davison, J. E., 1428
 de Fontaine, D., 967, 999
 Dew-Hughes, D., 1411
 Doman, R. C., 1378
 Dreshfield, R. L., 624
- Ehrenreich, H., 592
 Eliezer, I., 803, 846, 1440
 Elliott, J. F., 1332, 1453
 Evans, B. L., 226
- Fine, H. A., 355
 Fisher, J. R., 909
 Fivozinsky, S. P., 1325
 Flukiger, R., 375
 Fopiano, P. J., 567
- Gaye, H., 907
 Giessen, B. C., 1161
 Gittus, J. H., 1065
 Glasser, F. P., 407
 Goldstein, J. I., 462
 Gribulya, V. B., 1139, 1151
 Gschneidner, K. A., Jr., 226
- Haas, J. L., Jr., 909
 Hasebe, M., 911
 Henig, E.-Th., 164, 955
 Hirano, S., 508
 Howald, R. A., 803, 846, 1440, 1470
 Hsu, C. C., 1109
- Jackson, M. R., 423
 Jaffee, R. I., 1420
 Johnson, J. R., 483
 Jorda, J.-L., 375
- Kagan, E. K., 346, 351
 Kahan, D. J., 261
 Kaufman, L., 1065
 Khanna, K. M., 575
 Kikuchi, R., 967, 999
 Kiseleva, N. N., 1139, 1151
 Kolesnikova, T. P., 90
 Kreidler, E. R., 1307
 Kubaschewski, O., 1027
- Larson, H., 1354
 Livingston, J. D., 703
 Lukas, H. L., 164, 955
 Lupis, C. H. P., 907
- Mallik, A. K., 1200
 McCormick, S., 1047
 McNally, R., 1378
 Merrill, L., 100
 Mighell, A., 259
 Minor, D. B., 440
 Miodownik, P. A., 1065, 1479
 Mlavsky, A. I., 1426
 Mondolfo, L., 1382
 Morral, J. E., 566
 Myers, S. M., 516

Nakamura, K., 508
Negas, T., 1, 257
Neumann, J. P., 229
Nishizawa, T., 911

Ondik, H. 259

Pehlke, R. D., 1360
Pelton, A. D., 1077
Petrova, L. A., 90
Petzow, G., 164, 955
Prince, A., 660
Prochazka, S., 1409

Rairden, J. R., 423
Reilly, J. J., 483
Reno, R. C., 450
Rhines, F. N., 142
Romig, A. D., Jr., 462
Rosof, B. H., 1090
Roth, R. S., 1, 257

Saboungi, M.-L., 1093, 1109
Saito, S., 508
Sandrock, G. D., 483
Savitskii, E. M., 1139, 1151
Scheuermann, C. M., 1237
Selle, J. E., 1471
Sherwood, G. B., 1325
Sinha, V. K., 578
Slick, P., 1427
Smith, J. F., 1027
Smugeresky, J. E., 516

Sōmiya, S., 508
Spear, K. E., 744
Stalick, J., 259
Stein, V.S., 1506
Swartzendruber, L. J., 450

Tarby, S. K., 726
Thompson, W. T., 1077
Thurmond, C. D., 23
Tulupova, I. V., 1506

Van Tyne, C. J., 726
Verkade, M. E., 226
VerSnyder, F. L., 1418
Vol, A. E., 346, 351

Wachtman, J. W., 1
Wang, F. E., 545
Watkin, J. S., 1065
Watson, R. E., 592
White, H. J., Jr., 709
White, W. B., 251

Zimmermann, B., 955

SUBJECT INDEX

Each paper has been indexed under one or more of these entries for ease of retrieval. This index is cursory rather than exhaustive. Those papers giving numerical phase diagram data or phase diagrams on specific systems are listed in the Materials Index.

- Acceptor solubilities 26-27
- Activity coefficients 726-727, 774, 777-786, 803-845, 1047-1048, 1052-1055
- Additive systems (salts) 1093, 1098-1108
- Ageev, translated cumulative index 1237-1306
- Aircraft industry 262, 1396, 1418-1419
- Allen and Cahn 1012, 1017
- Alloy physics 84-89, 592-623
 - (Also see under specific terms)
- Alloys (see under Metallic systems)
- Amorphous materials 261-268, 1161-1185
- Analytical representations 672-675
- Angular correlation 450-461
- Applications (see under Needs and Applications, under main headings of Ceramics systems, Semiconductor systems, High pressure diagrams, or specific terms)
- Atomic deposition methods 151, 516-544
 - summary 1172
- Autoradiography 566

- Bale-Pelton polynomials and coefficients 846-847, 874-875, 902-903, 1445
- Band theory 619
- Batteries 262, 1109-1138
- Bonding, chemical (see also Crystal chemistry) 612-614, 763-773
 - , transient liquid phase (TLP) 1418-1419
- Bonnier and Caboz 956
- Bragg-Williams 978, 1000, 1008
- Brouwer diagrams 27

- Calculations of phase diagrams (see under Theories of phase diagrams, specific topics, and see Tuesday's poster session on this subject, pp 726-1236)
- Calphad 37, 49, 1188
- Calorimetry (including differential scanning calorimetry, DSC) 1171, 1173
- Capsule bursting method 508-515
- Ceramic systems (see also under specific systems, Materials Index)
 - compilation activities, review 2-5, 12-22, 121-122, 165, 252-256, 257-258, 1327-1331, 1460-1471
 - compilations, review 1-2, 14-22, 256, 407, 1326, 1374
 - needs and applications (see also under Panels II, III, and IV on User Needs, pp 1332-1452) 9-22, 121, 703-708, 1352, 1356-1357, 1361-1366, 1371, 1375-1377, 1378-1381, 1409-1410, 1427, 1442-1450, 1451-1452, 1455-1457, 1471, 1475
 - questionnaire review 5-22

Charge distribution, transfer 607, 615-619, 766
 Chatillon-Colinet 141
 Chemical analysis 143, 552, 1379
 Chemical scan (isothermal) 151
 Cluster variation (theory) 967-998, 999-1026, 1474
 Coatings of materials 262, 423-439
 Coherent phase diagrams 999-1026
 Cohesion, cohesion energy 594-603, 616
 Compilations (see under Ceramic systems, Semiconductor systems,
 Metallic systems, High pressure diagrams)
 Compilation methods 22, 163, 658, 720-725, 1475-1478
 Composites 1378-1381
 Compounds (see also the Materials Index) 100-200, 763-773, 1378-1381
 Compound prediction 763-773, 1112, 1139-1150, 1151-1160, 1220-1236, 1473
 Computerized data banks (see under Crystallography and under
 Thermodynamics)
 Concentration simplex 660-662
 Concorde, alloys in use 1396
 Coordination numbers, 1479-1491
 - generalized 767
 Crystal chemistry 84-89, 101, 545-547, 620-621, 745-746, 763-772, 1139-1150,
 1479-1491
 Crystallography
 - compilations 82-83, 259-260, 720-725, 1326
 - computerized data bank 259-260
 - theory and prediction of phases 100-109, 659, 763-773, 1139-1150, 1151-1160

 Data banks, computerized
 - crystallography 259-260
 - thermodynamics and thermochemistry 37, 40, 41, 43, 45, 49,
 121-124, 1077-1089, 1186-1199
 Data compilations (see under Ceramic systems, Semiconductor systems,
 Metallic systems, High pressure diagrams, under the subtopic "compilations")
 Density of states (esp Ti) 595
 Differential thermal analysis, DTA (see under Thermal analysis)
 Diffusion couple analysis 142, 149-151, 465, 522-524, 913
 Dilatometry 142, 151, 517
 Dip sampling 143
 Distribution and publication of phase diagrams 262-264, 703-708,
 709-719, 720-725, 1325-1326
 Donor solubilities 26-27

 Electrical conductivity (experimental phase change det.) 143, 517
 Electrochemical probe 148
 Electron densities 611
 Electron diffraction 148
 Electron distribution 607, 615-619, 766
 Electron energies 594-609

Electron microprobe 148, 156, 462-471

- microscope, reflecting, transmission, scanning (SEM, STEM) 146, 148, 440-449, 462, 471-474

Electronegativity 610-613, 766

Electronic density of states (esp Ti) 595

Electronic materials (see under narrower term, Semiconductor systems, or specific topics)

Ellingham diagrams (see also Metal-gas phase diagrams Solid-vapor diagrams and Pourbaix diagrams) 1077-1088, 1428

Emf measurements in galvanic cells 517

Energy storage/conversion 262, 1109-1138, 1426, 1428-1439, 1440-1450, 1458

Experimental techniques of phase diagram determination (see under specific techniques)

F*A*C*T (Facility for the Analysis of Chemical Thermodynamics) 1077-1089

Field ion microscope 146

Format of phase diagrams

- representation 16-18, 262-264, 265-271, 578-591, 658, 660-702, 1093-1108, 1315-1324, 1458-1460, 1506-1519
- distribution and publication 262-264, 703-708, 709-719, 720-725, 1325-1326
- publication standards 1307-1324

Geometric description of superalloys 628-658

Gibbs energy function, generation of 1027-1046

Glasses (see also specific glasses in the Materials Index)

- ceramic 1378-1381
- metallic 261-268, 1161-1185
- needs 1378-1381

Graphical methods 45, 265-271, 628-658, 1077-1089, 1506-1519

Hardy-type power series 141

High pressure phase diagrams

- compilation activities, review 100-120
- compilations, review 101-108
- needs and applications 261-268, 703-708
- P-T, P-T-X diagrams 121-122, 153, 578-591

Hillert 956

History of data compilations 2, 36, 90, 100

Hot stage microscopy 1310

Hot wire microscopy 355-374

Hume-Rothery 662

Hyperfine techniques (see also under nuclear magnetic resonance, Mossbauer effect, perturbed angular correlation) 450-461

Industrial needs and applications

- ceramics 1378-1381, 1409-1410, 1427, 1440-1450, 1455
- composites 1378-1381
- glasses 1378-1381
- intermetallics 1378-1381
- ionic systems (see salt systems)
- iron and steelmaking 567-574, 1360-1377, 1378-1381, 1421-1423
- non-ferrous 567-574, 1334-1353, 1354-1359, 1378-1381, 1382-1408, 1418-1419, 1423-1425, 1427
- salt systems 1426, 1428-1439
- superconductors 1411-1417

Interaction parameters 1210-1214

Intermetallics (see also under Compounds, or see under specific systems in the Materials Index)

- needs 1378-1381

Internal pressure 1210-1214

International Atomic Energy Agency (IAEA) 38, 45, 60-61, 78-79

Ion backscattering methods 151, 516-544

- implantation methods 151, 516-544

Ionic systems (see also Salt systems, and also specific systems

in the Materials Index) 115-120, 165-225, 251-256, 272-345, 1093-1108

Iron and steelmaking (needs) 1360-1377, 1378-1381, 1421-1423

Irradiation effects 1065-1076

Kaburagi and Kanamori 1012, 1017

Kohler 141, 956

Least squares method of optimizing phase diagrams 955-966

Lever rule, enhanced 454

Magnetic effects 594-603

Margules 848, 872, 874, 876, 903

Matte 1356-1357, 1456

Metal-gas phase diagrams (see also Solid-vapor, Pourbaix-,

Ellingham diagrams, etc) 1047-1064, 1077-1088, 1090-1092, 1332-1333

Metallic-nonmetallic component diagrams 1047-1064, 1077-1088, 1090-1092

Metallic radii 763

Metallic systems (see also under specific systems, Materials Index)

- compilation activities, review 37-38, 40-48, 49, 92-94, 122, 164, 226-228, 229-250, 751, 1186-1199, 1327-1331, 1460-1471
- compilations, review 36-38, 50-74, 90-94, 122, 227, 234, 346-350, 351-354, 744-762, 1237-1306, 1326, 1374, 1406
- needs and applications (see also under Panels II, III, and IV on user needs, pp 1332-1452) 121, 261-262, 567, 703-708, 725, 1109, 1180-1182, 1352, 1355-1357, 1361-1366, 1371, 1375-1377, 1378-1381, 1382-1408, 1411-1417, 1427, 1447-1448, 1451-1452, 1455-1457, 1471, 1475
- questionnaire review 261-266

Metallographic analysis 142-143, 156, 517

Metastable phases 261-266, 1161-1185, 1421, 1457
 Mossbauer effect 152, 450-461, 615
 Microanalysis 913, 1379
 Microchemical analysis 148, 440
 Micro-furnace 357
 Micro-indent hardness 148
 Micro x-ray diffraction 148
 Microscopy (see under specific type, e.g. optical, electron, etc.)

 Natural iteration (theory) 967, 974-978
 Needs and Applications (see under Ceramics systems, Semiconductor system, Metallic systems, High pressure, etc., and see under Industrial needs).
 Newton-Raphson iteration method 967, 976-977, 1017
 Non-ferrous phase diagram industrial needs 1334-1353, 1354-1359, 1378-1381, 1382-1408, 1418-1419, 1423-1425, 1427
 Non-stoichiometry prediction 770
 Nuclear Magnetic Resonance (NMR) 121, 152, 450-461

 Olson 730-731
 Optical microscopy (color, reflectivity, other) 148, 411-413
 Order-disorder 984-998, 999-1026

 P-T, P-T-X, diagrams 28, 121-122, 153, 253, 578-591, 1421, 1456
 Pair approximation (theory) 968-973, 1009-1010, 1017
 Pair potentials 610, 616, 1424
 Pauling 620, 763-773, 1479-1491
 Perturbed angular correlation (PAC) 450-461
 Phacomp 37, 624-627, 1423
 Phase rule 143-144, 162
 Physical chemistry and metallurgy, general 84-89
 Potential-composition diagrams 1077-1088
 Potential-potential diagrams 1077-1088
 Potentials (see also under specific potentials) 603-609, 1011-1015
 Polar diagrams 662-663, 684
 Pourbaix diagrams (see also Metal-gas diagrams, Solid-vapor diagrams, Ellingham diagrams, Stability diagrams, etc.) 1090-1092, 1428
 Predictive methods (see under Theories of phase diagrams, Thermodynamics theories, or under specific topics)
 Predominance area phase diagrams 1077-1088
 Pressure scan 152
 Projection methods
 - parallel 664-668
 - perspective 663-664
 Pseudopotentials 603-609, 1014
 Publication and distribution 262-264, 703-708, 709-719, 720-725, 1325-1326
 Publication standards 1307-1324

Quenching (see also spat-cooling) 1310
 - argon jet 383
 - rapid quenching methods, summary 1172
 Quenched phase plots 1166
 Questionnaire, reviews
 - ceramic system 5-22
 - metallic systems 261-268

 Radioactive techniques 148
 Raoultian activity coefficient 726-727
 Reciprocal systems, representations of 671
 - salt systems 1093-1108
 Redlich-Kister 803-845, 846-906, 1445
 Representations of phase diagrams 16-18, 262-264, 265-271,
 578-591, 660-702, 1093-1108, 1315-1324, 1507-1520
 Russian literature 44, 46, 50, 51, 92-99, 346-350, 351-354, 1237-1306

 Salt systems (see also Ionic systems and see specific systems
 in the Materials Index) 1093-1108
 - needs 1426, 1428-1439
 Scratch hardness 148
 Second order phase transitions 620
 Sectioning methods for phase diagram representations 668-671
 Selective chemical solution 148
 Semiconductor systems
 - compilations, review 23, 346-350, 351-354
 - needs and applications (see also under Panels II, III, and
 IV on User Needs, pp 1332-1452) 27-28, 121, 703-708, 1426, 1471, 1475
 Semiconductor compounds, predictive methods 1220-1236
 Sigma phase 625-658, 916, 1065
 Slags (see also under Materials Index for specific systems) 362-366,
 908, 1334-1353, 1356, 1361, 1368-1369, 1374, 1440, 1456
 Smelting
 - copper 1336-1339, 1342-1349, 1354
 - lead 1354
 - nickel 1339-1340, 1350-1352
 - zinc 1354
 Solid state physics (see under Alloy physics or under specific topics)
 Solid-vapor diagrams (see also Metal-gas phase diagrams Pourbaix-
 Ellingham diagrams, etc.) 28, 121-122, 362-374, 1047-1064, 1077-1088,
 1090-1092, 1332-1333
 Solubilities, donor, acceptor 26-27
 Speiss 1357
 Splat cooling 383, 1171
 Stability diagrams (see also under Pourbaix, Ellingham)
 1047-1064, 1077-1088, 1428, 1456
 Standards of publication 1307-1324
 Stoichiometric description of superalloys 625-627

Strain energy 1210-1214
 Strain fields 620
 Stress, phase diagrams under external tensile -, or shear stress
 575-577
 Structural instabilities 769
 Sulfur: desulfurization 1372, 1456
 Superalloys 37, 262, 423-439, 624-658, 1186
 - stoichiometric description 625-627
 - geometric description 628-658
 - phacomp 37, 624-627, 1423
 Superconductivity as technique in phase diagram determination
 384-386
 Superconductors 262, 375, 387-392, 401, 545-549, 616-618, 770
 1148, 1158, 1326, 1411-1417
 - needs 1411-1417
 Surface phases 262, 268, 1459-1460
 Surrounded atom model 141

 Temperature scan method 151
 Tetrahedron approximation 968, 978-983, 1008
 Theories of phase diagrams (see review article pp 592-623, Tuesday's
 poster session on the topic pp 726-1236, and see under specific topics)
 - listing of treatments of the subject 84-89
 Thermal analysis, including differential thermal analysis, DTA) 121, 142
 377-382, 407, 417-419, 517, 1171, 1310
 Thermal gravimetric analysis 517
 Thermochemistry (see Thermodynamics)
 Thermodata 37, 122
 Thermodynamics
 - compilations 37, 53, 75-81, 196, 228, 229-250
 - computerized data banks 37, 49, 121-124, 1077-1089, 1186-1199, 1451
 - theory, including computerized methods (see also Tuesday's poster
 session on the topic pp 726-1236; and see under specific topics)
 37, 121-128, 143-144, 163, 803-845, 846-906, 1077-1089, 1100,
 1457-1458, 1472-1475
 - listing of treatment of theory 84-89
 Toop 141, 730-731, 956
 Transient Liquid Phase (TLP) bonding 1418-1419

 Variable valency in representation of phase diagrams 671-672
 VINITI (see under Russian literature)

 Wiederkehr 960

 X-ray analysis 143, 156, 407-422, 440-449, 517, 551
 - synchrotron light 163

MATERIALS INDEX

This index represents a listing of pages on which quantitative information is given for specific systems: 1) all pages are noted on which phase diagram figures appear; 2) generally, those pages are noted on which data evaluation is discussed; 3) generally, those pages are noted on which related thermodynamic data, or sometimes related crystallographic data appear. A few summarizing data tables occur in these proceedings. No attempt has been made to list these under each individual material. Rather, these are noted under the general material category (e.g. "rare earths", etc.). Alloys have been listed with their components in alphabetical order under the component of lowest alphabetical occurrence. For compounds, the formulas have been alphabetized, but compounds forming components of salt systems are not broken up to further alphabetize, in order to preserve chemical meanings (e.g. $\text{CaF}_2\text{-AlF}_3\text{-Al}_2\text{O}_3$ is listed under $\text{AlF}_3\text{-Al}_2\text{O}_3\text{-CaF}_2$, rather than Al-Ca-F-O).

A-15 compound formation prediction	1148, 1158
$\text{A}_2^{\text{III}}\text{B}^{\text{IV}}\text{O}_7$ compound formation prediction	1149-1150, 1159-1160
Ac-B	762
Ag laves phase prediction	1147, 1157
Ag-B	770
Ag-Cu	780
Ag-Cu-S	774-797
Ag-Cu-Se	774-802
Ag-Cu-Zn (several temps)	237-246
Ag-Pd	1218
Ag-S	779-780
Ag-Si	219
Al	1407
Al-Au-In	455
Al-B	749, 753-757
Al-Be-Fe	544
Al-Ca-O-Si	1370
Al-Co-Cr-Ni	438
Al-Co-Fe-Si	1392, 1405
Al-Cr-Fe-Ni	438
Al-Cr-Fe-Si	1392, 1405
Al-Cr-Mo-Ni-Ti-W	630-635

Al-Cr-Nb	1189-1190, 1199
Al-Cr-Ni	628-630, 655, 658
Al-Cr-Ni-Pt	439
Al-Cr-Ni-Ti	628-630, 654
Al-Cr-Zr	1189-1190, 1194-1189
Al-Cu	608
Al-Cu-Mg-Si	1389-1390, 1402
Al-Fe-Mn	1391, 1403
Al-Fe-Mn-Si	1392, 1405
Al-Fe-Ni-Si	1392, 1405
Al-Fe-Si	1392, 1394, 1404, 1407
Al-Ge-Nb	1415
Al-Li	1115-1118, 1128-1131
Al-Li-Mg	1109-1138, 1134-1138
Al-Mg	1118-1119, 1128-1129, 1132
Al-Mg-Zn	1385-1386, 1399
Al-Mn	134
Al-Ni-Ti	628-630, 657
Al-Sn	1219
Al-Ti-V (Ti-6Al-4V)	567-574
Al-Zn	1393, 1406
AlCa ₂ F ₇ , and related cpds.	283-285
AlCaF ₅ -FNa	318
Al ₂ CaF ₉ Na	320
AlF-CaF ₂	280-285
AlF ₃	278
AlF ₃ -AlF ₆ Li ₃ -AlF ₆ Na	329, 331
AlF ₃ -AlF ₆ Na ₃ -CaF ₂	314, 317-324
AlF ₃ -AlF ₆ Na ₃ -Al ₂ O ₃	322-326
AlF ₃ -AlF ₆ Na ₃ -Al ₂ O ₃ -CaF ₂	333, 335-337

$\text{AlF}_3\text{-AlF}_6\text{Na}_3\text{-Al}_2\text{O}_3\text{-CaF}_2\text{-FLi}$	272-354
$\text{AlF}_3\text{-AlF}_6\text{Na}_3\text{-Al}_2\text{O}_3\text{-CaF}_2\text{-FLi}$	336, 338
$\text{AlF}_3\text{-AlF}_6\text{Na}_3\text{-FLi}$	229, 332
$\text{AlF}_3\text{-Al}_2\text{O}_3\text{-CaF}_2$	328
$\text{AlF}_3\text{-FLi}$	300-305
$\text{AlF}_6\text{Li}_3\text{-AlF}_6\text{Na}_3$	306-311
$\text{Al}_6\text{Li}_3\text{-AlF}_6\text{Na}_3\text{-Al}_2\text{O}_3$	228-330
$\text{AlF}_6\text{Li}_3\text{-Al}_2\text{O}_3$	310, 312
$\text{AlF}_6\text{Li}_3\text{-CaF}_2$	314, 316
$\text{AlF}_6\text{Li}_3\text{-CaF}_2\text{-FLi}$	329, 333-334
AlF_6Na_3	277
$\text{AlF}_6\text{Na}_3\text{-AlF}_3$	289-296
$\text{AlF}_6\text{Na}_3\text{-Al}_2\text{O}_3$	296-299
$\text{AlF}_6\text{Na}_3\text{-Al}_2\text{O}_3\text{-CaF}_2$	325-328
$\text{AlF}_6\text{Na}_3\text{-CaF}_2$	285-290
$\text{AlF}_6\text{Na}_3\text{-FLi}$	305-308
$\text{AlKO}_2\text{-O}_2\text{Si}$	442
Al_2O_3	279
$\text{Al}_2\text{O}_3\text{-AlF}_3$	300
$\text{Al}_2\text{O}_3\text{-CaF}_2$	299-300
$\text{Al}_2\text{O}_3\text{-CaO-MgO-Na}_2\text{O-O}_2\text{Si}$	362-366, 374
$\text{AlO}_{1.5}\text{-KO}_{0.5}$	884
$\text{Al}_2\text{O}_3\text{-WO}_3$	221
Alloy 713 and 713LC	642
Am-B	752-756, 762
As-Ga	1233-1234
As-In	1233-1234
Au laves phase prediction	1147, 1157
Au-B	771
Au-Cu	726-743, 984-985, 988, 997-998, 1007-1011, 1020-1024

Au-Cu-Ni	726-743
Au-Mn	1013, 1025
Au-Ni	726-743
Au-Sb (including metastable diagram)	1173
Au-Si	1219
Au-Si (including metastable data)	1178
Au-Te	271
B-Ba	748, 753-757
B-Be	748, 752-757
B-C-Fe	566
B-Ca	748, 753-757
B-Co	749, 752-756, 761
B-Cr	749, 753-756, 759, 768
B-Fe	749, 753-756, 760
B-Fe (including metastable data)	1177, 1178
B-Hf	749, 753-756, 758
B-Ir	749, 753-756, 761
B-La	749, 753-756, 758
B-Mg	748, 753-757
B-Mn	749, 753-756, 760, 768
B-Mo	749, 753-756, 759
B-Nb	749, 753-756, 759, 768
B-Ni	750, 753-756, 761
B-Np	752-756, 762
B-Os	749, 753-756, 760, 770
B-Pa	762
B-Pd	750, 753-756, 761
B-Pt	750, 752-756, 761
B-Pu	752-756, 762
B-Re	749, 753-756, 760

B-Rh	749, 753-756, 761
B-rich systems	752
B-Ru	749, 753-756, 760, 770-771
B-Sc	749, 753-756, 758
B-Sr	748, 753-757
B-Ta	749, 753-756, 759, 768
B-Tc	749, 753-756, 760
B-Th	752-756, 762
B-Ti	749, 753-756, 758
B-transition metal	751
B-U	752-756, 762
B-V	749, 752-756, 759
B-W	749, 753-756, 759, 771
B-Y	749, 753-756, 758
B-Zr	749, 753-756, 758
B-1900	642, 652-653
$B_2O_3-WO_3$	220
$BaO-WO_3$	206
Be-Cu	539, 543
Be-Cu-Ne	543
Be-Fe	541
Be-Si	1219
Be-Ti (including metastable data)	1177
Be-Ti-Zr	1174
$BeO-WO_3$	202
Bi-Nb	1219
$Bi_2O_3-WO_3$	225
Brasses	1383-1385, 1398

C	857
C-Cr-Fe	1058
C-Cr-Fe-O	1048, 1060
C-Fe	155, 572, 885, 1368
C-Fe (metastable data)	1367
C-Fe-H-O-S	1081
C-Fe-Ni	470, 480, 880
C-Fe-Sb	573
C-H-Ni-O-S	1081
C-Ni (at three pressures)	111
C-Ni	891-901, 904
C-W	770
CO ₃ -HO-Li-Na	1098, 1108
Ca-Cu-Mg (several temps)	247-250
Ca-Fe-O-Si	1368
CaF ₂	279
CaF ₂ -FLi	310, 313-315
Ca-O-Si	1369
CaO-WO ₃	204
CdO-WO ₃	219
Cl-F-K-Li	1095, 1107
Cl-F-Li-Na	1095, 1105-1106
ClK-(HO) ₂ Mg-MgO	511, 514-515
ClLi-(HO) ₂ Mg-MgO	511-512, 515
ClN-(HO) ₂ Mg-MgO	511, 513, 515
Co-Fe-Ni	479
Co-Gd (including metastable data)	1177
Co-Sm	769
Cr-Fe	916, 935

Cr-Fe-Mg-O	1062
Cr-Fe-Ni	911-954
Cr-Fe-Ni (including irradiation effects)	1066-1069, 1071, 1074-1075
Cr-Fe-O	1059, 1061
Cr-Ni	916, 939
Cr-Ni-Ti	628-630, 656
Cr-O-S	1424
Cr-U (including metastable data)	1177
$\text{Cs}_2\text{O} \cdot \text{WO}_3 - \text{WO}_3$	201
Cu-Fe	916, 924, 938, 1027-1046
Cu-Fe-Mn	911-954
Cy-Fe-Ni	911-954
Cu-Fe-O-SiO ₂	1333
Cu-Fe-O-S-Si	1343
Cu-Fe-S	1333, 1343
Cu-Ge-Nb	1417
Cu-Mn	916, 940
Cu-Nb-Sn	1416
Cu-Ni	726-743, 916, 941
Cu-Ni-S	1350
Cu-O-S	1090-1092
Cu-S	779
Cu smelting	1336-1339, 1342-1349, 1354
Cu ternary alloys	229-250
Cu-Zn	1383-1385, 1398
Cu-Zr (including metastable data)	1177, 1178
$\text{Dy}_2\text{O}_3 - \text{O}_3\text{Sc}_2$	553-565
$\text{Dy}_2\text{O}_3 - \text{WO}_3$	211

F-Li	280
Fe-H-O-Ti	503
Fe-H-Ti	456, 498, 500, 506-507
Fe-Mn	916, 936
Fe-Mn-Ti	490-492, 504-505
Fe-Ni	916, 937, 1082, 1084
Fe-Ni (including irradiation effects)	1065, 1068-1069
Fe-Ni-Mn (including irradiation effects)	1065, 1068, 1072-1073
Fe-Ni-O	1078, 1082-1086
Fe-Ni-O-S	1077-1089
Fe-O	700, 909-910, 1080, 1084
Fe-O-S	1080, 1424
Fe-O-Si	1343
Fe-O-Ti	488-489, 501
Fe-Sb	573
Fe-Ti	486-488, 499
Ga-In-Sb	137, 138, 139
Ga-Nb	387-389, 397, 402-404
Ga-Sb	1233-1234
Ga-Sn-Zn	136
GaO ₃ -WO ₃	222
Ge-Nb	389-392, 405-406
GMR 235	642, 652-653
graphite	857
H-Zr	587, 590-591
HfO ₂ -WO ₃	214
H-Nb-Zr	588-589
H ₂ O-(HO) ₂ Mg-MgO	511, 515
Ho ₂ O ₃ -O ₃ Sc ₂	552-565

In-Sb	1233-1234, 1236
$\text{In}_2\text{O}_3\text{-WO}_3$	223
IN 100	642, 652-653
IN 731 X	642
Inconel 700	642, 652-653
Inconel 713 C	642, 652-653
Inconel X-750	642, 652-653
Ir laves phase prediction	1147, 1157
$\text{KO}_{0.5}\text{-O}_2\text{S}$	902, 906
$\text{K}_2\text{O}\cdot\text{WO}_3\text{-WO}_3$	199
$\text{La}_2\text{O}_3\text{-WO}_3$	208
Li-Mg	1119-1120, 1128, 1133
$\text{Li}_2\text{O}\cdot\text{WO}_3\text{-WO}_3$	197
M 316 stainless (including irradiation effects)	1065
Mar - M 200	642, 652-653
Metal hydrides	610-612
Mg-Pb	1388, 1401
Mg-Si	1386, 1400
Mg-Zn (including metastable data)	1177, 1178
MgO-WO_3	203
Mn-O-S	1424
Mo-P	770
Mo-V	1218
Mo-W	1218

$\text{Na}_2\text{O} \cdot \text{WO}_3 - \text{WO}_3$	198
Nb-Ni (including metastable data)	1177
Nb-Ti	1218
Nb-W	1218
$\text{Nb}_2\text{O}_5 - \text{WO}_3$	215
$\text{Nd}_2\text{O}_3 - \text{WO}_3$	210
Ni-based (superalloys)	624-658
Ni-O-S	1078-1080, 1424
Ni smelting	1340-1341, 1350-1352
Ni-Ti	135, 769
Nicrotung	642, 652-653
Nimonic 115	642, 652-653
O-Si	882
Os laves phase prediction	1147, 1157
Oxide systems	165-225, 251-256, 257-258, 272-345, 355-374, 410-422, 440-449, 508-514, 550-562, 909
PbO-WO_3	224
Pb-Sn (including metastable data)	1175
Pb-Te	1235
Pd laves phase prediction	1147, 1157
Pd-Si (including metastable data)	1177, 1178
Pt laves phase prediction	1147, 1157
Pt-V	549

Rare earths	110, 226-228, 751-752, 763
- tabulation of structure vs pressure	110, 112-120
$\text{Rb}_2\text{O} \cdot \text{WO}_3 - \text{WO}_3$	200
René 41	642, 652-653
Re-W (including irradiation effects)	1066, 1068-1069, 1076
Rh laves phase prediction	1147, 1157
Ru laves phase prediction	1147, 1157
$\text{Sm}_2\text{O}_3 - \text{WO}_3$	209
Sn-V	770
$\text{SrO} - \text{WO}_3$	205
Steels: 43XX steel	571-572
$\text{Ta}_2\text{O}_5 - \text{WO}_3$	216
$\text{TiO}_2 - \text{WO}_3$	212
Ti-rich, commercial (Ti-6Al-4V)	567-574
Tool steels	572-573
TRW 1900	642, 652-653
Udimet 500	642, 652-653
Udimet 700	642, 652-653
Unitemp AF	642, 652-653
$\text{UO}_3 - \text{WO}_3$	217
V-W	1218

Waspaloy 642, 652-653

$\text{Y}_2\text{O}_3 - \text{WO}_3$ 207

$\text{ZnO} - \text{WO}_3$ 218

$\text{ZrO}_2 - \text{WO}_3$ 213

U.S. DEPT. OF COMM. BIBLIOGRAPHIC DATA SHEET	1. PUBLICATION OR REPORT NO. NBS SP-496	2. Gov't Accession No.	3. Recipient's Accession No.
4. TITLE AND SUBTITLE Applications of Phase Diagrams in Metallurgy and Ceramics—Volume 2 Proceedings of a Workshop Held at the National Bureau of Standards, Gaithersburg, Maryland, January 10-12, 1977		5. Publication Date March 1978	
		6. Performing Organization Code	
7. AUTHOR(S) G. C. Carter, Editor		8. Performing Organ. Report No.	
9. PERFORMING ORGANIZATION NAME AND ADDRESS NATIONAL BUREAU OF STANDARDS DEPARTMENT OF COMMERCE WASHINGTON, D.C. 20234		10. Project/Task/Work Unit No.	
		11. Contract/Grant No.	
12. Sponsoring Organization Name and Complete Address (Street, City, State, ZIP) National Bureau of Standards; National Science Foundation; Defense Advanced Research Projects Agency; Office of Naval Research; National Aeronautics & Space Administration; Energy Research & Development Administration; U.S. Army Research Office		13. Type of Report & Period Covered	
		14. Sponsoring Agency Code	
15. SUPPLEMENTARY NOTES Library of Congress Catalog Card Number: 78-2201			
16. ABSTRACT (A 200-word or less factual summary of most significant information. If document includes a significant bibliography or literature survey, mention it here.) <p>The proceedings of a Workshop on Applications of Phase Diagrams in Metallurgy and Ceramics, held at the National Bureau of Standards, Gaithersburg, Maryland, on January 10-12, 1977, is presented in this NBS Special Publication. The Workshop was co-sponsored by the Institute for Materials Research and the Office of Standard Reference Data, NBS, and the National Science Foundation, the Defense Advanced Research Projects Agency, the Office of Naval Research, the National Aeronautics and Space Administration, the Energy Research and Development Administration, and the U.S. Army Research Office.</p> <p>The purpose of the Workshop was to assess the current national and international status of phasediagram determinations and evaluations for alloys, ceramics and semi-conductors; to determine the needs and priorities, especially technological, for phase diagram determinations and evaluations; and to estimate the resources being used and potentially available for phase diagram evaluation. These proceedings reflect the detailed contents of the Workshop for both the tutorial and review sessions as well as four poster sessions and four panel sessions covering the subjects; critical phase diagram availability, user needs of phase diagrams, experimental methods of determination, theoretical methods of calculation and prediction, methods of phase diagram representations of calculation and prediction, methods of phase diagram representations (especially multicomponent) and distribution to the user. Three of the panels addressed the subject of phase diagram needs in industrial applications.</p> <p style="text-align: right;">Cont.</p>			
17. KEY WORDS (six to twelve entries; alphabetical order; capitalize only the first letter of the first key word unless a proper name; separated by semicolons) Ceramics; computer predictions; critical evaluations; data compilations; electronic materials; industrial needs; metallurgy; phase diagrams; theory of phase diagrams; thermodynamics.			
18. AVAILABILITY <input type="checkbox"/> For Official Distribution. Do Not Release to NTIS <input checked="" type="checkbox"/> Order From Sup. of Doc., U.S. Government Printing Office Washington, D.C. 20402, SD Stock No. 003-003-01895-3 <input type="checkbox"/> Order From National Technical Information Service (NTIS) Springfield, Virginia 22151		19. SECURITY CLASS (THIS REPORT) UNCLASSIFIED	21. NO. OF PAGES 847
		20. SECURITY CLASS (THIS PAGE) UNCLASSIFIED	22.

16. ABSTRACT (A 200-word or less factual summary of most significant information. If document includes a significant bibliography or literature survey, mention it here.)

These proceedings represent documentation of this assessment, and constitute a valuable resource to workers in these areas, especially those planning to initiate phase diagram programs. Most subjects within the overall scope have been dealt with substantially in these proceedings; a few specialized topics such as surface and small particle phases, needed for the study of catalysis, have not been treated in detail. As the Alloy Data Center maintains a continuing phase diagram program, we would like to receive suggestions for similar topics of current and future interest, descriptions of new needs, or addenda and corrigenda to these proceedings. A tear-off sheet has been provided at the end of these proceedings for this purpose to be sent to the NBS Alloy Data Center.

If you wish to send us your suggestions for additional topics of current and future data compilation needs, or if you have any other addenda or corrigenda to these proceedings, please note them on this page and return to the

Alloy Data Center
National Bureau of Standards
Bldg. 223, Room B-150
Washington, DC 20234

Name _____

Affiliation _____

Address _____

City _____ State _____ Zip Code _____

Suggestions:

(cut here)

There's
a new
look
to...

DIMENSIONS

NBS

... the monthly magazine of the National Bureau of Standards. Still featured are special articles of general interest on current topics such as consumer product safety and building technology. In addition, new sections are designed to . . . PROVIDE SCIENTISTS with illustrated discussions of recent technical developments and work in progress . . . INFORM INDUSTRIAL MANAGERS of technology transfer activities in Federal and private labs. . . DESCRIBE TO MANUFACTURERS advances in the field of voluntary and mandatory standards. The new DIMENSIONS/NBS also carries complete listings of upcoming conferences to be held at NBS and reports on all the latest NBS publications, with information on how to order. Finally, each issue carries a page of News Briefs, aimed at keeping scientist and consumer alike up to date on major developments at the Nation's physical sciences and measurement laboratory.

(please detach here)

SUBSCRIPTION ORDER FORM

Enter my Subscription To DIMENSIONS/NBS at \$12.50. Add \$3.15 for foreign mailing. No additional postage is required for mailing within the United States or its possessions. Domestic remittances should be made either by postal money order, express money order, or check. Foreign remittances should be made either by international money order, draft on an American bank, or by UNESCO coupons.

Send Subscription to:

NAME-FIRST, LAST																							
COMPANY NAME OR ADDITIONAL ADDRESS LINE																							
STREET ADDRESS																							
CITY												STATE				ZIP CODE							

PLEASE PRINT

- ☐ Remittance Enclosed
(Make checks payable to Superintendent of Documents)
- ☐ Charge to my Deposit Account No.

MAIL ORDER FORM TO:
Superintendent of Documents
Government Printing Office
Washington, D.C. 20402

NBS TECHNICAL PUBLICATIONS

PERIODICALS

JOURNAL OF RESEARCH—The Journal of Research of the National Bureau of Standards reports NBS research and development in those disciplines of the physical and engineering sciences in which the Bureau is active. These include physics, chemistry, engineering, mathematics, and computer sciences. Papers cover a broad range of subjects, with major emphasis on measurement methodology, and the basic technology underlying standardization. Also included from time to time are survey articles on topics closely related to the Bureau's technical and scientific programs. As a special service to subscribers each issue contains complete citations to all recent NBS publications in NBS and non-NBS media. Issued six times a year. Annual subscription: domestic \$17.00; foreign \$21.25. Single copy, \$3.00 domestic; \$3.75 foreign.

Note: The Journal was formerly published in two sections: Section A "Physics and Chemistry" and Section B "Mathematical Sciences."

DIMENSIONS/NBS

This monthly magazine is published to inform scientists, engineers, businessmen, industry, teachers, students, and consumers of the latest advances in science and technology, with primary emphasis on the work at NBS. The magazine highlights and reviews such issues as energy research, fire protection, building technology, metric conversion, pollution abatement, health and safety, and consumer product performance. In addition, it reports the results of Bureau programs in measurement standards and techniques, properties of matter and materials, engineering standards and services, instrumentation, and automatic data processing.

Annual subscription: Domestic, \$12.50; Foreign \$15.65.

NONPERIODICALS

Monographs—Major contributions to the technical literature on various subjects related to the Bureau's scientific and technical activities.

Handbooks—Recommended codes of engineering and industrial practice (including safety codes) developed in cooperation with interested industries, professional organizations, and regulatory bodies.

Special Publications—Include proceedings of conferences sponsored by NBS, NBS annual reports, and other special publications appropriate to this grouping such as wall charts, pocket cards, and bibliographies.

Applied Mathematics Series—Mathematical tables, manuals, and studies of special interest to physicists, engineers, chemists, biologists, mathematicians, computer programmers, and others engaged in scientific and technical work.

National Standard Reference Data Series—Provides quantitative data on the physical and chemical properties of materials, compiled from the world's literature and critically evaluated. Developed under a world-wide program coordinated by NBS. Program under authority of National Standard Data Act (Public Law 90-396).

NOTE: At present the principal publication outlet for these data is the Journal of Physical and Chemical Reference Data (JPCRD) published quarterly for NBS by the American Chemical Society (ACS) and the American Institute of Physics (AIP). Subscriptions, reprints, and supplements available from ACS, 1155 Sixteenth St. N.W., Wash., D.C. 20056.

Building Science Series—Disseminates technical information developed at the Bureau on building materials, components, systems, and whole structures. The series presents research results, test methods, and performance criteria related to the structural and environmental functions and the durability and safety characteristics of building elements and systems.

Technical Notes—Studies or reports which are complete in themselves but restrictive in their treatment of a subject. Analogous to monographs but not so comprehensive in scope or definitive in treatment of the subject area. Often serve as a vehicle for final reports of work performed at NBS under the sponsorship of other government agencies.

Voluntary Product Standards—Developed under procedures published by the Department of Commerce in Part 10, Title 15, of the Code of Federal Regulations. The purpose of the standards is to establish nationally recognized requirements for products, and to provide all concerned interests with a basis for common understanding of the characteristics of the products. NBS administers this program as a supplement to the activities of the private sector standardizing organizations.

Consumer Information Series—Practical information, based on NBS research and experience, covering areas of interest to the consumer. Easily understandable language and illustrations provide useful background knowledge for shopping in today's technological marketplace.

Order **above** NBS publications from: Superintendent of Documents, Government Printing Office, Washington, D.C. 20402.

Order **following** NBS publications—NBSIR's and FIPS from the National Technical Information Services, Springfield, Va. 22161.

Federal Information Processing Standards Publications (FIPS PUB)—Publications in this series collectively constitute the Federal Information Processing Standards Register. Register serves as the official source of information in the Federal Government regarding standards issued by NBS pursuant to the Federal Property and Administrative Services Act of 1949 as amended, Public Law 89-306 (79 Stat. 1127), and as implemented by Executive Order 11717 (38 FR 12315, dated May 11, 1973) and Part 6 of Title 15 CFR (Code of Federal Regulations).

NBS Interagency Reports (NBSIR)—A special series of interim or final reports on work performed by NBS for outside sponsors (both government and non-government). In general, initial distribution is handled by the sponsor; public distribution is by the National Technical Information Services (Springfield, Va. 22161) in paper copy or microfiche form.

BIBLIOGRAPHIC SUBSCRIPTION SERVICES

The following current-awareness and literature-survey bibliographies are issued periodically by the Bureau:

Cryogenic Data Center Current Awareness Service. A literature survey issued biweekly. Annual subscription: Domestic, \$25.00; Foreign, \$30.00.

Liquified Natural Gas. A literature survey issued quarterly. Annual subscription: \$20.00.

Superconducting Devices and Materials. A literature survey issued quarterly. Annual subscription: \$30.00. Send subscription orders and remittances for the preceding bibliographic services to National Bureau of Standards, Cryogenic Data Center (275.02) Boulder, Colorado 80302.

U.S. DEPARTMENT OF COMMERCE
National Bureau of Standards
Washington, D.C. 20234

OFFICIAL BUSINESS

Penalty for Private Use, \$300

POSTAGE AND FEES PAID
U.S. DEPARTMENT OF COMMERCE
COM-215



SPECIAL FOURTH-CLASS RATE
BOOK

Date of request ☒ Not needed after:

Requester's order no.

Call No.

For use of Book author: OR: periodical title, vol. and date

Status

Dept.

Book title, edition, place, year, series: OR: periodical article author, title, pages. ☐ This edition only.

Verified in: OR: item cited in

ISBN, or ISSN, or LC card, or OCLC, or other number if known _____

If non-circulating, & cost does not exceed \$ _____, please supply ☐ Microfilm ☐ Hard copy

B REPORT

Request for ☐ LOAN or ☐ PHOTOCOPY
According to the A.L.A. Interlibrary Loan Code

REPORTS: Checked by

SENT BY: ☐ Library rate ☐

Charges \$ _____ Insured for \$ _____

Date sent

DUE

RESTRICTIONS: ☐ For use in library only

☐ Copying not permitted ☐

NOT SENT BECAUSE:

☐ In use ☐ Not Owned

☐ Non Circulating

☐ Request of

Estimated Cost of: ☐ Microfilm ☐ Hard copy

BORROWING LIBRARY RECORD:

Date received 3-1-81

Date returned 5-6-81

☐ Library rate ☐

Charge enclosed \$

Insured for \$

RENEWALS: ☐ No renewals

Requested on

Reviewed to

(or period of renewal)

Note: the receiving library assumes responsibility for notification

Request complies with
☐ IIR (a) (7), Guidelines (CCG)

AUTHORIZED BY:
(FULL NAME)

